

AD717149

AFCRL-70-0543
27 OCTOBER 1970
SPECIAL REPORTS, NO. 105

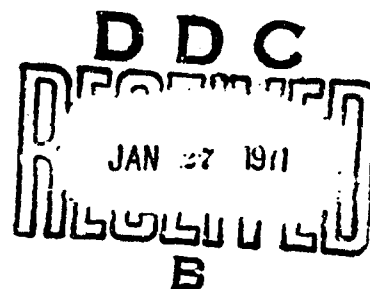


AIR FORCE CAMBRIDGE RESEARCH LABORATORIES

L. G. HANSCOM FIELD, BEDFORD, MASSACHUSETTS

Proceedings, Sixth AFCRL Scientific Balloon Symposium

Editor
LEWIS A. GRASS



AIR FORCE SYSTEMS COMMAND

United States Air Force



Best Available Copy

Reproduced by
**NATIONAL TECHNICAL
INFORMATION SERVICE**
Springfield, VA 22151

502

STI		
WRITE SECTION <input checked="" type="checkbox"/>		
DIFF SECTION <input type="checkbox"/>		
ANNOUNCED <input type="checkbox"/>		
CLASSIFICATION		
DISTRIBUTION/AVAILABILITY CODES		
DIST.	AVAIL.	HOW/BY SPECIAL
1		

This document has been approved for public release and sale; its distribution is unlimited.

Qualified requestors may obtain additional copies from the Defense Documentation Center. All others should apply to the Clearinghouse for Federal Scientific and Technical Information.

AFCRL-70-0543
27 OCTOBER 1970
SPECIAL REPORTS, NO. 105



AEROSPACE INSTRUMENTATION LABORATORY PROJECT 6665

AIR FORCE CAMBRIDGE RESEARCH LABORATORIES

L. G. HANSCOM FIELD, BEDFORD, MASSACHUSETTS

Proceedings, Sixth AFCRL Scientific Balloon Symposium

Editor
LEWIS A. GRASS

This work was supported in part by the National Aeronautics and Space Administration under Grants NGR-33-008-102, NGR-33-008-012, NGR-33-008-125, and Contract NAS8-24668, in part by the Office of Naval Research under Contract N00014-67-A-0108-0017, in part by the New York State Science and Technology Foundation under Grant SSF(8)-4, and in part by the Air Force Office of Scientific Research under Grant AFOSR-69-1785. It is Columbia Astrophysics Laboratory Contribution No. 20.

This document has been approved for public release and sale; its distribution is unlimited

AIR FORCE SYSTEMS COMMAND

United States Air Force



Abstract

This publication contains the papers presented at the Sixth AFCRL Scientific Balloon Symposium held in June, 1970 to promote the exchange of current information among balloon designers, developers, and flight managers and researchers engaged in scientific balloon programs. Subjects include: balloon-borne experiments in high-energy astrophysics, detection of atmospheric tides near 48 km, sun-oriented atmospheric optics, a proposed balloon mission in the Venus atmosphere, a panel on balloon materials and testing, telemetry and balloon-control instrumentation, advanced balloon technology, high altitude station-keeping balloons, the AFCRL tethered-balloon facility, advances in meteorological balloons, and superpressure balloons in the tropical stratosphere.

Contents

1. BALLOON-BORNE X-RAY POLARIMETRY by R.S. Wolff	3
2. GAMMA RAY ASTRONOMY AT 1 AND 3 MILLIBARS IN THE SOUTHERN HEMISPHERE by P. Albats, G. Frye, J. Maynard, and A. Zych	13
3. HIGH ENERGY ASTROPHYSICS FROM BALLOONS by J.F. Ormes	27
4. A CONSTANT-ALTITUDE BALLOON EXPERIMENT AT 48 KILOMETERS by H.N. Ballard, N.J. Beyers, and M. Izquierdo	33
5. A PAYLOAD STABILIZATION AND ATTITUDE CONTROL PLATFORM FOR HIGH ALTITUDE BALLOON EXPERIMENTS by L.E. Orwig, A.P. Wood, and P.E. Lavoie	49
6. A SCIENTIFIC MISSION USING A BALLOON IN THE ATMOSPHERE OF VENUS by R.M. Henry and J.P. Dickson, Jr.	61
7. SUN ORIENTED ATMOSPHERE OPTICS MEASUREMENTS USING THE HIGH ALTITUDE BALLOON by R.B. Toolin and N.C. Poirier	75
8. APPLICATIONS OF RADIO ALTIMETRY TO BALLOONS by F.G. Stremler, N. Levanon, and V.E. Suomi	91
9. VERTICAL LASER LINK USING TETHERED BALLOON by M. Subramanian	101
10. A REVIEW OF VHF BALLOON INSTRUMENTATION by D.M. Thon	111

Contents

11. EVALUATION OF UHF RADIO FREQUENCY EQUIPMENT FOR BALLOON TELEMETRY by O. L. Cooper	117
12. AIRSHIP AND BALLOON LEAGUE OF THE UNITED STATES	143
13. COMMENTS ON TETHERED BALLOONS by L. E. Speed	147
14. THE USE OF TETHERED BALLOONS AND KITES IN THE GARP TROPICAL EXPERIMENT by G. Stilke	153
15. THE INFLUENCE OF CHANGES OF MATERIAL STRUCTURE ON THE FAILURE OF POLYETHYLENE BALLOON FILMS by D. Weissmann	157
16. DEVELOPMENT OF THE e-BALLOON by J. H. Smalley	167
17. THE STEVENS INSTITUTE LABORATORY FOR BALLOON TECHNOLOGY AND SOME OF ITS CONTRIBUTIONS TO BALLOON RESEARCH by H. Alexander	177
18. A LISTING OF COMPUTER PROGRAMS AVAILABLE AT NCAR FOR SOLVING RECURRING PROBLEMS IN BALLOONING by J. M. Angevine	197
19. EXPERIMENTAL BALLOON GAS AND FILM TEMPERATURES by R. M. Lucas, G. H. Hall, and B. M. Allen	227
20. GENERAL PHILOSOPHY AND TECHNIQUES OF BALLOON CONTROL by B. D. Gildenberg	241
21. A DECISION THEORY MODEL FOR BALLOONING PROBLEMS by A. L. Morris	255
22. HEAVY LOAD PERFORMANCE OF STRATOFILM BALLOONS by L. Mielke	287
23. THIN FILMS FOR MESOSPHERE FLIGHT by J. H. Nelson	297
24. AN INFLATABLE RESTRAINT COLLAR FOR BALLOONS by K. Stefan	303
25. RECOMMENDATIONS FOR A REVISION OF THE BALLOON SPECIFICATIONS MIL-P-4840A (USAF) by A. D. Kerr and H. Alexander	315

Contents

26. OBSERVATIONS ON A TEST PROCEDURE FOR POLYETHYLENE BALLOON FILMS by J. A. Winker	325
27. BALLOON FILM SPECIFICATIONS by J. R. Nelson	329
28. TEST SPECIFICATION FOR UNSUPPORTED BALLOON FILMS by R. Hauser and K. Stefan	335
29. A TOWING TECHNIQUE FOR DETERMINING THE AERODYNAMIC FORCES ON TETHERED BALLOONS by L. T. Redd	341
30. A COMPARISON OF SEVERAL VERY HIGH ALTITUDE STATION KEEPING BALLOON CONCEPTS by J. J. Vorachek	355
31. RECENT AIRSHIP DEVELOPMENTS AND APPLICATIONS by R. R. Fisher and R. S. Ross	383
32. ENGINEERING CONSIDERATIONS FOR A TETHERED BALLOON SYSTEM BELOW THE TROPOPAUSE by P. F. Myers	395
33. FAIR SITE AND THE MARK II BALLOON TETHER WINCH by L. A. Grass, K. J. Turner, and D. C. Cox	411
34. NEW FRENCH TETHERED BALLOONS OF LARGE VOLUME: DEVELOPMENT, HANDLING TECHNIQUES, AND SAFETY PROBLEMS by P. Perroud, C. Aycoberry, J. Barrère, V. Controt, M. Saunois, M. Sylvestre-Baron, and B. Vieille	423
35. A SIMPLIFIED MATHEMATICAL MODEL FOR THE MOTION OF A TETHERED KITE BALLOON: STABILITY CRITERIA by J. M. Dubois	439
36. NEW TECHNIQUES AND DEVELOPMENTS IN METEROLOGICAL BALLOONS by M. Sharenow	445
37. FAST-RISING STABLE STREAMLINED BALLOON FOR HIGH RESOLUTION WIND MEASUREMENTS by R. M. Henry and C. V. Echstrom	459
38. AN ANALYSIS OF THE BOUNDARY LAYER ASSOCIATED WITH FLOATING BALLOON SYSTEMS by R. D. Reynolds and A. L. Wallis, Jr.	471
39. NIMBUS-D/IRLS SUPERPRESSURE BALLOONS IN THE TROPICAL STRATOSPHERE by J. D. Tefft	477

Contents

40. NIMBUS 4 INTERROGATION, RECORDING AND LOCATION SUBSYSTEM by A. Gottesman	483
APPENDIX A. Publication of Proceedings of Past AFCRL Balloon Symposia and Workshops	493

Balloon Borne Experiments and Instrumentation

Monday

Morning: Chairman, Jack K. Kelso
Defense Atomic Support Agency

Afternoon: Chairman, Ralph J. Cowie
Air Force Cambridge Research Laboratories

Evening: Chairman, Thomas W. Kelly
Air Force Cambridge Research Laboratories

PROCEEDINGS, SIXTH AFCRL SCIENTIFIC BALLOON SYMPOSIUM *

1. Balloon-borne X-ray Polarimetry

R.S. Wolff
Columbia University, New York

The recent discoveries of solar X-ray emission and stellar X-ray sources have led to important questions regarding the physical processes generating these highly energetic photons. To obtain a more complete understanding of the X-ray production mechanisms responsible, investigators have sought to measure the overall intensity, spectrum, time variation, and polarization of the X-ray fluxes. In particular, the polarization of the X-ray emission is strongly dependent on the source conditions. X-rays produced in a hot, isotropic, optically thin plasma would be unpolarized. Such a model has been suggested for the strong stellar X-ray source, Sco X-1. However, X-rays produced by bremsstrahlung collisions between a stream of high energy anisotropic electrons and an ambient gas would exhibit strong linear polarization. These conditions could prevail during a solar flare, where high energy electrons accelerated in the corona stream into the

(Received for publication

*This work was supported in part by the National Aeronautics and Space Administration under Grants NGR-33-008-102, NGR-33-008-012, NGR-33-008-125, and Contract NAS8-24668, in part by the Office of Naval Research under Contract N00014-67-A-0108-0017, in part by the New York State Science and Technology Foundation under Grant SSF(8)-4, and in part by the Air Force Office of Scientific Research under Grant AFOSR-69-1785. It is Columbia Astrophysics Laboratory Contribution No. 20.

PRECEDING PAGE BLANK

denser atmosphere collide with the cooler gas and emit the high energy X-ray flux that is often observed (Cline and Holt, 1968). The low energy photons will be polarized perpendicular to the plane formed by the incident beam and outgoing X-ray flux, and the high energy photons will be polarized in the plane. The synchrotron process provides a third possible method of producing X-rays. Relativistic electrons trapped in a magnetic field will spiral around the field lines, radiating X-ray photons which are linearly polarized with their electric vector lying in the plane perpendicular to the magnetic field intensity. In this case, the plane of polarization is independent of the photon energy. This mechanism has been considered in explaining the x-ray emission of the Crab nebula, since a similar process seems to adequately explain its polarized optical and radio emission (Woltjer, 1964). Measurements of X-ray polarization and its energy dependence would be definitive in distinguishing between the various production processes.

X-ray polarization can be detected by utilizing the angular dependence of the electron-photon incoherent scattering cross section. When the scattering angle is 90° , the photons are preferentially scattered in a direction orthogonal to the incident beam and the electric vector of the incident wave, as shown in Figure 1.1. This effect can be realized in a scattering target comprised of a light element, where the electrons are loosely bound and can scatter photons incoherently. This method of detecting polarization is limited by the condition that the scattering angle

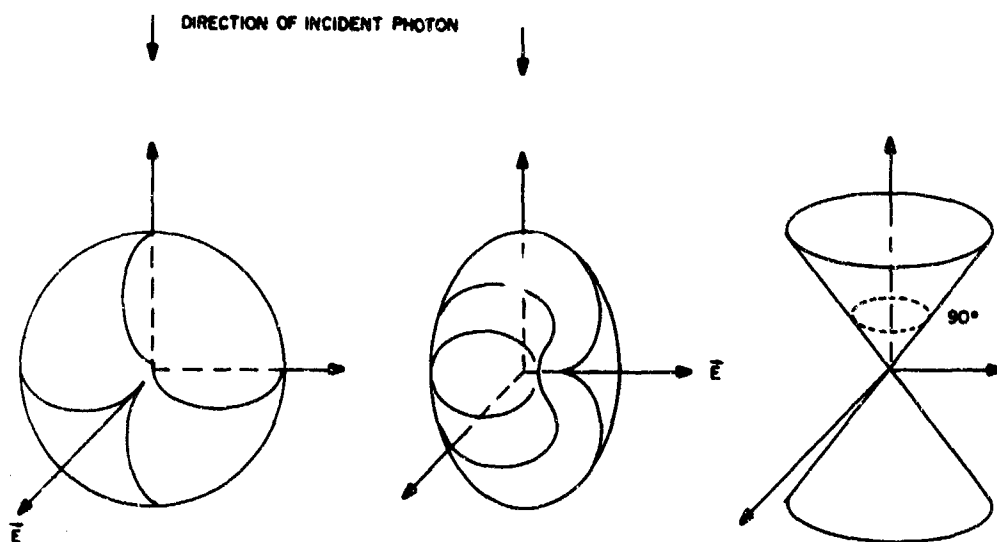


Figure 1.1. Sine-squared Distribution of Scattered Photons for Two Directions of Incident Polarization. Those Scattered Within the 90-degree Cone Carry Little Information About Polarization

must be 90° to obtain complete extinction of the photons polarized in the plane of viewing (the plane formed by the directions of the incident and scattered beams). In practice, the X-ray detector must subtend a large solid angle, and photons scattered at angles other than 90° are also detected, but this effect can be accounted for. Incoherent scattering as a method of detecting X-ray polarization has the distinct advantage over other techniques such as Bragg reflection because the cross section is essentially independent of energy. Whereas Bragg reflection can be used to measure polarization only at a single wavelength, incoherent scattering allows observation over a continuum of energies. This effect is advantageous because it increases the signal strength and enables simultaneous measurement of polarization over a range of energies.

An incoherent scattering X-ray polarimeter has been constructed and successfully flown in sounding rockets to study several stellar X-ray sources. The instrument is shown in Figure 1.2. The polarimeter consists of an array of scattering blocks and X-ray detectors enclosed in an anticoincidence shield to reduce the cosmic ray-induced background. Both the stellar and solar X-ray fluxes depend strongly on energy, diminishing rapidly at shorter wavelength. The flux from the Crab nebula, for example, obeys a power law (Boldt et al, 1969)

$$N(E)dE = 7E^{-2}dE \text{ photons/cm}^2\text{-sec-keV} \quad (1.1)$$

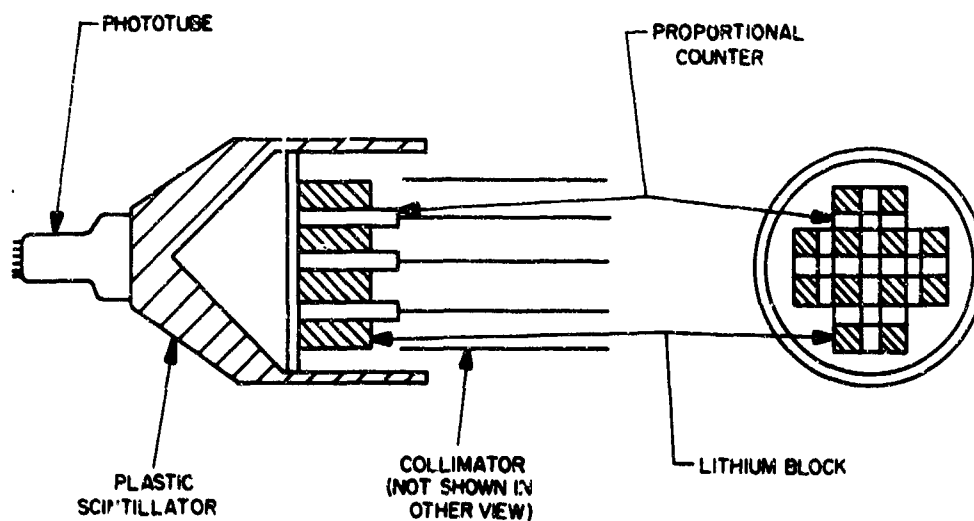


Figure 1.2. Schematic Diagram of Polarimeter

in the range 1 to 500 keV. It is imperative to maximize the sensitivity of the instrument at the lowest possible energy. For this reason, lithium metal was selected as a scattering material. Photoelectric absorption varies with energy as $E^{-7/2}$, and in lithium the incoherent scattering cross section and photoelectric cross section become comparable at 8 keV. Above this energy, the polarimeter can operate efficiently. The shape of the scattering blocks was chosen to maximize the overall sensitivity. The block length is greater than one scattering length, implying that more than 70 percent of the incident photons will interact in the metal. The width was chosen to be small compared to a scattering length to allow photons to emerge from the sides without multiple scattering.

Proportional counters are used to detect the scattered photons. These detectors produce a signal amplitude proportional to the energy of the detected X-ray, allowing pulse-height analysis and the study of the energy dependence of the X-ray polarization. Furthermore, those cosmic-ray background pulses whose amplitudes fall above the range expected for X-rays can be eliminated. Proportional counters also permit the use of pulse shape discrimination to distinguish between valid X-ray events and charged-particle-induced background. The gas filling in the counters establishes the upper limit of the polarimeter energy range, and this was maximized by using three atmospheres of xenon. The overall sensitivity of the polarimeter as a function of energy is shown in Figure 1.3.

Data are taken with the polarimeter by pointing the instrument at the X-ray source and rotating around the line of sight. If the X-ray flux is polarized, the counting rate in each detector will be modulated at twice the rotation frequency. The depth of modulation determines the degree of polarization. Monte Carlo calculations and laboratory tests have shown that the X-ray polarization P is related to the maximum and minimum counting rates N_{\max} and N_{\min} by the relation

$$P = \mu \left(\frac{N_{\max} - N_{\min}}{N_{\max} + N_{\min}} \right) \quad (1.2)$$

where μ is the polarimeter modulation factor, and is equal to 3.18.

The measurement of stellar X-ray polarization is limited by the low signal intensities and the high cosmic-ray-induced background rates. A prototype of the polarimeter was flown in a balloon to assess the effectiveness of various background suppression techniques and to investigate instrumental effects which could result in a spurious polarization measurement (Wing, 1968). The polarimeter was carried to an altitude of 96,000 ft, hung vertically below the balloon, and rotated around the symmetry axis. It was found that the anticoincidence shield

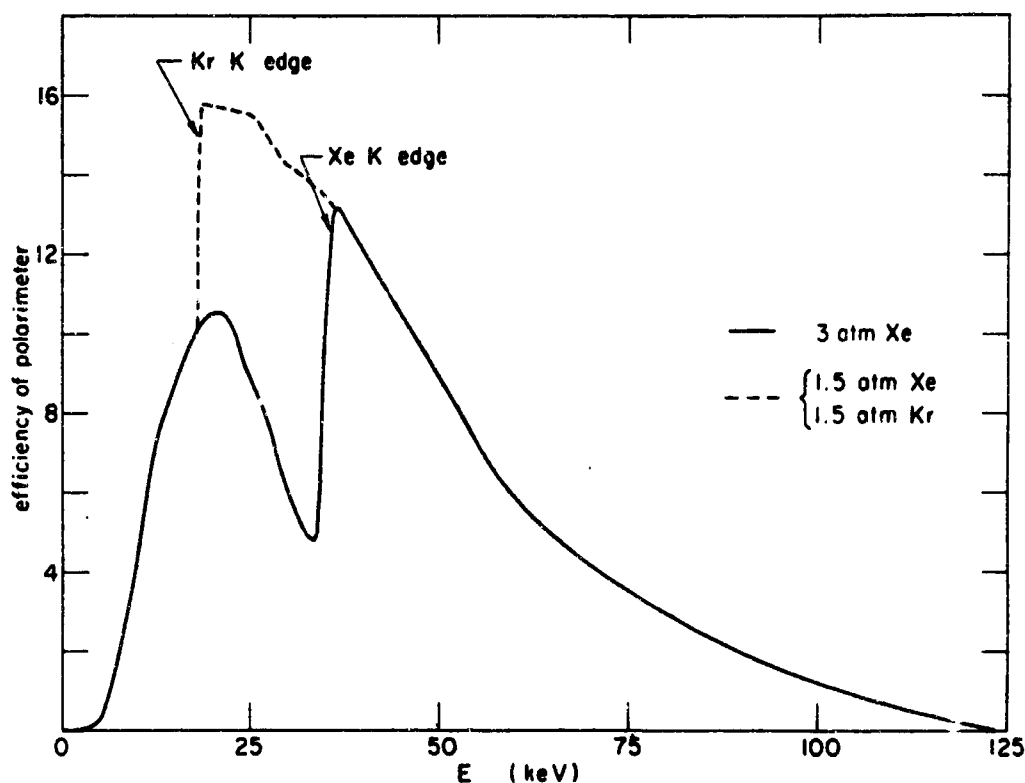


Figure 1.3. The Efficiency of the Polarimeter as a Function of Energy

reduced the background rate by a factor of three. Pulse-height analysis reduced the background in the range 5 to 25 keV by another factor of three. A final background rate of 0.01 counts/keV-sec-counter was obtained. The flux from the Crab nebula in the same energy range above the atmosphere is approximately one tenth of this value. The asymmetry of the primary cosmic-ray flux, or east-west effect, was also considered. A modulation in the background rate due to this anisotropy could manifest itself as a spurious indication of polarization. Analysis of the data revealed, however, that all fluctuations in the counting rates were completely random.

Further background suppression has been obtained by utilizing pulse-shape discrimination. Charged particles passing through the counters produce long ionization trails, and the subsequent pulses rise slowly. X-rays, however, are absorbed at a single point and result in quickly rising pulses. A method of distinguishing between the two types of events was developed, and data obtained in a recent rocket flight indicated that the background rate can be reduced to 0.003 counts/counter-keV-sec (Wolff, 1969).

Although the polarimeter was originally designed for use in sounding rockets, its application from balloon altitudes has been seriously considered. The development of larger balloons, with increased lifting capacity and altitude, has greatly improved the feasibility of balloon-borne X-ray polarimetry. The availability of better control systems has also been an important factor. The primary problem in stellar X-ray polarimetry is the low intensity and strong energy dependence of the sources. For this reason, high altitude and long duration flights are essential to make meaningful measurements.

As an example of the problems involved and the results which could be obtained, we can consider the possibility of measuring the X-ray polarization of the Crab nebula with the lithium block polarimeter. Since atmospheric absorption is acute at energies below 15 keV, we have assumed an energy range of 15 to 50 keV. The efficiency of the polarimeter between 25 and 35 keV is particularly low when only xenon gas is used in the detectors because the xenon K absorption edge lies at 35 keV. If the proportional counters are filled with a mixture of 1.5 atmospheres of xenon and 1.5 atmospheres of krypton, the efficiency can be greatly increased, as shown by the broken curve in Figure 1.3. However, laboratory measurements have indicated that background rejection using pulse-shape discrimination is less effective in gas mixtures.

The signal intensity for the Crab nebula, measured at the top of the atmosphere, was calculated from Eq. (1.1) and corrected for atmospheric absorption at various balloon altitudes. The use of the xenon-krypton mixture increased the signal intensity in the 15 to 50 keV range by 55 percent. The background rate assumed was based on the most recent rocket data. A study of the rocket data as a function of altitude indicated that the background rate was constant above 100,000 ft. A total background rate of 7 counts/counter-sec could be expected. The signal intensity was calculated for 125,000 ft, 140,000 ft, and 157,000 ft with the Crab nebula 10° from the zenith, corresponding to a launch from Palestine, Texas. At the lowest altitude, a rate of 0.22 counts/counter-sec would be obtained; at 140,000 ft, the signal rate would be 0.50 counts/counter-sec; and at 157,000 ft, the signal rate would be 0.84 counts/counter-sec.

The minimum polarization that can be measured is governed by the total numbers of signal and background counts obtained. Statistical fluctuations impose a lower limit on the detectable polarization, since a finite amount of completely random data will yield a non-zero result. If we refer the polarization vector to an orthogonal coordinate system and let P_1 and P_2 be the components of P along each axis, it can readily be shown that the minimum detectable polarization (in each component) is given by (Wolff, 1969)

$$3\sigma_{P_1} = 3\sqrt{2} \mu \frac{\sqrt{S+B}}{S} \quad (1.3)$$

where S and B are the total numbers of signal and background counts. This limit means that 99 percent confidence can be ascribed to a result which exceeds the value calculated from Eq. (1.3). Since polarization is a positive definite quantity obtained from the components by the relationship

$$P = \sqrt{P_1^2 + P_2^2}, \quad (1.4)$$

it is apparent that purely statistical fluctuation in the components will always result in a non-zero value for the apparent polarization. Even when the actual polarization is zero, a measurement of P will yield a mean value of (Wolff, 1969)

$$P = \sqrt{\frac{\pi}{2}} \sigma_{P_1}. \quad (1.5)$$

The predicted signal and background rates can now be used with Eq. (1.3) to obtain an estimate of the sensitivity of a balloon-borne polarimetry experiment. Since the background rate greatly exceeds the signal, it is clear that long observation periods will be required. This calculation was performed assuming 8 hours at maximum altitude with the meridian crossing in the middle of the observation period. This condition was chosen to minimize the atmospheric slant height and also to avoid possible cosmic-ray effects at large zenith angles (discussed below). By combining the signals from the 16 proportional counters, we find that the minimum detectable polarization at an altitude of 125,000 ft is 21 percent. At an altitude of 140,000 ft, observing for the same 8-hour period, the limit is lowered to 15 percent. If the experiment can be performed at 157,000 ft, a polarization as small as 10.2 percent could be detected.

The latter result makes balloon-borne polarimetry appear feasible if the problems inherent in long-term observations can be overcome. Current models of the Crab nebula which attribute the X-ray emission to synchrotron radiation from relativistic electrons predict that the optical and X-ray flux should have comparable polarizations. The optical emission integrated over the 1' diameter region of the nebula responsible for X-ray emission is 19 percent polarized (Oort and Walraven, 1956). Furthermore, the 2-cm radio emission from the entire nebula is 14 percent polarized. The only X-ray result reported to date, obtained from a rocket flight with this same polarimeter, yielded an upper limit of 27 percent on the X-ray polarization (Wolff et al., 1970). The proposed balloon experiment would therefore

provide a substantial improvement in the sensitivity of measurements of this important quantity.

The prolonged observation times required to obtain sufficient data necessitate accurate pointing and control of the payload. The polarimeter must be pointed within 3° of the X-ray source in order to avoid instrumental effects which lead to spurious signal modulation. When the X-ray flux is incident at an angle greater than 3° , unscattered photons can directly illuminate the detectors, leading to an anomalously high counting rate. Calculations and laboratory measurements revealed that the spurious polarization induced by this effect is less than 1.5 percent, provided that the X-ray flux is within 2.5° of the polarimeter axis. A control system capable of pointing the payload to within a 3° radius circle of the X-ray source and maintaining a sidereal scan is therefore required. The polarimeter must also be rotated around the line of sight to average out the differences in sensitivity among the various detectors and to obtain the modulation characteristic of polarization. The payload could be equipped with a rocking assembly which would rotate the polarimeter through $\pm 45^\circ$ while the gondola remains fixed. Finally, it would be desirable to periodically point the polarimeter away from the source to make a background measurement. Since the background rate is so crucial to the experiment, long-term drifts in the electronics which could affect the counting rate would greatly confuse the data.

A further restriction on the control system is that the angle between the polarimeter axis and the zenith be kept at a minimum. Evidence from satellite surveys has shown a substantial gamma-ray albedo from the earth's atmosphere, which is particularly strong at the horizon. If the polarimeter is aimed near the vertical, the projected area subtending this flux is minimized. The background counting rate would be higher when the instrument is pointed far from the vertical and could be subject to angular variations which could induce spurious modulation. Since the sun can also be a strong source of high energy X-rays, it would be prudent to perform the experiment at night using a stellar tracking system.

The problems inherent in measuring polarization in solar X-ray emission are quite distinct from those associated with stellar sources. Under normal circumstances, the sun is not a source of high energy X-rays, with a negligible flux above a few keV. During periods of solar activity, however, appreciable numbers of energetic photons, usually associated with solar flares, are emitted. Sounding rocket and satellite monitors have been used to study the intensity, spectra, and time variations of these X-ray events. A typical X-ray flare rises to a maximum in 1 to 2 min, reaching a peak energy flux in excess of 10^{-4} ergs/cm²-sec above 7 keV, and then diminishes in 5 to 10 min. Often superimposed on this flux are short, intense bursts of high energy rays of a few seconds' duration and ranging

as high as 100 keV. The slower varying component of the X-ray emission often exhibits a thermal spectrum which can be characterized by plasma temperatures as high as 10^8 °K.

Using X-ray data recently reported for a solar flare (Hudson et al., 1969) we have calculated the minimum detectable polarization in various energy intervals. The results are listed in Table 1.1. In performing these calculations, a balloon altitude of 125,000 ft and 100 sec of data were assumed. Polarization of X-ray fluxes up to 90 keV could readily be measured.

Table 1.1. Minimum Detectable Polarization from an X-ray Flare Observed at 125,000 ft

Energy Range (keV)	3 σ Limit (%)
10-20	1.77
20-30	1.61
30-40	1.80
40-50	1.77
50-60	2.95
60-70	5.15
70-80	8.70
80-90	18.7

The primary problem in measuring X-ray flare polarization from balloons involves the frequency of occurrence of the events. The rate at which flares occur is strongly related to the state of solar activity. During times of peak activity, flares are produced several times per day, but accurate predictions cannot be made. At best, a probability of flare occurrence can be established, based on the age and number of active regions on the sun. During times of high probability, one could launch a balloon experiment and wait for a flare, but even in an 8-hour patrol the chance of detecting a flare is not great. A successful solar flare balloon program would necessitate a series of launches in conjunction with a period of intense solar activity.

In summary, it is possible to say that stellar X-ray polarimetry is feasible from balloons. With high-altitude, accurately controlled balloons, the long observation periods required to accrue adequate data can be obtained. Measurement of solar X-ray polarization, although not encumbered by the long integration periods, still requires accurate control over prolonged time intervals while waiting for an X-ray flare to occur. Both experiments could yield meaningful data regarding the mechanism responsible for X-ray production.

References

- Boldt, E., Desai, V. and Holt, S. (1969) Astrophys. J. 156:427.
- Hudson, H.S., Peterson, L.E. and Schwartz, D.A. (1969) Astrophys. J. 157:389.
- Oort, J.H. and Walraven, T. (1956) Bull. Astron. Inst. Neth. 12:285.
- Wing, T. (1968) Ph.D. Thesis, Dept. of Physics, Columbia University, New York.
- Wolff, R.S. (1969) Ph.D. Thesis, Dept. of Physics, Columbia University, New York.
- Wolff, R.S., Angel, J.R.P., Novick, R. and Vanden Bout, P. (1970) Astrophys. J. Letters 160:L21.
- Woltjer, L. (1964) Astrophys. J. 140:1309.

Contents

2.1	Introduction	13
2.2	Southern Hemisphere Series	14
2.3	Gamma Ray Spark Chamber	16
2.4	Point Source of γ -Rays - SGR γ -1	19
2.5	Longreach and 30 m cu ft Balloons	21
2.6	Conclusion	25

2. Gamma Ray Astronomy at 1 and 3 Millibars in the Southern Hemisphere

P. Albers, G. Frye, J. Maynard and A. Zych
Case Western Reserve University
Cleveland, Ohio

Abstract

In collaboration with Professor Hopper's Cosmic Ray Group at the University of Melbourne, we have made a series of high altitude flights in Australia. The experiment was to survey the southern sky for sources of primary gamma rays above 50 MeV in energy. The basic detector was a spark chamber whose sparking patterns were recorded photographically. With the cameras, associated electronics and flight instrumentation, the total weight of the gondola is 480 lbs. On two flights from Parkes, NSW, in February 1969, we detected a point source of gamma radiation located 20° below the center of the galaxy. More recent flights on 10 and 30 M balloons from Longreach, Queensland in November 1969 will also be described.

2.1 INTRODUCTION

I would like to relate to you some of the work that the cosmic ray group at Case Western Reserve University has been doing. In particular, I will describe our work in gamma ray astronomy for a series of balloon flights at 3 and 1 mb in the southern hemisphere.

The phrase "gamma ray astronomy" is related to the familiar optical astronomy in the sense that we are interested in electromagnetic radiation coming from celestial objects in the sky. However, gamma rays are very high-energy light particles, or photons, and require detection techniques that are more familiar to high-energy nuclear physics than astronomy. Nevertheless, the detector which I will describe shortly is a telescope which is carried to very high altitudes with balloons to get above most of the earth's atmosphere which is a source for background.

Once gamma rays are detected from some celestial object or area of the sky, the intensity and energy spectrum of these gamma rays provides information about their origin. A number of production mechanisms for these gamma rays are possible on a cosmological scale. These include the collision of the high energy protons and electrons within our galaxy with the hydrogen and star light. One would also expect high-energy gamma rays from discrete objects such as quasi-stellar objects, super nova, and the more recently discovered pulsars.

Since 1963, a program has been underway at Case Western Reserve University to scan the entire celestial sphere with a spark chamber for discrete sources of high-energy gamma rays with energies greater than 50 MeV. This program has, to date, covered about one-half of the sky in both the northern and southern hemispheres with a threshold sensitivity of $1 \times 10^{-5} \text{ } \gamma/\text{cm}^2 \text{ sec}$ from a point source.

2.2 SOUTHERN HEMISPHERE SERIES

In recent years, a number of groups have been able to take advantage of Australia's special vantage point for viewing the southern sky with experiments from balloons. To my knowledge, all of these flights have been conducted with the able assistance of the Project HIBAL launch crew and facilities based at Mildura. This is a joint operation of the U.S. AEC and the Australian Department of Supply.

Our flights have originated from three different launch locations. There are shown in Table 2.1. Each location has something different to offer. The vertical cutoff rigidity at Mildura has about the same value as at Palestine, Texas. Flights from Parkes, in New South Wales, provided a considerably longer float time when the high altitude winds were from the east. Longreach, in Queensland, is directly on the Tropic of Capricorn and has a considerably higher cutoff and, therefore, provides a reduction in background radiation due to the primary flux.

At this point, I should mention that our Australian flights have been a collaboration with Professor Victor Hopper and his group at the University of Melbourne.

Table 2.1. Launch Sites for Balloon Flights in the Southern Hemisphere

Location in Australia	Number of Flights	Geographic Latitude	Vertical Cutoff
Mildura (VIC.)	8	34.5° South	4.0 BV
Parkes (NSW)	3	33.5° South	4.5 BV
Longreach (QLD)	4	23.5° South	8.8 BV

Table 2.2. Listing of Balloon Flights in the Southern Hemisphere

Date	Flight Number	Launch Site	Balloon Size M Cu Ft	Polyethylene Thickness	Time at Float	Max. Alt. - Ft.	Remarks
3/14/67	330-A	Mildura	5	3/4 Mil	6 Hr	120 K	Successful Flight
3/20/67	334-A	Mildura	9	3/4 Mil	0	70 K	Burst-Free Fall
9/9/67	356-A	Mildura	10.6	1/2 Mil	0	135 K	Payload Failure
9/27/67	360-A	Mildura	10.6	1/2 Mil	3 Hr	136 K	Partial Success
10/23/67	365-A	Mildura	5	3/4 Mil	0	78 K	Burst
11/1/67	367-A	Mildura	10.6	1/2 Mil	8 Hr	134 K	Successful Flight
11/10/67	369-A	Mildura	10.6	1/2 Mil	5 Hr	135 K	Partial Success
11/23/67	372-A	Mildura	10.6	1/2 Mil	2 Hr	92 K	Balloon Failure
2/6/69	427-A	Parkes	10.6	3/4 Mil	4 Hr	132 K	Successful Flight
2/17/69	428-A	Parkes	10.6	3/4 Mil	0	132 K	R/C Malfunction-Cut down
2/28/69	429-A	Parkes	10.6	3/4 Mil	8 Hr	132 K	Successful Flight
11/17/69	463-A	Longreach	30	1/3 Mil	3 Hr	158 K	Partial Success
11/26/69	466-A	Longreach	30	1/3 Mil	0	0	Balloon Failure
11/27/69	467-A	Longreach	10.6	3/4 Mil	8 Hr	131 K	Successful Flight
12/4/69	468-A	Longreach	30	1/3 Mil	5 Hr	158 K	Partial Success

Table 2.2 is a listing of the flights we have made in Australia. For the most part, 9 and 10 million cu ft balloons have been used to take our payload to 3 mb. Even at 5 mb though, practically all of the gamma rays detected are produced in the remaining air above the detector by the primary flux. Therefore, observing a possible source of gamma rays is essentially a signal-to-noise problem and the highest possible altitude is a prime requirement.

Last November, we had an opportunity to fly two 30 M* cu ft balloons which took our payload to almost 1 mb. These flights were launched at Longreach. As you can see from the last column in Table 2.2, we have had our successful flights and also our problems.

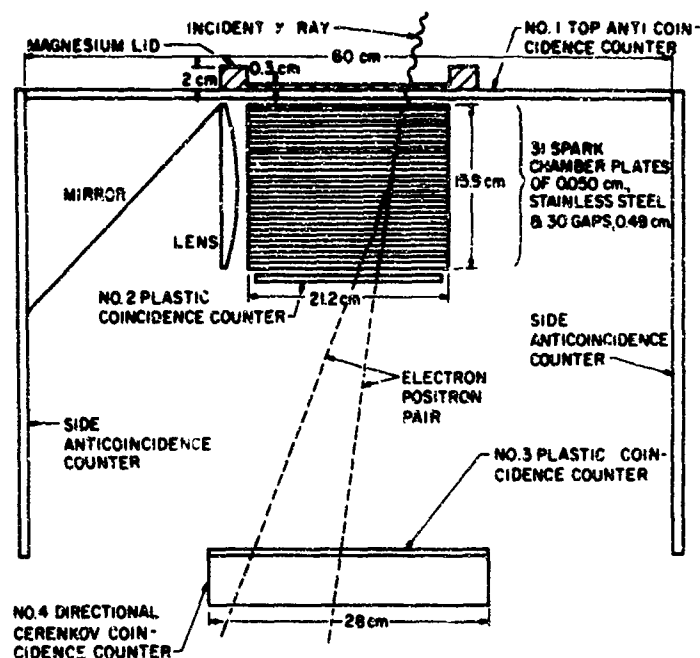
2.3 GAMMA RAY SPARK CHAMBER

The basic scheme that we use to detect gamma rays is a spark chamber. This is shown in Figure 2.1. The spark chamber consists of a series of thin, parallel, stainless steel plates in a vessel filled with neon gas at about one atmosphere of pressure. Gamma rays themselves have no electrical charge, but they interact in the iron to produce an electron-positron pair of charged particles. This electron and its anti-particle, the positron, leave ionization trails in the neon gas between the plates and are then detected by the three detectors below the spark chamber (Detectors 2, 3, and 4). When this electron-positron pair is detected, a 8 KV high voltage pulse is applied to alternate plates in the spark chamber. Sparks occur where the charged particles have produced the ionization path. The sparks are produced within a fraction of a microsecond after the event has occurred. These sparks are then photographed.

Detector #1 in Figure 2.1 is a plastic scintillator anticoincidence counter to ensure that the interaction in the chamber is due to an electrically neutral particle. Detector #4 is a directional Cerenkov detector which is sensitive only to charged electrons and positrons moving downward.

Figure 2.2 shows a pictorial view of the spark chamber with the photomultiplier tubes, mirrors and camera in place. The spark chamber and high voltage electronics are in pressurized vessels. The remaining electronics and hardware are in the low pressure environment. Note that a 16 mm camera is used to record two 90° stereoscopic views of the chambers. The camera also photographs an instrument panel for each event which includes the instantaneous orientation of the gondola in the azimuthal direction. The gondola hangs in the vertical direction as shown. Since the spark chamber will detect gamma rays with incident directions

* M: million



50 LBS. OF IRON

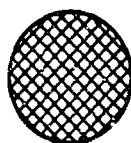


Figure 2.1. Gamma Ray Spark Chamber System

off the zenith, no orientation of the gondola is required for events which pass within 30° of the zenith. Professor Hopper's group is building an orientation in which will allow us to observe the Magellanic Clouds which lie very near the South Celestial Pole.

Actually, two cameras are now used with a rotating mirror arrangement to switch from one camera to the other by radio command. Our event rate at float is about 3 per second. The total film capacity is 128,000 frames.

A typical gamma ray event is shown in the photograph in Figure 2.3. Here it can be clearly seen that the event originates in one of the plates. The bending of the tracks is due to the multiple scattering of particles in the plates. Measurements of the spark positions are done manually by a staff of scanning personnel and then transferred to computer tape for analysis.

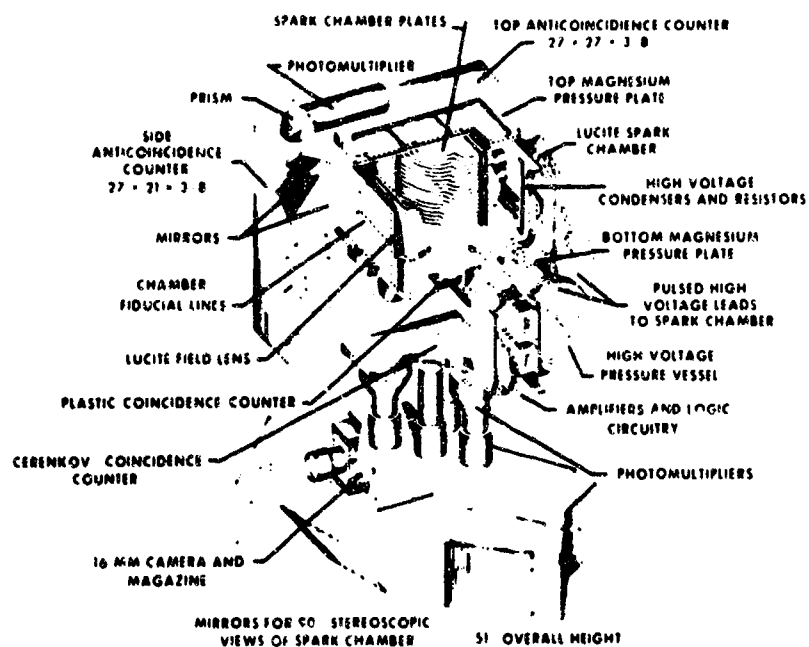


Figure 2.2. Pictorial View of Gamma Ray Spark Chamber System

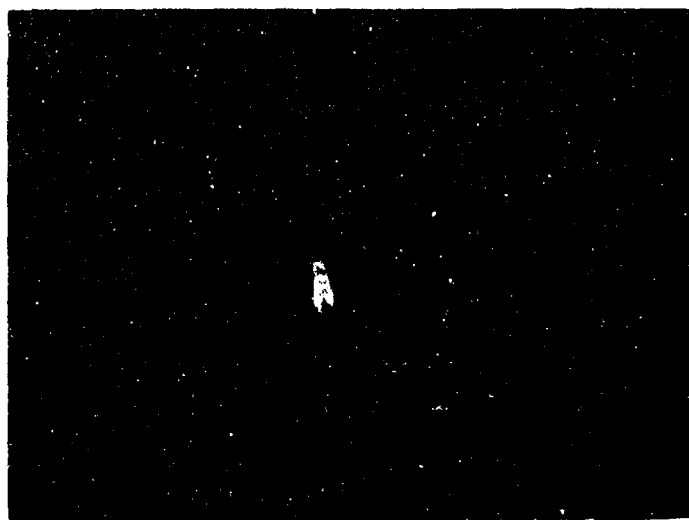


Figure 2.3. Typical High Energy Gamma Ray Event

From the spark position information in the chamber, two things are determined. First, the direction of the incident gamma ray is determined from the directions of the two tracks in the chamber to an accuracy of about $\pm 3^\circ$. Second, the scattering in the iron plates causes the tracks to deviate from a straight line. A measurement of these deviations provides the energy of the incident gamma ray.

From the orientation of the gamma ray in the chamber and the magnetic orientation of the gondola, the right ascension and declination of each incident gamma ray can be calculated and related to a point on the celestial sphere.

2.4 POINT SOURCE OF γ -RAYS - SGR γ -1

At this point I would like to describe some of the results we obtained from the two flights launched from Parkes in NSW in February of 1969 which reached 3 mb. The results from the analysis of the flight film indicate that a point source of gamma rays is present in the southern sky with an intensity above the background level for our detector.

Before I discuss the point source data further, let me indicate how our data are analysed for a possible source of gamma rays. In Figure 2.4 we have divided the sky into bins. The coordinates are right ascension and the sine of the declination to provide horizontal strips of equal solid angle. The variation in width of each bin is determined from the response of the spark chamber to that part of the sky during the flight in such a way that the total exposure for each rectangle is the same. The minimum size of a bin is determined by the angular resolution of the detector.

The numbers indicated in each bin in Figure 2.4 indicate the number of gamma ray events that originated from that particular direction of the sky. The sequence of numbers in each bin represents different classifications of gamma ray events. A point source will show an enhancement in one of the bins. Of course, one has to take into account the random statistical fluctuations in the number of background events found in each bin. It should be noted that the plot in Figure 2.4 is for one section of the sky in the northern hemisphere.

Our data from the two flights from Parkes were analysed in this manner, independently. The data for each flight showed an enhancement in the gamma ray flux from the same location in the sky. These data are shown in Figure 2.5. Here, we show the number of events from a $4^\circ \times 4^\circ$ bin centered at the proposed source location. This is bin #4 in Figure 2.5. Also shown is the average number of events for the same bin size from the surrounding bins corrected for the relative exposure. The two graphs in Figure 2.5 show, for the two flights, the number of events for regions #1 thru #7. For both flights, an enhancement of about three standard deviations above the background level is seen in region #4.

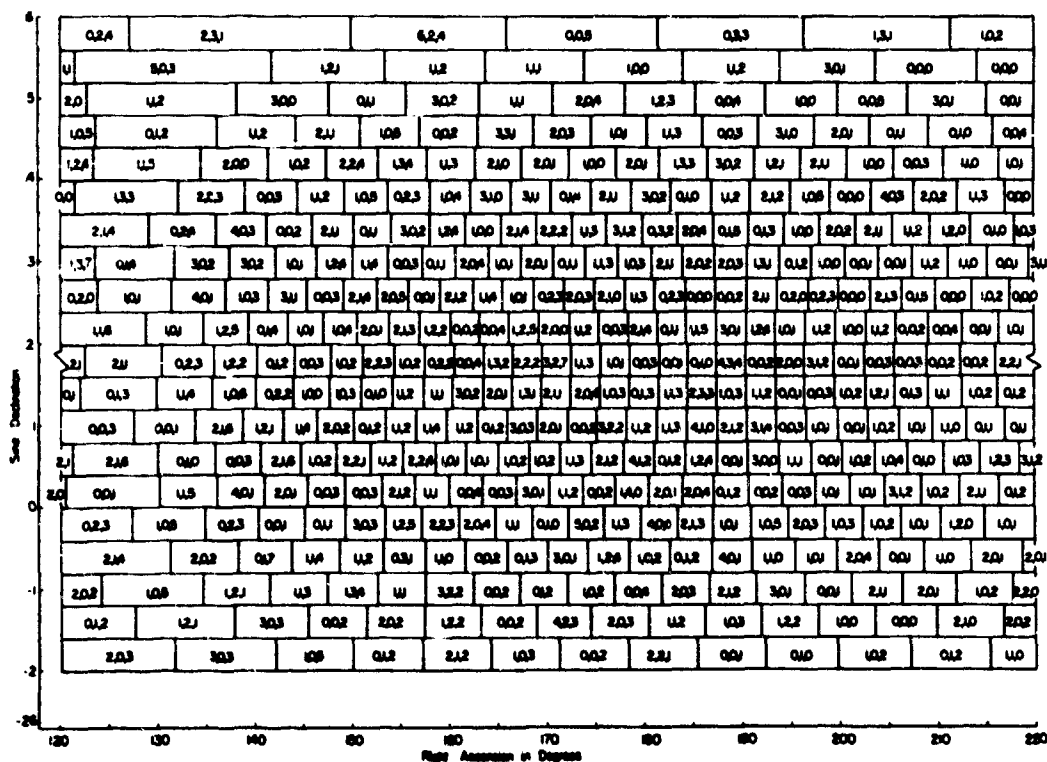


Figure 2.4. Incident Direction of Gamma Rays in Right Ascension and Declination for a Balloon Flight

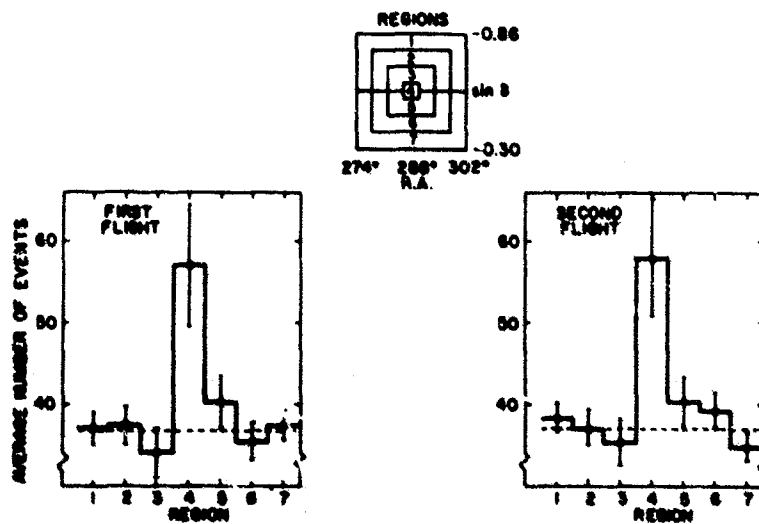


Figure 2.5. Comparison of the Bin at R.A. = 288°, sin δ = -0.58 with the Average of Surrounding Bins Corrected for the Relative Exposure

For one flight, a random three standard-deviation fluctuation is not too unlikely. However, to have such an enhancement for two separate sets of data and have it occur in the same bin location is very unlikely. The chance that these increases at the same bin location are just accidental occurrences is about 1 part in 1000. Therefore, we have taken these data to be evidence for the first point source of gamma rays to be observed. Note that the atmospheric background level is still twice the source intensity, so that higher altitudes are very desirable.

Several factors have convinced us that this evidence is not just some systematic instrumentation effect. First, a different detector was used on each of the two flights. For the first flight, a spark chamber system built by the University of Melbourne group was used. For the second flight, our detector was used. While the basic design of the two systems is the same, there were significant differences in the electronics, optics and orientation monitoring.

Second, the flight films were scanned separately and the events reduced to right ascension and declination by different computer programs. One flight was analysed at Melbourne and the other one at Case Western Reserve University. There was good agreement between the two groups for those portions of one flight which was scanned and processed by both groups.

Table 2.3 gives the present location and intensity of the source. It is located in the constellation of Sagittarius and has been designated as Sgr γ -1.

Presently, the data from these two flights are being combined and checked, and we expect to have a more refined result later this summer.

Table 2.3. Preliminary Location and Intensity of Sgr γ -1

$$\begin{aligned} \text{Location } \alpha &= 288^\circ \pm 3^\circ \\ \delta &= -35^\circ \pm 2^\circ \\ (l_{II} = 3^\circ, b_{II} = -20^\circ) \\ \text{Intensity } (3 \pm 1) \times 10^{-5} \gamma'/\text{cm}^2\text{sec } (>50 \text{ MeV}) \end{aligned}$$

2.5 LONGREACH AND 30 M CU.FT. BALLOONS

Last November, we had an opportunity to go back to Australia, this time to Longreach. The combination of a higher cutoff rigidity and 30 M cu ft balloons that would take our payload to 1 mb has the effect of reducing our background counting rate due to the residual atmosphere by a factor of about 4, and thus providing a more sensitive search for gamma ray sources.

In addition, the recent discovery of pulsating radio and X-ray sources is certainly suggestive that one ought to try to look for pulsed high-energy gamma rays. This required the addition of a reasonably accurate clock to our present system which has an accuracy of one part in 10^8 per day.

The data from the three flights which we had at Longreach are presently being analysed and no results are available yet. Therefore, for the remaining portion of this talk, I would like to present some general ascent data for one of the flights with a 30 M cu ft balloon.

The photographs in Figures 2.6, 2.7, and 2.8 were taken at Longreach. Figure 2.6 shows our instrument package in the Meteorological Station at the airfield. The thermal insulation that usually surrounds the instrument has been removed. This small work area was essentially the only air-conditioned space available and we were very fortunate to have had that. The Meteorological Station did have its own radar facility. High altitude wind data were obtained up to about 130,000 ft with meteorological balloons prior to each flight. The radar was used to track the balloon on ascent also.

Figure 2.7 shows our payload on the launch truck. The distance from the launch arm to the truck was about 550 ft. Our payload is completely enclosed with urethane foam to provide both thermal insulation and also a dark box for photography. A crush pad is added below our gondola. The unit attached outside our main gondola is a sun compass which can determine the sun's azimuthal direction to $1/3^\circ$. This provides a check for our magnetic determination of the spark chamber orientation. Below, are the radio command - telemetry equipment (Winzen Research) and ballast hopper. A squib was used in the parachute shroud lines to collapse the chute at impact. Also, a burst switch was placed at the top of the parachute.

Figure 2.8 shows a 30 M with balloon just after launch. The ascent rate and altitude were obtained for the entire ascent from the radar measurements. These data are shown in Figure 2.9 for our second flight with the large balloon. The gross weight was 2092 lbs. Fourteen percent free lift was used for this flight. For our first 30 M flight (463-A), 13 percent free lift was used. The average ascent rate for this flight for the first 30,000 ft was 600 ft/min and 5 hours were required to reach float. From the data in Figure 2.9 for 468-A, the average ascent rate to 30,000 ft is 1000 ft/min and 4 hours were required to reach float. This flight was launched about 12 min after sunrise. Ascent ballasting is also shown on this graph. Each point of the ascent rate data shown in Figure 2.9 is an average over about 3 or 4 readings and the indicated peaks are real.

To provide a more accurate measurement of the residual atmospheric pressure at float, we fly a large dial Wallace and Tiernan pressure gauge which is calibrated against a McLeod gauge before each flight.

The ascent data from this gauge are shown in Figure 2.10. From these data it can be seen that the maximum altitude for this flight was 1.17 mb or 154 K ft. The maximum float altitude for the first flight with a 30 M was 1.19 mb.

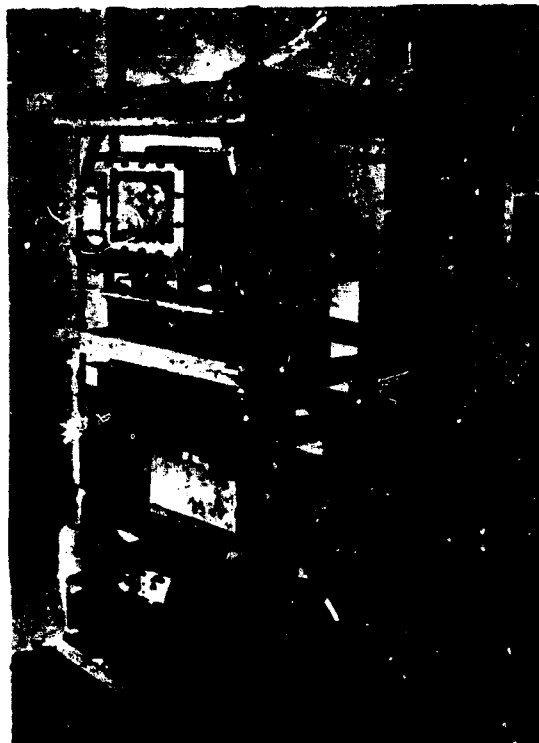


Figure 2.6. Gamma Ray Detector at Longreach, QLD



Figure 2.7. Gamma Ray Detector on Launch Truck and 30 Million Cu Ft Balloon



Figure 2.8. 30 Million Cu Ft Balloon at Longreach, QLD, just After Launch

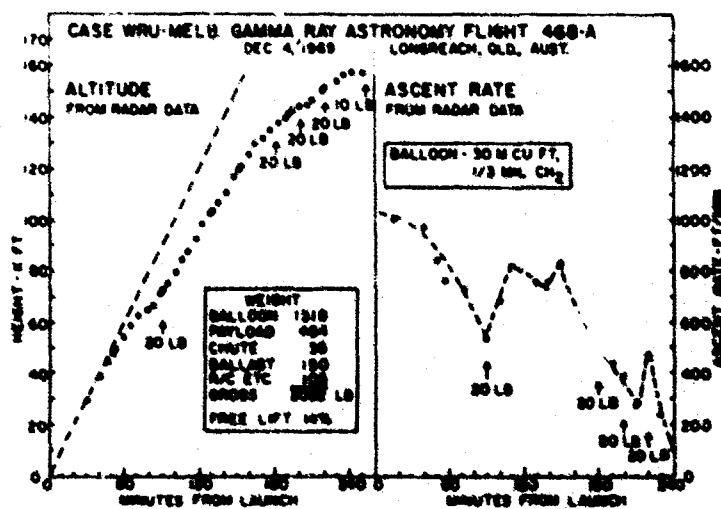


Figure 2.9 Altitude and Ascent Rate for 30 Million Cu Ft Balloon at Longreach, QLD (Flight 468-A)

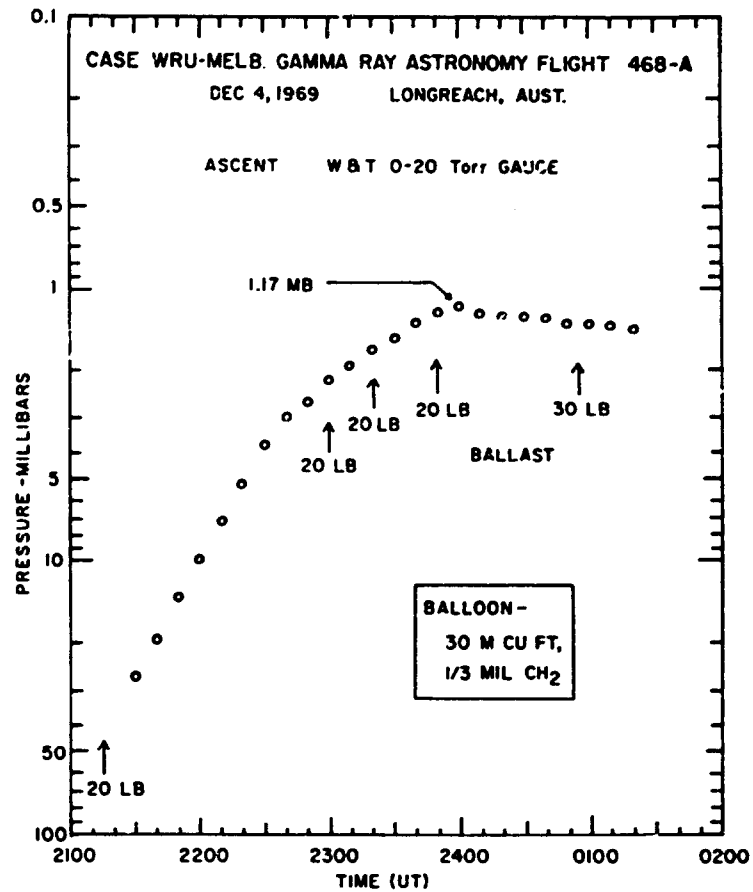


Figure 2.10. Ascent Curve from Data Taken from Onboard Pressure Gauge. (Flight 468-A)

2.6 CONCLUSION

To conclude, I would like to say that a number of discoveries in the past year or so have made high-energy gamma ray astronomy a very exciting field of investigation. Also, the availability of reliable large balloons capable of taking a payload such as ours to pressures less than 1 mbar offers an exceptional opportunity in the near future to do better experiments from balloon platforms.

3. High Energy Astrophysics From Balloons

J.F. Ormes
NASA/Goddard Space Flight Center
Greenbelt, Maryland

The cosmic corpuscular radiation consists of completely ionized nuclei of the elements from hydrogen through iron and beyond. A single cosmic ray has been found with a charge which may exceed that of any particle known. Our knowledge began in 1948 when heavy cosmic rays were discovered in balloon borne photographic emulsions (Freier et al, 1948). It has subsequently been realized that these cosmic rays represent a sample of matter from the galactic thermonuclear furnaces where elements are formed. They contain enormous energies in a single particle extending in energy up to 10^{20} eV and so represent products of the most energetic phenomena known. As such they represent an important astrophysical phenomenon. Filling the galaxy with an energy density of 1 eV/cm^3 , comparable to the energy in gas turbulence and magnetic fields, they have an important effect on the dynamical structure and stability of the galaxy (Parker, 1965). A large fraction of the direct measurements of the cosmic radiation have been made in high altitude balloons. More recently, the new fields of X- and γ -ray astronomy have developed, and together with cosmic rays they have formed an area of study now called High Energy Astrophysics. This arose because the X- and γ -rays are photons energetic enough to behave more like particles than electromagnetic waves. Hence, the techniques of measuring cosmic rays could be directly applied to these studies. X-ray

PRECEDING PAGE BLANK

emitting stars and nebulae have been identified and a strong γ -ray emission from the center of the galaxy has been observed. A good deal of the early work in these fields has been, and is being, done from balloons.

It is of course true that those things which can be measured most easily have been measured first. Our present measurements have, for example, taken full advantage of existing balloon technology. In order to see how extensions of balloon technology could affect high energy astrophysics, a brief survey of our present state of knowledge will be given. A few of the measurements that would be useful for extending our knowledge and their implications for balloons will be discussed.

The cosmic rays are known to extend in energy from a few million electron volts to 10^{20} or more electron volts (Linsley, 1963). The spectrum of these particles is shown in Figure 3-1. Note how rapidly the intensity decreases with increasing flux. Above 10^{14} eV all the data come from extensive air shower arrays, in which the cosmic rays are studied by measuring the characteristics of the shower of secondary particles produced when a primary cosmic ray interacts in the atmosphere. These detector arrays are spread over large areas on the ground and operate for many years in order to obtain statistically meaningful results (Brownlee et al, 1969).

At energies from 10^{10} eV to 10^{14} eV, very little information is available. At these energies particles are completely relativistic, having velocities essentially equal to the velocity of light. As a result, measuring energies is very difficult and requires heavy equipment (Ormes et al, 1968). In addition, the low intensities of these particles require large area detectors and long exposure times. To study these particles from balloons requires altitudes in the range of 100 to 120 thousand feet or higher, but the background increases linearly with pressure (and hence exponentially with decreasing height). The hope is that in the near future, scientific payloads in the range of 2 to 5 tons can regularly be carried to these altitudes. In the long term what is required is long observing times and this can probably only be achieved on satellites.

Quite detailed information on the charge composition and energy spectra of cosmic rays is already available at low energies. Some of this data is summarized in Figure 3.2. The most intense region of the spectra of all the components lies at a few hundred MeV, and conveniently the overlying atmosphere does not produce prohibitive background in this energy range. For this reason most of the early information between 100 and 1000 MeV came from balloon-borne detectors.

At present, satellite detectors have been used to extend our information to still lower energies. However, satellite detectors have, until now, been small and have had to operate for long times to obtain significant fluxes of particles. The energy region below 100 MeV is of particular interest for studies because so many

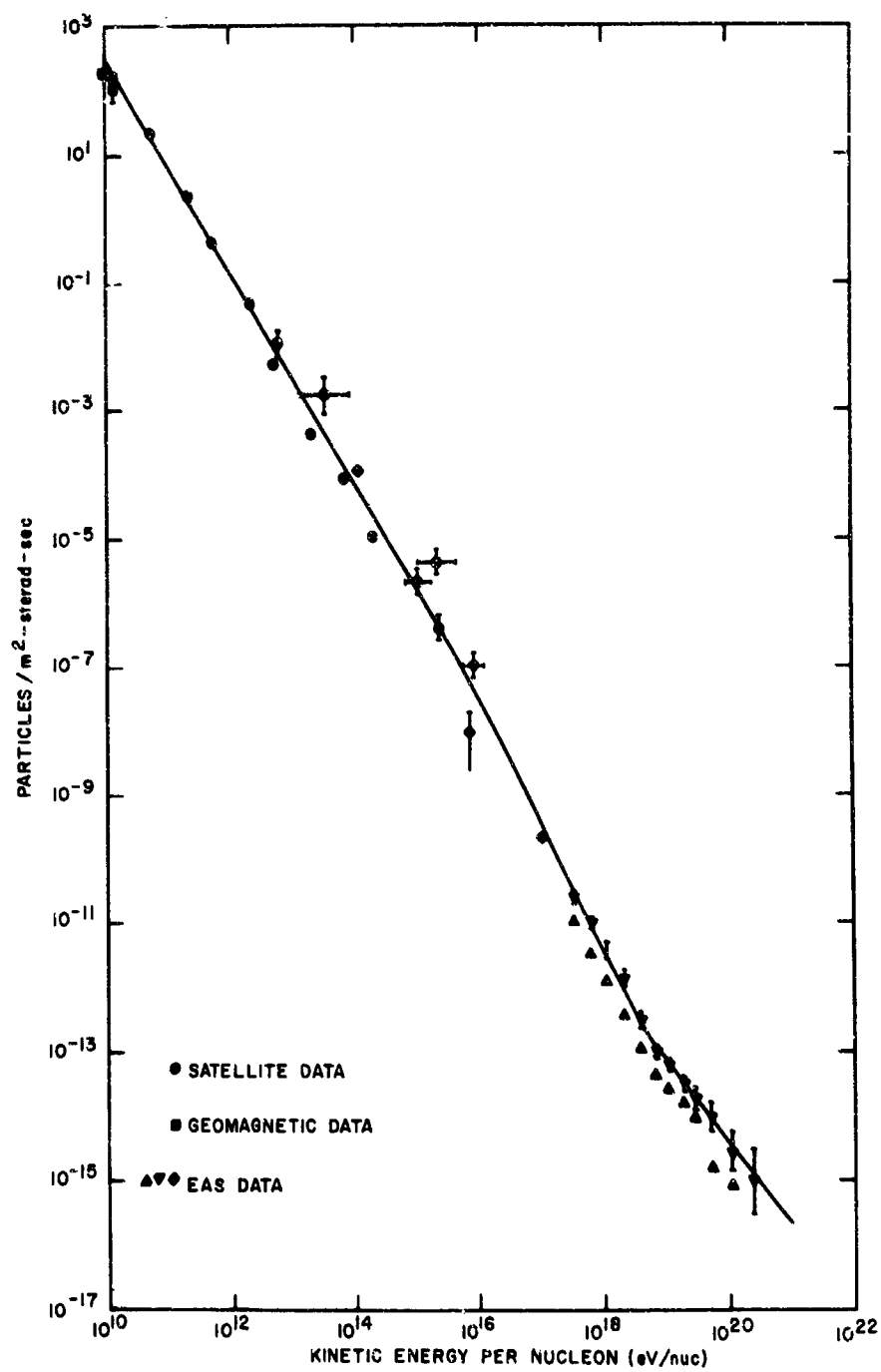


Figure 3.1. Spectrum of Cosmic Rays Extending Over 10 Orders of Magnitude and Having a Steeply Falling Spectrum

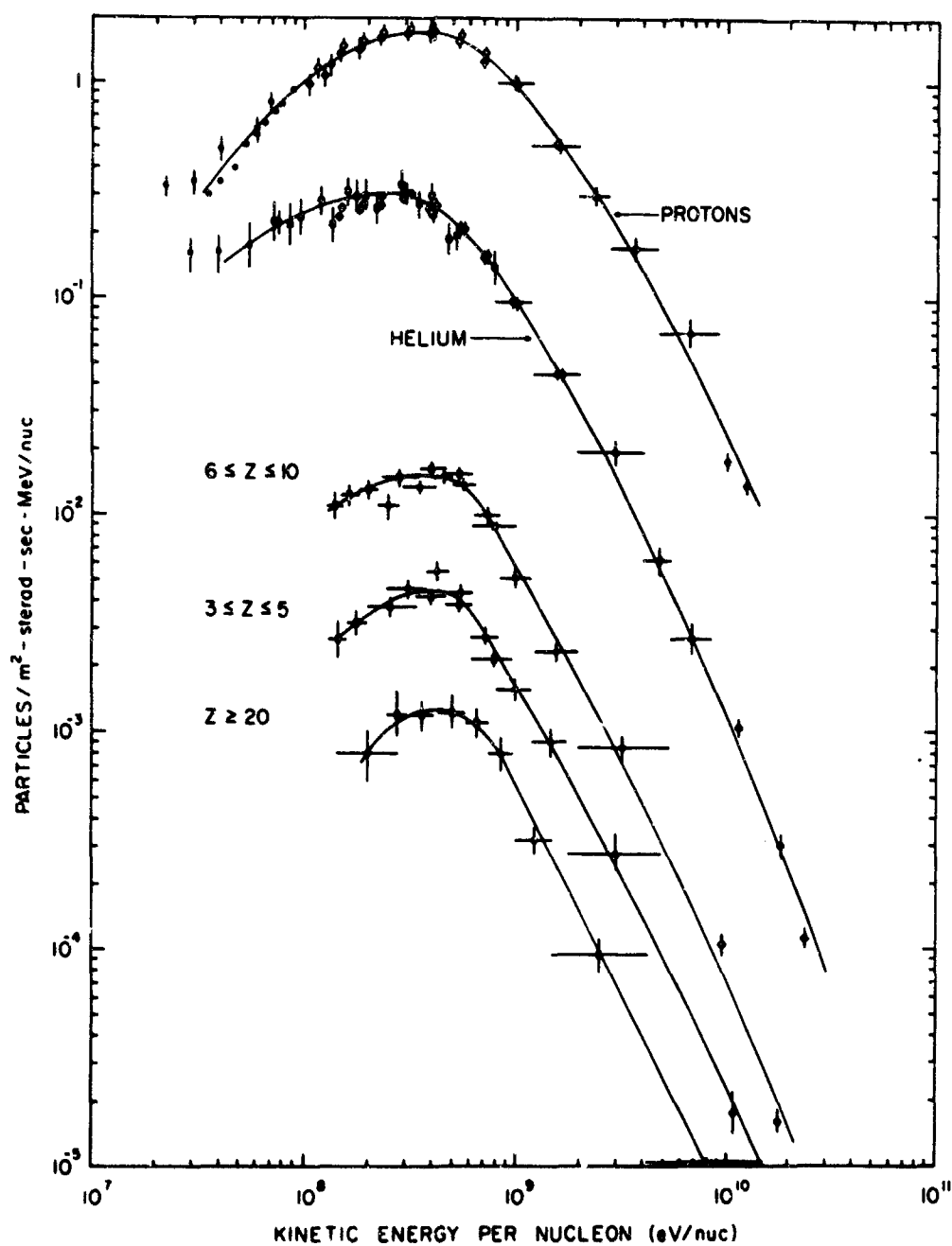


Figure 3.2. Differential Spectra of the Various Cosmic Ray Constituents at Low Energies. Most of this data above 10^8 eV/nuc comes from balloon borne instrumentation

energy-dependent phenomena are supposed to become important in this energy range. Detectors for studying low energies need not be heavy but they must be large in area. To do studies of this type would require large-area, light-weight detectors carried to very high altitudes. Detectors of a few hundred pounds carried to 0.5 mb pressure for long flights from high latitude stations would be exceedingly useful.

Gamma rays are exceedingly rare events from the cosmos. To date, the only identified emission is a line source in the direction of the galactic center lying in the plane of the galaxy (Clark et al, 1958). It was discovered in a satellite experiment and has recently been verified in a balloon experiment flown in Australia. To search for other sources from balloons will require payloads in the 1000 to 2000 lb. range, with very long exposures and altitudes of 3 or 4 mb. In addition, accurate pointing devices would be required to locate the sources and to maintain a fixed orientation of the experiment with respect to the celestial objects.

X-ray astronomy has progressed a long way in the last few years with experiments flown on rockets and balloons. Point sources of X-rays have been identified with stellar objects and X-ray emissions from supernova remnants have been discovered and verified. This is extremely interesting in light of the recent discovery of pulsars. Pulsars are pulsating sources of electro-magnetic radiation which are believed to be rapidly rotating neutron stars which are the remnants of supernova explosions. Extending measurements from balloons will require large-area detectors and stably oriented payloads. These payloads would be in the 500 pound class and would be required to go to very high altitudes, say 0.5 mb.

To summarize these balloon needs, development of a cheap, reliable system for very heavy payloads would seem to be the easiest to realize. Somewhat further in the future but of potentially very great importance would be the development of superpressure balloons capable of carrying payloads of several hundred, or even a few thousand pounds. Staying aloft for many days, weeks or even months at altitudes comparable to those presently being achieved with present payloads would be a big step. When these payloads can be carried to 0.5 mb on superpressure balloons, the only thing a satellite will be needed for is tracking.

If this sort of development expands and replaces much costlier satellite programs, then the present balloon facilities will be unable to handle the business. Even now scheduling is a problem with optimal flight conditions coming only twice a year and with the uncertainties inherent in experimental work.

To relieve this pressure many standardization features could be introduced. For example, a series of community telemetry stations could be set up at intervals across the country which would be available for all experimenters and for long flights. The balloon support system could include data telemetry as in the case of

satellites. Data format into the system from experimenters could be specified, and then the transmission and receiving could be done by the community stations. A tax on each user could be made for operation, upkeep and new equipment. Flights with multiple experiments on board would then be easier, as all experiments would feed data into a common telemetry channel with subsequent demodulation into individual signals on the ground. As development proceeded, the ground receiving stations could be replaced by a satellite tracking system such as the IRLS (Gottesman). This should remove a major obstacle to multiple payload flights.

An exciting possibility exists - to someday have a balloon which can carry several experiments on a several months flight at high altitudes. It is important that balloons be developed to keep pace with the needs of the scientific community. In this time of budget cutbacks, etc., I hope some orderly process can be found for ordering priorities and funding balloon development. If balloon costs can be kept moderate and the reliability can be made reasonably high, then this will represent a significant contribution to high-energy astrophysics.

References

- Brownlee, R. G., Chapman, G. J., David, S. A., Fisher, A. J., Horton, L., Goorelich, L., Kohn, P. C., McCusker, C. B. A., Outhred, A., Parkinson, A. F., Peak, L. S., Rathgeber, M. H., Ryan, M. J.[†] and Winn, M. M. (1969) Proceedings of the 11th International Conference on Cosmic Rays, Budapest (to be published).
- Clark, G. W., Garmire, G. P., and Kraushar, W. L. (1968) Ap. J. Letters 153: L203.
- Freier, P., Lofgren, E. J., Ney, E. P., Oppenheimer, F., Bradt, H. L., and Peters, B. (1948) Phys. Rev. 74:213.
- Gottesman, A.: these proceedings.
- Linsley, J. (1963) Proceedings of the Eighth International Conference on Cosmic Rays, Jaipur 4:77.
- Ormes, J. F., Balasubrahmanyam, V. K., McDonald, F. B., and Price, R. D. (1968) IEEE Transactions on Nuclear Science, NS-15 3:566.
- Parker, E. N. (1965) Astrophys. J. 142:584.

Contents

4.1	Introduction	34
4.2	Balloon Characteristics and Instrumentation	35
4.3	Data Acquisition Systems	39
4.4	Balloon Trajectory Characteristics	41
4.5	Listing of Significant Results	43

4. A Constant-altitude Balloon Experiment at 48 Kilometers

H.N. Ballard and N.J. Beyers
U.S. Army Electronics Command
White Sands Missile Range, New Mexico

M. Izquierdo
Schellenger Research Laboratories
University of Texas at El Paso

Abstract

A helium-filled, zero-pressure (internal and external pressures equal), polyethylene balloon, 28.7 million cubic feet in volume (the largest to date), was launched on 11 September 1968 from White Sands Missile Range (WSMR), New Mexico, to study the atmospheric tides that rocket soundings have indicated exist in the 40 to 60 km atmospheric region. The balloon served as a constant-level stable support for a scientific payload consisting of six instruments for the measurement of temperature, pressure, density, and related ozone and water vapor concentrations near 48 km. Radar position-time data served to determine the wind velocity. The balloon reached a record altitude of 48.5 km and then followed a predicted trajectory extending from WSMR to Twenty-Nine Palms, California. Seventeen hours of stratospheric meteorological data were obtained with four hours being obtained in the 48 km altitude region. This paper describes the various aspects of the balloon system and its flight, and lists the significant results obtained; it is intended to serve as a reference for subsequent papers related to a detailed analysis of the various records.

1.1 INTRODUCTION

A program designed to determine the nature and extent of atmospheric tides in the 30 to 60 km region has been in progress since 1964 at the U. S. Army Atmospheric Sciences Laboratory (ASL) at White Sands Missile Range, New Mexico. These atmospheric tides have been shown to exist through a study of the data obtained from five rocketsonde experiments, four at WSMR (Beyers and Miers, 1965; Miers, 1965; Beyers et al, 1966), and one at Ascension Island (Beyers and Miers, 1968).

The observed tidal oscillations, as evidenced by amplitude variations in the wind velocity of approximately 10 m sec^{-1} at 60 km, have a dominant diurnal mode and are accompanied by diurnal temperature variations with mean amplitudes which measure from 2°C at 40 km to 8°C at 60 km. The magnitudes of these measured tidal wind and temperature variations are considerably larger than those predicted from theoretical considerations (Leovy, 1964; Lindzen, 1967).

This discrepancy between the theoretical and empirical results has led to extensive studies related to corrections that must be applied to the observed wind velocities and temperatures. These are determined from the successive radar-determined positions of a descending parachute and from the parachute-borne bead thermistor temperaturesonde, respectively. Corrections to the observed wind velocities have been determined by Eddy et al (1965) and Murrow (1965). Corrections to the observed temperatures have been determined by Wagner (1961, 1964); Ballard (1961, 1967, 1968); Pearson (1964); Hind (1966); Drews (1966); Thompson and Keily (1967); Thompson (1968); Ballard and Rubio (1968); Hyson (1968); Ballard and Rofo (1969).

While all known physical effects appear to have been accounted for in the determination of these corrections to the observed wind velocities and temperatures, additional experiments were conducted at ASL in an attempt to understand the still existing theoretical and observational differences. These experiments utilized independent sensing techniques to determine the temperature-related atmospheric parameters of pressure and density. Atmospheric pressures in the 30 to 60 km height interval were determined by a thermal conductivity pressure gauge (Thiele and Beyers, 1967) while atmospheric densities in the same atmospheric region were determined by a parachute-borne beta-ray densitometer (Ballard et al, 1966; Sellers et al, 1969). In addition, a rocket-borne ozonesonde was developed by Randhawa (1968) to determine the ozone profile in the 30 to 60 km atmospheric region.

This background and the progression of balloon technology to the point that it is now feasible to launch a constant-altitude balloon to a height of 50 km, plus the

ability to predict the balloon trajectory from 10 years of Meteorological Rocket Network (MRN) data concerning the winds in the 30 to 65 km interval, led to the integrated tidal experiment described herein. The balloon served as a stable support for a payload of six modified rocketsonde instruments. Atmospheric winds were obtained from the radar-determined balloon trajectory, atmospheric temperature by thin-film-mounted bead thermistors, atmospheric pressure by a thermal conductivity gauge, atmospheric density by a beta-ray densitometer and oxone concentration by a chemiluminescent ozonesonde.

The balloon flight was conducted as a cooperative experiment among the U.S. Army Atmospheric Sciences Laboratory (ASL), the Balloon Branch of the U.S. Air Force Cambridge Research Laboratories (AFCRL) and Schellenger Research Laboratories of the University of Texas at El Paso.

4.2 BALLOON CHARACTERISTICS AND INSTRUMENTATION

The polyethylene balloon, with a material thickness of 0.45 mils and a total volume of 28.7 million cubic feet, was designed and fabricated jointly by AFCRL and Winzen Inc. and launched from WSMR for ASL by the Balloon Branch of AFCRL located at Holloman Air Force Base, New Mexico. The balloon, as shown in Figure 4.1, contains only 14,000 cubic feet of helium (STP). When fully expanded at 48.5 km, as shown in the telescopic photograph of Figure 4.2, the balloon had a mean diameter of 410 feet.

The balloon experiment required a supporting frame for six atmospheric sensors with their associated power supplies and telemetry systems. A weight limit of 75 pounds was initially set for the sensor payload so that the planned altitude of approximately 50 km might be reached by the balloon system. The sensor payload was constructed with a total weight of 59 pounds. It consisted of aluminum frame and ballast exit (7.5 lbs), central battery power supply and sensor modulation circuitry (30 lbs), two 1680 MHz transmitters (3 lbs), and six atmospheric sensors with their associated mountings (18.5 lbs).

Environmental chamber tests determined that Yardney silver cell batteries would best meet the temperature, pressure, ampere-hour and weight requirements specified. It was established that if the environment temperature was no less than 0°C, the batteries performed satisfactorily even though there was some boil-off of the electrolyte at the pressure corresponding to an altitude of 50 km. Since most of the balloon flight was to be in an atmospheric region where the temperature is approximately 0°C, the primary concern was the protection of the batteries through the tropopause region during balloon ascent. Thus, styrofoam

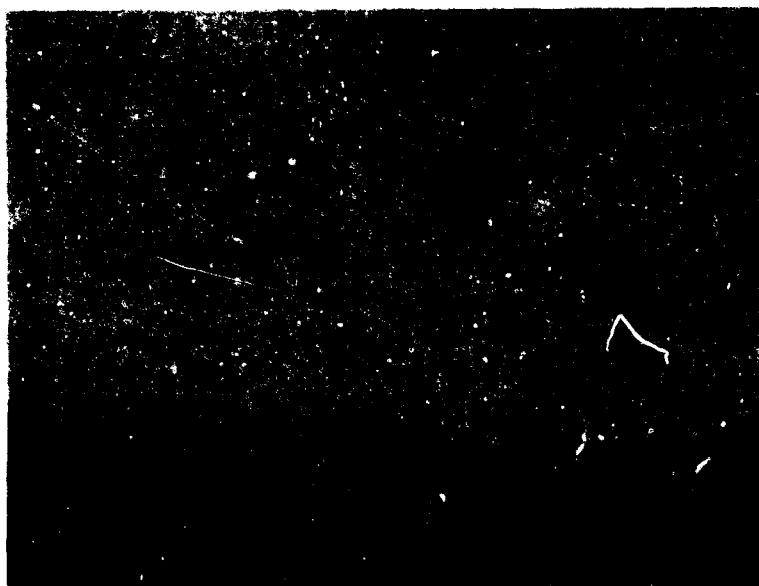


Figure 4.1. The Partially Filled Balloon at Time of Launching



Figure 4.2. The Fully Expanded Balloon at 48.5 km

sheets three inches thick were utilized for the walls of the battery box. A thermally controlled heater which dissipated 13 watts of power maintained the batteries at 15°C when the environment temperature was -70°C . The battery box also contained the various electronic circuits for the atmosphere sensor payload.

The rf transmitter was a standard radiosonde 1680 MHz unit. While the average life of these transmitter tubes exceeds 24 hours, an alternate transmitter was installed which was activated when the primary unit failed. This was accomplished by using an rf detector and signal level sensing circuit which electronically switched the filament battery supply from the primary to the secondary transmitter, if the rf power dropped by more than 50 percent from its nominal value.

The atmosphere sensors were modified rocket-borne instruments which had been developed over a period of several years. They were:

Bead-thermistor temperature sensor (Ballard, 1967).

Bead-thermistor temperature sensor with solar shields.

Thermal conductivity pressure gauge developed by Metrophysics Inc. (Thiele and Beyers, 1967).

Beta-ray atmospheric densitometer (Ballard et al, 1968; Sellers et al, 1969).

Chemiluminescent ozone sensor (Randhawa, 1968).

Cryogenic sampler for the determination of atmospheric composition (Ballard et al, 1968).

The temperature sensors and thermal conductivity pressure gauge were mounted on hollow glass epoxy rods which extended three feet below the aluminum frame.

Electronic circuits were developed, which allowed each of the five atmospheric sensors to pulse-modulate the transmitter successively for a period of one minute out of the five minutes necessary to complete the sensor sampling cycle. Data from five of the instruments was telemetered to the ground stations. Figure 4.3 is a block diagram of the electronic circuitry for the sensor payload.

The cryogenic sampler was designed to obtain two independent samples of the atmosphere after the balloon had reached its float altitude. Spring-loaded mechanical valves to the sample chambers of the probe were opened and closed by explosive squibs. The squibs were fired electronically by pulses occurring at predetermined times. No data was telemetered from the cryogenic sampler, which was to be recovered and its contents analyzed by a mass spectrometer.

Figure 4.4 shows the complete balloon payload consisting of radar reflector (on the earth's surface); parachute; balloon control package consisting of ballast hopper, 285 lbs of lead shot as ballast, electronic instrumentation for remotely controlling the times for ballasting and balloon destruction; ballast ejection tube; and atmospheric sensing package. The aluminum frame is hexagonal in shape

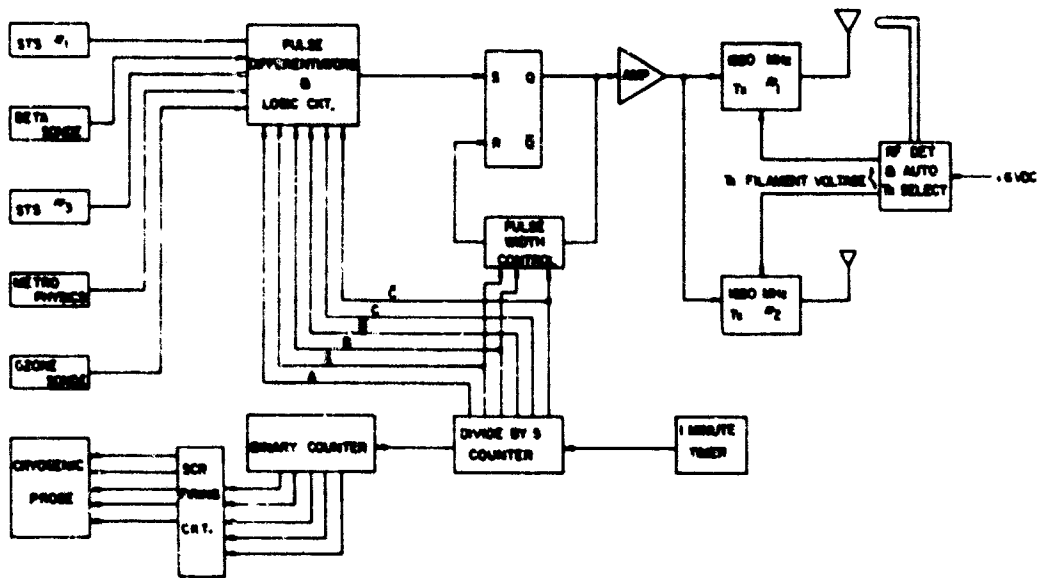


Figure 4.3. Block Diagram of the Electronic Circuitry for the Sensor Payload



Figure 4.4. The Complete Balloon Payload - Radar Reflector, Parachute, Balloon Control Package, Ballast Ejection Tube, and Atmospheric Sensing Package

with a maximum extent of 3 feet. The distance from the end of the balloon to the temperature sensors mounted on the glass epoxy rods is 64 feet when the parachute and instrument package are fully extended below the balloon (Figure 4.4). This was the maximum allowable distance as dictated by the procedures for launching the balloon. Figure 4.5 shows the arrangement of the sensing instruments. Extending below the aluminum frame (from left to right) are the atmospheric pressure thermal conductivity gauge, beta-ray densitometer, ballast exit tube, two 1680 MHz transmitters, bead-thermistor temperature sensor, dual chamber cryogenic atmospheric sampler, and bead-thermistor temperature sensor with solar radiation shields. Mounted above the aluminum frame are the central battery and telemetry package, and the chemiluminescent ozonesonde.

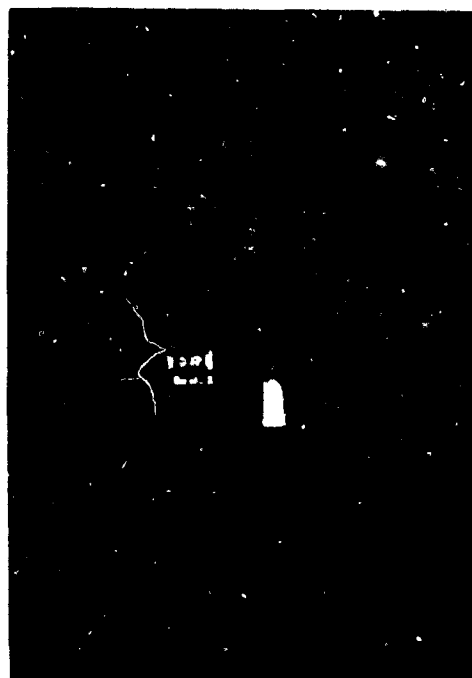


Figure 4.5 The Arrangement of the Atmospheric Sensing Instruments

4.3 DATA ACQUISITION SYSTEMS

Approximately 10 years of data obtained from MRN rocket soundings of the atmosphere in the 30 to 65 km region indicated that a balloon could be launched from WSMR and its trajectory at an altitude of approximately 50 km predicted. These data showed that each year the zonal winds in the 45 to 55 km height interval at 30°N latitude flow from the east from 1 May to mid-September (Webb, 1966). The peak value of the wind speed is of the order of 50 m sec^{-1} in July and then slowly decreases in magnitude, reaching a value near zero in the period extending from 10 to 17 of September. The wind then reverses and flows from the west. The corresponding meridional component of the wind is from the south, and its speed is of the order of a few meters sec^{-1} throughout the year. Based upon this data, the ground-based data acquisition sites were determined so that the balloon and its sensor payload would be under continuous surveillance by radar and GMD meteorological receivers for a period of approximately 24 hours, as the balloon followed a northwesterly trajectory from WSMR to the eastern border of California.

Fixed GMD meteorological receiver and FPS-16 radar systems exist at WSMR and Fort Huachuca, Arizona. From the range characteristics of the GMD and FPS-16 systems, it was determined that the placement of two additional mobile GMD stations, one at Lordsburg, New Mexico and one at Springerville, Arizona, would give the desired continuous tracking of the balloon system by both the telemetry receivers and the radars.

Figure 4.6 shows the locations of the radar and GMD sites and the projection of the balloon trajectory onto the earth's surface.

4.4 BALLOON TRAJECTORY CHARACTERISTICS

The balloon was launched at 0558 MST on 11 September 1968 from the site seen in Figure 4.1 at WSMR, New Mexico. The x-y plot of the balloon trajectory (Figure 4.6) was similar to that predicted. Immediately prior to the scheduled time of balloon launch it was known that the winds at 50 km were of a somewhat higher speed than was desirable; however, the predicted surface winds for several days after 11 September were such (greater than 2 to 3 knots) that their occurrence would have precluded successful launching of the balloon before the easterly zonal winds at 50 km shifted to a flow from the west, thus disrupting the experiment for one year.

Because of these factors, the actual balloon trajectory extended further to the west of WSMR than did the originally planned trajectory; however, the tracking range of both the radar and GMD systems proved to be approximately twice that expected, giving continuous radar and telemetry data for 17 hours.

Figure 4.7 presents the altitude vs time plot for the balloon which corresponds to the x-y trajectory shown in Figure 4.6. Shown also in Figure 4.7 is a vertical cross section of the terrain features over which the balloon passed.

The balloon reached a float altitude of 48.5 km approximately 2.5 hours (0830 MST) after the time of launch, thus giving an average ascent rate of 5.4 m sec^{-1} . It then remained at an essentially constant altitude of 48.5 km ($\pm 0.3 \text{ km}$) for a period of 3 hours and 15 minutes (1145 MST). During this time interval (0830-1145) ballast was released at 0915 for a period of 5 minutes, and again at 0955 for a period of 5 minutes. At approximately 1145 MST the balloon began a slow monotonic descent (0.3 m sec^{-1}) and reached an altitude of 35 km at 2300 MST at which time FPS-16 radar track was lost.

The balloon flight was terminated at 2330 MST near Twenty-Nine Palms, California. The balloon was found 12 September 1968. The instrument payload was found approximately seven months later. The instruments for the measurement of temperature, pressure, density and ozone concentration functioned properly

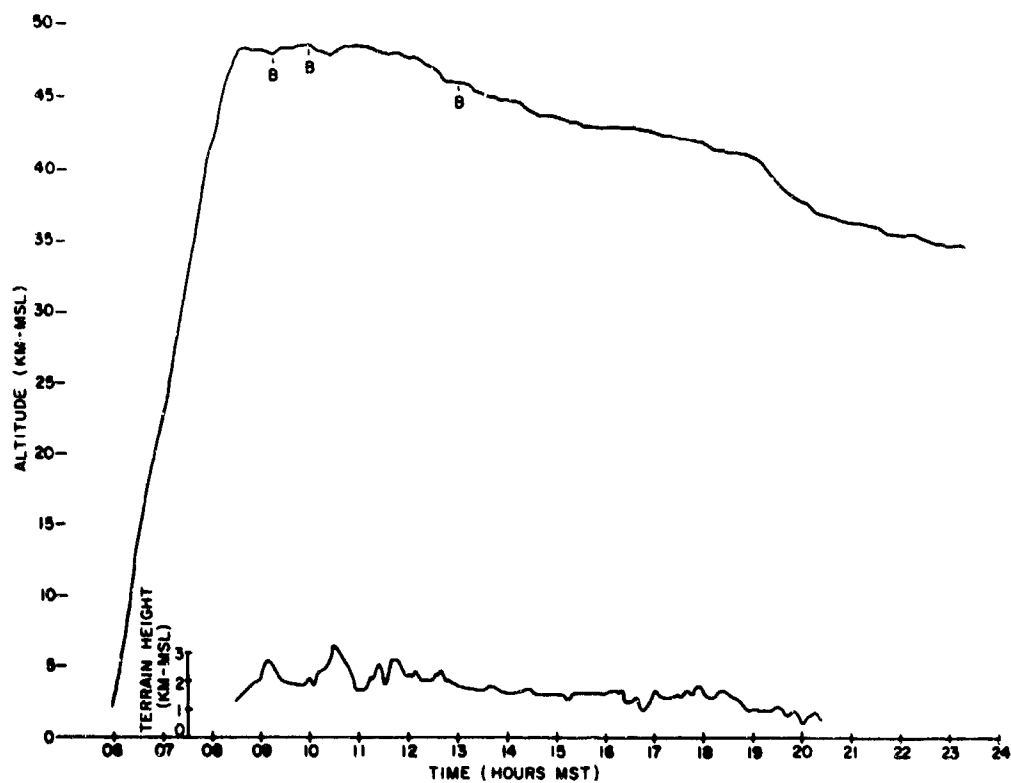


Figure 4.7. The Altitude vs Time Plot for the Balloon which Corresponds to the X-Y Trajectory of Figure 4.6. Points at which ballast ejection occurred are labeled "B"

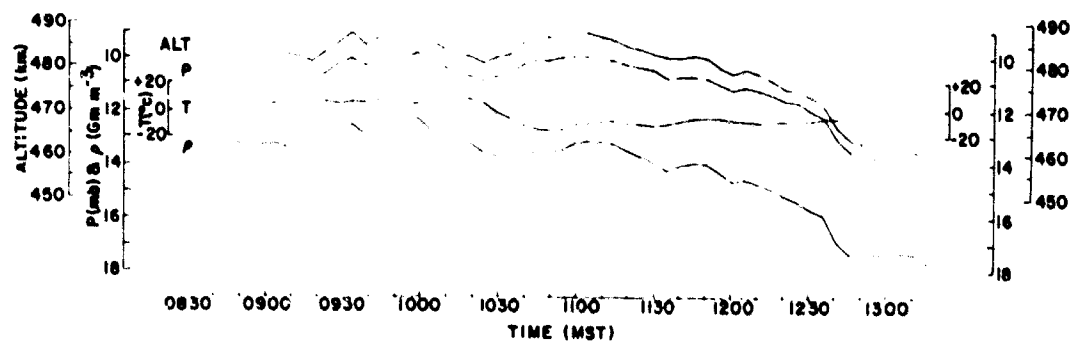


Figure 4.8. Balloon Altitude and Atmospheric Pressure, Temperature, and Density as Functions of Time

throughout the flight, and data concerning these parameters were telemetered continuously to the various ground receiving stations from the time of balloon launch to the time of balloon flight termination (0558-2330 MST). The FPS-16 radar data served to determine the balloon altitudes and the approximately wind velocity along the balloon trajectory.

The dual-chamber cryogenic sampler functioned properly, obtaining two atmospheric samples at an altitude of 48.5 km; however, the atmospheric samples obtained were subsequently contaminated by extremely slow leakage of ground-level air into the samples during the seven-month period in which the sample lay in the California desert.

The altitude of the balloon and the atmospheric pressure, temperature, and density as determined by the thermal conductivity gauge, the STS bead-thermistor and beta-ray densitometer, respectively, are plotted in Figure 4-8 for the time period extending from 0830-1320 MST. The ozone data have been published by Randhawa (1969).

As an integral part of the balloon experiment, a rocket-borne STS temperature and wind sensing instrument was fired to an altitude of 65 km at 1145 MST for the purpose of comparing rocketsonde temperatures and wind data with the corresponding parameters as determined from the balloon flight. By a fortunate circumstance, an Arcasonde 1A temperature and wind sensing instrument was fired from San Nicolas Island, California at 1121 MST. The data from the WSMR and San Nicolas Island rocket soundings are presented in Figures 4.9 and 4.10, respectively. The balloon, at the time of the rocket soundings, was over mountainous, wooded terrain (height 3 km) located in Arizona [see Figures 4.6 and 4.7 and refer to item (5) in Section 4.5].

4.5 LISTING OF SIGNIFICANT RESULTS

A time of approximately 8 months was required to reduce the radar and telemetry records to obtain wind speed, balloon altitude, pressure, temperature and density at successive points along the balloon's trajectory. An analysis of these records indicates that a number of significant results were obtained from the balloon flight. These are listed below:

- (1) The uncertainty in the determined altitude of the balloon did not exceed ± 75 meters from 0830-1600 MST (Figures 4.6 and 4.7).
- (2) The pressure, as determined by the thermal conductivity pressure gauge on the balloon package, agreed within 3 percent of the atmospheric pressures computed through the hydrostatic equation and the perfect gas equation of state

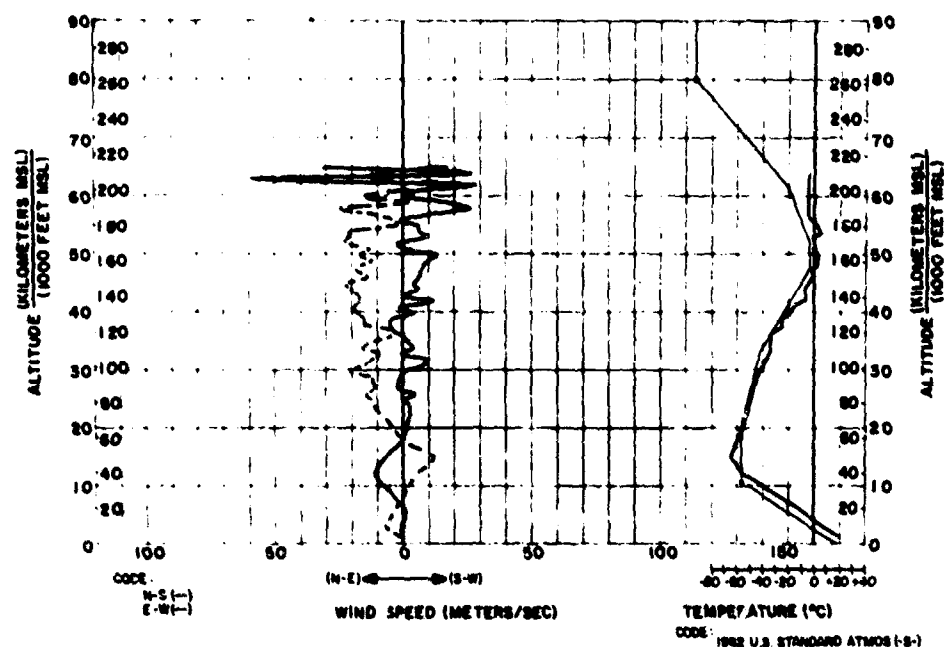


Figure 4.9. Wind and Temperature Profiles from a Rocket Sounding at White Sands Missile Range, New Mexico, 1145 MST, 11 September 1968

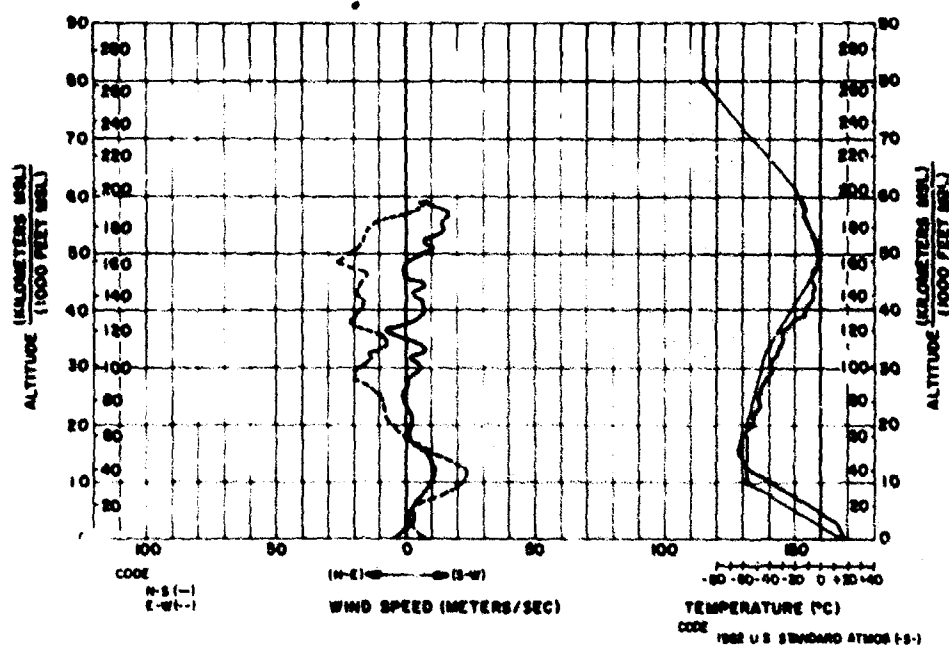


Figure 4.10. Wind and Temperature Profiles from a Rocket Sounding at San Nicolas Island, California, at 1121 MST, 11 September 1968

(Ballard, 1967) from the temperatures as determined from the STS rocketsonde fired at 1145 MST and the pressure at 34.3 km from a hypsometer radiosonde.

(3) The horizontal component of the wind speed as determined from the (x-y) trajectory of the balloon (Figure 4.6) is in excellent agreement with the wind speeds as determined from the rocketsonde data presented in Figures 4.9 and 4.10.

(4) A study of the vertical trajectory of the balloon between the times of 0830 and 1200 MST is suggestive of a vertical upward motion of the atmosphere at a velocity of approximately 70 cm sec^{-1} .

(5) An examination of the balloon trajectory (Figure 4.6) at approximately 1210 MST and a study of the terrain over which the balloon was floating at that time (Figure 4.7) are suggestive of an orographic perturbation in the atmospheric flow pattern which propagated to 48 km. The rocket soundings from WSMR (Figure 4.9) and from San Nicolas Island (Figure 4.10) show a wind with components from the south and east at 48 km. The balloon moved sharply to the south at 1210 MST.

(6) The atmospheric density values, as determined by the beta-ray densitometer, at all altitudes throughout the balloon trajectory, were approximately 30% greater than the density values as determined from the rocket sounding at 1145 MST from WSMR.

(7) The temperatures at 48 km as determined by balloon-borne bead-thermistor temperature sensors (which were identical in configuration to the rocket-borne temperature sensor fired at 1145 MST from WSMR) were approximately 10°C higher than rocketsonde temperatures at 48 km. This was expected because of the proximity of the temperature sensors to the sunlit balloon. The balloon-launching procedures dictated that the payload could not be more than 64 feet from the lower end of the balloon at the time of launching.

The results listed above will be discussed in more detail in subsequent papers related to the balloon experiment.

References

- Ballard, H. N. (1961) Response time of and effects of radiation on the VECO bead thermistor, Instrument Soc. of America, Report No. 167-LA-61, 27 pages.
- Ballard, H. N. (1967) The measurement of temperature in the stratosphere and mesosphere, J. Appl. Meteor. 6:150-163.
- Ballard, H. N. (1968) Reply, J. Appl. Meteor., pp. 306-310.

- Ballard, H. N., Seilers, B. and Izquierdo, M. (1968) A Parachute-Borne Beta-Ray Densitometer, Proceedings of the Third National Conference on Aerospace Meteorology, May 6-9, 1968, pp. 36-93.
- Ballard, H. N., Izquierdo, M. and Haire, A. (1968) A Cryogenic Sampler for the Determination of Stratospheric Composition, American Meteor. Soc. Conference on Composition and Dynamics of the Upper Atmosphere, University of Texas at El Paso.
- Ballard, H. N. and Rubio, R. (1968) Corrections to observed rocketsonde and balloonsonde temperatures, J. Appl. Meteor., pp. 919-928.
- Ballard, H. N. and Rofe, R. (1969) The thermistor measurement of temperature in the 30-65 km atmospheric region, Stratospheric Circulation, Vol. 22, Progress Series of American Institute for Aeronautics and Astronautics, Academic Press, New York, pp. 141-166.
- Beyers, N. J. and Miers, B. T. (1965) Diurnal temperature change in the atmosphere between 30 and 60 km over White Sands Missile Range, Journal of Atmospheric Sciences, 22(No. 3):262-266.
- Beyers, N. J., Miers, B. T. and Reed, R. J. (1966) Diurnal tidal motions near the stratopause during 48 hours at White Sands Missile Range, Journal of Atmospheric Sciences, 23(No. 3):325-333.
- Beyers, N. J. and Miers, B. T. (1968) A tidal experiment in the equatorial stratopause over Ascension Island, Journal of Atmospheric Sciences, 25(No. 1): 155-159.
- Drews, W. A. (1966) An Improvement of Atmospheric Temperature Measurement Above 30 km by Means of the Bead Thermistor Mounting Arrangement, NASA Report NASA-16111.
- Eddy, A., Duchon, C. E., Haase, F. M. and Haragan, D. R. (1965) Determination of Winds from Meteorological Rocketsondes, Report No. 2, Atmospheric Sciences Group, Austin, Texas.
- Hind, A. D. (1966) Temperature Corrections to a Bead Thermistor in the Upper Atmosphere, Weapons Research Establishment, Australian Defense Scientific Service, Tech. Note.
- Hyson, P. (1968) Thermistor mountings, J. Appl. Meteor., pp. 908-918.
- Leovy, C. (1964) Radiative equilibrium in the mesosphere, Journal of Atmospheric Sciences 21:238-248.
- Lindzen, R. S. (1967) Thermally driven diurnal tides in the atmosphere, Quarterly Journal Royal Meteorological Soc. 93:18-42.
- Miers, B. T. (1965) Wind oscillations between 30 and 60 km over White Sands Missile Range, New Mexico, Journal of Atmospheric Sciences, 22(No. 4): 382-387.
- Murrow, H. N. (1965) Parachutes for Meteorological Rocket Applications, IRIG Doc. No. 111-64, pp. 237-245.
- Pearson, P. H. O. (1964) Investigation into Response and Corrections to a Thermistor and a Platinum Nose Resistance Thermometer for Temperature Measurements in the Upper Atmosphere, Tech. Note P.A.D. 83, Dept. of Supply, Australian Defense Scientific Service, Weapons Research Establishment.

- Randhawa, J.S. (1968) Mesospheric Ozone Measurements During a Solar Eclipse, J. Geophys. Res. 73(No.2):493-495.
- Sellers, B., Ballard, H.N. and Izquierdo, M. (1969) Direct measurement of air density in the 30-60 kilometer region by beta ray forward scattering, International Journal of Applied Radiation and Isotopes, 20:341-351.
- Thiele, O.W. and Beyers, N.J. (1967) Upper atmospheric pressure measurements with thermal conductivity gauges, Journal of Atmospheric Sciences, 24(No. 5):551-557.
- Thompson, D.C. (1968) On the errors of a thin-film mounted rocketsonde thermistor, J. Appl. Meteor. 7:306.
- Thompson, L.C. and Kelly, D.P. (1967) The accuracy of thermistors in the measurement of upper air temperatures, J. Appl. Meteor. 6:380-385.
- Wagner, N.K. (1961) Theoretical time constant and radiation error of a rocketsonde thermistor, J. Appl. Meteor. 18:602-614.
- Wagner, N.K. (1964) Theoretical accuracy of meteorological rocketsonde thermistor, J. Appl. Meteor. 18:606-614.

Contents

5.1	Introduction	50
5.2	General Discussion	51
5.3	Description of Orientation System Operation	52
5.4	Performance of Prototype Unit in a Balloon Flight	57

5. A Payload Stabilization and Attitude Control Platform for High Altitude Balloon Experiments*

L.E. Orwig, A.P. Wood and P.E. Lavoie
University of New Hampshire
Durham, New Hampshire

Abstract

A relatively simple payload orientation system has been developed and the prototype unit has been flown on a balloon flight launched from Palestine, Texas. The system provides a reference platform stabilized to a north-south reference. From this platform the scientific payload is oriented about two independent axes (azimuth and elevation) to an accuracy of $\pm 1.4^\circ$ by means of a fully digital, ground-commanded pointing system.

The fixed platform is stabilized through the use of a magnetometer-controlled analog servo system which drives a bi-directional DC motor. The magnetometer converts a measurement of the earth's magnetic field flux to an error voltage which drives the correction motor. This unit maintains a fixed aspect between the platform and the earth's magnetic field lines. A small built-in electronics "deadband" limits the stabilization accuracy to $\pm 3^\circ$.

Movement about each of the azimuth and elevation axes is achieved by means of a digital servo system utilizing a stepping motor as the prime mover. A complement of seven ground-initiated commands enables angular movement in azimuth

*This publication is the result of research sponsored by the National Aeronautics and Space Administration under Grant NGR-30-002-021.

and elevation in 1° and 10° increments and in either direction of rotation. An angular position readout for each axis is provided by a seven bit digital shaft encoder.

A PCM/FM-FM telemetry link between balloon and ground permits transmission of data from balloon to ground and commands from ground to balloon. A flight encoder-ground decoder system provides a continuous monitoring and visual display of the azimuth and elevation position angles, analog magnetometer error voltage, and commands status at the ground station. In this way the operator has complete control over the payload orientation at all times during the balloon flight.

The prototype system was used to point a large volume gamma-ray detector on a high altitude balloon flight. The scientific payload weighed approximately 150 pounds. A complete description of the pointing system and results of its performance in this flight will be presented.

5.1 INTRODUCTION

Very often in balloon-borne experiments it is desirable to have the capability of stabilizing and orienting the instrumentation payload. Such orientation systems can become quite complex depending upon such constraints as the number of axes of motion required, the pointing accuracy desired, and the weight and size of the payloads involved.

The system proposed in this paper provides for the stabilization and biaxial orientation of balloon payloads. This system was designed to meet the following design criteria:

- (1) The system must have two independent controllable axes of motion.
- (2) Every possible pointing direction shall be attainable with the system.
- (3) Overall pointing accuracy shall be equal to 9 square degrees in any chosen direction.
- (4) The system shall be flexible enough to handle various payload configurations without compromising system operation.
- (5) The pointing direction shall be controlled at all times by an operator on the ground.
- (6) The resulting configuration to be achieved at minimum cost.

The original motivation in designing such a system was the desire to point directional scintillation-counter detectors in the search for X-ray and gamma ray radiations from celestial objects. However, application of the proposed system is not limited to these particular experiments.

Best Available Copy

5.2 GENERAL DISCUSSION

The basic concept of the orientation system is to provide an azimuthally-stabilized reference platform upon which movement of the scientific instrument can be made in both the azimuthal and zenith (or elevation) directions. The various coordinates necessary to define a unique pointing direction are indicated in Figure 5.1. The vertical axis of the balloon suspension+ gondola defines the z-axis of the coordinate system, while the azimuthal stabilization provides a coordinate vector in the horizontal plane.

Stabilization about the vertical axis (that is, definition of the horizontal coordinate vector) is achieved with a closed loop servo system which always maintains a magnetometer (fixed to a boom on the gondola) pointing perpendicular to the local horizontal component of the earth's magnetic field. The magnetometer boom thus defines a fixed reference direction about the vertical. This stabilization process uses the inertia-wheel approach whereby the entire gondola is pivoted below a large inertia load against which force can be applied to maintain the reference. For our purposes this inertia load could be provided by the balloon itself if "rigidly" attached to the gondola, or by a separate inertia wheel or weighted boom.

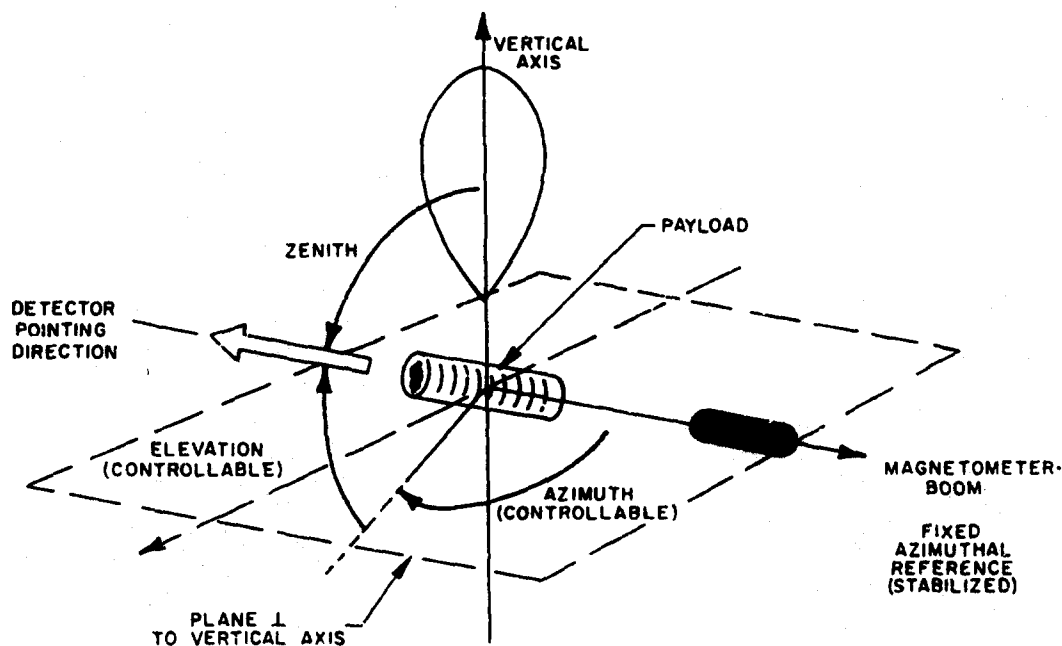


Figure 5.1. Sketch of the Stabilized Coordinate System and the Two Controllable Pointing Angles

Best Available Copy

Having obtained this coordinate system defined by these two perpendicular axes, two more angles must be specified to get a unique pointing direction. These angles are the AZIMUTH and ELEVATION (or ZENITH) as shown in Figure 5.1. The AZIMUTH angle is realized by rotating the payload with respect to the stabilized boom, while the ELEVATION angle requires a rotation of the payload with respect to the vertical. Both of these motions are accomplished through the use of a radio-commanded digital servo system.

The entire orientation system can logically be divided into three basic subsystems:

- (1) Azimuthal stabilization subsystem which provides the fixed reference axis in the horizontal plane.
- (2) Digital servo subsystem which produces movements in azimuth and elevation.
- (3) Subsystem which includes the data encoding, command verifications, telemetry interface, and entire ground station providing for control of the pointing operation and continuous visual monitoring of the system performance.

These three subsystems are treated in detail in the following sections.

5.3 DESCRIPTION OF ORIENTATION SYSTEM OPERATION

5.3.1 Azimuthal Stabilization Subsystem

The fixed reference of the stabilization system is magnetic north. A Schonstedt magnetometer model RAM-5C is used as an error sensor and is mounted on a boom to lessen the effect of any inherent magnetic field or the distortion of the earth's field by the payload. As shown in Figure 5.2, the servo system consists of the magnetometer, a summing amplifier, a power amplifier with nonlinear feedback, and a DC motor to drive the platform. The purpose of the summing amplifier was to subtract the bias voltage from the magnetometer. The system drives the sensor (the platform) to a magnetic null and this summing amplifier reduces the output of the magnetometer to zero volts. The power amplifier has integral positive and negative feedback to produce the transfer function shown in Figure 5.2. The deadband, adjusted to be about $\pm 3^\circ$ of boom rotation, and the short segment of high gain (essentially the open loop gain of the amplifier) insures that error signals too small to overcome the starting friction of the motor and drive assembly will not result in a large idling current. When the error signal is larger than the deadband, the output immediately becomes large enough to drive the system in the proper direction for null. The motor excitation control relay de-energizes the system during the ascent stage of the flight and is closed when the balloon is near the proper altitude.

5.3.2 Azimuth and Elevation Drive Subsystem

The digital or commandable drive systems for azimuth and elevation control of the experiment detectors utilize DC stepping motors as prime movers. The stepping motor is unique in that it moves in discrete increments rather than rotates. Thus, speed and angular rotation may be closely controlled with no overshoot.

Figure 5.3 shows a simplified block diagram of the system components. The control flip-flop and the control gate inhibit or allow the clock pulses to enter the stepping motor driver. The command to step produces a pulse from the execute monostable (the monostable prevents relay contact bounce from giving multiple step commands) which sets the control flip-flop. This enables the control gate and allows the pulses to drive the stepping motor through the stepping motor driver and at the same time be counted by the drive pulse counter. When the proper count is reached, the counter resets the control flip-flop and disables the control gate. The gearing of the drive systems is such that a rotation of 200 steps by the stepping motor produces a 1° change in platform orientation. The step selection relay can enable the drive pulse counter to accept 200 or 2000 counts resulting in a 1° or 10° change in platform orientation. Since one change in platform orientation (azimuth or elevation) is made at a time only a single drive system is necessary. The drive selection relay connects the pulse train to the proper stepping motor. Motor reversal is accomplished by reversing the phase of the pulse trains to the driver by the motor reversal relay.

The current to operate the stepping motor is fairly substantial (approximately two amperes) and would cause excessive drain on the payload batteries. Therefore, the stepping motor excitation relay de-energizes the motor when not in use. The drive system utilizes a worm gear arrangement which prevents any movement of the platform except by the stepping motor.

To command the system the NCAR resonant reed relay system was used. A tone transmitted from the ground is received by the balloon and closes a particular relay. An open relay (de-energized) will dictate one mode of operation and, when it is energized, switch the system to a complementary mode. The commands are as follows:

- (1) Magnetometer motor on - off. This enables the fixed reference point system to operate when required.
- (2) Standby - operate. In the standby mode the current to the stepping motor is interrupted to conserve power. In the operate mode, the motors are fully energized prior to movement.
- (3) Azimuth - elevation. This determines which motor will be connected to the drive system.

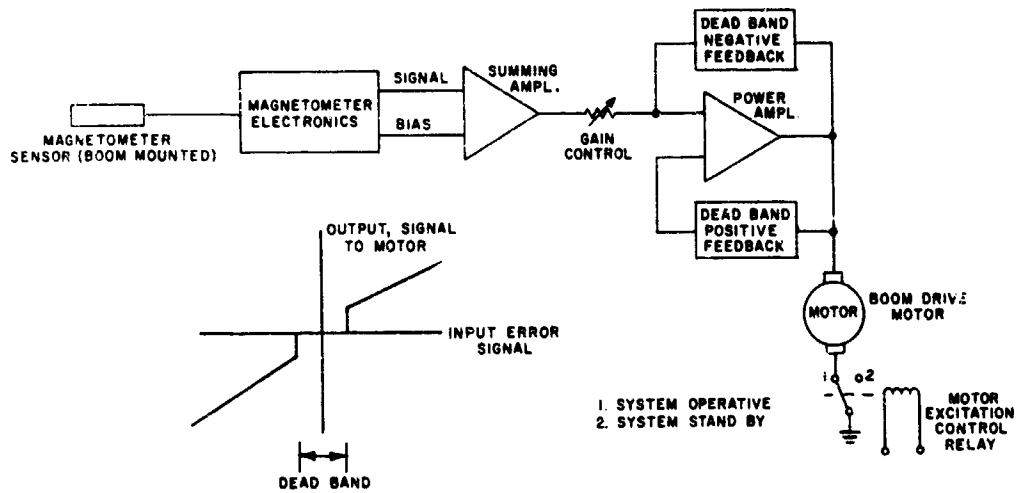


Figure 5.2. Block Diagram of the Magnetometer Azimuth Stabilization System

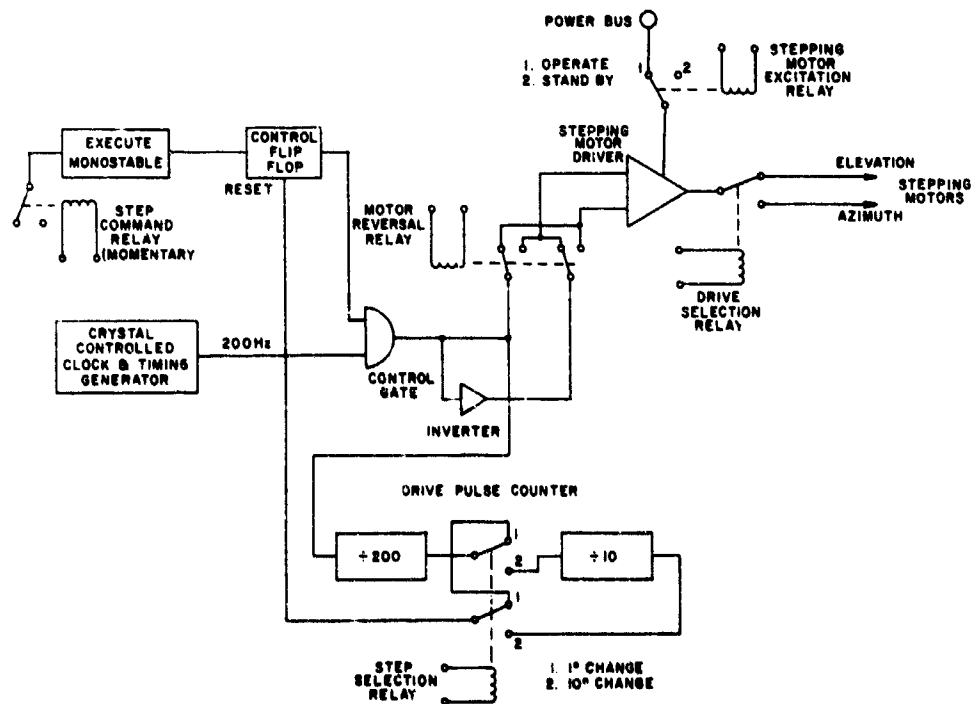


Figure 5.3. Azimuth and Elevation Drive Systems

- (4) Clockwise - counterclockwise. This determines the direction of motor rotation.
- (5) $1^\circ - 10^\circ$. This determines the extent of motor rotation and thus the rotation of the platform.
- (6) Execute. This enables the driver system to drive a motor as per previous commands.

5.3.3 Data Encoding and Transmission Subsystem and Ground Station

To verify the position of the experiment platform, eight bit shaft encoders (Gray code) were connected to the azimuth and elevation axes. These encoder outputs and the command status information (DC levels controlled by command relay contact closures) are telemetered to the ground on two IRIG telemetry channels. Figure 5.4 shows the block diagram of the PCM system. Seven four-bit shift registers are used to form the serial data stream. Extra bits not presently used are available for system expansion. For example, the encoders now in use are accurate to only 1.4° although the digital command system can execute movements as small as 1° . Ideally, the accuracy of a nine-bit encoder would be commensurate with the system and the telemetry was designed to handle the extra bits. A gated clock produces a sequence of 28 pulses which shifts the contents of the shift registers into the data stream. The data rate of 10 Hz is slow enough to be handled by the lowest IRIG subcarrier channel. The gated clock also commutates the magnetometer output onto the same telemetry channel. The duty cycle is five seconds on and five seconds off. As shown in the diagram, one five-second interval contains the digital information and the next contains the analog-magnetometer data. A second telemetry channel is used to send this gated clock signal to the ground for data synchronization and display.

The maximum current required by the complete stabilization system is given below:

+ 28 Volts (magnetometer)	- 5 ma
+ 12 Volts (analog servo system)	- 800 ma
- 12 Volts (analog servo system)	- 500 ma
+ 8 Volts (stepping motor)	- 2 amps
+ 5 Volts (logic)	- 500 ma

The data link between the command system on the balloon and the ground is a PCM/FM/FM telemetry network. As shown in Figure 5.5 the signals are received, discriminated, and restored to the original data line and gated clock. A dual channel strip-chart recorder and a seven-track FM tape recorder provide a permanent data record.

The first pulse of the gated clock, its risetime restored by the input clock shaper, triggers a one shot multivibrator (pulse duration about 3.9 seconds) and

The diagram illustrates the timing and data processing system for the Lunar Roving Vehicle (LRV). It shows the flow of data and timing signals from various receivers and recorders to the LAMP DISPLAY and LAMP DRIVERS.

Inputs and Receivers:

- TELEMETRY RECEIVER:** Provides data to the DISCRIMINATORS and the 28 BIT DATA BUFFER.
- WWV RECEIVER:** Provides a VIDEO signal to the DISCRIMINATORS and a 7 TRACT FM TAPE RECORDER.
- 7 TRACT FM TAPE RECORDER:** Outputs a 7-bit signal (1-7) to the DISCRIMINATORS and the CRY.

Processing and Timing:

- DISCRIMINATORS:** Process the VIDEO and 7-bit signals to produce a GATED CLOCK and DATA signals.
- DUAL CHANNEL STRIP CHART RECORDER:** Records the DATA signal.
- DIGITAL DATA INPUT SHAPER:** Processes the DATA signal into a 28 BIT SHIFT REGISTER.
- 28 BIT SHIFT REGISTER:** Contains two intervals: 1. DIGITAL INTERVAL and 2. MAGNETOMETER INTERVAL.
- INPUT CLOCK SHAPER:** Processes the GATED CLOCK signal into a TRIGGER ONE SHOT.
- TRIGGER ONE SHOT:** Generates a pulse for the TIMING GENERATOR.
- TIMING GENERATOR:** Generates timing signals for the LAMP DRIVERS and the 28 BIT DATA BUFFER.

Outputs and Displays:

- LAMP DISPLAY:** Shows the 28 BIT DATA BUFFER output.
- LAMP DRIVERS:** Drive the LAMP DISPLAY.
- GRAY TO BINARY CONVERTER:** Converts the 28 BIT DATA BUFFER output to a binary signal.
- CRT:** Displays the 7-bit signal (1-7) from the 7 TRACT FM TAPE RECORDER.
- ANALOG MAGNETOMETER VOLTAGE:** Provides a signal to the TIMING GENERATOR.

Timing Generator Outputs:

- DIGITAL INTERVAL:** 1.0000 - 0.0000
- MAGNETOMETER INTERVAL:** 1.0000 - 0.0000
- 28 CLOCK PULSES:** 1.0000 - 0.0000
- BUFFER CLOCK PULSE:** 1.0000 - 0.0000

Figure 5.5. Block Diagram of the Orientation System Ground Station

the timing generator which produces the 10 second period square-wave gate for commutating the magnetometer analog signal and the digital data. In this case, the commutator is a mechanical relay. This method of using monostable multivibrators for synchronization of data rather than a true synch word in the telemetry format is possible because the digital data stream is present for only 2.8 seconds (28 pulses at a 10 Hz rate) out of the 5 seconds allotted. By centering the clock pulses in the data interval, leaving approximately 1.1 seconds on either end, multivibrator timing variations can be neglected. (The centering is obtained by the 3.9 second monostable: $2.8 \text{ seconds} + 1.1 \text{ seconds} = 3.9 \text{ seconds}$.)

The digital data (now separated from the magnetometer signal) enters the digital data input shaper to restore rise-time, and then the shift registers controlled by the 28 clock pulses from the gated clock channel. At the end of the digital data interval, provided by the 10-second period square wave, a pulse is produced which shifts the contents of the registers into buffer storage. Before entry the encoder data is converted from Gray to straight binary code to simplify data reduction. The outputs of the storage registers are connected to lamp drivers which have the current capacity to drive the display lights.

Although the ground station and display unit is quite simple, it gives the command system operator full knowledge of the status of the balloon package. Magnetometer data indicates whether the analog servo system is operative and keeping a fixed reference point; the status lights denote the commands given to the system and verify each new command before actual movement is executed; and the shaft encoder displays check the values of the pointing angles.

5.4 PERFORMANCE OF PROTOTYPE UNIT IN A BALLOON FLIGHT

A prototype unit of the orientation system was flown from Palestine, Texas, on 26 November 1969. It was used to control the pointing direction of a large volume gamma-ray spectrometer which had crude directional properties. Figure 5.6 is a pre-flight photograph of the complete UNH flight payload. The portion of the payload which was pointed consisted of the large sphere in which the detector was housed. An inertia "dumbbell" consisting of two 15-lb lead weights attached to a 12 ft length of aluminum channel was rigidly coupled to the main load carrying shaft. This shaft was then decoupled from the balloon suspension by means of a swivel coupling.

Commands for the system were provided by the NCAR resonant reed relay package. The NCAR electronics package and ballast box was suspended below the gondola mainframe so that it became a rigid member of the gondola system.

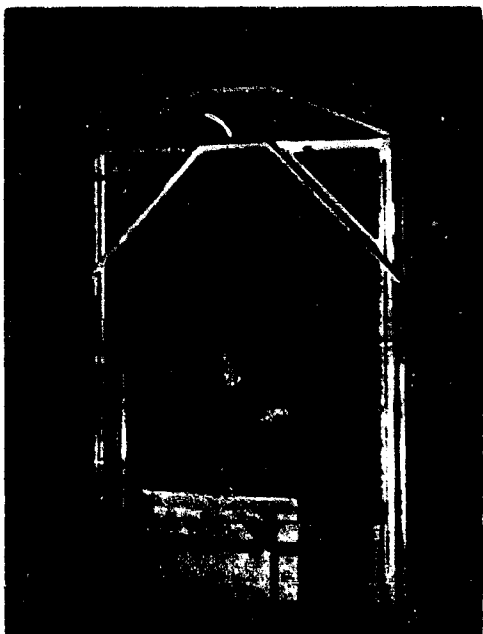


Figure 5.6. Photograph of the UNH Payload Showing the Magnetometer Boom, Gondola Frame, Scintillation Detector, and Detector Electronics Container

After an 0750 CST launch, the balloon reached float altitude at ~1000 CST and remained near this altitude for ~2 hours before flight termination. The azimuth stabilization system remained off on ascent and was commanded on at ~1001 CST. Although there was no azimuth stabilization on ascent, a series of elevation movements was successfully completed. This provided data at different fixed elevation angles while sweeping in azimuth. On ascent the magnetometer readout indicated a tendency for the gondola to rotate slowly in one direction. We feel that this indicates an incomplete rotational decoupling of balloon and gondola by the swivel.

After the stabilization system was activated, several more series of movements were performed which required usage of both the elevation and azimuth control systems. These digital systems appeared to operate well throughout the entire flight.

However, accurate pointing requires the properly stabilized reference direction. During the time when this subsystem was operative, the magnetometer output voltage at the ground station showed the following:

(1) Except for a few instances, the magnetometer was always reading one direction from null. This result would be obtained if the correction system had to constantly correct for a steady rotation of the gondola in one direction. This is consistent with the incomplete decoupling of balloon and gondola mentioned previously.

(2) Quite often the magnetometer boom was seen to drift beyond the deadband (sometimes as far as 15° from null) before an error correction was made. This effect could result if the voltage applied to the DC motor at the deadband edge was insufficient to overcome the starting friction of the motor and gearing. In this way the boom could drift out of the deadband until a large enough voltage was obtained to start the motor and produce an error correction.

(3) The magnetometer readout also showed a periodic oscillation of the magnetometer boom about its average pointing direction. This motion had a period of

~0.5 min. This motion could result from the continual drifting and restabilization of the boom arising from a balloon rotation which was coupled to the gondola. Also, however, it could result from a pendulum motion of the balloon-gondola system causing the magnetometer to pitch up and down. The magnetometer would then sense a vertical component of the earth's field in addition to the horizontal component giving incorrect magnetometer readings and producing the observed effect.

In conclusion, this orientation system performed with limited success on one balloon flight. The actual overall pointing direction accuracy in this flight was $\sim 10^\circ$. It is felt that with minor modifications to the stabilization servo drive system, the design criteria of $\leq \pm 3^\circ$ in pointing accuracy on each of the movable axes can be realized.

Acknowledgments

The authors wish to thank Dr. E. L. Chupp for his initial suggestion to construct such a system. Many thanks also go to Mr. Peter Elkins who constructed a majority of the flight and ground station electronics, and to Mr. Al Knight for his aid in the mechanical construction of the system. In addition, we thank Dr. D. J. Forrest and Mr. Andrew Mammay of the University of New Hampshire and the entire staff of the NCAR launch facility in Palestine, Texas, for their help in making the flight of the prototype system a success.

Contents

6.1	Introduction	61
6.2	Missions Utilizing Balloons	62
6.3	Balloon Systems	65
6.4	Materials	68
6.5	Payload	69
6.6	Testing	69
6.7	Concluding Remarks	72

6. A Scientific Mission Using a Balloon in the Atmosphere of Venus

R.M. Henry and J.P. Dickson, Jr.
NASA Langley Research Center
Hampton, Virginia

Abstract

A proposed mission for the scientific exploration of the planet Venus utilizing a balloon-borne instrument package, or buoyant station, is outlined. Launch vehicles, trajectories, orbits, and entry systems are briefly described. Deployment, inflation and control systems, and balloon construction are discussed in greater detail. Instrumentation, dropsondes and communication systems are outlined, scientific objectives are listed, and some possible balloon trajectories in the Venus atmosphere are shown.

6.1 INTRODUCTION

For many years balloons have served as important tools for scientific observations in the Earth's atmosphere, and it is natural to consider their use in the exploration of other planets, especially planets having dense atmospheres such as Venus. Perhaps the first mention of the idea in print was made in 1935 by Edgar Rice Burroughs (1935), whose science-fiction astronaut, Carson Napier, operated an airship in the atmosphere of Venus. More recent and more serious suggestions

have been made by Pritchard (1963), who considered both Mars and Venus; Greenfield and Davis (1963 and 1965), and Davis and Greenfield (1965) who considered only Mars; and Gross (1965 and 1966), who suggested using a balloon in the Venus atmosphere for entry retardation as well as for flotation.

Evidence accumulated since 1963 indicates that the Mars surface atmospheric pressure is near 6 mb rather than the previously assumed 85 mb, and, as a result, use of balloons in the Mars atmosphere is considerably less attractive, although not completely ruled out for some limited purposes. On the other hand, recent evidence indicates an extremely dense atmosphere for Venus with surface pressures of perhaps a hundred Earth atmospheres, making the use of balloons over Venus more attractive.

Since 1965, the NASA Langley Research Center has pursued a series of feasibility studies of progressively increasing depth on the design of balloon systems and complete space missions utilizing the balloon concept. Both in-house studies and contractual studies by the Martin-Marietta Corporation, Raven Industries, and Geophysics Corporation of America have been included (Final Report 1967 and 1969; Sadin and Frank, 1968; Steinberg et al, 1969; and Sadin and Frank, 1969). The purpose of this report is to summarize some results of these studies with emphasis on the balloon systems and their operation.

6.2 MISSIONS UTILIZING BALLOONS

The basic technique for placing a balloon system at its floating altitude in the atmosphere of Venus is shown in Figure 6.1. The primary retardation from interplanetary velocity to subsonic velocity is achieved by a blunt-cone aeroshell with appropriate heat shield; then a parachute is deployed to reduce the velocity further. Coincident with the parachute deployment, the aeroshell and heat shields are jettisoned and an instrumented entry probe is dropped. This entry probe is separate from the balloon system and provides an independent atmospheric profile measurement. When the parachute system reaches a dynamic pressure of 1 pound per square foot, at a velocity of about 30 feet per second, balloon inflation is begun. Before inflation is complete, the parachute is released. When inflation is complete, the inflation system and tanks are dropped. Since the initial temperature of the expanding gas is low, the balloon will drop to some distance below the final equilibrium altitude before the lift equals the weight. As the balloon begins to rise, gas will be vented to the atmosphere, requiring that the initial gas supply be greater than that required for equilibrium; however, the additional weight is much less than would be required for heating the gas. Figure 6.1 shows that a typical balloon system comes to equilibrium after about 40 minutes and after dropping about 1 km below the equilibrium level.

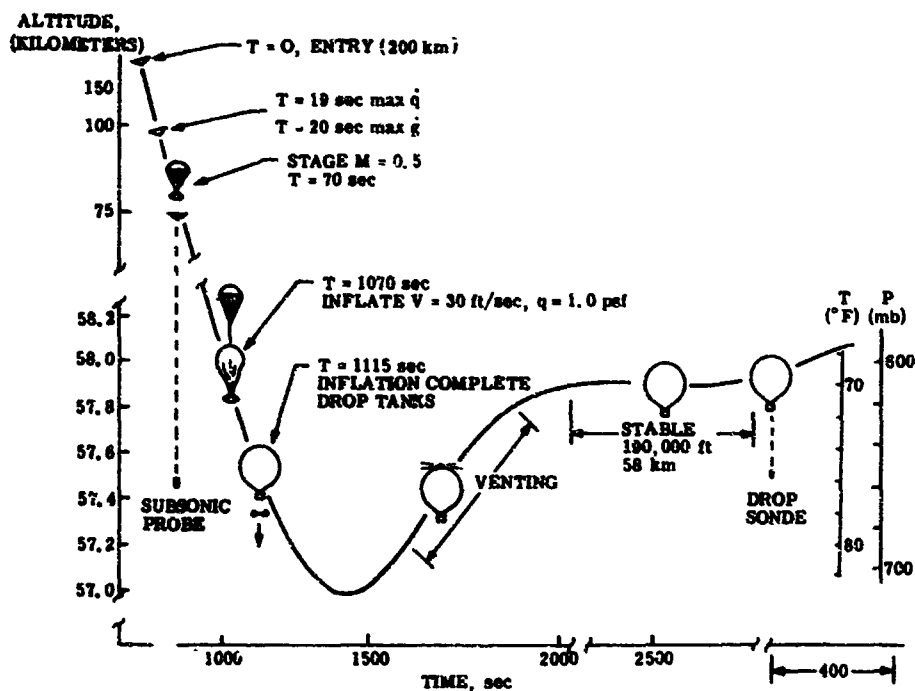


Figure 6.1. Entry and Deployment Sequence

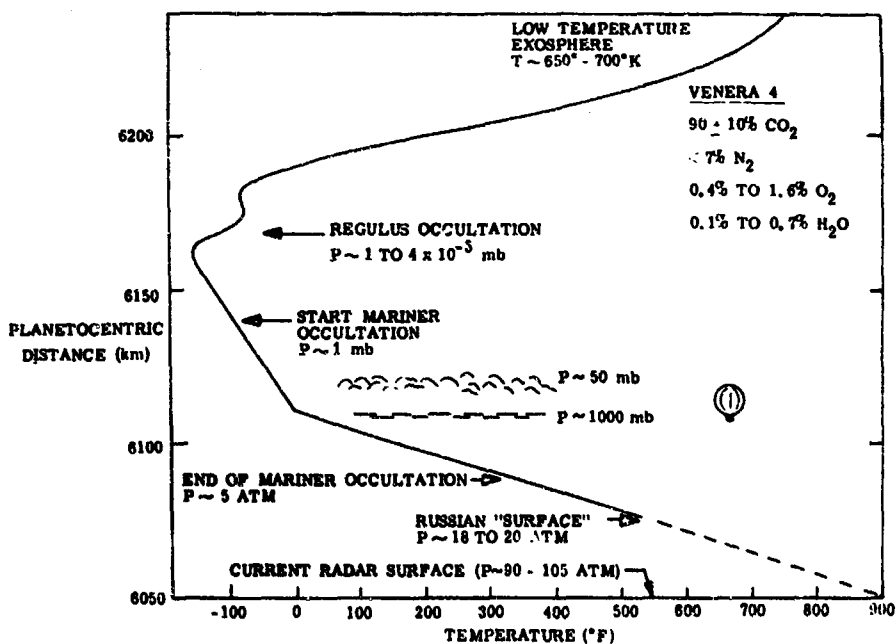


Figure 6.2. Atmospheric Structure of Venus

The choice of an equilibrium altitude is governed by the scientific investigations, and by the environment provided for the balloon and the instrumentation and electronics. Figure 6.2 shows the profile of atmospheric temperature derived from Mariner and Venera measurements. The profile shows the original Venera "surface" at the pressure of around 20 Earth atmospheres. Although this value is no longer widely credited, there is still some question as to the exact radius and pressure of Venus surface. However, what is important for balloon operation is that temperatures near the clouds are well known both in relation to the cloud tops and as a function of pressure or density. Since a superpressure balloon floats at a particular density, we can design a balloon system to float where we choose over a wide range. A particularly attractive level is indicated by the balloon symbol in Figure 6.2. At this level, the pressure is 600 mb, the density corresponds to 5000 feet in Earth's atmosphere, and the temperature is 70° F. In addition, this level is within the expected cloud layer, and, according to Venera data, liquid water drops might be expected to be present. Thus, it seems to be an attractive level for not only cloud composition measurements but also for biological experiments.

In addition to the density, the design of the balloon system depends on the weight of the balloon and its payload. Just as in the Earth's atmosphere, a wide variety of types and sizes of balloons might be used in the atmosphere of Venus, and in the course of investigation balloon systems ranging from a few pounds to thousands of pounds have been considered. However, our studies of complete missions have concentrated on a system with a buoyant station weight (on Earth) of around 200 pounds with a growth potential to several hundred pounds. By the term "buoyant station" we mean the floating balloon along with its lift gas, scientific instrumentation, power systems, communication systems, data handling systems, and the required supporting structures and equipment. The weight of the buoyant station determines the required weight for inflation equipment and tankage, parachute systems, aeroshell and heat shields, the amount of propellant required and, finally, the type of launch vehicle required and the type of trajectories which are feasible. Figure 6.3 illustrates trajectories which are feasible for the 200-pound class buoyant station using a Titan III-C launch vehicle.

The first mission illustrated is a simple flyby with direct entry of the aeroshell and the buoyant station. In this case, communications must be by a direct link from the buoyant station to Earth, at least for missions of long duration. The communication and trajectory requirements limit the possible target points, but some desirable points are available. Figure 6.3 illustrates one point, and the possible balloon trajectories, based on a model of atmospheric circulation which assumes that the faintly visible "wagon spoke" markings represent the wind

pattern at cloud level. The dashed lines show the limiting trajectories based on limiting velocities of 4 and 40 mps.

Next shown in Figure 6.3 are the entry points and limiting trajectories for an orbital mission. As you can see, the computed trajectories begin near the equator and move to a point near the pole. This is the most desirable trajectory for scientific return. The orbital mission also enhances scientific return by allowing orbiter experiments and combined orbiter-buoyant station-dropsonde experiments. In addition, the orbiter serves as a communication relay link and an aid in position determination.

Another possibility is the inclusion of a buoyant station experiment with a Mercury-Venus swingby such as is currently planned for the 1975 launch opportunity. Of course, such a combination requires compromises in both Venus and Mercury experiments. As shown in Figure 6.3, the buoyant station entry is confined to the dark side of Venus, eliminating the possibility of using solar cell power systems, and the uncertainty in trajectory is large, with the possibility of limited latitude coverage. In addition, the Mercury trajectory restrictions result in an increase of entry velocity which would require advances in heat-shield technology. No separate Venus experiments are included in the planned 1975 Venus-Mercury swingby mission.

6.3 BALLOON SYSTEMS

Whichever type of trajectory is used, the entry, deployment, and flotation systems are similar. Figure 6.4 shows how the parachute system, the inflation system, the balloon and gondola, and the initial dropped probe are fitted into the entry capsule. A further weight breakdown of these systems is given in Figure 6.5.

Some details of the balloon and inflation systems are shown in Figure 6.6. Since the balloon is inflated below the parachute, in the deployment sequence shown in Figure 6.1, the load of the tankage must be carried through the balloon, requiring load fittings and a load line through the balloon. For most of the length, a porous cylinder of Dacron or Nomex fabric serves as both load line and diffuser sock. To keep the initial bubble of gas near the top of the balloon and minimize fluttering of the balloon material, a nonporous liner of Mylar or Kapton film covers the lower portion of the sock.

To distribute the weight of the gondola on the inflated balloon, a load skirt of Dacron or Nomex fabric is attached near the base of the balloon. A pressure control valve within the gondola maintains the desired superpressure and prevents overfilling of the balloon. An inflation diffuser using multiple screens, or perhaps a simple orifice, is used to limit the velocity of the high-pressure inflation gas.

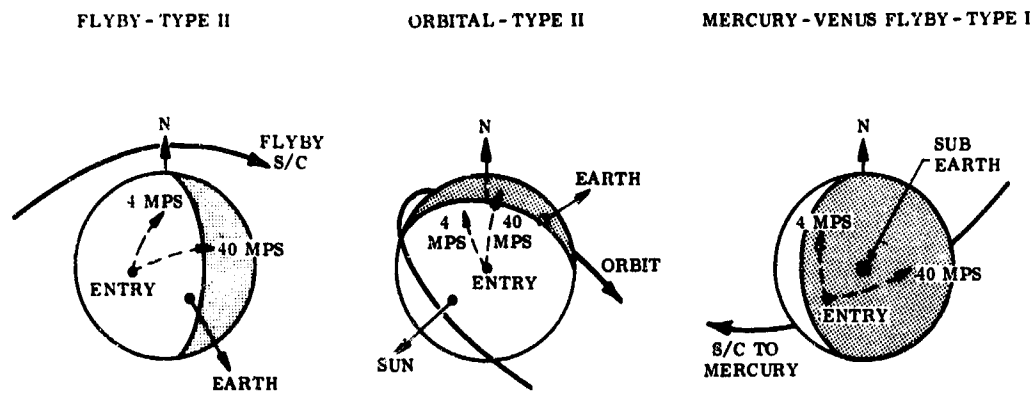


Figure 6.3. Three Types of Venus Missions

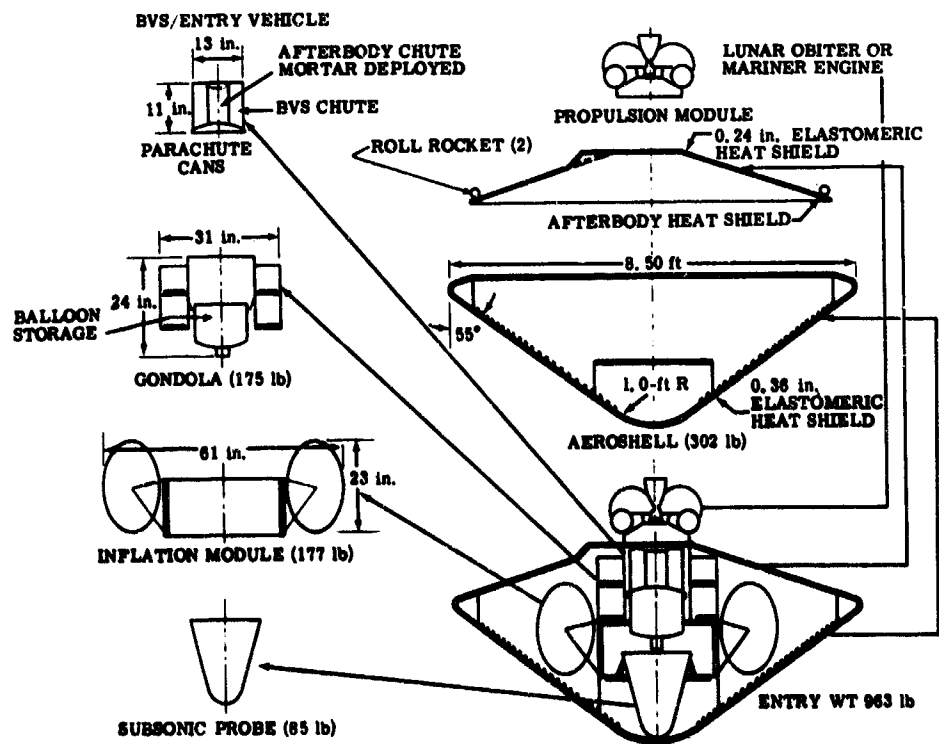


Figure 3.4. Subassemblies in Aeroshell

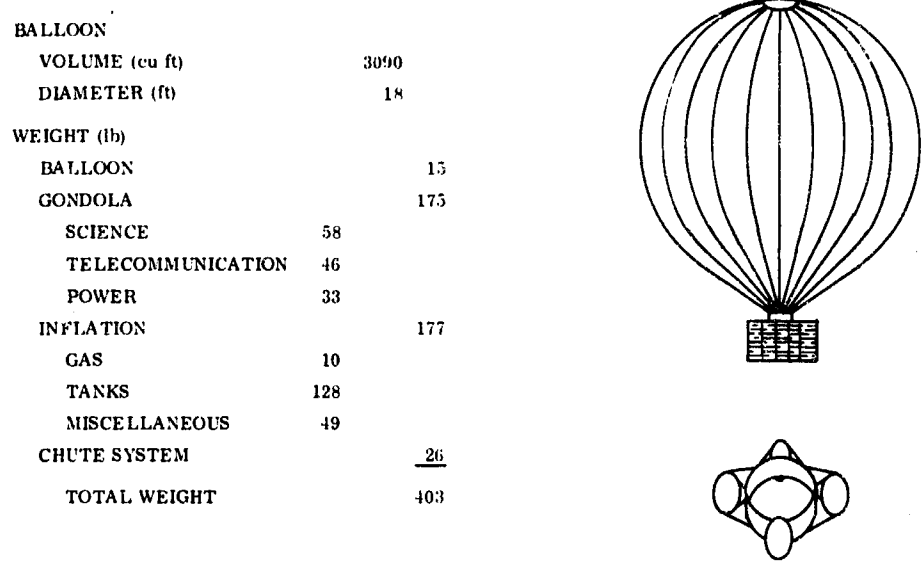


Figure 6.5. Weight Breakdown of Buoyant Station

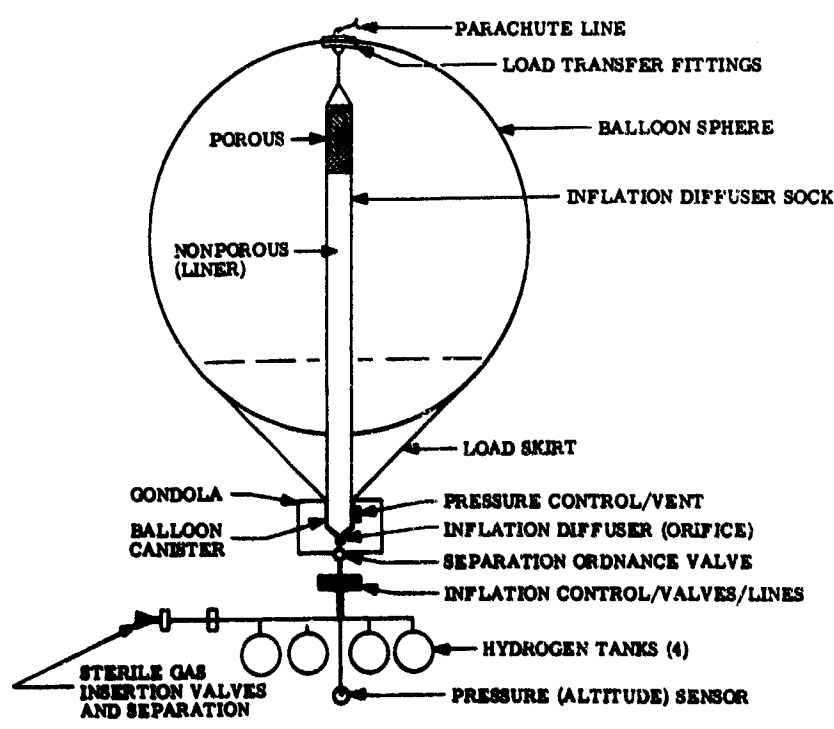


Figure 6.6 Balloon and Inflation Systems

An ordnance valve is used to close the line and separate the inflation module when inflation is complete. The inflation module below this valve is dropped on completion of inflation. Contained in this module are the valves and controls which initiate inflation at the set pressure level, the high-pressure hydrogen tanks, and additional valves and separation devices which permit sterile insertion of hydrogen after the entry capsule in its bioshield has been sterilized. A single tank would, of course, be most efficient from a weight/volume standpoint, but four tanks have been used to permit better placement within the aeroshell. Other lift gases besides hydrogen are feasible in the dense Venusian atmosphere, and other means of storage are also feasible. However, high-pressure hydrogen appears optimum for the 200-pound class of buoyant station because of hydrogen's lift efficiency, because it does not require heating or cooling beyond that supplied by the ambient atmosphere, and because it makes very rapid inflation possible. For much larger systems, cryogenic hydrogen, chemically generated hydrogen, and catalytically decomposed hydrazine become competitive for initial inflation or for makeup gases.

6.4 MATERIALS

A wide variety of materials have been considered and a number of them tested. The principal new requirement for the Venus balloon beyond present-day balloon requirements is the necessity for sterilization. As might be expected, this requirement eliminates many common balloon materials. In fact, the only suitable materials presently used in balloons are Mylar film and Dacron fabric. Among other materials, Kapton film and Nomex fabric appear as strong candidates, with strength properties similar to Mylar and Dacron, but wider temperature limits. An advanced material called PBI (polybenzimidazole) appears as a future possibility. It can be manufactured in both film and fiber form, and has very wide temperature limits. These wide temperature limits are not needed for the missions described herein, but would be useful for other missions which involve vertical cycling in the atmosphere, and which might be attractive follow-on missions. So far, adequate samples in the proper form for testing have not been available. Possible problems are in lamination and in the stiffness of the material which may pose packing and deployment problems.

Our tests confirm the experience of NCAR and others that presently available materials have sufficiently low permeability for long duration only when used in laminates. None of the single-layer materials tested have low enough leak rates after sterilization, simulated handling abuse, packing, and deployment. On the other hand, several laminated materials of Mylar and Kapton survived all of these

tests successfully. In addition, both materials are extremely resistant to hydrochloric and hydrofluoric acids which have been reported in minute amounts in the Venus atmosphere.

6.5 PAYLOAD

Figure 6.7 illustrates the configuration of the gondola and the location of some of the experiments. Not shown are a pressure sensor, a gas chromatograph/mass spectrometer experiment, and a biological experiment. The TV dropsonde shown in dashed lines is not part of the base-line instrumentation, but is one of a number of experiments which could be added if additional weight is made available by electing direct entry of the aeroshell rather than out-of-orbit entry.

Figure 6.8 shows the initial subsonic probe which is dropped upon separation of the aeroshell, and one of the dropsondes which can be dropped by programming or on command.

The balloon system plus the dropsondes provide a very flexible base for experiments, and the long stay time in the atmosphere makes possible very detailed measurements and permits biological experiments to be performed. It also permits reprogramming and allows time for gathering relatively large samples of cloud particles for analysis. The natural wind drift of the balloon makes measurements over different parts of the planet possible and provides information on atmospheric circulation. Large separation for experiments which require isolation can be achieved by dropping them on a cable, and instruments requiring an upward view can be mounted atop the balloon with connecting wires to the gondola supported by the load line.

6.6 TESTING

Considerable experience exists in the deployment of balloons from airplanes in Earth's atmosphere; in fact, this is a routine operation. However, both the balloon construction and the deployment technique outlined above differ from those used in Earth atmosphere deployments, and it is desirable to perform suitable tests to verify their performance. Both static and dynamic inflation tests have been performed using a balloon constructed like that in Figure 6.6. The static tests were conducted outdoors and used hydrogen from a 4000-psi source. Since the use of hydrogen in the Langley full-scale tunnel was considered hazardous, readily available nitrogen was substituted. Since the volume flow of Venus deployment was simulated with the heavier nitrogen, the test was more severe. The

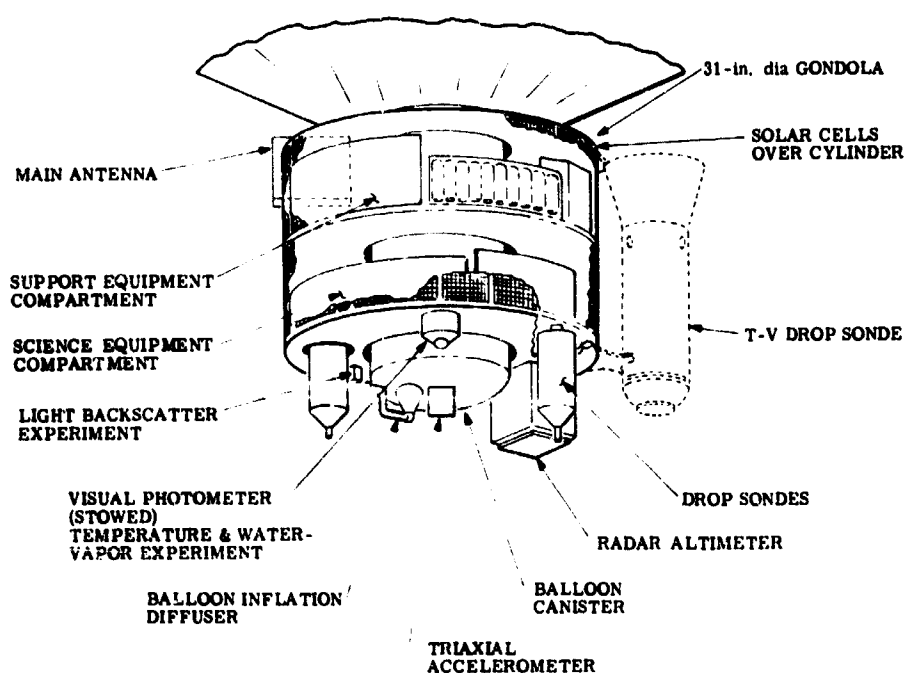


Figure 6.7. Balloon Payload

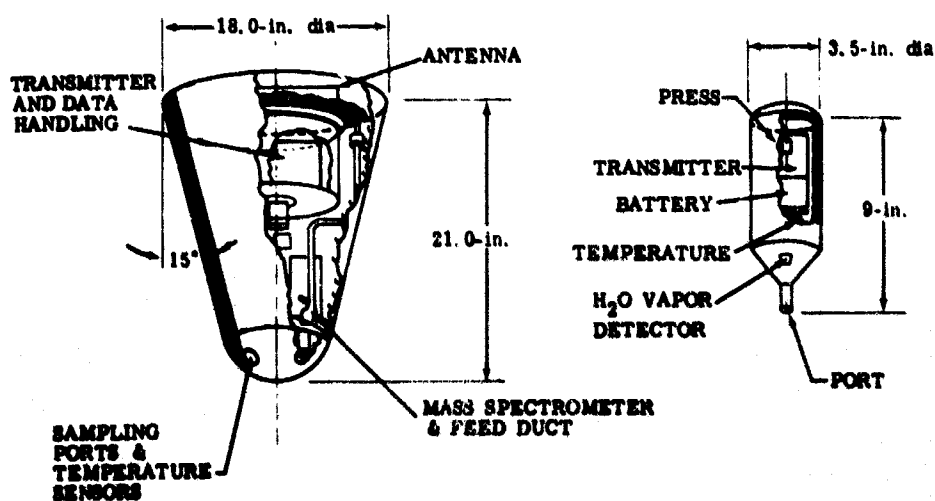


Figure 6.8. Dropped Probes

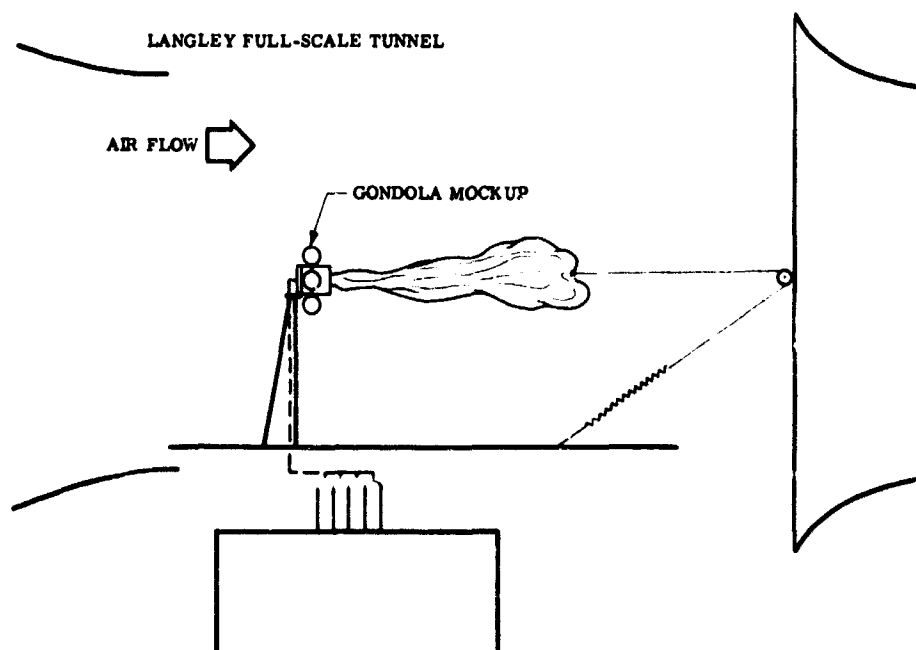


Figure 6.9. Wind-Tunnel Test Setup



Figure 6.10. Test Balloon with Gondola Mockup

test setup in the full-scale tunnel is shown in Figure 6.9. The airflow was regulated to simulate the Reynolds numbers of Venus deployment in a mainly CO₂ atmosphere. Mockups of the gondola and inflation module were included to simulate their effects on the flow. The parachute load was simulated by a line attached to a pulley and a bungee cord. In addition to full simulation of the Venus inflation sequence, tests were made with prolonged flow at several partially inflated conditions to observe the degree of flutter or flagging present. The degree was quite moderate at all levels of inflation. Evidently, the presence of the parachute line reduces the tendency to whip or flag, and the diffuser sock eliminates flutter near the base of the balloon due to the incoming inflation gas. No damage to the balloon was observed during simulated Venus conditions; and when a much more severe condition was accidentally applied, the damage was limited to the load skirt while the film envelope remained intact.

In Figure 6.10, the balloon which was tested in the full-scale tunnel is shown fully inflated with a mockup of the gondola attached.

6.7 CONCLUDING REMARKS

A scientific mission to Venus utilizing a balloon to support the payload has been studied in considerable depth by the NASA Langley Research Center and its contractors. All aspects of the complete mission have been found to be feasible, and the mission offers several desirable features for experiments. The long stay time of a balloon in the atmosphere permits detailed analysis, biological experiments, and experiment reprogramming. The natural wind drift permits measurements at different parts of the planet and provides information on atmospheric circulation.

Such a mission is not part of the current NASA plans, but it is under consideration for future programs, perhaps during the 1980's.

References

- Burroughs, E. R. (1935) Lost on Venus (Published by Author).
 Davis, M. H., and Greenfield, S. M. (1965) The Mars Balloon Feasibility and Design, Proceedings of the 1964 AFCL Scientific Balloon Symposium, Air Force Surveys in Geophysics No. 167, pp. 341-352.

Final Report (1967) Buoyant Venus Station Feasibility Study.

- Vol. I: Summary and Problem Identification, J. F. Baxter, NASA CR-66404.
- Vol. II: Mode Mobility Studies. R. E. Frank and J. F. Baxter, NASA CR-66405.
- Vol. III: Instrumentation Study. A. R. Barger and J. F. Baxter, NASA CR-66406.
- Vol. IV: Communications and Power. J. D. Pettus, A. A. Sorenson, and J. F. Baxter, NASA CR-66407.
- Vol. V: Technical Analysis of a 200-Pound BVS. A. R. Barger, R. E. Frank, J. D. Pettus, A. A. Sorenson, and J. F. Baxter, NASA CR-66408.
- Vol. VI: Technical Analysis of a 2000- and 5000-Pound BVS. R. E. Frank and J. F. Baxter, NASA CR-66409.

Final Report (1969) Buoyant Venus Station Mission Feasibility Studies for the 1972-73 Launch Opportunities.

- Vol. I: Mission Summary Definition and Comparison. John F. Baxter, Ronald E. Frank, John N. Froistad, and Gene R. Cody. NASA CR-66725-1.
- Vol. II: Trajectory Analysis for 1972 and 1973 Mission. Donald W. Marquet and Charles E. French, NASA CR-66725-2.
- Vol. III: Part I - Configuration. Patrick C. Carroll, Ronald E. Frank, and Jack D. Pettus, NASA CR-66725-3. Part II - Appendixes. Allan R. Barger, H. Edward Sparhawk, John C. Mellin, Ronald E. Frank, Jack D. Pettus, Patrick C. Carroll, Robert W. Stoffel, James E. Cole, Ted H. Tucker, James W. Berry, and Walter F. Hane, NASA CR-66725-4.

Greenfield, S. M., and Davis, M. H. (1963) The Physics of Balloons and Their Feasibility as Exploration Vehicles on Mars, NASA CR-51782.

Greenfield, S. M., and Davis, M. H. (1965) Balloons for the Scientific Exploration of Mars, Proceedings of the 1964 AFCRL Scientific Balloon Symposium, Air Force Surveys in Geophysics No. 167, pp. 353-364.

Gross, F. R. (1965) Buoyant Probes Into the Venus Atmosphere, Proceedings of the AIAA Unmanned Spacecraft Meeting, Los Angeles, California, pp. 76-87.

Gross, F. R. (1966) Buoyant probes into the Venus atmosphere, J. Spacecraft (No. 4):582-587.

Pritchard, C. L. (1963) Preliminary Study of the Application of Balloons in the Atmospheres of Mars and Venus, Raven Industries Technical Note 31, Sioux Falls, South Dakota, 29 January 1963), revised 22 March 1963.

Sadin, S. R., and Frank, R. E. (1968) Buoyant Venus Station for the 70's, Preprint No. 68-7-4, Americana Astronautical Society, Denver, Colorado.

Sadin, S. R. and Frank, R. E. (1969) Buoyant Venus Station Requirements, AIAA 6th Annual Meeting, Anaheim, California.

Steinberg, Sv. and Holle, G. F. (1969) Experimental Results of the Deployment/Rapid Inflation Characteristics of a Buoyant Venus Station Balloon, AIAA/ASTM/IES 4th Space Simulation Conference, Los Angeles, California.

Contents

7.1	Introduction	76
7.2	General System	76
7.3	The Flight System	77
7.4	The Solar Biaxial Pointer	79
7.5	The Spectropolarimeter	83
7.6	The Infrared Radiometers	84
7.7	The Near Sun (Aerosol) Radiometers	86
7.8	Telemetry	87
7.9	Gondola Dynamics	87
7.10	Conclusions	89

7. Sun Oriented Atmosphere Optics Measurements Using the High Altitude Balloon

R.B. Toolin
Air Force Cambridge Research Laboratories
Bedford, Massachusetts

N.C. Poirier
Northeastern University
Boston, Massachusetts

Abstract

Recent balloon flights at Holloman AFB, New Mexico illustrate the general type of optical measurements and instrumentation used for investigation of the radiational characteristics of the earth and its atmosphere. The particular flights had an international tone since they involved the pointing of two infrared radiometers developed by the Meteorological Institute of the University of Munich, Germany and two other radiometers from AFCRL - using a two-axis sun pointer designed by Ball Brothers Research Corp. of Boulder, Colorado. Also, referenced to one axis of the pointer was a set of spectropolarimeters from the Dept. of Meteorology, UCLA. Data were transmitted to the White Sands receiving stations, using an airborne telemetry set prepared by Northeastern University. The entire assemblage was contained in an AFCRL gondola.

Typical samples of telemetered data, both optical and "housekeeping" types, are presented and these levels are interpreted in terms of the primary sensors which produced the transduced signals. System operation is illustrated by this means.

Dynamic measurements of the balloon gondola were made and, in conjunction with temperature sensors, illustrate some of the advantages of scientific ballooning.

PRECEDING PAGE BLANK

7.1 INTRODUCTION

A particular mission within the USAF R&D community involves theoretical and experimental studies of the nature of optical radiation in the earth's atmosphere. There are two optical processes which categorize the effects of the atmospheric medium. These are designated as scattering and absorption. Scattering refers to the spatial redistribution of radiation by the molecules and particulate matter of the atmosphere. Absorption is the direct conversion of optical energy into other forms - primarily, heat energy.

In order to describe the earth's atmosphere as a radiational medium, several specific optical characteristics must be set forth. The absorbing, scattering and polarizing features of the radiation would be necessary. These would have to be specified for a range of wavelengths because these optical properties are spectrally sensitive. A general comment would represent that the scattering of optical radiation is proportional directly to the number density of the molecules of the atmosphere and inversely to the fourth power of the wavelength. This observation is markedly modified by the presence of aerosols, or particulate matter, in the atmosphere particularly within the first 5 km above the surface of the earth. Additionally, there are the more complex atmospheric molecules, such as ozone, water vapor, sulfur dioxide, methane and many other trace gases. These are highly variable in concentration and in distribution, and are strong optical absorbers for specific wavelengths.

The experimental package to be described is configured to measure the spectral intensity and polarization of optical radiation emerging through the atmosphere, and also to determine specific scattering and absorbing properties of the atmosphere. Since these radiational values are vitally dependent upon solar lighting, the measuring devices, to have a valid use, must have a known and fixed orientation with respect to the sun.

7.2 GENERAL SYSTEM

This experiment has six distinguishable elements which are incorporated necessarily to achieve the program's technical objectives. There is, first of all, the flight system consisting of the balloon, flight control devices, and the gondola for protection and support of the scientific equipment. Continuous orientation of the instrumentation, in spite of the swinging and rotating motions of the gondola, is obtained with a biaxial sun pointer. There are three types of scientific instruments. Infrared radiometers are oriented directly to the sun for measurement of solar absorption by atmospheric water vapor and methane. Filter wheel radiometers are

set at specific angles from the sun to measure forward scattering. There is a set of two spectropolarimeters, each directed to the underlying atmosphere. One is arranged so that it scans in the vertical plane containing the sun and the nadir; the other, normal to this plane. Finally, some of the information is recorded directly into an on-board magnetic tape recorder. All signals are transmitted by a telemetry link to a ground station where the data are recorded on magnetic tape and also processed for quick-look information by the scientists at the receiving site.

Figure 7.1 outlines the system which has been launched from Holloman AFB, New Mexico on several occasions. Successful parachute recoveries have been made in the open areas of Texas and New Mexico about seven hours after launch.

7.3 THE FLIGHT SYSTEM

Figure 7.2 is an on-site photograph of the flight system just prior to launch. The horizontal bar supports the primary and backup flight-control and command system, a standard radiosonde and a Load Let-Down Reel (Doherty et al, 1967). The latter is activated shortly after launch and deploys the instrumented gondola to a maximum distance of 500 feet. For the illustrated flight, a separation of 200 feet assured that no balloon surface was within the field of view of any optical sensors. Its use also reduces the possibility, at the time of landing, that the load bar will impact on the gondola.

The gondola, of 1/4 to 1/2 inch aluminum plate, supports on its top surface the sun pointer and measuring instruments. Its middle sections contain the tape recorder, telemetry unit and two single axis gyros. The bottom sections hold the primary batteries and the ballast box which contains 100 lbs of fine steel shot. The unused amount is released prior to landing. A set of two AFCRL impact switches is mounted at the extreme position.

The gondola also has to serve as an inertial device because the sun pointer assembly must work against the gondola to maintain stable pointing about the vertical axis. This would recommend that the gondola be as wide as practicable. The spectropolarimeters mounted to the pointer must have a clear downward line of sight and so have to be extended outboard of the gondola. This necessarily increases the moment of inertia of the pointer assembly. The compromise solution has been to limit the diameter of the gondola to 32 inches. At termination of scientific measurements, landing legs are sprung outward. The legs are restrained by common gate springs. The six legs, symmetrically arranged about the gondola proper, have, at the outside end, food strainers containing open cell polyurethane foam; and the other end, styrofoam dashpots.

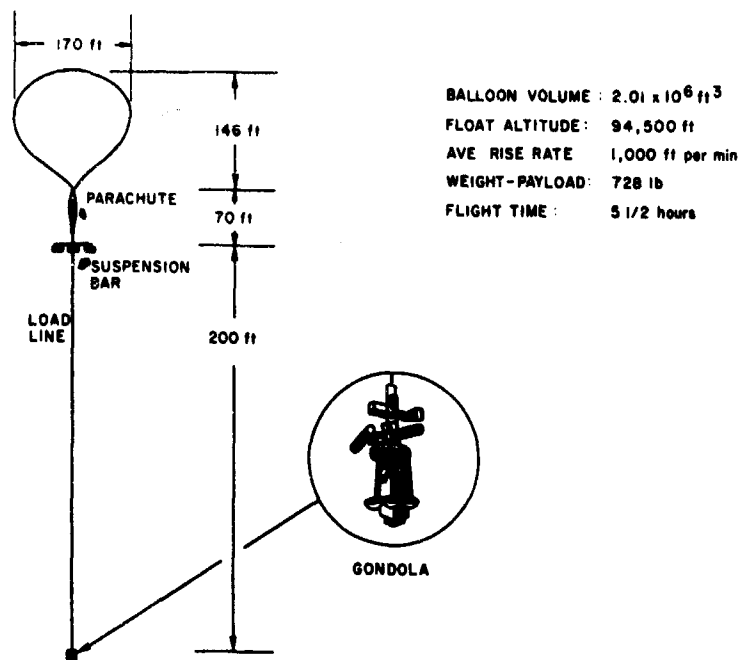


Figure 7.1. The Balloon-borne Flight System and Principal Statistics of a Flight

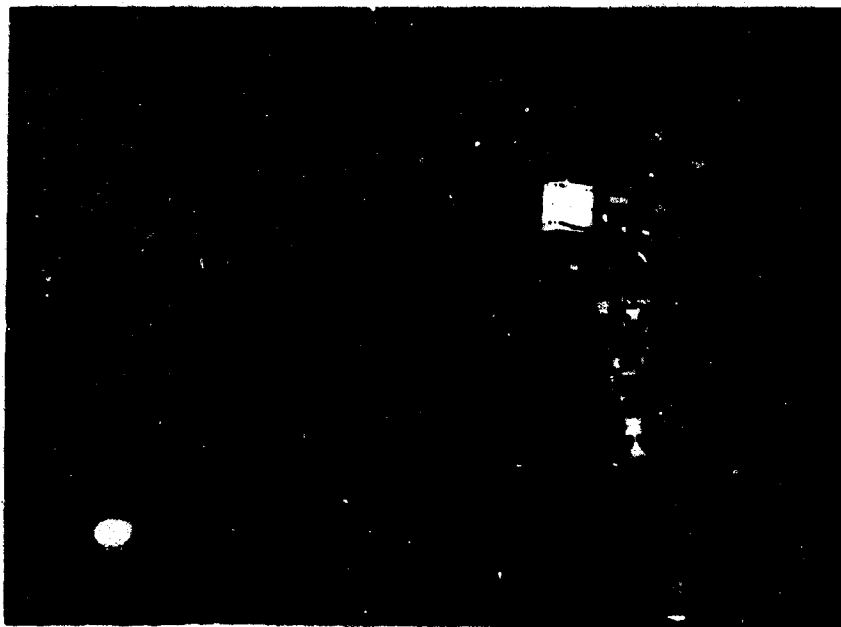


Figure 7.2 Pre-launch Configuration of the Atmospheric Optics Experiment

7.4 THE SOLAR BIAXIAL POINTER

Figure 7.3 illustrates the prominent features of the sun orientation unit and also displays the relative position of the three groups of scientific instruments. This pointer has been designed and fabricated by Ball Brothers Research Corp. (Greeb, 1965) with a design goal to point an 80 lb instrument within ± 2 minutes of arc of the center of the sun. The system has two mutually perpendicular axes of rotation. The entire pointer rotates azimuthly about a vertical axis. Only the scientific instrument attached to the shaft which rotates about the lateral (elevation) axis will be positioned biaxially. Three separate sensor blocks containing photo-sensitive detectors produce an electrical current proportional to the angular deviation about each axis. The output of these sensors is used in a feedback control system (an independent system in both axes) to orient the instrumentation toward the sun.

Although there are others for monitor and override functions, the principal sensors are those used for pointing. The azimuth coarse-error sensor is mounted at the top of the pointer case. Four detectors, in combination, make up a sensor

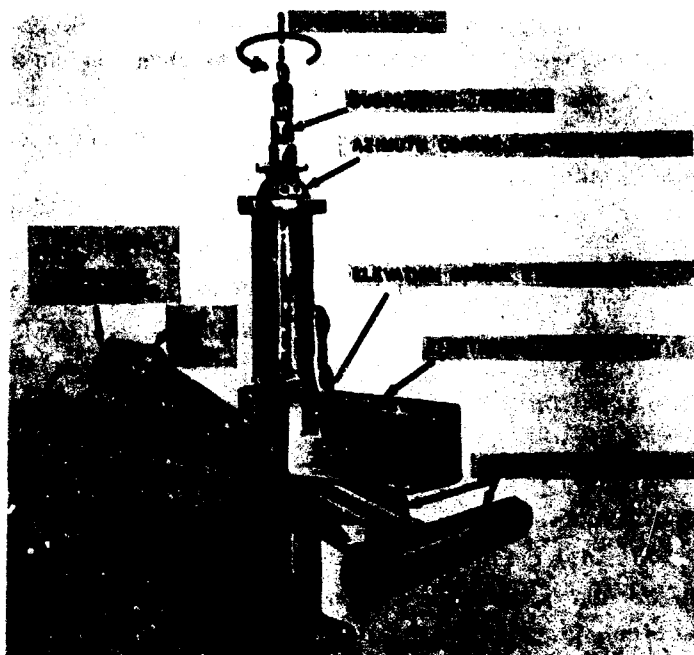


Figure 7.3. Major Features of the Biaxial Solar Pointer and Arrangement of the Experiment

with a 360° Field of view (FOV) azimuthly. This sensor operates to position the pointer about the azimuth axis until the elevation axis is perpendicular to the solar vector within 3° . With the pointer in this position, the set of two detectors which make up the elevation coarse sensor is illuminated. This sensor is mounted directly in the elevation shaft but opposite to the instrument mounting flange. It is deliberately recessed into the electronics compartment to reduce the effects of reflected light from the earth and balloon. Adjustable shields mechanically limit the FOV to an approximately rectangular $40^\circ \times 95^\circ$. The elevation coarse sensor provides error signals to rotate the instrument about the elevation axis. The resultant coarse alignment of the instrument optical axis and the solar vector is within 3° . This action also brings the sun within the FOV of the fine sensors and the target sensor. The fine sensor in each axis is composed of two photosensitive detectors assembled in a block, which is hardmounted to the scientific instrument and in precise alignment with it. The target sensor provides a signal which activates the override mechanism to transfer the pointing function to the fine sensors.

Figure 7.4 illustrates, in block format, the signals recorded at various locations in the servo system. The azimuth and elevation channels are essentially identical, with only minor component value difference in the servo feedback networks. The particular signals, converted to angular notation, had been recorded while the balloon system was at 71,000 ft. In general, they are typical for the entire flight.

Position potentiometers are installed in both the elevation and azimuth systems to provide direct measurement of gimbal angles. Their outputs show, over a time interval of five minutes, that the pointed instrument was oriented to an elevation of 30° above the horizontal and that the gondola rotation with respect to the pointer was approximately 1 rev per minute. The monitor at the power switch illustrates a signal proportional to the current being delivered to the torquer motor of either axis. Knowing the torque sensitivity, the ordinate is converted to the torques being applied during this five minute interval to maintain biaxial track. Considering that these are 1.2 lb ft torquer motors, this torqueing is quite small. The "house-keeping" signals at the input to the Pulse Width Modulator are proportional to the error voltage from the preamplifiers of error sensors. Examined in terms of angular error, the display shows very small servo error signals being generated and, for the five minute interval error, correction rates are very reasonable.

Figure 7.5 displays the functional arrangement of the monitor system. It operates independently of the servo system in that servo sensors do not furnish signal current to monitor circuits. Two of the monitor circuits do control the operating mode of the servo electronics.

The target detector, mounted and aligned on the fine sensor block, has been referenced earlier. Once the sun has come within $\pm 3^\circ$ during the acquisition mode

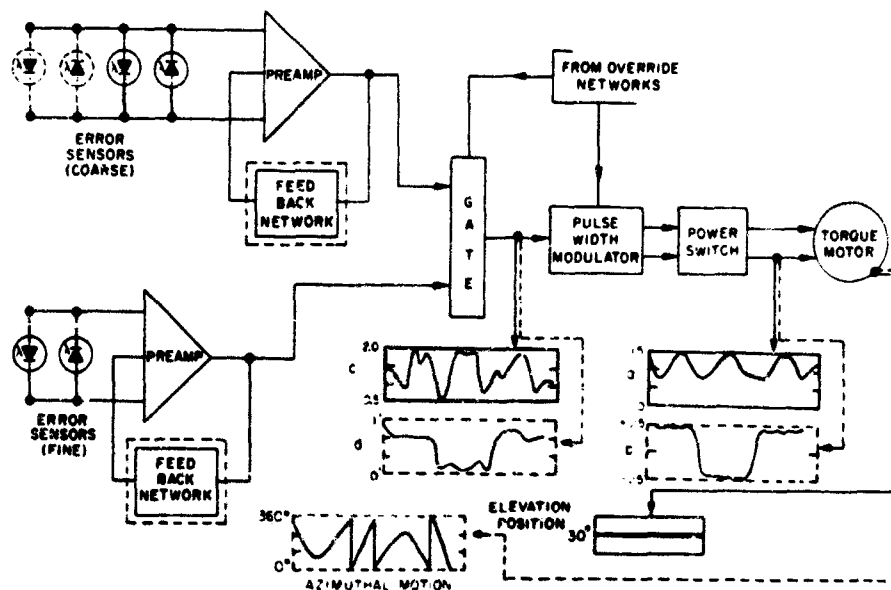


Figure 7.4. Functional Diagram of the Servo System

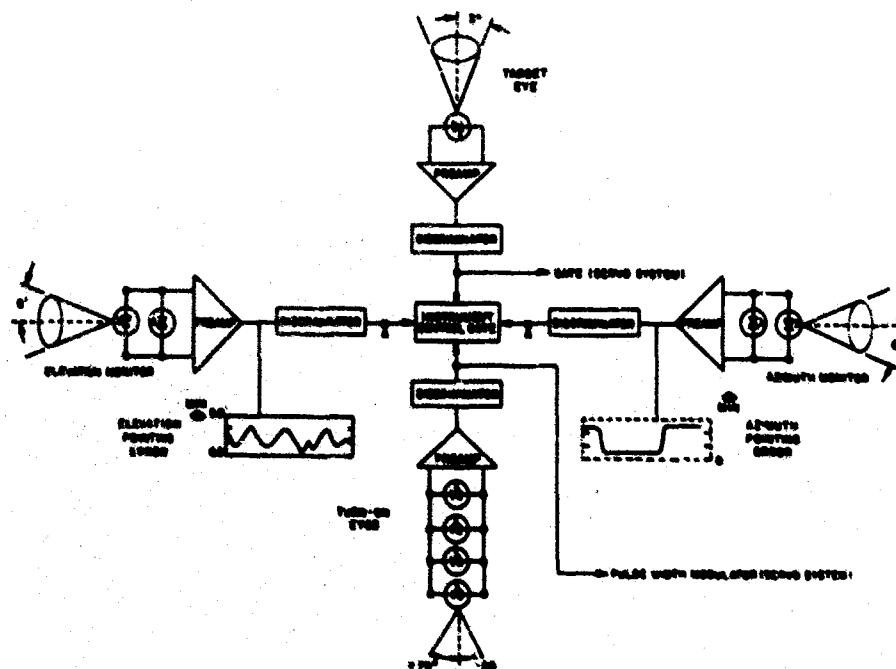


Figure 7.5. Function Diagram of the Monitor System

and it remains within this field of view of the target sensor for a period greater than 2 seconds, the discriminator is triggered. It provides a signal which inhibits the coarse sensor preamp output in the servo system, leaving the fine detector preamps to control the servo system for fine pointing.

The other control is a more precautionary type and is referred to as the turn-on sensor set. The four detectors are arranged in the same polarity and are physically located, in symmetrical fashion, on the azimuthal coarse sensor block. Specially designed and moveable baffles are located above and below these detectors. This limits the vertical field of view of the sensor block so that no spurious radiating sources (for example, from balloon surface reflections) will be intercepted. If the sun position should be outside this angular coverage, the signal level from the turn-on sensor will go below a preset value. Then the discriminator is activated generating a signal into the Pulse Width Modulator of the servo system, disabling it so that no pulse train is fed into the Power Switch. Again, at this time, and throughout the flight, the telemetered signal shows no gating action to have occurred, except for the first twenty-five minutes after launch when the sun was below local horizon.

Both the azimuth and elevation monitoring sensors are mounted on the fine sensor block. These two sets of sensors give a direct measure of the angular pointing error for their respective axes. Each sensor has a 10° conical FOV but, in actuality, the telemetered signal will be in saturation if the instrument points at an angle in excess of 6 minutes of arc as measured from the center of the solar disc. Both five minute portions of the flight records are typical, in general, for the actual performance of the system. If an angular error had ever exceeded the ± 5 minutes of arc for either axis, then the pertinent discriminator would have been activated, generating a 5-volt signal monitored at the point marked "A".

The instrument control gate is not used for these flights. It would provide a disabling signal to the scientific instrument if any one of the four monitor/override networks should generate its own disabling signal.

Detailed examination of the monitoring records of these flights represents that the pointing inaccuracy never has been greater than ± 4 minutes of arc with respect to the center of the sun, even with the most severe dynamic loading during ascent. Generally, pointing has been well within ± 2 minutes of arc. Continuous corrections, except at float, superimpose a very low magnitude of oscillation on the pointing monitor signals.

7.5 THE SPECTROPOLARIMETER

The Meteorology Dept. of the University of California at Los Angeles has developed this instrument for the measurement of skylight and earthlight intensity, and polarization at selected wavelengths in ultraviolet and visible spectrum (Chesebrough, 1967). Theoretical considerations of a pure molecular flat atmosphere as viewed from a platform above the sensible atmosphere, would produce the results shown in Figure 7.6a. The graph illustrates the percent of linear polarization, at a wavelength of 0.36μ , with the earth being characterized as non-reflective at this wavelength. The prominent features are a maximum polarization of 75 percent occurring approximately 90° from the anti-solar point, and a reversal in polarization in the general region of the anti-solar point. This illustration is for that particular plane of observation containing the sun and the nadir. The factual atmosphere is neither purely molecular nor flat, so that field observations can diverge radically from this simple representation.

The principal functional components for the spectropolarimeter to accomplish these measurements are shown in Figure 7.6b. Collimated light of unknown intensity and polarization is passed through a rotating Glan prism, serving as an

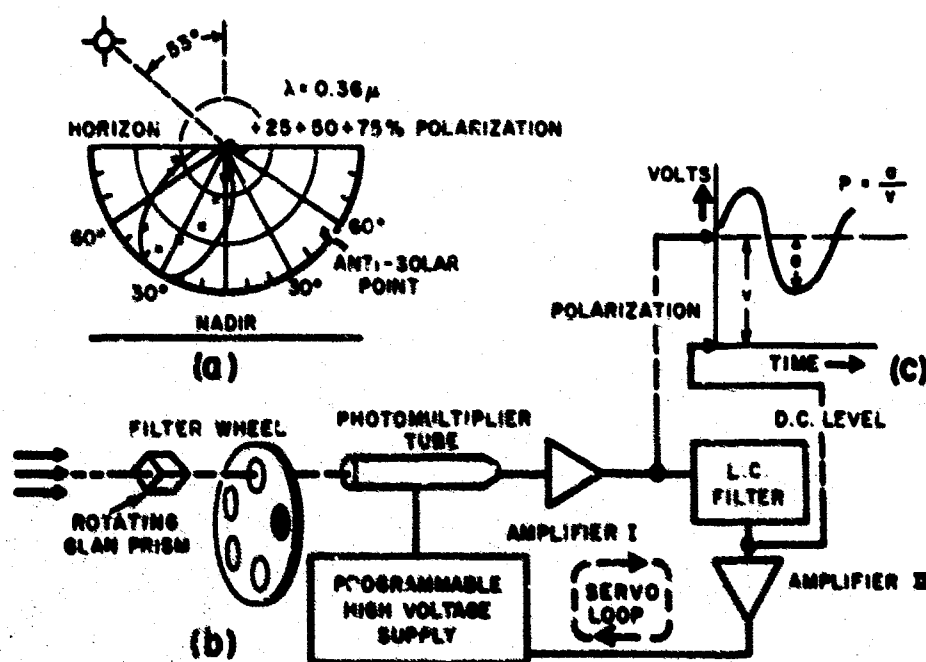


Figure 7.6. The Spectropolarimeter Experiment

analyzer; through one of several automatically programmed interference filters; and onto an ASCOP Model 541A photomultiplier. The sinusoidal photosignal is fed into the Analog Devices Model 210 amplifier and thence through an LC smoothing filter. A portion of this signal is fed into a Burr Brown operational amplifier. The output of this amplifier is bucked against a fixed voltage and the residual acts as the controlling voltage for the Arnold Model SHU-2500PE power supply. This programmable power supply, the photomultiplier, the amplifiers and the LC network form a closed-loop servo system. Variations of three to four orders of magnitude in the intensity can be handled by this technique.

Each spectropolarimeter weighs approximately 14 lbs. Each is mounted only to the azimuthal axis of the stabilized platform; one being set for the plane containing the sun, and the other normal to this plane. The spectropolarimeter is programmed to complete the 180° scan from horizon through nadir to the opposite horizon in seven minutes, in 3° intervals, with a complete spectral sample being taken at each step. The illustration of Figure 7.6c would be typical of the flight data and the easy calculation for the percent of polarization is shown. Specimen results are shown in Figure 7.6a, with the same geometry of lighting, measured from the balloon platform at 92,000 feet. A more complete analysis of this type of data has been published (Rao, 1969). For the particular illustration, the difference between the theoretical curve and the experimental points is due to the presumption of a nonreflecting earth. A more proper choice of this parameter would show a marked coincidence of values.

7.6 THE INFRARED RADIOMETERS

The Meteorological Institute of the University of Munich, Germany, has developed a general type of radiometer for the measurement of several of the absorbing gases present in the earth's atmosphere. The particular units which are flown in this payload are prototypal instruments for the measurement of absorption by water vapor and trace gases. The problem associated with such measurements is that for the small concentrations of these gases in the upper atmosphere, the intensity of solar radiation as measured through an absorption band will be little different from the intensity through an adjacent atmospheric window. Figure 7.7a suggests the method of the difference radiometer in which only the difference signal in the radiation inside and outside the absorption band is obtained, and this is measurable to approximately the same accuracy as the referenced intensity. Both channels, difference and reference, use identical but separate signal handling electronics, as shown in Figure 7.7b. For water vapor absorption, the actual measurements were made at wavelengths of 1.87μ , the

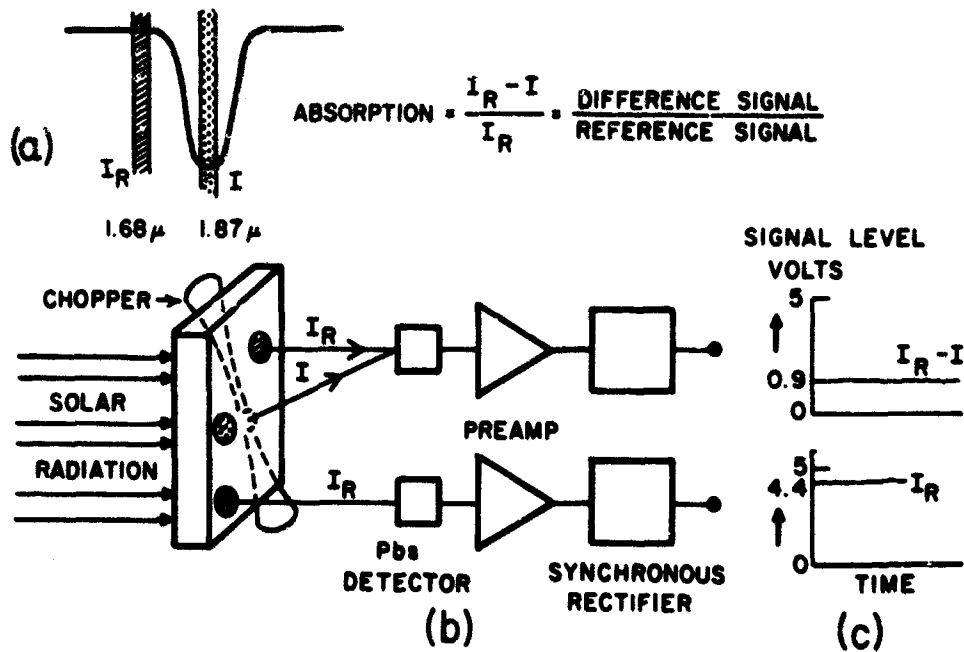


Figure 7.7. The Infrared Radiometer Experiment

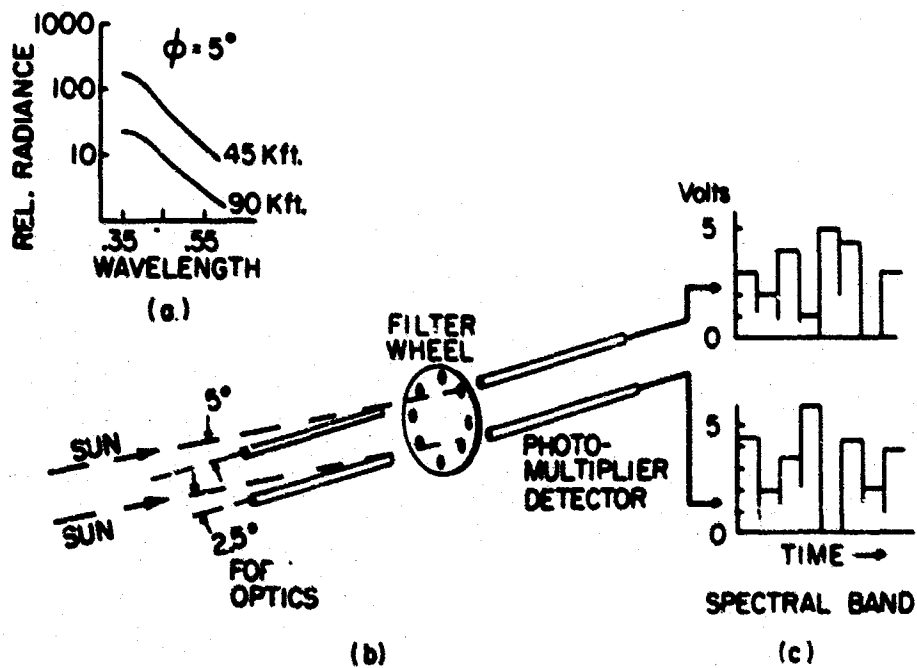


Figure 7.8. The Near-sun Radiometer Experiment

absorption band, and at 1.68μ , an atmospheric window. The markedly lower atmospheric concentration of methane requires a modification to this method. Here a sealed absorption cell containing a known concentration of methane gas is located in the reference beam, and the atmospheric absorption is compared with the referenced absorption. The instruments weighed 20 lbs and were mounted directly to the elevation arm for biaxial pointing to the sun.

Figure 7.7c represents signal levels transmitted to the ground station. This particular record, for a time interval of one-half minute, was obtained during the early portion of a flight and is not especially typical of the entire flight. Above 70,000 feet, and with the higher sun elevation, the difference signal is near the zero volt level, indicative of the very low concentrations for this geometry.

7.7 THE NEAR SUN (AEROSOL) RADIOMETERS

The optical presence of particulate matter in the upper atmosphere usually would be veiled by the light scattering from the normal and smaller gaseous molecules. However, the aerosol scattering of light is characterized by a preferred redirection of the radiation into the forward angles. So the most sensitive viewing angles for detection are close to the sun. This natural advantage has the drawback that the optical sensors must be designed and aligned with exacting care, so that no direction sunlight or flaring can introduce spurious radiation. Another important characteristic of optical scattering by aerosols is that the spectral distribution is markedly different from the orderly λ^{-4} property of atmospheric molecules. These two factors, forward scattering and spectral selection, are used in a set of instrumentation. Figure 7.8a illustrates the general characteristics of the light distribution near the sun (offset angle of 5°) for two different altitudes. The effects of molecular scattering have been removed, so that the illustrated residual is the aerosol scattering. Figure 7.8b outlines the radiometers' arrangement with optical axes offset from the sun pointing axis by 2.5° and 5° . Figure 7.8c sketches the signals acquirable during the 20-second sampling period. The voltage levels are not idealized, for the geneva driving mechanism for the filter wheel does produce a dwell time at each filter, with a very quick transfer to the following spectral discriminator. Results of this experiment are to be published separately.

7.8 TELEMETRY

The telemetering system should be familiar to the users of rocket vehicles since it is composed of their standard units which have been integrated by the electronics engineering group of Northeastern University. Fifteen IRIG channels are used. The primary transmitter operates in the P band, at 237.8 MHz, with a nominal power of 4 watts. The impending national range change to S-band transmissions recommended that such a transmitter be tried also. In the most recent flight, a Conic Model CTM UHF 402 transmitter was used, in parallel with the P band unit and operated at 2251.5 MHz. The one-quarter wave stub antennae with ground plane dangle beneath the gondola.

Operational performance of both units, using the common set of subcarriers, was completely satisfactory. The greater attenuation of the S-band transmission was offset by the higher gain of the receiving antenna, so that the signal strengths at the receiver were approximately identical.

Since the balloon vehicle soaks in the cold atmosphere due to the slow vertical rise rate, the telemetry can is packed with sealed water bottles, using their heat capacity to maintain a stable temperature regime. Throughout a flight, this does not deviate more than 20°C from ground launch temperature.

7.9 GONDOLA DYNAMICS

The biaxial pointing also affords the opportunity to harvest data on gondola motions. Figures 7.9 and 7.10 are graphical compilations of the rotational motions for two separate flights. Indicated directions are with respect to North. Other than the obvious wild motions of winding and unwinding during tropospheric penetration, there is a subtle implication of a correlation with wind shears.

The individual points on the temperature profile are data from the on-board radiosonde. The gradual deviation from the ambient temperature curve is most probably due to the increasing effect of the confined helium as an extended radiating source.

A Minneapolis-Honeywell cageable vertical gyro, with two degrees of freedom (roll and pitch) was mounted in the gondola framework for the most recent flight. Both axes are responsive to a range of $\pm 19.5^{\circ}$ and are sensitive to a change of 0.1° . Figure 7.11 presents the pendulous actions of this flight as a function of time and altitude. The curves describe the angular magnitudes of the oscillations in both planes. Following the initial period of launch shock, the pendulous action generally is of the form of a simple sinusoidal motion with peak-to-peak values as

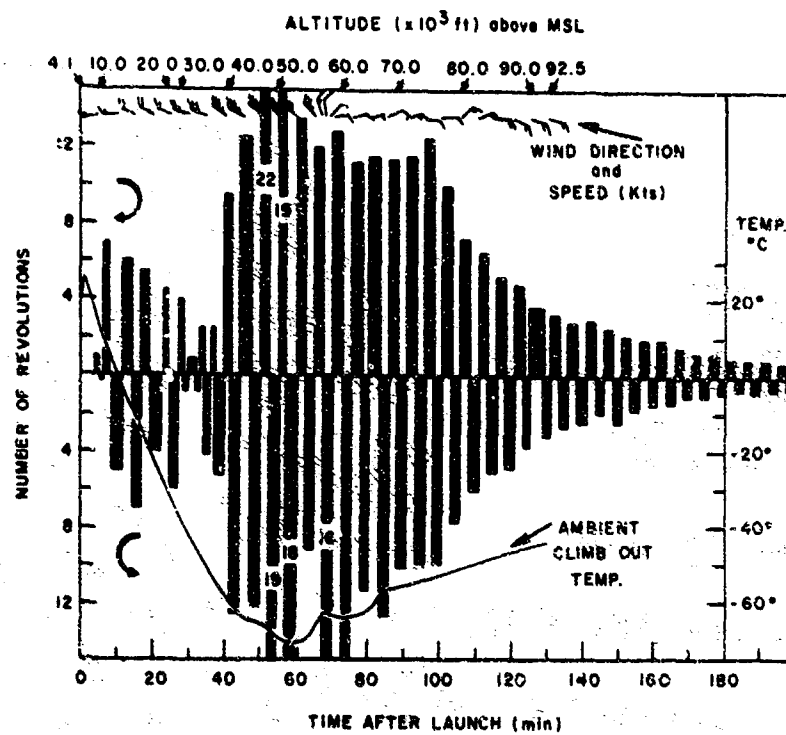


Figure 7.9. Gondola Rotations - Flight No. 2. Numbers of rotations are for the time intervals indicated by width of the black bars

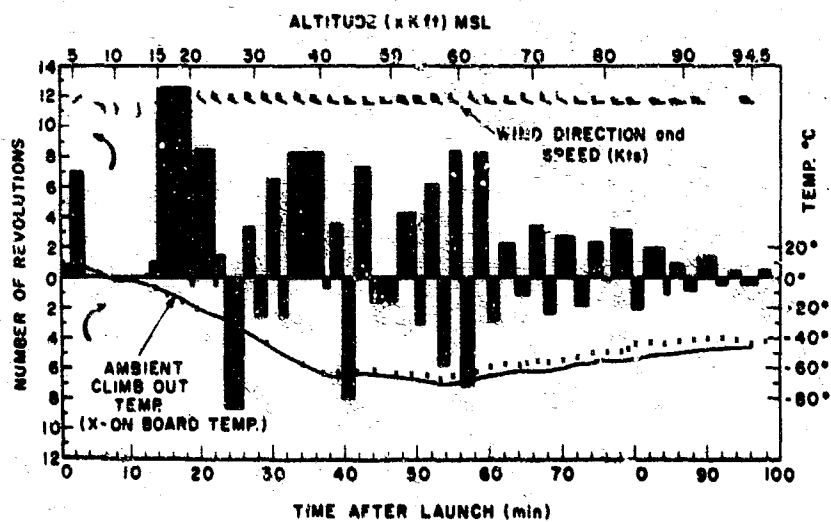


Figure 7.10. Gondola Rotations - Flight No. 4. Numbers of rotations are for the time intervals indicated by width of the black bars

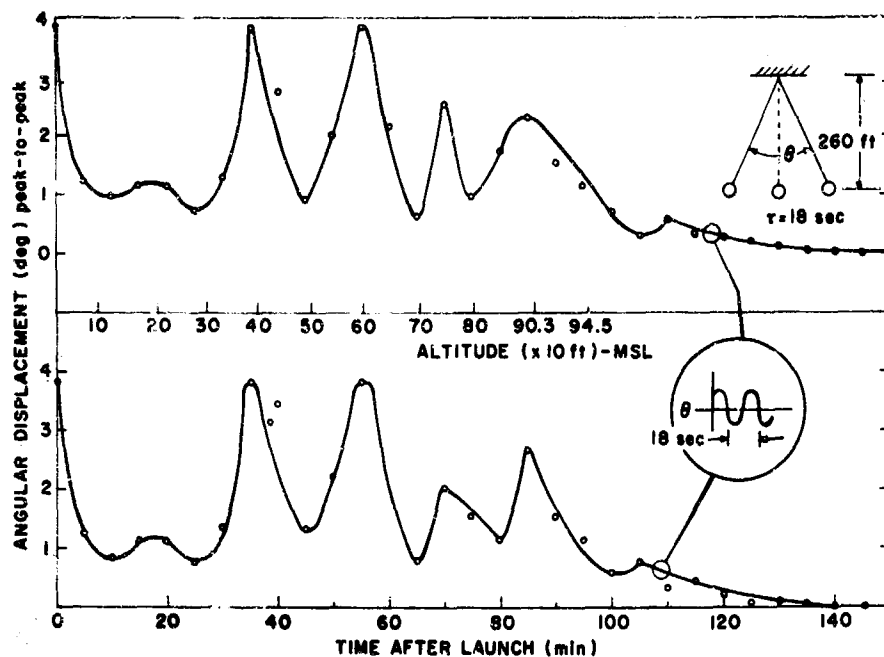


Figure 7.11. Pendulous Motions of Gondola - Flight No. 4

shown and with the period of oscillation of approximately 18 seconds. This value corresponds well with that of a simple pendulum of length 260 feet, which is also the approximate distance from the base of the balloon to the gondola.

7.10 CONCLUSIONS

Because of the diversity of the experiments which have been flown in these balloon payloads, no specific comments can be made concerning scientific results. There is one statement which can be echoed again - that these efforts illustrate again the versatility of high altitude ballooning for scientific payloads. It is the last of the test beds where the experiment can define the shape, size and performance required of the carrier rather than the usual but opposite situation.

Acknowledgments

The authors wish to express their sincere gratitude and appreciation for the continuing cooperation, high motivation and obvious technical competence of the research personnel who have participated in this team effort - Mr. Carl Rust of AFCRL; Mr. Robert Wallace of Northeastern University; Messrs. Peter Burkert and Dieter Rabus of the University of Munich; Dr. C. R. Nagaraja Rao and Mr. Daniel Dibble of U.C.L.A. Particular acknowledgment is to be made to the personnel of the Balloon R&D Test Branch (AFCRL) at Holloman AFB, New Mexico for their always excellent support.

References

- Chesebrough, G. F., Dibble, D. F. and Rao, C. R. N. (1967) Gain Compensated Photopolarimeter for Airborne Measurements of Skylight Polarization, Scientific Rpt. No. 1, Contract No. F19628-67-C-0196, AFCRL-67-0396.
- Doherty, F. X., Czepyha, G. R. and Reddy, R. J. (1967) The In Flight Deployment of Heavy Payload Trains Beneath Ascending High Altitude Balloons, Instrumentation Paper No. 134, AFCRL-67-0634.
- Greeb, M. E. (1965) Design and Development of the Balloon-Borne Pointer, BBSP-200, Final Report, Contract No. AF19(628)-4914, AFCRL-65-604.
- Rao, C. R. N. (1969) Balloon measurements of the polarization of light diffusely reflected by the earth's atmosphere, Planetary and Space Science : 17(No. 6)

Contents

8.1 Introduction	92
8.2 Principle of Operation	92
8.3 Range Ambiguities	94
8.4 Output Data	96
8.5 Test Results	96
8.6 Extensions	98

8. Applications of Radio Altimetry to Balloons

F.G. Stremier, N. Levanon, and V.E. Sumi
University of Wisconsin
Madison, Wisconsin

Abstract

A newly developed radio altimeter enables geometric altitude measurements of meteorological balloons up to altitudes of 35 km over water, and 12 km over land. The one-watt peak power pulsed-radar is simple and light enough to be carried by regular sounding balloons with radiosonde. Flight tests conducted on standard radiosonde flights over water indicate that the random error averaged over one second is less than 0.1 percent. Power consumption is one-watt average; weight excluding batteries is ten oz.

An independent, accurate altitude measurement proves very useful in a variety of balloon experiments. As an accurate ranging device, it is expected that this altimeter can find ready applications in GARP.* Two flight tests have already been performed on-board GHOST balloons. Current work is progressing in multiplexing additional channels of slowly-varying information, such as derived from barometric sensors, on the carrier frequency of the altimeter. This will provide the balloon experimenter with a very accurate and reliable radiosonde. Resulting experiments are limited only by the imagination of the experimenter.

* Global Atmospheric Research Program

8.1 INTRODUCTION

A direct measurement of geometric height is not often included in balloon instrumentation requirements. Normally temperature, pressure and humidity are sufficient to obtain a vertical profile, particularly when samples are taken frequently and the altitude is low. With increasing use of superpressure balloons and an increasing emphasis on accuracy at higher altitudes, however, the possibilities of absolute height measurements become quite attractive. A radio altimeter is described here which was developed specifically for making such measurements from balloons.

Various types of radio or, more specifically, radar, altimeters have been designed and built for aircraft, rocket, and satellite applications. In contrast, the use of such a device on a balloon poses some very different and often very stringent requirements. The radar must be self-contained and accurate with no special operator requirements. It should be able to operate over wide temperature ranges (for example, -55°C to $+55^{\circ}\text{C}$) without sacrificing accuracy. It should operate reliably up to 30 km or more and yet consume very meager amounts of power. And above all, it should be cheap and not weigh more than a few hundred grams!

Obviously some compromises must be made. However, we have made an attempt to meet as many of the demands as possible in a prototype design. To keep the design simple, a pulse-type radar is used which seeks and determines its own repetition rate, eliminating elaborate timing circuits. A single transistor is used as a superregenerative receiver and transmitter. The basic design strategy is to make this circuit operate at a repetition rate determined by the altitude of the balloon.

8.2 PRINCIPLE OF OPERATION

The radio altimeter described here is a pulse-radar system in which the elapsed time period between transmitted pulses is a measure of altitude. A single rf superregenerative stage serves as both the transmitter and the receiver. This stage is an oscillatory circuit held from oscillating by a negative quench voltage. When a positive quench pulse is applied, oscillations are allowed to grow. A pulse of radio frequency (rf) energy results whose envelope area depends on the rf input signal present when the quench pulse is applied. The frequency of oscillation is carefully controlled in these units by coupling to strip lines etched on a teflon circuit board.

As the pulse period approaches the delay time of a previously transmitted pulse returning from the ground, the envelope of the superregenerative circuit output reaches a peak. If the rf superregenerative stage is gated-on a little too early or a little too late, the envelope area decreases, as illustrated in Figure 8.1. The correct operating repetition period T is:

$$T = \frac{2h}{c}$$

where h is the altitude and c is the velocity of light.

The overall operation of the superregenerative rf stage suggests that an error signal could be derived to drive the repetition rate to the correct value. The remainder of the altimeter circuitry is needed to generate this error signal, both in magnitude and sense, to filter it, and to adjust the repetition rate accordingly to keep the error small. A block diagram of the complete radio altimeter is shown in Figure 8.2. The voltage-controlled oscillator (VCO) determines the repetition rate of the quench pulses. A sinusoidal voltage at a preset frequency, f_p , is added to the derived error signal to vary the repetition rate about the correct value. Variations at this frequency in the superregenerative detector output are amplified and then multiplied by the sinusoidal voltage, to derive a slowly-varying error voltage for controlling the repetition rate. An integrator is used to average the error voltage. Typical values are 200 Hz for f_p and a one-second time constant in the integrator.

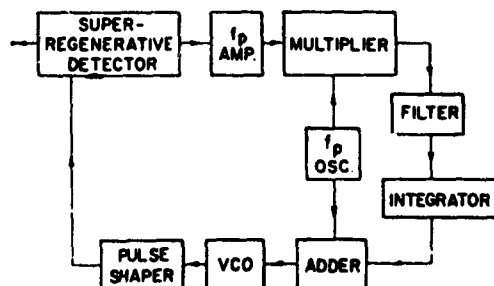


Figure 8.2. Block Diagram of the Radio Altimeter.

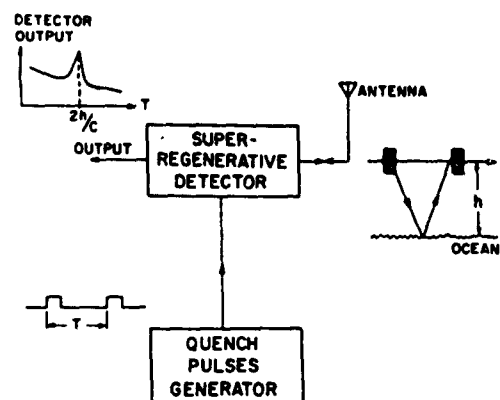


Figure 8.1. The Output of the Superregenerative Detector Peaks When the Quench Pulse Period Equals the Delay of the Return

For short transmitted pulses, the shape of the returned pulse is an integrated version of the transmitted pulse in cases of scattered reflections, and an attenuated replica of the transmitted pulse in cases of specular reflection, as shown in Figure 8.3 (Levanon, 1970). In both cases, there is a relatively well-defined break point in the returned pulse at the point corresponding to the trailing edge of the

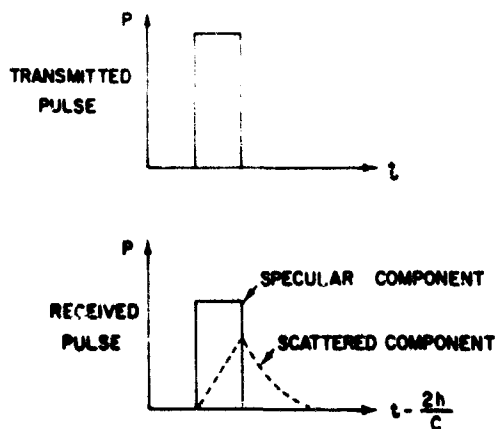


Figure 8.3. Simplified Return Pulse Envelopes

transmitted pulse. Taking advantage of this fact, the altimeter is made to scan from longer to shorter repetition periods and locks on the trailing edge.

The closed-loop response shows a close resemblance to the familiar phase-lock loop (Gardner, 1966). The main parameter of such a loop is its bandwidth which is, approximately, the reciprocal of the signal averaging time. Lowering the loop bandwidth reduces the effects of noise and fluctuations in the returned pulses. On the other hand, the altimeter is required to follow altitude changes and must also be able to

acquire lock within a reasonable amount of time. For ascending radiosonde balloon flights, a bandwidth of 1 Hz appears to be a reasonable compromise, while for superpressure balloons the bandwidth can be less.

8.3 RANGE AMBIGUITIES

The idea of transmitting a pulse as soon as a previous one is received is certainly an efficient means of operation for a radar altimeter and has been suggested for aircraft use (Jacob, 1967). A drawback of the method, however, is the presence of range ambiguities which can result. Under certain conditions this is not too serious for balloon flights as long as some other means for coarse altitude readings is available.

The range ambiguity problem arises because there is no reason why the altimeter cannot transmit a second pulse before the previous one is received. This subharmonic mode of operation (see Figure 8.4) can occur at any altitude above twice the minimum altitude of operation if locking is lost. In other words, the range ambiguity is equal to the minimum altitude of operation.

The exact relation between the geometric altitude, h , and the pulse repetition period, T , is:

$$h = \frac{c}{2} (nT - \tau)$$

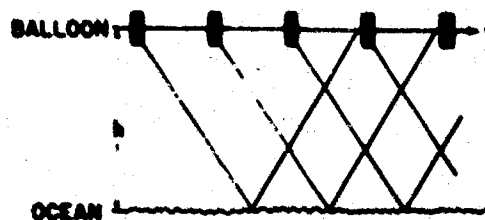


Figure 8.4. Subharmonic Altimeter Operation

where n is the subharmonic mode number and τ is the (fixed) delay between the beginning of the quench pulse and the end of the transmitted pulse. The parameter τ can be measured and controlled accurately in the altimeter design. The VCO range can be preset arbitrarily for the minimum and maximum allowable repetition rate. Assuming a two-to-one VCO range and a minimum altitude of 2 km, the pattern of switching modes as the balloon ascends, for no loss of locking except at end of range, is shown in Figure 8.5.

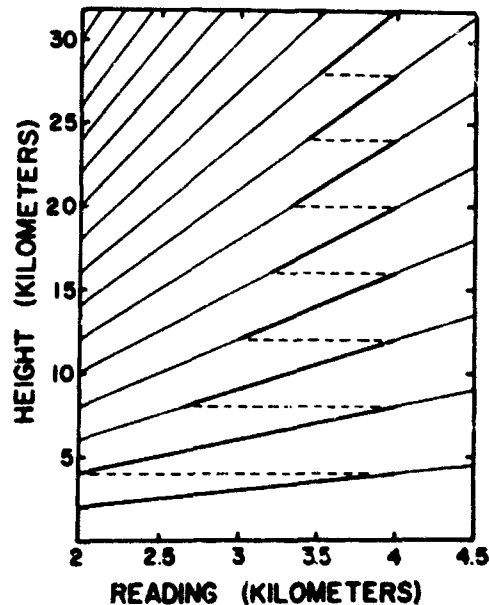


Figure 8.5. Range Ambiguity Pattern

Subharmonic operation is desirable to a certain extent, particularly at high altitudes, because the quench pulse frequency remains high, yielding more pulses per unit time.

Before there is a greater average transmitted power and better signal-to-noise ratio. Range ambiguities are equal to the minimum altitude and can be resolved by pressure readings or by extrapolation of the balloon ascent data.

Subharmonic operation is recommended even if the range of operation is limited, as in the case of the superpressure balloons. It is possible not only to assure that only one mode will cover a given limited range, but that the subharmonic mode numbers can be chosen to give several different ranges with no changes in circuitry. As an example, suppose that an altimeter is designed with a maximum repetition period range of 25 μ sec. to 30 μ sec. This altimeter will measure altitudes over about a 3 km range centered at 200 mb on the third subharmonic and centered at 100 mb on the fourth subharmonic with no changes in circuitry.

The maximum altitude of operation is influenced by transmitter power, antenna gain, choice of operating frequency, terrain, etc. The upper limit for altimeters currently being used is 35 to 40 km over water and 12 to 15 km over land using 5-element yagi antennas at 403 MHz. Larger antennas can be used but not without an accompanying increase in bulk and weight. An altimeter operating at 1680 MHz requires 12 db more gain than one operating at 403 MHz to give the same performance. Most of this can be made up in antenna gain.

8.4 OUTPUT DATA

The best means of extracting the altitude data is counting the pulse repetition rate. In short range balloon flights, such as radiosonde flights, this is relatively easy since the ground station is within receiving range of the altimeter radar pulses.

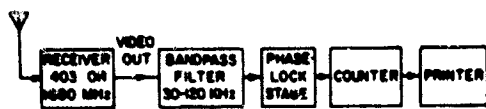


Figure 8.6. Block Diagram of Ground Station

A block diagram of such a ground station is shown in Figure 8.6. This scheme is quite inefficient, however, because it uses 100 kHz of bandwidth to receive a signal of 1 Hz bandwidth.

In longer balloon flights, such as GHOST flights, it is more efficient to make a bandwidth reduction on-board the balloon package before transmission. One method of doing this is to multiply the VCO signal with a fixed frequency from a crystal oscillator. The difference frequency is then counted down (by a factor of 1024 in present GHOST flights) before the data is telemetered.

An alternative is to sample the voltage at the input to the VCO and use the analog information for the telemetry signal. However, this requires a very linear, temperature-stable VCO characteristic and some degradation in performance can be expected. An altimeter for the IRLS* flights is being tested using this approach.

8.5 TEST RESULTS

As of 1 May 1970, nine flight tests and several ground tests of the altimeter have been made and several more are pending. Four aircraft flights were made to test prototype models and to gather information on the shape of the return pulse. Three regular radiosonde balloon flights were made, one over local terrain and two over Lake Michigan (Levanon and Suomi). The latter two of these flights demonstrated that an early version of the altimeter could measure altitudes accurately up to 18 km over water. Two GHOST flights have been made from Christchurch, New Zealand and a third is pending.

The first GHOST balloon was launched to 100 mb (15.8 km). The electronics payload included the regular GHOST package plus the radar altimeter and solar panels to supply power to the altimeter. Interference between the telemetry system and the altimeter prevented proper operation of the altimeter. A second GHOST balloon was launched to 200 mb (12.2 km) on 3 October 1969. From the

* Interrogation, Recording, Location Subsystem.

data received, the altimeter provided altitude readings for about seven hours. Data transmission ended as the sun dropped below 20 degrees incidence, reducing the power available from the solar cells below the operational level. Unfortunately, the balloon went down during the night.

All the above flight tests were made using altimeters with vacuum tube rf stages. To conserve power, an effort was started in January to redesign the altimeter using all solid-state components. The resulting new electronics for the 403 MHz altimeter is shown in Figure 8.7. A photograph of the 403 MHz altimeter with its antenna is shown in Figure 8.8.

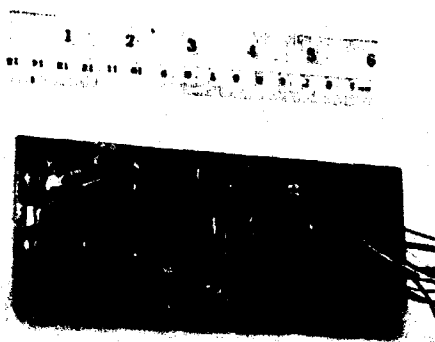


Figure 8.7. Electronics Package of the Radio Altimeter

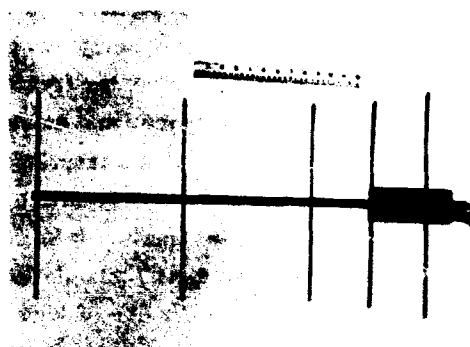


Figure 8.8. Radio Altimeter Being Used in GHOST Balloon Flights

Recent tests have shown that the new altimeter model has enough sensitivity to lock on specular components in ground clutter, for example, metal roofs of buildings, etc., beyond the minimum range of the unit. A very convenient and inexpensive test is to point the altimeter at the horizon from the top of a tall building.

Altitude measurement error in a laboratory calibration setup is less than ± 3 meters over a one-second integration time. Minimum signal to maintain lock is $3 \mu\text{v}$ at the antenna terminals. Weight distribution of present models is:

Electronics	4 oz
Antenna	3 oz
Packaging and cabling	3 oz
	<u>10 oz</u>

Power required is one watt at ± 12 V. Light-weight solar panels are being used for the superpressure balloon flights.

A prototype of a solid-state altimeter operating at 1680 MHz has been built and tested. Transistors are still very expensive for this operating range, and temperature stability is more of a problem than at 403 MHz. Work in this area is continuing.

8.6 EXTENSIONS

The foregoing has described what has been done with the radio altimeter concept. Tests indicate that the altimeter is a very useful and practical meteorological tool. Here we discuss several extensions of these ideas for continued study and development.

The altimeter operation is not affected by changes in the carrier frequency. We have found that the frequency can be tuned using a diode, and thus information can be multiplexed on the center frequency. It is quite conceivable for example, that temperature, pressure, and humidity information can be multiplexed on the center frequency of the altimeter.

The altimeter is quite insensitive to other pulsed signals and moderately insensitive to other CW signals. It is very sensitive to other signals near its center frequency which have a tone modulation near the 200 Hz tone used for the error signal. This suggests the use of tone-modulated signals to capture or perturb the altimeter operation, allowing opportunities for interrogation or ranging from a controlled transmitter. Measurements of winds are a distinct possibility in this way.

Perhaps one of the greatest disadvantages in finding widespread meteorological applications for these altimeters is cost. Parts costs alone total \$200.00 for present units. At least half of this is directly attributable to the use of military grade components, particularly the integrated circuits, to meet the rigid temperature specification.

We anticipate that many cost-saving cuts can be made in the design without sacrificing very much in performance. Possibilities in integrated circuit design, particularly on mass produced levels, could also make significant reductions in cost. In short, even though the present altimeter is several orders of magnitude below the cost of other airborne radars, the possibility of a truly expendable altimeter whets the appetite of the experimenter!

Acknowledgments

This research has been sponsored by the Laboratory for Atmospheric and Biological Sciences, Goddard Space Flight Center, NASA, under Contract NAS 5-11542. The authors wish to thank Charles E. Blair for circuit design and construction of the various models.

References

- Gardner, F.M. (1966) Phaselock Techniques, John Wiley & Sons, New York.
- Jacob, D.M. (1967) A Solid-State Altimeter and Rendezvous Radar, paper at NACON, Dayton, Ohio. Copies available from author at TRW.
- Levanon, N. (1970) Balloon-borne altimeter IEEE Transactions on Geoscience Electronics GE-8:19.
- Levanon, N. and Suomi, V.E., A radio altimeter for balloons and some meteorological applications, Journal of Applied Meteorology, (to be published).

Contents

9.1	Introduction	101
9.2	Optical Tracker and Transceiver	102
9.3	Balloon and Retroreflector System	105
9.4	Operational and Measurement Procedure	108
9.5	Results	109
9.6	Summary	109

9. Vertical Laser Link Using Tethered Balloon

M. Subramanian
Bell Telephone Laboratories, Inc.
Whippany, New Jersey

Abstract

A mobile vertical laser link using a tethered balloon and an optical tracker has been developed to study atmospheric propagation effects. A hollow retroreflector, mounted on a stabilizer and oriented by radio control from the ground, is continuously tracked by an optical tracker-transceiver using a helium-neon laser operating at 0.6328 micron wavelength.

The balloon has been flown in Chester, New Jersey, up to a 1000-foot altitude, and has been tracked satisfactorily in wind speeds up to 15 miles per hour during daylight hours. The results of the measurement of laser intensity scintillation due to modulation by atmospheric turbulence is presented.

9.1 INTRODUCTION

A number of studies have been made of the atmospheric effects on optical propagation on horizontal terrestrial paths. However, due to difficulties involved in establishing suitable airborne platforms, relatively little experimental work has

PRECEDING PAGE BLANK

been performed for vertical paths. The early studies on vertical optical propagation have been made principally by observing stellar scintillation. However, Hudson (1965) recently has observed a twinkling layer in the lower atmosphere using an incoherent source on a free-falling balloon, and Minott (1969) has made scintillation measurements with a detector on a satellite and a laser source on the ground. The present work describes a vertical laser link using a tethered balloon, for purposes of making atmospheric propagation studies.

The overall system is shown in Figure 9.1. A hollow retroreflector, mounted on a stabilizer and oriented by radio control from the ground, is suspended from the balloon and is continuously tracked by an optical tracker-transceiver using a laser source. The laser radiation is transmitted through a 10-inch refracting telescope as a defocused, circularly-polarized beam. The return beam is received by the same optics, and split by a beam splitter into signal and tracking channels. Thus, propagation measurements are simultaneously made while tracking the retroreflector on the balloon.

The balloon has been flown up to an altitude of 1000 feet, and has been tracked with a high degree of smoothness up to 15 miles per hour wind speed during daylight hours. The initial experiment is aimed at measuring the vertical turbulence profile of the atmosphere. The data on intensity scintillation as a function of vertical range is presented for a location in Chester, New Jersey.

9.2 OPTICAL TRACKER AND TRANSCEIVER

A block diagram describing the various components of the optical tracker-transceiver is shown in Figure 9.2 and the details of the components are given in Figure 9.3. The major components of the tracker-transceiver are a laser source for the transmitter, an optical circulator that provides isolation between transmitter and receiver, a common transmitting and receiving telescope, a beam splitter to divide the return beam between the data and tracking receivers, data receiver, tracking receiver, servo-system, and the antenna mount (not shown in the figure). The transmitter is a helium-neon laser source operating at 0.6328 micron wavelength, designed to generate linearly polarized radiation in a single transverse mode. The output is focused on an optical circulator whose function is to direct the radiation to the telescope without feeding it into the receivers. It consists of a Glan-Laser polarizer (a modified Glan-Thompson prism) that causes total internal reflection for the light coming from the transmitter. The bent beam then traverses through a quarter-wave plate that converts the linear polarization into circular polarization. The output of the circulator is passed through a 10-inch refracting telescope. The telescope has incorporated in it

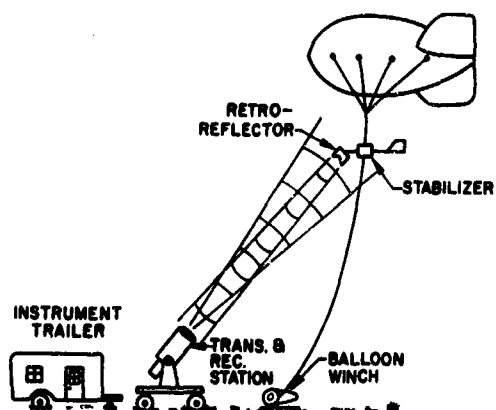


Figure 9.1. Laser Vertical Propagation Link

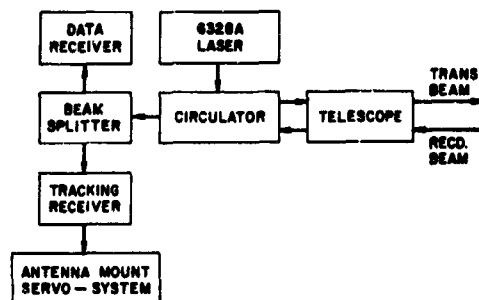


Figure 9.2. Tracker-Transceiver Block Diagram

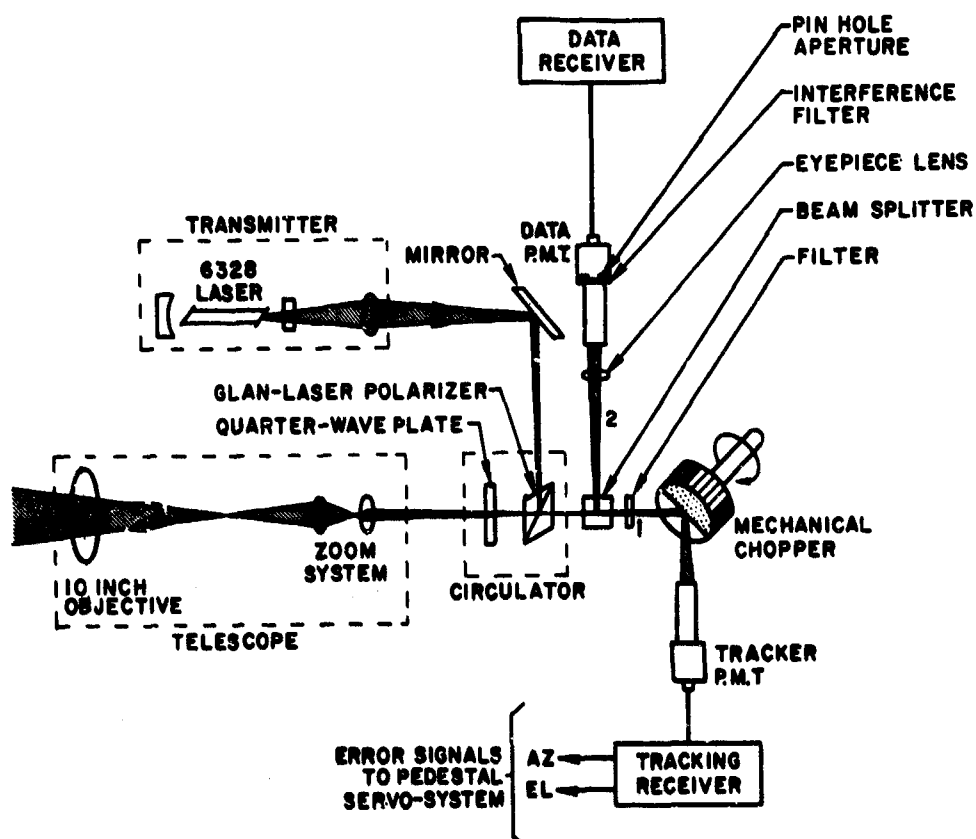


Figure 9.3. Tracker-Transceiver: Component Details

a zoom system that can vary the focal length of the telescope continuously from 60 to 240 inches. The zoom system facilitates varying the diameter and divergence of the outgoing beam, and has been set at the 240-inch focal length position. The outgoing beam from the telescope is approximately 6.5 inches in diameter and diverges with a cone angle of approximately 1 milliradian. These dimensions of the beam ensure that the divergence produced by the atmospheric turbulence (approximately 0.1 milliradian) and the diffraction limited divergence (4 micro-radians) are small compared to the defocussing produced on the beam.

As will be explained in the following section, the returned beam from the retroreflector is circularly polarized in the opposite sense. Its size on the objective of the telescope is 5 inches in diameter (twice the size of the retroreflector) so that the returned power is collected in total by the 10-inch objective of the telescope. The circularly-polarized return beam traversing through the quarter-wave plate in the circulator is once again converted into linear polarization. However, due to the reverse sense of rotation it is now orthogonal to the transmitted beam orientation. The Glan-Laser polarizer now transmits the light through to the receiver without causing total internal reflection. The optical isolation between the transmitter and receiver was measured at better than 40 dB.

The functioning of the circulator as described above does not possess any nonreciprocal behavior and hence, in the strictest sense, the name is a misnomer. However, it is still used in this context here, as its performance from an overall system behavior achieves the same goal. It is a vital component in the system in that it enables the design to achieve its performance objectives, which include the following:

- (1) First, it enables the receiver to detect the core of the beam, thus facilitating comparison with analytical results.
- (2) Secondly, it prevents the return beam from reaching the laser cavity, thus avoiding instabilities in the laser.
- (3) Finally, the use of a circulator improves tracker performance by permitting a full circular image on the rotating chopper (see Figure 9.3).

In the receiver, the laser beam is divided by a beam splitter into two paths labeled 1 and 2 in Figure 9.3, used respectively for tracking and propagation measurements. The beam transmitted directly through the beam splitter (path 1) falls on a rotating mechanical chopper. The chopper has a semi-circular mirrored front surface and a reference source and diode (not shown in the figure) on its side. The beam reflected from the face of the chopper falls on a photomultiplier tube (PMT) whose output is fed to the error sensing electronics circuitry. If the beam returning from the retroreflector arrives along the axis of the telescope, no tracking errors are developed. However, if the beam from the retroreflector

arrives off-axis, the beam is displaced from the center of the chopper face, and both azimuthal and elevation errors are developed by the error sensing electronics circuitry.

The beam reflected by the beam splitter in the receiver system (path 2) is passed successively through an eyepiece lens, an interference filter to reduce the background light, and a 1 mm aperture and then detected by the data channel PMT. The output of the PMT is recorded on tape by a FM tape recorder.

The transmitter, circulator, telescope, and the two receivers are assembled on a common base and mounted on an antenna mount which is controlled and driven by a servo-system. The error signals derived by the tracking receiver actuate the servosystem which keeps the telescope pointing at the retroreflector. The picture of the antenna mount positioned on a portable trailer along with the tracker-transceiver assembly is shown in Figure 9.4.

9.3 BALLOON AND RETROREFLECTOR SYSTEM

The balloon used to establish the space station is a tethered balloon system that is capable of flying up to 1500 feet above local ground level in Chester, New



Figure 9.4. Tracker-Transceiver Picture

Jersey, (800 feet above M. S. L.) carrying a payload of approximately 5 pounds. The 775 cu ft aerodynamically-shaped balloon made by Schejldhal and Company measures 26 feet in length and 7.5 feet in diameter and is filled with helium. The balloon is capable of flying up to a maximum wind speed of 25 knots. A gasoline-powered winch is used to raise and lower the single-tethered balloon. The balloon launching and mooring is a two-man operation; though while it is flying, only one man is required at the winch. The angle of attack is designed to be 10 degrees. However, since this was not the case with the balloon supplied, a ballast weighing about 3 to 5 pounds had to be added to the tail end to stabilize the balloon from excessive rotation. The balloon was still having a rotational oscillation of over 90 degrees which is beyond the field of view of the retroreflector used, thus resulting in frequent loss of tracking. Consequently, considerable effort was spent in designing a stabilizing system for the retroreflector.

The 2.5-inch retroreflector used to return the beam to the ground station is a hollow, three-sided reflector and has a field of view of about 40° . In other words, any incident beam on the retroreflector within a cone of 40° about its axis is reflected back in the same direction as the incident radiation. Since the number of reflections that occur at the retroreflector is three, the circularly polarized incident radiation is returned circularly polarized in the opposite sense. As mentioned in Section 9.2, this reversal of polarization is a necessary criterion for the functioning of the optical circulator.

In spite of the large field of view of the retroreflector, its orientation needs to be maintained in such a direction as to keep facing the telescope on the ground all the time. Its azimuthal orientation will change due to change in wind direction, as well as any torque imparted to it either by the rotation of the balloon or by the twist in the tether to the ground. The azimuthal orientation will also change if there is a large horizontal displacement of the balloon due to strong wind. The elevation orientation needs to be changed as the balloon is flown at different altitudes.

Any design for the retroreflector assembly must meet two primary demands. First, it should stabilize the orientation of the retroreflector so that it is always looking towards the telescope on the tracker. Secondly, the overall weight of the assembly should be as small as possible since increase in payload reduces the maximum altitude up to which the balloon can be flown. The following preliminary scheme, shown in Figure 9.5, used for mounting the retroreflector, though not completely satisfactory from the latter consideration, proved adequate for initial experimentation. The retroreflector is mounted on a yoke that can be positioned over approximately 100-degree elevation angle range. The rotation is achieved by the use of a radio-controlled servo-motor that can be operated from ground.

Thus, when the altitude at which the balloon is flown is changed, the retroreflector can be reoriented for the appropriate elevation angle without having to bring the balloon down. The yoke containing the retroreflector and radio-controlled servo is attached to the center of a 12-foot boom with a 1.75 pound weight attached to each end. Such an arrangement helps to increase the moment of inertia of the system and thus increase the period of free oscillation of the retroreflector about a vertical axis.

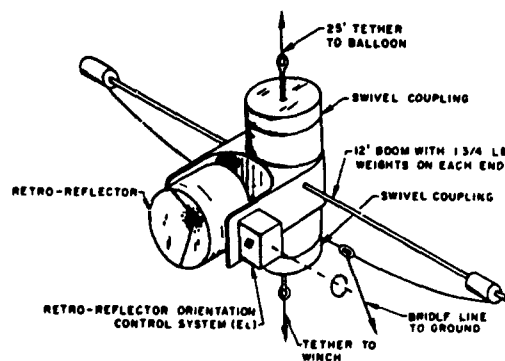


Figure 9.5. Retroreflector Assembly

The natural period of oscillation of this system was measured to be approximately 1 minute. To minimize the rotational torque imparted to the boom due to the rotation of the balloon from above and due to twist in the tether from below, the boom is attached between the balloon and the tether with two swivel couplings. The effects due to translational motion of the balloon caused by gusts of wind is minimized by providing a 25-foot tether between the boom and the balloon. A braid was attached to the two ends of the boom and a thin guy line was brought down in the direction of the tracker and held by a person on the ground. This enabled the retroreflector orientation to be kept facing the tracker successfully. The weight of the complete retroreflector assembly was approximately 7 pounds. Figure 9.6 shows the balloon, the retroreflector, and the winch under operating conditions.

The retroreflector orientation scheme described above requires the continuous use of one person to maintain the azimuthal orientation. An improved design, shown in Figure 9.7, is expected to relieve this manual requirement by providing greater azimuthal and elevation stabilization as well as radio-controlled azimuthal orientation. As in the previous design, the retroreflector assembly is attached to the balloon by a 25-foot tether line, and two swivel couplings are used to attach the assembly between the balloon and the tether to ground. A battery-operated gyro-stabilizer motor is used to achieve greater stability due to sudden impulses. The natural azimuthal oscillation period of the gyrostabilizer is in the order of minutes. Since the gyrostabilizer does not have a preferred orientation axis, a wind vane has been provided to provide such an axis, which in this case will be the average direction of the wind. The desired orientation of the retroreflector azimuthal direction will, in general, be different from that of the average wind direction and is achieved from ground by the additional radio-controlled servomotor provided in the new design. The elevation orientation control operates in a similar fashion as described in the previous design.



Figure 9.6. Proposed Retroreflector Assembly

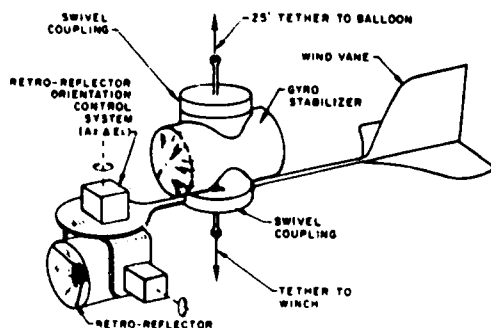


Figure 9.7. Balloon and Retroreflector Assembly

9.4 OPERATIONAL AND MEASUREMENT PROCEDURE

The winch for the balloon tether was positioned at about 400 feet away from the tracker. As the balloon was flown at various altitudes, the propagation link was always maintained on a slanted range. This was necessary in order to avoid tracking at zenith angle, in which case the error developed in the azimuthal channel will vary so rapidly as to cause loss of tracking. The balloon was flown at every 100-foot incremental altitude from ground level up to 1000 feet. The maximum altitude was limited to 1000 feet due to heavier payload and the weight due to balloon stabilization ballast. At each altitude the balloon was maintained relatively stationary, and simultaneous tracking and intensity scintillation measurements were performed. During the majority of time while the altitude was varied, the tracker followed the retro-reflector continuously. The FAA regulations limited the balloon flying up to a maximum wind speed of 15 mph, and the tracker was able to follow the retro-reflector up to this speed. The jitteriness in tracking was measured to be approximately 1 arc second. Tracking was found to be difficult when either the wind was very gusty or it changed directions rapidly.

The intensity scintillation data, which is obtained as a time varying voltage out of the data channel PMT, was recorded by the FM tape recorder for about 2 to 3 minutes at each altitude.

9.5 RESULTS

A typical picture of the data channel PMT output due to intensity scintillation is shown in Figure 9.8. In addition to the fast fluctuations seen on the scope trace, there is also the slowly varying component. In other words, the modulation components introduced by the atmospheric turbulence have not only fast fluctuations extending up to a few hundred Hertz, but also down to 0 Hz. This is the reason for observing the scintillation for an extended period, namely in the order of minutes. The recorded information on the tape was processed through an analog computer to obtain the measure of fluctuations in the received signal, described by the quantity called the depth of modulation. It is defined as the ratio of the rms voltage to the average voltage. It is easy to estimate the depth of modulation for an equivalent vertical range (Subramanian, 1970) from the measured values of slant range. This is shown in Figure 9.9 where the dots indicate the average depth of modulation over a 2-minute period at each altitude flown, and the error bars denote the variance of the depth of modulation over the same interval. This result has been used to estimate the vertical profile of the atmospheric turbulence (Subramanian, 1970) in the local troposphere at Chester, New Jersey.

9.6 SUMMARY

A mobile vertical laser link using a tethered balloon has been developed to study the atmospheric effects on optical propagation, and as a remote probing technique for measuring the atmospheric parameters. The optical tracker-transceiver while following the retroreflector suspended from a tethered balloon

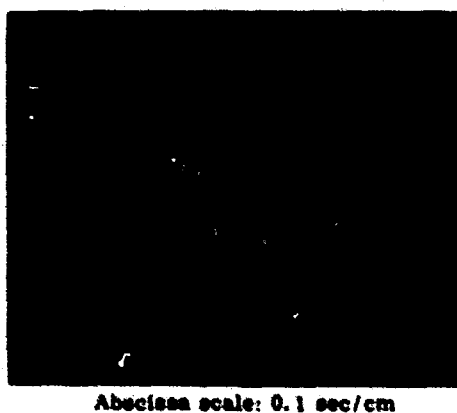


Figure 9.8. Temporal Representation of Scintillation

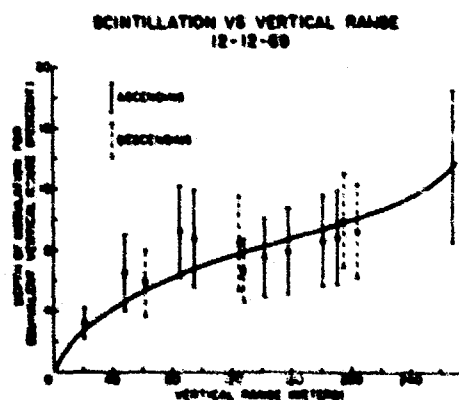


Figure 9.9. Vertical Range Dependence of Depth of Modulation

makes simultaneous measurements of the effects of the atmosphere on laser radiation. The autotrack system has been demonstrated to track smoothly (to the order of an arc-second jitteriness) up to a slant range of about 1000 feet, and an elevation angle of about 50 degrees under wind speed conditions up to 15 mph. The result on the intensity scintillation produced by the atmospheric turbulence as a function of vertical range is presented.

Acknowledgments

The author would like to express his appreciation to Mr. R. R. Redington for experimental assistance, and to Mr. H. J. Scagnelli for his help in the mechanical design of the tracker-transreceiver. His gratitude is also due to Messrs. L. Ginerich, Jr. and Y. S. Lim for their cooperation in improving the performance of the tracker.

References

- Hudson, C. H. (1965) Experimental evidence of a twinkling layer in the Earth's atmosphere Nature, 207:247-249.
- Minott, P. O. (1969) Scintillation in An Earth-To Space Propagation Path, presented at the 12th Plenary Meeting of the Committee on Space Research, Prague, Czechoslovakia.
- Subramanian, M. (1950) Laser Remote Sensing of Lower Atmospheric Turbulence Profile, presented at URSI/USNC 1970 Spring Meeting, Washington, D. C. Also to be published by the author in the near future.

10. A Review of VHF Balloon Instrumentation

D.M. Thon
Winzen Research Inc.
Minneapolis, Minnesota

For the past several years, balloon control and telemetry equipment has included elements borrowed from the vast list of VHF equipment developed specifically for missile research and for the NASA space program. This equipment was developed to meet demanding specifications and to provide great flexibility in data handling capability. Standardizing criteria had been established by the Inter Range Instrumentation Group which allowed systems to be assembled using elements from different manufacturers, and made the basic ground telemetry stations compatible with a variety of flight package configurations. With improved efficiency of VHF power generation by solid state devices and with VHF direction-finding equipment suitable for light aircraft on the commercial market, the last ingredients for change were available. Conversion meant simply deciding that acquisition costs would be offset by the advantages of greater versatility and reliability.

It should be pointed out that all balloon groups did not necessarily feel the same need and, therefore, because of special requirements did not view VHF as the best solution to all of their problems. It is accurate to say that all recognized a need for improvement; that significant improvements were made; and that VHF had at least some part to play in each group's improvement package. The VHF system to be described is typical of that in use by private industry for flights

made under ONR, NASA and NCAR sponsorship, and is typical of the basic system used by NCAR in their flight work.

To explain the need for change requires a quick look at what had been in general use. Early instrumentation included beacon transmitters in the 1.65 to 1.75 MHz range which enabled aircraft equipped with ARN-6 type radio compasses to track balloon flights. Simple altitude telemetry was obtained by the use of a code drum and a moveable contact arm which was positioned by an aneroid capsule. This resulted in a cw signal for direction-finding purposes and a keyed cw code group for telemetering the altitude level. The technique served well, since both a beacon signal and the telemetered altitude data were available to the tracking aircraft without special reception equipment. It meant, however, that the amount of data which could be transmitted was severely limited and that data sensor output had to be converted to provide coding of the cw signal.

Another undesirable feature was the long wire antenna which presented problems at launch and occasionally at flight termination. Near free-fall conditions had been experienced with some parachute descents because the antenna had become wrapped about the chute risers, preventing full canopy deployment. This entanglement sometimes caused signal loss at this most critical time of the tracking operation.

Early instrumentation also included radio command receivers operating in the HF band (6 to 7 MHz). Again, the length of a conventional antenna was greater than desired. The HF band is extremely crowded and is characterized by a very high noise level whenever electrical storm activity occurs within a radius of several hundred miles. While the competing signals and the noise can be over-ridden and conditioned to allow satisfactory radio command response, their presence is most unwelcome in communications relay and slant range measurement applications.

In the system to be described (Figure 10.1) telemetry transmission is performed by a solid state FM transmitter operating in the 225 to 260 MHz band with an output power of two to four watts. The modulation frequency response, sensitivity and linearity meet or exceed IRIG and FCC standards, as do specifications for frequency stability and spurious signal radiation. Modulation is provided by up to eighteen subcarriers, which in turn are frequency modulated by a voltage derived from the various data sensors. These subcarrier oscillators (voltage controlled oscillators) may be time shared to expand the number of data inputs whenever full-time data plots are unnecessary, and Pulse Code Modulation (PCM) may be introduced where sampling rates are appropriate.

The telemetry transmitter also serves to retransmit a ranging signal on command, and to relay voice communication when placed in the transpond mode.

These functions can be set up to be performed in the presence of the telemetry multiplex or may, for optimum clarity, be switched to exclude telemetry during the short intervals devoted to their use.

The antenna for the VHF telemetry transmitter is a ground plane with the radials at 150 degrees with respect to the vertical, resulting in a characteristic impedance of 50 ohms. The antenna is flown with the ground plane above the radiator, and therefore power is directed downward at a low angle with respect to the horizontal. In most cases, in spite of random antenna orientation, a signal suitable for aircraft tracking has been transmitted after termination and impact. This has been true for distances as great as 60 miles with the payload on the ground and the tracking aircraft at 7,500 feet — and on one occasion was still functioning after a free-fall caused by a parachute-burst balloon entanglement.

The radio command receiver and decoder forms the other major element of the instrument package. The typical basic FM receiver uses crystal-controlled local oscillators and dual conversion to give excellent stability and selectivity characteristics.

Because security is a prime concern in balloon radio command systems, the method of channel selection and command activation must provide a high degree of reliability. Two basic methods, with slight variations, are in use and have proven to exhibit the necessary characteristics. The first of these is a tone-coded system which holds the receiver output stages off until a private line or enable gate tone is received. This serves to arm the decoder output stages and allows a second tone, when held beyond a short time delay, to select and activate the desired channel. With present equipment this method may be used to operate up to twenty-four channels with switch closures for control and for verification.

The other method is a PCM type developed by NCAR to provide 30 command channels. In this system the PCM commands pulse width-modulate an 800 Hz tone in a 5-bit binary code with each bit followed by its complement. Transmission of each command requires approximately 880 milliseconds. With the addition of a

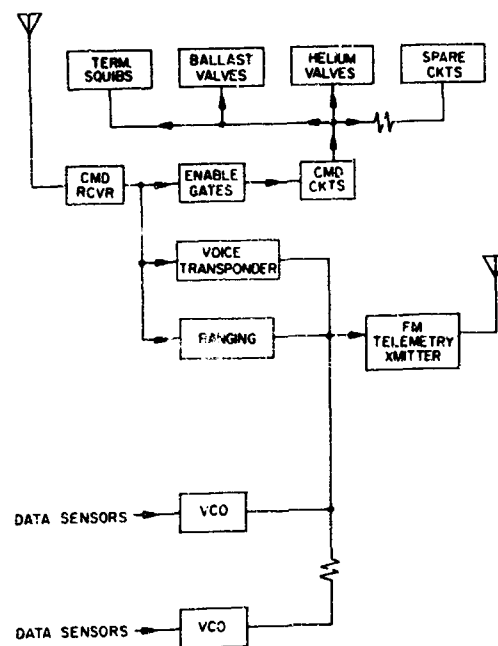


Figure 10.1. Balloon Instrument Package

"sync" pulse, the PCM telecommand system provides five security features. Before the decoder will activate a command, the PWM must be on an 800 Hz tone, the "sync" pulse must precede the transmission of the binary command, each digit of the 5-bit code must be followed by its complement, there must be only 11 pulses received by the decoder, and each pulse must have the proper width.

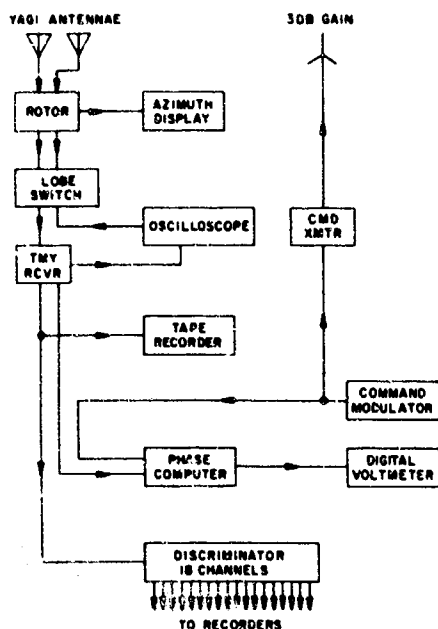


Figure 10.2. Ground Station

The command receiver also processes signals for determining slant range to the balloon. At the ground station (Figure 10.2) a precise tone is transmitted to the balloon-borne radio command receiver and is simultaneously presented to one input of a phase comparator. When received at the balloon, this tone operates a gate circuit which switches the signal to the telemetry transmitter for retransmission. The ground station telemetry receiver provides the returned signal for the other input of the phase comparator, resulting in an analog voltage proportional to phase difference. The distance represented by each degree of phase shift is determined by the frequency of the ranging tone. If this frequency is made precisely 224.7 Hz, each degree of phase shift is equal to one nautical mile and with proper scale selection, can be read directly in nautical miles with a digital voltmeter.

The slant range figure is reduced to a horizontal distance using balloon altitude information, and is coupled with an azimuth indication to allow position fixes to be plotted on a map. Azimuth is obtained by lobe switching two vertically oriented Yagi arrays mounted to include several degrees of divergence. A scope presentation of the telemetry receiver IF signal shows the amplitudes produced by alternate lobe-switch positions. When the motor-driven antenna array is positioned to produce precisely equal amplitudes, the direction-setting is complete and can be read out with any suitable angular position indicator.

Another function provided by the radio command receiver concerns transponding voice communication from ground and aircraft locations through the balloon instrumentation package to any other location not in direct line-of-sight. Again a tone-actuated enable gate is used to switch audio, from which the tone has been filtered, to the modulation input of the telemetry transmitter. As in ranging, the

tone employed is not one of those used in the normal command channels and, since the enable tone to activate the command channels is not transmitted, there is no possibility of inadvertent command operation.

Considering the many functions performed by this basic instrumentation package, the efficiency is quite good. The weight of a typical system — six telemetry channels and six command channels — is approximately 18 pounds including a water-tight, drawn aluminum housing. Continuous power consumption is of the order of 10 watts which, for 36 hours, is conservatively provided by a silver-cell package weighting 24 pounds, including adequate reserve to power intermittent command circuit requirements. The 24-pound figure includes a water-tight, drawn aluminum housing.

As previously reported by the AFCRL Instrumentation Group, it is often desirable to avoid hardwire power connection between apex helium valves and the instrument package at the base of the parachute. The alternative is to fly a small radio command package mounted on the balloon top fitting. This package contains the power supply for both the command receiver and for the operation of the helium valve motor. A typical package with power for four hours of valve operation weighs 20 pounds complete with insulated housing. No verification signal is available in this case aside from the telemetry of response to valving, which is available on the altitude telemeter in the base package. Should immediate verification of valve position be desired, a second VHF transmitter on an alternate frequency can be used. Approximately ten pounds of weight are required for this additional feature.

Current instrumentation development at WRI is aimed at lowering package power consumption through the use of integrated circuits. Along with a reduced power requirement which, of course, will reduce size and weight, a significant increase in reliability is expected.

One specific area where improvement efforts are continuing, concerns the replacement of resonant reed and contactless resonant reed relays in the radio command output section. Extremely selective passive filters have been constructed and, after more extensive testing, may allow this desirable replacement.

References

- Cowie, R. J., A Unique Balloon-Borne Command Data Link, Proceedings, Fifth AFCRL Scientific Balloon Symposium.
- Czepyha, C. G. R., Balloon-Borne Instrumentation, Proceedings, Fourth AFCRL Scientific Balloon Symposium.
- Snyder, R. L. (1968) Digital and Analog Telemetry and Telecommand Systems NCAR Scientific Balloon Facility Publication.

Contents

11.1	Introduction	117
11.2	Radio Horizon Range	118
11.3	Receiver Noise Considerations	119
11.4	Equipment Selection	125
11.5	Signal Power Level Calculations	129
11.6	Test Results	132
11.7	Balloon Flight 487-P	132
11.8	Balloon Flight 505-P	135
11.9	Balloon Flight 523-H	137
11.10	Balloon Flight 535-PT	137
11.11	Summary and Conclusions	138

11. Evaluation of UHF Radio Frequency Equipment for Balloon Telemetry

O.L. Cooper
National Center for Atmospheric Research
Boulder, Colorado

11.1 INTRODUCTION

For several years the National Center for Atmospheric Research (NCAR) has provided VHF telemetry for data retrieval from scientific experiments on high-altitude research balloons. This consists of Standard IRIG FM/FM and PCM/FM/FM telemetry. In accordance with a Military Communications Board Memorandum, MCEB-M-92-65, all telemetry operations were to have been transferred from the VHF band to the UHF bands by 1 January 1970. The VHF band is 215-260 MHz while the UHF bands are 1435-1540 MHz (L-Band) and 2200-2300 MHz (S-Band). Most telemetry activity has been assigned to the higher band; however, the Interdepartmental Radio Advisory Committee (IRAC) has provided assignment in the L-Band for balloon telemetry. Because of the anticipated frequency transfer, NCAR obtained the necessary equipment for UHF telemetry evaluation for ballooning and has had several flight tests with the equipment. Even though a time extension has been granted for using the VHF band, a forward effort is being made to fully effect the changeover, because further time extensions are not anticipated.

The major deterrents in converting to UHF are the cost, complexity of equipment and the low efficiency of the airborne transmitters. The propagation loss at

the higher frequencies is greater, making it necessary to have a high-gain antenna at the ground station. The high-gain antenna inherently has a pencil beam making it necessary to track the balloon signal continuously. The noise at UHF frequencies is less than at VHF. Noise at lower frequencies results from atmospheric noise up to 50 MHz, man-made noise up to 200 MHz and cosmic noise up to 300 MHz. At the higher frequencies noise will be reduced so that the signal-to-noise ratio is improved and dependent, to some extent, on the noise generated in the receiver (Reed and Russell, 1966). The receiving equipment should have low noise figures so that the ground system will operate with as great a signal-to-noise ratio as possible.

11.2 RADIO HORIZON RANGE

Range of operation with UHF, as with VHF, is limited to radio horizon (Reed and Russell, 1966) distances as determined by the heights of the balloon and the receiving antenna on the ground. The receiving antenna height has small significance for long range except that it should clear surrounding objects. The direct radio-horizon distance to a balloon from a ground station may be calculated by means of handbook formula, $D = (3h/2)^{1/2}$, where h is in feet and d is in statute miles (Reed and Russell, 1966). The propagation range, which is greater than the tangential distance due to atmospheric refraction, may be approximated by considering the earth's radius to be $4/3$ its actual radius. The propagation distance is then approximated by $D = (2h)^{1/2}$. A more accurate calculation of the maximum propagation distance may be made by using an empirical formula for the index of refraction of the atmosphere (Bean and Dutton, 1966; and Reed and Russell, 1966). Computer calculations have been made by NCAR using this method for the atmospheric refractivity, maximum ground distance and slant range and elevation angle error for various balloon altitudes, and line of sight elevation angles for each month of the year at Palestine, Texas. The tables for the month of February have been taken as typical. The maximum slant range to a balloon using this method is about 4.5 percent less than that calculated by using the $4/3$ radius formula.

Table 11.1 gives the radio-horizon range in both statute miles and nautical miles for balloons at several altitudes.

Because of the problems, mentioned above, in converting to UHF telemetry, a careful selection of equipment for evaluation was made. In order to assemble a system which could use a low-power balloon-borne transmitter, emphasis was placed on low-noise receiving equipment and an antenna with reasonable high gain consistent with cost and complexity.

Signal power level calculations were made in order to establish the desired performance features of the equipment. Marginal signal conditions during a

Table 11.1. Radio-horizon Range for Balloons at Various Altitudes

Balloon Altitude kilofeet	Maximum Range	
	Statute Miles	Nautical Miles
80	400	347
90	425	369
100	448	389
110	470	408
120	491	426
130	510	442
140	530	460
150	549	476

balloon flight generally occur when the range approaches the radio horizon. Even though there may be adequate signal-to-noise ratio during most of many flights it is believed desirable to emphasize receiving equipment with low noise figures for a better margin of safety.

11.3 RECEIVER NOISE CONSIDERATIONS

The ability of a telemetry receiver to detect the presence of a signal is fundamentally limited by the presence of noise. If there were no noise present in the receiver, it would be possible to detect any small signal, by providing the receiver with sufficient gain. Since noise is always present, amplification in the receiver amplifies noise as well as the desired signal. Sources of noise within a receiver are: (1) thermal noise caused by the random motion of electrons in a conductor; (2) shot noise caused by the nonuniform rate at which electrons are emitted from the cathode of a vacuum tube and collected on the plate; (3) partition noise caused by the division of current in a multielement vacuum tube; (4) induced grid noise caused by the collection of electrons on the grid of a vacuum tube which modulates the plate current; (5) crystal noise caused by thermal noise, shot noise and flicker noise in the semiconductor; and (6) transistor noise which is closely related to crystal noise.

Thermal noise is a great contributor to the overall noise in a receiver. It is caused by the random motion of electrons in the conductors and circuit components of resistance, R , and at absolute temperature, T , in degrees Kelvin. The mean square value of the electrical noise voltage is (Lawson and Uhlenbeck, 1950; and Nyquist, 1928):

$$\overline{e^2} = 4RkTB_n \quad (11.1)$$

where k = Boltzmann's constant = 1.38×10^{-23} joule/deg.

B_n = noise bandwidth.

The noise generated by a conductor at a temperature, T , may be represented by a resistance, R , in series with a mean-square noise voltage as given in Eq. (11.1). According to Thevenin's theorem, maximum power transfer occurs when the source impedance and load impedance are conjugates. In this case, the optimum load impedance is R , and the maximum noise power transferred to the load is $\overline{e^2}/4R$, or

$$\text{Maximum available noise power} = kTB_n. \quad (11.2)$$

This noise is known as thermal noise because of its dependence on temperature, T . It is also known as white noise or Johnson noise (Friis, 1944; and Skolnik, 1962).

An "ideal" receiver adds no noise to the signal being amplified; however, a practical receiver will generate noise to some extent. The measure of the noise generated by a practical receiver compared with that of an ideal receiver is called the noise factor. The noise factor, F , of a linear system is defined as

$$F = \frac{S_{in}/N_{in}}{S_{out}/N_{out}} = \frac{N_{out}}{kTB_n G} \quad (11.3)$$

where the gain, G , is equal to S_{out}/S_{in} and the input noise, N_{in} , is equal to kTB_n . The noise factor of the receiver may be considered as the degradation of the signal-to-noise ratio by the receiver. When the noise factor, F , is expressed in db it is called the noise figure, NF, where $NF = 10 \log F$.

Since the output noise of a receiver is the amplified input noise, $kTB_n G$, plus the additional noise, ΔN , generated in the receiver the noise factor can be written

$$F = \frac{kTB_n G + \Delta N}{kTB_n G} = 1 + \frac{\Delta N}{kTB_n G} \quad (11.4)$$

To standardize the definition of noise factor the Institute of Radio Engineers specifies that a temperature of $T_0 = 290^\circ\text{K}$, which is near room temperature, be used for the calculation of the noise factor (Skolnik, 1962).

Figure 11.1 shows two networks (amplifiers) in series. They have the same noise bandwidth, B_n , but different noise factors and gains. Using Eq. (11.3), the output noise, N_o , from both networks is,



Figure 11.1. Two Networks in Series

$$N_o = F_o G_1 G_2 k T_o B_n$$

$$= \text{noise from network 1 at output of network 2} \quad (11.5)$$

$$+ \text{noise, } \Delta N_2, \text{ introduced by network 2}$$

where F_o is the overall noise factor.

$$F_o G_1 G_2 k T_o B_n = k T_o B_n F_1 G_1 G_2 + \Delta N_2 = k T_o B_n F_1 G_1 G_2 + (F_2 - 1) k T_o B_n G_2 \quad (11.6)$$

$$F_o = F_1 + \frac{F_2 - 1}{G_1} \quad (11.7)$$

If the gain of the first amplifier is large, the contribution of the second network to the overall noise factor is small.

The use of the noise factor is not as convenient for low-noise receivers as is the effective noise temperature, T_e . From Eq. (11.4) the noise factor is

$$F = 1 + \frac{\Delta N}{k T_o B_n G} \quad (11.4)$$

where ΔN is the noise introduced by the amplifier or receiver itself. The effective noise temperature is defined as that temperature, T_e , at the input of the receiver which would account for the noise, ΔN , at the output. Therefore $\Delta N = k T_e B_n G$ and

$$F = 1 + \frac{k T_e B_n G}{k T_o B_n G} = 1 + \frac{T_e}{T_o} \quad (11.8)$$

$$T_e = (F - 1) T_o \quad (11.9)$$

The effective noise temperature of an ideal receiver is zero degrees. By using Eq. (11.8) it can be shown that the effective noise temperature of N networks in cascade is

$$T_e = T_1 + \frac{T_2}{G_1} + \frac{T_3}{G_1 G_2} + \dots + \frac{T_n}{G_1 G_2 \dots G_{n-1}} \quad (11.10)$$

If a receiver has low noise-high gain input stages, the noise contribution from external sources may be significant as compared with noise generated within the receiver. Noise from external sources which may enter the receiver along with the signal through the antenna includes cosmic noise, solar noise, atmospheric and man-made noise and atmospheric absorption noise (Skolnik, 1962).

From black body radiation theory it is known that any body which absorbs energy radiates the same amount of energy that is absorbed (Lawson and Uhlenbeck, 1950). A lossy transmission line absorbs a certain amount of energy and transmits it as noise. The same is true of the atmosphere. Consider an absorbing atmosphere of temperature, T_a , surrounded by an imaginary black body at the same temperature. The loss, L , is the ratio of input to output energy of a signal passing through the atmosphere. The noise power available over a bandwidth, B_n , from the imaginary black body is $kT_a B_n$. After passing through the atmosphere the noise power available is $kT_a B_n / L$. The difference between these two is $kT_a B_n (1 - \frac{1}{L})$ and is equal to the noise power, ΔN , radiated by the atmosphere.

$$\Delta N = kT_e B_n G = kT_e B_n / L = kT_a B_n \left(1 - \frac{1}{L}\right) \quad (11.11)$$

$$T_e = T_a (L - 1). \quad (11.12)$$

Losses in radio-frequency hardware such as transmission lines, antenna or duplexer result in noise; thus, a lossy component may be assigned a noise factor or an effective noise temperature. The effective noise temperature may be derived, as above, for a lossy atmosphere, or it may be derived by using Eqs. (11.3) and (11.8). From Eq. (11.3), the noise factor may be expressed as

$$F = \frac{N_{out}}{kT_a B_n G}$$

where T_a is set equal to the ambient temperature. The noise output from a lossy component is $kT_a B_n$ and $G = 1/L$, therefore $F = L = 1/G$. From Eq. (11.9),

$$T_e = (F - 1) T_a = (L - 1) T_a. \quad (11.13)$$

A receiving system has an effective noise temperature, T_e , as well as an overall noise factor, F_o . If a lossy transmission line with temperature, T_a , and loss L is connected to a receiver with effective noise temperature, T_{rec} , the effective noise temperature of the combination using Eq. (11.10) is

$$T_e = (L - 1) T_a + L T_{rec} . \quad (11.14)$$

If T_a is the standard temperature, T_o , and $F_{rec} = 1 + T_{rec}/T_o$

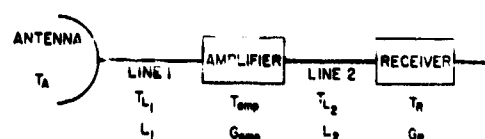
$$T_e = (LF - 1) T_o . \quad (11.15)$$

The overall noise factor of a receiver and a lossy transmission line, from Eqs. (11.8) and (11.15) is $F_o = FL$.

In general the contributions to the total effective noise temperature of a system may be divided into three categories: (1) the effective space noise temperature, (2) the effective noise temperature contributions due to RF lossy components and (3) the effective noise temperature of the receiver itself (Skolnik, 1962). The space noise temperature consists of cosmic noise and atmospheric noise which is composed of an ionospheric component, an oxygen component and a water vapor component.

The noise which appears at the antenna terminals enters by the side lobes as well as the main beam. When using the antenna at low elevation angles, the side lobe noise can be greater than that from the main beam. This is because land is a complete absorber, hence if the antenna radiation pattern illuminates the ground, it sees noise at the ambient temperature. The antenna temperature for elevation angles between zero and 10° ranges from 50°K to 100°K (Gruenberg, 1967; Jordan and Baldmain, 1968; Skolnik, 1962; and Stiltz, 1961).

Suppose we have a telemetry receiving system as pictured in Figure 11.2.



The effective temperature of the system is given by Eq. (11.10), and if Eq. (11.12) is used for the effective temperature of the transmission lines, the total expression for the above system is

Figure 11.2. Telemetry Receiving System

$$T_e = T_a + (L_1 - 1) T_o + T_{amp} L_1 + \frac{(L_2 - 1) T_o L_1}{G_{amp}} + \frac{T_r L_1 L_2}{G_{amp}} . \quad (11.16)$$

Since the overall noise factor, F_o , of the receiver preceded by a transmission line with losses, L , is $F_o = FL$, the effect of the attenuation of one decibel in line 2 is negligible in its overall effect on the receiver-preamplifier noise factor. For this reason the preamplifier is located near the antenna. If the attenuation of line 1 is considered when calculating the effective temperature of the system, it will add to the receiver noise level by the amount of the cable loss. Since the receiver system was calibrated at the amplifier input, the cable loss can be considered as part of the losses between the transmitter and receiver input. The effective temperature is

$$T_e = T_a + T_{amp} + \frac{T_r}{G_{amp}} \quad (11.17)$$

where, from Eq. (11.9), $T_r = (F_r - 1)T_o$ and $T_{amp} = (F_{amp} - 1)T_o$.

$$T_e = T_a + (F_{amp} - 1)T_o + \frac{(F_r - 1)T_o}{G_{amp}}$$

$$T_e = T_a + T_o \left[F_{amp} + \frac{F_r - 1}{G_{amp}} - 1 \right] \quad (11.18)$$

$$T_e = T_o \left[\frac{T_a}{T_o} + F_o - 1 \right] \quad (11.19)$$

The total noise power in watts is given by $N = kT_e B_n$, therefore

$$N = kB_n T_o \left[\frac{T_a}{T_o} + F_o - 1 \right] \quad (11.20)$$

where

k Boltzmann's constant. 1.38×10^{-23} joule/°K

B_n Receiver noise bandwidth, 0.3×10^6 Hz

T_o Reference temperature, 290°K

T_a Noise temperature of the antenna (worst case when $T_a = T_o$; typical case, $T_a = 50^\circ\text{K}$ to 100°K from oxygen and water vapor when at low elevation angles) (Jordan and Baldmain, 1968; and Stiltz, 1961).

Equation (11.20) may be rewritten to express the noise in dbm (db below one milliwatt) for $T_a = F_o$.

$$N = 10 \log \frac{k T_o B_n}{1 \times 10^{-3}} + 10 \log F_o. \quad (11.21)$$

Equation (11.21) is separated into two parts to show the effect of variation of the overall receiver noise factor. The noise contributed by the first half of Eq. (11.21) is -119.2 dbm. This will be less negative by an amount contributed by the noise figure, NF, of the receiving system. From Eq. (11.7), the noise factor of the system is

$$F_o = F_1 + \frac{F_2 - 1}{G_1} \quad (11.7)$$

where F and G are expressed as ratios and the noise figure is $10 \log F_o$.

11.4 EQUIPMENT SELECTION

There are two alternatives in selecting receiving equipment for UHF telemetry. Since most organizations already possess VHF receivers, it is cheaper to buy a down-converter to convert UHF to VHF, provided the VHF receivers have the desired IF and data bandwidth capabilities to be used with UHF. The other alternative involves the use of a UHF tuner and a UHF preamplifier. The down-converter or the preamplifier should be connected as near the antenna as possible. NCAR purchased an Aertech down-converter and a Melabs parametric amplifier with the plan to use the better of the two systems at the launch station and the other at a downrange station. A transistor amplifier was also obtained for evaluation with the UHF receiving configuration. Specifications for all equipment are given at the end of this paper.

The Aertech Down Converter, shown in Figure 11.3, consists of an Aertech Model T4604 tunnel diode amplifier (TDA) with a noise figure of 3.7 db and a gain of 12 db, an Aertech Q4207 mixer-amplifier with a noise figure of 9 db and gain of 20 db, and a MG Microwave local oscillator. The overall noise figure of the converter is less than 4.7 db and the RF to IF gain is 24.5 db.

The Melabs parametric amplifier consists basically of two tuned circuits coupled by a varactor diode, a pump (microwave) frequency source and a circulator to separate the input and output signals. It is unlike conventional amplifiers in that it converts RF power at one frequency to RF power at another frequency, rather

than convert DC power to RF power. The varactor diode is a reactive device acting as a variable capacitor and has amplification with less noise generation than in conventional amplifiers. This particular model has a noise figure of two db and a gain of 20 db. A photograph of the parametric amplifier is shown in Figure 11.4.

The Mu-Del amplifier is a solid state unit consisting of three common-emitter transistor stages wired into a hybrid integrated circuit microstrip package. It has a noise figure of 3.5 db and a gain of 28 db. It is small, lightweight, has low power consumption and is rather inexpensive. A photograph is shown in Figure 11.5.

Table 11.2 shows noise figures for various receiving combinations using a DEI 711 receiver and an L-Band tuner with a noise figure of 11 db (noise factor = 12.6) and a noise figure of 7 db when used with a VHF tuner.

Table 11.2. Noise Figures for Various Receiving Combinations

Preamplifier	NF (db)	F	Gain (db)	F _O	NF (db)
Melabs	2	1.59	20	1.706	2.32
Mu-Del	3.5	2.24	28	2.26	3.54
Aertech	4.7	2.97	25	2.98	4.74

A calibration chart for the four receiving system configurations is shown in Figure 11.6. These curves represent signal level values in db as read on a front panel signal strength meter in terms of signal input in dbm. The receiver noise level is adjusted for a meter reading of zero with a 50 ohm dummy load at the receiver input. The other calibration curves are made with the respective amplifiers or converter after the receiver has been adjusted as described. The various noise levels are shown. It can be seen on this diagram that the Melabs parametric amplifier has the best sensitivity. The output of the calibrated signal strength monitor on the receiver is recorded on a strip chart for each flight.

The transmitter purchased for evaluation with the UHF system is a Teledyne Model TR1402. It develops a minimum of 2 watts of RF power with an efficiency of 10%. It is a true FM transmitter operating in the UHF L-Band. A photograph of the transmitter with an airborne antenna is shown in Figure 11.7.

The tracking antenna selected for the UHF evaluation system consists of an Andrew Corp. Model 38500 positioner with an 8-foot diameter mesh paraboloid reflector. It has a gain of 29 db over an isotropic radiator. The positioner will control the antenna between elevation limits of -10° to $+190^{\circ}$, and azimuth up to 400° . The rotation speed is one degree per second. A remote control unit

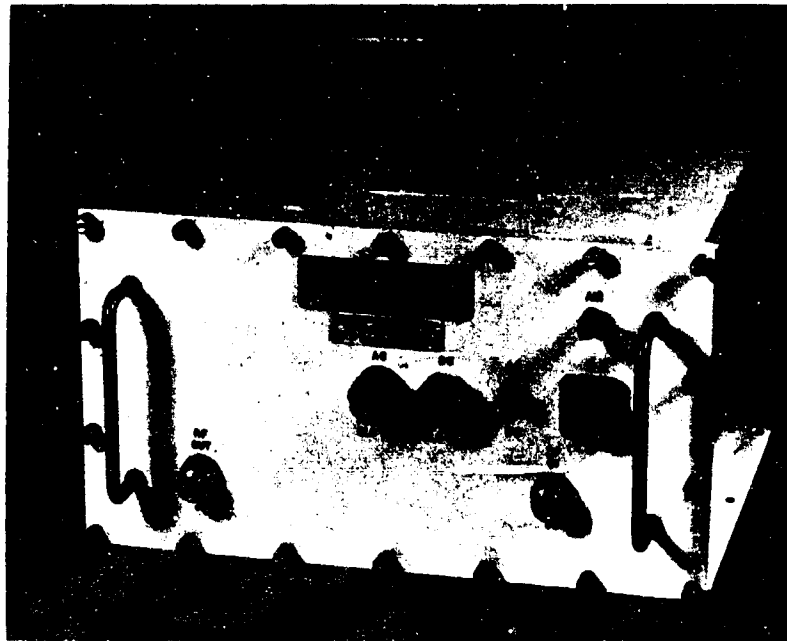


Figure 11.3. Aertech Down Converter

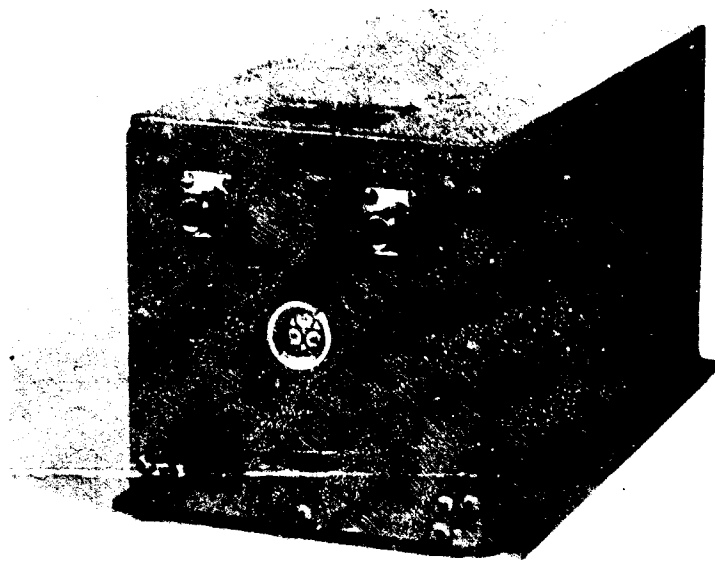


Figure 11.4. Melabs Parametric Amplifier

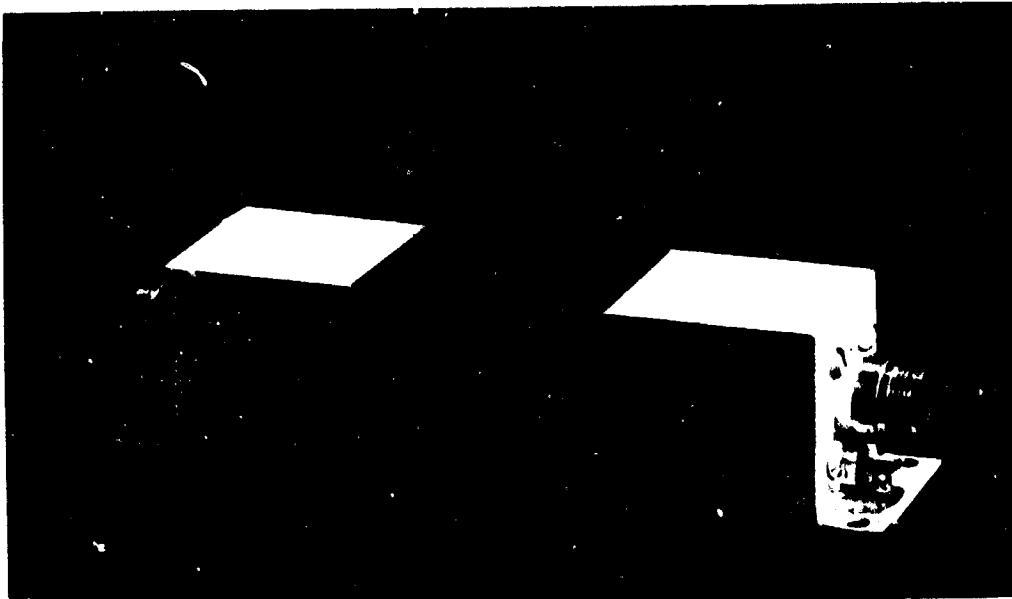


Figure 11.5. Mu-Del Transistor Amplifier

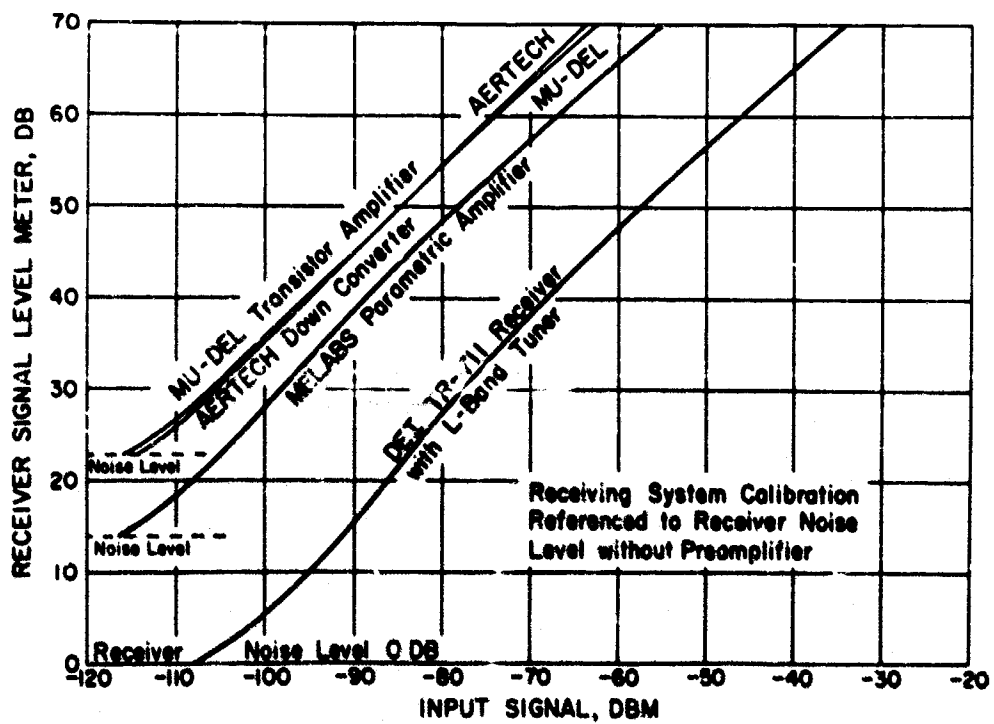


Figure 11.6. Calibration Curves for Receiving Systems

contains switches for controlling the azimuth-elevation motors, and dials for indicating azimuth and elevation angles. A photograph of the antenna is shown in Figure 11.8.

The 8-foot diameter antenna was chosen rather than the more conventional 6-foot diameter dish because of the added 3 db signal power gain. This is equivalent to doubling the power at the transmitting source. Vertical polarization is used on the balloon as well as with the tracking antenna. Circular polarization was considered but rejected as being unnecessary for balloon telemetry applications. Vertical polarization is easier to accomplish at both ends of the radio link.

Three kinds of airborne antennas have been used with the UHF system. One is an Andrew Corp. ground plane antenna Model T55070-14. It is designed for high speed aircraft installation but performs well when mounted to a one-foot diameter metal disc. Another is a coaxial or sleeve antenna. The most preferred type is a modified ground plane as shown with the transmitter in Figure 11.7. This antenna is shop-made and consists of a truncated conical skirt with a total enclosed angle of 60 degrees and a quarter-wave radiator. All three antennas provide good 50 ohm terminations and flight tests have shown no appreciable difference in received signal level. All airborne antennas are assumed to have a horizontal gain of 2 db over an isotropic radiator.

A block diagram of the UHF telemetry system is shown in Figure 11.9.

11.3 SIGNAL POWER LEVEL CALCULATIONS

Figure 11.10 illustrates the power levels at different points in the radio frequency link. The power level is plotted in decibels relative to one milliwatt (dbm). The transmitter power is three watts or +35 dbm. This is represented by the plateau on the left side of the diagram. The transmission cable loss from the transmitter to the balloon antenna is one db while the antenna gain is two db. The free space loss for a range of 400 nautical miles (radio horizon) is 153 db based on the formula

$$L = 20 \log (4\pi R/\lambda) \quad (11.22)$$

where λ is the wavelength and R is expressed in meters. The atmospheric loss caused primarily by oxygen and water vapor is approximately one db per 100 nautical miles (Bean and Dutton, 1966; and Gruenberg, 1967). The signal level is increased by 29 db with the 8-foot paraboloid antenna and one db is lost in the antenna pedestal and associated cabling. The resultant plateau of -93 dbm represents the signal at the preamplifier or converter input terminals.



Figure 11.7. Teledyne Transmitter and Modified Ground Plane Antenna



Figure 11.8. Andrew Tracking Antenna

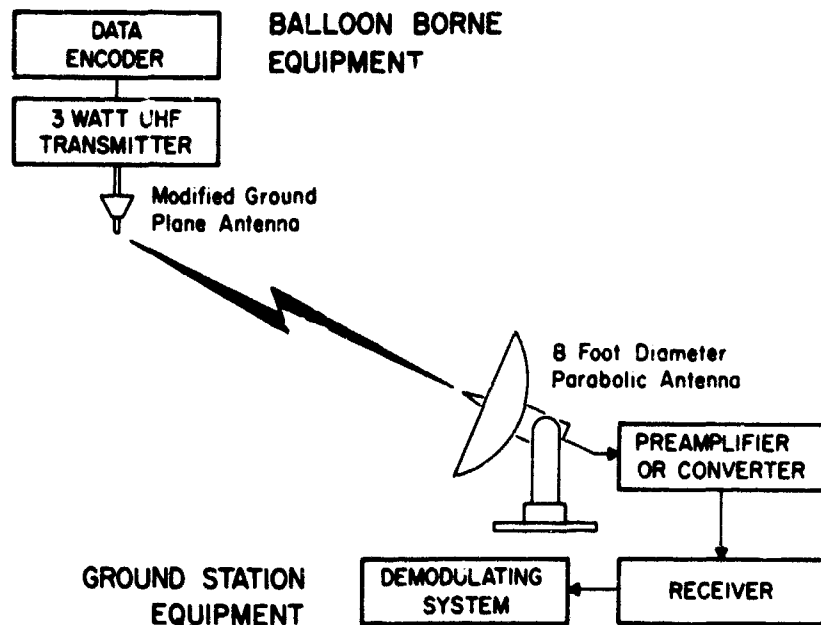


Figure 11.9. Block Diagram of Telemetry System

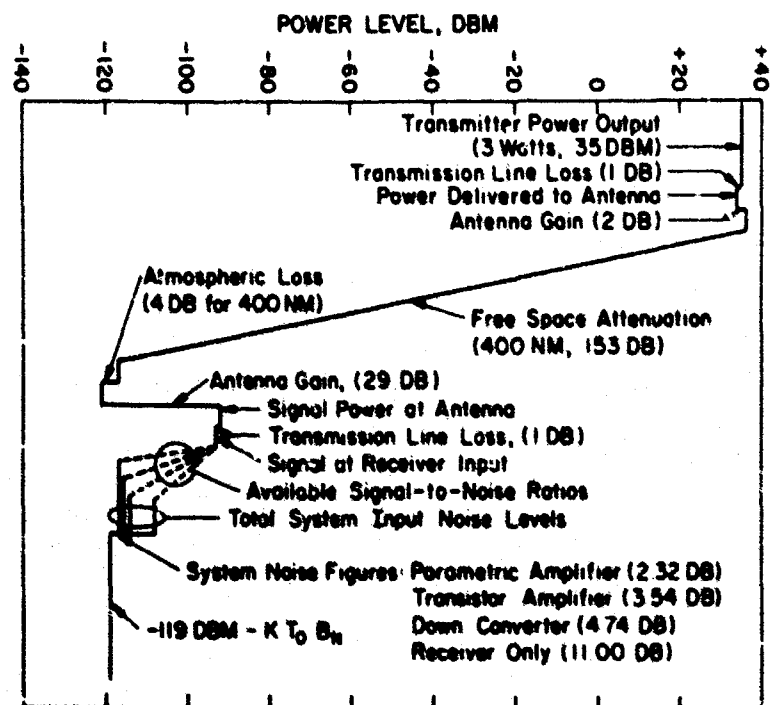


Figure 11.10. Signal Power Level Diagram

On the lower left side of the diagram, the receiver noise contributed by the temperature-bandwidth factors is represented by the -119 dbm level. The noise figure contribution is shown by four steps which represent the noise figures of 2.32, 3.54, 4.74 and 11 db for the parametric amplifier, transistor amplifier, down-converter and receiver alone, respectively. The dashed lines represent the four signal-to-noise ratios with the four receiving configurations. It can be seen that the amplifier with the lowest noise figure provides the greatest signal-to-noise ratio. In this diagram the highest signal-to-noise ratio using an amplifier or converter is 23.7 db. This provides a margin of safety because 9 to 12 db is considered adequate for FM/FM telemetry, and 13 db for PCM/FM with an error probability of one bit in 10^5 bits (Gruenberg, 1967; and Stiltz, 1961). If the UHF receiver were used without a preamplifier, the signal-to-noise ratio is 15 db which is quite marginal.

11.6 TEST RESULTS

Four recent balloon test flights have been made with UHF telemetry. Signal strength measurements have been of primary interest; however, the data handling capability has been checked in many cases. On most flights, VHF telemetry was used as the prime FM/FM data link for other experiments; however, it was proven that UHF would have performed equally as well.

11.7 BALLOON FLIGHT 487-P

This was the first of the series of test flights for UHF telemetry equipment evaluation. Arrangements were made to test every conceivable configuration of UHF equipment available at the ground station and on the balloon. The balloon was equipped with the Teledyne 3-watt transmitter as the primary signal source. A Ball Brothers transistor-cavity (0.25 watt) transmitter was also flown to see the effects of 11 db reduction in power. The 3-watt transmitter could be loaded into two separate antennas by means of a coaxial switch. One antenna was the shop-made modified ground plane and the other was the Andrew ground plane aircraft antenna. The low power transmitter was loaded into the coaxial antenna.

At the launch site ground station, arrangements were made to use conveniently the parametric amplifier or the down converter at the antenna. The transistor preamplifier was not available at this time. A roof-mounted ground plane antenna was made available to receive the signal in lieu of using the parabola when at close range. This would reduce the tracking efforts in case signal acquisition became difficult. A strip-chart recorder was used for recording signal levels from the

receiver. The receiving systems were calibrated with a Hewlett-Packard Model 614 signal generator.

A VHF FM/FM telemetry system was used for the flight to convey the flight data. It had subcarrier oscillators for magnetic aspect sensors, low-bit-rate PCM, command decoder monitor, altitude transducer, voice relay channel and a JPL high-bit-rate PCM data encoder. The subcarrier channels modulated the VHF transmitter continuously, and modulated the UHF transmitter under certain conditions.

In order to get information about bit error rates using the UHF system for balloon telemetry, a high-bit-rate PCM data encoder was flown. This encoder was provided by the Jet Propulsion Laboratory (JPL) of the California Institute of Technology. JPL was a large contributor to the implementation of the flight. The PCM encoder was developed for the sole purpose of doing bit error studies under test flight operational conditions. The encoder generates a 64-word frame of 16 bit words. There are two unique words, a frame sync word and a common word to complete the frame.

The PCM encoder could be ground-commanded to operate at kilobit rates of 4, 8, 16, 64 and 80. The 64 kbps and the 80 kbps rates directly modulated the UHF transmitter while the other rates were used to modulate a channel E subcarrier oscillator. The three lower bit rates deviate the channel E subcarrier with modulation indices of 5.25, 2.63 and 1.31, respectively. The UHF transmitter deviation was 500 kHz. The 16 kbps rate was used for most of the flight. This represents the worst case signal-to-noise condition we would expect to use.

During the flight, several equipment configurations were arranged and are listed as follows:

- A - Parabolic receiving antenna with parametric amplifier and 3-watt balloon transmitter.
- B - Ground plane receiving antenna with no preamplifier and 3-watt balloon transmitter.
- C - Ground plane receiving antenna with parametric amplifier and 3-watt balloon transmitter.
- D - Ground plane receiving antenna with parametric amplifier and 2.5-watt balloon transmitter.
- E - Parabolic receiving antenna with parametric amplifier and 0.25-watt balloon transmitter.
- F - Parabolic receiving antenna with down-converter and 0.25-watt balloon transmitter.
- G - Parabolic receiving antenna with down-converter and 3-watt balloon transmitter.

Figure 11.11 shows signal power level vs balloon range for flight 487-P. The free space signal power line represents the signal into a 50-ohm load one would expect from a 3-watt transmitter and a 2 db antenna on the balloon and a 29 db antenna on the ground. Total cable losses are 2 db. The signal power is attenuated by the atmosphere by approximately one db per 100 nautical miles (Bean and Dutton, 1966; and Gruenberg, 1967). This is shown by the available signal power curve.

The actual signal curve is broken into segments according to the legend above. The points on the curve represent conveniently selected points for plotting and do not represent all of the signal fluctuations. Since this graph is quite compressed in range, actual signal variations would create a broad trace on the graph and would make it difficult to read. The fluctuations are caused by gondola rotation, variations in atmospheric attenuation properties such as refraction, absorption, reflection, and ducting and interference (Reed and Russell, 1966). Segments A and G represent typical equipment configurations, and both A and G will represent the optimum signal level available. The noise levels shown at the bottom of the graph are different for the two configurations. Segments E and F should be 11 db lower than A and G because of the transmitter being 11 db below the 3-watt transmitter. Only a slight difference could be seen in the signal level during flight, when the 3-watt transmitter was changed from the modified ground plane antenna to the Andrew ground plane antenna. The shop-made modified ground plane was about one db better at the range where the comparison was made. This may have been a result of differences in radiation patterns of the two antennas.

All signal level data runs a few db less than the expected level. This is probably because of the inaccuracies in measurements and in not knowing some of the exact equipment parameters, such as antenna gains, cable losses, etc. Care was taken, however, with equipment calibration. Under the circumstances, it is believed that a reasonable agreement between theoretical and actual signal level measurements was obtained.

At the ground station, the PCM data from the JPL encoder was recorded on an analog tape recorder for the purpose of storage and playback. It was not convenient to record on computer compatible tape during this operation. The analog tape was later played back through an EMR 185 PCM decommutator and a PDP/4 computer. The computer was programmed to detect any errors in the common word and to print each frame sync word and any errors that occurred in that frame of 63 additional common words. Tape was played back for 10-minute sampling intervals and the first portion of the flight was very free of errors. The bit error from launch to 260 NM averages 5.74×10^6 bits per error. From 260 NM to 360 NM it ranged from 1×10^5 to 2×10^6 bits per error. After 360 miles the data became erratic and it was difficult to obtain good bit error data. The signal-to-

noise ratio at this range was about 10 db; however, the radio horizon was being approached and the signal was becoming erratic. The 64 kbps and the 80 kbps rates were tested at the marginal signal range with no success because of low signal-to-noise ratio. The same was true for the 4 kbps and 8 kbps rates. The signal was lost at 400 nautical miles.

11.8 BALLOON FLIGHT 505-P

The parametric amplifier was not available for this flight, which left the down-converter the only UHF receiving equipment that could be used. The airborne equipment consisted of the 3-watt Teledyne transmitter and a 185 milliwatt Microcom Corp. Transmitter. The signal from the 3-watt transmitter was radiated by a modified ground plane antenna and a coaxial (sleeve) antenna with 3 db attenuation in the transmission line. The antennas were transferred by a coaxial switch. The attenuator was used to show the effects of cutting the transmitter power in half. The low power transmitter was used to illustrate the results of using a signal 12 db below the 3-watt transmitter. It used the Andrew ground plane antenna.

The 3-watt transmitter was modulated by a channel H subcarrier oscillator which, in turn, was modulated by square wave signals from a multivibrator with commandable frequencies of 4.5 kHz, 9.1 kHz and 23.5 kHz with subcarrier modulation indices of 5, 2.5 and 1 respectively. The multivibrator was used in lieu of a PCM signal for this test.

Other electronic instrumentation equipment was tested on this balloon flight, such as a new PCM command system and a digital timer. A long-range flight was desired but could not be achieved because of early termination due to an undesirable trajectory. This prevented the balloon from reaching the radio horizon, therefore, marginal signal conditions could not be examined.

Figure 11.12 shows signal power level vs range for flight 505-P. Since this graph includes the results of flight 523-H, the signal level for this flight is shown with a solid line. The available signal power line with the 3 db drop is also a solid line. Segment A is the unattenuated signal from the modified ground plane. Segment B is the attenuated portion. The Microcom low power transmitter was turned on early in the flight and shown by segment E. This segment is approximately 12 db below the 3-watt transmitter signal level as could be shown by the extension of an average of segment A.

The square wave modulation on the subcarrier channel H which modulated the UHF transmitter was examined at the ground station during flight. No deterioration of the signals was noted at maximum range, however, no marginal signals occurred to degrade the pulse by increased noise.

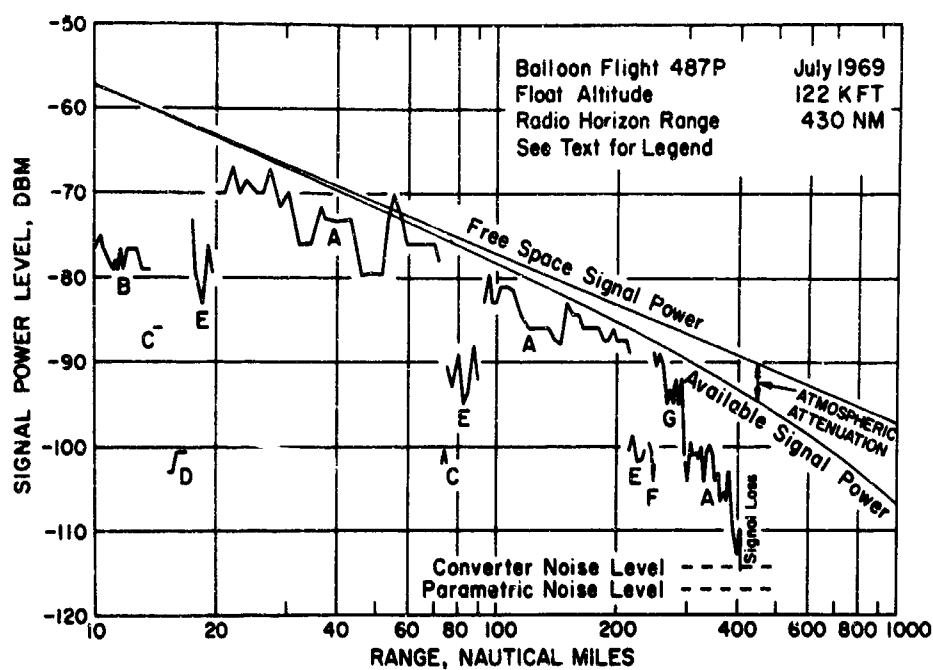


Figure 11.11. Signal Level vs Range, Flight 487-P

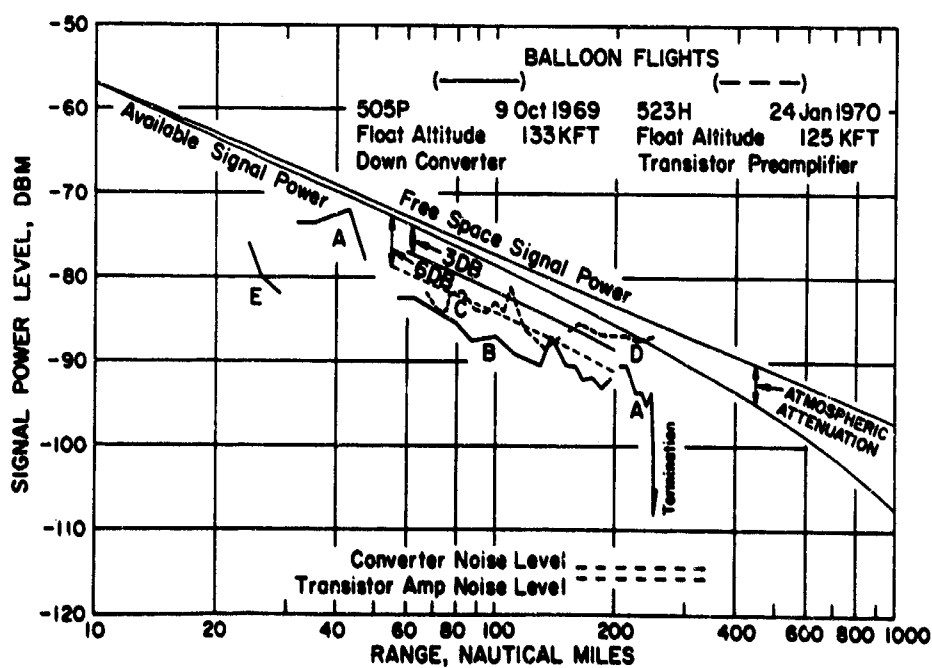


Figure 11.12. Signal Level vs Range, Flights 505-P and 523-H

The test was successful in that it showed that adequate signal strength is available for UHF telemetry and more experience was gained in using UHF frequencies.

11.9 BALLOON FLIGHT 523-H

The parametric amplifier was still unavailable for this flight; however, a Mu-Del transistor amplifier was obtained for evaluation and was used throughout the flight. The 3-watt transmitter was used on the balloon. Its output could be switched between two modified ground plane antennas one of which had a 6 db attenuator in the transmission line. FM/FM flight data was handled by a VHF system and the UHF system. The main objective in the test was to observe signal levels during flight.

This flight was different from all the other test flights in that it was launched at Hobbs, New Mexico, which is near the radio horizon for a 125K ft balloon. The UHF ground station was at Palestine, Texas. This meant that the balloon signal should have been at a low level when first acquired. Due to commitments in manning other ground station equipment, the UHF signal was not acquired until the balloon was at 250 nautical miles range. The flight was terminated at a point 57 nautical miles from the ground station.

The UHF system was used to handle the flight data during part of the flight. The flight was used to test other equipment such as the new PCM command system and a digital timer as well as a new balloon design.

Figure 11.12 shows the signal power level with dashed segments C and D. Segment C is the 6 db attenuated signal while segment D is unattenuated. The dashed available signal power level is 6 db below the level for the 3-watt transmitter. The signal level for this flight more nearly agreed with the theoretical level than for other flights as can be seen on the graph.

11.10 BALLOON FLIGHT 535-PT

The Mu-Del preamplifier was used almost exclusively during this flight in order to get continuous data without many interruptions. The parametric amplifier was connected for a short duration test. The balloon UHF configuration was the same as for flight 523-H where the 3-watt transmitter was switched between two modified ground plane antennas, one with 6 db attenuation.

The flight was used to test other electronic equipment as well as a new balloon design. The flight data could be transmitted by the VHF and UHF systems; however,

the UHF transmitter carried the FM/FM telemetry data throughout the flight. The UHF transmitter deviation was 500 kHz.

Figure 11.13 illustrates the available signal power at the ground station amplifier input throughout the flight. The signal was lost at the radio horizon of 430 nautical miles. The chart indicates adequate signal strength for all telemetry applications throughout the flight. The 6-db attenuator was used at intervals during the flight, and appeared on the flight recording as one would expect, a 6 db lower signal level. No pronounced signal variations were noticed which could be attributed to interference by the direct and reflected waves. This flight would have been the best one to illustrate such variations since the RF equipment configuration was almost unchanged during the flight. The directivity of the antenna tends to reduce interference effects. In general, the test was a smooth operation and the UHF tests were quite successful.

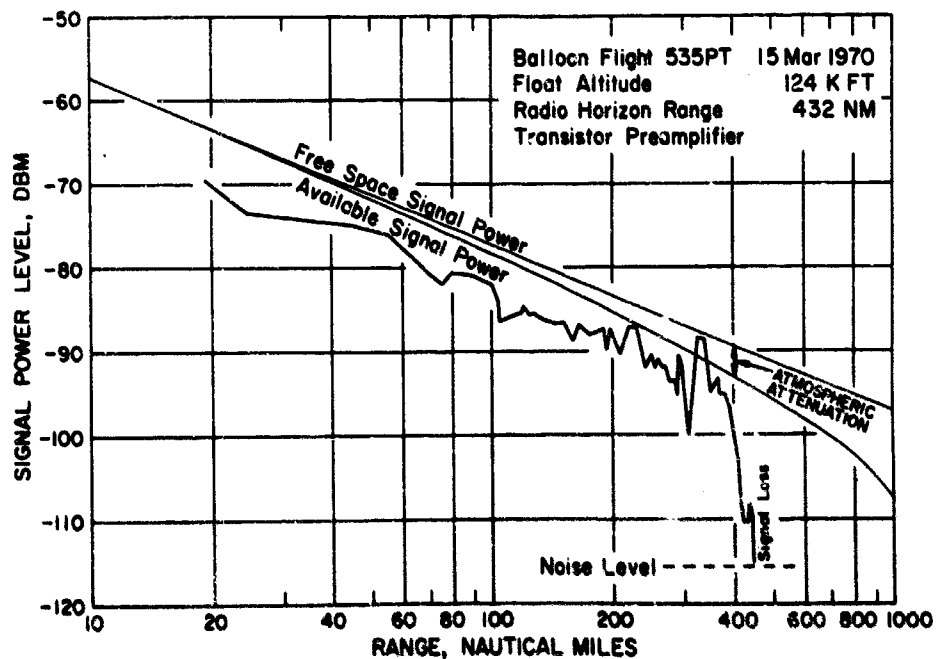


Figure 11.13. Signal Level vs Range, Flight 535-P

11.11 SUMMARY AND CONCLUSIONS

In order to comply with the Military Communications Board Memorandum, MCEB-M-92-65, which stated that all telemetry should occupy the UHF bands after

January 1970, NCAR purchased evaluation equipment for the L-Band. Several flight tests were made using the UHF equipment and all were considered successful. Many variations of signal levels and equipment configurations were used in order to learn the most about the UHF performance. The low power and attenuated power conditions were flown to compare power levels at the radio horizon where the levels are marginal. It was found that the drop-out was somewhat abrupt and no good information in this area could be obtained. Also since VHF was used for commanding the different signal source configurations, the command link became marginal simultaneously with the UHF signal.

The flight tests have shown that there will be no great problems in converting to UHF telemetry. More attention will be necessary for tracking the antenna unless an automatic tracking system is used. Experience has shown that if the tracking antenna is positioned at 90° elevation while the balloon is in the immediate area, no tracking is necessary. After the balloon is at long ranges, only an occasional adjustment is necessary. On several occasions the signal was deliberately lost by directing the antenna away from the signal, then reacquired with no difficulties. The solution for tracking is an automatic system such as the Monopulse system but these cost many thousands of dollars.

All the UHF equipment is somewhat expensive as compared with VHF equipment. An expensive parametric amplifier was purchased for UHF evaluation. However, with lower cost units such as the Mu-Del amplifier being available, the noise figure trade-off hardly seems worth the extra cost, especially if repairs are expected. It may be less expensive to use down-converters with existing VHF receivers, but the IF bandwidth and data bandwidth characteristics should be compatible with the anticipated deviation and data requirements. If a receiver with plug-in capability is available, a UHF tuner with a low noise preamplifier is more desirable.

Aside from being expensive, the airborne transmitters are very inefficient. The one used for these test was approximately 10 percent efficient. It is anticipated that more efficient transmitters will be developed and hopefully the price will be reduced. The extra input power creates additional weight in the form of batteries. It may be possible to improve on power consumption by using a one-watt transmitter. Flight tests indicate that this signal would be adequate.

Table 11.3. Equipment Specifications

<u>Aertech Down Converter</u>	<u>Model C4223</u>
Frequency Range	1435-1540 MHz
IF Frequency	185-290 MHz
Local Oscillator	1250 MHz
Gain/Ripple	24.5 db/ ± 0.5 db
Noise Figure	TDA 3.7 db System 4.7 db
Power Input Source	115 V ac or 28 v dc
Cost	\$3350
<u>Melabs Parametric Amplifier</u>	<u>Model APL 3C</u>
Frequency Range	1445 to 1530 MHz
Gain	20 db
Noise Figure	2 db
Compression	1 db at -33 dbm
Power Input Source	115 v ac
Cost	\$6475
<u>Mu-Del Transistor Amplifier</u>	<u>Model MDA 1415</u>
Frequency Range	1435-1540 MHz
Gain	28 db
Noise Figure	3.5 db
Power Requirement	15 volt, 20 ma
Size	1.5 x 1.5 x 6.25 inches
Cost	\$1'00
<u>Teledyne Telemetry Transmitter</u>	<u>Model TR1402</u>
Frequency	1485.5 MHz
Modulation	True FM
Power Output	Min. 2 watts
Efficiency	10%
Deviation Sensitivity	1 volt rms for 500 kHz dev.
Operating Temperature	-20°C to +85°C
Cost	\$3600
<u>Ball Brothers Research Corporation Transmitter</u>	<u>Model SST 400</u>
Frequency, cavity controlled (adjustable)	1485.5 MHz
Modulation	FM
Modulation Sensitivity	1 volt p-p for 500 kHz dev.

Table 11.3 (Contd). Equipment Specifications

<u>Ball Brothers Research Corporation</u>	
<u>Transmitter (Contd)</u>	<u>Model SST 400</u>
Power Requirement	28 v
Efficiency	10%
RF Power Output Nominal	250 mw
<u>Microcom Corp. Transmitter</u>	<u>Model T4</u>
Frequency	1484.5 MHz
Modulation	FM
Modulation Sensitivity	1 volt p-p for 1 MHz dev.
Power Output	185 mw. min.
Power Requirement	28 v dc
<u>Andrew Corp. Antenna System</u>	<u>Model 38500</u>
Paraboloid Diameter	8 ft
Frequency	1485 MHz
Polarization	Vertical
Gain Over Isotropic	29 db
Beam Width (3 db)	6°
Side Lobes	18 db down at 12.5°
Construction	Welded mesh
Control	Remote
Cost	\$8500
<u>Andrew Corp. Antenna</u>	<u>Model T55070-14</u>
Application	Aircraft
Frequency	1400-1500 MHz
VSWR	1.3
Average Power Rating	50 watts
Polarization	Vertical
Gain	5 dbi
Weight	7 oz
Cost	\$100

Acknowledgments

The author wishes to acknowledge the efforts of Mr. Jim Riccio of JPL for his efforts in helping instrument flight 487-P and reducing PCM test data. Thanks are also due the Palestine NCAR operations staff for assisting with all UHF test flights. Appreciation is also expressed to Mr. Morton Kizner of Mu-Del Electronics, Wheaton, Maryland, for providing a UHF preamplifier for these tests.

References

- Bean, B. R. and Dutton, E. J. (1966) Radio Meteorology, National Bureau of Standards Monograph 92, U. S. Government Printing Office.
- Friis, H. T. (1964) Noise figures of radio receivers, Proceedings of the IRE (Vol. 32).
- Gruenberg, E. L. (1967) Handbook of Telemetry and Remote Control, McGraw-Hill.
- Jordan, E. C. and Baldmain, K. C. (1968) Electromagnetic Waves and Radiating Systems, Prentice Hall.
- Lawson, J. L. and Uhlenbeck, G. E. (1950) Threshold Signals, Radiation Laboratory Series, Vol. 24, McGraw-Hill.
- Nyquist, H. (1928) Thermal agitation of electric charge in conductors, Physical Review (Vol. 32).
- Reed, H. R. and Russel, C. M. (1966) Ultra High Frequency Propagation, Boston Technical Publishers, Inc.
- Skolnik, M. I. (1962) Introduction to Radar Systems, McGraw Hill.
- Stultz, H. L. (1961) Aerospace Telemetry, Prentice-Hall, Inc.

12. Airship and Balloon League of the United States

C.E. Rosendahl
Flag Point
Toms River, New Jersey

A non-profit organization to be known as the AIRSHIP AND BALLOON LEAGUE OF THE UNITED STATES has been incorporated under the laws of the State of New Jersey with the primary general purpose of the preservation of the history of buoyant aircraft, that is, airships and balloons. The incorporators were the author of this paper together with four others who have served in the lighter-than-air organization of the U.S. Navy, and now reside in the general Lakehurst vicinity.

The purposes for which the LEAGUE was organized are as follows:

- (1) To collect and preserve data pertaining to the preservation of the history of buoyant aircraft, the senior branch of aeronautics.
- (2) To provide and administer suitable display facilities and repository for airship and balloon items of historical significance and/or interest such as parts, models, documents, books, papers, publications, photographs, clippings, correspondence, films, and other articles and items relevant to the history of airships and balloons.
- (3) To assemble knowledge and information pertaining to airships and balloons.
- (4) To serve as an information and research center for airship and balloon historical matters.

(5) To make available educational and historical material pertaining to airships and balloons to students and to the public.

(6) To assemble and provide information as to the location, character, extent of other historical and technical information, displays, repositories pertaining to airships and balloons.

(7) To collect and preserve articles, specimens, and material things illustrative or demonstrative of airships and balloons.

(8) To procure and preserve historical relics and places pertaining to airships and balloons and the owning, leasing, furnishing, and managing of historic building or buildings for the use of the League.

(9) To perpetuate the memory of those who, by their deeds, labor, and heroism, contributed to the history of airships and balloons.

(10) To encourage and facilitate social contacts for League members and others active or interested in airship and balloon history.

(11) To participate in other practical activities in general harmony with the above.

(12) To cooperate with other agencies, groups, and individuals in carrying out the above-stated purposes.

In deciding to form the LEAGUE, we have not been unaware of the attention already being given to the preservation of the history of buoyant aircraft by such organizations as the Smithsonian Institution; the Wingfoot Lighter-than Air Society; the U. S. Air Force Museum; the U. S. Naval Aviation Museum; the Zeppelin Museum at Friedrichshafen, Germany; and others in varying degrees. But it is felt that in addition to such existing historical recognition, buoyant aircraft deserve a MUSEUM of their own in the United States but taking cognizance of such craft the world over.

Hence, a major objective of the LEAGUE is the establishment and operation of an AIRSHIP AND BALLOON MUSEUM which, it is hoped, amongst its other purposes would serve as headquarters of the LEAGUE, and importantly also as an information and research center for airship and balloon historical matters.

Since Lakehurst is so well known throughout the world as a major center of airship operations, it is felt also that the A & B MUSEUM belongs in the immediate Lakehurst vicinity. The Lakehurst Naval Air Station has no buildings or structures either suitable or available for such museum purposes. Furthermore, it is felt that the proposed museum should be a private venture, though obviously there would be hoped for and appreciated various kinds of recognition and assistance from governmental sources that might come without too many strings attached.

The various kinds of membership in the League have not yet been finalized, but generally speaking anyone who believes in and wishes to participate in the above-outlined historical goals will be eligible and welcome for membership.

Even though no effort has yet been made at publicizing the League, its purposes, and the museum, not a few persons who have incidental knowledge of the project have already sent in items of interest in the history of buoyant aircraft for which, fortunately we do have temporary storage space. We are able to receive and maintain properly, from now on, pertinent material anyone might now care to give us for the museum. In particular, there would be appreciated photographs, books, papers, and publications with which we can continue building up our reference files.

In the near future, the incorporators expect to active the LEAGUE and will then publicize its existence, purposes, types of membership, and like information. Meanwhile we are most appreciative of this opportunity of bringing this historical project to your attention, in the hope that we may have whatever assistance, cooperation, and possible participation you may consider appropriate at this point.

We are at the point in our planning for activation and implementation where any suggestions and comments would be gratefully received and greatly appreciated. For the time being, any communications on the subject may be addressed to --

Vice Admiral C. E. Rosendahl US Navy Retired
Flag Point
Toms River, New Jersey 08753

Contents**13.1 Introduction****13. Comments on Tethered Balloons**

L. E. Speed
Lea Bridges Industries
South End On Sea, England

13.1 INTRODUCTION

One of the earliest problems confronting uses of tethered balloons was the retention of the shape of the balloon during windy conditions. Unless the pressure inside the envelope is in excess of the velocity head of the wind, the forward end of the balloon will deform inwards; this concavity increases the drag of the balloon and may cause instability.

This deformation was very common when spherical balloons were used tethered - for observation purposes, etc.

With the introduction of the first reasonably successful kite balloon, the DRACHEN in 1894, this deformation of nose was considerably reduced by the fitting of a ballonnet inflated via a scoop by ram air, supplemented by the pressure head of the gas in the envelope (Figure 13.1).

As this balloon seldom exceeded an altitude of 3000 feet and flew at 20 - 25° angle of attack, the internal pressure at the most critical area of the envelope (that directly facing the wind) was above the velocity head of the wind, and unless there was an excessive loss of gas, little nose deformation occurred. The high angle of attack, however, caused excessive cable tensions, and with the introduction of the CAQUOT balloon in 1916, which flew at a much smaller angle of attack,

PRECEDING PAGE BLANK

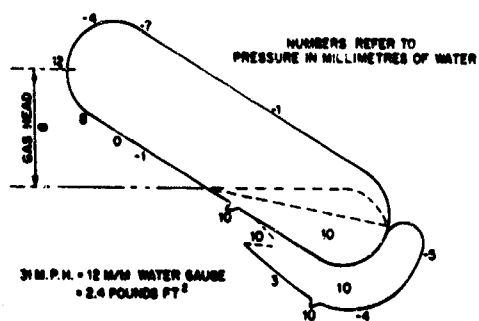


Figure 13.1. Drachen Balloon, 30 mph

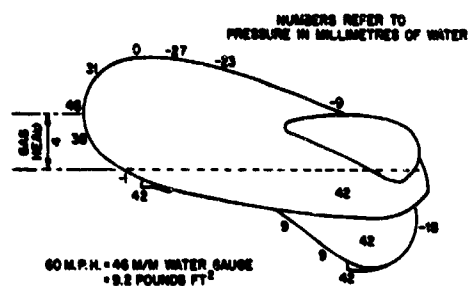


Figure 13.2. Caquot Balloon, 60 mph

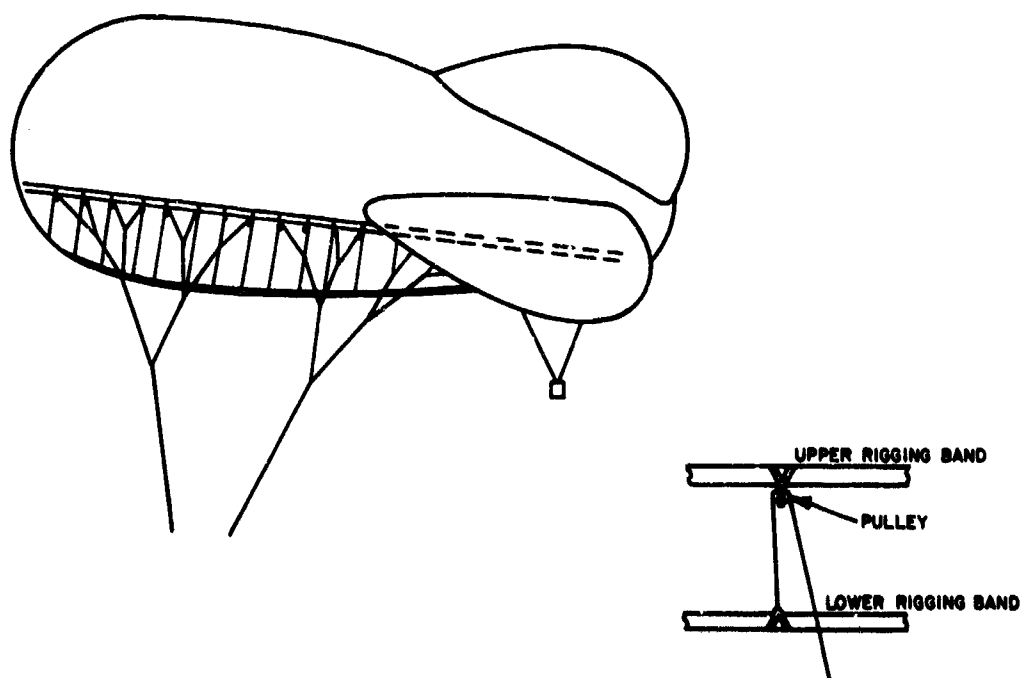


Figure 13.3. "Willows" Balloon

12 - 15°, and with increased ceiling, the nose-deformation problem became more acute (Figure 13.2).

The increased ceilings required by balloons used for barrage purposes aggravated the position. The French were moderately successful when using elastic cords to retain the internal pressure, but the hysteresis effect which is always present in rubber cords was increased by the cold temperatures experienced at altitude.

During 1916, a young Naval Lieutenant Willows conceived an idea whereby the internal pressure could be produced by the tension in the rigging legs (Figure 13.3).

One side of a 5000 cu ft balloon was rigged by passing the rigging over a series of pulleys attached to the conventional rigging band, and the end of each rigging leg was attached to another rigging band near the bottom center line of the envelope, thus forming an expanding gore. This arrangement should result in an internal pressure proportional to the cable tension and wind speed. This expanding gore ran the full length of the envelope, and to achieve this, the balloon was turned upside down, bringing the vertical rudder to the top of the envelope and the fins hanging down at an angle of 30°. On the preliminary trial, very uneven expansion of the envelope was apparent, most of the expansion taking place at the forward and after ends of the balloon where the rigging pull angle was acute. The balloon was modified by removing the after rigging and inserting rubber cords instead, and the balloon was rebalanced by suspending a weight near the tail.

The second trial took place in a wind of 8 mph, the balloon being tethered to a small hand winch. Three defects were again apparent:

- (1) The balloon expanded on one side rigging only, resulting in the balloon flying "off wind".
- (2) The gas-filled stabilizers caused the center of buoyancy to alter as the gas expanded, thus affecting trim.
- (3) The envelope did not expand evenly along its length, the nose of the balloon presenting a decidedly flat surface.

The balloon was allowed to ascend and the winch operator, not having received the order to stop ascent at 6,000 feet (the limit of the expanding gore), permitted the balloon to rise to 9,700 feet where the balloon burst, falling to the ground in two pieces. This experiment was not continued.

During 1937 a variation of Willows' idea was produced by a Major Wheelwright, but as Willows' expansion scheme depended upon rigging pulls applied on the outside of the envelope, Wheelwright evolved an internal rigging (Figure 13.4).

The balloon was of six lobes formed by six cusps fitted with pulleys over which the internal rigging passed. To reduce the length of the rigging projecting outside the balloon, when the balloon was at ground level, the expansion system was

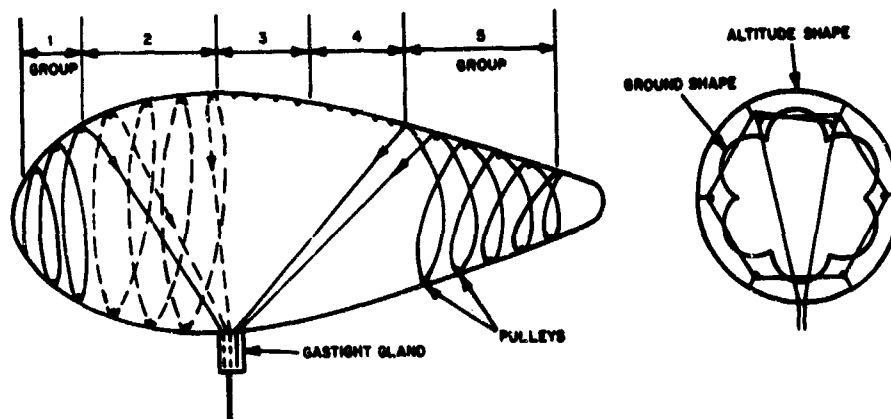


Figure 13.4. Wheelwright Expanding Balloon

divided into 4 1/2 sections with 9 rigging wires passing through a mercury-filled gland fitted at the underside of the envelope.

A small model was made, air inflated and weighted to represent gas lift, and slung upside down; when air was forced into the envelope, the model expanded and ascended the rigging. There were several minor snags because of the pulleys' (domestic curtain fittings) jamming occasionally and the air leaking from the gland; nevertheless it was decided to construct a full size model of 11,000 cu ft volume.

This full size model was of conventional shape, but because of the lobular cross section, narrow base stabilizers (gas-filled via the envelope) were fitted. Forty pulleys spaced about 18 inches apart were positioned on each cusp, each rigging group taking the form of a conical helix inside the envelope.

Flying trials were undertaken and the angle of attack was found to be greatly in excess of that calculated (25° instead of 8°). The balloon yawed and pitched considerably, partly because the stabilizers bent at the narrow base, and the balloon broke away, but on recovery it was discovered that two of the internal rigging bands had torn away from the envelope.

The balloon was repaired, wider base stabilizers fitted and other minor modifications made, and the flying trials continued. The balloon flew at an altitude of approximately 300 feet on 2,000 feet of cable — the drift of the balloon being very excessive — and after several unsuccessful attempts to fly the balloon, after other modifications the trials were abandoned.

My third 'novelty' is of a bellows-type of pump fitted to the upper end of the flying cable and operated by the variation in the tether cable tension.

Small balloons of approximately 3,000 cu ft which depended upon the expansion of rubber cords were used in considerable numbers to deter dive bombing during World War 2. These were flown from ships and moored to buoys around harbours.

Because of the acute shortage of rubber, other systems of pressure control were considered.

A pump (Figure 13.5) was made by forming a fabric cylinder about 3 feet long, the ends being made of wood about 8 inches in diameter. Springs made from rubber cords were fitted between the wooden ends, which contained entrance and exit valves, orifices and suspension eyes; the pump operating like a concertina. This pump was effective within a limited range of wind speeds but would not operate over the full range of operational wind speeds, 0 - 70 mph.

Thus for a balloon to operate in a wind speed of, say, 0 - 20 mph, a weak spring was necessary to give the required length of stroke. At above 30 mph the spring was fully extended and the pump failed to operate. Conversely, when a stronger spring was fitted the stroke of the bellows was insufficient to supply a sufficient volume of air at the lower wind speeds.

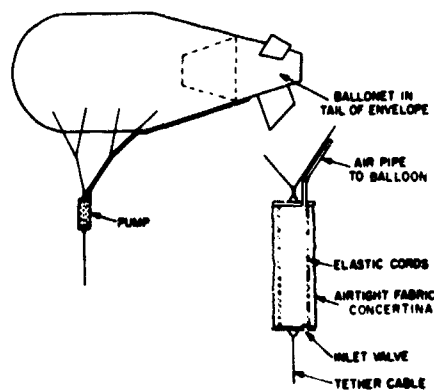


Figure 13.5. Pump Kite Balloon

14. The Use of Tethered Balloons and Kites in the GARP Tropical Experiment

G. Stilke
Meteorologisches Institut
Universität Hamburg

The Global Atmospheric Research Programme (GARP) is a joint effort of the ICSU (International Council of Scientific Unions) and the WMO (World Meteorological Organization) with the goal to increase our understanding of the general circulation of the atmosphere and to develop the physical and mathematical basis for methods of extended prediction.

There will be several international field experiments in this programme, the tropical experiment starting in 1973/74, and later a global experiment. The planning of the first tropical experiment is most advanced. The proposal for the experimental studies contains the use of tethered balloons and kites from ships for measuring atmospheric temperature and humidity fine structure (GARP Publ. Ser. No. 4, p.11, Jan. 1970).

The planning conference on GARP-Tropical Experiments (Brussels 16-20. 3. 1970) has calculated a participation of 24 research ships in the first tropical experiment over the Atlantic (and of more than 100 merchant ships). The tethered balloon- and kite-sondes should measure, if possible, also the eddy fluxes of heat, water vapor and momentum in the lower 1000 m above the ocean. Special attention must be paid to avoid as far as possible unknown motions of the balloon and sonde system.

PRECEDING PAGE BLANK

Balloon Technology

Tuesday

- Morning:** Chairman, John McFall
National Aeronautics and Space Administration
- Afternoon:** Chairman, J.H. Smalley
National Committee on Atmospheric Research
- Evening:** Chairman, Lewis A. Grass
Air Force Cambridge Research Laboratories

Contents

15.1	Introduction	158
15.2	Material Characterization	159
15.3	Mechanical Testing and Discussion	162
15.4	Conclusions	164

15. The Influence of Changes of Material Structure on the Failure of Polyethylene Balloon Films

D. Weissmann
Stevens Institute of Technology
Hoboken, New Jersey

Abstract

During the last few years, a long series of investigations of the performance of polyethylene (P.E.) films used as balloon materials was conducted under simulated launch and flight conditions.

It was found that the nature of the rupture achieved by burst at -70°F exhibits a ductile-brittle transition dependent upon the thermal-stress history of the material.

The present study was planned to correlate that phenomenon to the structure of the P.E. film and its changes due to creep and orientation under loading.

Through an experimental study consisting of a series of tests at various critical temperatures, the above-mentioned correlation is investigated. The tests performed included creep, constant strain rate, and mechanical dynamical tests to investigate mechanical properties changes and infrared, molecular weight distribution, and X-ray studies to investigate structural properties.

Some initial results are presented and the observed failure pattern is discussed in light of these results.

PRECEDING PAGE BLANK

15.1 INTRODUCTION

A long series of investigations, testing balloon films under conditions which simulate launch and flight conditions, were carried out over the last few years by A.D. Kerr and H. Alexander. Many of the results were presented in previous symposia and reports (Kerr, 1968; and Kerr and Alexander, 1968).

Much of the testing consisted of bursting cylindrical samples in a cold chamber at a temperature of -70°F after they were uniaxially preloaded by different loads for varying periods of time. The preloading was done at temperatures of 75°F , 92°F and 110°F .

One of the most significant observations was that the pressure needed to burst the sample dropped radically after certain preloading conditions were applied.

In Figure 15.1, the burst pressure is plotted as a function of the preloading time. As the preloading time increases, the burst pressure decreases to some limiting value. It is interesting to note that in order to get the same drop in burst pressure the elongation λ has to be the same, indicating that the drop in burst pressure is associated with the amount of orientation introduced by the uniaxial creep.

In addition to the burst-pressure drop effect, a change in the nature of the rupture appearance between the two cases was observed. In a case where there is no drop in burst pressure, the rupture is ductile; being characterized by one rupture line usually in the machine direction (Figure 15.2). In the samples which show a pressure drop, the rupture is brittle and the material shatters like glass (Figure 15.3).

This transition in the nature of the failure is of great importance. A ductile material has the ability to deform and relax a large applied stress while a brittle material will rupture. In actual flight conditions, the film might be locally overstressed. This difference between ductile and brittle behavior could mean the difference between success and catastrophic failure.

The problem undertaken here is to determine the correlation between the material structural changes (such as orientation) and the above observations.

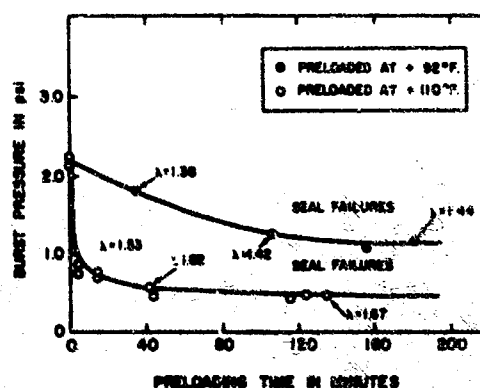


Figure 15.1. Burst Pressure of StratoFilm (Load 60 lb burst at -70°F)

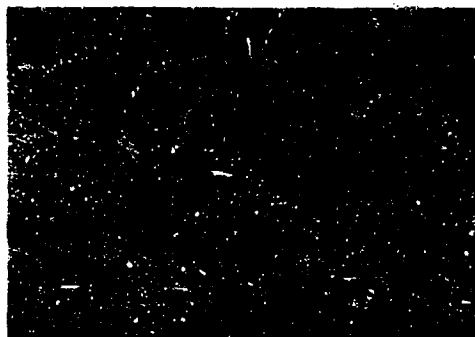


Figure 15.2. Ductile Rupture

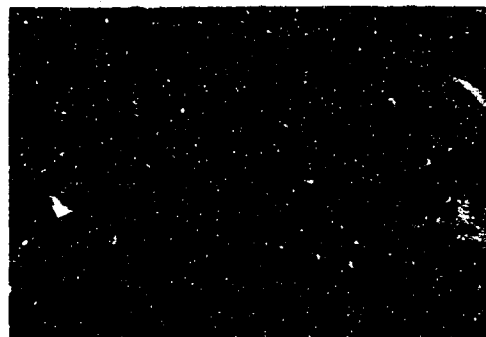


Figure 15.3. Brittle Rupture

The work consists of two main parts. The first part involves the characterization of some commonly used films in as much detail as is possible, and the second involves the correlation effort.

15.2 MATERIAL CHARACTERIZATION

Infrared Spectroscopy, Gel Permeation Chromatography (GPC) and X-ray Diffraction studies were performed in order to characterize two films: X-124 and StratoFilm.

The infrared spectrum for both films looks like that of a typical polyethylene (PE) as shown in Figure 15.4. The absorption band located above wave number 2900 cm^{-1} has to do with stretching (change in length) of C-H bonds. The bands at wave numbers 1470 cm^{-1} and 730 cm^{-1} have to do with the deformation of the CH angle in the HCH plane relative to the back bone (McCram et al, 1967).

The GPC showed some difference in the molecular weight distribution between the two films, as shown in Figure 15.5. X-124 was characterized as a typical PE while the StratoFilm, as blended PE.

The X-ray diffraction, Figure 15.6, shows that the thinner films have a preferred orientation in the machine direction (due to production). The main diffraction is done from (110) and (200) planes. In the unoriented material the (110) peak is much higher than the (200) peak, while in the oriented material they become almost equal. The preferred orientation in the machine direction was verified previously by mechanical tests.

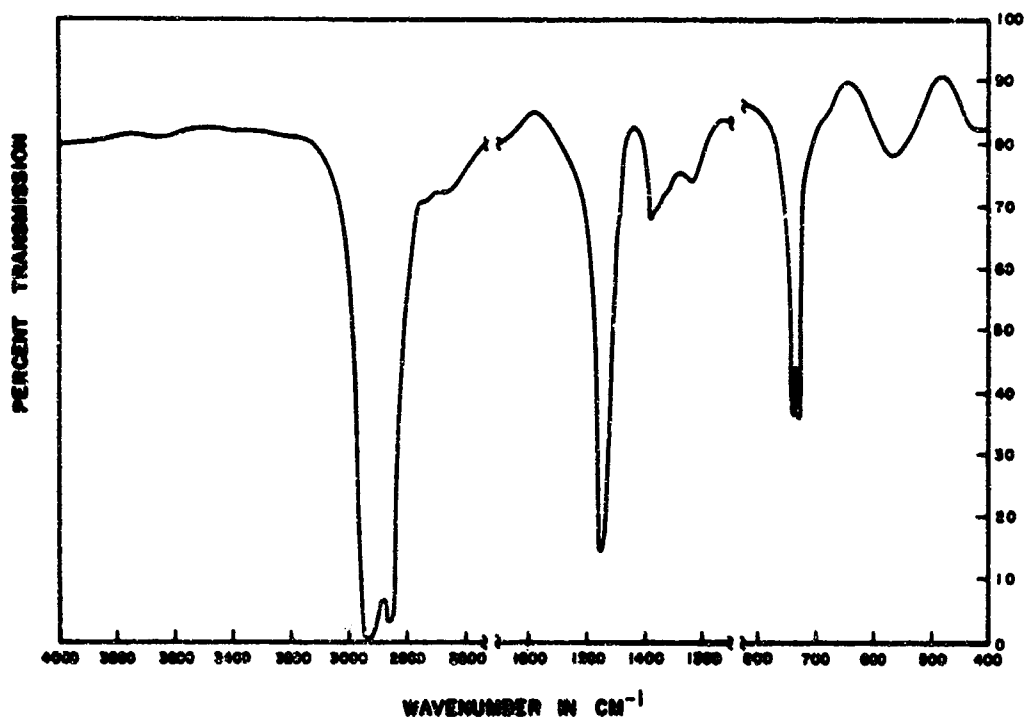


Figure 15.4 Infrared Spectrum of PE

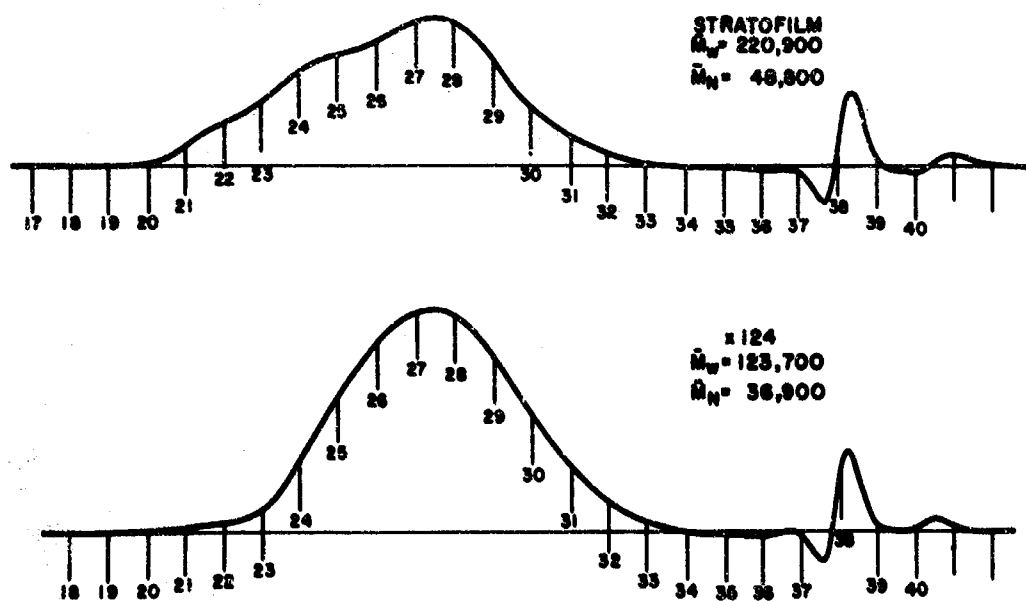


Figure 15.5 Molecular Weight Distribution of StratoFilm and X-124 from GPC

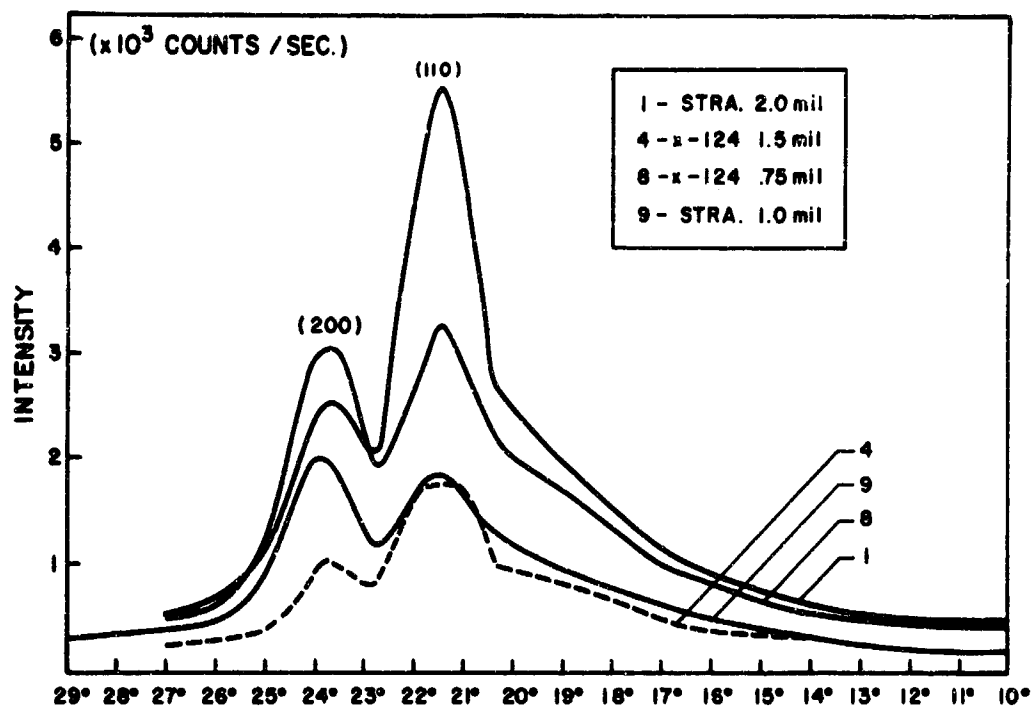


Figure 15.6. X-ray Diffraction (Through Direction)

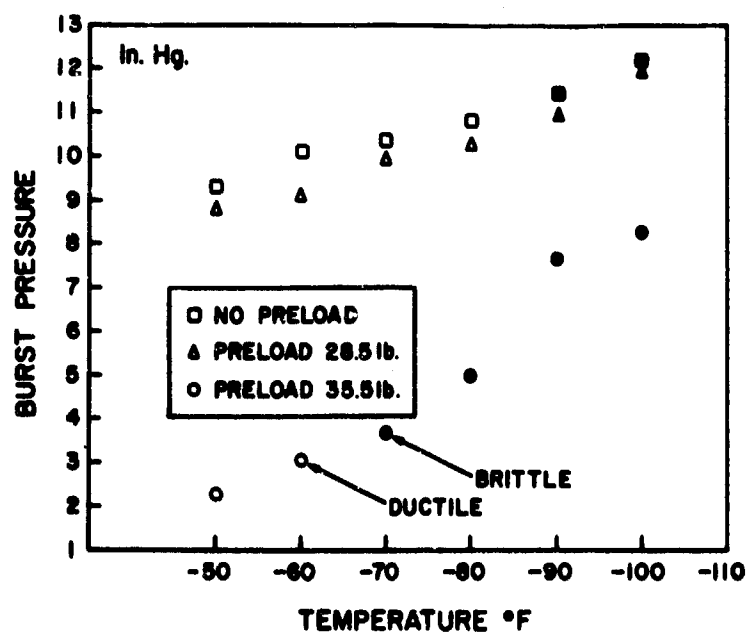


Figure 15.7 Burst Pressure of StratoFilm at Varying Preloads vs Burst Temperature (Preloading Time - 2 Hours)

15.3 MECHANICAL TESTING AND DISCUSSION

A set of cylinder burst tests were carried out at different temperatures at two preload stresses and without any preloading. The results are summarized in Figure 15.7. The lower preload stress did not induce a drop in the burst pressure while the higher stress did. This can possibly be explained in terms of an activation energy which is involved in the mechanism yielding the strength drop. This energy will be time and temperature dependent as is usually the case for visco-elastic materials. It can be expected that the lower load will yield a burst pressure drop after a loading time longer than the one used here.

In addition, Figure 15.7 shows at what temperature the nature of the rupture changes. For the higher stress used, the rupture transition occurs at -70°F ; shifting from -90°F for the low preloading stress case.

Comparing this result with an accepted real and loss moduli versus temperature characteristic of low density PE, Figure 15.8, it is found that the above-mentioned material failure transition occurs in the valley between the β and the γ transitions of the loss modulus curve. It is possible that if the temperature is higher than the temperature of the lowest point of the valley, that is closer to the β transition, this transition dominates the deformation of the material at that temperature, and would yield a ductile failure. At temperature below the valley temperature the γ transition is dominant, yielding the brittle pattern (McCram et al, 1967).

The location of the transitions on the temperature axis is not constant. The transition may be shifted due to many factors. It is a major purpose of this investigation to determine if orientation of the material results in such a shift.

In order to investigate this phenomenon, a series of Instron-constant rate

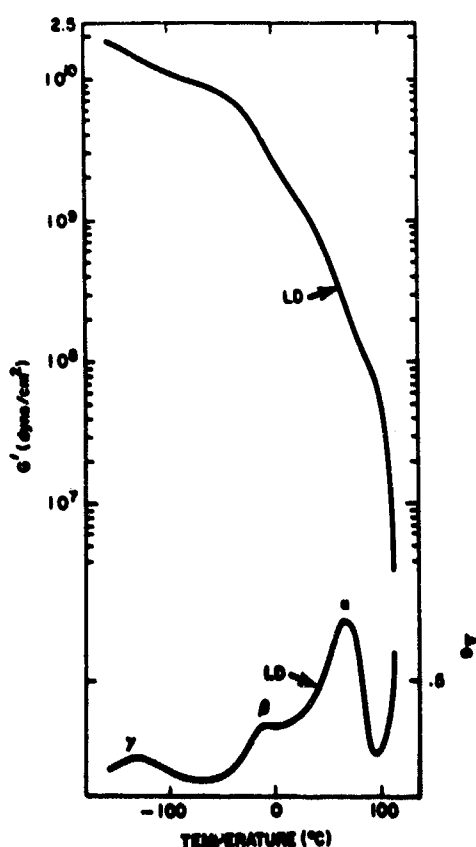


Figure 15.8. Real and Loss Moduli of PE. Δ_G = logarithmic decrement = $\ln \frac{A_n}{A_{n+1}}$, A_n , A_{n+1} are successive amplitudes

of stretching, creep, and mechanical-dynamical tests are planned. A typical output from an Instron tensile test is shown in Figure 15.9. The highest stress at the end of the elastic region is defined as the yield stress (σ_y) and the average stress after the yield is called the neck stress (σ_N).

In Figure 15.10, the yield stress and neck stress in the machine direction are given as a function of temperature. As the temperature is lowered, both σ_y and σ_N increase. The tests in the transverse direction give similar results.

In Figure 15.11, the curves of yield stress at different rates of grip separation are plotted vs temperature. At temperatures above -50°C , the lines appear to be parallel while below this temperature they start to deviate from each other.

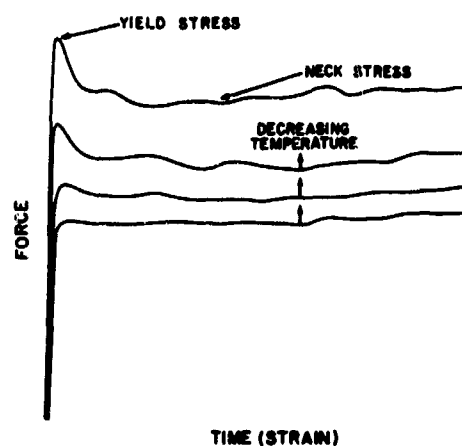


Figure 15.9. Typical Instron Test Output

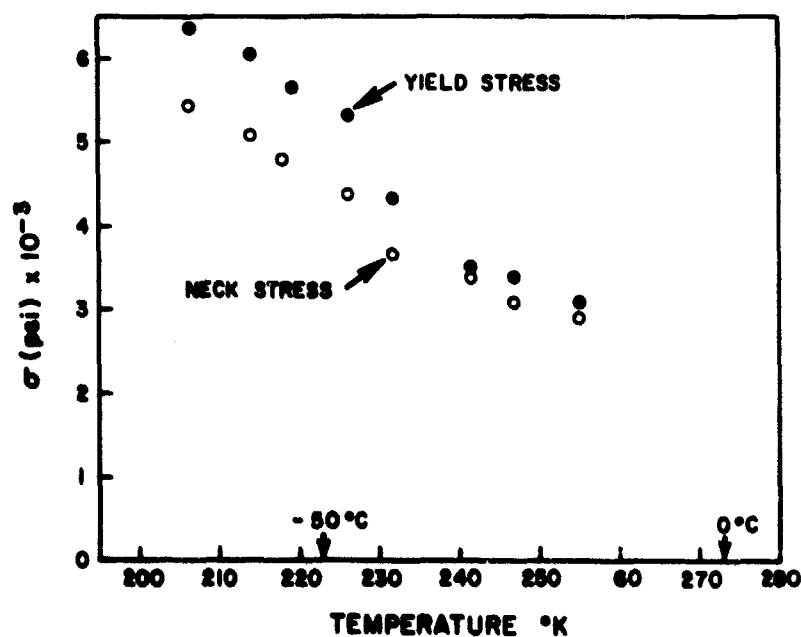


Figure 15.10. Yield and Neck Stresses vs Temperature

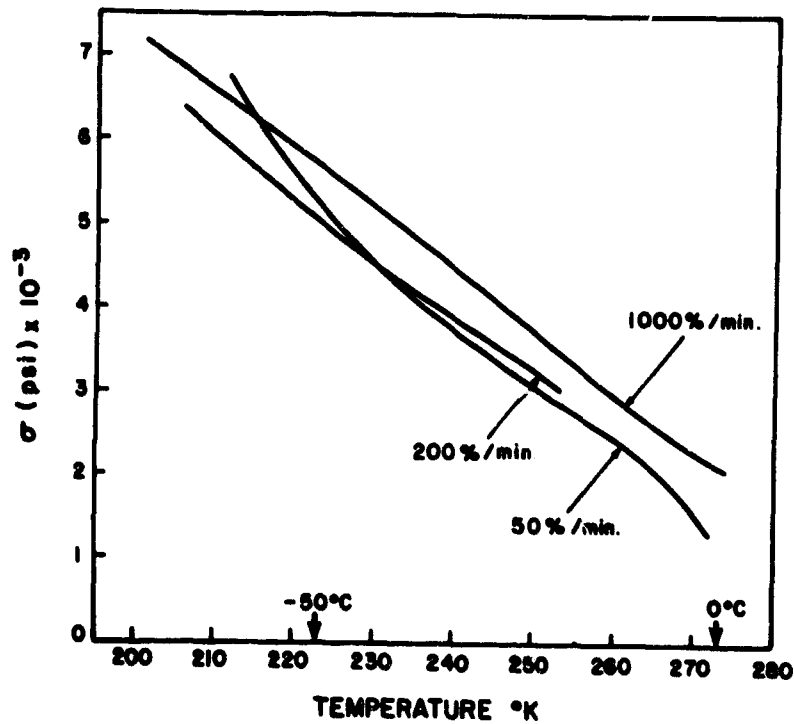


Figure 15. 11. Yield Stresses at Different Strain Rates vs Temperature

15.4 CONCLUSIONS

At the present time there are not enough data to suggest an interpretation which will tie together all of these observations. By repeating the Instron tests on preoriented material and by performing dynamical-mechanical tests in order to construct real and loss modulus curves, we hope to find a correlation between changes in material structure and the observed mechanical behavior.

A better understanding of the behavior of the film under the stresses applied and the temperatures experienced may be utilized to avoid premature failures by indicating possible improvements of the material or changes in design assumptions and launch procedures.

Acknowledgment

The author wishes to thank Dr. H. Alexander for his helpful advice and guidance in this work.

References

- Kerr, A.D. (1968) Balloon Strength in the Troposphere as Affected by Creep at Launch, Proc. AFCRL Fifth Scientific Balloon Symposium, Lewis A. Grass Editor, p. 7.
- Kerr, A.D. and Alexander, H. (1968) On the Cause of Failure of High Altitude Plastic Balloons, New York University Report #A-68-28 (also AFCRL-68-0486).
- McCram, N.G., Read, B.E. and Williams, G. (1967) Anelastic and Dielectric Effects in Polymeric Solids Wiley, pp. 353-376.
- Tanford, C. (1961) Physical Chemistry of Macromolecules Wiley, pp. 75-82.

Contents

16.1	Introduction	167
16.2	The e-Balloon	168
16.3	Advantages and Disadvantages	169
16.4	Lobe Design	170
16.5	Internal Pressures and Temperatures	171
16.6	Model Tests	171
16.7	Engineering Models	172
16.8	Flight Test Instruments	172
16.9	Flight Duration	173
16.10	Payload Potential	173
16.11	Operational Considerations	174
16.12	Future Improvements	175
16.13	Flight Tests	175

16. Development of the e-Balloon

J.H. Smalley
National Center for Atmospheric Research*
Boulder, Colorado

16.1 INTRODUCTION

The e-balloon is a particular form of a superpressure balloon. It is designed to make use of the well proven, but rather weak, lightweight films used in present day zero-pressure balloons. This report discusses the reasons for the particular form, the development of the first engineering models and future potential.

It will be seen in the following that a superpressure balloon can carry only light loads for a given size, so "Where does the advantage lie?" With each sunset, a zero-pressure balloon must expend ballast if it is to maintain altitude. With each succeeding sunset, ever larger amounts of ballast are needed. Thus, as duration requirements increase, the size of the balloon increases and the amounts of helium and ballast needed increase. Figure 16.1 shows a comparison of the costs of two balloon systems. One is a zero-pressure system using ballast to maintain altitude, the other is a superpressure system using the constant volume principle to maintain altitude. The figure shows that for a 50-lb payload to 130,000 ft, the duration for equal cost is between five and six days. Only balloon, helium

* The National Center for Atmospheric Research is sponsored by the National Science Foundation.

PRECEDING PAGE BLANK

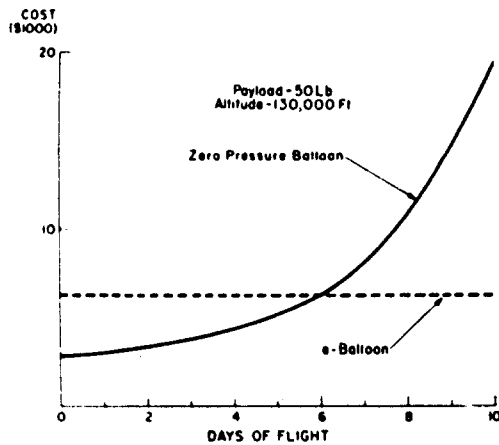


Figure 16.1. Comparison of the Non-Equal Costs for a Long Duration Flight

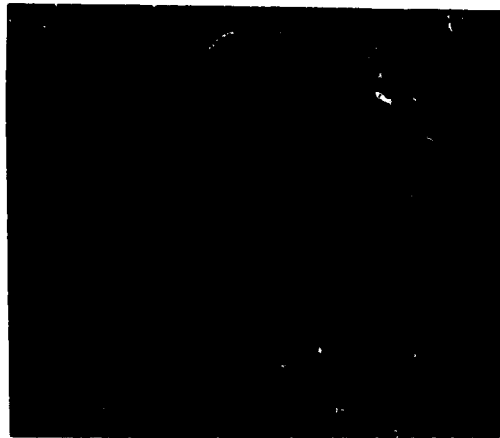


Figure 16.2. Photograph Showing the Top View of a Model e-Balloon

and ballast costs are considered. All other costs would be essentially the same for either system.

16.2 THE e-BALLOON

The e-balloon has the shape of an oblate spheroid. Figure 16.2 is a photograph showing the top view of a laboratory model, and Figure 16.3 is a sketch from the side. It is often remarked that the shape is that of a pumpkin or a tomato.

In principle, a balloon could be designed to have a very large internal pressure and yet have no circumferential stress. The shape of such a balloon in side view would be as in Figure 16.3. Classically, this curve is Euler's elastica.* In reality there must be a finite distance between meridional strength members, and a gas barrier is called upon to support the pressure. However, the usual polyethylene barrier material has low strength. In addition, the gas pressure in a superpressure balloon can be an order of magnitude greater than that in a natural shape balloon. By building in additional material so that the gores can bulge outward between tapes (Figure 16.4), the radius of curvature is reduced to a point where the film stresses are within allowable values. The curve taken by

*The equation of the elastica is $x^2 = \sin \varphi$, where x is the radial coordinate and φ is the angle of the tangent to the curve with respect to the horizontal. The ratio of height to radius is 1.1981. The ratio of the radius to gore length is 0.38138.

the load tapes is no longer the elastica, but differs only slightly from it. Only if the lobes of bulged material are complete semicircles is the elastica curve achieved.

The gores are necessarily cut from flat material. To achieve the design curvature, both meridional and circumferential, use is made of the extensibility of the film. The stress resulting from this known strain is used in deriving the lobe shape.

The result is a superpressure balloon made from extensible material, ellipsoidal in shape, nearly the elastica curve - thus the e-balloon.

16.3 ADVANTAGES AND DISADVANTAGES

It was anticipated that the major advantage of this particular design would be that it could be constructed and flown using the same state of the art as zero-pressure balloons. This included the same film, load tapes, sealing methods and end fittings. In part this has been borne out. The load tapes are heavier than usual but of the same materials. End fittings have proven to be more difficult to install because they are larger and heavier. Also, additional steps are needed to ensure gas integrity at the end fittings. Launch methods are the same as those of more usual balloons.

The major disadvantage is the large equatorial diameter. This results in a large number of heavy load tapes to support the bursting force which is proportional to the diameter squared. This is the price paid for omitting circumferential strength members.

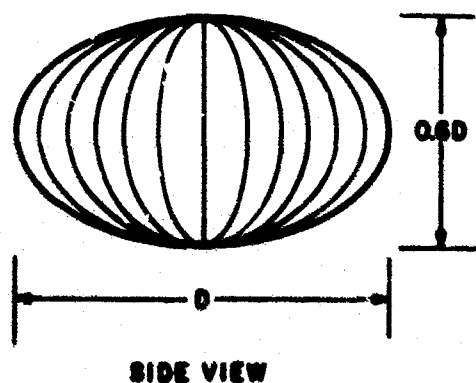


Figure 16.3. Sketch of the Side View of a Model e-Balloon

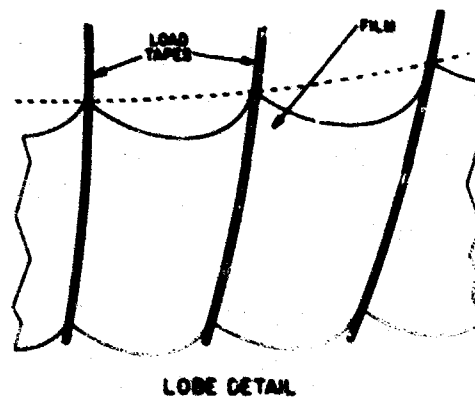


Figure 16.4. Sketch Showing the Lobe Detail of a Portion of an e-Balloon

16.4 LOBE DESIGN

The e-balloon is designed in much the same way as a natural shape balloon. Rather than assume a symmetric body of revolution, the design is confined to a single lobe. All lobes are, of course, identical. A short length of lobe is assumed to be similar to a portion of a torus. As in a torus, the meridional stress (σ_m) is constant. The lobe radius (R_c) is

$$R_c = 2\sigma_m / (p + w_f \sin \theta)$$

where

p = local pressure

w_f = film weight per unit area

θ = angle of the load tape tangent with respect to the vertical, measured in a plane containing the load tape and the balloon centerline

The circumferential stress (σ_c) along the centerline of the lobe is

$$\sigma_c = R_c (p + w_f \sin \theta + \theta' \sigma_m)$$

where θ' is the derivative of θ with respect to the gore length coordinate.

The angular width of the lobe (lobe angle) is a function of R_c and the local spacing of the tapes. Summing the forces on an element, the width of one lobe and of infinitesimal length yields differential equations which are numerically integrated for θ , load tape tension, balloon volume and balloon weight. Results show that σ_c and R_c are nearly constant. The lobe angle is zero at nadir and zenith, and reaches a maximum at the equator. Because the e-balloons for practical loads at high altitudes are large, σ_c is almost twice σ_m (as in a cylinder). Thus, σ_m must be chosen such that σ_c does not exceed design values for the gas barrier material used.

The final gore pattern, cut from unstressed material, has its dimensions reduced from the design values such that the necessary strain to reach the desired shape will result in the desired stresses. Because of the long flight duration, creep of the balloon materials is an important consideration.

16.5 INTERNAL PRESSURES AND TEMPERATURES

These conditions are all important to the design. At zero supertemperature, the superpressure determines the amount of gas in the balloon. This value must be large enough so that in the coldest part of the night, the internal pressure is still positive. The minimum amount of gas is thus determined. Additional gas extends the time before leaks cause the pressure to drop to zero. There is a practical limit to the amount of gas that can be carried to make up losses. Table 16.1 shows an example of the volume increase as superpressure increases.

Table 16.1. Effect of Superpressure on e-Balloon Size

Superpressure (percent)	Volume (MCF)
5	4.6
8	5.3
12	6.6
15	8.1
20	12.1

Altitude = 125,000 feet

Suspended Load = 250 pounds

Supertemperature = 10%

During the hottest part of the day, the combination of superpressure and supertemperature determine the maximum stresses encountered.

Unfortunately, there are very little data available on maximum and minimum supertemperatures developed. Preliminary calculations utilizing the best known material thermal properties indicated that satisfactory design values would be 12 percent superpressure and 10 percent supertemperature based on ambient pressure and temperature. At 125,000 ft, for example, 10 percent supertemperature is 44°F and 12 percent superpressure will initially accommodate 47°F subtemperature assuming no change in volume.

16.6 MODEL TESTS

First, a rather crude feasibility model was made simply to give a gross check on design parameters. Then two models were built by Winzen Research, Inc. A photograph of one is shown in Figure 16.2. They were extensively leak-tested and given a careful visual examination. In no case were leaks found in the seams.

Instead, the only leaks were where the gas barrier had been opened for an attachment, for example, the inflation tube. As a result, a design principle has been adopted that the gas barrier shall not be broken for attachments of any kind. (An exception has been made for the destruct panel "buttons".) Pressurizing the model to bursting resulted in a rip in one gore lying along the equator of the gore - the anticipated maximum stress point.

16.7 ENGINEERING MODELS

A contract was entered into with Winzen Research, Inc. of Minneapolis, Minn., for the two laboratory models mentioned above and for two engineering evaluation balloons. A third engineering evaluation balloon was purchased from Raven Industries, Inc., Sioux Falls, S.D.

A minimum payload sufficient for instrumentation and an altitude high enough to provide realistic conditions were chosen for the basic design. Preliminary calculations indicated that the balloon would not be overly large if the design condition was 50 lb at 125,000 ft. Estimates of minimum and maximum internal temperatures indicated that the design conditions should be 12 percent superpressure and 10 percent supertemperature. A gas barrier of 0.9 mil polyethylene was chosen. The nominal stresses of 4 lb/ft meridionally and 8 lb/ft circumferentially are, respectively, $1/9$ and $1/4$ breaking strength at room temperature and one-half those values at ambient flight temperature. A load tape with a nominal breaking strength of 1,200 lb was used. At maximum pressure conditions this is a safety factor of two. The constructed weight was 1,210 lb.

16.8 FLIGHT TEST INSTRUMENTS

The payload for the engineering flights consisted solely of balloon control and balloon evaluation equipment. Twelve channels of information were transmitted with a GHOST-type system. They were:

- (1) Internal pressure (2 channels)
- (2) Internal temperature (2 channels)
- (3) Air temperature
- (4) Battery temperature
- (5) Balloon film temperature
- (6) Balloon film strain (3 channels)
- (7) Balloon load tape strain
- (8) Altitude

A locating beacon also carried altitude information. A receiver was used to turn the beacon on and off, and to command cut-down. An E-cell timer was carried to terminate the flight. If the balloon settled below 75,000 ft, a barometric switch would also terminate the flight. Sun angle for tracking purposes used a separate, solar-powered transmitter. The telemetry transmitter with the major sensors, the receiver, the timer, the beacon and the 75,000-ft switch were all separately powered with batteries. To protect the batteries, they were carried in a dewar.

16.9 FLIGHT DURATION

The long term potential for flight duration is very difficult to forecast. No amount of analysis will appreciably improve this situation. Actual flights will be needed to arrive at a duration figure which can be stated with confidence.

As an upper limit, a pessimistic estimate of duration due to permeability of the film to the lifting gas yields a number in excess of 10 years. Obviously, the lifetime will be a function of other things such as material degradation and manufacturing imperfections. In the short term, material degradation will not be serious. The major concern, then, is small leaks in the balloon. The importance of great care in manufacturing, particularly in the area of the end fittings, cannot be over emphasized.

16.10 PAYLOAD POTENTIAL

The first flight model carried 50 lb. Fifty pounds is a minimum payload since it is needed for balloon controls and performance monitors. The following table lists balloon volumes needed to carry heavier payloads.

Table 16.2. e-Balloon Payload Potential

Suspended Load (lb)	Volume (MCF)		
	Altitude (ft)		
	120,000	125,000	130,000
100	3.1	4.9	8.0
250	4.3	6.5	10.4
500	6.2	9.2	13.9
1000	9.7	13.9	20.5

The load given must include balloon controls. Prices of such balloons will vary from 10 percent to 50 percent more than zero-pressure balloons of comparable volumes.

16.11 OPERATIONAL CONSIDERATIONS

Operational problems with a superpressure balloon vary considerably, depending upon the flight duration and flight location desired. Some of the problems are new and may require extensive development to implement.

(1) Political - The first consideration is political. Flights confined to the United States are governed by the usual FAA regulations. Flights outside of the U. S. A. come under the ICAO Convention of 1944 to which most of the nations of the world are signatories. The essence of the Convention as far as unmanned aircraft (that is, balloons) are concerned is that no nation shall overfly another without permission. This has recently been modified to the extent that flights in the tropics are permissible. Permission for flights in the Southern Hemisphere has been obtained by NCAR for the GHOST program.

(2) Launching - So far, e-balloons have been launched with the same techniques as used for zero pressure balloons. There is no indication that techniques will have to be modified.

(3) Tracking - The GHOST balloons are tracked by a combination of dead reckoning and measurement of the local sun angle. Data are transmitted at 15 MHz at a very slow bit rate. Receiving stations are scattered throughout the Southern Hemisphere. The system is successful and well proven, and could be used on any superpressure balloon. Obviously the network of receiving stations could prove costly.

A test flight launched from Christchurch in April 1970, utilizing Nimbus D and the IRLS system, has proven successful. Certainly a satellite system offers many advantages and should be developed for tracking in the future.

(4) Trajectory - Experience at mid-levels has shown that, in time, a superpressure balloon will depart from the launch latitude by 30 degrees or more. This can occur in a single orbit of the earth. In the tropics, the trajectories are less variable. Based on upper atmosphere wind data, a more constant latitude trajectory for flights above 120,000 ft would be expected. Of course, during the semi-annual wind reversal all trajectories are very erratic.

(5) Data Recovery - There are two types of data recovery to be considered. If the payload is expendable, then data recovery by a GHOST-type system, by storage and dump upon command or, most desirably, by satellite can be used.

Commonly it will be necessary to recover the payload. A flight of a few days duration made during "turn around" (that is, usually early May or late September) will often remain over land, and payload recovery is routine. However, long durations will almost certainly mean overwater flights. One possible operational plan would involve a launch from South America. The balloon would be permitted to orbit the earth one or more times. An airborne task force stationed in South America would intercept the balloon as it passes over the continent. The flight would be terminated by command, and the payload recovered either by aerial snatch or by surface travel to the ground impact location. It is apparent that the probability of complete orbits would have to be high and that the operation would be expensive.

Another possible operational plan would involve launch either in Europe or Japan and recovery in North America.

16.12 FUTURE IMPROVEMENTS

The item most in need of improvement is the load tape. In the first engineering models, the specific strength (ratio of breaking strength to unit weight) is approximately 70,000 ft. Glass filaments have a specific strength of about 250,000 ft. A glass filament load tape would be a great improvement. Either the tapes could be lighter or the safety factor increased. The weights of load tapes in the engineering balloons are 41 percent of the balloon weight. The sensitivity of balloon volume to balloon weight is indicated in Table 16.2. Fewer tapes would be reflected in simpler end fitting assembly.

A second value of glass load tapes is the higher modulus of elasticity. Dwyer* indicates that a polyethylene seam is weakened when placed under strain along the seam. A higher modulus load tape would reduce seam strain and therefore increase its strength.

16.13 FLIGHT TESTS

Two flights have been attempted at this time. The first was a ground abort not associated with the balloon. The second lasted 16 hours and then was terminated for an unknown reason. Also, float altitude was about 7 percent below the expected value. A third balloon is on hand and will be flown in the near future.

* Private communication.

Acknowledgment

The effort reported herein was supported in part by the National Aeronautics and Space Administration.

Contents

17.1	Introduction	178
17.2	The Experimental Facilities and the Philosophy of Testing	178
17.3	The Testing Procedures and the Results of Their Application to Some Plastic Films	182
17.4	Recommendations for a Revision of the Balloon Specification MIL-P-4640A	193
17.5	Conclusions and Future Activities	194

17. The Stevens Institute Laboratory for Balloon Technology and Some of Its Contributions to Balloon Research

H. Alexander
Stevens Institute of Technology
Hoboken, New Jersey

Abstract

In September, 1968, the Laboratory for Balloon Technology was established at Stevens Institute of Technology under the sponsorship of the Air Force Cambridge Research Laboratories. This report contains a complete description of the facilities of the laboratory and explains the philosophy of investigation of balloon materials and structures that inspired its establishment. This philosophy can be summed up as one of using testing methods that simulate situations that a balloon experiences during launch, ascent and flight at altitude. The highlights of a number of investigations performed in the Laboratory during the past year and one-half are discussed, and the contribution of each of these results towards the furtherance of knowledge in balloon technology is pointed out. These investigations include: an evaluation of Union Carbide Perflex B100, the establishment of a failure criterion for biaxially stressed polyethylene balloon film, an evaluation of Winzen StratoFilm K (polyurethane), an investigation into the failure characteristics of thin polyethylene films (less than 1 mil), the establishment of a preliminary revision of the Specifications MIL-P-4640A, and an investigation into the effect of high-temperature strain history on the ductile-brittle failure transition in polyethylene film at tropopause temperatures.

17.1 INTRODUCTION

The rash of balloon failures in the early 1960's, a matter of prime concern to the Air Force, supplied the impetus for a research program directed toward defining the failure mechanisms in polyethylene balloons, the causes thereof, and possible remedial action. Consequently in the search for possible causes of failure in balloons, a number of investigations were initiated in February 1965 at New York University under contract to AFCRL (Kerr, 1967 and 1968). During the course of these investigations, a philosophy of testing evolved. This philosophy can be summed up as one of using testing methods that simulate situations that a balloon experiences during launch, ascent and flight at altitude.

In September, 1968 this project, which was under the directorship of Dr. A. D. Kerr at New York University, was transferred to Stevens Institute of Technology when the author took up his post there as Assistant Professor of Mechanical Engineering. At that time the Laboratory for Balloon Technology was established under the directorship of the author. The experimental facilities of the laboratory have been specifically designed to reflect the above-mentioned testing philosophy. This report contains a description of the facilities of the laboratory, and explains this philosophy of investigation of balloon materials through a description of the highlights of a number of investigations performed in the Laboratory during the past year and one-half.

17.2 THE EXPERIMENTAL FACILITIES AND THE PHILOSOPHY OF TESTING

The various examinations of the properties of balloon film can be considered as divided into two phases: launch-temperature tests, and investigations into the strength of balloon films at low temperatures. During the launch-temperature testing performed at New York University, it was established that uniaxial testing alone was not a valid strength indicator for biaxially stressed balloon films because of the large deformations and the accompanying deformational anisotropy occurring in the uniaxial test. In view of this observation, it was decided to use a pressurized and axially-loaded cylindrical tube of film as a standard test specimen (Kerr, 1966).

With the launch-temperature testing of cylindrical tubes in mind, the laboratory has been equipped with a launch-temperature testing and conditioning room which has heavily insulated walls and ceiling, no windows and a raised, insulated floor. The combined air conditioning-heating system is capable of maintaining the temperature of the room at any value between 45° and 130°F regardless of the outside conditions. The temperature control is accomplished by constantly circulating

the room air in a closed system. The controller operates differential steam and cold-water system valves that feed the heating or cooling agent into heat exchanger coils. The temperature can be maintained at the desired temperature $\pm 1^{\circ}\text{F}$. Figure 17.1 shows a series of cylinder conditioning and failure tests being performed in this room.

Although it has been recognized that a valid strength indication cannot be obtained from uniaxial tests alone, this by no means implies that uniaxial tests have no value. In fact, the opposite conclusion has been arrived at. By putting the various film-testing procedures in their proper perspective concerning their relevance to actual situations that a balloon experiences during launch, ascent and flight at altitude, it has been determined that uniaxial testing can be quite valuable.

Consequently, uniaxial testing has become a standard test method of the laboratory not as an ultimate strength indicator, but as a means of comparison for various films (or various batches of the same film) and as a means of determining the degree of biaxial orientation of the tested films.

Uniaxial creep testing is performed in the above-described controlled temperature room at launch temperatures. Testing requiring cold temperature (below 40°F) is done in a small cold chamber that uses liquid nitrogen as its coolant. Testing in this chamber (shown in Figure 17.2) can be performed at any temperature between -300°F and room temperature with an accuracy of $\pm 2^{\circ}\text{F}$.

Uniaxial, constant-strain-rate testing is accomplished with a table model, Instron tensile-testing machine equipped with a controlled temperature chamber that can provide a testing environment at any



Figure 17.1. Cylinder Pressurization Tests in Progress



Figure 17.2. Small Cold Chamber for Uniaxial Creep Testing



A



B

Figure 17.3. A. Instron Tensile Tester with Temperature Chamber
B. Close-Up of Sample in Temperature Chamber

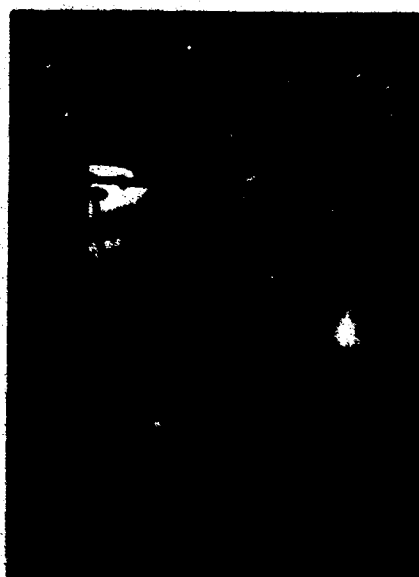


Figure 17.4. Cold Temperature Testing of Cylindrical Samples



Figure 17.5. Torsional Fatigue Testing of a Cylindrical Sample

temperature between -109° and $+350^{\circ}\text{F} \pm 1^{\circ}\text{F}$. The heating is accomplished with electric heating coils over which the chamber air is constantly circulated. The cooling is done with liquid carbon dioxide supplied from the main line that runs through the laboratory for cold-chamber use. The CO_2 line is fed from a remote location where twelve, 50-lb tanks of CO_2 are stored. The tanks are used in banks of 6, leaving a spare bank always in reserve. A test being performed in this constant strain rate apparatus is shown in Figure 17.3.

The low-temperature testing of biaxially-loaded cylinder samples is performed in a CO_2 cooled chamber, custom built for the laboratory by Associated Testing Company of Wayne, New Jersey. This chamber is equipped with a frame for hanging samples and a slit in the floor used for connection of the axial load weights. The pressurization is accomplished through a 5-ft copper tubing coiled within the chamber to assure that the pressurizing gas is at the chamber temperature. Experiments are regularly performed at any temperature down to $-109^{\circ}\text{F} \pm 1/4^{\circ}\text{F}$, with CO_2 as a coolant. An optional, liquid-nitrogen injection system allows the possibility of testing at temperatures down to -130°F , the limiting temperature of the controller. Figure 17.4 is a photograph of a typical test in progress in this chamber.

Since it was expected that the twisting that a balloon experiences during ascent may have a detrimental effect on the burst strength of some balloon films at cold temperatures, a torsional fatigue-testing machine was constructed. This machine

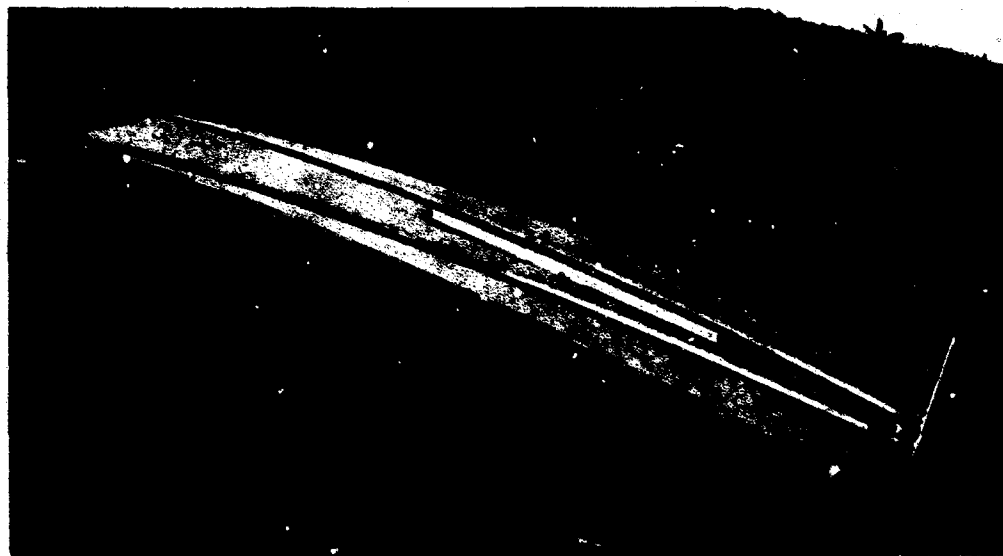


Figure 17.6. Apex Gore Panel Simulator

was used in checking for strength degradation due to twisting in the Arctic Wind Tunnel of the U.S. Army Natick Laboratories, Natick, Massachusetts. The results of those tests will be discussed in the next section. Figure 17.5 shows a sample being tested in this apparatus. It is planned to incorporate a twisting apparatus into the Associated Testing Chamber sometime in the near future, thus allowing all biaxial cold-chamber testing to be done in this one chamber.

The loading in the apex region, $0' \leq \text{radius} \leq 30'$, of a fully tailored balloon is thought to be most critical to its successful flight. It is hoped that from an analysis of the loading and deformation response in this critical region of the balloon, using the apex gore panel simulator (Figure 17.6) there will emerge a better understanding of the failure process of balloons and a practical design tool that can be used to help in avoiding future, premature, balloon failures.

17.3 THE TESTING PROCEDURES AND THE RESULTS OF THEIR APPLICATION TO SOME PLASTIC FILMS

Each of the specialized pieces of equipment described above has been specifically included in this laboratory so that a series of tests could be developed that would quickly indicate the acceptability of any plastic film for balloon use. Those tests and the results of their application to a number of past, present and future candidate balloon films are the subject of this section.

17.3.1 A Failure Stress Criterion for Balloon Film

One of the most important problems in balloon design and analysis is to determine the mechanical conditions that cause a balloon film to undergo large deformations or to fail by fracture. Present methods of uniaxial, constant strain-rate testing are inadequate for this purpose because they do not take creep effects into account, nor do they relate to a multiaxial state of stress. Both of these considerations appear to be of importance in actual failures of balloon film materials. Therefore, a research program was initiated to establish a "failure" stress relevant to balloon films. A "safe" stress chart that can be easily used in balloon design and analysis was then constructed.

At balloon launch, as well as at very high altitudes, the film is quite ductile. Consequently, large plastic deformations occur before actual rupture. This investigation was devoted to the establishment of "safe" stress levels for launch temperatures and high altitude temperatures where the failure is of a ductile type. It was decided to consider a safe stress level as one at which the material sample which creeps will not fail within a specified time interval. Tests were conducted with inflated cylinders. It was found that within a narrow range of stresses the

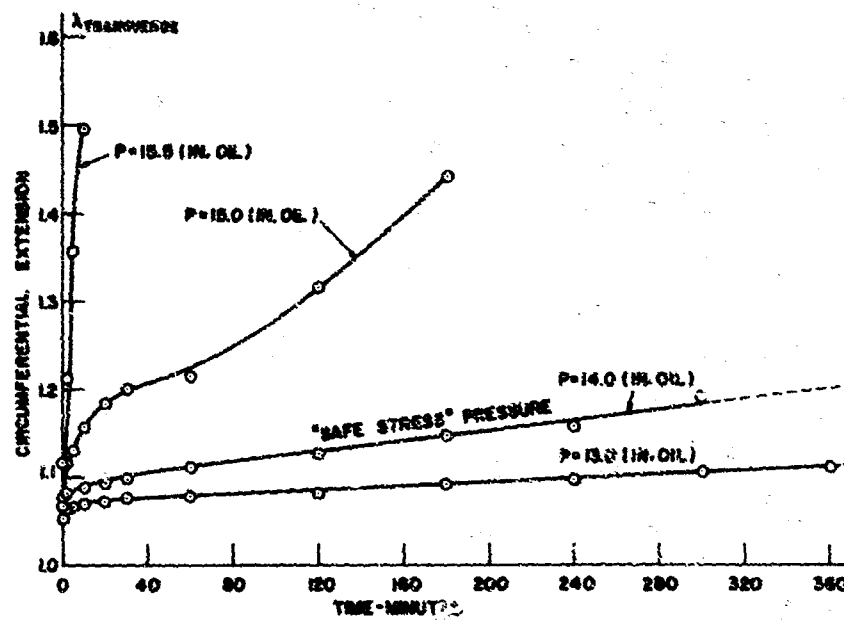


Figure 17.7. Creep Curves for 2 mil StratoFilm Samples with Cylinder Axis Parallel to Machine Direction. 0 lb. axial load. Temperature, 78°F

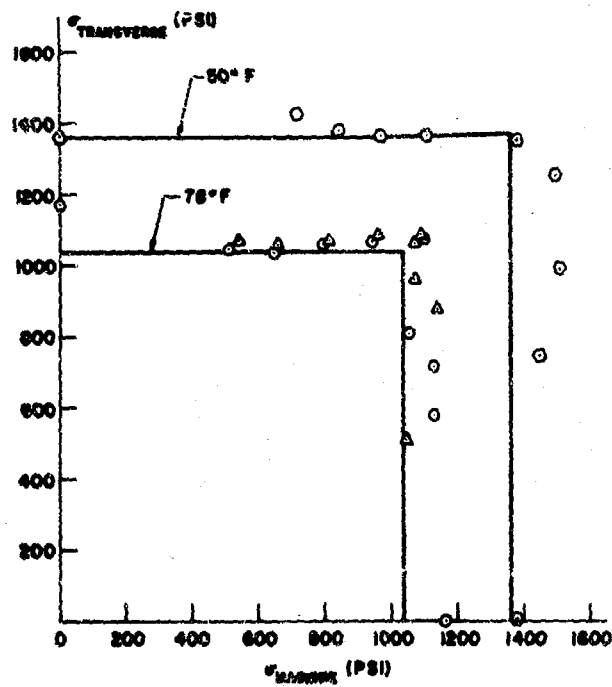


Figure 17.8. Safe Stress Chart for 2 mil StratoFilm at 78°F and 50°F

deformation vs time curves change from those of uniform creep to curves which show a highly accelerated rate of deformation. This behavior is shown in Figure 17.7, a set of creep curves for 2.0 mil StratoFilm samples with the cylinder axis parallel to the machine direction. It was therefore decided to consider the stress value at which this abrupt transition takes place as the "failure" stress.

Using this new definition of failure, which is felt to be relevant for balloon films, the results of tests at various biaxial stress ratios can be presented by plotting the limiting curve in a system of rectangular coordinates in which the coordinates represent the machine and transverse direction stresses. Figure 17.8 is a "safe" stress chart for 2.0 mil StratoFilm at various launch and high altitude type temperatures. The failure stress seems to be almost entirely independent of the biaxial stress ratio.

If for each balloon film a "safe" stress chart such as is presented in Figure 17.8 is produced for a complete range of flight temperatures, and temperature is

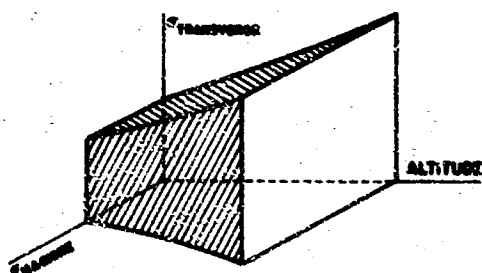


Figure 17.9. Proposed Failure Surface for Balloon Design and Analysis

correlated to altitude through a knowledge of atmospheric conditions, the "safe" stress characteristics can be presented as a surface in stress - altitude space (Figure 17.9). In order to analyze proposed balloon designs, the balloon designer need only choose a point on the balloon skin that he might consider critical and plot its stress vs altitude characteristics as a curve in stress - altitude space. As long as this curve is inside the limiting surface of "safe" stresses, it is reasonable to assume that the design is safe. Further details on this failure stress criterion can be found in a report by Alexander and Murthy (1968).

17.3.2 Cold Temperature Testing

In a search for causes of failure of plastic balloons, an experiment which simulates the stresses and temperatures in part of a balloon during launch and ascent was conceived, and then tests using a number of balloon films were conducted (Kerr and Alexander (1968)). In the test, a film cylinder is preloaded axially at a temperature encountered at launch, for some time interval, then it is cooled to a typical tropopause temperature and pressurized until it bursts. It was found that because of the preloading, the strength of the samples deteriorates; the degree of deterioration, varying from one film to another, being dependent upon preload time, temperature and stress; and that the failure type changes from ductile to brittle.

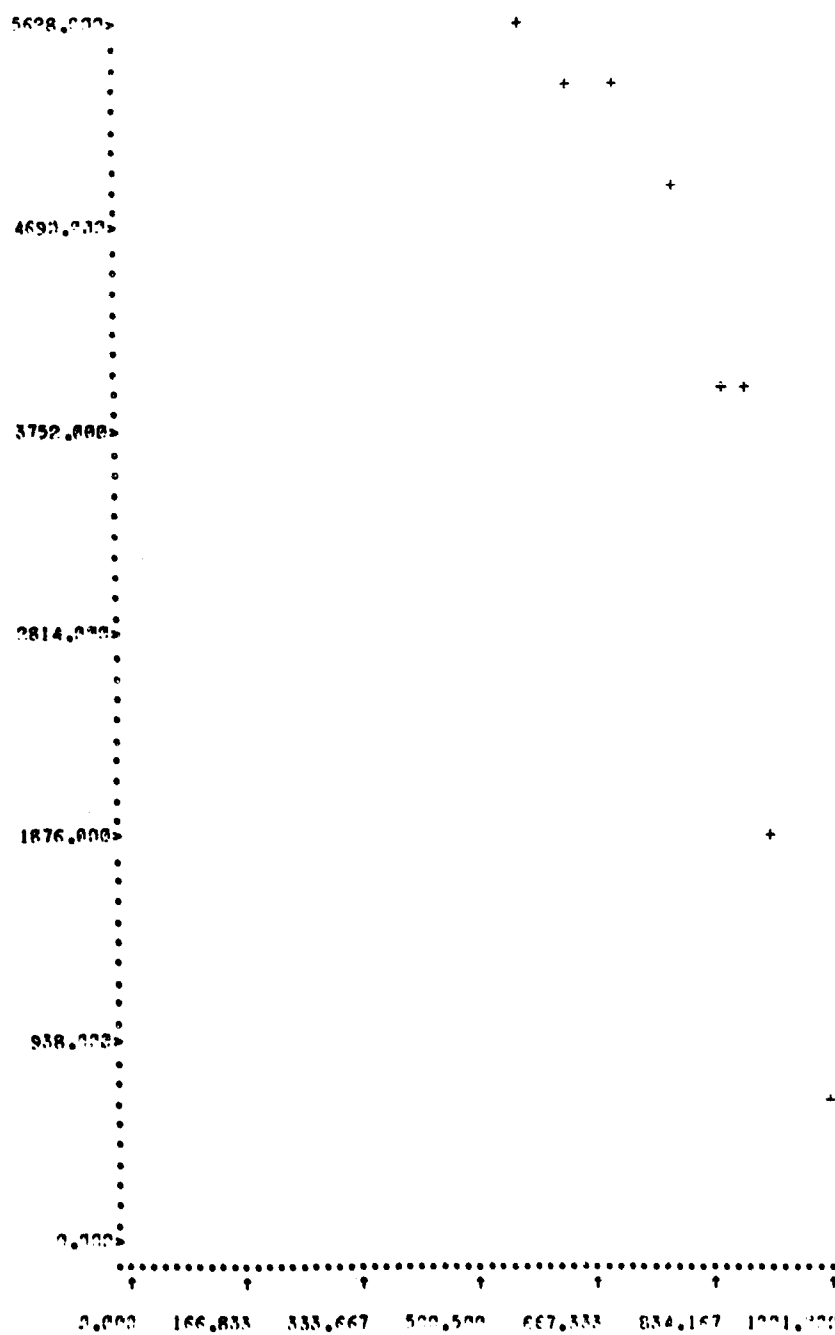


Figure 17.10. Burst Stress vs Preload Stress for 2 mil StratoFilm. Preloaded at 110°F for 120 minutes. Burst at -70°F after cooling for 15 minutes

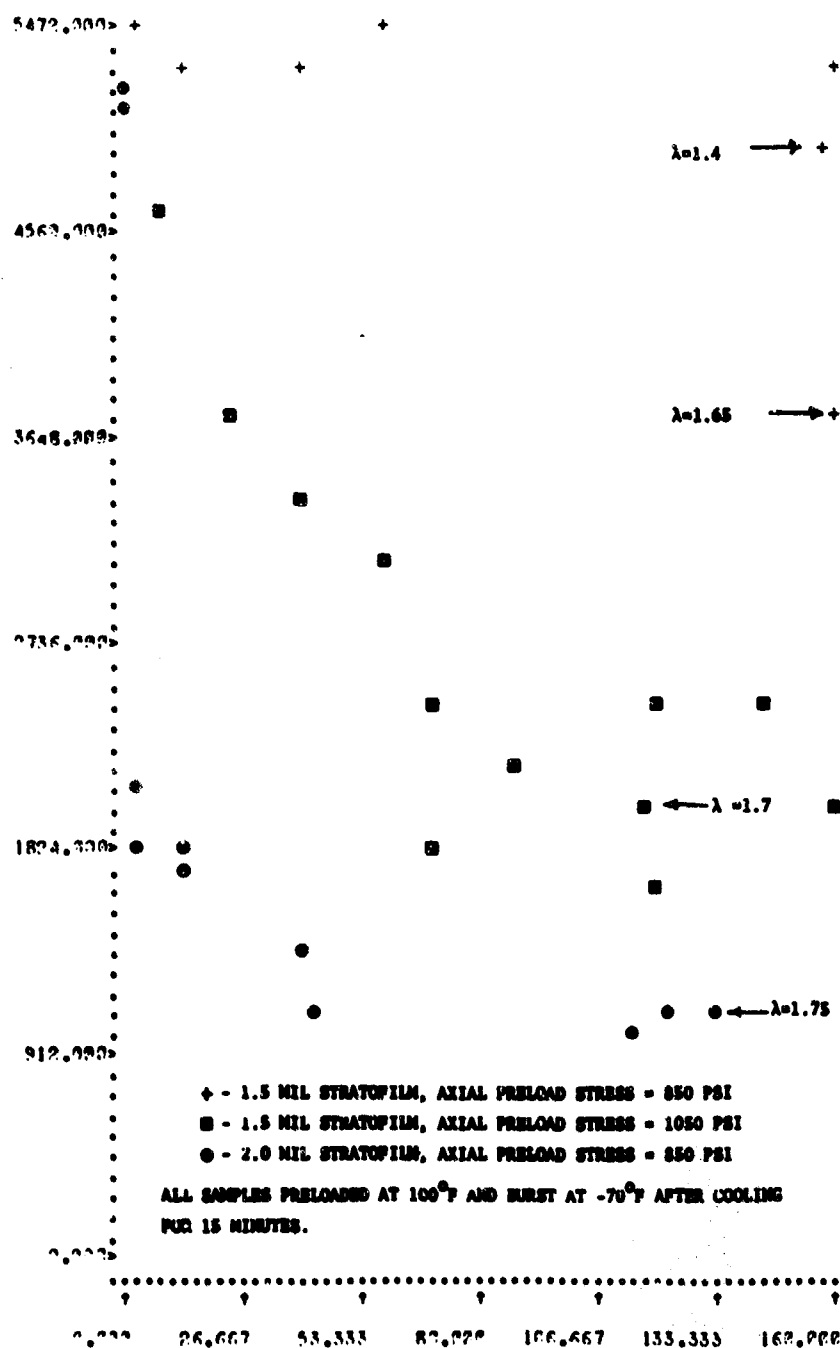


Figure 17.11. Effect of Various Preloading Stresses and Strains on the Cold Temperature Strength Deterioration of StratoFilm

Since this effect was first noted, more than 700 tests have been performed with many different film samples in an attempt to explain this phenomenon and to correlate the results with actual balloon experience. Since each test is represented by 23 separate pieces of information, it has been found to be quite helpful to do the sorting and searching for possible correlations using a high-speed digital computer. A program has been written, and is in operation on the Stevens Institute PDP-10 machine, which sorts the data on command and graphs the sorted data sets as desired. A few examples of the results of this investigation are shown in Figures 17.10 and 17.11. Figure 17.10 shows a graph of burst stress vs preload stress for 2 mil StratoFilm that has been preloaded at 110°F for 120 minutes and burst at -70°F after being allowed to cool for 15 minutes. The burst stress is found to decrease as the preload stress is increased, going to zero at the failure stress established in the report by Alexander and Murthy (1968). This curve can be used to put a realistic limit on the meridional loading allowed in a balloon for this film.

In an effort to discover if the uniaxial creep strains at preloading are the determining factor in this burst strength degradation, Figure 17.11 was prepared. Here it is found that when 1.5 mil StratoFilm is preloaded so that its creep strains are similar to those of the 2-mil StratoFilm, the burst stress deterioration of the two films is similar, whereas when they are preloaded so that their preload stresses are similar the burst stress deterioration characteristics are quite different. The physical explanation for this phenomenon is the subject of an investigation by Weissman (1970). However, from an engineering point of view, it can be immediately applied in a determination of the suitability of plastic films for balloon use.

Using the torsional fatigue-testing machine, it was found that those samples of polyethylene film that had deteriorated burst-strengths due to preloading tended to crack during twisting at cold temperatures, while those that had not been preloaded remained ductile even after twisting for 2 hours at -70°F . This result seems to further demonstrate the brittle character of the preloaded samples. Recently, preliminary torsion tests on mylar-scrim samples indicated that these materials are extremely sensitive to twisting at cold temperatures. Many samples shattered at a very low stress level after twisting for



Figure 17.12. Shattered Mylar-Scrim Sample of Film Used in the CRISP Balloon Series

as little as 20 minutes at -70°F . A typical, failed-sample is shown in Figure 17.12. Recent failures in the CRISP balloon series may be traced to this effect.

17.3.3 The Failure Characteristics of Very Thin Polyethylene Films

The requirement of attaining very high float altitudes has caused balloon film manufacturers to produce very thin films ($\approx 0.3 \rightarrow 0.5$ mils). Samples from two different batches of one such film, 0.35 mil StratoFilm, were submitted to the Laboratory by Winzen Research, Inc. for evaluation as a balloon film. To our knowledge, this film is extruded from the same resin as the presently used StratoFilm of other thicknesses. For convenience, the samples will be referred to as coming from batches 1 (old) and 2 (new). The samples were provided in layflat tubes with seals on either side. The film thickness, according to measurements made by Winzen Research, varied from 0.35 to 0.41 mil.

The film was tested uniaxially in strips cut from the tubes in both the machine and transverse directions, and biaxially, by inflating the tubes. Using the failure stress criterion of Alexander and Murthy (1968), it was found that the failure stress was identical to that of 2 mil StratoFilm. The ultimate rupture, however, was found to be different in batch 1 than it was in batch 2. Batch 2 exhibited extensive necking and thinning as with 2 mil film, while batch 1 ruptured at relatively small strains with the appearance of small holes. Low temperature tests at -70°F yielded similar results. Batch 2 reacted very much the way 2 mil StratoFilm reacts, while batch 1 samples ruptured at relatively small strains with the opening of small holes at a stress level a little lower than the batch 2 film, ≈ 4300 psi. No evidence of brittleness was observed in either film.

Uniaxial tests were performed on the Instron tensile tester with 1 inch wide by 2 inch long samples at 20 inches per minute. The results of these tests, presented in Figure 17.13 indicated that the batch 1 film is highly oriented in the machine direction while the batch 2 film has orientation that is closer to the equibiaxial orientation of the 2 mil StratoFilm, giving it much greater ultimate elongation.

These findings seem to be in accord with an extensive study conducted by General Mills, Inc. (1951) in which they were able to obtain from the extruder detailed information regarding the manufacturing of their tested films. They found that "films extruded with nearly equal elongation in both machine and transverse directions showed that the strength of the film was 30 to 75 percent stronger and tougher than previous standard films."

For a high altitude balloon, these properties possessed by equally oriented films -- greater ultimate strength and ability to withstand large elongations -- could make the difference between successful and unsuccessful flights. It is

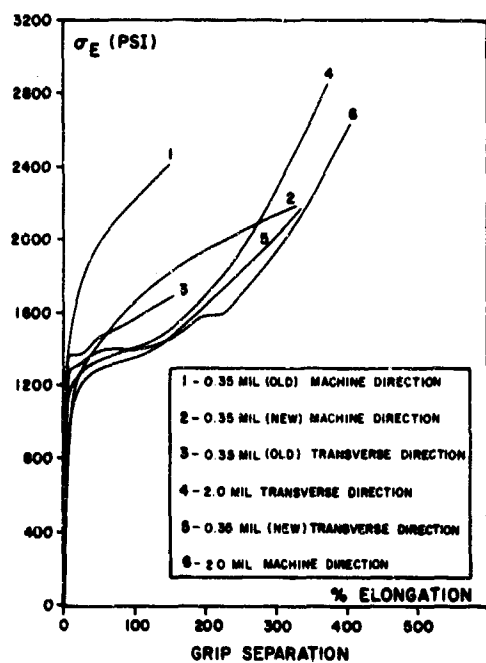


Figure 17.13. Uniaxial Stress-Strain Responses of StratoFilm

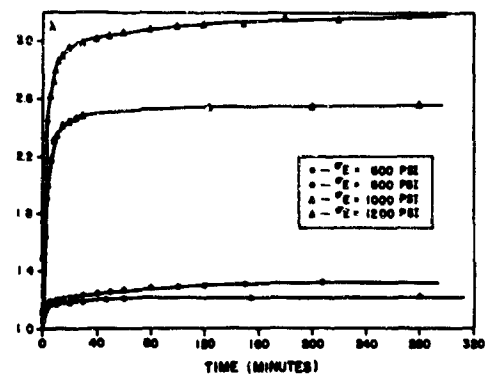


Figure 17.14. Uniaxial Creep of StratoFilm K, Machine direction

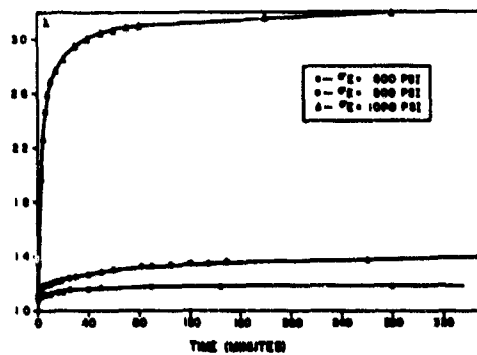


Figure 17.15. Uniaxial Creep of StratoFilm K, Transverse direction

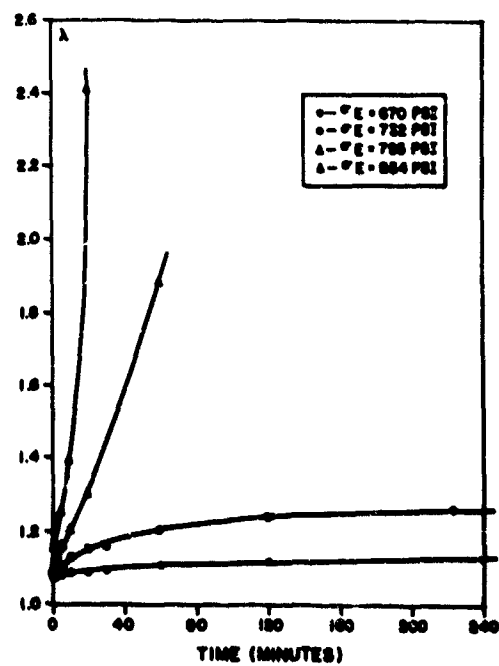


Figure 17.16. Biaxial Creep of StratoFilm K

recommended that the manufacturers of balloon films should make every effort to avoid the production of highly uniaxially oriented films, even though this might be difficult to accomplish when producing very thin films.

17.3.4 Evaluation of New Plastic Films for Use in High Altitude Balloons

17.3.4.1 STRATOFILM K

StratoFilm K is a film submitted by Winzen Research, Inc. for evaluation as a balloon film. It is extruded from a polyurethane elastomer which is marketed under the trade name, Estane, by the B. F. Goodrich Chemical Company. Estane is a partially crystalline material that has a fairly prominent viscoelastic, rubber-like response, but it exhibits definite yielding very much like that of polyethylene. Its response to loading is a cross between that of a rubber and a thermoplastic.

The film was provided in 15-inch, layflat tubes sealed along both edges. It was tested uniaxially in strips cut from the tubes in both the machine and transverse directions, and biaxially, by inflating the tubes. Due to the prominent viscoelastic response of the material, the room temperature properties were determined through creep testing. The results of the uniaxial tests are shown in Figures 17.14 and 17.15. Fairly low stress values (1200 psi) cause very large strains. In fact, there is a definite yield between 800 and 1000 psi as is indicated by the sudden increase in the long time elongation. However, increased stress levels result in a strain hardening with an ultimate tensile strength of 5,000 psi. The biaxial tests, performed at various constant inflation pressures with no axial load, yielded little additional information due to the occurrence of tensile instabilities at rather low nominal stress values. Figure 17.16 contains these curves which are very similar to the hypothetical curves presented by Kerr (1965). The biaxial tests yielded no additional information about ultimate strength, but they did indicate that the seals were at least as strong as the material.

Low temperature tests were performed in the Arctic Wind Tunnel of the U. S. Army Natick Laboratories at -70°F . The cylinders were inflated after being allowed to cool for 15 minutes. Although the burst strength was quite high, 7500 psi, the material was extremely brittle. It is completely unworkable at tropopause temperatures.

The conclusion drawn from these various tests is that this material, due to its high elongation at fairly low stresses at high temperatures, is unsuitable for use in standard design, natural shape balloons. It may be useful in the production of an expandable-type balloon as long as extension or flexing is not required at tropopause temperatures.

17.3.4.2 PERFLEX B-100

Tests were performed on samples of a new Union Carbide plastic film (trade name - Perfex B-100) in order to determine its suitability for use in the production of high altitude balloons (Alexander and Weissman, 1969). Both 2.0 and 1.0 mil samples were tested in order to determine their mechanical properties, both time independent and time dependent, at both launch and tropopause temperatures. In addition, the suitability of various types of seals was also investigated in these two critical temperature ranges.

The films were tested uniaxially at room temperature (75°F) using strips cut in both the machine and transverse directions. The tests were run on the Instron tensile testing machine at three rates of elongation and in a step-loading procedure by hanging dead load weights. The experimental points obtained by the latter method are long time equilibrium deformations. Figures 17.17, 17.18, 17.19 and 17.20 contain the engineering stress (force/original cross-sectional area) versus λ (deformed length/original length) characteristics obtained from these various tests. The results of these tests indicate that this material is almost equibiaxially oriented, is not highly dependent upon strain rate (exhibits very little creep) and is much stronger than presently used balloon films.

Cylinder inflation tests at launch temperatures indicated that the films could withstand up to 6000 psi circumferential engineering stress with a circumferential extension of ≈ 1.35 at which time a creep tensile instability occurred. This type of instability is a function of the geometry of the cylinder as well as the material properties. It is quite probable that the films can withstand even higher stresses under biaxial loading. It was noted however, that all failures initiated at a crease in the tube.

Cold temperature cylinder inflation tests, in the Arctic Wind Tunnel of the U.S. Army Natick Laboratories at -70°F, both with and without high temperature preloading, indicated failures for the 2 mil film at 14,200 psi and at 18,000 psi for the 1 mil film without preloading. After preloading with approximately 1,600 psi axial stress at 110°F for 100 minutes, the failure stress at -70°F was found to drop to 12,800 psi for the 2 mil film and to 13,960 psi for the 1 mil film. All failures were very ductile with fairly large elongation, indicating absolutely no cold brittleness problem.

These films were sealed by Winzen Research using a band-type sealer with overlay strips, by Raven Industries using a hot-jet sealer with no additional material in the seal area, and by Union Carbide using a Weldotron stationary type sealer. Biaxial tests of these seals indicated that neither the Winzen or the Raven seals had better than 50 percent material strength. The Union Carbide, Weldotron seals were found to sometimes have 100 percent material strength.

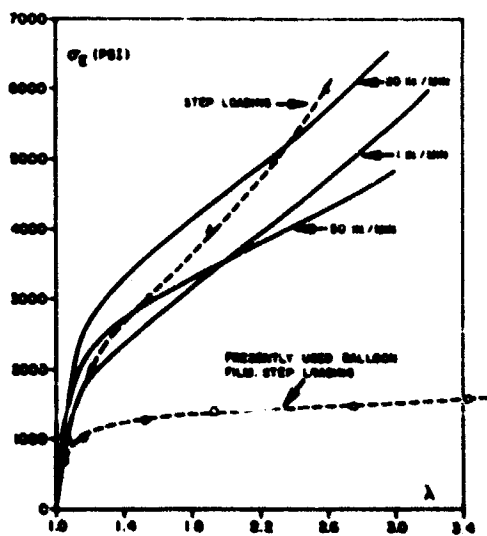


Figure 17.17. 2 mil Perflex B-100 in Uniaxial Extension. Machine direction. (Instron tests are on 4 inch samples)

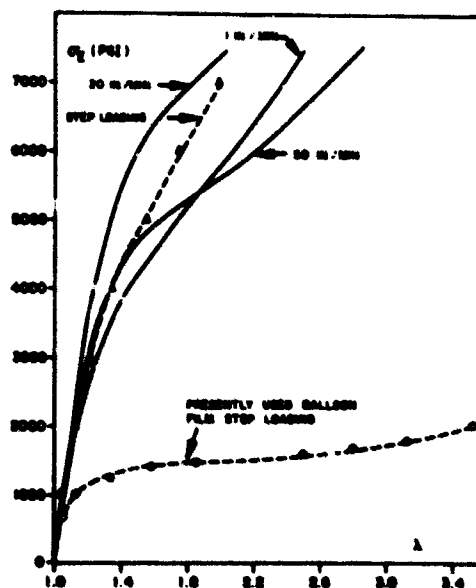


Figure 17.18. 2 mil Perflex B-100 in Uniaxial Extension. Transverse direction. (Instron tests are on 4 inch samples)

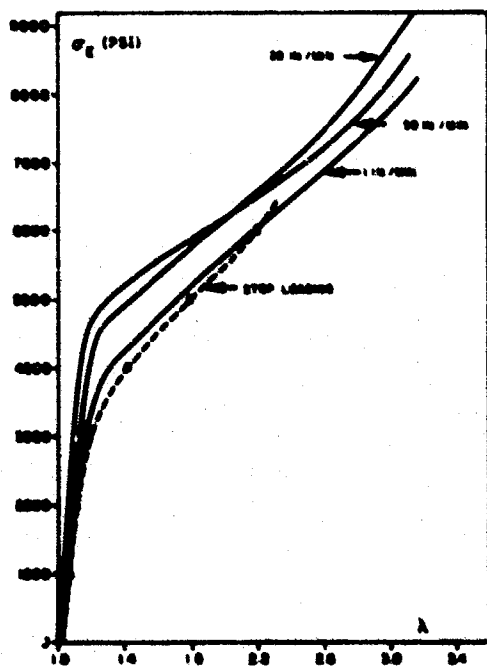


Figure 17.19. 1 mil Perflex B-100 in Uniaxial Extension. Transverse direction. (Instron tests are on 4 inch samples)

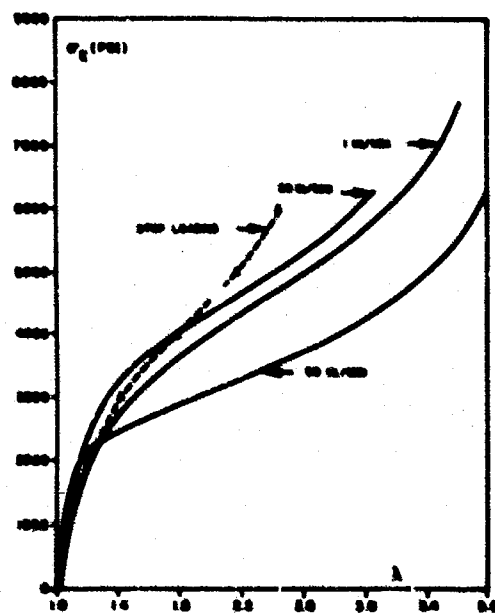


Figure 17.20. 1 mil Perflex B-100 in Uniaxial Extension. Transverse direction. (Instron tests are on 4 inch samples)

The results of this investigation have indicated that this new film, under all types of testing conditions is at least 3-1/2 times as strong as presently used balloon films with greater ductility at low temperatures. All indications are that it will be an excellent balloon barrier material. If the Weldotron type seal can be made in a continuous seal, the one remaining obstacle to the immediate use of this film in balloon production will have been solved.

17.4 RECOMMENDATIONS FOR A REVISION OF THE BALLOON SPECIFICATIONS MIL-P-4640A

The present balloon specifications of the U.S. Air Force MIL-P-4640A (USAF) are based on studies conducted by General Mills, Inc. for the U.S. Air Force during the early nineteen fifties. These specifications were written essentially for a specific film, DFD 5500, which at that time was the predominant material used in the fabrication of balloons.

The recent development and use of new balloon films, the large number of balloon failures in the early 1960's (all of barrier materials which passed the prescribed tests), and the ever increasing demand for larger balloons, necessitate the complete revision of that part of the balloon specifications which deals with the strength of the balloon films and seals. Based on the findings referred to in this report, as well as upon the finding of relevant studies conducted before by others, a revised test program has been recommended. It is expected that these recommendations will initiate a discussion among film producers, balloon manufacturers, balloon users, mechanics and materials scientists, and the AFCRL and, thus, create a rational basis for the planned revisions.

It has been recommended that, in order to qualify as a balloon material, a submitted film should be subjected, at least, to the following tests:

- (1) Uniaxial tensile tests at room temperature in both the machine and transverse directions, as is described in Section 17.3.3 above, in order to determine the degree of uniaxial orientation, and the ultimate strength and elongation properties.
- (2) Biaxial tests at launch temperatures in order to establish a "safe" stress as is described in Section 17.3.1 above.
- (3) Biaxial tests at tropopause temperatures in order to establish the burst strength and the degree of deterioration accomplished by uniaxial, launch temperature preloading.
- (4) Mutilation and fatigue tests at tropopause temperatures in order to determine the ability of both preloaded and non-preloaded samples to withstand cold temperature flexing.

(5) A series of resin characterization tests, such as gel permeation chromatography, to establish molecular weight density distribution, infra-red absorption testing to establish molecular composition, and differential thermal analysis to obtain melting point data. (These test results, upon reproduction at a future date on different batches of film, will assure that the same basic resin is used for all).

The complete details of these recommendations can be found in a report by Kerr and Alexander (to be published as a Stevens Institute Report).

17.5 CONCLUSIONS AND FUTURE ACTIVITIES

As was pointed out in the introduction of this report, the Laboratory for Balloon Technology was established for the purpose of having available to the AFCRL, and the balloon community at large, a research and testing facility specifically designed to aid in the qualification of materials as balloon films and in the design and analysis of balloon structures. The initial establishment period has been described in this report. It is now felt that the methods of attack of the Laboratory to various balloon problems have been proven out by the experiences described above. It is hoped that in the years to come, the Laboratory for Balloon Technology of Stevens Institute will make many more contributions to balloon research and development. It is planned in the near future to broaden the activities of the Laboratory to include suggested improvements in scrim-reinforced films, and investigations into the feasibility of high-altitude expandable balloon systems, as well as to continue the important task of establishing qualification criteria for various balloon barrier materials.

Acknowledgments

This report would not be complete without acknowledging the people who have aided in establishing the Laboratory. At the top of this list should be the project director of the initiating project, Dr. A. D. Kerr, and the Air Force Cambridge Research Laboratories; particularly Mr. J. Dwyer whose intellectual and physical support made this project possible.

Mr. D. Weissman of Stevens Institute has spent many hours in the gathering and construction of the component parts of the Laboratory. He also either personally performed or supervised the performance of many of the reported experiments. His aid has been invaluable.

References

- Alexander, H. and Murthy, G.K.N. (1968) A Failure Stress Criterion for a Polyethylene Balloon Film, NYU-AA-68-18 (AFCRL-69-0103).
- Alexander, H. and Weissmann, D. (1969) An Evaluation of a New Plastic Film for Use in High Altitude Balloons, Stevens Institute Report ME-RT-69011 (AFCRL-69-0441).
- General Mills, Inc., Aeronautical Research Laboratories (1951) Evaluation of Materials for Balloon Fabrication, Report No. C/R 5159, December, p. 3.
- Kerr, A.D. (1965) On Creep Failure of Balloons, Proc. AFCRL Scientific Balloon Workshop, AFCRL-66-309, p. 31.
- Kerr, A.D. (1966) Experimental Study of Balloon Material Failures, Proc. Fourth AFCRL Scientific Balloon Symposium, AFCRL-67-0075, p. 39.
- Kerr, A.D. (1967) Stress and Deformation Analysis of Flexible Balloons, Final Report on Contract No. AF19(628)-4990, NYU-AA-67-105 (AFCRL-67-0345).
- Kerr, A.D. (1968) Stress and Deformation Analysis of Flexible Balloons, Final Report on Contract No. F19628-67-C-0241, NYU-AA-68-41 (AFCRL-68-0612).
- Kerr, A.D. and Alexander, H. (1968) On a Cause of Failure of High Altitude Plastic Balloons, NYU-AA-68-28 (AFCRL-68-0486).
- Kerr, A.D. and Alexander, H., Recommendations for a Revision of the Balloon Specifications MIL-P-4640A(USAF) (to be published as a Stevens Institute Report).
- Weissmann, D. (1970) The Influences of Changes of Material Structure on the Failure of Polyethylene Balloon Film, 6th AFCRL Scientific Balloon Symposium.

Contents

18.1	Introduction	197
18.2	Lift Tables	198
18.3	Launch Operations	203
18.4	Climatology	210
18.5	Rigging	213
18.6	Flight Operations	219
18.7	Balloon Design	222

18. A Listing of Computer Programs Available at NCAR for Solving Recurring Problems in Ballooning

J.M. Angevine
National Center for Atmospheric Research
Boulder, Colorado

18.1 INTRODUCTION

As one of the primary missions under its contract with the National Science Foundation, NCAR is involved in numerical modeling of the general circulation of the atmosphere with the goal of improving long-range weather forecasting. To handle the number of calculations necessary for even a modest model, and to make the calculations in a reasonable length of time, NCAR has installed in its Mesa Laboratory a Control Data Co. 6600 computer. The computer is managed by the NCAR Computing Facility which also maintains a competent staff of programmers. This Facility and its staff are available for the use of other NCAR groups in addition to the scientists working on General Circulation. For the convenience of the NCAR staff in the 30th street building, which is across town from the Mesa Laboratory, a General Electric time-sharing terminal is available with access to the Mark II system.

The Balloon Facility has built up a group of programs for these computers to solve problems which are likely to recur in the Ballooning Industry. This paper contains a very brief outline of some of these programs. They are available on request, on an "as-is" basis, or to fulfill legitimate scientific ballooning needs;

PRECEDING PAGE BLANK

they can be run on the NCAR computers by a Balloon Facility staff member on request to the Manager of the Facility. The programming language for the 6600 is Fortran IV with some extensions and modifications. The Mark II System uses Fortran IV.

It is beyond the scope of this paper to give derivations or equations. The emphasis is on results to be expected from the programs rather than on their mathematical basis, but wherever possible references are given for use in researching the background of any program more deeply. In addition, the programmer's name is included with each description. Any of these people will be happy to discuss the programs if more information is needed.

18.2 LIFT TABLES

18.2.1 Helium Lift

Programs KELCYL and KBOTTL

18.2.1.1 PROGRAMMER

Jack M. Angevine.

18.2.1.2 DESCRIPTION

This group of programs was originated to up-date the available information on the amount of lift obtained from a given pressurized cylinder when the gas is released starting from a known temperature and pressure, and stopping at another temperature and pressure.

Helium properties over the appropriate ranges of temperature and pressure were calculated from three separate sources (Keesom, 1942; Miller et al, 1961; and Akin, 1950), with three separate programs, and the results compared with published tables from four sources (Mann, 1962b; Miller et al, 1961; Simmons, 1960; and Wilson, 1960). The conclusion of this investigation was that Keesom's Helium, (1942), is the most reliable theoretical work and that of the experimental work of Miller et al (1961) at the Bureau of Mines provides the best data available. These two sources correlated very closely. Since the empirical equation presented by Miller is simple and easy to work with, it was chosen for the program.

The change in internal size of a cylinder because of changes in temperature is determined by multiplying the coefficient of thermal expansion by the dimension and the temperature difference.

Elastic deformation of the cylinder caused by internal pressure is found by using standard stress equations (Roark, 1965), and combining these with stress-strain relations involving Young's Modulus and Poisson's ratio.

The resulting tables show the amount of lift available in the cylinder at specific temperatures and pressures. Generally the cylinder is not completely drained and the quantity remaining in the cylinder at the new temperature and pressure must be subtracted from the original amount to calculate the lift available from the amount expelled.

Methods of determining temperatures and pressures of the gas in the cylinder are beyond the scope of this paper. All amounts calculated by these methods assume accurate knowledge of temperature and pressure and that they are at steady state.

18.2.1.3 DATA REQUIRED

There are two main programs available to generate lift tables. They differ only in the method used to determine wall thickness of the cylinder. In Program KELCYL the wall thickness is calculated in the program from the weight and length given. In Program KBOTTL, wall thickness is an input quantity and bottle weight and length are included for reference only.

The data required are as shown in Table 18.1.

Table 18.1. Data Required for Lift Programs

Identification of cylinder or bottle - up to 50 characters
Material identification - up to 50 characters
Water volume - cubic feet for KELCYL, cubic inches for KBOTTL
Outside diameter - inches
Length - feet
Cylinder weight - pounds
Wall thickness - inches, for KBOTTL only
Young's Modulus
Coefficient of thermal expansion
Poisson's ratio
Base temperature for thermal expansion
Molecular weight of air
Molecular weight of helium
Compressibility of air at inflation conditions
Compressibility of helium at inflation conditions

18.2.1.4 RESULTS

Tables may be generated in several formats and with various units depending on the needs of the user. The options available are listed in Table 18.2. A choice of one must be made at the time the program is submitted.

Table 18.2. Options for Table Format and Units

Medium
Film, 35 mm cathode ray tube photographs
Paper, 11 x 15 in.
Both film and paper
Pressures
Initial
Total number
Interval
Pressure Units
PSIG
PSIA
Atmospheres
Temperatures
Initial
Total number
Interval
Temperature Units
Deg. Rankine
Deg. Fahrenheit
Deg. Kelvin
Deg. Celsius
Number of columns and number of lines on each page (maximum of 6 columns and 50 lines)
Units of Lift
Pounds
Grams

The first page of results lists the input quantities and also shows several values calculated for reference including ratio of diameter to wall thickness, water volume converted to other units and helium properties at standard conditions, Table 18.3. Succeeding pages consist of the tables in the format and units called for, Figure 18.1. Note that there are no lines separating columns and that one column of pressures is associated with the next column containing lift. To avoid confusion, lines should be drawn on the tables to separate adjoining unrelated columns.

Table 18.3. First Page of Results

Table for lift of helium in average tube from 38 tube Trailer No. BT 1	
Nominal Properties	
Tube Weight	785 pounds
Wall Thickness	.329 inches
Tube Outside Diameter	9.63 inches
Dia/Wall Ratio	29.2
Tube Length	24.00 feet
Tube Water Volume	17514.66 cubic in.
Tube Water Volume	10.1358 cubic ft.
Steel Intermediate Manganese	
Young's Modulus	(1041 + .2 SI)
Linear Thermal Expansion	29300000 psi
Poisson's Ratio	.00000628 in/in/F
	.288
Helium Properties at 70 deg F and 1 Atmosphere	
Unit Lift	6.2421083 lb/lb HE
Specific Volume	96.672394 Ft ³ /lb
Compressibility	1.0004890

		TEMPERATURE		50.0 DEG C									
PRESS	LIFT	PRESS	LIFT	PRESS	LIFT	PRESS	LIFT	PRESS	LIFT	PRESS	LIFT	PRESS	LIFT
PSIG	LB	PSIG	LB	PSIG	LB	PSIG	LB	PSIG	LB	PSIG	LB	PSIG	LB
0	.04	500	21.04	1000	42.04	1500	62.04	2000	82.04	2500	102.04	3000	122.04
10	1.07	510	22.07	1010	43.07	1510	63.07	2010	83.07	2510	103.07	3010	123.07
20	1.90	520	23.09	1020	44.09	1520	64.09	2020	84.09	2520	104.09	3020	124.09
30	1.63	530	24.11	1030	45.11	1530	65.11	2030	85.11	2530	105.11	3030	125.11
40	2.36	540	25.00	1040	46.10	1540	66.10	2040	86.10	2540	106.10	3040	126.10
50	2.79	550	26.01	1050	47.00	1550	67.00	2050	87.00	2550	107.00	3050	127.00
60	3.22	560	27.03	1060	48.00	1560	68.00	2060	88.00	2560	108.00	3060	128.00
70	3.65	570	28.04	1070	49.00	1570	69.00	2070	89.00	2570	109.00	3070	129.00
80	4.08	580	29.06	1080	50.00	1580	70.00	2080	90.00	2580	110.00	3080	130.00
90	4.51	590	30.07	1090	51.00	1590	71.00	2090	91.00	2590	111.00	3090	131.00
100	4.94	600	31.09	1100	52.00	1600	72.00	2100	92.00	2600	112.00	3100	132.00
110	5.37	610	32.10	1110	53.00	1610	73.00	2110	93.00	2610	113.00	3110	133.00
120	5.80	620	33.12	1120	54.00	1620	74.00	2120	94.00	2620	114.00	3120	134.00
130	6.23	630	34.13	1130	55.00	1630	75.00	2130	95.00	2630	115.00	3130	135.00
140	6.66	640	35.15	1140	56.00	1640	76.00	2140	96.00	2640	116.00	3140	136.00
150	7.09	650	36.16	1150	57.00	1650	77.00	2150	97.00	2650	117.00	3150	137.00
160	7.52	660	37.18	1160	58.00	1660	78.00	2160	98.00	2660	118.00	3160	138.00
170	7.95	670	38.19	1170	59.00	1670	79.00	2170	99.00	2670	119.00	3170	139.00
180	8.38	680	39.21	1180	60.00	1680	80.00	2180	100.00	2680	120.00	3180	140.00
190	8.81	690	40.22	1190	61.00	1690	81.00	2190	101.00	2690	121.00	3190	141.00
200	9.24	700	41.24	1200	62.00	1700	82.00	2200	102.00	2700	122.00	3200	142.00
210	9.67	710	42.25	1210	63.00	1710	83.00	2210	103.00	2710	123.00	3210	143.00
220	10.10	720	43.27	1220	64.00	1720	84.00	2220	104.00	2720	124.00	3220	144.00
230	10.53	730	44.28	1230	65.00	1730	85.00	2230	105.00	2730	125.00	3230	145.00
240	10.96	740	45.30	1240	66.00	1740	86.00	2240	106.00	2740	126.00	3240	146.00
250	11.39	750	46.31	1250	67.00	1750	87.00	2250	107.00	2750	127.00	3250	147.00
260	11.82	760	47.33	1260	68.00	1760	88.00	2260	108.00	2760	128.00	3260	148.00
270	12.25	770	48.34	1270	69.00	1770	89.00	2270	109.00	2770	129.00	3270	149.00
280	12.68	780	49.36	1280	70.00	1780	90.00	2280	110.00	2780	130.00	3280	150.00
290	13.11	790	50.37	1290	71.00	1790	91.00	2290	111.00	2790	131.00	3290	151.00
300	13.54	800	51.39	1300	72.00	1800	92.00	2300	112.00	2800	132.00	3300	152.00
310	13.97	810	52.40	1310	73.00	1810	93.00	2310	113.00	2810	133.00	3310	153.00
320	14.40	820	53.42	1320	74.00	1820	94.00	2320	114.00	2820	134.00	3320	154.00
330	14.83	830	54.43	1330	75.00	1830	95.00	2330	115.00	2830	135.00	3330	155.00
340	15.26	840	55.45	1340	76.00	1840	96.00	2340	116.00	2840	136.00	3340	156.00
350	15.69	850	56.46	1350	77.00	1850	97.00	2350	117.00	2850	137.00	3350	157.00
360	16.12	860	57.48	1360	78.00	1860	98.00	2360	118.00	2860	138.00	3360	158.00
370	16.55	870	58.49	1370	79.00	1870	99.00	2370	119.00	2870	139.00	3370	159.00
380	16.98	880	59.51	1380	80.00	1880	100.00	2380	120.00	2880	140.00	3380	160.00
390	17.41	890	60.52	1390	81.00	1890	101.00	2390	121.00	2890	141.00	3390	161.00
400	17.84	900	61.54	1400	82.00	1900	102.00	2400	122.00	2900	142.00	3400	162.00
410	18.27	910	62.55	1410	83.00	1910	103.00	2410	123.00	2910	143.00	3410	163.00
420	18.70	920	63.57	1420	84.00	1920	104.00	2420	124.00	2920	144.00	3420	164.00
430	19.13	930	64.58	1430	85.00	1930	105.00	2430	125.00	2930	145.00	3430	165.00
440	19.56	940	65.60	1440	86.00	1940	106.00	2440	126.00	2940	146.00	3440	166.00
450	19.99	950	66.61	1450	87.00	1950	107.00	2450	127.00	2950	147.00	3450	167.00
460	20.42	960	67.63	1460	88.00	1960	108.00	2460	128.00	2960	148.00	3460	168.00
470	20.85	970	68.64	1470	89.00	1970	109.00	2470	129.00	2970	149.00	3470	169.00
480	21.28	980	69.66	1480	90.00	1980	110.00	2480	130.00	2980	150.00	3480	170.00
490	21.71	990	70.67	1490	91.00	1990	111.00	2490	131.00	2990	151.00	3490	171.00

Figure 18.1. Example Page of Lift Table

18.2.1.5 VALIDATION

The results of these programs have been checked against existing tables and found to give consistently greater values for lift. As examples, at 1490 psig and -10°C the difference is 2.7 percent and at $+30^{\circ}$ it is 2.9 percent. The difference is greater at lower pressures and less at higher pressures. Carefully measured superpressure balloon inflations have verified this difference, but the absolute accuracy of the tables is still not known because of the difficulty of getting accurately the water volumes of a run-of-the-mill group of small cylinders. Until a controlled test is run using known water volume, the absolute accuracy will remain in doubt. For some large cylinders, the water volume and other characteristics can be found from manufacturer's records. But the difficulty of measuring the lift accurately again renders the problem troublesome. At this time there is no plan to make controlled tests for further validation.

18.2.2 Hydrogen Lift

Program H2LIFT

18.2.2.1 PROGRAMMER

Jack M. Angevine

18.2.2.2 DESCRIPTION

This program is identical to the helium lift program KBOTTTL including the same calculations for thermal and pressure effects on cylinder volume. It is used for those cases where wall thickness of the cylinder is known rather than calculated in the program.

Hydrogen properties are taken from Wooley et al (1932). Comparisons were made with NBS circulars 120 (Dean) and 564 (Hilsenrath et al, 1962) and agreement was found to be good. Another method (de Graaf) was also compared with good agreement, but the method of Wooley lends itself slightly better to the treatment required here.

Cylinder volume is corrected, as for the helium tables, for pressure and temperature deformation.

Lift is calculated as for the helium tables with molecular weight of hydrogen taken from the 1962 Standard Atmosphere (1962) as 2.01594.

18.2.2.3 DATA REQUIRED

The data required for the hydrogen lift program is the same as that required for the KBOTTTL Program, Table 18.1.

characteristics. Force calculations can be made as accurately as required by varying the size of these segments.

The complete derivation of the force analysis and a full description of the computer programs is given in NCAR Technical Note TN-47 (Angevine et al, 1970).

18.3.1.3 DATA REQUIRED

There are two major programs, each with two options as to the method of handling the payload. One program evaluates the case in which the distance between payload and winch will be fixed during the operation; the second considers the case in which the distance between payload and winch may be varied. Both can accommodate either a vehicle-supported payload or a Stonehenge-handled payload.

1234567890123456789012345678901234567890123456789012345678901234567890			
LAUNCH EXAMPLE-STONEHENGE CARLE RESTRAINED LAUNCH			
.0734	DENSITY OF AIR IN POUNDS PER CUBIC FOOT		
.4	COEFFICIENT OF AIR DRAG ON THE BALLOON		
0.1	COEFFICIENT OF AIR LIFT ON THE BALLOON		
50.	RADIUS OF ANCHOR CIRCLE IN FEET		
24.	TOTAL NO. OF ANCHORS		
5.	NO. OF INCLUDED EMPTY ANCHORS		
.425	THICKNESS OF ANCHOR LINES IN INCHES		
.72	DENSITY OF ANCHOR LINES IN POUNDS PER FOOT		
2.1847	WIDTH (FT.) OF SPREADER AT APEX OF ANCHOR LINES		
0.0	LENGTH (FT.) BETWEEN ANCHOR LINE CONFLUENCE AND EXTENSION LINE END		
15.	WEIGHT OF PAYLOAD IN FEET		
3780.	WEIGHT OF PAYLOAD IN POUNDS		
55.337	LENGTH OF EXTENSION LINE IN FEET		
14.	WEIGHT OF EXTENSION LINE IN POUNDS		
-.008	GROUND SLOPE (FT./FT.) * IF WINCH ABOVE PAYLOAD		
405.	TOTAL TRAIN LENGTH IN FEET		
1.0	INTEGRATION STEP SIZE FOR TRAIN SIDE IN FEET		
3	NO. OF SECTIONS OF CONSTANT THICKNESS		
1.	85. THICKNESS (FT.) AND LENGTH (FT.) OF SECTION		
2.	50. THICKNESS (FT.) AND LENGTH (FT.) OF SECTION		
.6666	268. THICKNESS (FT.) AND LENGTH (FT.) OF SECTION		
5	NO. OF SECTIONS OF CONSTANT DENSITY		
60.	85. TOTAL WEIGHT (LBS.) AND LENGTH (FT.) OF SECTION		
120.	50. TOTAL WEIGHT (LBS.) AND LENGTH (FT.) OF SECTION		
1088.	268. TOTAL WEIGHT (LBS.) AND LENGTH (FT.) OF SECTION		
0.0	WEIGHT OF TRANSFER FITTING IN POUNDS		
232.	WEIGHT OF TOP BALLOON IN POUNDS		
6084.	GROSS LIFT IN POUNDS		
2900.	HORIZONTAL CROSS SECTION OF BALLOON IN SQUARE FEET		
2680.	VERTICAL CROSS SECTION OF BALLOON IN SQUARE FEET		
.425	THICKNESS OF STAY IN INCHES		
.72	DENSITY OF STAY IN POUNDS PER FOOT		
1.0	INTEGRATION STEP SIZE FOR STAY SIDE IN FEET		
4	NUMBER OF WINDS		
0.	0.	0.	COEFFICIENTS OF WIND PROFILE POLYNOMIAL
0.	.878	.35	COEFFICIENTS OF WIND PROFILE POLYNOMIAL
0.	.986	.35	COEFFICIENTS OF WIND PROFILE POLYNOMIAL
0.	1.083	.35	COEFFICIENTS OF WIND PROFILE POLYNOMIAL
.99	DECIMAL FRACTION OF TRAIN ON GROUND		
.45	DECIMAL FRACTION OF TRAIN ON GROUND		
.9	DECIMAL FRACTION OF TRAIN ON GROUND		
.8	DECIMAL FRACTION OF TRAIN ON GROUND		
.7	DECIMAL FRACTION OF TRAIN ON GROUND		
.6	DECIMAL FRACTION OF TRAIN ON GROUND		
.5	DECIMAL FRACTION OF TRAIN ON GROUND		
.4	DECIMAL FRACTION OF TRAIN ON GROUND		
.3	DECIMAL FRACTION OF TRAIN ON GROUND		
.2	DECIMAL FRACTION OF TRAIN ON GROUND		
.1	DECIMAL FRACTION OF TRAIN ON GROUND		
.01	DECIMAL FRACTION OF TRAIN ON GROUND		
0.0	DECIMAL FRACTION OF TRAIN ON GROUND		
0.0	ALPHA IN DEGREES		
1.0	ALPHA IN DEGREES		
5.	ALPHA IN DEGREES		

Figure 18.3. Input Data Cards, Program LAUNCH (Stonehenge Payload Support)

Data required for any of these options are nearly identical. Weights, lengths and other pertinent information about the system are entered as shown in Figure 18.3. The train is divided into as many sections as desired, each with a weight, thickness and length. The example in Figure 18.3 represents input for the LAUNCH program, which calculates configurations for varying distance between winch and payload, and in this case the train is assumed divided into three sections of constant thickness and constant density.

18.3.1.4 RESULTS

Results from the main programs appear in two forms — as printed output showing calculated values of the variables, and as a set of pictorials showing the shape and relationship of the train, launch balloon and restraint cable. Figure 18.4 is an example of the printed output and Figure 18.5 is the pictorial for the block of information enclosed in the box in Figure 18.4.

Each of the two main programs generates a magnetic tape which then is used as input to an auxiliary program which can be set up to plot the values in the most meaningful way. Examples of the displays available from these auxiliary programs are shown in Figures 18.6 through 18.10.

Figures 18.6 and 18.7: Plotted from program LAUNCH, each of these families of curves represents tension in the train (solid curves) and angle of the lowest segment of the train (dashed curves) as functions of distance between payload and winch, apparent train angle and restraint cable length. Any combination of variables may be plotted by simple changes to subroutines.

Figures 18.8, 18.9, and 18.10: Plotted from program CLANCH in which the distance from payload to winch is kept constant, these three curves illustrate the characteristic forces and angles of the system as restraint cable length is changed. Each curve is for a particular vertical wind profile chosen to represent as nearly as possible realistic conditions for the launch site and time.

18.3.1.5 VALIDATION

Results of these programs have been used in several flight operations and one test (Angevine, 1968). In each case the predictions have been representative of the observations, as long as wind direction and velocity have remained reasonably steady as required in the assumptions made for the programs.

18.3.2 Stonehenge

Programs GEOMTR, STODIM, CLEAK, SLACK.

18.3.2.1 PROGRAMMERS

Jack M. Angevine and David W. Fulker.

		ALPHA = 1.00		FTONG = 0.		FTONG = 0.	
WIND PROFILE 1		ALPHA = 1.000	ALPHA = 1.000	FTONG = 0.	FTONG = 0.	FTONG = 0.	FTONG = 0.
TTP	214.452	970.360	1726.360	2482.360	3238.360	3994.360	4750.360
ALPHA	02.422	55.294	19.324	29.895	23.974	19.949	15.924
TTM	1397.559	1697.044	2225.029	2854.294	3539.487	4246.229	4943.487
TOTALM	347.741	199.445	135.438	102.020	82.024	68.873	57.946
PARTC	182.835	358.518	396.544	419.331	416.605	419.946	419.946
TSS	4475.106	4568.201	4745.925	5076.805	5475.238	5943.485	6419.946
TNETAN	87.557	77.421	68.368	60.306	53.321	47.368	41.415
TSM	4209.653	4416.783	4666.839	5001.862	5413.846	5891.380	6389.380
SLNGTH	389.682	207.487	149.445	121.520	106.753	98.946	98.946
C	198.113	482.967	491.040	478.005	480.086	486.392	486.392
ALPHA	59.444	26.920	17.464	12.930	10.313	8.623	7.423
TEXT	0.	0.	0.	0.	0.	0.	0.
TANCH	123.543	559.011	994.532	1430.053	1865.574	2301.095	2731.695
FALB	0.	0.	0.	0.	0.	0.	0.
FBY	5857.000	5857.000	5857.000	5857.000	5857.000	5857.000	5857.000
FDB	0.	0.	0.	0.	0.	0.	0.
WINDS	0.	0.	0.	0.	0.	0.	0.
WIND PROFILE 2		ALPHA = 1.000		FTONG = 0.		FTONG = 0.	
TTP	214.452	970.360	1726.360	2482.360	3238.360	3994.360	4750.360
ALPHA	01.562	55.294	19.324	29.895	23.974	19.949	15.924
TTM	1392.301	1696.795	2225.029	2854.294	3539.487	4246.229	4943.487
TOTALM	346.322	199.179	135.438	102.020	82.024	68.873	57.946
PARTC	187.386	358.518	396.544	419.331	416.605	419.946	419.946
TSS	4546.825	4638.836	4846.243	5160.051	5588.127	6029.875	6499.875
TNETAN	82.689	75.114	66.762	59.141	52.453	46.712	41.415
TSM	4281.887	4481.246	4746.155	5084.451	5498.849	5975.992	6475.992
SLNGTH	370.367	209.267	141.094	122.940	107.970	99.697	99.697
C	227.374	411.684	458.583	472.929	483.837	487.938	487.938
ALPHA	58.872	26.873	17.452	12.926	10.311	8.622	7.422
TEXT	0.	0.	0.	0.	0.	0.	0.
TANCH	123.543	559.011	994.532	1430.053	1865.574	2301.095	2731.695
FALB	0.	0.	0.	0.	0.	0.	0.
FBY	5857.000	5857.000	5857.000	5857.000	5857.000	5857.000	5857.000
FDB	0.	0.	0.	0.	0.	0.	0.
WINDS	0.	0.	0.	0.	0.	0.	0.
WIND PROFILE 3		ALPHA = 1.000		FTONG = 0.		FTONG = 0.	
TTP	214.452	970.360	1726.360	2482.360	3238.360	3994.360	4750.360
ALPHA	01.288	55.239	19.308	29.849	23.972	19.949	15.924
TTM	1391.038	1696.573	2225.029	2854.294	3539.487	4246.229	4943.487
TOTALM	345.935	199.109	135.438	102.020	82.024	68.873	57.946
PARTC	186.553	358.518	396.544	419.331	416.605	419.946	419.946
TSS	4546.821	4657.913	4867.792	5162.105	5582.495	6051.950	6541.950
TNETAN	82.595	74.527	66.354	59.040	52.228	46.545	41.415
TSM	4304.312	4512.714	4748.007	5106.121	5520.828	5999.610	6499.610
SLNGTH	370.717	209.779	141.540	123.326	108.291	99.872	99.872
C	234.845	413.935	456.754	473.673	482.565	488.340	488.340
ALPHA	58.662	26.861	17.449	12.924	10.310	8.622	7.422
TEXT	0.	0.	0.	0.	0.	0.	0.
TANCH	123.543	559.011	994.532	1430.053	1865.574	2301.095	2731.695
FALB	0.	0.	0.	0.	0.	0.	0.
FBY	5857.000	5857.000	5857.000	5857.000	5857.000	5857.000	5857.000
FDB	0.	0.	0.	0.	0.	0.	0.
WINDS	0.	0.	0.	0.	0.	0.	0.
WIND PROFILE 4		ALPHA = 1.000		FTONG = 0.		FTONG = 0.	
TTP	214.452	970.360	1726.360	2482.360	3238.360	3994.360	4750.360
ALPHA	01.017	55.185	19.292	29.803	23.969	19.949	15.924
TTM	1389.771	1696.353	2225.029	2854.294	3539.487	4246.229	4943.487
TOTALM	345.548	199.040	135.417	102.020	82.020	68.849	57.946
PARTC	184.709	358.437	396.422	419.330	416.606	419.946	419.946
TSS	4591.565	4679.374	4889.506	5204.224	5604.875	6074.667	6549.667
TNETAN	81.605	73.945	65.952	58.546	52.009	46.475	41.415
TSM	4327.140	4533.882	4760.025	5128.474	5543.389	6021.687	6501.687
SLNGTH	371.220	210.307	141.990	123.703	108.611	100.146	100.146
C	242.223	416.168	457.919	474.412	483.090	488.779	488.779
ALPHA	58.503	26.848	17.446	12.923	10.310	8.622	7.422
TEXT	0.	0.	0.	0.	0.	0.	0.
TANCH	123.543	559.011	994.532	1430.053	1865.574	2301.095	2731.695
FALB	0.	0.	0.	0.	0.	0.	0.
FBY	5857.000	5857.000	5857.000	5857.000	5857.000	5857.000	5857.000
FDB	0.	0.	0.	0.	0.	0.	0.
WINDS	0.	0.	0.	0.	0.	0.	0.

Figure 18.4 Sample Output Page, Program LAUNCH (Stonehenge Payload Support)

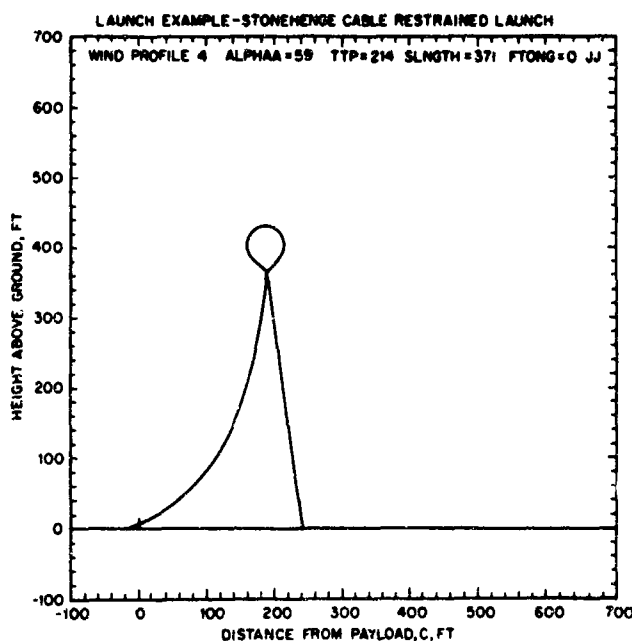


Figure 18.5 Typical dd80 Pictorial, Program LAUNCH (Stonehenge Payload Support)

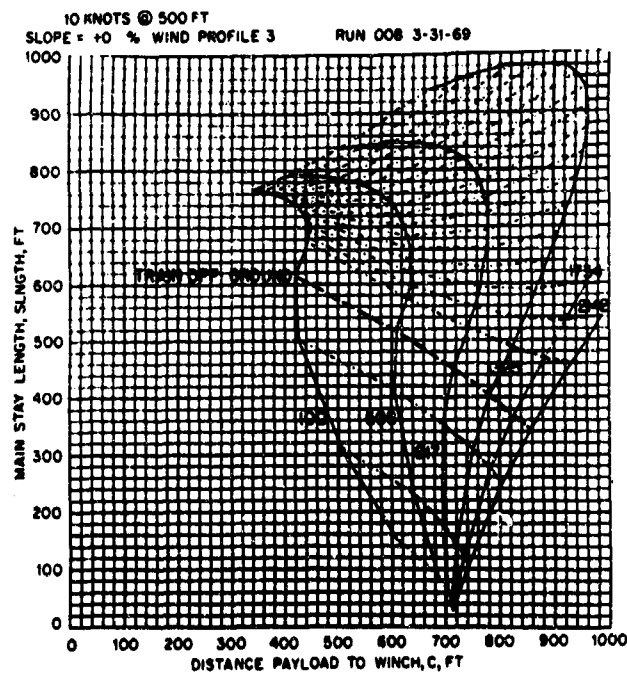


Figure 18.6 Program LAUNCH, Mainstay Length vs. Distance for Constant Train Tension

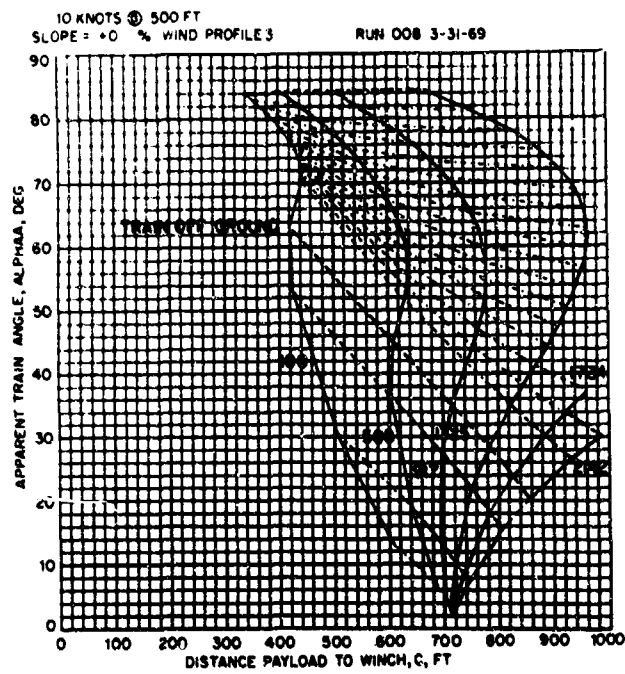


Figure 18.7 Program LAUNCH, Apparent Train Angle vs. Distance for Constant Train Tension

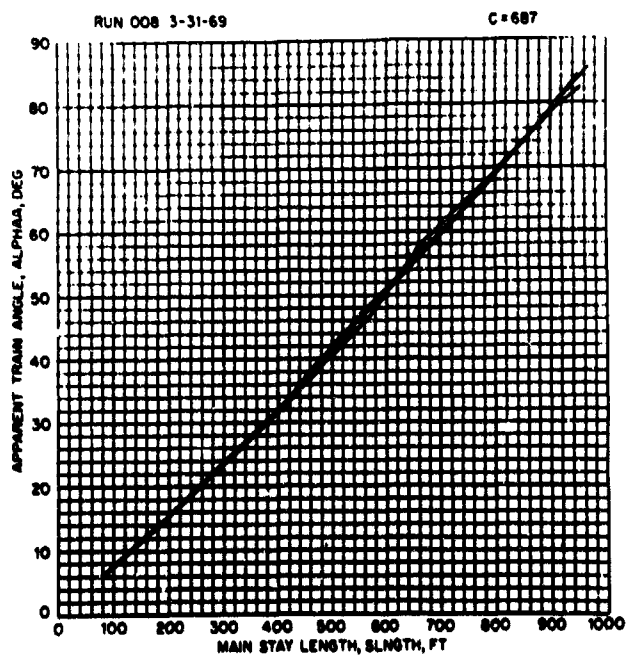


Figure 18.8. Apparent Train Angle vs. Mainstay Length, C = 687 ft

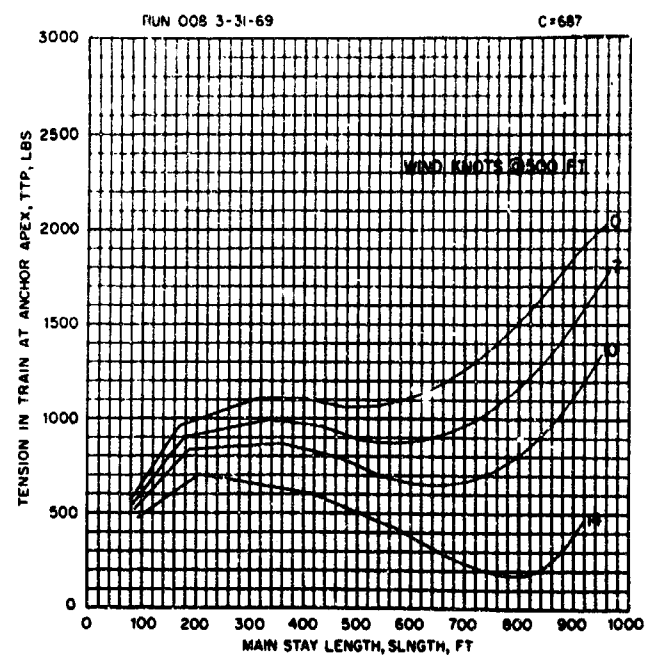


Figure 18.9. Tension in Train vs. Mainstay Length, C = 687 ft.

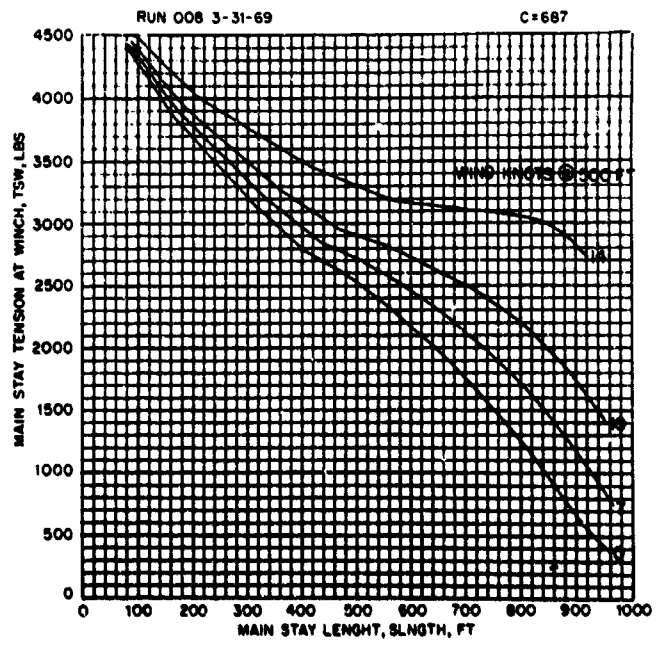


Figure 18.10. Tension in Restraint Cable vs. Mainstay Length, C = 687 ft.

18.3.2.2 DESCRIPTION

A photograph of a Stonehenge launch configuration appears as Figure 18.11 with the components labeled. This method of handling balloon payloads may be used where, for various reasons, a suitable vehicle is not available or a vehicle can not be used. A full description of the method and derivations is contained in NCAR TN-40 (Angevine et al, 1969) and will not be repeated here.

The dimensions and forces in a particular Stonehenge array may be calculated by hand, but where a number of them must be calculated for comparison to pick an optimum configuration the calculations are more quickly done by machine. TN-40 was written to assist in making configuration choices; much of the computing work has been done by the use of programs GEOMTR, CLEAR, and SLACK and presented in the TN as tables and figures. For final calculations or to calculate a configuration not listed in TN-40, program STODIM is available, and is discussed in the following sections.

18.3.2.3 DATA REQUIRED

Radius of the anchor circle and total number of anchors available in the circle are the basic data. The number of anchors empty between the two being used must be chosen by the programmer. Dimensions of the payload and rigging details are inserted along with either the desired extension line length or anchor line length. Figure 18.12 illustrates the input data needed for a case in which the extension line length is to be calculated.

18.3.2.4 RESULTS

Results are printed out as shown in Figure 18.12 and include not only all dimensions, but also the ratio of load in the anchor lines to load at the apex to provide a quick means of choosing anchor line size.

18.3.2.5 VALIDATION

These programs have been used in the design of several launch operations and the results were found to be satisfactory (Angevine et al, 1969; and Angevine, 1968).

18.4 CLIMATOLOGY

18.4.1 Balloon Trajectories

Program SIMFLT.

18.4.1.1 PROGRAMMERS

Alvin L. Morris, David W. Fulker and Jack M. Angevine.

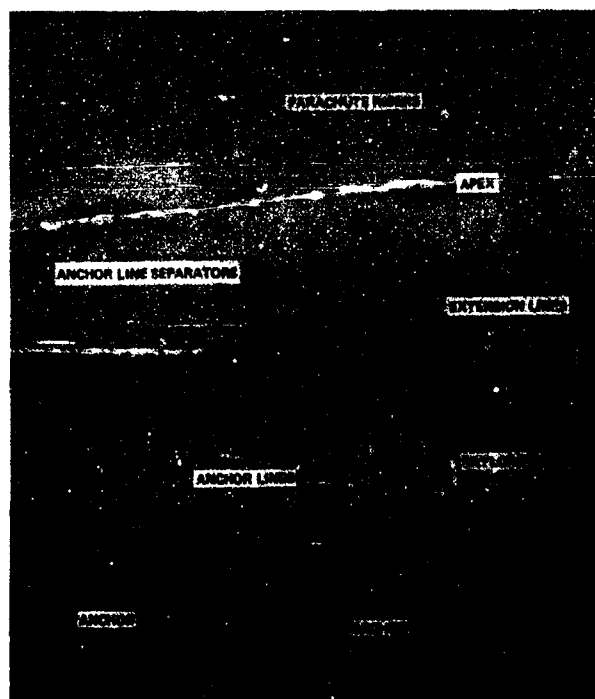


Figure 18.11. Closeup View of Stonehenge Launch System

```

STONEHENGE DIMENSIONS FOR STONEHENGE TEST
INPUT DATA
RADIUS = 50.00000 RADIUS OF ANCHOR CIRCLE IN FEET
ANCH1 = 24.00000 TOTAL NO. OF ANCHORS
ANCH2 = 4.00000 NO. OF INCLUDED EMPTY ANCHORS
SPREAD = 2.10000 WIDTH OF ANCHOR LINE SPREADER IN FT
STRA = 0. EXTENSION LENGTH FROM SPREADER TO LOAD LINE IN FT
MPAY = 14.00000 HEIGHT OF PAYLOAD IN FEET
ALN = 40.00000 LENGTH OF ANCHOR LINE IN FEET INPUT DATA
MULTIN HAS BEEN SET TO 2000

GEOMETRY OUTPUT
ETA = 45.00000 HALF INCLUDED ANGLE BETWEEN ANCHORS IN DEG
B = 35.35534 HALF DISTANCE BETWEEN ANCHORS IN FT
P = 34.34466 LENGTH OF RISE FROM 2 ANCHORS IN FT
HST = 37.30000 EXTENSION LINE LENGTH REQUIRED IN FT
A = 40.00000 ANCHOR LINE LENGTH REQUIRED IN FT
PHI = 43.81074 ANCHOR LINE ELEVATION ANGLE IN DEG
PANCH = 50.00000 PROJECTED LENGTH OF ANCHOR LINE IN FT
PDS = 40.71072 HALF ANGLE BETWEEN ANCHOR LINES AT APEX IN DEG
L = 30.00000 PANCH PLUS STRA
MP = 40.33000 TOTAL HEIGHT TO APEX
TATTH = 1.50 RATIO ANCHOR/SPREADER/EXTENSION SLACK

```

Figure 18.12. Data and Results from Program STODIM

18.4.1.2 DESCRIPTION

Statistically derived trajectories can be calculated at a rate of 2000 flights/min, giving balloon flight planners a key to the most probable paths balloons will take when launched from sites within the U.S. Variations of the computer program allow selecting launch sites and times most likely to yield balloon trajectories over desired targets, as may be required in pollution studies and for at-sea recoveries (National Center for Atmospheric Research, 1969).

To simulate a balloon flight from a given starting point, the SIMFLT program makes a linear interpolation of data on a 5° grid in two dimensions to find each mean wind component and standard deviation at the latitude and longitude of that location. (The trajectory during ascent and descent is not calculated, and must be accounted for separately.) Next, a wind velocity is selected by a random process from a normally distributed population of winds having these means and standard deviations. The program tests the direction of the wind vector against pre-assigned limiting directions, chosen to simulate conditions which might be imposed as a condition for launching an actual flight. If the vector is within these angular limits, the simulated flight is allowed to "fly" for a given time increment, and a new position is calculated. At this position new grid data are available and a new wind vector is chosen, using the new data and the random selection process. To allow for the persistence of the wind, each new wind vector is, in principle, combined with the previous vector so that the autocorrelation of winds along the simulated trajectory approximates that of the winds along actual trajectories. The actual autocorrelation is not known. In practice, the prior vector (reduced in magnitude by 2 percent) is added to the new vector (reduced in magnitude by 98 percent) to derive the resultant vector for the next time increment.

The computed trajectories are believed to have essentially the same statistical characteristics as real trajectories.

18.4.1.3 DATA REQUIRED

The program is based on six years of wind data from rocket soundings at Point Mugu, White Sands, Cape Kennedy, and Wallops Island. The data include monthly mean zonal and meridional wind speeds and standard deviations for each 10,000 ft level between 80,000 and 160,000 ft, and supplemental data at 10 mb (104,000 ft). The data for each level and each month from all observing stations were plotted on a map, and isolines drawn for each variable. Interpolation from the isoline pattern provided derived data at each point of a 5° longitude-latitude grid. The data are available in punched card decks, one for each month and level.

Latitude, longitude and a ten-character name of the starting point (and goal, if one is desired) are entered with the wind data. The number of flights may be

varied as desired, although 2000 has proven to be statistically adequate. The maximum time in hours that the flights are to be allowed to run, the time increment between calculations and the acceptable direction of the wind are optional.

18.4.1.4 RESULTS

Printed output consists of tabulations of the mean and standard deviation of location of the flights at elapsed times selected by the programmer, Figure 18.13.

Locations of the flights at selected times can also be shown on graphic displays using the cathode ray tube output photographed on microfilm. The examples shown in Figures 18.14 and 18.15 show the location of every fifth simulated flight at 2 hours and 10 hours after launch. Only every fifth one is plotted for clarity, but the number may be changed at will. The symbols indicate the nearness of each flight to the mean location of all the flights at the chosen time; in this case, an "X" is a flight in the 50 percent closest to the mean, an "H" is a flight in the next closest 40 percent and an "O" is a flight in the farthest 10 percent. The symbol "S" is the starting point, and "M" is the mean location. The percentages may all be varied as desired.

The capability to analyze for flights on a specific track as to a specific goal is shown in Figure 18.16. The numbers represent the mean location of all the flights after that elapsed time in hours. The goal is shown as a "G" and the symbols for each flight are shown at their closest approach to this location. The mean location of these flights is again shown by an "M". The calculated means and standard deviations are also printed out as shown in Figure 18.17.

18.4.1.5 VALIDATION

All simulations made so far agree with experience and expectations. There is no real way to validate the program quantitatively since no statistically valid number of balloon flights can be made under controlled conditions similar to those imposed by the program. The data grid could benefit from improved observational coverage, but for planning purposes the existing data seem adequate. Final decisions for an actual flight operation must, of course, rely on adequate short range meteorological forecasting.

18.5 RIGGING

18.5.1 Suspension Stiffness

18.5.1.1 PROGRAMMER

Jack M. Angevine

STARTING POINT IS - EDWARDS AFB
 LAT = 34.90000 LON = -117.87000

DATA IDENTIFICATION - DECEMBER 130000 FT

NO OF FLTS	TIME	MEAN LAT	MEAN LON	S.D. LAT	S.D. LON
2000	0.	34.7	-117.9	.0	.0
2000	1.0	35.1	-115.7	.5	.8
2000	2.0	35.2	-113.5	1.1	1.6
2000	3.0	35.4	-111.4	1.4	2.4
2000	4.0	35.6	-109.2	2.1	3.2
2000	5.0	35.7	-107.0	2.6	3.9
2000	6.0	35.9	-104.8	3.1	4.7
2000	7.0	36.1	-102.6	3.5	5.4
2000	8.0	36.7	-100.4	4.0	6.2
2000	9.0	36.7	-98.2	4.5	6.9
2000	10.0	36.6	-95.9	4.9	7.6
2000	11.0	36.7	-93.7	5.4	8.3
2000	12.0	36.9	-91.4	5.8	9.0
2000	13.0	37.1	-89.1	6.2	9.8
2000	14.0	37.3	-86.8	6.6	10.5
2000	15.0	37.5	-84.5	7.0	11.2

Figure 18.13. Printed Output for Location from Edwards AFB

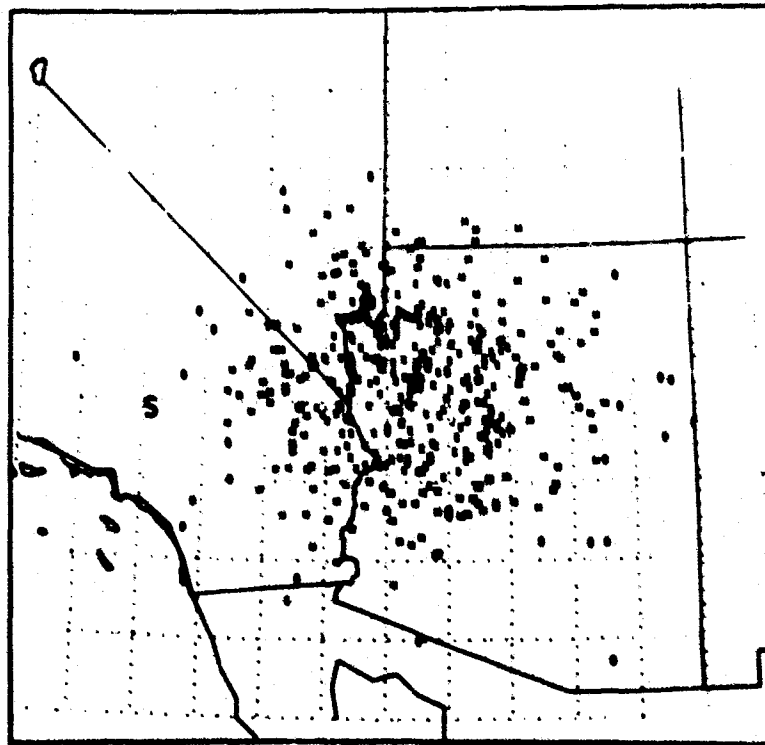


Figure 18.14. December 130,000 ft from Edwards AFB after 2 Hours.
 Angle 360.0-0, increments of latitude and longitude 1 degree(s)

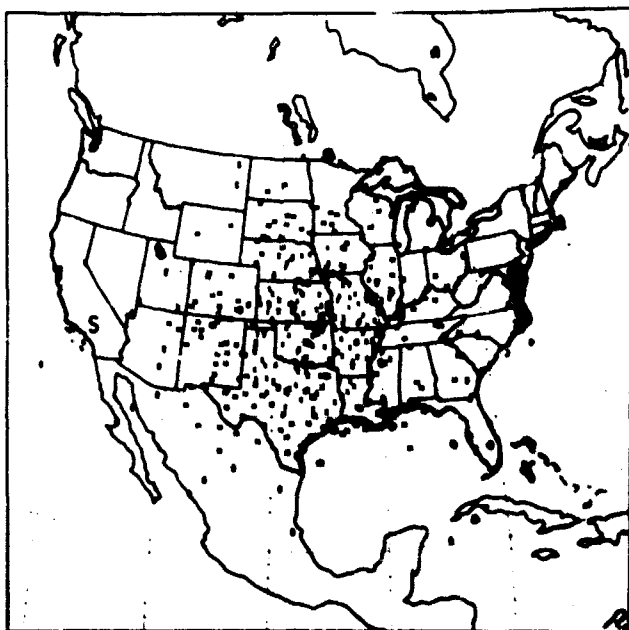


Figure 18.15. December 130,000 ft from Edwards AFB after 10 Hours. Angle 360.0-0, increments of latitude and longitude 10 degree(s)

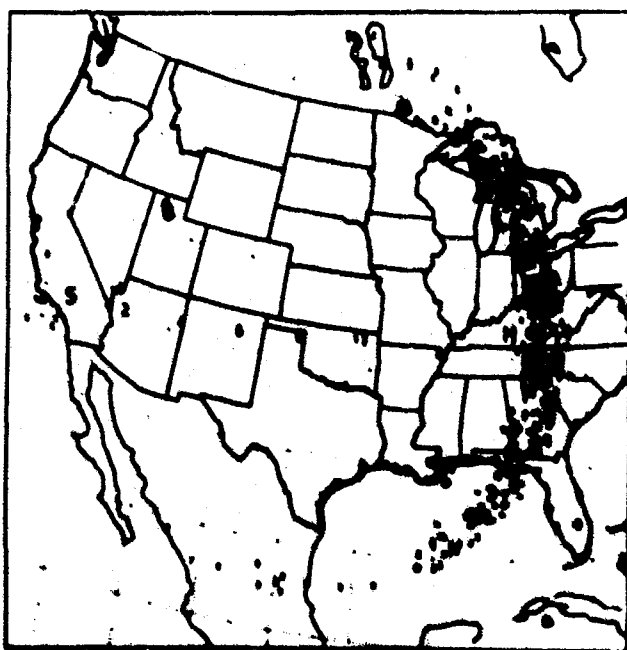


Figure 18.16. December 130,000 ft from Edwards AFB to Columbus, Ohio. 11.9 hours SD 1.7, angle 360.0-0, increments of latitude and longitude 5 degree(s)

STARTING POINT IS - EDWARDS AFB
 LAT = 34.93000 LON = -117.87000
 GOAL IS - COLUMBUS, OH
 LAT = 40.00000 LON = -03.00000
 DATA IDENTIFICATION - DECEMBER 130000 FT
 2000 WINDS CHECKED, 2000 FLIGHTS MADE
 PERCENTAGE OF WINDS WITHIN ANGULAR LIMITS = 100.0
 NEAREST APPROACH TO GOAL = (936 FLIGHTS)
 MEAN TIME = 11.9 HOURS WITH S.D. = 1.7
 MEAN LAT = 37.3 DEG WITH S.D. = 6.5
 MEAN LON = -85.2 DEG WITH S.D. = 4.4
 CORRELATION COEFFICIENT = .1004 SA = 6.6 SN = 4.3 OSI = 11.1
 MAX ANGLE = 360.0 DEGREES, MIN ANGLE = 0. DEGREES
 PERSISTENCE = .98

Figure 18.17 Printed Output for Nearest Approach to Goal, from Edwards AFB to Columbus, Ohio

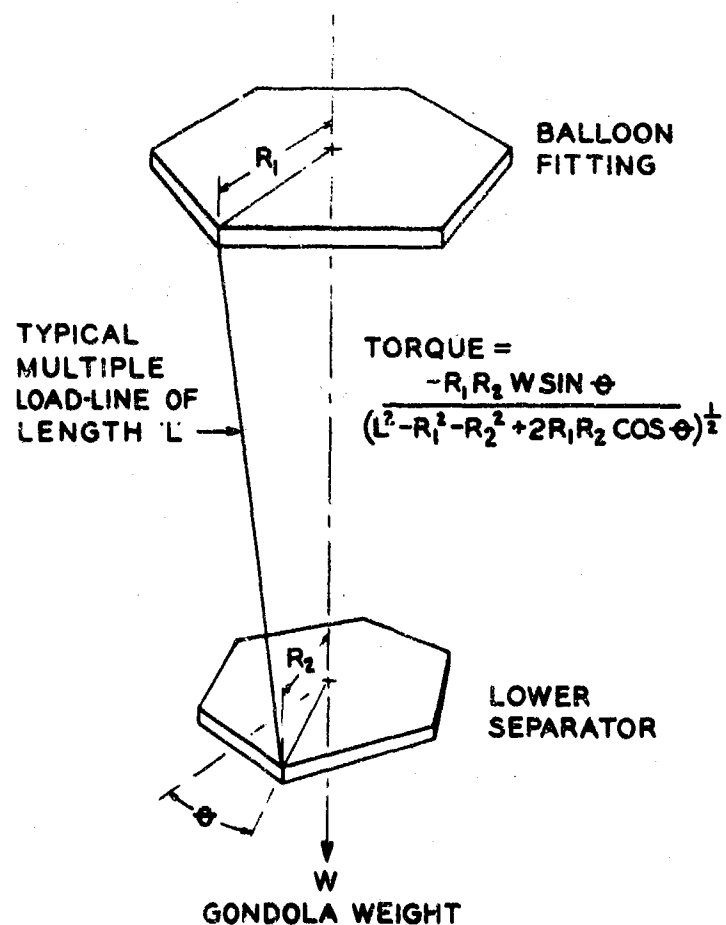


Figure 18.18. Prismatic Multipoint Suspension System

18.5.1.2 DESCRIPTION

Some experimenters require a certain amount of torsional stiffness in the suspension system between the experiment and the balloon. Sometimes they also need to know how to simulate their actual suspension in a building which does not allow use of the full size suspension elements.

This program makes torsional stiffness calculations for suspension systems containing as many as five different sections, allowing for different spreader dimensions at the top and bottom of each section and also allowing for changes in length in sections containing nylon shroud lines. The program is written for GE Time Sharing System Mark I.

A generalized single section of a suspension system is shown in Figure 18.18. When additional sections of suspension are added end to end and a torque is applied between the top-most and bottom-most fittings, the same torque is experienced by all the sections. Since each section may have different dimensions, the angle through which each is rotated may be different and the total angle of the entire suspension is unknown. It is most convenient, then, for the program to accept increments of torque as input values and to calculate the resulting rotation angle of each section and find the total rotation angle by summing the individual angles.

In addition, some sections may be composed of nylon shroud lines which will stretch under load, changing the length of the section. Although many factors such as temperature, humidity, and loading rate enter into the elongation of shroud lines, an attempt is made to estimate this loaded length in the program. The effect of this estimate on the overall result can be checked by re-calculating, this time assuming that the section does not stretch.

The only currently used suspension configuration that the program cannot now accept is the case of a section with all the lines in the same plane but at different radii from the center of rotation. The equations for this case exist and can be included with little difficulty if the need arises.

18.5.1.3 DATA REQUIRED

The initial torque value, increments of torque in pound-feet, and total number of torque values are chosen. The total number of sections is entered and the program then interrogates the programmer for the data on each individual section, as shown in the example, Figure 18.19. Although the data input is slow using this method, the program can be run by anyone familiar with a teletype terminal. A sketch of the suspension system with the pertinent data is an important aid in keeping the data organized.

SUSTOR 10128 PX SYSP 4/23/70

INITIAL TORQUE VALUE, LB-FT
 ? 0
 TORQUE INCREMENT, LB-FT
 ? .1
 TOTAL NUMBER OF TORQUE VALUES, LB-FT, MAX 20
 ? 10
 NUMBER OF SECTIONS, MAXIMUM OF 5
 ? 2
 INPUT DATA FOR EACH SECTION:

 SECTION 1
 ELASTIC OR NOT (+1 OR -1)
 ? +1
 NUMBER OF ELEMENTS (LINES, CABLES), INTEGER
 ? 108
 UNSTRETCHED LENGTH, FT (DECIMAL)
 ? 155
 RADIUS OF UPPER END, FT (DECIMAL)
 ? 1.25
 RADIUS OF LOWER END, FT (DECIMAL)
 ? .96
 WEIGHT SUSPENDED FROM THIS SECTION, LB (DECIMAL)
 ? 1950

SECTION 2
 ELASTIC OR NOT (+1 OR -1)
 ? -1
 NUMBER OF ELEMENTS (LINES, CABLES), INTEGER
 ? 6
 UNSTRETCHED LENGTH, FT (DECIMAL)
 ? 45
 RADIUS OF UPPER END, FT (DECIMAL)
 ? .96
 RADIUS OF LOWER END, FT (DECIMAL)
 ? .56
 WEIGHT SUSPENDED FROM THIS SECTION, LB (DECIMAL)
 ? 2000

SECTION	ROTATION ANGLES					COMBINED	
	1	2	3	4	5	ANGLE	SPRINGK
TORQUE							
.000	.000	.000	.000	.000	.000	.000	.000
.100	.394	.240	.000	.000	.000	.634	.158
.200	.788	.480	.000	.000	.000	1.267	.158
.300	1.182	.719	.000	.000	.000	1.901	.158
.400	1.576	.959	.000	.000	.000	2.535	.158
.500	1.970	1.199	.000	.000	.000	3.169	.158
.600	2.364	1.439	.000	.000	.000	3.803	.158
.700	2.758	1.679	.000	.000	.000	4.437	.158
.800	3.152	1.919	.000	.000	.000	5.072	.158
.900	3.547	2.159	.000	.000	.000	5.706	.158

Figure 18.19. Suspension Torque Example

18.5.1.4 RESULTS

Results are presented in tabular form following the input data, Figure 18.19. The rotation angle of each section under the influence of the applied torque is presented individually. The total angle of rotation and combined spring constant of the system are presented in the last two columns. Units are: torque, lb-ft; spring constant, lb-ft/deg.

If the range of torques selected is so great that one of the sections would twist greater than 90° , the calculation stops at that point and a message is printed just above the table of output values stating which section is affected and which torque value causes the 90° deflection.

18.5.1.5 VALIDATION

The method used in this program has been used to calculate suspension characteristics for several flights and indoor simulations with no apparent discrepancies. As far as is known there has been no attempt to measure the exact spring constant of an assembled suspension for comparison with calculated values.

18.6 FLIGHT OPERATIONS

18.6.1 Communications Networks

Programs COMMUN, CLINK.

18.6.1.1 PROGRAMMERS

David W. Fulker and Jack M. Angevine.

18.6.1.2 DESCRIPTION

Occasionally a ballooning project will require a complex communications network comprised of a number of communication channels and stations, and possibly even one-way channels such as passive relays. It is not always easy to determine by inspection whether all the communications requirements are met by a proposed network, or whether there is unneeded duplication of channels or stations. It is even more time-consuming to set up a systematic method of back-up communication in the event of a failure somewhere in the system.

These programs provide tables that show both the direct and relayed methods of communicating from one station to any other station in the network. An analysis of those tables can then reveal weaknesses or unnecessary duplications in the system. Program COMMUN provides a working list for the communicator at each station showing, by channel and call sign, how he can communicate with any other station in the network.

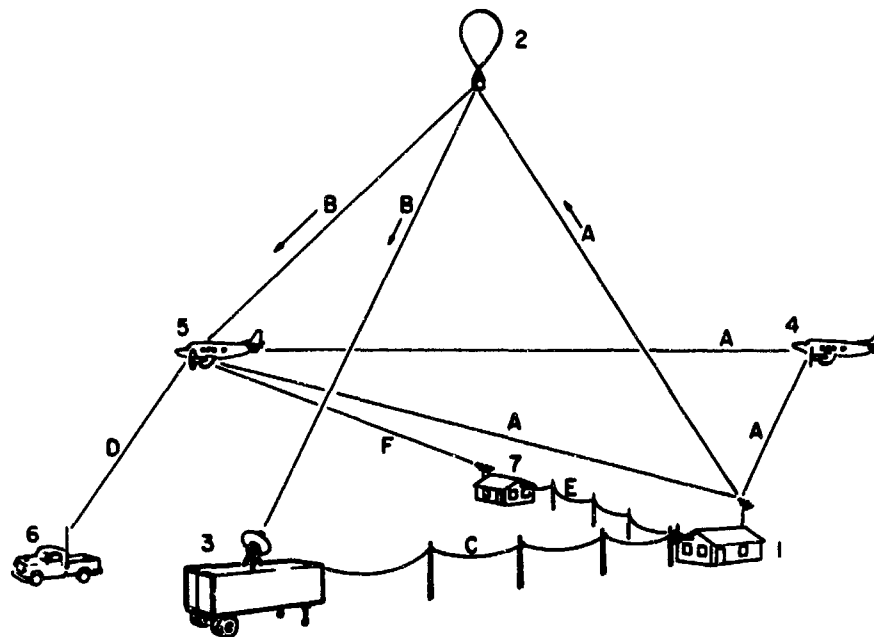


Figure 18.20. Example Communication Network

18.6.1.3 DATA REQUIRED

The analysis begins by drawing a simple network diagram, coding each station by number and each channel of communication by letter as in the very simple example of Figure 18.20. Since the call signs at each end of a link will be different, the letter designating a communication channel will be associated with a different call sign at one station than at the other. A listing of the services at each station is then prepared as in Figure 18.21. Finally a list of direct communication links between each station is prepared as in Figure 18.22 where the coded word 01AA04 means "station 1 on channel A to channel A at station 4."

18.6.1.4 RESULTS

Results from program CLINK are presented as two tables coded by station number and channel letter, one showing the direct route between stations and the other showing both the direct and the one-station-relay routes between stations.

Program COMMUN prints out a complete list of all services at each station, the coded direct route data and a page for each station showing the routing and call signs for communication with any other station in the network, Figure 18.23. Blanks indicate that there is no direct or single-relay route by which the two stations can communicate. A column is left open to assign priorities where several routes exist.

7 EXAMPLE COMMUNICATION PROBLEM

COMMAND
5

A NCA 41 (138.54 MHZ)
C 723-2293 (TELEPHONE)
E 729-2991 (TELEPHONE)

BALLOON
2

A PASSIVE RELAY (138.54
B TELEMETRY (255.1 MHZ)

SCI VAN
2

B VAN (255.1 MHZ)
C 729-0527 (TELEPHONE)

BACKUP A/C
1

A NCA 42 (138.54 MHZ)

TRACK. A/C
4

A NCA 43 (138.54 MHZ)
B NCA 43 (255.1 MHZ)
C NCA 43 (CB)
F NCA 43 (ASSIGNED FREQ)

RECOVERY
1

B NCA 43 (CB)

FAA
2

B 729-1234 (TELEPHONE)
F FAA (ASSIGNED FREQ)

01AA02 01CC63 01AA04 01AA05 01EE07
020003 020005
03CC01
04AA01 04AA05
05AA01 05AA04 05DD06 05FF07
06DD05
07EE01 07FF05
C08000

Figure 18.22. Direct Communication Links Coded

Figure 18.21. List of Communication Services by Station

1 COMMAND EXAMPLE COMMUNICATION PROBLEM

UNITS -

A NCA 41 (138.54 MHZ)
C 723-2293 (TELEPHONE)
E 729-2991 (TELEPHONE)

TO	PRIORITY	THRU	ON	CALL
2 BALLOON	DIRECT	NCA 41 (138.54 MHZ)	PASSIVE RELAY (138.54)	
3 SCI VAN	DIRECT	723-2293 (TELEPHONE)	729-0527 (TELEPHONE)	
	BALLOON	NCA 41 (138.54 MHZ)	PASSIVE RELAY (138.54)	
4 BACKUP A/C	DIRECT	NCA 41 (138.54 MHZ)	NCA 42 (138.54 MHZ)	
	TRACK. A/C	NCA 41 (138.54 MHZ)	NCA 43 (138.54 MHZ)	
5 TRACK. A/C	DIRECT	NCA 41 (138.54 MHZ)	NCA 43 (138.54 MHZ)	
	BALLOON	NCA 41 (138.54 MHZ)	PASSIVE RELAY (138.54)	
	BACKUP A/C	NCA 41 (138.54 MHZ)	NCA 42 (138.54 MHZ)	
	FAA	729-2991 (TELEPHONE)	729-1234 (TELEPHONE)	
6 RECOVERY	TRACK. A/C	NCA 41 (138.54 MHZ)	NCA 43 (138.54 MHZ)	
7 FAA	DIRECT	729-2991 (TELEPHONE)	729-1234 (TELEPHONE)	
	TRACK. A/C	NCA 41 (138.54 MHZ)	NCA 43 (138.54 MHZ)	

Figure 18.23. Sample Routing Sheet

18.6.1.5 VALIDATION

The results can be checked by inspection.

18.7 BALLOON DESIGN

18.7.1 Full Scale Dimensions

Program FULL SIZ.

18.7.1.1 PROGRAMMER

Justin H. Smalley.

18.7.1.2 DESCRIPTION

This program calculates the actual dimensions of a specific balloon using equations for the natural shape in which circumferential stress is zero. The balloon may have a cap and various types of end sections and may be top-loaded.

Using the initial input conditions, the program attempts to find a solution in a fixed number of iterations. If a solution is found the results are printed in a table with the requested number of increments. If no solution is found, a table of intermediate results can be printed out from which a better set of input data is available for subsequent calculations.

18.7.1.3 DATA REQUIRED

The flight requirements of load and altitude, the type of balloon desired, whether or not a cap will be necessary, and an approximation of other acceptable balloon parameters is required. Table 18.4 is a list of the input data for FULL SIZ.

18.7.1.4 RESULTS

Final results consistent with all the input data appear as in Figure 18.24 where the symbols mean the following:

- S - distance along gore from bottom
- R - inflated radius
- Z - vertical height above the base when inflated
- T - tape load assuming no stress in the film
- TM - film stress assuming no load in the tapes
- THETA - angle from the centerline
- G.W. - gore width at the equator

Table 18.4. Input Data for Balloon Design Program FULL SIZ

THETAO	- Initial half cone angle at the base (degrees).
SIGMA	- Film unit weight.
FOP	- Top load, weight supported on the top of the balloon including end fitting.
ELOP	- Bottom load, weight suspended from the bottom of the balloon including end fitting.
ALPHA	- Differential pressure at the base of the balloon.
DELS	- Estimated calculation increment size ($=S/N$).
OMEGT	- Tape unit weight, weight/length.
TANGL	- Taper angle for balloons with taper-tangent end sections. TANGL = 0 for fully tapered balloons (degrees).
TAUMO	- Initial stress at the bottom of the bottom end section. TAUMO = 99999 for fully tailored balloons.
TAUMI	- Stress at the point of tangency between the top end section and the natural shape of the balloon wall. TAUMI = 99999 for fully tailored balloons.
RZ	- Initial radius of material at the base. RZ = 0 for a fully tailored balloon or if TAUMO is specified.
RBOT	- Radius of the bottom end fitting.
RTOP	- Radius of the top end fitting.
N	- Number of major calculation increments along the gore length.
LNS	- Number of lines to be printed in the output table.
KIP	- Skip (if KIP = 1) the table of intermediate outputs, depending on confidence in achieving final results on a particular run.
SIGCAP	- Unit weight of film in the cap layer of film.
SCAP	- The distance along the gore where the cap starts (Equals zero if no cap).
SMAX	- A value greater than the estimated gore length. (Used to prevent certain calculations from diverging.)
BOY	- Buoyancy at the desired float altitude.
ENT	- No. of tapes (number of gores).

FILM UNIT WT. =	.00500	INITIAL ANGLE =	68.367
INITIAL RADIUS =	2.000	TAPER ANGLE =	68.367
INITIAL STRESS =	215.860	SECOND STRESS =	99999.000
BOTTOM LOAD =	1000.000	TOP LOAD =	40.000
INIT. PRESSURE =	-0.	TAPE UNIT WT. =	.01540
NO. OF MAJ. INC. =	200	NO. OF TAPES =	120

S	R	Z	T	TM	THETA
FULLY-TAILORED-- R = 2.000					
2.152	2.000	0.	22.605	215.860	68.367
25.505	73.632	8.799	22.770	18.402	67.293
48.852	45.053	18.099	22.997	9.749	65.656
72.212	66.132	28.149	23.299	6.729	63.206
95.566	86.662	39.273	23.693	5.222	59.675
118.920	106.331	51.850	24.206	4.348	54.875
142.273	124.684	66.273	24.865	3.809	48.522
165.627	141.079	82.877	25.700	3.479	40.461
188.981	154.686	101.822	26.728	3.300	30.614
212.334	164.527	122.957	27.939	3.243	19.053
235.688	169.630	145.695	29.286	3.297	6.635
MAX. RADIUS-- R = 170.169 Z = 155.872 G.W. = 8.910					
259.042	169.256	168.987	30.681	3.462	-8.000
282.395	163.139	191.451	32.008	3.747	-22.474
305.749	151.615	211.733	33.156	4.177	-36.745
329.102	135.559	228.508	34.054	4.798	-50.184
352.456	116.154	241.504	34.681	5.702	-62.244
375.810	94.602	250.419	35.066	7.079	-72.478
399.163	71.893	255.782	35.267	9.369	-80.573
422.517	48.692	258.362	35.349	13.865	-86.336
445.871	25.353	259.093	35.368	26.643	-89.666
469.224	2.000	258.969	35.366	337.720	-90.530
469.224	2.000	258.969	35.366	337.720	-90.530
TOP OF BALLOON-- R = 2.000					
VOLUME =	15163834.416	AREA =	302925.242		
SKIN WT. =	1514.626	TAPE WT. =	863.150		
TOTAL WT. =	2377.777	CAP WT. =	0.		
MAX S =	471.224	TOP LOAD =	40.000		
CAP LENGTH =	0.	VOL% S&S =	.14492		
GROSS LOAD =	3417.777	BUOYANCY =	.06022539		

Figure 18.24. Results of Balloon Design Program FULL SIZ

18.7.1.5 VALIDATION

This program, or its modifications, has been used to design hundreds of balloons and is considered to be fully validated.

18.7.2 Nondimensional

Programs FULLEND, SUBLOAD, OVERLOAD.

18.7.2.1 PROGRAMMER

Justin H. Smalley.

18.7.2.2 DESCRIPTION

These programs are used in parametric studies, to find first design approximations, or to make trade-off choices.

Program FULLEND is the same as program FULL SIZ described in the previous section, but with non-dimensional parameters.

Programs SUBLOAD and OVERLOAD are reported in Smalley (1965) and the descriptions will not be repeated here. They consider the cases of a balloon carrying less than, or more than, the design load.

References

- Akin, S.W. (1950) The thermodynamic properties of helium, Transactions of the ASME: 751-757.
- Angevine, J.M. (1968) Test Report, Stonehenge Launch Test, Unpublished Report, NCAR.
- Angevine, J.M., Sparkman, J.W., and Fulker, D.W. (1969) Design of the Stonehenge Launch System, NCAR TN-40.
- Angevine, M. and Fulker, D.W. (1970) Forces in a Cable-Restrained Balloon System, NCAR TN-47.
- Byrnes, W.R., Reid, R.C., and Ruccia, F.E. (1964) Rapid depressurization of a gas storage cylinder. Industrial and Engineering Chemistry Process Design and Development 3(3), 206-209.
- Dean, John W.: A Tabulation of the Thermodynamic Properties of Normal Hydrogen from Low Temperatures to 300°K and from 1 to 100 Atmospheres, NBS Tech. Note No. 120. Also, A Tabulation of the Thermodynamic Properties of Normal Hydrogen from Low Temperatures to 540°R and from 10-1500 Psia, NBS Tech Note No. 120, Sup. A, British Units.
- deGraaf, W.: Compressibility isotherms and thermodynamic functions of hydrogen and deuterium. Conclusions regarding the intermolecular field. QC 318, G72.
- Hilsenrath, et al (1962) Tables of Thermal Properties of Gases, NBS Circular 564.
- Kalman, H.S. (1968) Computing Volume of Helium in Cylindrical Steel Containers at 10 to 1,000 Psia, Bureau of Mines Information Circular, IC8367.
- Kalman, H.S. (1969) Private communication.
- Keesom, W.H. (1942) Helium, Elsevier Publ. Co.
- Mann, D.B. (1962a) The Thermodynamic Properties of Helium From 3 to 300°K Between 0.5 and 100 Atmospheres, NBS Tech. Note 154.
- Mann, D.B. (1962b) The Thermodynamic Properties of Helium From 6 to 540°R Between 10 and 1500 Psia, NBS Tech. Note 154A.
- Miller, J.E., Brandt, L.W., and Stroud, L. (1961) Compressibility Factors for Helium and Helium-Nitrogen Mixtures, Bureau of Mines Report of Investigations, RI5845.

- National Center for Atmospheric Research (1969) Facilities for Atmospheric Research.
- Nidey, R. A. (1968) Stabilization and Orientation of Balloon-Borne Instruments, NCAR.
- Roark, R. J. (1965) Formulas for Stress and Strain, McGraw-Hill, New York.
- Simmons, J. T. (1960) The Physical and Thermodynamic Properties of Helium, Whittaker Controls, Div. of Telecomputing Corp.
- Smalley, J. H. (1965) Free balloons with off-design payloads. In Proc. Balloon Symposium, Air Force Cambridge Research Laboratories, AFCRL-66-21.
- U.S. Standard Atmosphere (1962).
- Wilson, M. P., Jr., (1960) Thermodynamic and Transport Properties of Helium, General Dynamics Corporation Electric Boat Div., P60-002, MGCR-PR-1550.
- Woolley, H. W., Scott, R. B., and Brickwedde, F. G. (1932) Compilation of thermal properties of hydrogen in its various isotopic and ortho-para modifications J. of Res., NBS 41:379.

Contents

19.1 Introduction	227
19.2 Balloon System	228
19.3 Instrumentation	228
19.4 Results	230
19.5 Conclusions	240

19. Experimental Balloon Gas and Film Temperatures

R.M. Lucas, G.H. Hall, and B.M. Allen
Arthur D. Little, Inc.
Cambridge, Massachusetts

Abstract

This third balloon flight in a series for the Office of Naval Research has culminated in the acquisition of extensive flight data during ascent, float, sunset and sunrise. The vehicle was a 250,000 cubic foot polyethylene balloon which floated at an altitude of 80,000 feet and provided experimental data over a period of 16-1/2 hours. The data, comprised of some 120,000 data points and inflight calibrations, have been reduced to give the time history of balloon gas, local air, and film temperatures at seven locations on the balloon surface. In addition, the infrared radiation equilibrium temperature and balloon azimuth and rotation rate was also obtained.

19.1 INTRODUCTION

This balloon flight was the third in a series for the Office of Naval Research. The previous two instrumented flights were reported in the Proceedings of the Fourth and Fifth Balloon Symposium. This flight took place on the 25th and 26th of May 1969 at the National Center for Atmospheric Research (NCAR) flight station, Palestine, Texas.

From the previous two flights, we learned that our measurement techniques were good, the data obtained were accurate but incomplete, and that our theoretical computer model of a balloon and its vertical motion were in need of further improvements. In order to achieve this improvement, we needed extensive temperature measurements of the balloon fabric and verification of all temperature measurements through three critical phases of a trajectory, ascent, ballasting and sunrise-sunset. The purpose of this flight, then, was to obtain extensive and accurate temperature measurements of the several parameters affecting the behavior of a balloon system. Launch took place at 5 PM, local time; altitude was achieved after 1.5 hours; sunset occurred at 3.5 hours, two ballast drops at 3.8 and 5.2 hours, sunrise at 13.3 hours and termination at 16 hours after launch.

19.2 BALLOON SYSTEM

The balloon, helium, telemetry system, ground support and flight management were provided by NCAR. The general configuration and dimensions of the balloon system are shown in Figure 19.1.

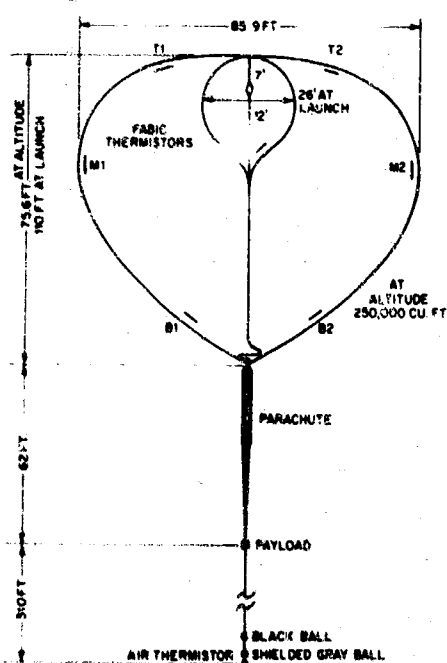


Figure 19.1. Balloon Configuration

In addition to the two helium thermistors at 7 and 12 feet below the top fitting, there were a total of seven film thermistors attached to the inside surface of the balloon. Positioned 370 feet below the balloon were two air, two blackball and one shielded grayball thermistors. The blackball measures incident flux while the grayball, covered with material identical to the balloon film, measures the absorbed radiant heat flux. Also measured were the gondola or instrument-package temperature and the temperature of the 14-inch diameter, aluminum cover plate of the top fitting.

The gross weight of the system was 585 pounds and the free lift was 10 percent. Float altitude was 80,000 feet.

19.3 INSTRUMENTATION

The telemetry system, 9-mil diameter aluminized thermistors, circuitry,

and thermistor-mounting arrangements were identical to those used in the previous flight, and the full description is contained in the Proceedings of the 5th Symposium. In addition, an extensive discussion of the instrumentation and calibration procedures was given at the 23rd Annual ISA Conference, 29 October 1968, Paper No. 68-805, by G. H. Hall, entitled "Helium Gas and Air Temperature Measurements in High Altitude Balloons."

The grayball is similar in construction to the blackball. An inner, aluminum-tubing framework in the form of a 7-inch diameter icosahedron supported the aluminized thermistor. This framework was covered with the 1.5 mil polyethylene balloon fabric. The assembly was then supported within a larger similar framework which was covered with a 1/4 mil polyethylene film. This outer surface acted as a convective shield.

Two magnetometers, manufactured by the Schonstedt Instrument Co., oriented at 90° to each other and aligned with the film sensors were mounted to the parachute load ring just below the bottom fitting. The connection between the parachute and the bottom fitting of the balloon consisted of universal joints to allow relative bending of the connection but not rotation. This rotation of the balloon and bottom fitting would directly rotate the magnetometers. The two magnetometer outputs used together uniquely determine the magnetic heading of the balloon reference gores. This information together with an equation that states the sun azimuth for any geographical location at any time will, therefore, give the desired heading of the film thermistors with respect to the sun as a function of time.

The top and bottom film thermistors were located 30 feet from the fittings and the middle thermistors were situated at the maximum inflated diameter. Thermistors T1, M1, and B1 were located in the middle of the same gore while the second set were located on the 180° opposing gore. Thermistor M3 was located midway between M1 and M2 and served as a redundant temperature measurement, and would have provided a clue to the direction of balloon rotation in sunlight in the absence, or failure, of the magnetometers used for the rotation measurement. The locations were chosen for geometrical reasons and to insure that the sensors would not be in the fabric folds at critical portions of the flight.

Our calculations show that the boundary layer outside the balloon during ascent is of the order of $1/10$ or $1/2$ inch thick, while inside the balloon the boundary layer increased from $1-3/4$ in. at launch to about 12 inches at altitude. Hence, a measurement of film temperature should be made inside the balloon where disturbances from the adjacent gases are a minimum.

The balloon was layed out on the floor of a local building, and the helium sensor string and lead wires were pulled through the middle of the folded fabric. Next, the five, upper-film thermistor leads were taped to the gore seams at intervals from the top fitting, ending at the measured position, T and M. The bottom leads

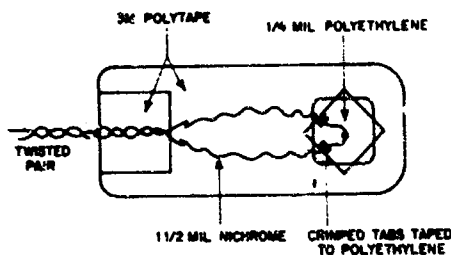


Figure 19.2. Film Thermistor Mounting

merely extended from the bottom fitting. Hence, there were 8 pairs of leads inside the balloon, 6 of which were fed through the top cover plate. At the film sensor locations, 6-inch vertical slits were made for insertion of the film sensor. The slits were sealed with tape, and care was taken to insure minimum helium leakage around the lead wires. The sensors were located 18 inches away from, and parallel to, the gore seam.

The maximum gore width at the M locations was 50 inches. The film sensor is shown in Figure 19.2.

The 2-inch wide 3M tape is backed up with a second piece of tape to anchor the twisted pair of leads to the tape itself. The nichrome leads take a wavy path to the thermistor. These two features isolate any mechanical loads produced by motion or stretching of the balloon fabric. The 1/4 mil polyethylene square provides mechanical protection for the thermistor bead, and holds the bead in close proximity to the balloon fabric; and the four open corners allow venting as the pressure is reduced during ascent. Because polyethylene is relatively transparent to the incident radiation, the 1/4 mil layer adds negligible absorption to the 1.5 mil balloon fabric. The crimped tabs of the thermistor platinum leads are taped to this 1/4 mil square, and thus provide a relatively strain-free mounting of the thermistor.

This method and other techniques of thermistor film mounting have been under investigation by NCAR, and a summary of their work by Mr. Karl Stefan is given in their Annual Report for 1969.

19.4 RESULTS

The data presented originated from balloon telemetry printed in digital form during real time at 15-second intervals. These data were later punched on computer cards and processed using our IBM 1130 system. The processed data were graphically displayed using a cathode-ray storage tube and a CALCOMP on-line plotter. Hard copy graphs of the CRT images were obtained by POLAROID photographs. All data points are connected by straight lines. The 5 msec time-response of the thermistors and telemetry system permit this detailed temperature definition.

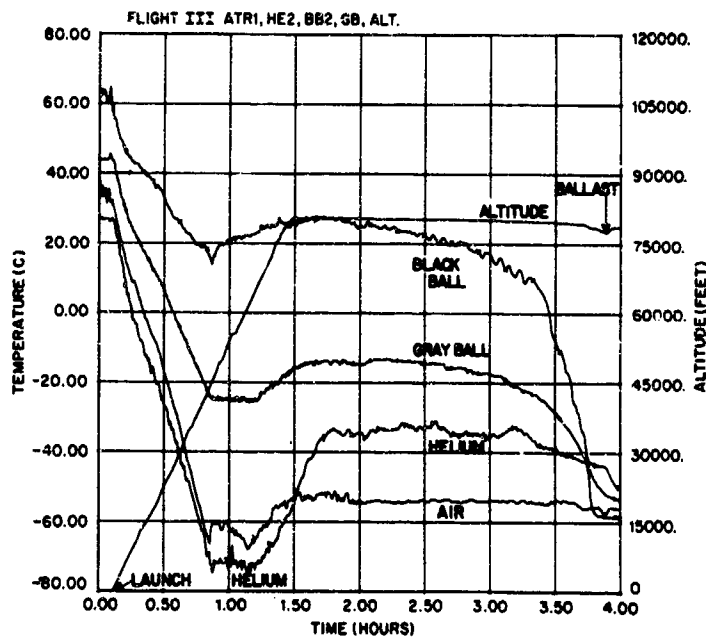


Figure 19.3. Temperatures and Altitude From Launch to Sunset

19.4.1 Launch to Sunset

As shown in Figure 19.3, the blackball temperature remains high until sunset, but the high air velocity during ascent and lack of complete convective isolation depresses the blackball temperature especially noticeable at tropopause. The grayball follows the same trend as the blackball, but indicates lower temperatures since it has a smaller solar absorptance.

The balloon is lift-controlled during ascent; the helium undergoes adiabatic expansion and is much colder than the surrounding air. As float altitude is reached at 1.5 hours, the convective and adiabatic processes have ceased, and the helium temperature starts increasing due to internal convective-heat transfer from the balloon film. The effect of sunset, starting gradually at 2.0 hours and ending abruptly at 3.8 hours, is indicated by the blackball temperature. The helium is slowly cooling and an abrupt decrease in helium temperature is noticed at the first ballast drop due to the adiabatic expansion on the recovery of altitude.

The film temperatures for this time period are shown in Figures 19.4 and 19.5. Before altitude is reached at 1.5 hours, the film temperatures are coupled to air temperature because of the convective heat transfer at high velocities, but are slightly higher than air due to solar heating. Helium temperature is lowest, so there is some thermal energy being put into the helium during ascent. Film

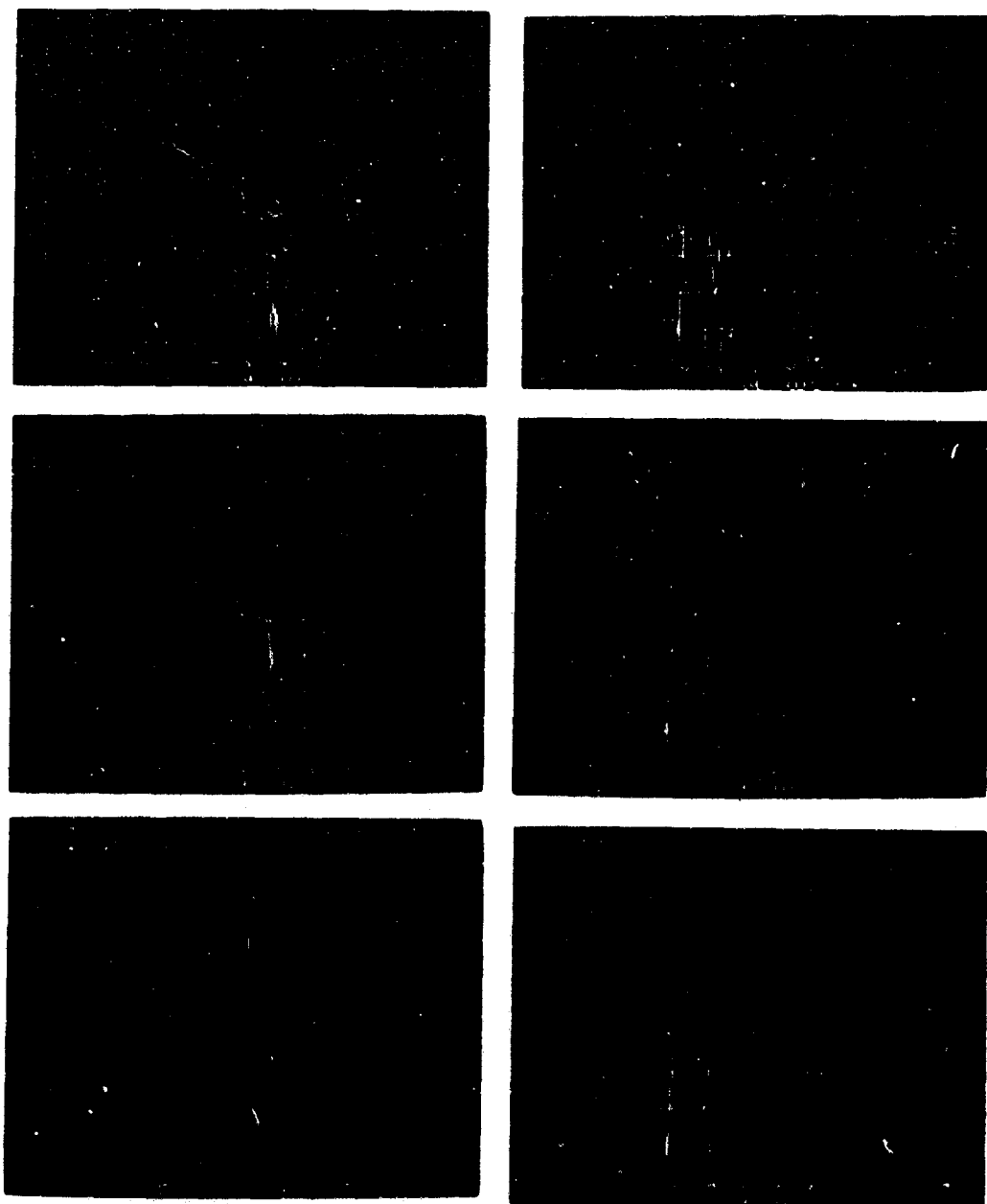


Figure 19.4. Film Temperatures and Rotation From 0.6 to 1.8 Hours

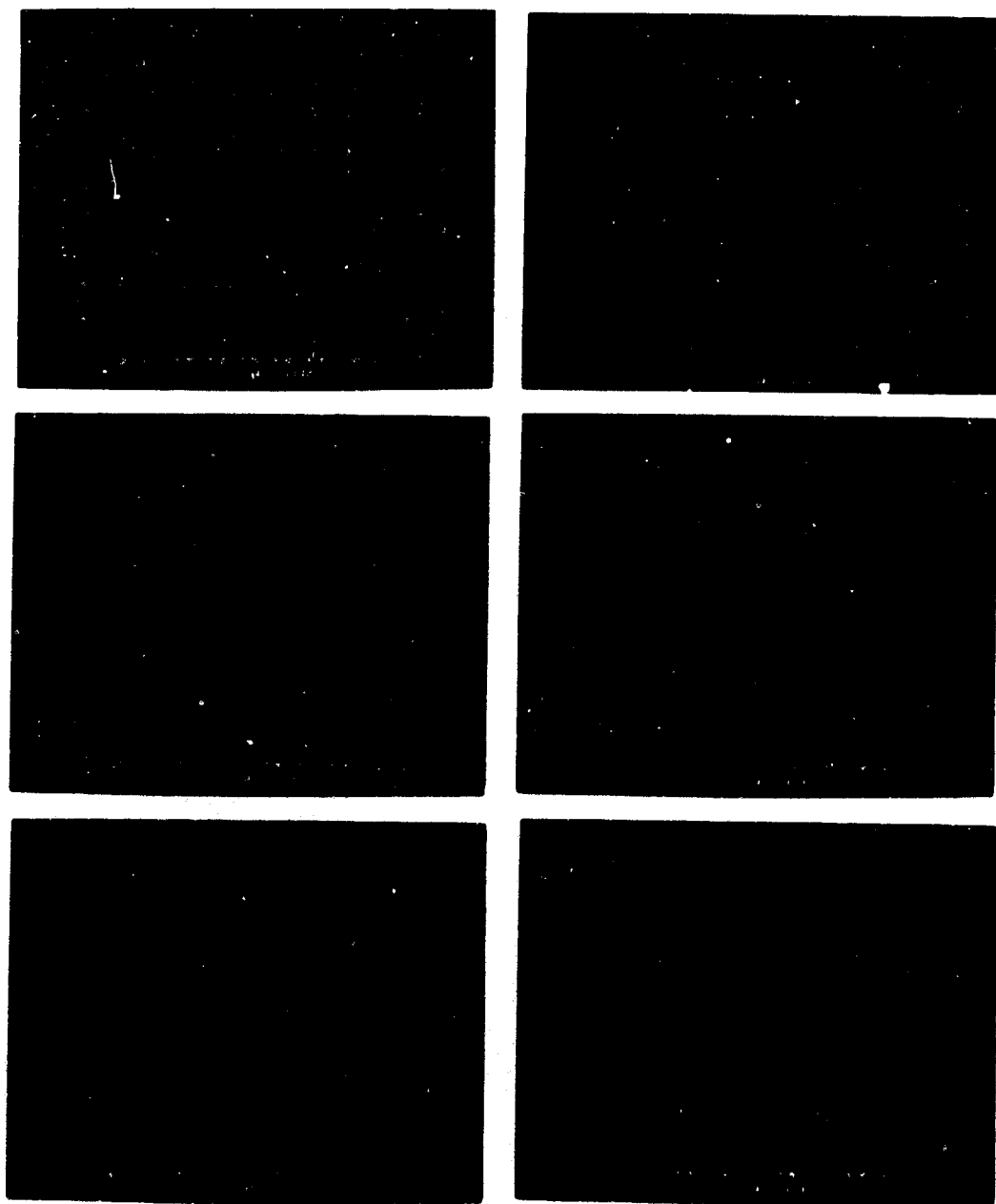


Figure 19.5. Film Temperatures and Rotation From 1.8 to 3.4 Hours

temperatures along gore 1 are about the same as gore 2, but there are differences from top to bottom of the balloon. Before 1.0 hours, only the top film sensors are exposed to the helium and their temperatures are lower than the middle and lower film locations which are still wrapped in the slack balloon below the bubble. At 0.95 hours, just above tropopause, the middle sensors become part of the partially deployed bubble; M1 in particular has come out of the folds and its exposure to the helium is noted by its sudden drop in temperature - below air, but still above the helium temperature. As the balloon reaches float altitude, the helium becomes exposed to more warmer fabric and its temperature steadily increases above air temperature.

In the relatively stable period of 1.8 to 3.4 hours, there is a small decrease in the average film temperatures as shown in Figure 19.5. The variations of the film temperatures generally are in phase, but the temperatures are different due to location. The bottom and middle locations are warmer due to sun and earth radiation, while the top locations are about 5 degrees cooler due to partial shielding from the radiative inputs. Film T_2 temperature is out of phase when compared to the remaining temperatures and is lower than the corresponding temperature of T_1 . During nighttime float, T_1 and T_2 are within $1/2^\circ\text{C}$ of each other which indicates their individual calibrations are accurate. We can only speculate that the position of T_1 and T_2 combined with a low sun angle of about 5° below horizontal near sunset leads to this temperature difference. During this time period the balloon is dropping slightly in altitude, losing about 1000 feet from 1.5 to 3.5 hours.

In Figure 19.6, the sunset effect on a typical film temperature and rotation is quite apparent. Sunset is complete at 3.8 hours, sensor B2 shows a very steady temperature and balloon rotation has essentially ceased. During ascent, average rotations are 30 RPH; at ceiling prior to sunset, 12 RPH; nighttime float, 1.2 RPH and at sunrise the angular velocity increases to 8 RPH. It is noted that an attempt to correlate instantaneous film temperature with sun heading will not give consistent results. As the warmer film rotates out of the sun, the adjacent helium rises due to local contact with the warm film. This film is replaced by cooler film. Further, the film in the lower half of the balloon is warmer than the top which tends to encourage the natural convection currents caused by wall heating. Thus the convective heat transfer process is quite complicated, and it appears that average temperatures must be used in describing the balloon temperature behavior. It is also noted that the frequency of the film temperature variations is just twice that of the rotational frequency. In other words, in one revolution of the balloon, any section of film faces the sun twice; once directly and once again on the opposite side where it sees the sun's radiation filtered by the first layer of film.

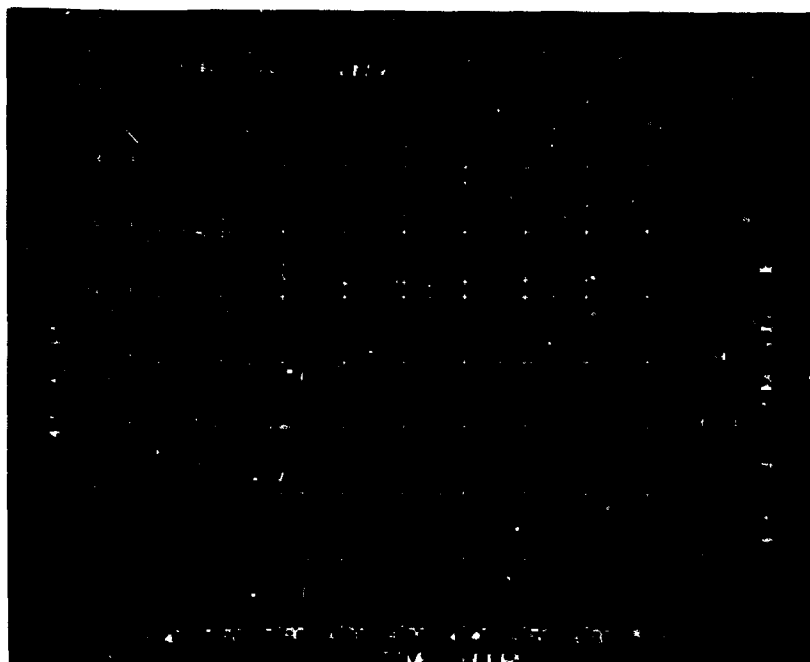


Figure 19.6. Sunset Effect on Rotation and Film Temperature

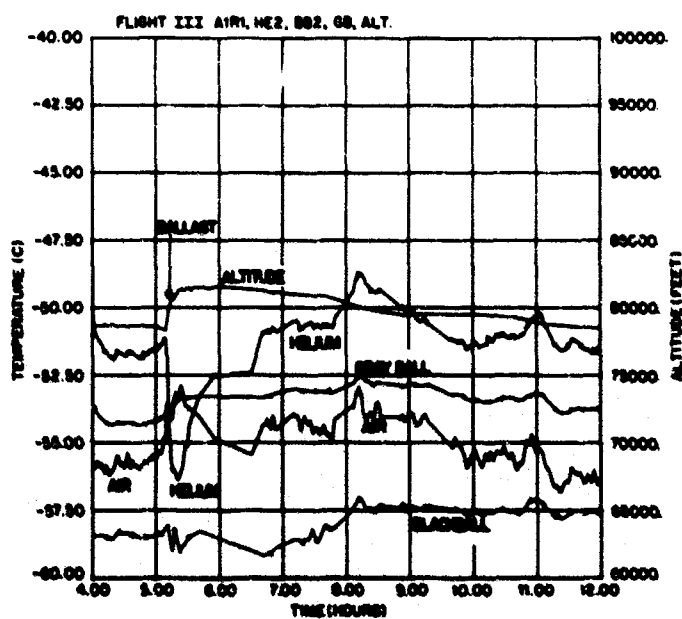


Figure 19.7. Nighttime Temperatures and Ballast Effect

19.4.2 Nighttime

In Figure 19.7, the nighttime temperatures are shown with the effect of ballast at 5.2 hours. Helium temperature drops 5 degrees due to adiabatic expansion as the altitude increases about 3000 feet. Air temperature increases due to the existing temperature inversion. Blackball and grayball are temporarily affected by the high velocity of ascent, and then return to their previous values.

At 8 hours, the ground trajectory shows that the balloon is leaving the wooded and grass covered terrain east of Waco, Texas, with a ground velocity of 24 MPH and is approaching the more arid and probably warmer area of Waco and Austin. At night, the balloon radiation input is the warm earth, and it can be shown that 50 percent of the earth's radiation received by the balloon at 80,000 feet comes from a 50-mile diameter area directly under the balloon. Thus at 8 hours the balloon sees a new radiative area about every 2 hours.

In Figure 19.8, the film temperatures are shown along gore number one. The temperatures of gore two were within $1/2^{\circ}\text{C}$ of those of gore one. The bottom film is everywhere warmer than either the middle or the top, which is the coldest. This confirms the source of the radiative input and shows that the helium is being warmed by the film through convective heat transfer. The ballasting also indicates that although the bulk helium temperature drop is rapid and large, at 5°C , the film temperature change is only $1-1/2^{\circ}\text{C}$ and the film temperature is strongly coupled to the radiation field.

19.4.3 Sunrise

In Figure 19.9, the temperatures and altitude are presented from 12 hours, through sunrise, to 1600 hours which was 10 AM CDT. Sunrise starts abruptly at 13.3 hours and its effect is completed within one hour. There are further small changes in temperatures and altitude due to the steady increase in solar radiation, as the optical air mass between the balloon and sun decreases. The before-and-after sunrise altitudes are about the same as the before-and-after nighttime ballast altitudes. These increases in altitude were 3000 feet. It is also of interest to note that the temperatures of Figure 19.9, two hours after sunrise, are essentially identical to the temperatures at two hours before sunset. With the exception of the helium temperatures, which tend to lag because of adiabatic expansion and contraction, the temperature-time profiles are very similar. The only difference in the balloon system before sunset and after sunrise is the dropping of 45 pounds of ballast and, undoubtedly, the loss of helium gas.

The sudden start of rotation due to solar heating and altitude increase when the sun rises at 13.3 hours is shown in Figure 19.10. Before sunrise the pattern of film temperatures, the bottom being highest and the top lowest, is obvious because

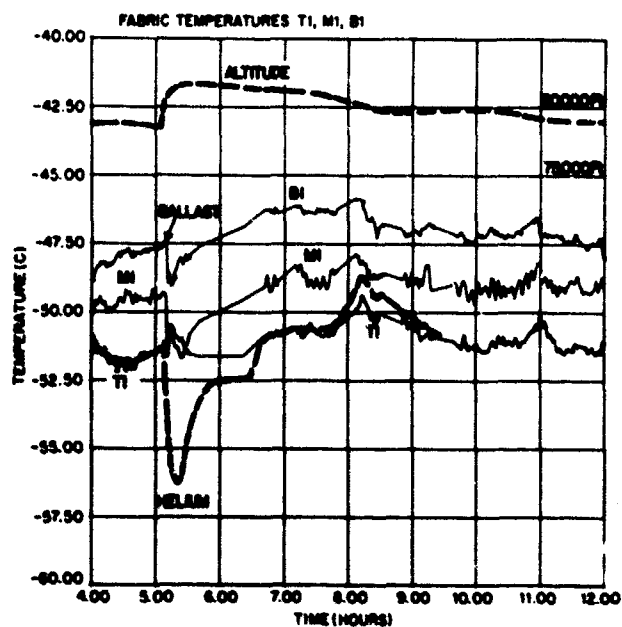


Figure 19.8. Film Temperatures and Ballast Effect

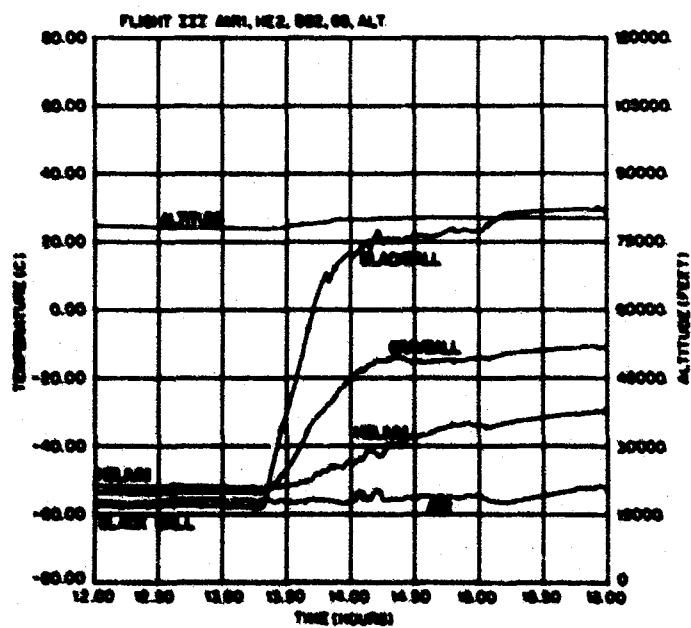


Figure 19.9. Temperatures and Altitude During Sunrise

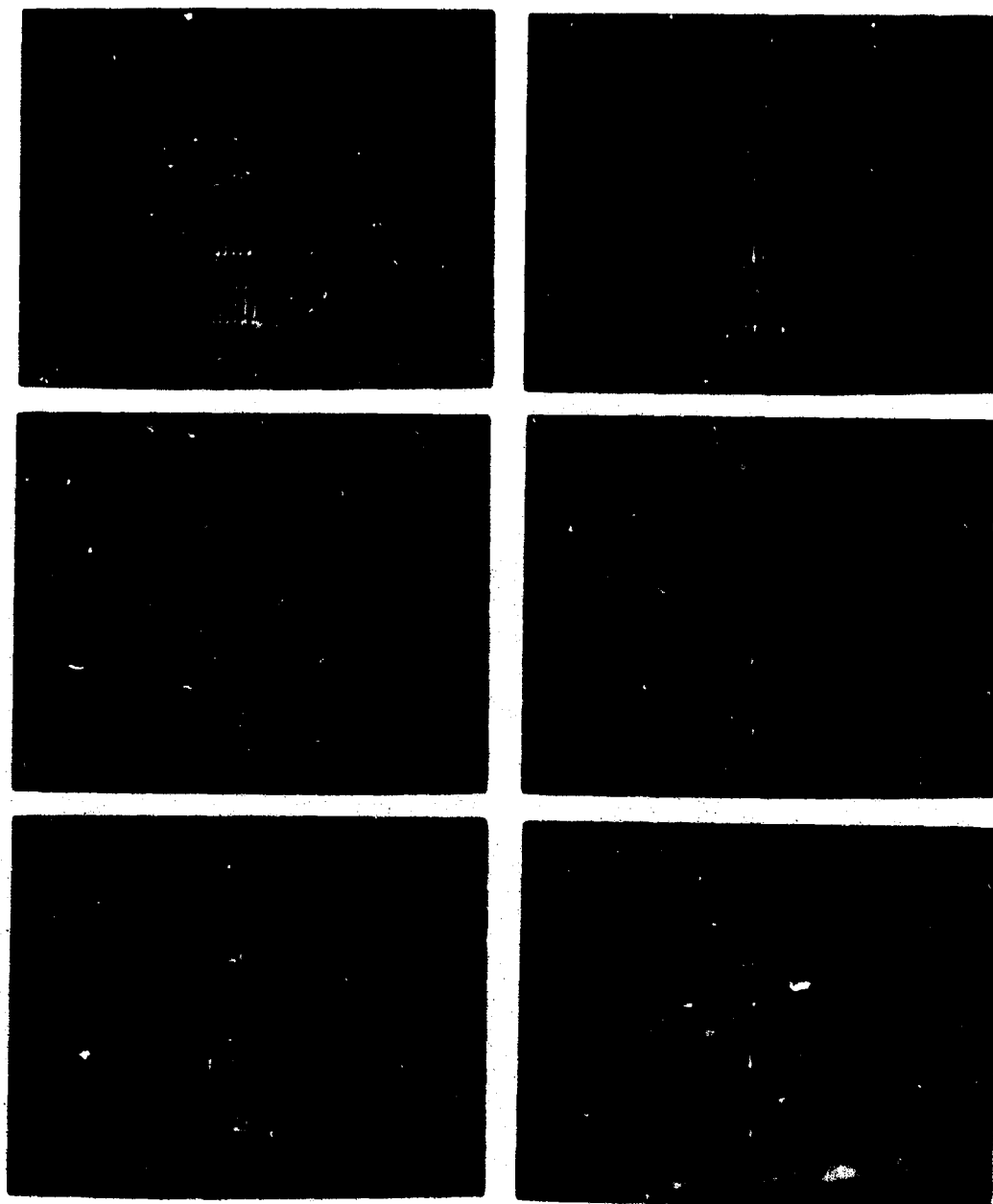


Figure 19.10. Film Temperatures and Rotation During Sunrise

of earth as the radiation source. During sunrise, however, the balloon rotation and the large-scale convective motion taking place in the helium completely obscures any consistent temperature differences. At about 14.5 hours, the maximum altitude has been reached, rotation has slowed considerably, and T2, although facing the sun, is lower in temperature. This may be caused by the low sun angle which locates the film surrounding T2 at the top of the balloon and almost parallel to the sun's rays.

The gondola, or instrument box, temperature was of interest on this flight due to sonde telemetry problems. This temperature, which is considered approximate, along with the temperature of the upper fitting cover plate is shown in Figure 19.11.

We would like to extend our theoretical model and perform the same kind of instrumented flight to 130,000 feet. With the larger balloon required, the top cover plate would be the location of a portion of the electronics. Thus, the plate

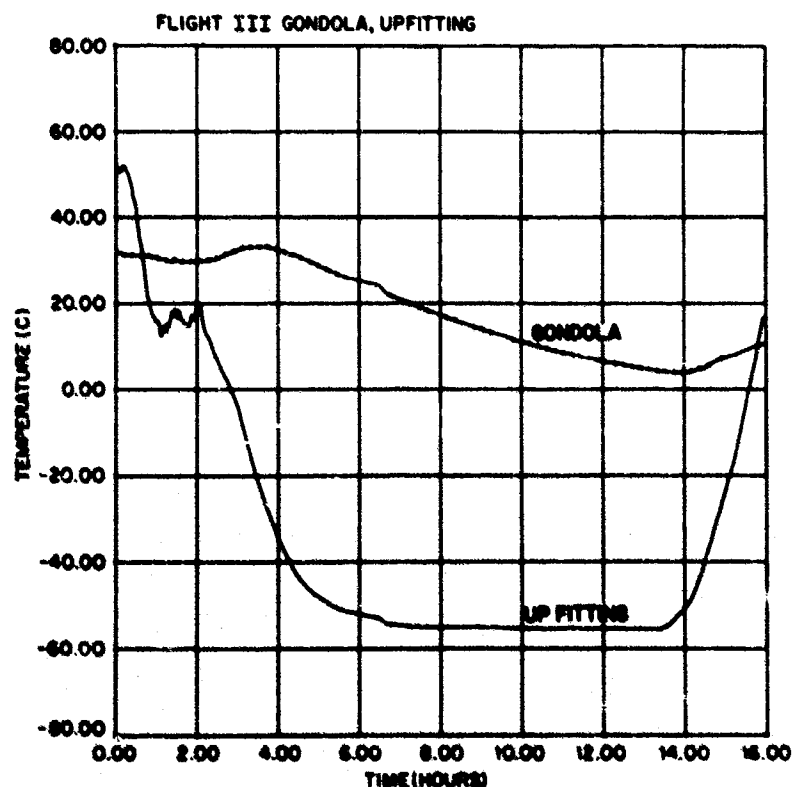


Figure 19.11. Gondola and Upperfitting Cover Plate Temperatures

temperature of -55°C , or approximately air temperature, would be the nighttime ambient temperature. Daytime temperatures would be close to $+15^{\circ}\text{C}$, and the electronics located there would operate between these temperature extremes.

19.5 CONCLUSIONS

After analyzing the data carefully, we conclude that there are several time periods during the balloon flight when distinctly different interactions with the environment predominate.

19.5.1 Phase I

During ascent, the interaction of the balloon fabric with the ambient air and the expansion of the helium gas dominate the balloon's thermal behavior. During the first hour of flight, the balloon ascends at about 1000 feet per minute and rotates rapidly. This results in heat transfer by forced convection which is dominating. Simultaneously, the helium cools by expansion as the atmospheric pressure decreases.

19.5.2 Phase II

Initially, at ceiling, the solar input dominates the balloon's behavior. Changes in fabric temperatures caused by rotation as thermistors move from shade to sunlight are more apparent. During sunset, the balloon initially descends at about 220 feet per minute into cooler ambient air, and the fabric temperatures drop sharply as the sun disappears over the horizon. Adiabatic compression is insufficient to maintain temperature and ballasting is necessary to counteract the effect of sunset.

19.5.3 Phase III

During nighttime floating, the infrared radiation absorbed by the balloon is the predominant influence. The warmer film near the bottom of the balloon is influenced by the earth's radiation. The upper film is shielded from earth and is exposed to the cold sky. Consequently the temperature of the upper film is lowest.

Contents

20.1	Introduction	241
20.2	Applications of Balloon Control	244
20.3	The Mechanics of Control	248
20.4	Computers and AC	252
20.5	The Future	253

20. General Philosophy and Techniques of Balloon Control

B.D. Gildenberg
Air Force Cambridge Research Laboratories
Bedford, Massachusetts

20.1 INTRODUCTION

Is balloon control (henceforth referred to as AC, aerostat control) a reality? Can this encapsulated chunk of gas be directed to a destination with any degree of accuracy? One hint is that manned balloon pilots are often guided by rules derived from conventional aircraft manipulation. Many of the problems such as over-control are identical. Rather than risk tautologies, let us now examine actual flight experience for evidence.

The first example (Figure 20.1) does involve a manned flight. A low level, open gondola exercise ideally illustrates the fundamental approach to AC. Launching 50 miles upwind, one of the objectives was to pass over Holloman Air Force Base around sunrise. Gradient wind above the friction level was from the southwest. Southeasterly night drainage winds from the high Sacramento Mountains prevailed below. The pilots "drove" toward those mountains in the gradient wind until they were reasonably confident of being above the region of drainage flow. Now the balloon was valved down a few thousand feet, and vectored in on the Holloman flashing beacon. Trajectory corrections were simple. To steer right, apply power in the form of ballast. To steer left, drop flaps by pulling on the apex

valve cord. The flight actually did arrive directly over the runways at 0600. A few days later, flying north near this same course in a light aircraft, I experienced a stronger, southwest gradient wind. The result was an annoying cross wind. Again it was early morning, so with a minor drop in altitude the cross wind was promptly transformed into a convenient tail wind. In both cases, one adjusts altitude to take maximum advantage of vertical wind shear.

Figure 20.2 illustrates a second example, an unmanned flight with more sophisticated requirements. The operation demanded penetration of a 10 square-mile target area while bracketing the 15 to 40K ft region. There were two different intercept times, 9 hours apart, which we hoped to achieve with one flight. The first phase was easily satisfied by irreverently launching from the center of the target.



Figure 20.1. Open Gondola Trajectory



Figure 20.2. "Race Track" Technique for Target Flights

The mission was performed in a month with an intriguing grab bag of easterly flows above persistent westerlies. The transition zone found both light northerly and southerly winds, ideal for completing the race track. A field of light easterlies was employed to drive across and upwind of the target, while expending time in the long interval between intercepts. Total deviation was only 25 minutes in 9 hours.

One sees, therefore, that AC is achieved primarily by adjusting vertical position or rate, launch position and launch season, to take advantage of variations in the vertical wind profile. The second example utilized maximum conditions, but we shall find that a high percentage of routine launches can still take advantage of AC.

20.2 APPLICATIONS OF BALLOON CONTROL

The standard constant-level balloon profile involves a continuous ascent, float at a single level, and descent by parachute. Ten to fifteen years ago, requirements for deviations from this simple vertical trajectory provided the catalyst for AC development. Experimenters concerned with obtaining vertical slice data through the atmosphere might purchase two flights for the price of one by having the entire system slowly valved down, at least to the tropopause. This is a region of special interest for atmospheric scientists, and very fine detail might now be obtained by driving the balloon through a number of times, and at very slow ascent rates. An alternate technique would be to step through in a succession of float altitudes, perhaps only 1000 feet apart. The potential for innumerable float altitudes is limited only by balloon volume and ballast. In Figure 20.3, four are demonstrated, with sufficient initial ballast for two or three more.

Concurrent with preliminary requests for modified flight profiles, a different problem appeared, generating further momentum in AC development. White Sands Missile Range became interested in utilizing balloons as targets for guided missiles. This application required positioning the aerostat over a specified target area (generally 10 miles square) at a predetermined time and altitude. The early flights were especially difficult, since economics negated use of ballast or an apex valve. AC was applied primarily by judicious choice of the launch site and initial ascent rate. Occasionally a few thousand foot tolerance in float altitude provided lucrative variations in trajectory. This kind of mission gradually expanded to include dropping powered or dummy nose cones, ejection seats, and even Captain Kittinger, over WSMR target areas. Indeed, target flights are still in process today, and include balloons as large as 26-million cubic feet, in the case of Project Voyager. Timing is especially difficult since WSMR is inclined to schedule a balloon mission as if it were a missile. The necessity for precision, however, has contributed further discipline to AFCRL ballooning, and conforms nicely to the overall philosophy of AC.

Statistics from these target flights offer one of the best quantitative tools for judging effectiveness of AC. The results are rather surprising. Figure 20.4 indicates that 59 percent have been within 5 nautical miles of target center - not just within the area. Accuracy has remained more or less constant over the years, since the earlier missions flew at lower altitudes (averaging 50K ft) but with less control capability. The more recent operations see substantial airborne control, but launch sites are fixed, and altitudes range up to 130K ft. Figure 20.5 indicates that 70 percent of the missions have been within 15 minutes of scheduled intercept, which is average WSMR mission tolerance. Looking at Figure 20.2 again, we see the prime target area. That particular flight was not typical, since it involved

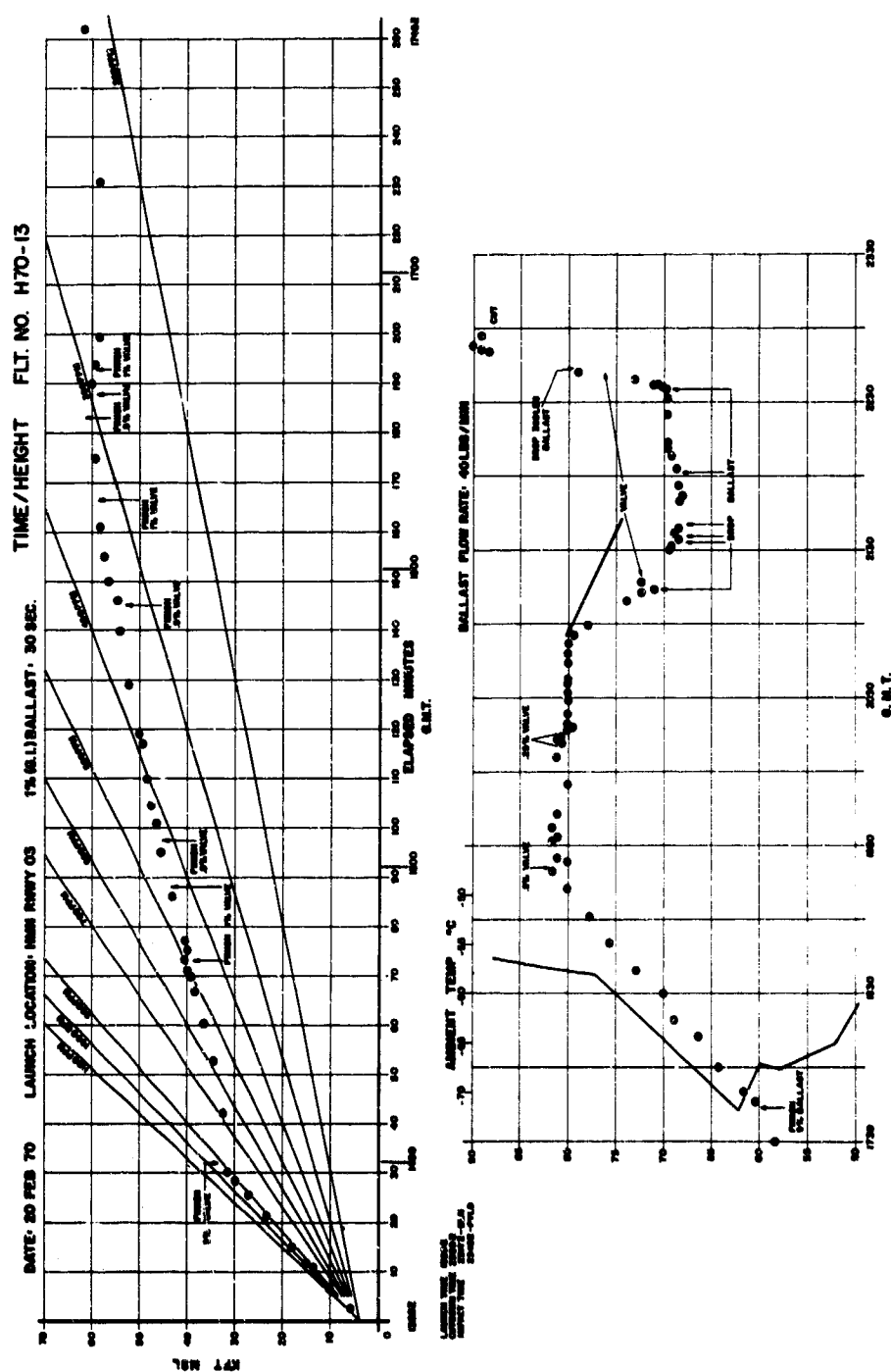


Figure 20.3. Multiple Float Levels

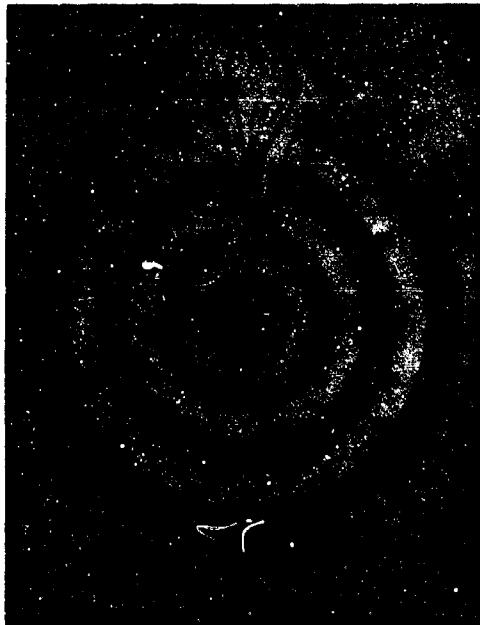


Figure 20.4. Position Accuracies for Target Flights

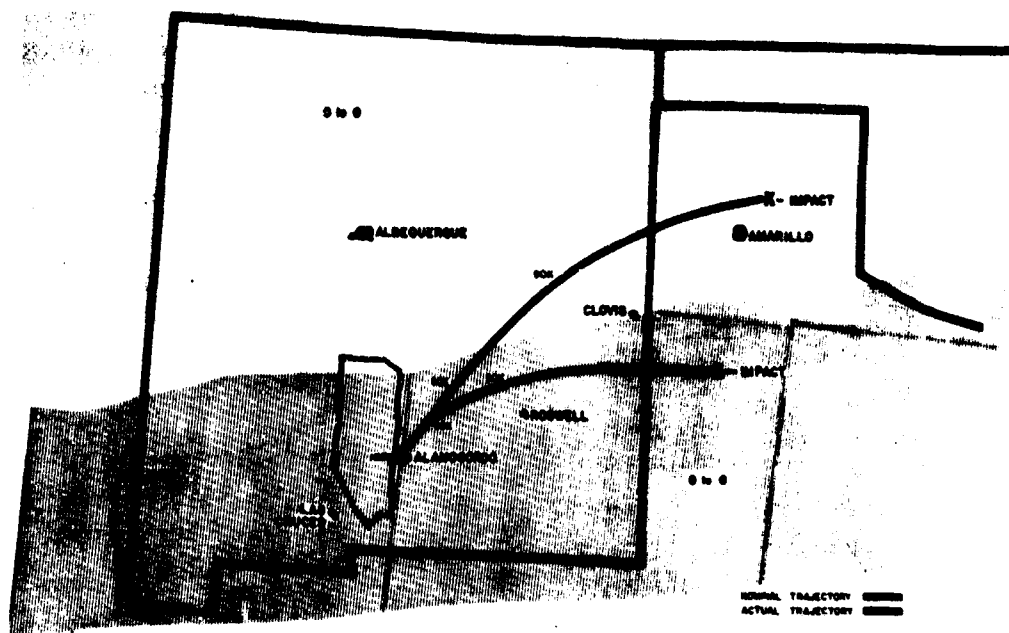


Figure 20.5. Timing Accuracies on Target Flights

relatively low altitude, with two intercept times. But it does vividly illustrate the degree of finesse possible in AC. In several target exercises, the balloon arrived at float altitude short of the target, with calm winds, or flow blowing it in the opposite direction. We promptly went down 10 to 15,000 feet, drove into the target, and ballasted rapidly back to float for a successful mission. One needs copious ballast and a low air intake altitude for this sort of acrobatics.

Contrasting terrain features offer special problems for target flights. Even at 50 kilometers, a balloon floating from the flat plains of Texas will experience a trajectory deflection as it passes over the Rocky Mountains. Deflection varies with speed, time of day and, probably, altitude. Hitting the target in this case is like playing a billiard shot. One solution involves prior launch of a small pathfinder balloon to calibrate the situation. Another is to level off at several altitudes below natural float until you find one that vectors into the bull's eye. Then latch ballast open before penetrating the target border. This allows time for other command functions, which usually are required just prior to the intercept.

Now we turn to an aspect of AC which has wide application in everyday balloon operations - avoidance of weather. It might be expressed by the equation $(No\ Go)^{AC} = Go$, and a classic example is offered in Figure 20.6. The normal profile (to the south) would have resulted in a termination well within a region of extended cloud ceilings. By leveling off at 60K ft for 1.5 hours, the flight was driven



H70-13 Profile Modification

20 FEB 70

Figure 20.6. Profile Modification for Weather Avoidance

safely into the clear area up north. Penetration of the clouds after launch occurred within local restricted areas.

In many cases, payload or balloon-system restrictions prohibited such extended maneuvers. Merely decelerating ascent rate during penetration of the jet stream can provide some correction, if the direction is favorable. Sometimes there is significant variability in the float wind region, and a minor altitude compromise can make the equation work. Occasionally, stretching a 12-hour flight into a 24-hour flight provides another solution. The procedure is simplified by allowing the balloon to settle into regions of minimum wind speed in the low stratosphere. Not only does this require less ballast than a normal night time flight, but overall trajectory will not be significantly lengthened. The latter is actually a special case of our fourth application; minimizing trajectories.

We saw in Figure 20.2 how a "race track" course was established, taking advantage of the stratosphere wind reversal and the range of directional choices in the transition zone. Here one also finds the layer of minimum wind which may provide virtual hovering of the system. Methods and climatology of hovering have been covered in numerous presentations by Mr. Nolan of AFCRL. In its extreme form the technique is an alternate to captive ballooning.

A final application is float-altitude adjustment, a variant of profile modification. In Figure 20.3 there were two examples. The balloon established a natural float at 82K ft, and was then valved to assume a new float at 80K ft. Later, an interim float at 67.5K ft was ballasted to 69K ft. The procedure usually dictates a number of small incremental valvings or ballast drops. It is employed when a contractor desires a very precise float altitude. Perhaps the simplest technique is to set the gross load for a float several thousand feet too low, and then very slowly ballast into position. These maneuvers are complicated by dynamics of natural float oscillations, which may range over 1000 feet. Determination of the actual altitude poses other problems since the aerostat actually floats on a constant density surface.

In summary, principal applications of AC are as follows:

- (1) Special flight profiles
- (2) Target flights
- (3) Avoiding weather
- (4) Minimizing trajectories
- (5) Adjusting float altitude

20.3 THE MECHANICS OF CONTROL

We know what and why; the next subject is how. The first item of implementation is versatile, reliable, on-board control instrumentation. Not only does consistent performance from instrumentation inspire confidence, but it determines the safety and, therefore the feasibility of most AC activities. Anytime a valving descent is initiated, especially at night, one must have complete assurance that recovery, in the form of ballast control, will be available. Otherwise one is confronted with single-engine aircraft flight philosophy which requires that potential emergency landing sites be continually mentally surveyed. A completely independent back-up package with three basic commands - ballast, valve and termination, is one very efficient approach. A minimum altitude ballast floor provides further reserve. The use of downwind command stations, tracking aircraft command capability, and a spread of communication frequencies to cover diurnal shifts are other precautions. Telemetry functions which describe actual minutes valved and ballast residue are not mandatory, but contribute to precision. For AC, rapidly and easily converted, moderately accurate altitude information is more important than high accuracy. Telemetry verification of command reception is mandatory in order to establish timing. Historically, balloon instrumentation has demonstrated continuous advance in sophistication and reliability, thereby affording more opportunity for AC.

Although the atmosphere holds most of the cards in this AC game, meteorological support becomes a vital element of control. Perhaps the key word in NASA's brilliant Apollo operations is "update", and the same thing holds to a large extent in AC. There is no better forecast than current, prevailing weather. A weather station immediately adjoining the balloon flight center is an optimum solution. Standard upper air data become available only twice a day. A source of supplementary radiosonde information is therefore highly desirable. AFCRL schedules a run which will be complete about one hour prior to launch, and includes the temperature profile on the height-time curve. A raw chart is seen in Figure 20.7. Summer and winter standard curves are employed for comparison so that one may quickly visualize what parts of the ascent will be fast or slow, and if the tropopause is unusually deep or sharp. Note the ascent rate slopes which provide a quick-look capability. In AC operations it also helps to delineate altitude of air-intake, plus preliminary ballasting and valving times.

Other techniques for obtaining useful or quick upper air data include access to special Air Force facsimile circuit AFX109, which provides charts up to 100,000 ft MSL. Telephoning pertinent stations for their upper air data before transmission time can expedite critical decisions. If you want to know what will happen to the trajectory if float altitude drops slightly, the track of the actual ascent provides the most fresh data.

Now let us focus on the bread and butter mechanics of AC, those stick and rudder basics, ballasting and valving (B&V). Following are some elementary rules of thumb.

RANDOM GOLDEN RULES OF B & V

- (1) React quickly and accurately
- (2) Employ high rates of flow
- (3) Stratosphere and troposphere are different animals
- (4) The nighttime stratosphere eats ballast
- (5) Valving effect is minimum at sunrise
- (6) Descent rates often double after tropopause penetration
- (7) A cold or sharp tropopause may simulate a solid surface
- (8) Invest no ballast in post-sunrise surface inversions
- (9) Turbulence decreases ascent rate
- (10) Carefully compute ballast needs; fly double
- (11) To level off, overvalue slightly
- (12) After the ballast is gone, ballast
- (13) The atmosphere's command switch is always on

Rule (1) is again related to the lore of conventional aircraft, which advises "Don't let the ship fly you all over the sky. You fly it. Do something; react!" A variation on this theme is, "Don't let the ship get ahead of you" and this is

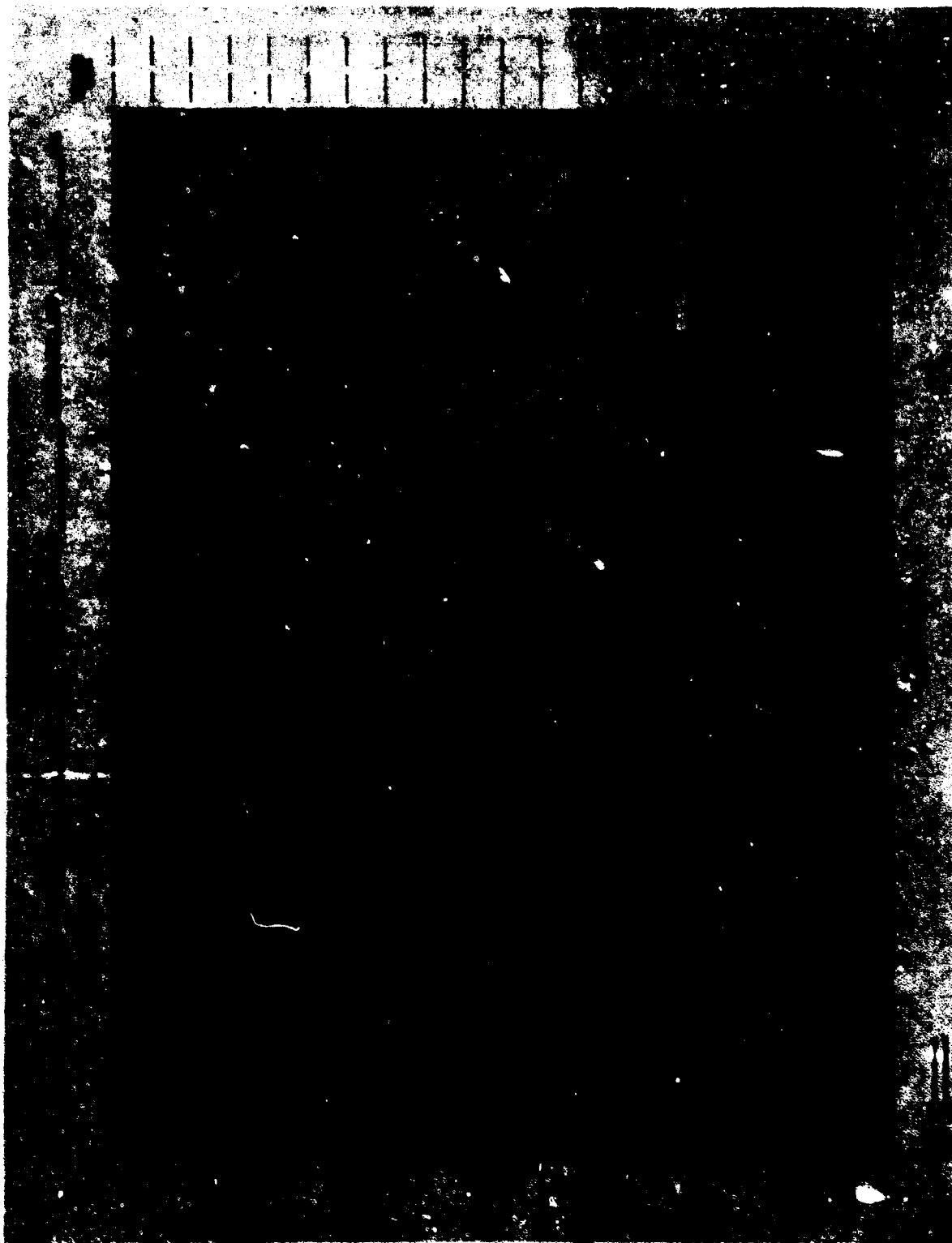


Figure 20.7. Basic Height-Time Curve

especially pertinent in AC. A surprising amount of concentration, discipline and quiet are required. After all, a scrim balloon with a ten-ton gross inflation, climbing at 1400 fpm in a 200 knot jet stream is, in a sense, a "hotter" vehicle than some World War Two aircraft. Of course, reaction time also depends heavily upon on-board sensors. The art of AC would be substantially enhanced by a functional rate of climb indicator.

In rule (2), the demand for fast response implies high rates of flow for both ballast and valving. Ballast capabilities are systematically increasing. Larger area apex valves have been utilized, and blowing a duct is another consideration. Faster flows also mean less command time with corresponding benefits in the instrumentation realm.

Complications offered by rule (3) will be expanded when the stratopause is penetrated with some regularity.

Referring to rule (4), sudden increase of cloud coverage or an unusual inversion can actually level off a flight in the night stratosphere.

The solution to rule (5), if a sunrise or early morning descent becomes necessary, is to generate some downward inertia prior to balloon sunrise. Cutting an auxilliary duct, a device being tested by Dr. Howell, is a more direct approach if no further maneuvering is desired.

Rule (6) offers difficulties in timing a descent, since the balloon first slows up radically at the top of the tropopause, then falls out the bottom.

Referring to rule (7), precision radar data at WSMR have demonstrated very rapid decelerations for balloons encountering the tropopause on ascent. One incident showed a flight literally bouncing off the tropopause base three times, after contact at 1000 fpm, then dropping 1100 feet and finally penetrating at a slower ascent rate. The identical action was visually observed for a system which, at launch, encountered a low level inversion. On top of this tropopause "firmament", especially with cold minimum temperatures found in southerly latitudes, a slowly descending balloon will actually level off for a nominal 30 minutes, sometimes longer.

The logic behind rule (8) is that radar data have shown the balloon is still rising, although too slowly to be detected by conventional on-board devices. After ten minutes or so, the ascent rate increases and is soon back to normal unless there is significant cloud cover.

Rule (9) has been the spoiler of many a good trajectory forecast. Maximum turbulence usually does not occur where the maximum jet exists, but at the altitudes of maximum shear.

Rule (10) is rather obvious. A supplementary factor is that extra ballast can always be jettisoned somewhat early without sacrificing altitude.

Rule (11) pertains to float altitudes engendered by using the apex valve rather

than natural ducting. If the vehicle is valved initially to an exact constant level, superheat will drive the system up after perhaps five minutes. The process becomes an awkward one with repeated valving exercises and a large potential for overcontrol. Experience indicates that actually generating a slight descent rate initially, something like 100 fpm or less, usually results in a stable float. The technique is still "seat of the pants" pilotage, and probably associated with the fact that zero-pressure balloons tend naturally to oscillate at float.

Rule (12) is not an extract from "Alice in Wonderland." It makes sense when ballast is equated to aviation gas. If the gauge reads empty at 10,000 feet, one does not automatically turn off the master switch. Even telemetry is not infallible. On a critical flight it may pay to blow ballast hoppers by command in order to take advantage of any residue.

Rule (13) is aptly numbered. The most maladroit armchair balloon pilot cannot lacerate a planned profile more ingeniously than our wily atmosphere. A height-time profile on a day with deep surface inversion, jet stream and sharp tropopause would prompt an unwary analyst to flag five cases of ballasting or valving. It typifies the major problem for AC. With an ascent rate of 600 fpm and 800 fpm required, the first question is not how much ballast, but what will the atmosphere do to the current rate in the next few layers? The number of variables contributing to the answer is rather uncomfortable. If conditions over the next 10,000 feet appear to be conservative, then a rate-of-climb indicator would be exceedingly helpful. One simply ballasts until momentum predicts the system will coast into the desired rate. Actually, the current ascent rate represents a perfect integrator of all these variables at any given point and might provide a clue to numbers coming up. This points toward the next subject, a ubiquitous computer.

20.4 COMPUTERS AND AC

As small, relatively economical desktop models become rapidly available, their marriage with AC is inevitable. Fast, accurate response, golden rule number (1) is a computer. AFCRL, for instance, has one program to extract densities from a local radiosonde run, and the densities are in turn plugged into the valving equation program. For the first time, accurate, simultaneous tallies can be maintained for ballast residue, gross load and free-lift during rapid AC maneuvers.

Suppose a mission requires reaching float at a precise time. The following table demonstrates the type of answers which can be invaluable in such a situation.

100 fpm over last interval	600
110 fpm for prior interval	660

120 overall fpm above tropopause	640
130 overall fpm from launch	800
140 minutes to float for 100, 110, 120	80, 75, 77
150 required minutes to float	70
160 required fpm	755

The language is a brand of imaginary "basic" but it helps to visualize the argument.

Now our procedure would be to ballast rapidly in very small increments until 100 to 160 match. This could be very effective, but still constitutes "seat of the pants" pilotage. The next step, going to a larger computer, would involve a program solving the aerodynamic drag constants of this particular system during ascent. Taking into account stored upper air data for upcoming slices, plus thermodynamic factors engendered as a function of the current ascent rate, it then reads out a new item, 170 in the preceding readout: minutes of ballast to achieve 150.

20.5 THE FUTURE

This computer exercise suggests that we consider, in general, the future of AC. Technological forecasts at this stage of the game consist largely in constructing lists of hardware or development contracts one would nominate, given an unlimited budget. So, in my funded crystal ball, I see radiational sensors on the balloon apex measuring ambient atmospheric parameters, similar structure above the balloon, and helium temperature. Density and pressure altitude measurements are complemented by gravitational sensors which simultaneously transmit three-axis velocities and accelerations. All of these data are fed directly into an on-board computer, which digests, solves, and then directs command and ballast functions. From the ground, one occasionally addresses the computer to modify the original programmed profile. You are not too concerned about losing this sophisticated control hardware. After separation, the entire payload is flown 1000 miles back to the launch site by inflatable, radio controlled glider, with wing loading in the dragon fly class.

But is even this level of operation optimum? The system still treads carefully around activities of that real dragon, the atmosphere.

The next step may be achieved via a tool to be discussed during tomorrow's session; powered, natural shape balloons. But I would like to go even further and consider superpressure balloons with solar-powered, exotic power plants of some sort, providing flight durations of one year or more. This combination, piloted by astute applications of AC would truly constitute an ultimate phase in ballooning, providing, among other things, a synchronous satellite of the atmosphere.

In summary, I propose AC as a major weapon in discouraging the widespread image of ballooning as a game played largely with random numbers. The constant level balloon opened up new magnitudes of opportunity for atmospheric research. Plugging in the AC provides a further dimension.

Contents

21.1	Decision Theory	256
21.2	The Dilemma - Project Cometail	258
21.3	A Simple Decision Tree	259
21.4	Estimating Probabilities	265
21.5	More Complex Decision Trees	269
21.6	Looking Back	285

21. A Decision Theory Model for Ballooning Problems

A.L. Morris
National Center for Atmospheric Research
Boulder, Colorado

Abstract

A balloon flight model constructed to show probability of success at various stages of a flight operation can help the planner make choices between possible courses of action. The value of such a model depends on how well it approximates a real operation and how accurately appropriate probabilities are known. These probabilities include balloon and hardware reliability and the probability that the crew can accomplish each step of the operation successfully. A first model is usually rather crude, and initial probabilities are frequently guesses. With use, the model can be refined and the probabilities needed can be estimated quantitatively through observation. Even the most refined model is only an aid to the man who must make a decision, however. To use it effectively he must understand its nature and supplement it with value judgments made independently of the model. To say this another way, blind use of an excellent decision model may not result in a good decision, but a good model used with understanding can be a valuable tool to the decision maker.

A first model for scientific ballooning is described and used in an example, and a method of getting the necessary reliability and operational probability constants is explained.

21.1 DECISION THEORY

Although the purpose of this paper is to show an application of decision theory to a ballooning problem, a little background in the theory of decision making is necessary to set the stage for understanding the application. First, what is a decision? Strangely, most books and papers on decision theory do not give a specific, concise definition. Essentially, however, the decision process involves recognizing that an action must be taken, seeking out and comparing the consequences of taking the action through each of the various alternative ways open and resolving which of the alternatives to follow. When an alternative has been chosen, a decision has been made. Whether one considers the decision to be the whole process or the resolution made at the end of the process isn't important in the application of decision theory, but it does affect the language one uses in discussing it. I shall use the word "decision" to include the entire process. For a more detailed discussion of the theory and terminology of decision theory, the reader is referred to Ellon (1969), Sisson et al (1967a and 1967b), Fishburn (1964), Wheeler and Peeples (1969), and Tribus (1969).

Decisions can be made through the use of formal procedures, or they may be made quite informally. They may be rational or irrational. They may be good or bad. These words, formal, informal, rational, irrational, good and bad also need to be defined.

A decision was a good one from a decision maker's point of view if the results flowing from the course of action taken following the decision are more favorable to him than the results he believes would have followed other decisions. A decision was bad if he believes another possible decision would have brought more favorable results. Whether a decision was good or bad can not be determined until the consequences of the decision are clear, and even then it is often difficult to weigh those consequences against the possible consequences of other decisions. Goodness or badness is usually relative. In spite of the difficulty of evaluating decisions, it is important in evolving better decision models that an effort be made to do so. Rational, as used here, has a rather special meaning. A rational decision is one which is made by following an agreed-upon decision process and using agreed-upon criteria to specify how a choice between alternatives is to be made. Thus the engineering department of Balloons Ltd., a balloon manufacturer, may have a formal procedure (a Computer Program called BALSPEC-1) for determining the engineering specifications of zero-pressure balloons to meet stated flight requirements. Clearly, such specifications may be arrived at in many other ways, but if company policy dictates the use of BALSPEC-1, it is irrational from the point of view of the company for a company engineer to determine them in any other way.

If one of the Balloons Ltd. engineers, using another computer program, can write equally good (from his point of view) though not identical specifications at half the cost of using BALSPEC-1, his decision on what the balloon specifications should be to meet the requirements will be rational to him but not to the company. On the other hand, if he can convince the company that his specifications are as good as those turned out by BALSPEC-1, his program is likely to be adopted and named BALSPEC-2. Then it would become irrational from both his point of view and the company's to use BALSPEC-1.

The example used above will be used further to illustrate the difference between a formal and an informal decision procedure. When flight requirements are received by Balloons Ltd., they have to be turned into balloon specifications.

Once - say, during the Siege of Paris in 1870, when the Parisians were building Montgolfiers in their railway stations in an effort to communicate with the outside - decisions about balloon design were made very informally. Each designer had his own, rather intuitive ideas about gore patterns. A man, not a machine, decided on the basis of what cloth was available at the moment, etc., how each balloon was to be made. He had many alternatives from which he selected one. He made decisions informally, and most of them were irrational to everyone but him.

Since Balloons Ltd. uses a strictly specified procedure to design balloons, it is formal, but is a decision being made? Are there any choices? If not, no decision was made, because none was necessary. During the evolution of BALSPEC-2, however, decisions were being made. Only after the "mathematical model" of a balloon which was used as a basis for writing BALSPEC-2 became sufficiently realistic, and the criteria for judging what constituted an acceptable balloon were clearly defined, could the procedure become so formal that no alternatives were considered to exist. The decision process had been used in selecting a model and in determining criteria for selecting one among the various alternative materials, etc. The engineers who wrote BALSPEC-1 and 2 had, in their view, solved an engineering problem. So they had! But they had gone through a decision making process in doing it.

Now that I've shown that decision making, even formal decision making, is not new to anyone involved in scientific ballooning, I want to construct a mathematical model of a different aspect of scientific ballooning. My mathematical model will be a version of the "decision tree" which is currently in vogue among writers on decision making, for example Archibald et al (1967). Rather than discuss a decision tree abstractly, I'm going to try to show what one is and how it is used as I construct a decision model.

21.2 THE DILEMMA-PROJECT COMETAII.

A balloon flight crew has been asked to consider flying a 4,500 pound payload to an altitude of 105,000 feet to study the tail of a comet. The payload can be flown on a mylar scrim balloon which will cost \$60,000. The scrim balloon will weigh 2,000 lbs. The manager of the crew believes that a modern polyethylene balloon might also be satisfactory, although experience with polyethylene carrying such a heavy payload is quite limited. Such a balloon will weigh 1,500 lbs and cost \$10,000. (The reader is warned that these numbers and all others used here are fictitious. They are used to demonstrate a method of solving a problem, and no conclusions about any actual situation should be drawn from them.)

If a flight with one balloon were in every way equivalent to a flight with the other, the crew would choose the polyethylene balloon because of the obvious cost saving. Several differences exist, however. The crew considers the scrim balloon to be almost certain to succeed. Therefore any failure which may occur if the scrim balloon is used is likely to be due to operational difficulties, that is electronics, hardware, rigging, launch, etc. The polyethylene balloon is believed to have a lower probability of withstanding the rigors of handling and flight than the scrim, provided that operational factors do not tip the scales one way or the other, but the crew has had more experience with polyethylene balloons, and it feels that the probability of encountering operational difficulties during inflation and launch is less with polyethylene than with scrim.

The scientist and his sponsor understand in a general way the problems of selection, and they know that a flight attempt on either balloon may fail. The time during which the comet may be viewed will permit the equipment to be flown twice during the comet's passage with reasonable opportunity for repair between flights. They are willing to consider a second flight if that seems appropriate. Therefore, the crew may also consider the possibility of using two or more balloons and making at least two flight attempts if necessary.

If no more information than this were available, the manager of the crew would face several possible alternate solutions and he would, through some means perhaps not even fully understood to him, make a decision. He can buy the scrim balloon, and the cost for the balloon and helium will be \$67,150, assuming that helium costs a dollar per pound of lift and that he will inflate to 10 percent free lift. He can buy a polyethylene balloon, and the cost for balloon and helium will be \$16,000. He can buy two polyethylene balloons and know that he can attempt two flights at a cost for the balloons and helium of \$33,200. Such a course will involve additional time and expense on the part of the scientist and additional balloon flight crew time. He can buy three polyethylene balloons and attempt three flights at a cost for balloons and helium of \$49,800. Perhaps he might even consider buying two scrim balloons or a scrim balloon and a polyethylene balloon.

It is clear to him that at the very least he needs to calculate more carefully the cost of flying two or more flights on polyethylene, but even if he finds that two such flights can be conducted at a cost comparable to one flight on scrim, should he select the polyethylene? Not necessarily! If the costs of two programs are equal, he should select the one having the better probability of success. This tells him that he also needs to incorporate some measure of reliability into his decision making process.

21.3 A SIMPLE DECISION TREE

As a first try at constructing a decision model, the manager drew Figure 21.1. Events which may occur during the ballooning operation are marked by rectangular boxes. In this tree the event is described briefly in each box, but each event is also identified by a number - just below the event box. Events follow in sequence from left to right along each branch of the tree. The final event along any branch is either success or failure, designated by S and F respectively.

The chart implies that once inflation is started (event 1) four events only may follow. These are: event 2 - inflation will be successful and the balloon will be

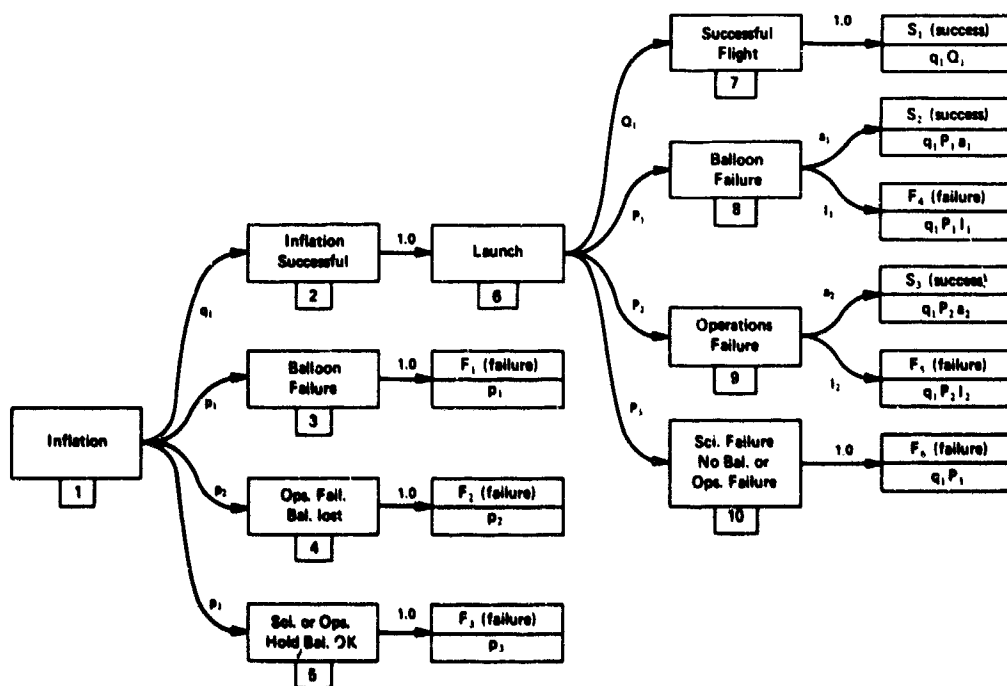


Figure 21.1. Balloon Flight Decision Tree for One Balloon and One Inflation

launched, event 3 - the balloon will fail in some manner during inflation and because the payload can not be flown, insufficient scientific data will be collected and the operation will fail, event 4 - an operations failure of some sort will occur which will result in loss of the balloon and lead to failure of the entire operation, and event 5 - a hold because of some problems on the part of the scientific or operations crew will result in expenditure of the helium but will leave the balloon usable.

Another manager might have chosen different events. The important thing is that the events should be pertinent, and they should be both mutually exclusive and exhaustive, that is they should all be recognizable, events such that if one occurs no other can occur, and taken all together they should include all possible events. One might ask, "what if inflation is started and stopped almost immediately so that essentially no gas is expended and the balloon is not damaged?" Under such conditions the manager would consider that event 5 had occurred, although the cost would not be the same as if all gas had been expended. Thus, somewhat arbitrary definitions are accepted in order to simplify the chart. They are akin to approximations often accepted in engineering practice. They should be accepted only with knowledge of their implications, however.

The probability that any one of the events will follow another event is given along the arrow joining the event boxes. For example, q_1 is the probability of a successful inflation leading to an attempted launch once inflation is started. The sum of the probabilities along a set of arrows proceeding from any event is 1. Thus

$$q_1 + p_1 + p_2 + p_3 = 1 \text{ and } Q_1 + P_1 + P_2 + P_3 = 1.$$

Note that along some arrows the probability is shown as 1.0, meaning that the next event is certain to follow. By definition, then, a successful inflation will be followed by an attempted launch. Also by definition - if launch is not attempted, sufficient scientific data will not be collected, and the mission will have failed.

Even if the launch is attempted, however, the mission can fail. The ways in which success or failure can occur following a launch attempt are shown following event 6 on the chart. They are: event 7 - a successful flight in which sufficient scientific data are collected, event 8 - failure of the balloon, but the failure may occur after the scientific mission is accomplished and so not preclude success of the mission, event 9 - an operations failure occurs, but again the mission may succeed in spite of it, and event 10 - the scientific equipment may malfunction or insufficient data may be obtained for reasons other than operations or balloon failure.

The probability that some combination of events will occur is calculated by following the usual rules for combining probabilities. The tree helps in keeping

the procedure straight. Thus the probability that success will occur as a result of a particular sequence of events is obtained by taking the product of all the probabilities found along the branch representing that sequence of events. In Figure 21.1 the probability of success and failure at the end of each branch is shown in the lower part of the success and failure boxes. The overall probability of success may be obtained by summing the probabilities in all the boxes marked S, and the overall probability of failure may be obtained by either summing all the probabilities of failure or by subtracting the probability of success from 1.

The probability of success is

$$P_S = q_1 [Q_1 + P_1 a_1 + P_2 a_2] .$$

The probability of failure is

$$P_F = p_1 + p_2 + p_3 + q_1 [P_1 I_1 + P_2 I_2 + P_3] .$$

It may not be obvious that $P_S = 1 - P_F$, but if one makes use of the identities

$$1 - q_1 = p_1 + p_2 + p_3$$

$$1 - Q_1 = p_1 + p_2 + p_3$$

$$1 - a_1 = I_1$$

$$1 - a_2 = I_2$$

he can readily determine that it is true.

By using appropriate probability values for each of the balloons, the manager can now calculate the probability of success and failure and compare them with cost. Let's assume that the probabilities he needs are those given in Table 21.1. We'll discuss in the next section how he might have arrived at such values.

The probability of success with the scrim balloon ($P_{S,s}$) is

$$\begin{aligned} P_{S,s} &= 0.93 [0.86 + 0.01 \times 0.25 + 0.07 \times 0.40] \\ &\approx 0.83 \end{aligned}$$

and with the polyethylene

$$\begin{aligned} P_{S,p} &= 0.89 [0.82 + 0.07 \times 0.10 + 0.05 \times 0.40] \\ &\approx 0.75. \end{aligned}$$

Table 21.1. Operational Probabilities

	Scrim	Poly-ethylene	Sequence of Events to Which Probability Applies
q ₁	.93	.89	Successful inflation following start of inflation.
P ₁	.01	.06	Balloon fails on inflation attempt.
P ₂	.02	.03	Balloon is lost during inflation due to an operations failure.
P ₃	.04	.02	Operations or Scientific hold causes loss of gas but not balloon.
Q ₁	.86	.82	Successful flight following successful inflation.
P ₁	.01	.07	Balloon fails during flight.
P ₂	.07	.05	Operations failure occurs during flight.
P ₃	.06	.06	Scientific failure during flight prevents success.
a ₁	.25	.10	Balloon failed but adequate scientific data obtained.
l ₁	.75	.90	Balloon failed and inadequate data obtained.
a ₂	.40	.40	Operations failure but adequate data obtained.
l ₂	.60	.60	Operations failure and inadequate data obtained.

The probabilities of failure with the scrim and polyethylene are respectively:

$$P_{F,s} = 1 - 0.83 = 0.17$$

$$P_{F,p} = 1 - 0.75 = 0.25.$$

The costs which the manager has estimated for the operation depicted by Figure 21.1 are shown in Table 21.2. From Table 21.2, the manager can assign costs to each success or failure event on the decision tree. Event 3 will cost the sum represented by the symbols G + E + B + H + I and so will event 4. Event 5 will cost G + E + H + I if the balloon is not damaged and its cost can be recovered. If the balloon is designed just for this flight, however, and none of its cost can be recovered, the cost of event 5 is the same as events 3 and 4. The costs to be associated with each of the successes or failures following launch are all the same, and they are obtained by summing cost categories G, E, B, H, I and F.

Table 21.2. Definition and Cost of Each Cost Category

Cost Symbol	Cost - Scrim	Cost - Polyethylene	Definition
G	\$150,000	\$150,000	Preparing and delivering scientific payload to the launch site, including all scientific crew costs prior to layout for inflation.
	3,000	3,000	Balloon crew costs for preparations leading up to layout for first attempted inflation.
E	1,000	1,000	Cost of expendable hardware, rigging, etc. used on each attempted flight.
B	60,000	10,000	Cost of one balloon.
H	7,150	6,600	Cost of helium for one inflation.
I	1,500	1,500	Balloon crew and scientific crew costs for layout, etc. through inflation.
F	2,000	2,000	Cost of launch and ensuing flight operation.
R	10,000	10,000	Cost of repairing scientific and flight equipment after a flight. Crew per diem and salaries are included.
*D	1,200	1,200	Cost of scientific crew per diem, salaries, etc. due to a delay resulting from an aborted inflation.

*Since such a delay will occur only if a balloon is available for another inflation attempt, this delay is principally a wait for a suitable day. It may be as little as 1 day or it may be many. The manager assumes 3 based on normal activity, climatology, etc.

The manager can now determine the risk of flying with polyethylene by multiplying the probability of each failure event by the cost of that event and summing all the products. He can do the same thing with scrim, and then he can compare the two risks. This is the simplest way of combining the measured of performance (the probabilities of failure and the costs) into a single measure of utility. If he accepts this measure as an adequate one, he would choose the balloon for which the risk is lower.

For balloons characterized by the data of Tables 21.1 and 21.2, the various probabilities of failure, the corresponding costs and the product of the two are shown in Table 21.3. The risk is the sum of the products. It is slightly lower with scrim.

Table 21.3. Computation of Risk for a Flight of One Balloon and One Inflation

Prob. Symbol	Scrim			Polyethylene		
	Prob. of Failure	Scrim Cost	Product	Prob. of Failure	Polyethylene Cost	Product
$q_1P_1I_1$.007	\$224,650	\$ 1,573	.056	\$174,100	\$ 9,750
$q_1P_2I_2$.030	"	8,761	.027	"	4,701
q_1P_3	.056	"	12,580	.053	"	9,227
P_1	.01	222,650	2,226	.06	172,100	10,326
P_2	.02	"	4,453	.03	"	5,163
P_3	.04	"	8,906	.02	"	3,442
Risk			\$38,499			\$42,609

Risk as a measure of utility does not take into account the value of the data one might get from a successful flight. In this case if the value of the data is expected to be less than the cost of the flight with a scrim balloon but greater than the cost with a polyethylene balloon, the scrim would clearly be the poorer choice. If this were true, however, to conduct the experiment with a balloon as a vehicle probably wouldn't be worthwhile anyway, and another alternative should be sought.

If the worth of a successful flight is known, a better measure of utility than risk can be used. Often termed expectation by game and decision theorists, it is the sum of all the products of the individual probabilities of success and their corresponding gains (worth of the experiment less the cost) less the risk. To illustrate for this example, let's assume the value of a successful experiment is \$1,000,000. Then the gain if one succeeds is (\$1,000,000 - \$224,650) for scrim and (\$1,000,000 - \$174,100) for polyethylene. It is the same in this example regardless of whether one succeeds via event 7 or event 8 or event 9, because the cost is the same for each of these events. The expectation is then

$$\left[(q_1 Q_1 + q_1 P_1 a_1 + q_1 P_2 a_2) (\text{value of experiment} - \text{cost of flight}) - \text{risk} \right].$$

For scrim this is $(0.828 \times 775,350 - 38,499)$ or \$603,490. For polyethylene it is \$580,120. Expectation also favors scrim under these conditions.

The worth of an experiment is rarely known, a priori, but sometimes it is possible to say that it has a value greater than or less than some specified value. We can calculate a number from the information we have which may be useful as a discriminant between courses of action.

Let V = value of a successful flight, C_s and C_p be the costs of a flight with scrim and polyethylene respectively and r_s and r_p the risks with scrim and polyethylene. Then in this simple case

$$e_s = (V - C_s) P_{S,s} - r_s \quad (\text{expectation with scrim})$$

and

$$e_p = (V - C_p) P_{S,p} - r_p \quad (\text{expectation with polyethylene}).$$

If one equates the expectation with scrim to that with polyethylene, he can calculate the value of V (designated by V_e) for which scrim and polyethylene are equally attractive. Thus

$$\begin{aligned} V_e &= \frac{(C_s P_{S,s} + r_s) - (C_p P_{S,p} + r_p)}{P_{S,s} - P_{S,p}} \\ &= \frac{(224,650 \times 0.828 + 38,499) - (174,100 \times 0.754 + 42,609)}{0.828 - 0.754} \\ &\approx \$684,000. \end{aligned} \quad (21.1)$$

If the sponsor or the scientist regards the worth of a successful experiment to exceed this, the scrim should be chosen. If not, the polyethylene should be chosen unless the worth of the experiment doesn't greatly exceed the cost of a flight on polyethylene. If it doesn't, the advisability of flying the experiment on any balloon should be seriously questioned.

21.4 ESTIMATING PROBABILITIES

Normally a balloon flight facility manager doesn't think in terms of probabilities such as those listed in Table 21.1, but he does frequently know the percentage of flight attempts which result in successful flights. He also can usually

determine from records available to him what fraction of the balloons fail during inflation and what fraction fail during flight. In these and similar records he may have the data required to form good estimates of some of the probabilities. q_1 in Table 21.1 may be estimated by dividing the total number of attempted inflations into the number of successful ones, taking care to define a successful inflation as it is defined in Table 21.1. An error could easily be made here by including as successes those inflations which were successful except that for operations or scientific reasons they were not followed by a launch attempt. Assume for purpose of illustration that 100 inflations of scrim balloons in the appropriate size and load carrying range have been attempted. Of these 93 were successful, one failed due to a defective balloon, two were destroyed due to operational errors and four were either partially or wholly inflated but for operational or scientific reasons were then deflated and stored for future use without damage to the balloon. Then the numbers $93/100$, $1/100$, $2/100$ and $4/100$ are estimates of the probabilities q_1 , p_1 , p_2 and p_3 . Now a population of 100 is a fairly large one in ballooning if the balloon size and payload range are at all restrictive, and when 99 out of 100 balloons perform satisfactorily during inflation (there were three failures, but two were believed or known to have been caused by operational failures), one is willing to concede that the balloons perform reliably through the inflation operation. In fact, most of us probably wouldn't reject the statement that the reliability through inflation is 0.99.

Would we as readily accept the statement that the probability of failure is 0.01 knowing that only one failed? That failure could have been an accident, or perhaps it was an accident that only one failed. Several others may have been on the verge of failure. We can not doubt that the probability of failure is 0.01 without also doubting that the reliability is 0.99, however. The point is that even with a record of flights which is large in terms of scientific ballooning, it is clear that we question the accuracy of probability values calculated from it.

I have outlined a way to use past performance records to estimate probability values which can be used in decision models, but I have also cast doubt on the accuracy of the values obtained, especially when the sample size is small. Another reason exists for questioning the accuracy of probability estimates based on past performance. What if the company which laminates the mylar film to the dacron scrim has made a subtle change in the lamination process? Do the results of the past still provide a basis for making estimates about the behavior of scrim balloons in the future? We don't know, of course, but if we accept the hypothesis that the past offers no information about the future because of this change, we must start over again with material tests, test flights, etc., if we are to have any basis for decisions about courses of action for the future. Changes such as the one suggested here are rarely so drastic that they cause us to lose complete faith in the

value of past performance as a measure of future performance. Usually we accept the thesis that past performance of a system provides an acceptable first approximation to future performance of a similar system; then we modify that first approximation to account for known or anticipated differences in the system.

Because we know that the accuracy of the best probabilities we can obtain to use in a formal decision model is open to question, we may question the wisdom of using them at all in decision making. But can we make a decision without using some measure of reliability? If we choose from two courses of action the one which will be less expensive if every aspect of the operation is successful, we are implicitly assuming that the difference in probability of success of the two systems is sufficiently small that the cost difference is more significant than reliability. If we are determined to buy the balloon system which is more likely to succeed, we must first decide which system that is, requiring at least that we made a comparative estimate of the likelihood of success. We are also implicitly assuming that the difference is great enough to compensate in some way for the difference in cost if the one we select is the more expensive one. It is difficult to conceive that a decision can be made between two balloon systems unless the decision maker does make either explicit or implicit assumptions about the relative likelihood (probability) of success of the systems. If such assumptions are indeed made, the decision maker should use the best information he has to estimate the likelihood of success, and he should use the estimates he makes in such a way that he understands at least qualitatively how they influence the decision.

If we accept these arguments and the conclusion, we see the need for consciously determining and using probabilities in decision making, and we recognize that probabilities which are applicable to ballooning will always be estimates. We recognize the need therefore to understand how these estimates affect our decisions so that we can take into account any doubts we may have about the accuracy of the estimates.

In the statement of the problem, it was pointed out that experience with flights of polyethylene balloons carrying heavy payloads is quite limited. Any estimate of the probability of success of a polyethylene balloon system of the type required which can be made from past performances of comparable systems will therefore be very doubtful. On the other hand, from his records the manager knows that there is a wealth of data on polyethylene systems carrying smaller payloads. He knows that several flights carrying payloads nearly as heavy as this one have succeeded and a few have failed. Further, recent improvements have been made in the seal strength of polyethylene balloons. He must try to use this and other information available to him to make the estimates he needs.

He can simply make an educated guess at the value of each of the probabilities he needs for the decision model, using his experience and knowledge to guide him

and making use of the fact that the sum of the probabilities of each of several groups must be unity. He can ask others who have experience in ballooning to make such guesses also, after assuring himself that each understands the purpose of the guesses and has reviewed the pertinent information available to him. An open discussion of information by those who are going to contribute guesses can be helpful. It will expose each to the other's concepts of what information is pertinent. It is probably better for each contributor to make his guesses privately than publicly in a meeting, however.

The various guesses can be combined in any number of ways. If all contributors are equally knowledgeable and all are considered to be unbiased, an unweighted average of all guesses of a particular probability may be best. The average then provides the group's best estimate and the variability of the responses serves as a measure of the uncertainty. A weighted average has some potential advantages over a straight average, however, because it allows the values contributed by the more knowledgeable participants to be given more emphasis. If the manager intends to use a weighted average, he should decide before he has the responses in hand what weights he will assign to the various contributions. Otherwise he may bias the results unduly by what he himself believes.

Let's assume that the probabilities given in Table 21.1 for polyethylene are the result of averaging the contributions of five knowledgeable people. Let's also assume that the person making the estimates most favorable to polyethylene turned in the following values for the operation using a polyethylene balloon:

$q_1 = 0.91$	$Q_1 = 0.85$
$p_1 = 0.04$	$P_1 = 0.04$
$p_2 = 0.03$	$P_2 = 0.05$
$p_3 = 0.02$	$P_3 = 0.06$

If the other values in Table 21.1 are used with these, we find that the probability of success with polyethylene is

$$P_{S,p} = 0.91 [0.85 + 0.04 \times 0.10 + 0.05 \times 0.40]$$

$$= 0.91 \times 0.874 \approx 0.795.$$

Thus the most optimistic set of probability values shows an overall probability of success of 0.795 while the adopted set showed 0.754. Since the cost of the operations are unchanged, the expectation for polyethylene, using this more optimistic probability and assuming the value of a successful flight to be \$1,000,000 is

\$622,310. This exceeds the \$603,490 calculated for scrim. Also, a successful flight must have a value of \$1,540,000 in order that the expectation with scrim will equal that with polyethylene. This contrasts with a value of \$684,000 using the polyethylene probability data of Table 21.1. The risk for polyethylene using $P_{F,p} = 0.205$ is \$35,280 contrasted to \$38,499 for scrim. Polyethylene would be the more logical choice unless the value of a successful flight is known to exceed \$1,540,000.

These results show that with the costs and experiment value assumed in this case, the various measures of utility are fairly sensitive to changes in reliability. But if the value of a successful experiment were known to exceed \$1,540,000, neither the expectation nor the discriminant would have indicated a change of choice from that made with the averaged probability data. If this were true, the manager would have been fairly confident that scrim was a good choice. If he had questioned that the value of the experiment was as great as \$1,000,000, however, he might have wished to compare measures of utility using one of the more pessimistic sets of estimates of the reliability of polyethylene. In the end, he probably used the set he considered to be the most accurate, but he understood how variations in the reliability of polyethylene could affect the measures of utility he was using.

Even with the best possible probability estimates, a bad decision may be made; a decision based on intuitive feelings about reliability is as likely to result in a bad decision as a good one. Therefore, unless one can devise an acceptable decision model which is not sensitive to the probabilities of success or failure, he must make the best estimates of reliability he can. The manager in this case should strive to find better ways of estimating probabilities for future decision models. Perhaps he can find ways to combine the results of materials tests, seal strength tests, manufacturer's quality control checks, etc., into meaningful balloon success or failure probabilities. He must not ignore the need for better estimates of the probability of success and failure in the various facets of operations either. Above all, however, he should not let the difficulty of obtaining acceptable probabilities lead him to adopt a decision model which implicitly assumes values of probability of success and failure for a balloon or for any aspect of the operation, unless he is aware that he is making the assumption and understands its consequences.

21.5 MORE COMPLEX DECISION TREES

The manager, having used decision theory to study a very limited set of alternatives, had a better understanding of its limitations than he had before, but he also had acquired an appreciation for its potential value. He decided to construct a model to study a more realistic set of alternatives. He assumed that he

will have two balloons available, that two attempted launches are permissible and that he can go through as many as three inflations if necessary.

As a first step he decided to extend the simple decision tree to include the possibility of a second inflation. The tree, showing events only by number, is presented in Figure 21.2. The branches of the tree going through events, 2, 3 and 4 are exactly like the tree shown in Figure 21.1 except that the success twigs at the end of the branch have been gathered together into one success bundle and the failure twigs also are formed into one failure bundle. The probability that events will lead to either of these bundles once inflation is started is given in the box representing the bundle.

Several simplifications of the tree are possible. For the purpose to be served here, events 3 and 4 can be combined. Also events 7 through 10 can be combined into two events, success and failure. The branch on the tree growing through event 5 following the first inflation is exactly like the tree itself without that branch, except that on the tree event 5 leads to a second event 1 while on the branch event 5 leads to failure. The branch growing through events 1, 2, 6, etc. to success and failure is a complex, re-occurring branch which for this application can readily be simplified to the one shown in Figure 21.3. Making use of these simplifications makes it possible to redraw Figure 21.2 as shown in Figure 21.4. The sequence of letters following each S and F event box will be explained in the next paragraph. Calculating the probability that events will lead to any one of the success or failure boxes is simple from this diagram.

The sequence of letters following each success and failure box are the letter symbols for the cost categories shown in Table 21.2. They are written in a special sequence to help avoid errors. Starting with the shortest sequence, that following events 3 and 4 after the first attempted inflation, the costs are the common costs which aren't repeated (G), the cost of expendable hardware (F) which must be replaced after each launch attempt, the cost of the balloon (B), the cost of the helium (H) and the cost of the inflation operation I. The cost categories which occur if the balloon is flown after the first inflation are shown after the S_1 and F_1 event boxes at the top of the chart. The sequence is exactly the same as the sequence described above except that the cost of the flight (F) is added. This F should not be confused with a failure symbol, but the usage is so different that no confusion is likely. Enough has been said that it should be fairly obvious if one starts at the left side of the chart and adds cost categories as events occur along any branch, he has the appropriate sequence when he reaches the end of the branch. The sequence after each success will end with an F; the sequence after each failure will end with either an I or an F.

By using the cost symbol shown after each failure event and Table 21.2, the total cost of all the events leading to that failure event can be readily calculated.

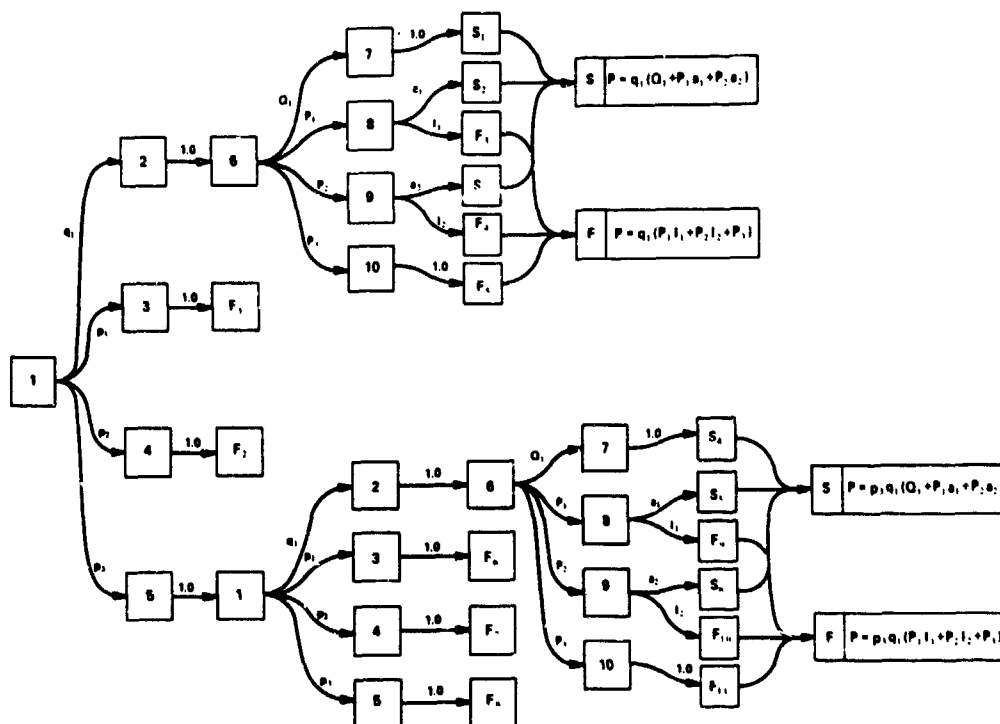


Figure 21.2. Decision Tree for One Balloon and a Second Inflation if a Second One is Advantageous.

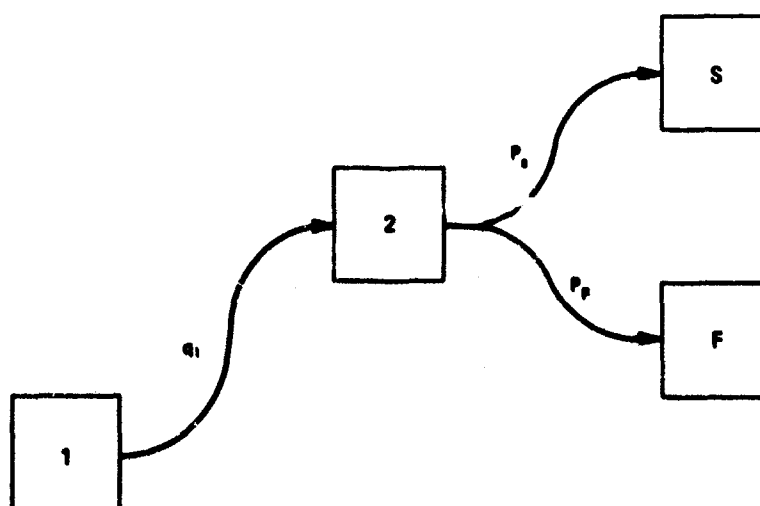


Figure 21.3. Simplified, Recurring Branch in Which $P_S = (Q_1 + P_1a_1 + P_2a_2)$ and $P_F = (P_1I_1 + P_2I_2 + P_3)$. Also $P_S + P_F = 1$.

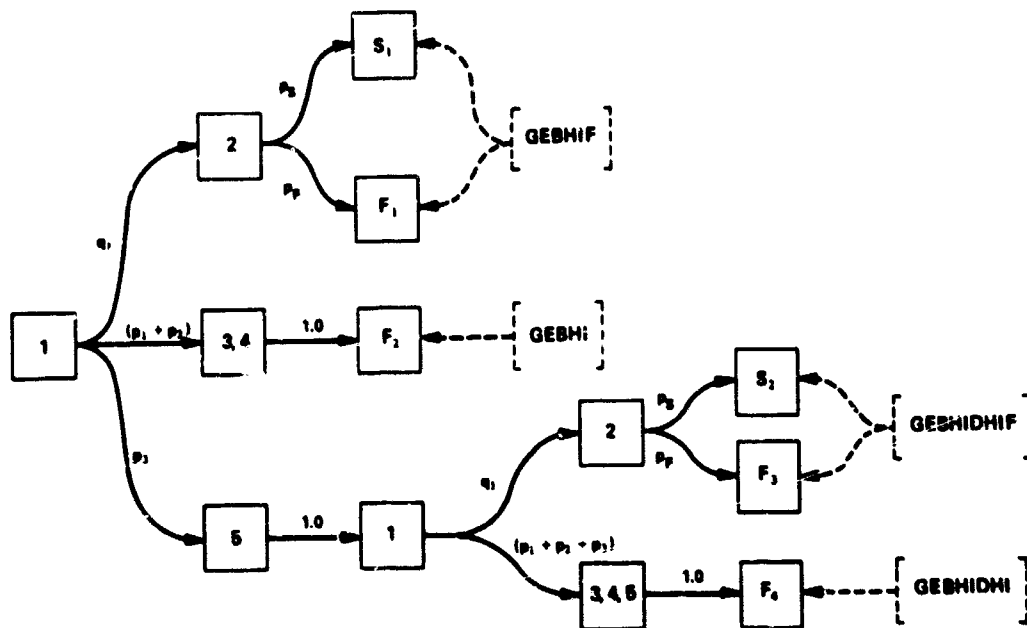


Figure 21.4. Simplified Decision Tree for One Balloon and as Many as Two Inflations. Note that $(p_1 + p_2 + p_3)$ along the lowest branch could be replaced by $(1 - q_1)$

That cost multiplied by the probability that failure will occur in that way gives the risk of failure through that particular chain of events, that is the events along that branch. As in the simple tree, the sum of all such risks is the risk of the entire project. Mathematically this can be written

$$r = \sum_{i=1}^n (C)_i (P_F)_i \quad (21.2)$$

where there are n failure events, $(P_F)_i$ is the probability of failure through the i th failure event and $(C)_i$ is the cost of all events leading up to and including that failure event.

Similarly, if the value of a successful experiment is known, the expectation can be written

$$e = \sum_{j=1}^m [v - (C)_j] (P_S)_j - \sum_{i=1}^n (P_F)_i (C)_i \quad (21.3)$$

where there are m success events.

Finally if one wishes to know the value the experiment must have in order that the polyethylene and scrim will have equal expectation, the following equation may be used:

$$V_e = ([ESC] - [EPC]) + (P_{S,S} - P_{S,P}) \quad (21.4)$$

in which

$$[ESC] = \sum_{j=1}^m (C_S)_j (P_{S,S})_j + \sum_{i=1}^n (C_S)_i (P_{F,S})_i$$

$$[EPC] = \sum_{j=1}^m (C_P)_j (P_{S,P})_j + \sum_{i=1}^n (C_P)_i (P_{F,P})_i$$

$$(P_{S,S} - P_{S,P}) = \sum_{j=1}^m (P_{S,S})_j - \sum_{j=1}^m (P_{S,P})_j$$

Equations (21.2), (21.3) and (21.4) are general and may be used with decision trees of any complexity which are constructed like the ones used here. V_e is a sufficiently useful number that some additional discussion of it is worthwhile.

The terms in brackets in the numerator of Eq. (21.4) may be interpreted as expected costs of the project. The first as written above is a best estimate of the cost of the operation with scrim if only those balloons, inflations, services, etc., which are necessary to give success or lead to ultimate failure are used. One might view it as the best estimate we can make of the average cost of a large number of similar projects carried out with scrim. Many will succeed with one balloon, one inflation and one flight attempt. These will not be very expensive. A few will use two balloons, two inflations, etc., and cost more.

The difference between the two terms in brackets in the numerator is then a best estimate of the difference in cost of carrying out the experiment using scrim and polyethylene. The terms in the denominator are the overall probabilities of success with scrim and polyethylene in that order.

V_e may take any value, being undefined at plus and minus infinity. If $V_e > 0$, the more costly operation is also the one more likely to succeed. A decision between them can only be made if the actual value of the experiment is deemed to be greater than or less than V_e . If it is greater than V_e , one chooses the more expensive alternative. If it is less, the lower cost alternative is preferable. If $V_e = 0$, there is no difference in the costs, but there is a difference in the probability of success, and the more reliable alternative should be chosen. If $V_e < 0$, the more

costly operation is the one less likely to succeed. The choice is obvious. Finally, V_e may be undefined (that is $\pm \infty$) because the probability of success with one balloon system is equal to the probability of success with the other. The lower cost system should then be chosen.

The simplification in tree construction leading to Figure (21.4) makes trees with additional alternatives appear tractible. Consequently the manager proceeded to construct a tree which would let him compare the alternatives open to him if he has two balloons and the opportunity for as many as three inflations and two launches. Figure (21.5) is the decision tree which resulted.

The events which are numbered are defined exactly as they were in the first simple tree. The success and failure events have also been identified by number as well as by the letters S and F. The probability symbols shown along the arrows between events have two numbered subscripts instead of a single one as before. The first subscript is used exactly as before. The second one identifies the balloon being used. If the second balloon were exactly like the first, this would not be necessary; but if one wishes to consider the possibility of using a scrim balloon with a polyethylene backup, the probabilities along the branches must be differentiated.

Note that some event boxes have two or more numbers in them. This was done because it was not helpful to identify the events separately for the decision the manager was trying to make. In the selection of a balloon, for example, it is not important whether a balloon fails because of defects or because it is damaged during the operation; therefore events 3 and 4 can be combined into an event identified as 3, 4 and defined as the occurrence of either event 3 or event 4.

The scientist's sponsor might use a similar decision tree to help him select the best combination of crew and balloons. He would be interested in differentiating crew performance and cost as well as balloon performance and cost, and so might want to keep events 3 and 4 separated; he might wish to consider other events as well.

When events are combined as 3 and 4 are here, the probability of occurrence of the combined event is the sum of the probabilities of the individual events since the individual events are mutually exclusive. If combining leaves the possibility of only two events following a given event, the probabilities are easier to show as the probability of the occurrence of one of the events and the probability of non-occurrence of that same event. This is done following the third inflation where $q_{1,2}$ and $(1 - q_{1,2})$ are used instead of $q_{1,2}$ and $(p_{1,2} + p_{2,2} + p_{3,2})$. This is possible here because when all permissible inflation attempts have been made, event 5 also results in failure even though a balloon may still be available.

Finally, note that some of the letters symbolizing cost categories are underlined. Those which are not underlined apply to the first balloon used in the

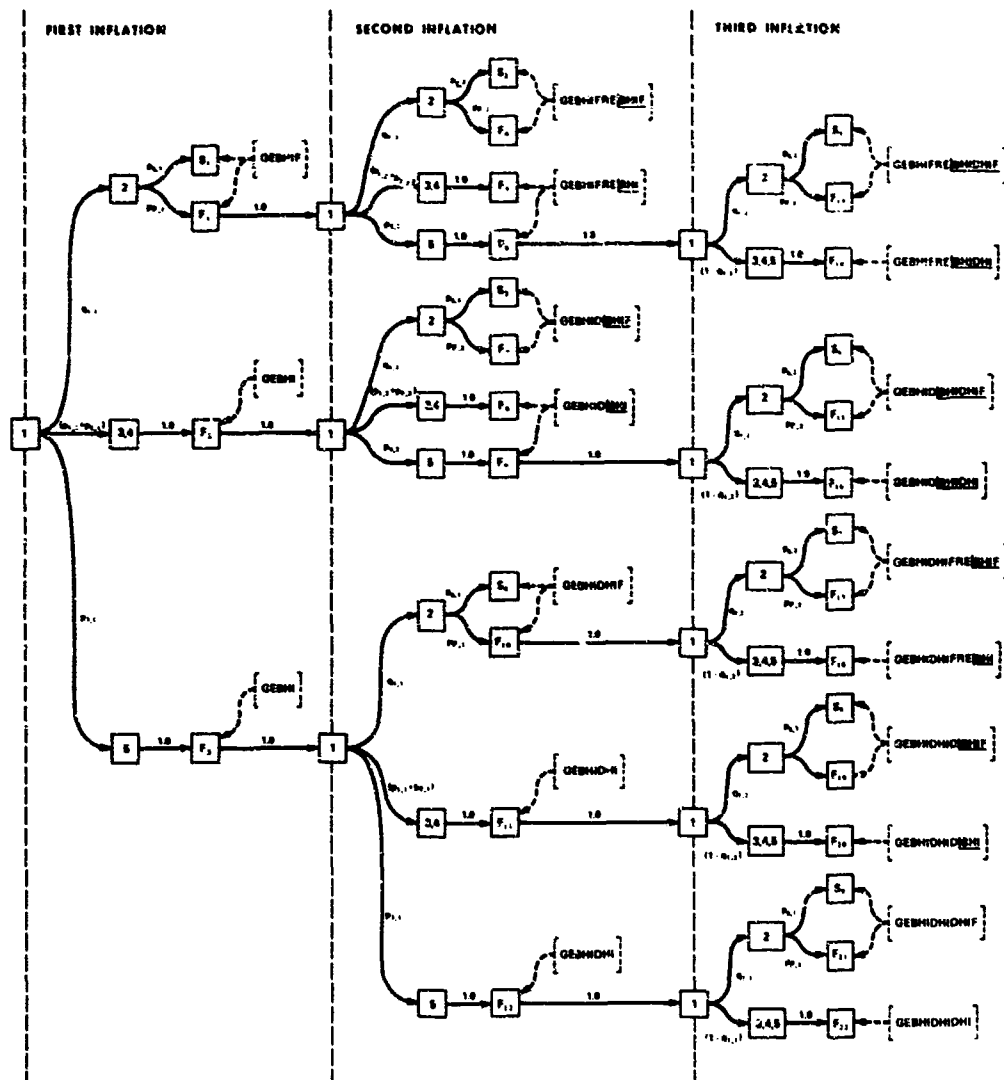


Figure 21.5. Decision Tree for an Operation Involving Up to Two Balloons, Three Inflations and Two Launches. If both balloons are identical, $q_{1,1} = q_{1,2}$; $p_{S,1} = p_{S,2}$, etc. If the balloons are different, in general $q_{1,1} \neq q_{1,2}$; etc.

operation; those which are underlined apply to the second. This becomes important only if the costs are different, for example if the first balloon is scrim and the second is polyethylene.

From Figure 21.5 and Table 21.4, probabilities can now be readily combined to determine the probability of each of the success or failure events. From Figure 21.5 and Table 21.2, the cost of each success or failure event can be determined. These results are given in Table 21.5.

Table 21.5 is essentially a computation form from which the value of the various terms of Eqs. (21.2) and (21.4) can be determined.

Table 21.4. Probability of Succession of Events for the Decision Tree Depicted by Figure 21.5

Succession of Events	Probability Symbol	Scrim	Poly-ethylene
1 to 2	$q_{1,1}$ or $q_{1,2}$.93	.89
1 to 3	$p_{1,1}$ or $p_{1,2}$.01	.06
1 to 4	$p_{2,1}$ or $p_{2,2}$.02	.03
1 to 5	$p_{3,1}$ or $p_{3,2}$.04	.02
2 to S	$p_{S,1}$ or $p_{S,2}$.890	.847
2 to F	$p_{F,1}$ or $p_{F,2}$.110	.153
1 to 3, 4	$(p_{1,1} + p_{2,1})$ or $(p_{1,2} + p_{2,2})$.03	.09
1 to 3, 4, 5	$(1 - q_{1,1})$ or $(1 - q_{1,2})$.07	.11

Table 21.6, derived from Table 21.5, gives the overall probability of success and failure, the risk $(\sum (C_i) (P_F)_i)$ and the expected cost $(\sum (C_j) (P_S)_j + \sum (C_i) (P_F)_i)$ of a number of possible alternatives. The second column of Table 21.6 shows which failure probabilities in Table 21.5 to add to obtain the overall probability of failure of the mission (shown in column 3) for the alternative stated in column 1. The probabilities given in columns 3 and 5 are carried to the third place to the right of the decimal, as they were in Table 21.5, for consistency in computations only; they aren't known that accurately.

Column 4 of Table 21.6 shows which success probabilities in Table 21.5 to sum to obtain the overall probability of success, and column 5 gives the numerical

Table 21.5. Summary of Probabilities and Costs and Their Products for Various Balloon Combinations. Probability and cost symbols are taken from Figure 21.5. Costs are based on Table 21.2, probabilities on Table 21.4. The column heading "scrim/polyethylene" indicates that the scrim balloon was used first.

S or F Event	Probability Symbol	Cost Symbol	Probability			Cost			Cost X Probability		
			Scrim/ Scrim	Scrim/ Poly	Poly/ Poly	Scrim/ Scrim	Scrim/ Poly	Poly/ Poly	Scrim/ Scrim	Scrim/ Poly	Poly/ Poly
S ₁	$q_{1,1}P_{S,1}$	*CF	.028	.028	.754	\$224,650	\$174,100	\$174,100	\$186,010	\$131,271	\$131,271
S ₂	$q_{1,1}P_{S,1}q_{1,2}P_{S,2}$	CFRE/BEIF	.085	.077	.113	306,300	255,750	205,200	26,036	28,900	21,136
S ₃	$(P_{1,1}+P_{2,1})q_{1,2}P_{S,2}$	CD/BEIF	.025	.023	.074	294,500	243,950	193,400	7,362	18,052	13,151
S ₄	$P_{3,1}q_{1,1}P_{S,1}$	CD/BEIF	.033	.033	.015	234,500	234,500	183,400	7,738	2,751	2,751
S ₅	$q_{1,1}P_{S,1}P_{3,2}q_{1,2}P_{S,2}$	CFRE/BEIDWIF	.003	.002	.004	316,150	265,050	214,500	948	1,062	429
S ₆	$(P_{1,1}+P_{2,1})P_{3,2}q_{1,2}P_{S,2}$	CD/BEIDWIF	.001	.000	.003	304,350	253,250	202,700	304	761	203
S ₇	$P_{3,1}q_{1,1}P_{S,1}q_{1,2}P_{S,2}$	CD/BEIDWIF	.003	.003	.002	316,150	265,050	214,500	948	530	429
S ₈	$P_{3,1}(P_{1,1}+P_{2,1})q_{1,2}P_{S,2}$	CD/BEIF	.001	.001	.001	304,350	253,250	202,700	304	254	203
S ₉	$P_{3,1}P_{3,2}q_{1,1}P_{S,1}$	CD/BEIDWIF	.001	.001	.000	244,350	192,700	192,700	244	---	---
F ₁	$q_{1,1}P_{F,1}$	CF	.107	.102	.136	224,650	174,100	174,100	22,914	23,678	23,678
F ₂	$P_{1,1}+P_{2,1}$	C	.030	.030	.090	222,650	172,100	172,100	6,680	15,489	15,489
F ₃	$P_{3,1}$	C	.040	.040	.020	222,650	172,100	172,100	8,906	3,442	3,442
F ₄	$q_{1,1}P_{F,1}q_{1,2}P_{F,2}$	CFRE/BEIF	.010	.014	.014	306,300	255,750	205,200	3,063	3,580	3,899
F ₅	$q_{1,1}P_{F,1}P_{3,2}$	CFRE/BEI	.003	.009	.004	304,300	253,750	203,200	913	1,015	2,438
F ₆	$q_{1,1}P_{F,1}q_{1,2}P_{F,2}$	CFRE/BEIF	.004	.002	.005	304,300	253,750	203,200	1,217	508	609
F ₇	$(P_{1,1}+P_{2,1})q_{1,2}P_{F,2}$	CD/BEIF	.003	.004	.009	294,500	243,950	193,400	864	976	2,320
F ₈	$(P_{1,1}+P_{2,1})(P_{1,2}+P_{2,2})$	CD/BEI	.001	.003	.003	292,500	241,950	191,400	292	726	1,531
F ₉	$P_{3,1}q_{1,1}P_{F,1}$	CD/BEI	.001	.001	.004	292,500	241,950	191,400	292	968	383
F ₁₀	$P_{3,1}(P_{1,1}+P_{2,1})$	CD/BEI	.004	.004	.003	234,500	234,500	183,400	938	550	550
F ₁₁	$P_{3,1}q_{1,1}P_{F,1}$	CD/BEI	.001	.001	.002	232,500	232,500	181,400	232	363	363
F ₁₂	$P_{3,1}P_{3,1}$	CD/BEI	.002	.002	.000	232,500	232,500	181,400	465	---	---
F ₁₃	$q_{1,1}P_{F,1}P_{3,2}q_{1,2}P_{F,2}$	CFRE/BEIDWIF	.000	.000	.000	---	---	---	---	---	---
F ₁₄	$q_{1,1}P_{F,1}P_{3,2}(1-q_{1,2})$	CFRE/BEIDWIF	.000	.000	.000	---	---	---	---	---	---
F ₁₅	$(P_{1,1}+P_{2,1})P_{3,2}q_{1,2}P_{F,2}$	CD/BEIDWIF	.000	.000	.000	---	---	---	---	---	---
F ₁₆	$(P_{1,1}+P_{2,1})P_{3,2}(1-q_{1,2})$	CD/BEIDWIF	.000	.000	.000	---	---	---	---	---	---
F ₁₇	$P_{3,1}q_{1,1}P_{F,1}q_{1,2}P_{F,2}$	CD/BEIDWIF	.000	.001	.000	265,600	---	---	266	---	---
F ₁₈	$P_{3,1}q_{1,1}P_{F,1}(1-q_{1,2})$	CD/BEIDWIF	.000	.000	.000	---	---	---	---	---	---
F ₁₉	$P_{3,1}(P_{1,1}+P_{2,1})q_{1,2}P_{F,2}$	CD/BEIDWIF	.000	.000	.000	---	---	---	---	---	---
F ₂₀	$P_{3,1}(P_{1,1}+P_{2,1})(1-q_{1,2})$	CD/BEIDWIF	.000	.000	.000	---	---	---	---	---	---
F ₂₁	$P_{3,1}P_{3,1}q_{1,1}P_{F,1}$	CD/BEIDWIF	.000	.000	.000	---	---	---	---	---	---
F ₂₂	$P_{3,1}P_{3,1}(1-q_{1,1})$	CD/BEIDWIF	.000	.000	.000	---	---	---	---	---	---

*C is used here as a substitute for the collection of cost symbols (BEI) which occur with every success or failure event.

Table 21.6. Probability of Success and Failure, Expected Cost, Risk and Maximum Cost and Risk for Several Possible Alternatives

Alternatives	Failure Symbols	Prob. of Failure	Success Symbols	Prob. of Success	$\Sigma(C)_j(P_c)_j$	(Risk) $\Sigma(C)_j(P_f)_j$	Expected Cost	Max Cost	Max Risk
2S, 3I	(F ₄ , F ₅ , F ₇ , F ₈ & F ₁₃ -F ₂₀)	.020	(S ₁ -S ₉)	.980	\$229,894	\$ 5,152	\$235,046	\$316,150	\$ 6,323
1S, 1P, 3I	"	.031	"	.971	220,875	7,832	228,707	265,600	8,234
1P, 1S, 3I	"	.030	"	.969	183,580	7,517	191,097	265,600	7,968
2P, 3I	"	.054	"	.946	169,573	10,188	179,761	214,500	11,583
2S, 2I	(F ₆ -F ₁₂)	.029	(S ₁ -S ₄)	.971	227,146	8,296	235,442	306,300	8,883
1S, 1P, 2I	"	.040	"	.960	219,050	9,951	229,001	255,750	10,230
1P, 1S, 2I	"	.044	"	.956	180,974	10,667	191,641	255,750	12,530
2P, 2I	"	.059	"	.941	168,309	12,093	180,402	205,200	12,107
1S, 2I	(F ₁ , F ₂ , F ₁₀ -F ₁₂)	.139	(S ₁ , S ₄)	.861	193,748	31,229	224,977	234,500	32,596
1P, 2I	"	.231	"	.769	134,022	40,030	174,050	183,400	42,182
1S, 1I	(F ₁ , F ₂ , F ₃)	.172	(S ₁)	.828	186,010	38,500	224,510	224,650	38,640
1P, 1I	"	.246	"	.754	131,271	42,559	173,830	174,100	42,829
Column No. (1)	(2)	(3)	(4)	(5)	(6)	(7)	(8)	(9)	(10)

probability of success. Column 6 is the sum of the products of the individual probabilities of success and the corresponding costs given in Table 21.5 and column 7 is a sum of the products of the individual failures and the corresponding costs. The numbers in column 7 are the mathematical risks of the various alternatives. The sum of corresponding numbers in columns 6 and 7 is entered in column 8, and it is the average cost of the alternative shown on that row in column 1.

Finally the last two columns are the maximum cost and the maximum risk respectively. The maximum risk being defined as the maximum cost times the overall probability of failure. Note that the numbers in the last column are slightly larger than the numbers in column 7. Also the average cost of each of the alternatives is less than its maximum cost.

It is interesting to note that for any of the alternatives which include one scrim balloon and one polyethylene balloon, the overall probability of success is slightly higher if the scrim is flown first, but the average cost is greater if they are flown in that order.

By combining the data from any two alternatives through the use of Eq. (21.4), the value of the discriminant V_e can be determined, and the alternatives can be compared. Tables 21.7 and 21.8 show such comparisons between each pair of alternatives.

Tables 21.7 and 21.8 are very similar. Both are special matrices. The rows and columns are identified by the maximum number of balloons and inflations which may be used in a particular course of action, and the order in which the balloons are given is the order in which they will be used. Therefore, 1S, 1P, 3I is different from 1P, 1S, 3I. The elements of the matrix, except the diagonal elements, are values of the discriminant which one obtains by comparing the two courses of action identified by the row and the column. The courses of action are arranged in order of cost with the most expensive in the top row and left column. This arrangement permits the discriminant values to be entered in the matrix in such a way that if the value of a successful experiment exceeds the matrix element, the course of action identified with the row on which the element is found is preferable to the course of action on the column. This rule is stated in the upper left corner of the matrix. Since the elements along the diagonal are not used for discriminant values, the cost and probability of success of the operation indicated by both the row and column are shown there for convenient reference.

Let's assume that the value of a successful experiment has been determined to lie between 3 and 3.5 million dollars. Since the most reliable choice is 2S, 3I, the manager selects the row labeled 2S, 3I and scans it, seeking a number larger than 3,000. This represents a discriminant value of \$3,000,000 because all numbers in the body of the table are in thousands of dollars. He finds the number 3,995. Since the value V of the experiment is less than 3,995, the column alternative

Table 21.8. Comparisons of the Various Courses of Action Using Maximum Costs. Discriminant values V_e are given in thousands of dollars.

Choose if Choose if $V < V_e$ Choose if $V > V_e$	2S 3I	2S 2I	1S, 1P 3I	1S, 1P 2I	1S 2I	1S 1I	2P 3I	2P 2I	1P 2I	1P 1I
2S, 3I	316,150 .98	1,094	5,106	3,179	686	602	2,990	2,845	629	629
2S, 2I		306,300 .97	∞	5,055	653	3,571	3,672	3,370	608	609
1S, 1P, 3I			265,600 .97	985	283	290	2,222	2,157	411	426
1S, 1P, 2I				255,750 .96	213	243	4,125	3,370	386	404
1S, 2I					234,500 .86	298			555	564
1S, 1I						224,650 .83			699	683
2P, 3I					-235	-86	214,500 .95	1,860	175	210
2P, 2I					-366	-172		205,200 .94	127	166
1P, 2I									183,400 .77	620
1P, 1I										174,100 .75

(1P, 1S, 3I) is preferable to the row alternative according to the instructions in the upper left corner of the table. In effect we are saying that the operation using two scrim balloons and up to three inflations will not on the average be enough more reliable than an operation with one polyethylene balloon, one scrim balloon and up to three inflations to warrant the difference in expected cost if the value of the experiment is less than \$3,995,000. Now the manager enters the 1P, 1S, 3I row and seeks a number larger than 3,000. Since he finds none, he accepts the one polyethylene, one scrim, three inflation alternative as the best choice. He finds the expected cost (\$191,097) and the probability of success (0.97) along the diagonal where the 1P, 1S, 3I row intersects the 1P, 1S, 3I column.

Using the procedure just used, we can construct a set of rules for choosing alternatives in this case. These are shown in Table 21.9 for both the expected cost and maximum cost alternatives. The choices are ranked in the order of descending experiment value. If the value of the experiment is high enough, three scrim balloons and up to three inflations are preferred regardless of whether the charges are to be made only for the balloons, equipment and services actually used or for the whole program. The preferred program at the next lower experiment value includes one scrim and one polyethylene balloon and up to three inflations, but the order in which the balloons should be used differs between the two costing systems. If the charges are made only for those services, etc., actually used, the polyethylene balloon should be used first because the expected cost is lower proportionally than the slightly lower reliability. If all balloons, services, etc., are to be paid for, however, the alternative having the higher reliability is preferred. Having only one balloon and one inflation is never a good choice, although it is listed in Table 21.9. It is the best choice only when the value of the experiment is less than the cost, and under such circumstances the experiment isn't worth conducting in this manner.

In discussing the one balloon, one inflation model, risk was considered as a measure of utility. From Table 21.6, we can see that the alternatives would be ranked as follows by risk: (1) 2S, 3I; (2) 1P, 1S, 3I; (3) 1S, 1P, 3I; (4) 2S, 2I; and (5) 1S, 1P, 2I. The first two choices, if one were to use risk, correspond to the preferred choices indicated in Table 21.9 for highly valued experiments. In uses similar to this, choices made using risk as a measure of utility have been found to agree generally with choices made using expectation when the value of the experiment is high. Risk is not a good measure of utility when the value of the experiment is low, however.

Now, what appears to be a good decision from the point of view of the manager may not be an acceptable solution to the sponsor. For example, the total amount of money available to the sponsor may be a deciding factor in eliminating some alternatives. Perhaps if he can hold his expenditure on Project Cometail to

Table 21.9. Rules for Choosing Alternative Courses of Action Under Two Systems of Charging

Charges Made for Only Those Balloons, Etc. Used			Charges Made for Maximum Program			
Experiment Value*	Choose	Expected Cost*	Prob. of Success	Experiment Value*	Choose	Cost*
> 3,995	2S, 3I	235	.98	> 5,106	2S, 3I	316
3,995-493	1P, 1S, 3I	191	.97	5,106-2,222	1S, 1P, 3I	266
493-32	2P, 3I	180	.95	2,222-1,860	2P, 3I	214
32-15	1P, 2I	174.1	.77	1,860-166	2P, 2I	205
< 15	1P, 1I	173.9	.75	< 166	1P, 1I	174

* Thousands of dollars.

\$225,000 or less, he will have money to sponsor another potentially valuable experiment. He can use the information in Table 21.9 as input to his own decision model and weigh these alternatives against others open to him. If he should decide that \$225,000 is all he can invest in this experiment, two polyethylene balloons and three inflations is the preferred alternative.

On the other hand, suppose the sponsor is trying to decide between balloons and a satellite as vehicles for Project Cometail. He believes that for \$5,000,000 the probability of acquiring sufficient acceptable data by satellite is virtually certain, say 0.999. Furthermore, he is willing to invest the \$5,000,000 for this purpose unless an acceptable alternative can be found. The manager can now accept the fact that the data which can be acquired by successfully carrying out the experiment are worth at least \$5,000,000. Using that value for V , he would choose 2S, 3I or 1S, 1P, 3I depending on the mode of charging.

Once again, if the sponsor is trying to decide between balloons and a satellite, he will note that there is still a 0.02 probability of failure with the best alternative offered here using balloons as vehicles. If the satellite offers a 0.999 probability of success, he can calculate that the value of the Cometail data must equal approximately \$250,000,000 for the expectation from the satellite to equal the expectation from the best balloon choice. This approximation is made using Eq. (21.4) as follows:

$$V_e = \frac{5,000,000 - 316,150}{0.999 - 0.98} = \$246,518,210$$

This is strictly valid only if the total cost of each program is independent of the success or failure of the program [that is, in Eq. (21.4), $(C)_j = (C)_i$]. That the value of a successful experiment will be so high seems unlikely, but still the sponsor may not be particularly happy with a 0.02 probability of failure.

The time during which the comet can be viewed satisfactorily does not permit more than two flights by one crew, but perhaps a parallel effort by two crews offers an answer. Each effort can be independent of the other; therefore, if the crews are equally competent, the probability of success with the second crew should equal that with the first. Also if they are equally efficient, the costs should be equal.

The maximum cost of such a double effort with two scrim balloons and three inflations each would then be \$632,300 and the probability of success, $P_{S,D}$, of the dual effort is the probability that at least one effort will succeed. It may be calculated in either of the following ways:

$$P_{S,D} = P_{S,1} + P_{S,2} - P_{S,1}P_{S,2}$$

or

$$P_{S,D} = \left(1 - P_{f,D}\right) = \left(1 - P_{f,1}P_{f,2}\right)$$

where $P_{S,1}$ is probability of success of one effort.

$P_{S,2}$ is probability of success of the other effort, and $P_{f,1}$ and $P_{f,2}$ are corresponding probabilities of failure. With the choice of two scrim balloons and three inflations,

$$P_{S,D} = 0.98 + 0.98 - 0.98 \times 0.98 = 0.9996$$

or

$$P_{S,D} = 1 - 0.02 \times 0.02 = 0.9996.$$

This suggests a probability of success which exceeds that assumed for the satellite at less than one eighth the cost. Dual efforts with one scrim, one polyethylene and three inflations would provide a probability of success comparable with that of the satellite at one ninth the cost.

21.6 LOOKING BACK

Having started with a simple decision model which enabled him to make quantitative comparisons between the utility of a single scrim balloon with one inflation and that of a single polyethylene balloon with one inflation, the manager then developed a more complex model which let him compare the utility of a number of different balloon operations with each other. From that model he developed quantitative data which were useful in making rough comparisons of the various balloon combinations with a satellite system. He realized, however, that his model for decision making was not designed to include the satellite; therefore, if he should wish to make a rigorous comparison with the satellite, he should review the decision model carefully and modify it as necessary to assure that just comparisons can be made. He also assumed that the results of the model were applicable to another crew without change, and he further assumed that the probability of failure of the two were independent. If the results deriving from these assumptions are to be considered seriously in making a decision, they should be carefully examined for validity.

This attempt by the manager to construct a realistic decision model has caused him to look systematically at what he believes to be the most significant aspects of

the success or failure of a balloon flight operation. He may decide that he can construct a more realistic model for this particular problem; if so, he should do so. Whether he does so or not, he will realize that he needs to institute ways of obtaining better data (for example cost estimates, probabilities, etc.) for use in future models.

As a result of going through this exercise, he has a better appreciation of the way he should interact with the scientist, the scientist's sponsor, the balloon manufacturer, etc., if all pertinent facets of a problem are to be considered in proper perspective.

Ultimately, of course, a man makes the decision, but he should make it from the vantage point of the most careful possible consideration of all pertinent facts. Modern decision theory provides a systematic way of approaching that vantage point. How closely the decision maker comes to it depends on his skill and dedication.

References

- Archibald, R. D., and Villoria, R. L. (1967) Decision Trees for Decision-making, Network-Based Management Systems (PERT/CPM), John Wiley and Sons, Inc.
- Ellon, S. (1969) What is a decision, Journal, Institute of Management Science, 16:(No. 4).
- Fishburn, P. C. (1964) Decisions and Value Theory, Wiley, New York.
- Sisson, R. L., Sieber, H. F., and Nagin, R. P. (1967a) Decision Making Revisited, Management Science Selections, Rev. Ed., Data Processing, Inc., Los Angeles, Calif.
- Sisson, R. L., Sieber, H. F., and Nagin, R. P. (1967b) Bayesian Decision Theory, Management Science Selections, Rev. Ed., Data Processing, Inc., Los Angeles, Calif.
- Tribus, M. (1969) Rational Descriptions, Decisions and Designs, Pergamon Press, New York and London.
- Wheeler, R. E., and Peepels, W. D. Jr. (1969) Modern Mathematics for Business Students, Brooks/Cole Publ. Co., A Division of Wadsworth Publ. Co., Belmont, Calif.

Contents

22.1	Introduction	287
22.2	History of Past Flights	287
22.3	Specialized Design Problems	288
22.4	Launch Technique	293

22. Heavy Load Performance of Strato Film Balloons

**L. Mielke
Winzen Research Inc.
Minneapolis, Minnesota**

22.1 INTRODUCTION

During the past several years there has been an increased demand for balloons capable of carrying heavier payloads to higher altitudes. The 10-million cubic foot size, which was for some time considered to be a big balloon, has given way to polyethylene balloons as large as 47 million cubic feet, and the 15 - 30 million size is becoming common. The payloads have increased from the 2,000 lb bracket to as much as 12,000 lbs with numerous flights being made in the 4,000 lb range. These increased payloads are requiring an extension of the state-of-the-art in balloon materials, components and launch procedures. This paper is a review of the heavy load flights with StratoFilm balloons, as well as a description of the work that is being done to further the state-of-the-art for heavy loads.

22.2 HISTORY OF PAST FLIGHTS

In 1959 the first 10-million cubic foot capped balloon was statically tested to evaluate the ability of a polyethylene balloon to withstand excessively high gross inflations. The balloon was fabricated from 1 mil material and had a 1 1/2 mil

internal cap and 500 lb load tapes. The inflation progressed satisfactorily to a value of 14,650 lbs gross. At that point the anchor bolt fractured, causing the balloon to ascend a few hundred feet before failure. Although the ultimate capability of the balloon was not determined, it was useful to know that it was in excess of 14,650 lbs. Improvements in balloon materials, manufacturing methods, design techniques and hardware have certainly increased the potential of the polyethylene balloon from what it was at the time of this static test.

A review of all flights using WRI StratoFilm balloons was conducted for the past 4 1/2 years. Those flights which involved payloads in excess of 3,000 lbs have been selected for study and are tabulated in Table 22.1. The balloon volumes range from 110,000 to 31,200,000 cubic feet. The payloads extend up to almost 12,000 lbs. There has been at least one flight attempted using each of the standard launch techniques (dynamic, tandem and vertical). Neglecting the two successful ground tests, the collar test and the flight abort due to instrumentation difficulties, the success ratio has been 53 percent, and the average payload carried on each of the successful flights was 3,775 lbs. Of the eight flights categorized as failures, two were due to mechanical problems encountered during launch, three were due to insufficient protection and/or operation of the reefing sleeve, and the remaining three were due to an opening of the basic balloon shell.

22.3 SPECIALIZED DESIGN PROBLEMS

22.3.1 End Fittings

22.3.1.2 APEX FITTINGS

Many years ago WRI adopted the plate, hoop and clamp ring end-fitting as a standard technique for the termination of the load tapes at the balloon apex. This design is ideally suited for a taped balloon with tailored gores and has proven successful for thousands of balloon flights. An important aspect of the installation involved the ability of the load tape to be sealed in a loop around the hoop. The strength-giving fibers of the load tape were made of Fortisan. Some time ago the manufacture of Fortisan filaments was discontinued, and this necessitated a search for a substitute material. A very extensive material study determined that polyester filaments have similar physical properties, and the decision was made to fabricate sample load tape. Concurrent with this effort, due to the difficulty encountered in sealing high-strength Fortisan load tapes together, a study was in progress to develop an end fitting design that did not incorporate the necessity for sealing the load tapes around the hoop.

Table 22.1. Heavy Load Flights, 1966 - April 1970 Summary

Vol.	Thickness- mils/Con- figuration	Date Flown	Launched By/At	Launch Type	Pay- load Lbs.	Press. alt.-ft.	Flight Dur. Hours	Remarks
$\times 10^6$								
0.11	2.0, NS	10/6/66	NCAR Psn, Texas	Ground Test	5695	-	-	Ground test of tandem balloon launch technique. Successful balloon performance.
0.11	2.0, NS	10/27/67	NCAR Psn, Texas	Ground Test	5013	-	-	Ground test of tandem balloon launch technique. Successful balloon performance.
2.03	1.5, NS 1.5 Cap	9/12/69	NCAR Psn, Texas	dynamic Tiny Tim	3510	79, 600	13.2	Successful flight.
2.90	2.0, NS	7/3/69	NCAR Psn, Texas	dynamic Tiny Tim	4188	81, 500	10.3	Successful flight.
5.025	1.0, NS 1.0 Cap	3/1/70	AFCRL Hmn AFB	-	6000	-	-	Collar test. Collar damaged balloon on ground causing a flight abort prior to launch.
2.90	1.5, NS	4/6/70	NCAR Psn, Texas	dynamic Tiny Tim	3065	90, 800	3.1	Descent started after reaching maximum altitude. Cut down after descending to 72 K. Ft.
10.5	1.5, NS 1.0 Cap	3/23/70	NCAR Psn, Texas	dynamic Tiny Tim	4731	105, 400	4.6	Successful flight.
10.6	1.0, NS 1.5 Cap	7/31/69	AFCRL Hmn AFB	Dyna- mic	3217	-	-	Reefing sleeve opened on release from launch arm. Wind created large sail which caused hole below cap. Flight aborted on ground.
10.6	1.0, NS 1.5 Cap	8/2/69	AFCRL Hmn AFB	Dyna- mic	3210	12, 000	0.1	Flight aborted due to instrumentation problems. Satisfactory balloon performance to termination.
10.6	1.0, NS 1.5 Cap	8/15/69	AFCRL Hmn AFB	Dyna- mic	3192	115, 000	4.3	Successful flight.
10.6	1.0, NS 1.5 Cap	4/28/69	AFCRL Hmn AFB	Dyna- mic	3347	106, 200	31.6	Successful flight.
10.6	1.0, NS 1.0 Cap	8/20/60	NCAR Psn, Texas	dynamic Tiny Tim	3690	108, 500	5.4	Balloon developed hole near top end fitting after reaching float altitude. Flight terminated early.
10.6	1.0, NS 1.0 Cap	9/15/69	NCAR Psn, Texas	dynamic Tiny Tim	3750	108, 800	11.3	Successful flight.

Table 22.1 Cont'd. Heavy Load Flights, 1966 - April 1970 Summary

Vol.	Thickness- mills/Con- figuration	Date Flown	Launched By/At	Launch Type	Pay- load Lbs.	Press. alt.-ft.	Flight Dur. Hours	Remarks
18.9	1.5 tand. 2.0 Cap	5/22/69	WRI, Nth- fld, Minn.	Tan- dem	5000	22,100	2.8	Main balloon damaged during launch.
18.9	1.5 tand. 2.0 Cap	7/1/69	WRI, Nth- fld, Minn.	Tan- dem	7500	10,800	3.3	System broke free from main cable at beginning of let-up. Launch balloon failure.
18.9	1.5 tand. 2.0 Cap	3/7/70	WRI, C. G. Arizona	Tan- dem	7500	13,600	1.7	Main balloon reefing sleeve did not open. Launch balloon failure.
20.8	0.8, NS 0.9Cap(2)	10/20/69	AFCRL Chico AFB	Dyna- mic	4326	-	-	Reefing sleeve opened on release from launch arm. Wind created large sail which caused hole below cap. Flight aborted on ground.
20.8	0.8 tand. 0.9Cap(2)	12/6/69	AFCRL Chico AFB	Dyna- mic	4325	119,500	27.9	Successful flight.
27.3	0.8 tand. 0.8 Cap	7/18/69	AFCRL Hmn AFB	Tan- dem	3500	123,000	8.3	GT-12 launch balloon. Successful flight.
27.3	0.8 tand 0.8 Cap	9/25/69	AFCRL Hmn AFB	Tan- dem	3800	126,000	27.3	GT-12 launch balloon. Successful flight.
31.2	1.5, NS 1.5Cap(2)	2/25/70	WRI, C. G. Arizona	Verti- cal	11950	-	-	Flight aborted after gore seam opened on ground.

Short sections of the end fitting have been pulled in the tensile tester with very good results. One unit has been installed in a static inflation of a superpressure balloon to check its suitability for production use. Based on the work to date, plans are being formulated to use the fitting in the near future, on a flight where it is anticipated that the loading on the fitting will be approximately 25,000 pounds.

22.3.1.2 BASE FITTING

The base fitting used by WRI has long been a standard throughout the industry. It consists of a collar and two opposing wedges which grip the balloon material and load tapes. The material and tapes which extend through the fitting can be fused into a hard ring or folded back over the collar and banded. Either technique increases the resistance of the material to being pulled out of the fitting.

It is anticipated that this basic design can be extended, without considerable difficulty, to be used for heavy loads. Component parts must be increased in strength and size. One fitting has been designed and tested for heavy load applications. It was subjected to a tensile load of 40,000 pounds without component failure or material slippage. Two other lighter duty units were tested to failure, which occurred at 50,000 lbs and 39,600 lbs.

22.3.2 Reefing Sleeve

The function of a reefing sleeve is to:

- (1) Provide increased protection for the balloon from damage due to handling, ground abrasions, etc.
- (2) Contain the material below the bottom of the lifting-gas level in the balloon, reducing the problem of control and possible damage by wind sailing during launch.
- (3) Open gradually during ascent, maintaining the zero pressure gas level at or slightly above, the top of the sleeve.

The present reefing sleeve design used on WRI balloons has been employed for both large and small balloons. It consists of a fairly heavy poly sleeve sealed to a poly flange which has been incorporated into the last gore seal. This sleeve is wrapped around the balloon, and a light weight poly tear panel is then sealed between the sleeve and the flange. A slit is initiated in the tear panel. During ascent there is a radial force on the top of the sleeve caused by the tensile forces in the load tape which is sufficient to continue propagation of the initial tear. The design requires low tear forces so that will be no chance of balloon failure because the sleeve failed to open. The opened sleeve remains attached to the gore seam and flies with the balloon. This attachment prevents sliding down and generating folds or rolls that would be increasing the required opening force.

The present configuration has been successfully flown on many flights, including almost all the heavy load flights reported in this paper. With one exception

it fulfills the design goals for heavy payloads. This exception involves the fact that due to the low-strength tear panel, tensile loads open the sleeve such that the included balloon angle at the top of the sleeve is $10-20^{\circ}$. This unfortunately allows considerable undeployed balloon material to be subjected to the wind. If the winds are high enough to overcome the tensile forces in the load tape, a "sail" of balloon material will develop which will further open the sleeve and cause the already undesirable situation to deteriorate. The solution to this problem is a range of materials of different tear strengths to cover the tensile range in steps.

The natural shape for an inflated bubble during ascent of a heavy load flight will approach the limit for a "shape sigma" of zero. This yields an angle at the base of the balloon of about 100° . A greater angle would indicate bubble super-pressure, and a lesser angle would allow more undeployed material above the intact sleeve. Efforts are currently being made to produce a reefing sleeve which will provide the desired bubble shape. A test arrangement has been set up which simulates a short section of balloon. Various sleeve configurations and materials are being evaluated in an effort to find a more suitable system for heavy loads. Test flights with up-cameras are planned for final evaluation of the most promising designs.

22.3.3 Inflation Tubes

Standard inflation-tube configuration has been a twenty-inch, layflat tube that passed through the balloon wall about 15 to 35 feet from the theoretical apex. The end was sealed three feet inside the balloon wall, and the short section was ventilated with one inch holes to diffuse the balloon lifting gas during inflation. The juncture between the tube and the balloon wall was reinforced to provide adequate strength for any reasonable loading encountered during inflation. This system is very satisfactory for loads launched dynamically.

During February 1970, the vertical launch of a 31,200,000 cubic foot balloon was attempted from Casa Grande, Arizona. This balloon was equipped with four, 800-foot long standard inflation tubes as well as one internal inflation tube. The internal tube consisted of a poly tube encased in a nylon sleeve. The tube was sealed to one of the gore seams and took the shape of the balloon contour during inflation. At the upper end the poly tube terminated below the nylon sleeve, allowing the sleeve to act as a diffuser. The bottom end of the composite tube was installed over a muffler which was mounted on the bottom end fitting. This arrangement provided a rapid and quiet means of inflation. Two subsequent tests using this inflation tube on smaller balloons also showed the basic design to be satisfactory, except that the nylon sleeve was not sufficiently porous to allow gas passage at as high a rate as desired. This will be corrected for upcoming flights.

Another inflation technique which is used in a tandem launch is to make the inflation through the transfer tube. The helium hose from the truck can be connected through a quick-disconnect coupling to a metal diffuser inside the transfer tube. After the bubble is erected, this system performs very well.

22.4 LAUNCH TECHNIQUE

In reviewing all of the launch techniques which have been utilized in heavy load flights, it may be concluded there is no one system which is totally satisfactory. Although each of the methods has definite advantages, they all also have some inherent disadvantages. A brief discussion of each technique will be presented to point out the desirable features as well as the associated problem areas relative to heavy-load applications.

22.4.1 Dynamic

This technique consists of holding the bubble in a release mechanism, normally a roller, until full inflation has been injected into the balloon through external inflation tubes near the balloon apex. The balloon base is connected to the payload through a parachute. The payload is mounted on a vehicle. At time of launch the bubble is released and moves to a position over the payload vehicle, and the vehicle is driven down-wind at a velocity approximately equivalent to the wind velocity. When these conditions have been met, the payload is released. The system has the advantage of tolerating a fair amount of wind, as well as wind direction shifts, during the inflation phase of the launch. It is somewhat limited in its ultimate capability due to the strength requirements, the ability to release the bubble, and a suitable ground anchor for the bubble release equipment. More serious, however, is the problem of obtaining a large vehicle which can tolerate a substantial side-load without danger of overturning. In addition, a large, flat, hard-surfaced area is required for conduct of this operation. Finally, it should be pointed out that the dynamic forces involved in this type of launch are often unacceptable for the scientific payload.

22.4.2 Tandem

A tandem system incorporates two balloons — the launch or inflation balloon and the main balloon — both connected by a transfer collar. The transfer collar is held on the ground during inflation of the launch balloon by a winch. The base of the balloon is connected to a parachute which, in turn, is connected to the payload. The payload is held on the boom of a heavy crane. It can be manually

released. After completion of inflation the system is raised over the crane by winching the launch balloon, transfer collar and main balloon to an upright position. The winch cable is then cut away, the system moves forward, and the payload is released. As with the dynamic launch, this system has the disadvantage of requiring some sophisticated heavy equipment. In this instance, a winch of suitable strength, drum capacity and payout speed is difficult to locate. The crane is not too serious a problem, as most industrialized areas have such equipment available. The primary advantages of this system over a dynamic launch are the lack of dynamic forces on the scientific instrumentation and payload-holding vehicle, and a somewhat relaxed requirement on the launch equipment. This system can tolerate fairly high launch winds, but changes in wind direction can cause problems. The crane can rotate about its axis, however, which helps to alleviate (but not eliminate) this problem. A further disadvantage of this system is the complexity of the flight train compared to that on a single-celled balloon. Also, the launch balloon provides little, if any, free lift at altitude, and a sizable portion of its weight as well as the weight of the transfer collar reduces the available payload-carrying capability of the system.

22.4.3 Vertical

The vertical launch technique is the simplest of the methods described. It consists of layout of balloon, erection of bubble, and continued inflation until the balloon stands vertical over a winch which is connected to the base of the balloon. Upon completion of inflation, the system (balloon and parachute) is winched over a crane holding the payload. The winch line is removed and launch is made by releasing the payload and the remainder of the system from the crane. The heavy equipment required is about the same as that for a tandem launch, except that the winch can have a fairly small spool capacity and slower payout speed, and still be satisfactory. If, during inflation, cross winds develop before the balloon becomes vertical, they will cause the balloon to slide across the ground cloths and risk possible damage. An 180° wind-direction change can cause the balloon to be pulled over the payload and anchor vehicle, causing destruction of the balloon. Once the balloon is vertical, it is capable of withstanding reasonable winds from various directions much as the tandem launch. The vertical launch technique represents the simplest operation in terms of the balloon system and the supporting heavy equipment. Its use is, however, restricted to times and locations where the winds are essentially calm for four-to six-hour periods.

It is quite possible that a solution more satisfactory than those mentioned above exists for heavy-load launches. One such method represents a combination of the dynamic and vertical launch techniques. It consists of initial inflation of

the bubble in a bubble-release device. This inflation would continue until the lift reached a value about 110 percent of the balloon weight. The bubble could then be released from the roller and allowed to erect itself over a winch which is fastened to the bottom end. The remainder of the inflation would progress as same as the vertical inflation had from this point. This system would take advantage of the desirable characteristics of the vertical inflation, but eliminate the high risk phase of the operation during initial inflation.

23. Thin Films for Mesosphere Flight

J.R. Nelson
Winzen Research Inc.
Minneapolis, Minnesota

Whether we talk about heavy payload balloons or very high altitude balloons, we still are primarily talking about larger and larger balloons. Since our last report at the Fifth AFCRL Scientific Balloon Symposium two years ago this month, Winzen Research has advanced to balloons considerably larger than the workhorse, 10.6-million cubic foot capped, unit familiar to many. Balloons in sizes of 15, 18.5, 18.9, 20.8, 20.36, 20.1, 28.7, 26.6, 27, 27.3, 31.2, 30.5, 30.16, 30.3, 33.9, and 47.6 MM cubic feet have been manufactured since then, and most have been successfully flown.

This report will present data on the current status of high altitude performance, and a discussion of recent and current R & D effort on reducing StratoFilm thickness, new materials of balloon-quality thin film, problems in working with these films, launch operations considerations, and a look at what might be in store for the near future.

Looking to the subject of this report, a compilation has been made of balloons flown above 140,000 feet - and also some scale-model balloons from thin films.

You will note that ten of these are the familiar 10.6MM size which carry an average payload of 850 lbs to an average altitude of 143,000 feet for an average duration of almost 17 hours. In the 30-million cubic feet size, the altitudes approached or attained the stratopause, averaging 158,000 feet with average payloads

PRECEDING PAGE BLANK

of 600 lbs and durations of three to over 17 hours. Also shown are some scale models, 3MM cubic foot balloons of 0.35 mil StratoFilm, the 47.6 MM cubic foot balloon of 0.35 mil (which stopped for a rest at 69,000 feet on its way to 174,000 feet and didn't get any higher) and some 0.3 mil nylon balloons of 100,000 cubic feet.

Turning to our recent R & D effort, there has been a two-fold attack on achieving light-weight large balloons. A program to explore new, strong, thin materials by building and flying balloons constructed from our materials and a fabrication research program has been funded by the Office of Naval Research since 1967; and a program to explore the ultimate practical reduction of conventional StratoFilm thickness has been funded by Air Force Cambridge Research Laboratories since March 1969.

Early in the program for ONR the search for new materials of balloon quality narrowed to nylon and polyurethane. A report on these films was presented by Leo Mielke at the Fifth AFCRL Symposium. Since that time, a new formulation of nylon has been investigated and found to have superior qualities of strength, elongation, extrudability to thicknesses as low as 0.1 to 0.2 mil and - most important - excellent thermoplastic sealing qualities with current sealing procedures used in our production. The successful flights using this nylon are shown in Table 23.1. A fourth balloon of this material is awaiting flight now, and, following a successful flight, two 3MM cubic foot balloons will be fabricated from this nylon for flight evaluation. These will be forerunners of a larger balloon whose size and existence are yet to be established.

The program for extending the use of basic polyethylene StratoFilm in thinner gauge started with a determination that the minimum thickness of StratoFilm for practical production was 0.35 mil. The program was then carried forward in four steps:- first, the computer design for a balloon to lift 250 pounds to 170,000 feet; and then in progression, evaluations of (1) the 0.35 mil StratoFilm in 7 foot diameter, 30 foot cylinders stressed to values computed for the full size balloon, (2) two - three million cubic foot balloons in flight, and finally, the 47.6 million cubic foot balloon.

During the in-house development work since 1967, new sealing techniques and machines have been developed for the ultra-thin materials. It becomes a whole new ball game.

In July, 1968, we contracted for computer time-sharing, which has opened new vistas of design and evaluation improvements. Several balloon-design computer programs developed by Justin Smalley of NCAR were modified for the time-sharing service. The stress levels at each station of the balloon shape are printed outputs, so, by varying program input parameters of payload and altitude, the

Table 23.1. High Altitude Flights Above 140,000 Feet, 1968-1969

Date	Film Gauge Mils	Volume MMft ³	Operation by	Pay-load	Bal. Wt.	Altitude K ft	Duration	Remarks
6/24/68	.5 .7 cap	10.6	ONR-RI	382	966	145.5	16:30	Success
9/1/68	.7 .7 cap	10.6	ONR-RI	654	1209	142	16:16	Success
7/1/68	.5 .7 cap	10.6	ONR-RI	917	955	140	14:32	Success
7/5/68	.5 .7 cap	10.6	ONR-RI	388	960	142	14:55	Success
7/21/68	.5 .7 cap	10.6	ONR-RI	933	947	140	19:08	Success
7/23/68	.5 .7 cap	10.6	ONR-RI	640	970	148	17:40	Success
7/29/68	.5 .7 cap	10.6	ONR-RI	472	933	142	18:54	Success
7/31/68	.5 .7 cap	10.6	ONR-RI	737	933	144.5	17:00	Success
8/1/68	.5 .7 cap	10.6	ONR-RI	1012	958	141	17:22	Success
7/2/68	.5 .5 cap	10.6	ONR-RI	380	887	148.2	16:03	Success
9/11/68	.45 .7 cap	28.7	AFCRL	432	1565	158	17:36	Success
9/23/69	.45 .7 cap	30.3	AFCRL	450	1528	161.5	17.6	Success
11/16/69	.45 .7 cap	30.16	Mildura	768	1289	156.4	30	Success
11/26/69	.45 .7 cap	30.16	Mildura	767	1264	0	0	Ground abort No test
12/4/69	.45 .7 cap	30.16	Mildura	773	1319	157	9.	Success
10/21/69	.35 .35 cap	3.02	Chico	400	310	127	9.2	Success
10/23/69	.35 .35 cap	3.02	Chico	400	302	128.7	5.2	Success
4/6/70	.35 .7 cap	47.6	Chico	400	1562	69	Probable ascent damage -Stopped at 69 K	
3/16/70	.3	0.1	Casa Grande WRI	124	24	89.4	5:38	Success Nylon
3/21/70	.3	0.1	Casa Grande WRI	123	24	89.5	5:04	Success Nylon
6/3/70	.3	0.1	MPLS. WRI	145	24	86	5 hrs.	Success Nylon

three million cubic feet balloon design duplicated the loading on the 47.6 million cubic foot balloon within close limits. This is a valuable tool in developmental programs such as this one. As indicated on the tabular flight results, the three-million balloons flew successfully. The 47.6 million balloon, however, did not reach ceiling. According to various observers, around 30,000 to 40,000 feet it encountered a severe turbulence which ripped the reefing sleeve all the way down, with considerable gyrations and sailing of the long balloon, which at this point had approximately 585 feet of undeployed material. The balloon got through the turbulent region, but slowed to a stop at 69,000 feet, where the flight was terminated.

This problem of undeployed material sailing during ascent through turbulent air was first recognized in the 1965 ONR Churchill flight series where up-camera pictures of a 10.6 million balloon showed this condition - some will remember the film I presented on this at the Fourth AFCRL Symposium. A reefing sleeve was designed at Winzen Research and, after testing on smaller balloons, was first used on the 28.7 million cubic feet balloon, built for Dr. Beyers, Atmospheric Science Office, White Sands, New Mexico, under contract with AFCRL, and successfully flown in September 1968. This reefing sleeve design has been flown with success on up to a hundred large balloons until the 47.6 million flight. The combination of a large area of undeployed material in a big balloon and a relatively light payload is more than the reefing sleeve design could handle.

A current, in-house program is in process to determine new rip panel materials in this design to cover a wide range of payloads likely to be encountered. The original design used a 1/2 mil StratoFilm rip panel. Several configurations of plastic rip panels have been tested, but a light canvas material seems to have excellent tear characteristics. A range of rip strengths will be tested to cover the requirements.

Another concept awaiting flight test (and not new except in detailed design) is to keep the main balloon reefed up to 50,000 feet or so (or above the turbulent region), and start transfer of gas from a launch balloon. When enough gas has been transferred to the main balloon, the top balloon is released from the train, ballast is dropped, and the main balloon proceeds to altitude.

Looking to the future a bit, I have extrapolated designs to see what we might have in store in the next year or so in large balloons.

First - with our current production facility, which length is 800 feet long - computer designs are presented based on 0.35 mil StratoFilm, which is pretty well on our threshold, and on 0.2 mil nylon, which is just around the corner.

With .35 mil, the balloon that can be built would be 63.4 MM cu ft in volume, and would carry 250 lbs to an altitude of 172,000 feet. Its diameter would be 540

feet, gore length, 766 feet, a cap 115 feet long of .85 mil StratoFilm, and it would use 100 lb polyester load tape, weight 2,287 lbs.

With .2 mil nylon, the balloon would be 62 MM cu ft and carry 250 lbs to an altitude of 181,000 feet. Its diameter would be 534 feet, gore length 764 feet, a cap 104 feet long of 0.2 mil nylon StratoFilm and 60-pound tensile load tape, weight 1570 lbs.

Our present plant has the capability of being extended to at least 1,000 feet, so it is not inconceivable that we might well be looking at a .35 mil balloon of 134 million cubic feet that would carry 250 lbs to 179,600 feet.

The unit would have a diameter of 694 feet, a gore length of 983 feet, and would weigh 3889 pounds. The same building extension would permit building a nylon balloon of 0.2 mil that would carry 250 lbs to an altitude of 189,500 feet and could push to 190,000 feet, I'm sure. Its diameter would be 695 feet, gore length 994 feet, with a weight of only 2700 pounds.

Looking at the future heavy-load balloons, it is computed that 20,000 lbs can be carried to 110,000 feet with a balloon of 78.5 MM cubic feet of polyethylene and a 52.4 MM cubic foot balloon of 0.5 mil nylon.

While perhaps this sounds a little far-fetched to some people at this time - so did the 30 million cubic feet range of volumes, which have successfully flown four times, seem far-fetched two years ago, and even 10 million cubic feet, as little as five years ago.

24. An Inflatable Restraint Collar for Balloons

K. Stefan
National Center for Atmospheric Research
Boulder, Colorado

The cable-restrained method for launching balloons, illustrated in Figure 24.1, is characterized by a cable from the base of the launch bubble to a winch. By paying out cable from the winch, the balloon may be raised to a vertical or intermediate position for release or manipulation of the system. Several possible advantages over other methods may accrue for this type of launch depending, of course, upon the situation. By raising the balloon before release, the system can be re-oriented into the wind line, if necessary, by simply moving the winch vehicle, and can then be released from the elevated position. This technique requires much less maneuvering room than a conventional dynamic launch.

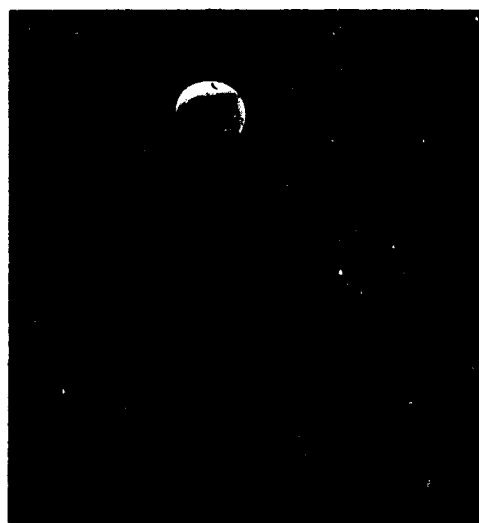


Figure 24.1. Typical Cable Restrained Launch

PRECEDING PAGE BLANK

The cable-restrained launch maintains the launch bubble under positive control at all times, even up to the moment of payload release if desired, thus assuring a shock-free launch for payload and balloon and avoiding uncertainties that may exist in a dynamic launch.

A cable-restrained launch has been possible in the past only with tandem balloon systems, where the transfer duct provides an attachment point for the restraining cable. Mainstay launches of single-cell balloons using a fitting at the base of the bubble for a cable attachment point have long been considered, but only recently has any attempt been made to actually develop the hardware. About two years ago, NCAR began development of an inflatable collar for this application. Raven Industries, Inc., on subcontract to NCAR, has designed an inflatable collar, and their initial field tests have been promising.

Table 24.1. Static Coefficients of Friction
(Lowest Values Reported)*

Friction Surfaces: Polyethylene film against following:	Dry	Lubricated with polyethylene powder
Polyethylene	0.50	0.12
Butyl coated nylon	0.50	0.17
Nylon cloth	0.25	0.17
Neoprene coated nylon	0.41	0.15
Neoprene (soft) coated nylon	0.62	0.12

* Extracted from NCAR TN-44, Tables 1 and 2

A previous project described in NCAR TN-44, 1969, had developed frictional data for polyethylene under various conditions of area loading by an inflatable support. Table 24.1 presents some of these data. This project also demonstrated that film could be clamped with an inflated support at moderate pressures without film damage. We, therefore, had gained some confidence that an inflatable restraint device would be feasible. Also, Angevine and Fulker (1970) had developed a program at NCAR for calculating the forces in a cable-restrained balloon system. This program was modified and used to resolve the force at the restraining collar into slip force and lateral force components, and was also used to include the "shucking force". This shucking force, which tends to push the collar down, results from the balloon bubble cone angle. These forces are illustrated in Figure 24.2. With this information, G.L. Morfitt of Raven Industries, Inc.

made preliminary designs and tests, and we settled on making a prototype restraining collar for a balloon with 3,000-lb gross lift to be launched in a wind having a profile which increases as a function of the 0.35 power of height from zero at the ground to 15 knots at 500 ft. We also decided that as an initial compromise affecting the dimensions of the restraining collar, we would specify operational restrictions of 2,000 lb of slip force and 3,000 lb of lateral force. A safety factor of two was specified for slip force, and a factor of three was specified for all other forces.

The resulting design is illustrated in Figure 24.3. The restraining collar consists of two double-walled inflatable half cylinders hinged together at one side, and equipped with a releasable fastener at the other side. The collar weighs 50 lb, is 4 ft long, and has a diameter of 20 inches. The inner surface of one of the half cylinders has an extension which is the fastening point for the restraint cable. The balloon material is placed longitudinally in the collar with several layers of polyethylene as a buffer between the balloon material and the collar inner surface. The

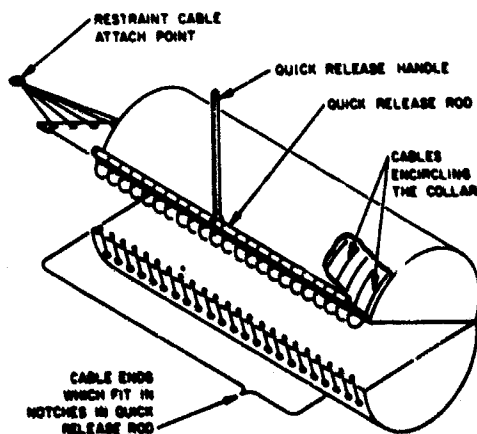


Figure 24.3. Schematic of Restraint Collar Design

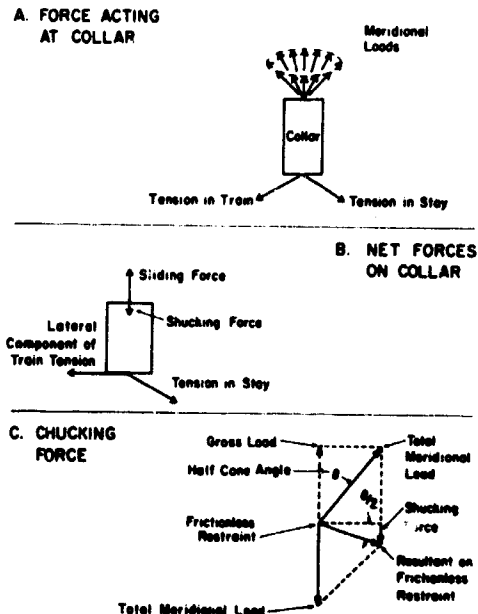


Figure 24.2. Forces at Restraint Collar

cylinder halves are closed and fastened and are then inflated to 25 psi. The releasable fastener consists of a 4-ft steel rod with notches spaced about one inch apart along its length. Steel cables, fastened to the rod, are passed around the collar. Ball fittings on each cable end fit into the notches on the steel rod. The rod is positioned to hold the cable ends in the notches. For opening, the rod is allowed to rotate so the cable ends all pull out of their notches simultaneously, thus releasing 50,000 lb of hoop tension that the inflation pressure is exerting along the collar edge.



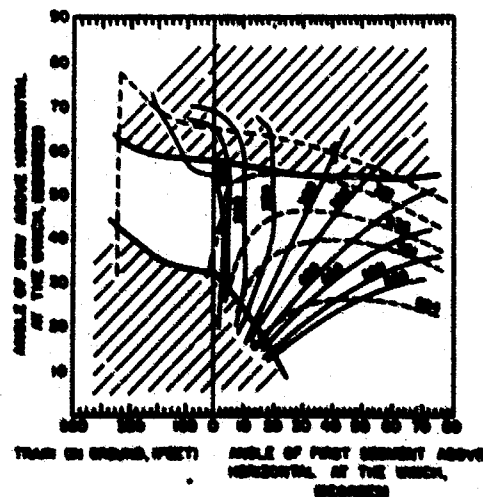
Figure 24.4. Restraint Collar Inflated

The configuration for balloon-system restraint during the launch process is shown in Figure 24.4. The balloon bubble is above the collar, the uninflated balloon train proceeds from the base of the collar to the payload, and the restraining cable proceeds from its fastening point at the base of the collar to the winch.

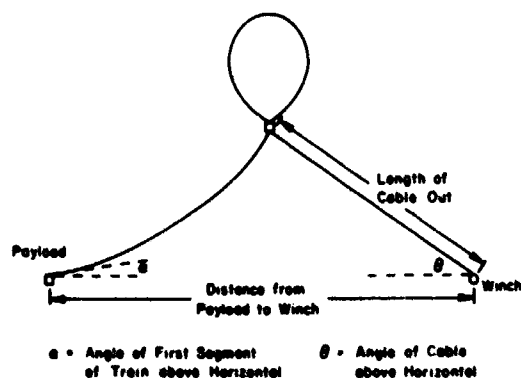
Limiting operational parameters were computed for this design and are presented graphically in Figure 24.5. The ordinate on this graph is the angle of the cable above horizontal at the winch, and the abscissa is a combination of two variables: the lefthand portion is the length of train resting on the ground, and the righthand portion of the abscissa is the angle above the horizontal of the train at the payload when the balloon train leaves the ground.

(The parameters for this graph are illustrated in Figure 24.6.) The hatching on the graph in Figure 24.5 denotes forbidden areas. In the upper area excessive slip force is the critical parameter, and in the lower hatched area excessive lateral force is the critical parameter. In the entire area between these limits, forces are acceptable in 15 knots of wind or less. The other lines across the graph are lines of constant length of cable out, and of constant

Figure 24.5. Operational Envelope for Restraint Collar. $2.94 \times 10^6 \text{ ft}^3$ balloon, 3,000 lb gross lift. Wind profile for 15 kt at 500 ft. Upper Hatched Area - Excessive Slip Force. Lower Hatched Area - Excessive Lateral Force. ----- Lines of constant distance from payload to winch. ——— Lines of constant cable length



A. TRAIN OFF GROUND



B. PART OF TRAIN ON THE GROUND

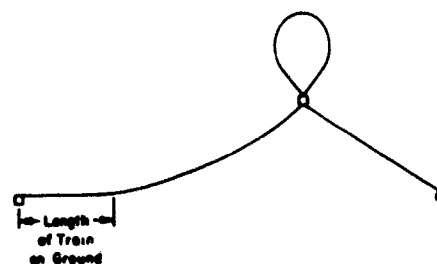


Figure 24.6. Parameters for Operational Envelope Graph



Figure 24.7. Collar Opening Sequence. Top: Restraint collar is the white cylinder in the foreground, in its fully closed position. Bottom: About 20 milliseconds later. Collar partially open



Figure 24.8. Collar Opening Sequence (continued). Collar is reacting against balloon

distance between the payload and winch. This graph shows that for a balloon bubble with 3,000 lb of lift and close to the ground, as shown by maximum length of train on the ground, the cable angle should be between 35° and 55° . As the bubble is let up and the balloon train leaves the ground, these limits become wider. Note that there is an angle range available which is good at all bubble elevations.

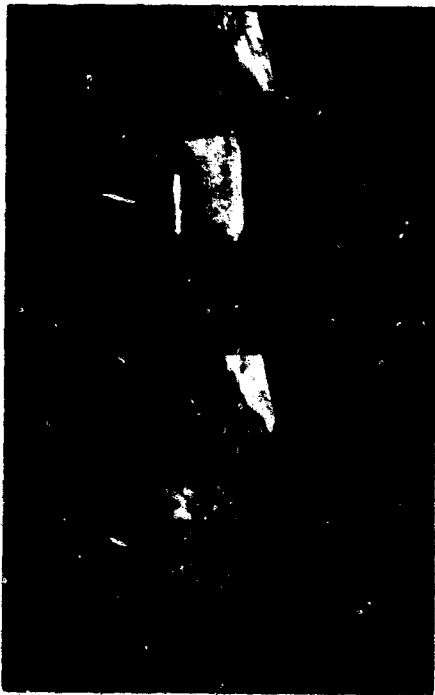


Figure 24.9. Collar Opening Sequence (continued). Collar springs clear of balloon

A motion picture sequence of a balloon release is shown in Figures 24.7, through 24.9. The camera speed was 64 frames per second. The first frame shows the inflated collar in position for opening. This was an early test, and the collar had not yet been fitted with the restraint-cable attachment. In the second frame, the opening device has actuated and the collar has started to open. The collar continues to open, as shown in Figures 24.8 and 24.9, and in so doing the collar imparts a forward momentum to the balloon and a rearward reaction to itself which results in a clean separation of collar and balloon. Figures 24.10 through 24.13 show a sequence of full-scale launch operation employing the restraint collar. Figure 24.10 shows the balloon bubble shortly after inflation with the collar in place and fastened by the restraint cable to the winch. Gross inflation here is 3,000 lb; winds are gusting to 12 knots. The restraint cable

angle is maintained in accordance with the operational envelope graph by merely moving the winch vehicle forward or backward to obtain the desired angle. In actual practice this angle adjustment technique was very accurate. In Figure 24.11, cable has been paid out and the balloon raised to an intermediate elevation. If desired, the balloon bubble could be released at this point by opening the collar. (High speed photographs of the collar opening with maximum aliding and lateral forces applied have shown satisfactory operation. The rapidity of opening apparently is adequate to prevent excessive relative motion during the opening process.) Figure 24.12 shows the system at the near vertical position, and Figure 24.13 shows the system after collar release.

Some discrepancies have been encountered in the development thus far, and corrective action is in process. In the launch test pictured, strong gusty winds existed, and the balloon bubble oscillated and rotated while it was restrained by the collar. Careful inspection of the material enclosed by the collar disclosed damage, which appeared to be abrasive in nature, to the polyethylene film positioned at the top edge of the collar. The balloon had been folded with the load tapes all at one side of the balloon, and the damage is ascribed to abrasion by these load tapes on the balloon barrier material where the load tapes separate out into the bottom cone angle of the bubble. Corrective action planned is to fold the balloon material so that the load tapes are evenly distributed around the periphery of the balloon stem. Therefore, if the bubble



Figure 24.10. Balloon Bubble with Restraint Collar Ready for Launch Procedure



Figure 24.11. Balloon System Partially Erected. Bubble release by opening restraint collar could be made here if desired



Figure 24.12. Balloon System Near Vertical and Ready for Bubble Release



Figure 24.13. Balloon System After Collar Opening and Ready for Payload Release

oscillates, the load-bearing tapes will not rub against the balloon barrier polyethylene. A further advantage of this load tape distribution is that it lends itself to load tape deployment without the necessity of the polyethylene film rearranging itself as the load tapes separate. It may be that this type of problem is not peculiar to our inflatable restraining collar. It also may occur in the conventional dynamic launch spools when the load tapes are all on one side of the balloon stem. We have encountered incidents during which balloon bubbles were buffeted by the wind while being held by the conventional launch arm, and the balloon subsequently failed at an altitude that would indicate holes in the vicinity of the launch arm retention. It may be that the even distribution of load tapes around the balloon stem would also be useful with a conventional dynamic launch arm. Repeated, violent, collar openings disclosed structural inadequacies which appear to be easily correctable. One interesting concept which will be tested is the use of deflation ports on the inner surfaces of the half cylinders. When the collar opens, inflation air will escape through these ports producing an immediate collar deflation. This should alleviate many post-opening stresses and, if successful, quite possibly could permit an even lighter collar construction.

For routine collar installation, one possibly irksome detail would be positioning the 50 cable ends in their notches on the collar opening device. This operation in routine use will require only 5 minutes, but extreme caution must be used to assure that all cable ends are in their notches. We are searching for a more convenient release scheme.

The inflatable restraint collar is well along in the development process, and results have been so encouraging to date that we felt it to be worthwhile to report on it at this time. It has been shown that the fragile material of a polyethylene balloon can be restrained and released under laboratory conditions without damage. It is expected that this capability can and will be extended in the near future to adverse field conditions. Prototype tests have been conducted with a 3,000-lb gross inflation system, and it appears that inflatable restraint collars can be designed for much greater gross weight systems.

References

- Angevine, J. M. and Fulker, H. L. (1970) Forces in a Cable-Restrained Balloon System, NCAR TN-47.
- National Center for Atmospheric Research (1969) Balloon Strain Relief System, NCAR TN-44.

Panel on Balloon Materials and Testing

Tuesday Panel

**Afternoon: Chairman, J.F. Dwyer
Air Force Cambridge Research Laboratories**

PRECEDING PAGE BLANK

Contents

25.1	Introduction	316
25.2	Recommended Tests	316
25.3	The Qualification Tests	317
25.4	The Acceptance Tests	322
25.5	Trial Period of Revised Specifications	322

25. Recommendations for a Revision of the Balloon Specifications MIL-P-4640A (USAF)

A.D. Kerr and H. Alexander

Abstract

A study of the deformation and strength properties of balloons and balloon materials was performed by the authors for Air Force Cambridge Research Laboratories over the past six years. Based on the findings of that study, as well as upon the findings of relevant studies conducted before by others, a revised test program to be used in the qualification and acceptance testing of balloon films is recommended and discussed. This new set of tests retains those tests of the old Specifications MIL-P-4640A (USAF) which are felt to be relevant to the determination of the suitability of films for balloon use. Tests that are not considered relevant to this determination have been discarded and new testing methods have been added.

These recommendations do not necessarily represent the opinion of the U. S. Air Force. Their main aim is to initiate a discussion among film producers, balloon manufacturers, balloon users, mechanics and materials scientists, and the AFCRL and, thus, create a rational basis for the planned revisions.

PRECEDING PAGE BLANK

25.1 INTRODUCTION

The present balloon specifications of the U. S. Air Force MIL - P - 4640A (USAF) are based on studies conducted by General Mills, Inc. for the U. S. Air Force during the early 1950's. These specifications were written essentially for a specific film, DFD 5500, which at that time was the predominant material used in the fabrication of balloons.

The recent development and use of new balloon films, the large number of balloon failures in the early 1960's (all of whose barrier materials has passed the prescribed tests), and the ever increasing demand for larger balloons, necessitate the complete revision of the part of the military balloon specifications which deals with the strength of the balloon films and seals. During the past six years, the authors studied the deformation and strength properties of balloons and balloon materials for the AFCRL. The results are summarized in Kerr (1969). Based on these findings, as well as upon the findings of relevant studies conducted before by others, a revised test program is recommended and discussed. It is expected that these recommendations will initiate a discussion among film producers, balloon manufacturers, balloon users, mechanics and materials scientists, and the AFCRL and, thus, create a rational basis for the planned revisions.

25.2 RECOMMENDED TESTS

It appears reasonable to prescribe two sets of tests, to be called the "qualification tests" and the "acceptance tests."

A new film submitted by a manufacturer to USAF for consideration as possible balloon material will have to first pass the "qualification tests." If the submitted film samples satisfy the prescribed requirements and the USAF places an order, then samples taken from the beginning and the end of the production run should be subjected to the "acceptance tests." For very large orders, film samples should also be tested at specified intervals to insure quality throughout the entire production run.

Because the seal is essential for the production of large balloons, and because the seal or its vicinity is usually weaker than the film, the tests proposed in the following are designed to test the strength of the seal as well as the proposed film. In this connection it should be noted that a strong film is useless as a balloon material until a seal is found whose strength matches the strength of the film.

In order to qualify as a balloon material, it is recommended that a submitted film and proposed seal be subjected, at least, to the following tests:

- (1) Uni-axial tensile tests at room temperature

- (2) Bi-axial tests {
 - at + 110F
 - at cold temperature
- (3) Mutilation and fatigue test at cold temperature
- (4) Molecular weight determination tests

The qualification tests are to be conducted by the AFCRL or an AFCRL approved Laboratory.

25.3 THE QUALIFICATION TESTS

25.3.1 Uniaxial Tests at Room Temperature

Various studies indicate that the response of a film to loads is strongly influenced by its orientation induced during extrusion. For example, films which are strongly oriented in the machine direction are usually weaker in the transverse direction. General Mills, Inc. conducted an extensive study during which they were able to obtain, from the extruder, detailed information regarding the manufacturing of their tested films. They found that "film extruded with nearly equal elongation in both machine and transverse directions showed that the strength of the film was 30 to 75 percent stronger and tougher than previous standard films" (Freeman, 1968).

The findings of General Mills, Inc., as well as results of more recent studies by the authors, seem to indicate that a nearly equal orientation in the machine and transverse direction is preferable for balloon films.

In general, extruder companies are unwilling to supply any details of the manufacturing process. To ensure that a balloon film responds similarly in both directions and possesses the required strength, the following uniaxial tensile test is recommended: Cut two film strips; one parallel to the machine direction, the other parallel to the transverse direction. The samples are then tested according to ASTM Test Method D882-67, Method A at room temperature. The speed of testing should be 10 in/min on a 3-inch by 1-inch sample. The test result should be presented in a graph as shown in Figure 25.1. For easy identification of the needed characteristics, it is suggested that the scale for ϵ (elongation) be such that the slopes of the obtained curves for small values of ϵ be about 45° , as indicated in Figure 25.1.

The slope of the obtained curves should be everywhere positive, (curve A). For the transverse direction, the obtained values should not deviate by more than 20 percent from the corresponding values in the machine direction.

The curves for both strips should be similar in character. If the σ - ϵ curve in the machine direction is of shape A and the one in the transverse direction is

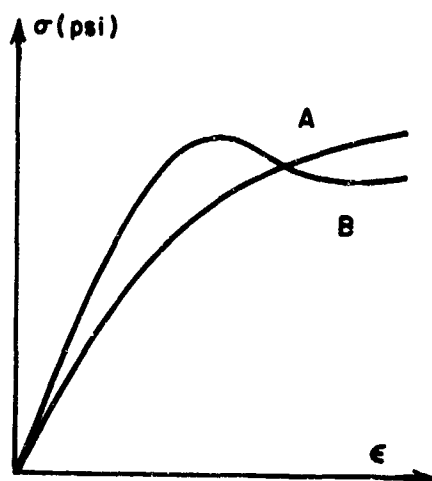


Figure 25.1. Method of Recording Uniaxial Tensile Test Results

of shape B, as shown in Figure 25.1, and if curve B deviates strongly from curve A, then this indicates strong orientation in the machine direction and the submitted film may not be suitable for balloon purposes. It should be noted that the labor and equipment involved in these proposed tests are essentially the same as in the uni-axial tensile test prescribed presently.

The above tests should be repeated after 24 hours at a different level of relative humidity in order to determine if the effect of humidity and aging is excessive.

25.3.2 Biaxial Tests

In these tests, the sample consists of a cylinder produced by placing two long film strips on top of each other and then sealing them along the edges, parallel to the machine direction. One of the strips should contain a crease. The method of sealing should be identical with the one to be used in the actual balloon. The sample is closed off at both ends by end fittings. The sample may be stressed by pressurizing it with a gas through the upper end fitting. This type of loading induces the fixed stress ratio

$$\frac{\text{circumferential stress}}{\text{axial stress}} = \frac{2}{1}$$

Different stress ratios may be obtained by additionally subjecting the lower end fitting to a load F , as shown in Figure 25.2.

In order to test the effect of creep upon the strength of the film and the seal at the high temperature encountered at launch and at very high altitudes, the following tests to be conducted at $+110^{\circ}\text{F}$ are recommended:

Three samples are to be tested. The first sample is subjected only to an

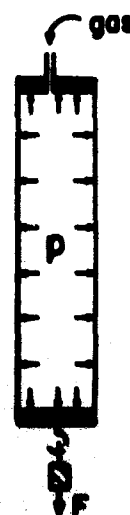


Figure 25.2. Method of Loading Test Sample

axial force F . At specified time intervals, the axial strain is measured and recorded as shown in Figure 25.3. The load F is determined as follows:

$$F = (A \sigma_{aa}) \text{ for tapeless balloons}$$

$$F = (0.8 A \sigma_{aa}) \text{ for taped balloons}$$

where A is the initial area of sample cross section (including seal material) and σ_{aa} is the anticipated axial stress in the actual balloon to be built from the tested material (presently about 800 psi). The second sample is subjected only to an internal pressure p . The corresponding axial and circumferential strains are measured at specific time

intervals and they are also plotted as shown in Figure 25.3. The pressure p is to be of such a magnitude that it creates the stress σ_{aa} in the circumferential direction of the sample. In the third test, the sample is subjected to F , and $p/2$ and the axial and circumferential strains are plotted in Figure 25.3.

When a film is tested for a balloon with unusual flight requirements such as a long stay at very high altitudes, that is long exposure to high temperatures, then the obtained graphs in Figure 25.3 should be checked for this additional requirement. Assuming that such a time period does not exceed, let us say, five hours, then if none of the plotted curves indicates failure within this time period (that is, if they behave as indicated by curves 1 and 2), then the film and seal have passed this test.

It should be noted that these experiments also test the effect of creases, die lines, pinholes, and other imperfections when the film is subjected to high temperatures and loads of long duration. For some additional background information on the above test, the reader is referred to Alexander and Murthy (1968).

In order to test the effect of creep during launch, upon the strength of the film and the seal (to be used) at the low temperature of the tropopause, the following tests are recommended: Several samples, as shown in Figure 25.2 are to be tested.

In the first test, the sample is brought into a cold chamber, cooled for 30 minutes, then pressurized until rupture. The burst pressure p is then recorded

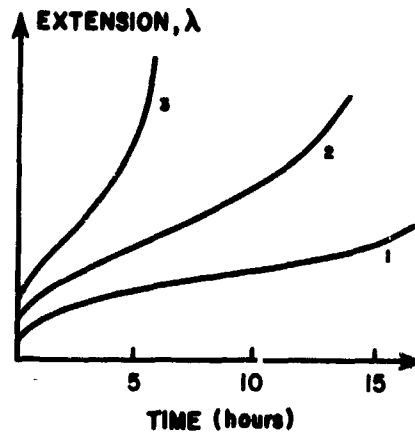


Figure 25.3. Method of Recording Creep Test Results for Samples 1, 2, and 3

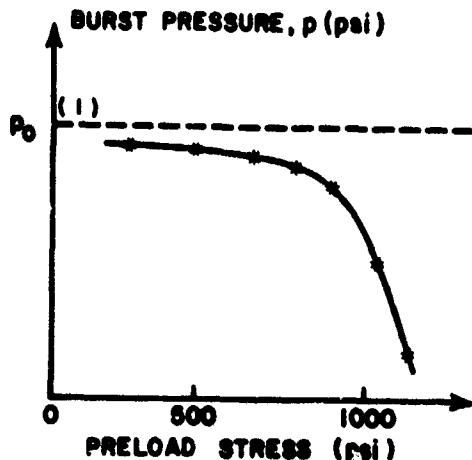


Figure 25.4. Method of Recording Burst Pressure

as the upper dashed line in Figure 25.4, and the failure pattern is noted.

In the next test, the sample is subjected to an axial force F for two hours at a temperature of 110°F . Then the loaded sample is placed in a cold chamber and cooled for half an hour. At the end of this cooling period, the sample is pressurized until rupture. The burst pressure is then recorded as shown in Figure 25.4 and the failure pattern is noted. For each consecutive test, F is increased until a sharp drop in the bursting pressure occurs, as indicated in Figure 25.4. The temperature of the cold chamber should be 10°F below the

lowest temperature anticipated during ascent.

For background information on this test, the reader is referred to Kerr and Alexander (1968).

The purpose of the above biaxial tests is to determine if the film can satisfy design requirements for a specific balloon under consideration. In cases where two films seem to have equally acceptable strength and creep properties from the point of view of design requirements, ultimate property testing may be used to determine which film would be operating with a greater factor of safety.

25.3.3 Matilation and Fatigue Test at Cold Temperature

The tests suggested so far are static in nature. Since the balloon is constantly deforming during launch and ascent, the following test, which simulates some of the situations during ascent, is recommended: The sample, shown in Figure 25.2, is subjected to the axial force F for two hours at a temperature of $+110^{\circ}\text{F}$. The loaded sample is then placed in a cold chamber. After being allowed to cool, it is subjected to oscillatory motions by rotating the lower end fitting with respect to the upper by 45° in each direction. After one hour the sample is pressurized until it bursts. The burst pressure should not be less than $4/5$ of the burst pressure (1) recorded in Figure 25.4. The testing temperature should be 10°F below the lowest temperature anticipated during ascent.

For additional background information in connection with the above test, the reader is referred to Kerr, 1966.

25.3.4 Molecular Weight Determination Tests

These tests check an important property of the basic resin (not of the extruded film). It appears that molecular weight is related to the cold brittleness properties of the film; high molecular weight being associated with good cold brittleness properties.

The present Specifications MIL-P-4640A prescribe a molecular weight measure in terms of a melt index, determined by measuring flow rates with an extrusion plastometer in accordance with ASTM test method D1238. According to the Final Report on Evaluation of Balloon Materials (p. 9) by General Mills, Inc. (Freeman, 1952), melt index is a measure of average molecular weight and is affected by chain branching.

In Freeman (1952), it is also pointed out that even when the average molecular weight is high, relatively small portions of low molecular weight polymer in a polyethylene resin will cause the resin or film to have a poor cold brittleness temperature. For this reason General Mills considered a chloroform extraction test, which was felt to be a better indicator of molecular weight distribution. This test was discontinued because at that time it was difficult to isolate the effect of all of the variables in the testing procedure.

Recently, new measuring instruments have been developed that can be used to determine molecular weights. In particular, the gel permeation chromatograph yields a complete molecular weight density distribution plot of number of molecules versus size.

25.3.5 A Note On Resin Characterization Tests

It has been the experience of the Air Force, and has been verified by the authors, that the basic resins are sometimes modified by the resin producer without the knowledge of either the balloon manufacturer or the Air Force. These modifications have contributed to at least one series of balloon failures and probably to others not yet investigated.

It therefore seems prudent to consider the inclusion of a number of resin characterization tests, in addition to the molecular weight determination test, within the qualification tests. The results of these tests would be later compared with the results obtained during acceptance testing. This comparison should indicate if any resin modification has taken place.

After a preliminary investigation of available testing procedures, it is recommended that it be considered that resin characterization be accomplished through the use of (1) gel permeation chromatography to establish molecular weight density distribution, (2) infra-red absorption testing to establish molecular composition, and (3) differential thermal analysis to obtain melting point information.

25.3.6 A Note on the Presently Used Cold Brittleness and Toughness Tests

The present cold brittleness tests essentially consist of a steel ball puncturing a film sample at cold temperature, and an examination of the failure pattern in order to determine if the failure is ductile or brittle. The inconclusiveness of this failure-pattern criterion is very aptly described in Hauser (1966). However, the inconclusiveness of the criterion was recognized long before by the investigators of General Mills, Aeronautical Research Laboratories (Freeman, 1952). They suggested that as a criterion for passing this test, a prescribed minimum amount of energy should be used up during rupture at cold temperatures. (This is essentially a combination of the cold brittleness and toughness tests.)

At a much later date, the testing apparatus to accomplish this was built and tested (Parsons, 1967). It was found that due to surface effects and other mechanical difficulties, this new criterion was no more accurate than the previous one. In fact, the authors of the present report have been informed (Dwyer, private communication) that many of these same operating difficulties appear in the room temperature falling-ball tests, making toughness criteria bases on these tests quite questionable.

It is therefore recommended, for the present time, to eliminate all falling-ball type tests from the revised specifications.

25.4 THE ACCEPTANCE TESTS

Only the tests in Sections 25.3.1, 25.3.2, and 25.3.4 are recommended.

25.5 TRIAL PERIOD OF REVISED SPECIFICATIONS

It is recommended that the trial period should be one year and that the revised specifications should not be binding during this time interval.

Acknowledgments

The authors wish to thank Mr. J. F. Dwyer AFCRL for a careful review of the manuscript and for his comments on various aspects of the proposed testing program.

References

- Alexander, H. and Murthy, G. K. N. (1968) A Failure Stress Criterion for a Polyethylene Balloon Film, N. Y. U. Report No. AA-68-18.
- Dwyer, J. F., Private Communication.
- Freeman, A. J. (1952) Final Report on Evaluation of Balloon Materials Project Gopher, Contract AF33 (600)-6298, General Mills, Inc., Aeronautical Research Laboratories.
- Freeman, A. J. (1968) Progress Report on Evaluation of Materials for Balloon Fabrication, General Mills, Inc., Report No. c/R 5159, p. 3.
- Hauser, R. L. (1966) Round-Robin Cold Brittleness Tests of Balloon Films, Proceedings 4th AFCRL Scientific Balloon Symposium, AFCRL-67-0075.
- Kerr, A. D. (1966) Experimental Study of Balloon Material Failures, Proceedings, 4th AFCRL Scientific Balloon Symposium, AFCRL-67-0075.
- Kerr, A. D. and Alexander, H. (1968) A Cause of Failure of High Altitude Plastic Balloons, N. Y. U. Report No. AA-68-28.
- Kerr, A. D. (1969) On the Strength of High Altitude Balloons, Journal of the Facilities for Atmospheric Research, National Center for Atmospheric Research, No. 9, pp. 8-11.
- Parsons, W. B. (1967) Relationship Between Toughness, Tensile, and Cold Brittleness for Unreinforced Balloon Film, Applied Science Division, Litton Systems, Inc., Report No. 3116.

Contents

26.1 Introduction	325
26.2 Test Procedure	325
26.3 Test Results	326
26.4 Conclusions	327
26.5 Recommendations	328

26. Observations on a Test Procedure for Polyethylene Balloon Films

J.A. Winker
Raven Industries, Inc.
Sioux Falls, South Dakota

26.1 INTRODUCTION

This paper is the result of an invitation to present recommendations regarding balloon film specifications at a Panel Meeting during the Sixth AFCRL Balloon Symposium. Rather than make an across-the-board critique of existing tests, or a comprehensive listing of new tests, I have elected to look at one specific test procedure in some detail. The subject is the cold brittleness test, which "determines" the brittleness characteristic of a balloon film from the appearance of the rupture when a heavy ball penetrates a membrane of the film. The analysis which follows concerns the inclined plane version of the cold brittleness test, though it is largely applicable to the vertically falling balloon technique as well.

From the outset it was assumed that this analysis was not likely to be controversial; the test method was already somewhat in disrepute and the study was expected to add validity to the criticisms already expressed regarding it.

26.2 TEST PROCEDURE

The study of cold brittleness testing was based on data derived from high speed photography. A standard, inclined-plane cold brittleness apparatus was

PRECEDING PAGE BLANK

installed in a cold box which was outfitted with special viewing and lighting windows. Five samples were photographed; one at room temperature to verify the setup, and four at various cold temperatures. The test conditions were as follows:

Test Number	Film Type	Thickness (Mils)	Temperature ($^{\circ}\text{C}$)
1	X-124	.75	Room Temp.
2	X-124	.75	-85
3	DFD 5500	1	-85
4	DFD 5500	1	-50
5	DFD 5500	1	-35

A high speed camera was run at approximately 3,000 pps, with the exact rate being determinable after processing by observing the position of light pulses on the film edge. These pulses were generated at precisely 1 millisecond intervals. Thus, the interval between successive frames is approximately 333 microseconds.

26.3 TEST RESULTS

By direct analysis from the film, it was possible to determine that the steel ball comes off the end of the inclined plane with a rotation rate of about 25 rps and a velocity of 9.8 ft/sec (.118 inch per msec). Observations and calculations from each of the five tests are as follows:

(1) Because this test was run at room temperature, elasticity of the material was very great and the center section of the film was displaced approximately 2 1/2 inches before rupture occurred. Time between initial contact and rupture was 22 msec, and during this time the ball rotated approximately 200 degrees. Rupture actually occurred above the ball because of the extra stretching induced by ball rotation. It is obvious that friction between the ball and the film caused some "rolling" of the center section of the film downward. It is probable that there was some skidding between the ball and the film, but this was not observable.

A direct measurement of film displacement with time was not possible because of the direction of observation, so displacement was based on the assumption that ball speed remained constant through rupture. This would not be strictly true, but the evidence indicates that it is a good approximation.

(2) This test of X-124 film at -85°C resulted in a ductile rupture. Time from ball contact to initial rupture was 7 msec, with the complete rupture actually occurring over several frames. Film displacement was .83 inches and ball rotation during contact was 65° . The ball obviously skidded on the film in this test, as well as in the subsequent tests.

(3, 4) In these two tests of DFD 5500, complete rupture occurs between frames, placing the phenomenon in the microsecond range. These were brittle failures. Time from contact to rupture was 3.5 to 5 msec and displacement approximately .4 inches.

(5) This test was similar to tests 3 and 4 in timing and film displacement; however the complete rupture occurred over several frames placing it in the milliseconds range. The failure was ductile.

It has been established by previous testing that the apparent cold brittleness point of a film is affected by the rate of onset of loading into the film (strain rate), with the brittle point occurring at warmer temperatures with higher strain rates. A simplified analysis was made to determine relative strain rates for the various tests. The simplification was in the assumption of a 2-dimensional rather than a 3-dimensional situation. Figure 26.1 shows how strain rate increases as the ball deflects the film sample.

Using the assumptions previously listed, the calculated strain rates were:

Test

- | | |
|---------|-------------------------|
| 1 | 39.5 inches/inch/second |
| 2 | 19.0 inches/inch/second |
| 3, 4, 5 | 9.5 inches/inch/second |

26.4 CONCLUSIONS

It was interesting, but perhaps not surprising, that the speed of rupture is distinctly different between the ductile and brittle cases. Brittle failures occur well within the minimum observable interval of 300 microseconds. The ductile failures occurred over approximately 1 msec, and showed definite evidence of tearing as the ball pushed its way through the opening in the film.

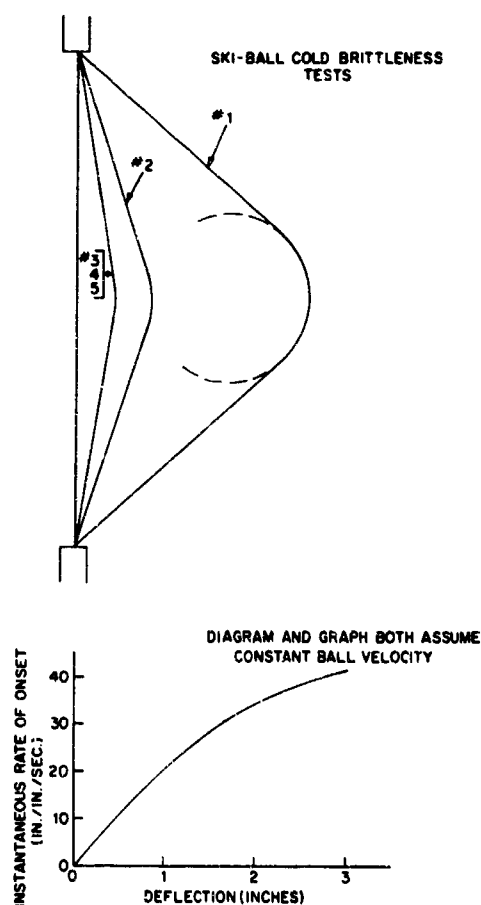


Figure 26.1

The observation on strain rate in a cold brittleness test is important in that this factor confuses the comparison between different films. It is generally accepted that a film exhibiting high cold elongation is preferable to one with a low cold elongation (all else being equal). However, as the elongation characteristics improve, strain rate in this type of test automatically tends to go higher (see Figure 26.1). But, as noted earlier, apparent cold brittleness point gets warmer with increased strain rate. Thus, the test method imposes a penalty on cold brittleness measurement, and a substantially superior film may show up to be only marginally better.

The real conclusion from the test is that there are far too many variables involved, and it is not possible to sort them out satisfactorily to determine meaningful film characteristics.

26.5 RECOMMENDATIONS

(1) The inclined-plane cold brittleness test has been exposed subjectively, and now objectively, as sorely deficient in defining useful film properties. It should be discontinued as a test requirement.

(2) The vertically falling ball test is substantially the same as the inclined plane test with the exception that the ball is not rotating. Most of the shortcomings still apply. This test should be discontinued.

(3) Some measurement of cold elongation properties should be included in any new test specification which is written. This could be as simple as a set of stress-strain curves (MD and TD), or more elaborate tests might be devised.

27. Balloon Film Specifications

J.R. Nelson
Winzen Research Inc.
Minneapolis, Minnesota

Most people knowledgeable in the field of stratospheric balloon production realize, I believe, that the MIL-P-4640A "Specification for Plastic Film, Polyethylene, for Balloon Use" was obsolete in approximately 1963. At this time balloon film which conformed to this specification was used in all manufacturers' processing, and balloons were failing with alarming regularity. Films used prior to this period of high failure rate exceed the specification values by considerable amounts, such as (approximately):

	Specification Value		Actual Value
	MD	TD	
Tensile Strength	2,000	1600	2600 psi
Elongation	250%	400%	500%
Cold Temperature Ductility	68°C		72°C

This experience indicated that the MIL-P-4640A specification is too lenient, particularly in the tensile, elongation and cold ductility requirements. The preparation of a specification should start with an examination of the duty cycle of the material, followed by a determination of acceptable test procedures and tolerances

that will assure adequate performance during the duty cycle. Also of importance is establishing evaluation test procedures without excessive economic burden on the production process in meeting the quality requirements.

Looking at the duty cycle of the film, it is subjected to degrees of handling abrasion, tension and flagging (fluttering) over a temperature range from as much as $+50^{\circ}\text{C}$ to -85°C . Film damage from these traumas can be negated in the manufacturing stage, or even up through portions of the field operations, by acceptable repairs or by deleting the damaged material. When the finished balloon is released, however, it must withstand the duty cycle environment or fail in its mission.

This environment at launch can be severe in areas of tensile stress, flagging and high or low temperature, depending on launch location. If an inflated balloon is held in the hot sun for a period, tensile creep can contribute to damage. If a low temperature exists, such as in an Alaska launch, the balloon is subjected to unusual tensile and flagging stresses combined with cold temperature.

During ascent, the balloon — particularly a large, thin-film balloon — is subjected to wind shears which can cause combinations of flagging and tensile stresses. These conditions usually occur in the coldest environment of the flight, and have many times been below -80°C .

As the balloon enters float, it is subjected to biaxial stress during the free-lift valving sequence.

Examination of the film requirements, therefore, seem to center around its tensile strength, elongation, and flexure or flagging resistance over a range of temperature from 50° to -85°C . Looking first at tensile strength and elongation it has been our experience that balloon-quality film can be generated if the tensile strength is held to a minimum of 3000 psi in both transverse and machine direction, and elongation at a minimum of 400 percent in both directions measured at a temperature of 24°C (see Figure 27.1).

Packaging and handling requirements always generate two folds in the rolled material which, if improperly accomplished, can result in a lowered tensile strength across the fold. It is therefore recommended that the transverse tensile strength across the fold be no less than 90 percent of the transverse strength of the same sample not in the fold.

As indicated, the film is subjected to biaxial stresses as the balloon enters float phase. A considerable amount of work has been accomplished on a research and development program to evaluate performance under biaxial loads. First efforts were with cylinders pressurized to obtain stress, and it was found that it was difficult to obtain repeatability even though statistical results were of value.



Figure 27.1

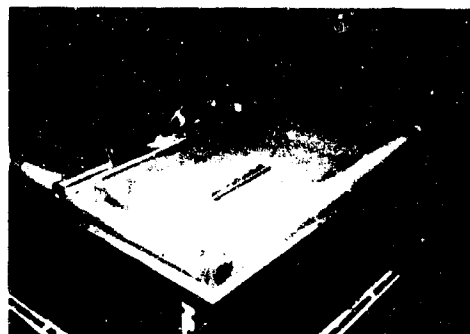


Figure 27.2

Another method of biaxially stressing a sample of film was devised as shown in Figure 27.2. The sample was cut in a cruciform shape and stretched over four teflon-coated rubber rollers mounted on ball bearings. The film contained hems into which foam-rubber coated tubes were inserted. Weights were then suspended from these tubes for loading. Both step-loading and creep data were determined from time-load sequenced measurement of the dimensions of predrawn squares to determine strain magnitude and location. Repeatability of data on many film samples tested was excellent. It is felt that biaxial stress is directly related to uniaxial stress in machine and transverse direction, so if proper selection of stress and elongation tolerances is made, it is not necessary to complicate the production picture by providing the sophisticated, slow, biaxial test procedures as a production specification requirement.

As part of WRI research and development effort in 1967-68, a development program was conducted on a means of determining cold brittleness characteristics by imposing flagging stresses on small pennants of material at -90°C , similar to conditions that might be experienced in an ascent through the tropopause. Results were reported by Mr. Leo Mielke of WRI at the Fifth AFCRL Scientific Balloon Symposium in June, 1968. This method of testing yielded quantitative data on the free stream energy required to cause brittleness failure, or, more attractively stated, the amount of free stream energy the material can stand at cold temperature and remain ductile. At the same time it was found that there was excellent correlation between brittleness temperatures established by these data and the conventional falling-ball test for ductility at cold temperatures on several different materials such as polyethylenes, nylons, and polyurethane.

We concur with Mr. Ray Hauser's comment (in his paper at the 1965 AFCRL Scientific Balloon Workshop) that the "ski slide" ball drop offers no advantages over the straight-line ball drop, and has several disadvantages.

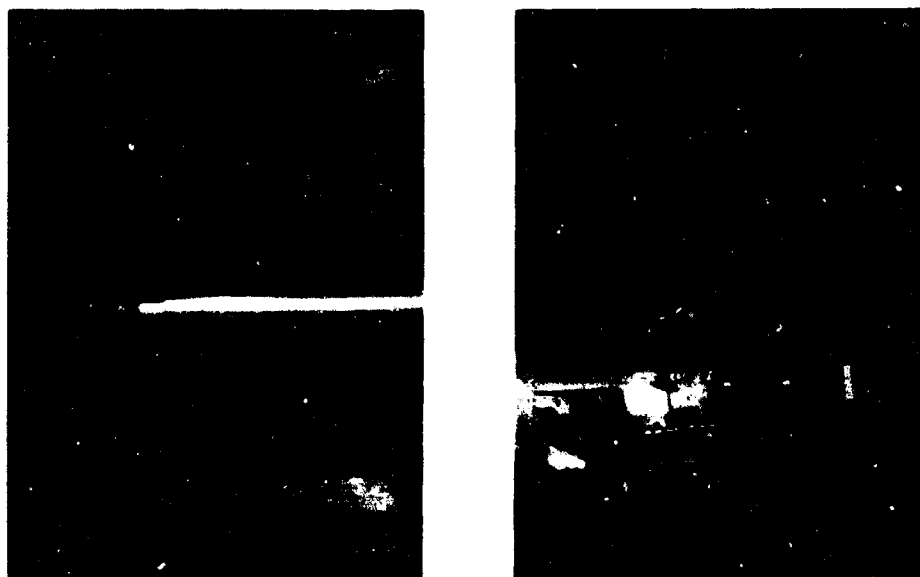


Figure 27.3

The straight drop test lends itself to production test methods, as is shown by the test equipment used by our production facility at Sulphur Springs, Texas (Figure 27.3). The cold cabinet has provision for simultaneous ball-drop test of eight samples. To minimize the turn-around time, or temperature pull down-time of the equipment, the balls are caught and returned to the front of the box for easy access, magnetic holding devices are used, and a pre-cooling rack holding up to 20 additional prepared samples is provided.

It is recommended that this method of testing at a temperature of -87°C be used for determining cold brittleness acceptability for film used in stratospheric balloons. This temperature is recommended since equatorial flights often reach temperatures this cold, and southern United States temperatures often approach -80°C , which leaves a small factor of safety at -87°C .

For balloon manufacturing requirements, there must be tolerances required on film length, width and thickness. These dimensions are primarily specified by the balloon manufacturer with appropriate tolerance of dimensions on length and width. Since performance and weight are closely associated with thickness, it is considered necessary to specify limits on thickness. The nominal gauge or mil thickness should be specified on the basis of a weight per area measurement divided by the yield of the film material, since this is by far the most accurate method of determining the nominal gauge. The minimum thickness, which obviously is an important dimension, cannot be measured adequately with a

micrometer or beta type gauge, since the first gives just spot checks and the second, too large a sample of area where thickness is averaged. It is our recommendation that a profilometer measurement of the entire layflat tube be made at each end of a roll, and a minimum acceptable thickness tolerance be established and specified for each gauge film. To obtain an adequate check on the thickness, it is recommended that the Winzen Research Inc. capacitance-type electronic thickness gauge or equal be used (Figure 27.4). This gauge permits measurement of variations in thickness as small as 5 millionths of an inch. Accuracy, repeatability, linear calibration, and strip chart readout are outstanding features which permit rapid, trouble-free production gauging and in-process control.

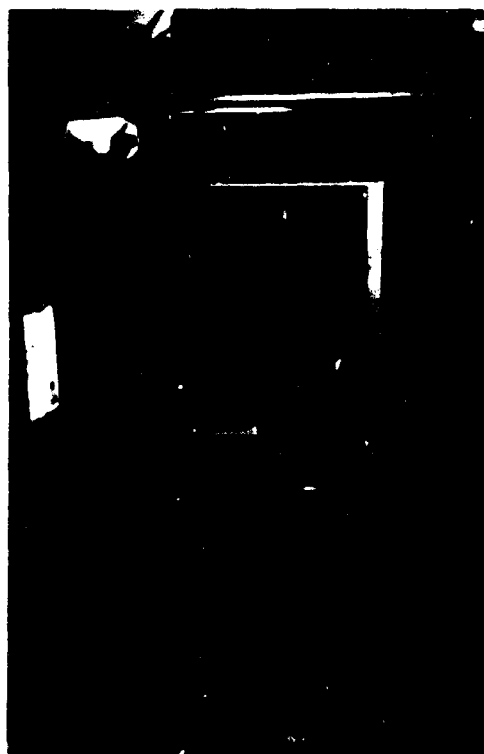


Figure 27.4

28. Test Specification for Unsupported Balloon Films

R. Hauser
Hauser Research and Engineering Company
Boulder, Colorado

K. Stefan
National Center of Atmospheric Research
Boulder, Colorado

The skin of a balloon, like the components of any other structure, is subject to unique stresses of its own environment. Fortified with several years of experience, balloon engineers have a better understanding of balloon skin requirements and of the properties of polymeric materials and test methods which are pertinent to ballooning. Therefore it seems appropriate to reconsider what the specifications for testing should be that we can have greater assurance of reliable balloon material during operations.

In its lifetime, balloon film must withstand a variety of possibly adverse conditions. First, the film must survive the handling, folding, transportation, and storage processes before its arrival at the launch pad as a sound balloon. During inflation procedures, the material is further handled and is sometimes buffeted by the wind, and it is directly stressed by the lift forces. At this point, the film will normally be at the warmest temperature it will experience during flight, and hence it is weakest in tensile and creep properties. Retention of the launch bubble by the launch arm produces a weird set of stress and abrasive conditions, and the dynamic release of the bubble causes further complicated stress conditions.

PRECEDING PAGE BLANK

During ascent, the balloon film cools, generally following the atmospheric temperature profile until high altitude is reached where radiation effects and balloon orientation are important, and skin temperature may fluctuate as much as 10-15°C within a few minutes (Stefan, 1968). During ascent, balloon shape assumes various degrees of asymmetry in which tensile stresses vary widely from ideal stresses of a symmetrical, natural shape. The time history of transitions from uniaxial meridional load to a uniaxial circumferential load or a biaxially loaded condition, may all affect the ultimate properties of the film. There is also ample photographic evidence of high-rate loading of the film. One ill-defined condition is the fluttering of the loose material in the uninflated portions of the balloon caused by vertical wind flowing past the balloon due to its ascent velocity. Occasionally, a balloon may encounter a horizontal shear wind, which billows out the loose material; fluctuating back and forth, the billows appear to produce impact loadings. Another observed phenomenon is a sudden shifting of the vertical folds of excess material from one position to another around the gas bubble, causing a horizontal movement of a considerable mass of balloon material which appears to start and stop quite suddenly.

When the balloon reaches float, there is a certain amount of overpressure generated until sufficient gas has vented to give an equilibrium float condition. Once this equilibrium is reached, the balloon material has met its test. If the balloon is still there, we don't need specifications any more.

The balloon film must withstand, then, a set of conditions, some of which can be identified precisely, many more that can be loosely quantified on the basis of statistical experience, and a few that still require intuitive and subjective judgments. The case is strong for continued effort toward identification and measurement of balloon skin stresses; meanwhile, we must do the best we can with specifications.

We think that formal balloon-materials specifications should be limited to well established materials such as polyethylene and mylar. As new materials are developed they should be judged in context with their performance capabilities, and separate specifications should be prepared for them. Specifications should define the best-functioning materials and should effectively discriminate between superior and inferior balloon film. They should be clear to understand, practical in application, and strict enough to effect controls.

Since research and testing of balloon materials has progressed to the point where specifications improvements are appropriate, we can suggest a number of specific changes to MIL-P-4640. These changes are intended to be consistent with the philosophy of quality assurance — maximum reliability with a minimum of testing and a minimum of confusion.

(1) Conditions of test $23 \pm 1^{\circ}\text{C}$ and $-79 \pm 2^{\circ}\text{C}$; present temperature tolerances ($25 \pm 5^{\circ}\text{C}$) are too lenient (ASTM D882).

(2) Thickness. The film thickness should be monitored in a detailed, continuous manner across the total width, using Beta gauge, capacitive or other techniques, for the purpose of learning thickness variations. Average thickness should be measured by weight/area for the four or more grades of balloon film (Anderson et al, 1956).

(3) Strength. Breaking factor, strength per unit width, should be measured at $+23^{\circ}\text{C}$ and at -79°C by ASTM D882-67 Method A. Strength criteria should be in units of pounds per inch width for each weight grade of balloon film. The present tolerances on both thickness (and hence strength) are too lax. The test specimen should be 1" wide with 4" gage pulled at 10 or 20 inches/minute ($+23^{\circ}\text{C}$) or at 0.5 inch/minute (-79°C).

(4) Elongation. The film elongation is normally measured along with strength, and tests have shown that elongation at -79°C is a significant discriminator for quality polyethylene balloon film. Elongation in uniaxial M and T directions must be at least 150% at $+23^{\circ}\text{C}$ and 30% at -79°C (Hauser, 1967).

(5) Cold brittleness. This test can probably be dropped as an acceptance requirement since cold elongation is a better discriminator (Hauser, 1967). If continued as a qualification test, the vertical drop should be included as an alternative to the inclined plane test. A tear length of 36 inches is appropriate to discriminate between ductile and brittle film in the vertical drop; ten inches is appropriate on the inclined plane.

(6) Toughness. This test may possibly be eliminated as an acceptance and qualification requirement.

(7) Other tests. A yield strength (breaking factor at 8 percent elongation) or creep instability requirement is probably appropriate to include. The former can be considered with breaking factor, thus avoiding additional tests. Flex endurance tests at low temperature might be of some value if followed by strength/elongation tests. Biaxial tests of these films are interesting, but most are too expensive for quality control. Pressurized cylinders may be appropriate for creep instability tests. Heat-seal tests for gore assembly might be included, with requirements for strength and shrinkage.

(8) Sampling. The present sampling plan provides little assurance of quality (Hauser, 1965 and 1966). Can the industry/government afford statistical sampling or would this additional cost exceed that of the few flight failures that might be avoided by closer inspection?

References

- Anderson, Gear and Morfitt (1956) Balloon Barrier Materials, AF-CRC-TR-56-262, General Mills, Inc.
- Hauser, R. L. (1965) Statistical Implications of Balloon Materials, Proceedings 1964 AFCRL-65-486.
- Hauser, R. L. (1966) Quality Analysis of Visqueen Balloon Film, NCAR Technical Note 12.
- Hauser, R. L. (1967) Round-Robin Cold Brittleness Tests of Balloon Films, NCAR Technical Note 27.
- Stefan, Karl (1968) Structural Measurements on Balloons in Flight, Proceedings Fifth AFCRL Scientific Balloon Symposium, AFCRL-68-0661, p. 253.

Tethered and Powered Balloons

Wednesday

**Morning: Chairman, Commander W.R. Wilson
Office of Naval Research**

Contents

29.1	Introduction	342
29.2	Symbols	342
29.3	Description of Technique	345
29.4	Description of Balloon and Tow Tests	346
29.5	Results and Discussion	348
29.6	Concluding Remarks	351

29. A Towing Technique for Determining the Aerodynamic Forces on Tethered Balloons

L.T. Redd
NASA Langley Research Center
Hampton, Virginia

Abstract

A simple tow-testing technique has been developed at Langley Research Center to obtain aerodynamic derivatives for large balloons. The technique consists of towing a balloon with an instrumented panel truck at various combinations of angles of attack and towing speeds. The balloon itself is suspended from the truck by two parallel lines arranged in such a manner as to keep the balloon's angle of attack constant regardless of the truck velocity. This arrangement also makes it possible to measure pitching moments along with other stability data.

The testing technique has been applied utilizing a 25-foot modified "class C" shape balloon which was towed at angles of attack ranging from 0° to 24° and velocities from 3 to 15 m/sec. The balloon was towed with and without the tail fins attached, in order to obtain information needed to calculate certain aerodynamic force coefficients. The data obtained from this towing technique compared favorably with existing wind-tunnel data on a small rigid model.

PRECEDING PAGE BLANK

29.1 INTRODUCTION

A tethered balloon may be useful for a number of purposes, such as supporting antennas or providing an aerial platform for various measuring instruments. Such operations are often impaired, however, by the occurrence of dynamic instabilities of the tethered balloon system, especially during strong wind conditions. Although some information relating to the stability of tethered balloons has been published (see, for example, Bairstow and Jones, 1915; and Newmark, 1961), systematic procedures for the analysis of balloon stability are apparently lacking. In an attempt to fill this need, the Langley Research Center has initiated a generalized research study aimed at the development of improved techniques for predicting the dynamic characteristics of tethered balloons.

One of the objectives of this study is the determination of aerodynamic forces on inflated balloons. In the past, these forces have been obtained from wind-tunnel studies on rigid balloon models (Stein and Shindo, 1968; and Farmer, 1969). Such measurements do not, however, account for deformation of the flexible balloon structure which may be significant for certain load conditions.

The purpose of this present paper is to describe a tow-test technique which has been developed in order to measure aerodynamic forces on full-size inflated balloons. Some typical results obtained by towing a 25-foot-long inflated balloon are presented, and comparisons are shown between these data and existing wind-tunnel data obtained on a rigid wind-tunnel model.

29.2 SYMBOLS

a distance from the balloon nose to structural center of gravity (see Figure 29.2)

B bouyancy force

b distance from the balloon nose to center of bouyancy

C_D coefficient of drag, $\frac{D}{\frac{\rho}{2} U_o^2 S}$

C_L coefficient of lift, $\frac{L}{\frac{\rho}{2} U_o^2 S}$

C_{L_t} coefficient of lift of a single tail fin, $\frac{L_t}{\frac{\rho}{2} U_o^2 S}$

C_M	pitching-moment coefficient, $\frac{M}{\frac{\rho}{2} U_o^2 S \bar{c}}$
\bar{c}	length of the balloon
D	drag force
d	balloon maximum diameter
h	perpendicular distance from longitudinal center of the balloon to the load band (see Figures 29.1 and 29.2)
L	lift force
L_t	lift force of one tail fin
M	pitching moment about an axis perpendicular to the x-z plane (see Figure 29.2)
P	absolute pressure
R	gas constant
R_N	Reynolds number, $\rho \frac{U_o \bar{c}}{\mu}$
S	characteristic balloon area (balloon volume) ^{2/3}
S_t	surface area of tail fin (one surface only)
T	tow line tension
T^o	absolute temperature
U_o	relative free-stream velocity
W_s	structural weight of the balloon
x, z	body-fixed coordinates with origin at the balloon structural center of gravity (see Figure 29.2)
$x_{c.p.}$	distance from the balloon nose to the center of pressure (see Figure 29.10)
α	angle of attack (see Figure 29.2)
γ	specific weight of gas
ρ	mass density of the atmosphere
ϕ	angular displacement of the balloon tow line in the x-z plane (see Figure 29.2)
μ	absolute viscosity of atmosphere
Subscripts	
1, 2	refers to front and rear tow cables, respectively (see Figures 29.1 and 29.2)
i	refers to conditions inside the balloon gas bag
e	refers to conditions outside the balloon gas bag



Figure 29.1. Test Balloon and Tow Truck

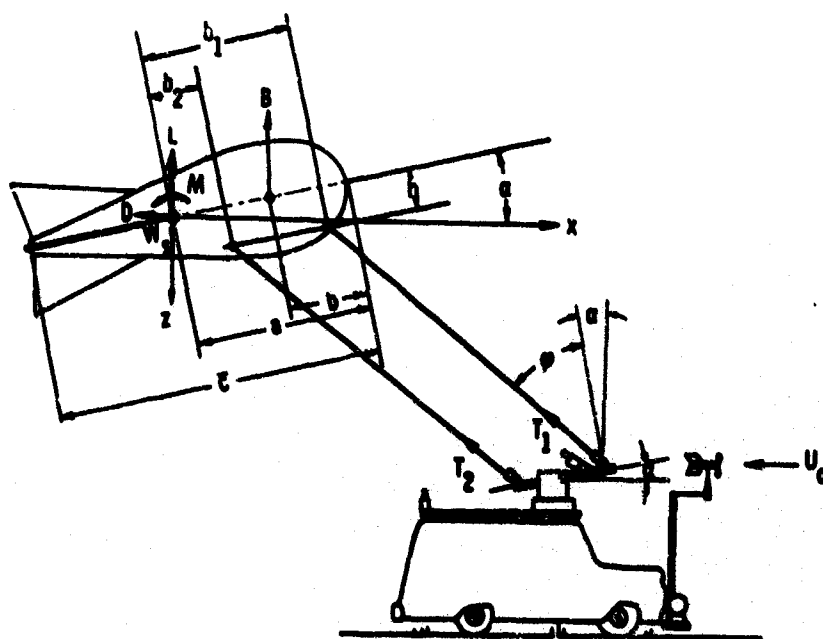


Figure 29.2. Schematic Diagram of Tow-truck Test Apparatus

29.3 DESCRIPTION OF TECHNIQUE

29.3.1 Tow Apparatus

The purpose of the tow-test technique described herein is to measure the steady aerodynamic forces and moments (L , D , and M) acting on the balloon at various angles of attack and relative wind velocities. As shown in Figures 29.1 and 29.2, the balloon is attached to the truck by two towing cables and a load bar. The cables, balloon, and load bar form a parallelogram so that in the absence of side forces the center line of the balloon remains parallel with the load bar regardless of the angle of the cables in the vertical plane. The load bar is attached to the truck through a pivot and can be adjusted to a desired angle of attack α . In still air, constant speed operation of the truck along a straight path produces the relative wind U_0 .

The panel truck provides space for instrumentation as well as acting as a towing vehicle. The load bar is equipped with load cells to measure cable tensions, and potentiometers to measure the angles of the cables with respect to the load bar. The speed of the vehicle relative to the air and the sideslip angle are measured by an anemometer mounted at the forward end of the truck. Outputs from these instruments are recorded on strip charts during the tests. Motions of the balloon are also recorded by two cameras mounted on the truck.

29.3.2 Aerodynamic Coefficients

Forces on the balloon are resisted by tension forces T_1 and T_2 in the towing cables acting through angle ϕ with respect to the load bar. The aerodynamic forces are expressed as follows:

Lift force:

$$L = (T_1 + T_2) \cos (\phi + \alpha) - (B - W_B) + 2\Delta w \quad (29.1)$$

where Δw is the cable weight.

Drag force:

$$D = (T_1 + T_2) \sin (\phi + \alpha) \quad (29.2)$$

Pitching moment about the center of gravity of the structure:

$$\begin{aligned} M = & [T_1 + \Delta w \cos (\alpha + \phi)] (b_1 \cos \phi - h \sin \phi) \\ & + [T_2 + \Delta w \cos (\alpha + \phi)] (b_2 \cos \phi - h \sin \phi) \\ & - B(a - b) \cos \alpha \end{aligned} \quad (29.3)$$

The tension in each of the tow cables, at the upper attachment point, can be approximated in general terms as follows:

$$T + \Delta w \cos(\alpha + \phi). \quad (29.4)$$

In Eqs. (29.1), (29.2) and (29.3), the quantities ϕ , U_o , T_1 , and T_2 (see Figure 29.2) are measured during the tow tests. The remaining quantities which appear in the equations are determined either from direct measurements or from supplementary tests as described in the Appendix. The quantities determined from the supplementary tests are the locations of the structural center of gravity, a , center of buoyancy, b , and the buoyancy force, B .

The aerodynamic lift, drag, and pitching moment deduced from the above equations are expressed in the following conventional nondimensional coefficient form:

$$C_L = \frac{L}{\frac{\rho}{2} U_o^2 S}, \quad C_D = \frac{D}{\frac{\rho}{2} U_o^2 S}, \quad C_M = \frac{M}{\frac{\rho}{2} U_o S \bar{c}}$$

where S is a reference area; in this case $S = (\text{volume})^{2/3}$.

29.4 DESCRIPTION OF BALLOON AND TOW TESTS

29.4.1 Balloon

To evaluate the tow-test technique, an inflatable balloon, 7.62 meters (25 ft) in length, was constructed at Langley Research Center. The particular balloon configuration chosen had been used in previous wind sensor studies conducted at LRC (Henry and Eckstrom, 1970); hence, there was additional interest in obtaining aerodynamic data on this configuration.

The balloon is shown attached to the tow truck in Figure 29.1, and its construction features and geometric properties are presented in Figures 29.3 and 29.4. The basic shape is similar to the so-called class "C" balloon configuration. However, unlike the class "C" shape, the aft portion is nearly conical and the nose is spherical. The essential components consist of the gas bag constructed of Nylon and Saran, and the tail fin assembly. A relief valve is provided to avoid over-inflation, and a load band is attached to the power portion of the bag which permits variations in tether-line attachment points. The tail assembly consists of four fins having a balsa spar framework covered with aluminized Mylar sheeting. The four fins are connected together by rings at the front and rear of the fins, and by a

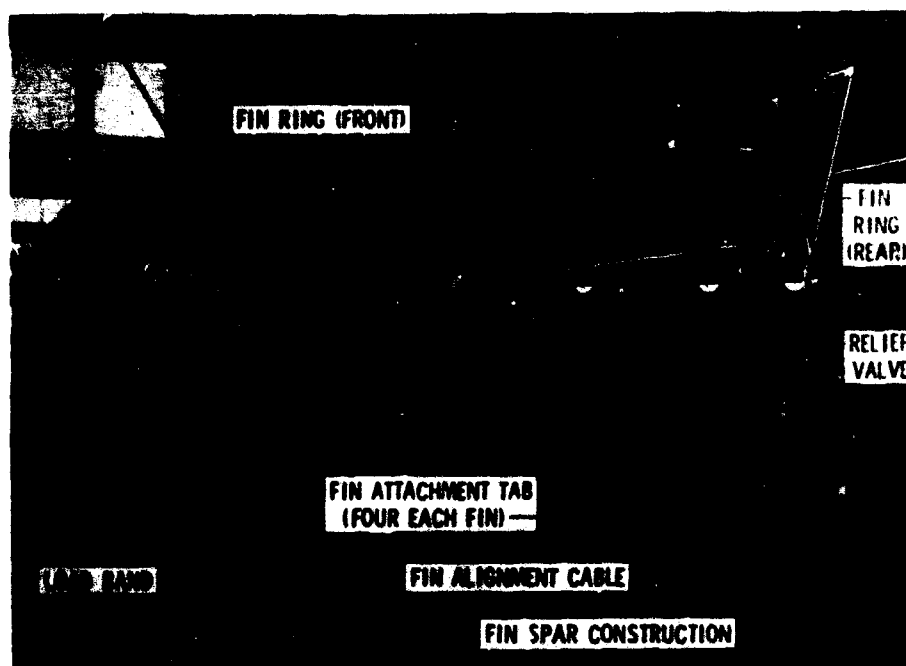


Figure 29.3. Details of the Test Balloon

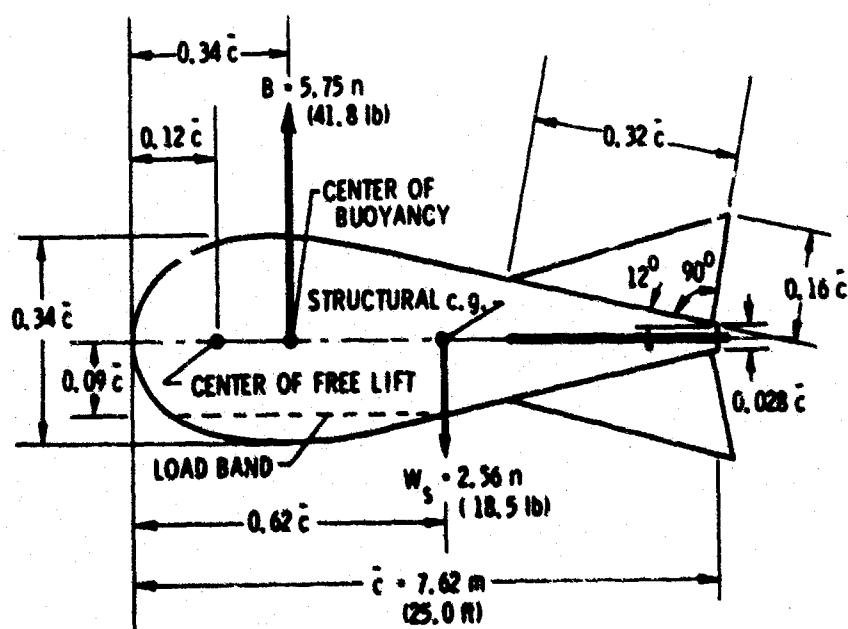


Figure 29.4. A Sketch Illustrating the Basic Physical Properties of the Balloon

number of small cables that can be adjusted to permit the fins to be aligned with the balloon center line. The tail assembly is connected to attachment patches on the gas bag at four points for each fin.

29.4.2 Tests

Tow tests were made during periods of calm air at constant speeds over a range from 3 to 15 meters per second (corresponding to Reynolds numbers of from about 1.5×10^6 to 7.5×10^6) in the range from 0° to $+24^\circ$ angle of attack. Some tests were made with the tail assembly removed from the balloon in order to obtain information concerning the tail forces needed in the determination of certain aerodynamic stability derivatives.

29.5 RESULTS AND DISCUSSION

A typical strip chart record of tow-test measurements is shown in Figure 29.5. In this example, the angle of attack is 10.3° and the speed is about 10 m/sec (30 ft/sec). Timing marks at 1-second intervals are located at the bottom of the chart. As indicated in Figure 29.5, the rear line tension, T_2 , oscillated appreciably. The mean value of T_2 was obtained by fairing through the oscillations.

Some of the reduced data in the form of lift, drag, and pitching-moment coefficient variations with respect to angles of attack are shown in Figures 29.6, 29.7 and 29.8, respectively. The solid curves in the figures are the averages of the measured data points shown. The scatter is attributed to such factors as small variations of ambient wind, limited length of the test runway, and oscillations in the strip chart records. The standard deviations of the data from the average curves shown in Figures 29.6, 29.7, and 29.8 are 0.0652, 0.0316, and 0.0082, respectively, which are typical of most of the data obtained. Despite this scatter, these aerodynamic coefficients are felt to be of satisfactory accuracy for use in a stability analysis.

The variation of the lift coefficient of the tail with angle of attack is shown in Figure 29.9. This was obtained from the difference in variation of lift with angle of attack from tests with the tail on, and from tests with the tail removed. The essentially linear characteristic may indicate good flow conditions over the aft portion of the balloon.

The nondimensional center of pressure of the aerodynamic force, as determined from the tow tests, is shown in Figure 29.10 as a function of angle of attack, α . It is nearly independent of α for values of $\alpha > 5^\circ$.

In Figure 29.11, for purposes of comparison, data from the tow tests of the inflated LRC balloon are presented together with wind-tunnel data from a small-

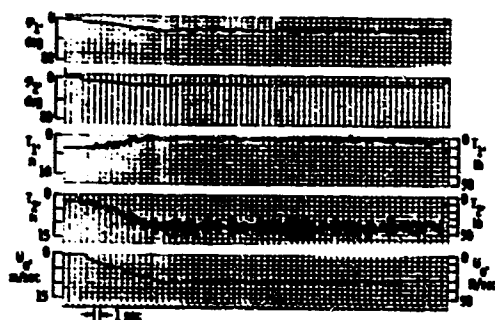


Figure 29.5. Strip Chart Recording of Tow-test Data ($\alpha = 10.3^\circ$)

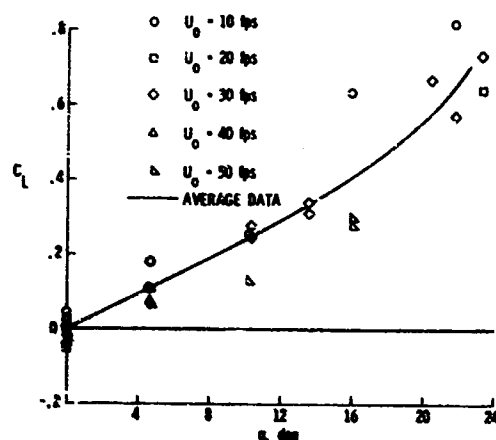


Figure 29.6. Aerodynamic Lift Coefficient (C_L) versus Angle of Attack (α)

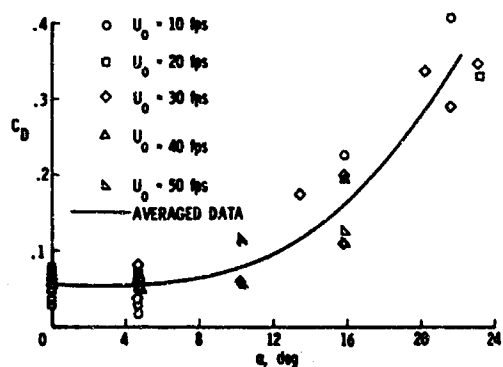


Figure 29.7. Aerodynamic Drag Coefficient (C_D) versus Angle of Attack (α)

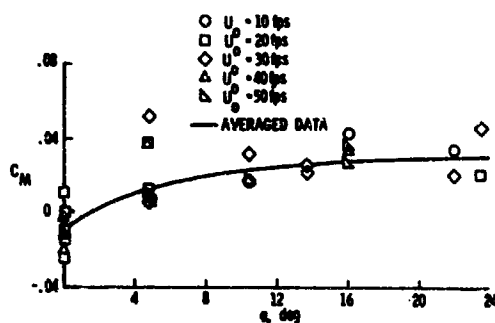


Figure 29.8. Aerodynamic Pitching-moment Coefficient (C_M) versus Angle of Attack (α). (The pitching moment is taken about the balloon's structural c.g.)

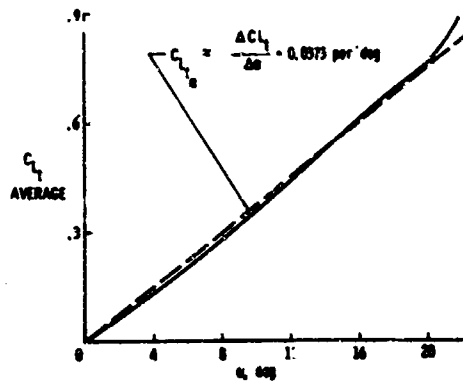


Figure 29.9. Variation of Tail-life Coefficient (C_{L_t}) with Changes in Angles of Attack (α)

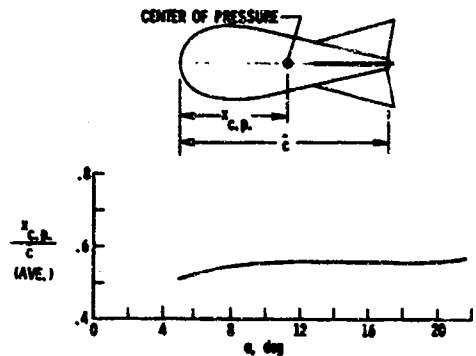


Figure 29.10. Location of Balloon's Center of Pressure ($x_{c.p.}$) versus Angle of Attack (α)

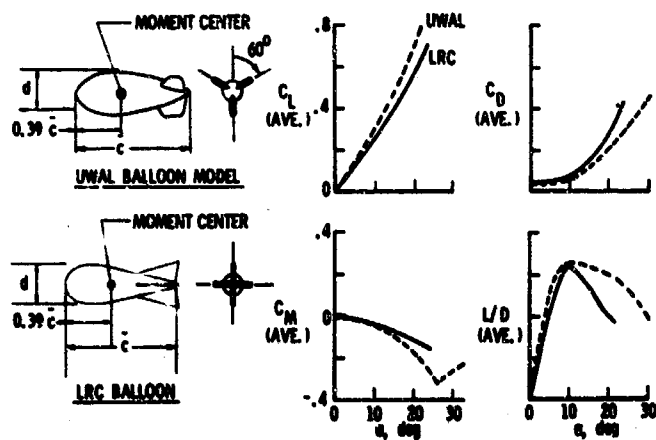


Figure 29.11. Comparison of LRC Balloon with a Class "C" Rigid Wind-tunnel Model

scale rigid model (UWAL model) of a somewhat similar class "C" balloon, reported elsewhere (Stein and Shindo, 1968; and Farmer, 1969). The UWAL balloon model had the following physical characteristics: $\bar{c} = 1.39$ m (4.65 ft), $\bar{c}/d = 3.46$, $S/S_t = 4.12$, and was tested at $R_N = 4.4 \times 10^6$; whereas, the LRC balloon's physical characteristics were: $\bar{c} = 7.62$ m (25.0 ft), $\bar{c}/d = 2.96$, $S/S_t = 4.74$, and was tested at $R_N = 1.5 \times 10^6$ to 7.5×10^6 . Hence, the above physical characteristics and Reynolds number test range were roughly the same for both balloons. Notice in Figure 29.11 that the moment center for the LRC balloon has been moved forward from the structural c. g. to correspond with the moment center for the UWAL balloon model. With regard to S/S_t , although the wind-tunnel test balloon configuration had only three fins in contrast to four on the tow-test configuration, the areas of the fins projected in the horizontal plane were related to the reference areas by about the same ratio. In view of these similarities, the degree of agreement between the two sets of results seems reasonable and the differences are felt primarily to reflect the detailed differences in configurations. Some of the differences in the data, however, are believed to be due to slight deformations of the LRC balloon nose and tail fins, especially at high velocities and angles of attack. As a matter of fact, at a truck velocity of 15 m/sec (50 ft/sec) and an angle of attack of 23° , the horizontal tail fins deformed to the extent that they failed structurally.

For a full description of the aerodynamic forces acting on a balloon, it is desirable to obtain information concerning changes in the aerodynamic side forces associated with changes in balloon yaw angles. This information can be obtained with the tow-truck system by simply rotating the balloon 90° about its longitudinal center line. However, because of balloon symmetry, side force tests were not necessary in the present investigation.

29.6 CONCLUDING REMARKS

The tow-testing technique described herein can be used to measure many of the aerodynamic force coefficients required in balloon stability analyses. The data presented indicate that the technique does not have any appreciable advantage over wind-tunnel tests utilizing small rigid models, provided that the desired Reynolds number can be obtained in the wind tunnel, and the full-sized balloon does not deform due to the aerodynamic forces. In cases where the Reynolds number or the deformations of an inflated balloon cannot be adequately simulated in wind tunnels, the tow technique provides a useful alternate method for determining balloon aerodynamic data.

References

- Bairstow, L., and Jones, R. (1915) The Stability of Kite Balloons: Mathematical Investigation, Advisory Committee for Aeronautical Reports and Memoranda, No. 208.
- Farmer, J.R. (1969) A Wind Tunnel Test of Three Single Hulled Balloons at Extreme Angles of Attack, University of Washington Aeronautical Laboratory Report, UWAL 957-B.
- Henry, R.M., and Eckstrom, C.V. (1970) A Fast-rising Stable Streamlined Balloon for High Resolution Wind Measurements, presented at the Sixth AFCRL Scientific Balloon Symposium, Portsmouth, New Hampshire.
- Newmark, S. (1961) Equilibrium Configurations of Flying Cables of Captive Balloons, and Cable Derivatives for Stability, RAE, Aero, 2653.
- Stein, D.E., and Shindo, S. (1968) A Wind Tunnel Test of a Single Hulled Balloon at Extreme Angles of Attack, University of Washington Aeronautical Laboratory, Report 901.

Appendix

Supplementary Tests

In order to measure the locations of the balloon's structural center of gravity, a , center of buoyancy, b , buoyancy force, B , and also volume, V_B , two different tests must be performed. In the first test the balloon is filled with lifting gas (helium) and constrained by two lines as shown in Figure 29A. 1. In the second test the balloon is filled with air and suspended with two lines as shown in Figure 29A. 2.

Referring to Figure 29A. 1, the buoyancy force B in terms of measured tensions F_1 and F_2 in the lines is

$$B = F_1 + F_2 + W_g. \quad (29A. 1)$$

The volume of the balloon V_B is

$$V_B = \frac{B}{\frac{P_e}{R_e T^0} \left[1 - \frac{P_1}{P_e} \left(\frac{R_e}{R_1} \right) \right]} \quad (29A. 2)$$

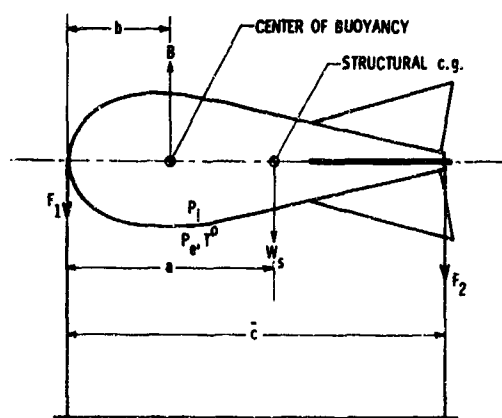


Figure 29A.1. Schematic Test Setup to Determine Buoyancy Force and Volume of the Balloon

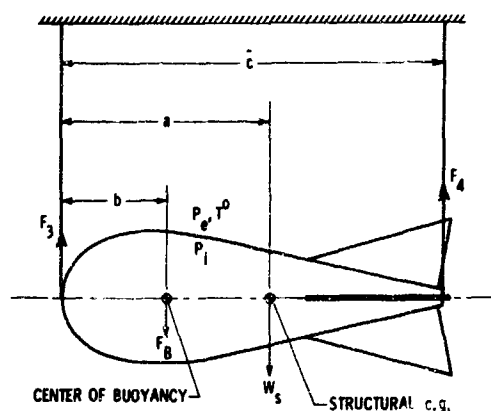


Figure 29A.2. Schematic Test Setup to Determine the Structural Center of Gravity and Center of Buoyancy of the Balloon

where subscript e refers to ambient air external to the balloon and i refers to the lifting gas inside. (The volume can also be determined analytically from the balloon geometry.)

The equations for the moments about the nose, as shown in Figures 29A.1 and 29A.2, respectively, are as follows

$$W_s a - Bb = -F_2 \bar{c} \quad (29A.3)$$

and

$$F_B b + W_s a = F_4 \bar{c} \quad (29A.4)$$

where F_B , the negative buoyancy of the air inside the balloon, is determined from

$$F_B = (\gamma_i - \gamma_e) V_B = \left(\frac{P_i - P_e}{R_e T_0} \right) V_B \quad (29A.5)$$

Solutions of Eqs. (29A.3) and (29A.4) for a and b yield

$$a = \frac{(BF_4 - F_B F_2)}{(B + F_B)} \cdot \frac{\bar{c}}{W_s} \quad (29A.6)$$

$$b = \frac{(F_4 + F_2)}{(B + F_B)} \bar{c} \quad (29A.7)$$

Contents

30.1	Introduction	355
30.2	Natural Shape, Propeller Driven Balloons	356
30.3	Streamlined Propeller Driven Balloon Systems	365
30.4	Tethered Balloon Systems	373
30.5	Tethered Balloon with Propulsion System	375
30.6	Balloon Tethered to an Airship	375
30.7	Comparison of Station-Keeping Balloon Concepts	377

30. A Comparison of Several Very High Altitude Station Keeping Balloon Concepts

J.J. Vorechek
Goodyear Aerospace Corp.
Akron, Ohio

30.1 INTRODUCTION

The high-altitude, free balloon has demonstrated its capability as a research tool for many years. One of its more significant limitations is the fact that it is subject to the vagaries of the wind. Thus, its endurance over a specific geographical area of interest is generally limited. If a given position can be maintained, the usefulness of a free balloon is substantially increased for some applications.

Two techniques used in the past for controlling position with a balloon are tethering it to the ground, or giving it a propulsion system (airship). Both approaches have been used for many years at low altitudes but, to date, have had no significant success at very high altitudes.

A number of very high altitude station-keeping balloon concepts have been evolved and two have been the subject of detailed study by GAC under contracts with AFCRL. A feasibility study has been accomplished on a two-balloon tethered system to 100,000 feet, as well as studies of powered, natural-shape balloons in the 60,000-to 100,000-foot altitude range. Additional concepts have been considered in a more preliminary manner.

This paper presents a conceptual description of balloon systems which offer possible solutions to the general problem of station-keeping at very high altitude,

PROCEEDING PAGE BLANK

and an indication of how some of the major parameters influence the balloon system characteristics. Wind is one of the most important factors to be considered in the design of a balloon system. For the purposes of this paper a typical altitude profile of winds has been used as shown in Figure 30.1. Frequency distribution indicates the period of time for which the winds will be below a certain value at a specific altitude.

30.2 NATURAL SHAPE, PROPELLER DRIVEN BALLOONS

30.2.1 Electrically-Powered Balloon Concept

The high-altitude powered-balloon concept employs a natural shape, zero pressure balloon made of Mylar scrim material. The general arrangement of this vehicle is shown in Figure 30.2. The payload, propulsion system, and radio control system are mounted on a gondola or support structure below the balloon. This load is connected to the balloon through a swivel and recovery parachute. The propeller, electric motor, and batteries are located on the gondola. When used, solar cells are mounted on the balloon structure.

Launch and ascent are accomplished in the conventional manner for high altitude balloons. The gondola and propulsion system are free swiveling, permitting rotation with respect to the balloon. Therefore, the propulsion device can be oriented into the relative wind. Control surfaces in the propulsion-system slip stream will provide orientation of the gondola. Balloon altitude control is effected

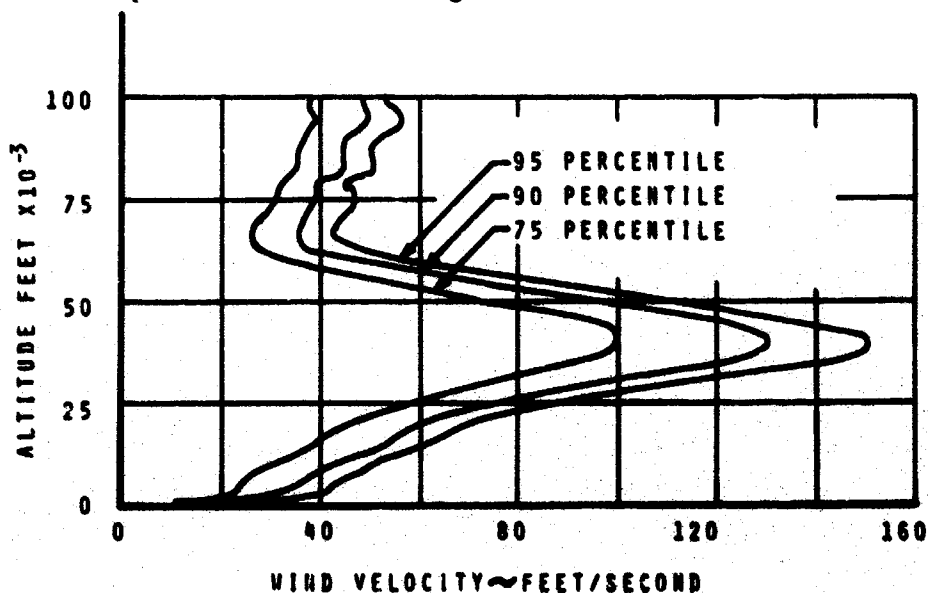


Figure 30.1. Typical Wind Profiles

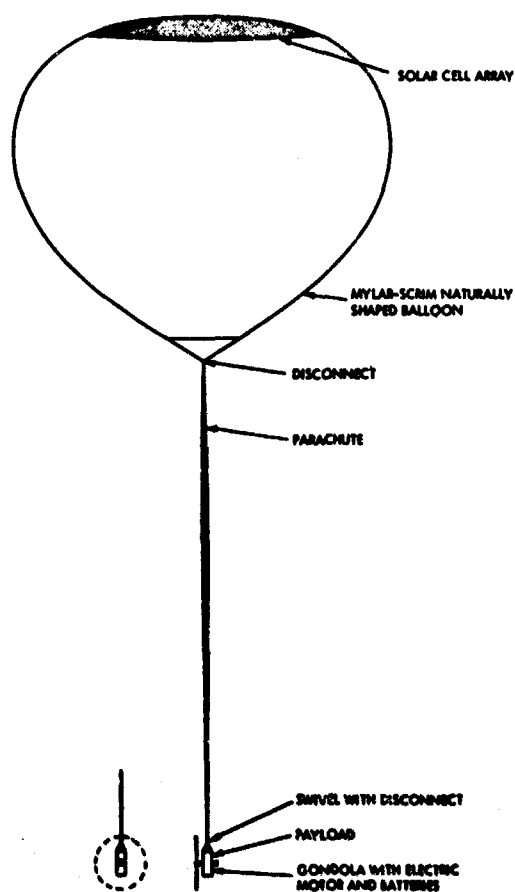


Figure 30.2. General Arrangement of Natural Shape Powered Balloon

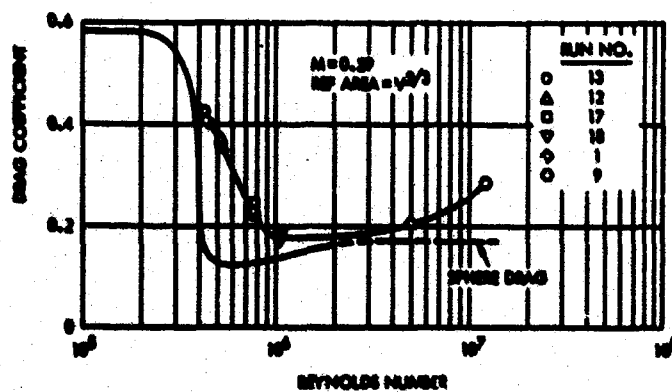


Figure 30.3. Natural Shape Balloon Drag Coefficient at Zero Angle of Attack Versus Reynolds Number

by valving gas and by dropping ballast. It is visualized that this powered balloon system with valving and ballasting capability can search out and fly in minimum wind fields. With this capability, a fixed station relative to the earth can be maintained with modest expenditure of power. After the mission is complete, the balloon is expended and the entire gondola is recovered by parachute.

30.2.2 Electric Propulsion System

It is necessary in a parametric study to establish the empty weight of the powered balloon systems to obtain the relationship between balloon volume and payload-carrying capability for various flight conditions. The electric propulsion system is a significant part of this weight. It is therefore highly desirable to minimize propulsion power requirements to reduce battery and solar cell weights.

Low disk loading (DL) propellers (that is, large diameter, slow rotating propellers similar to hovering helicopter rotors) will minimize power required to develop a given thrust. Thrust requirements for natural-shape balloons are based on experimental drag coefficient data as given in Figure 30.3. The effects of positive and negative aerodynamic lift have been neglected in this study.

Either an ac or dc motor can be used in the system. If an ac motor is used, an inverter is required to change the direct current supply to alternating current. A motor starter is required for either motor, and a gear reduction is necessary in either case.

From a review of available motors, the ac motor appears very promising from a weight standpoint, even when the weight of the inverter and additional power for the inverter are included. In addition, special commutator brushes are required for high altitude operation in the dc motors, whereas, no brushes are required in the ac motors. Also, motor starters for ac motors are generally lighter in weight.

In the aerospace motor category, most of the dc motors are below the 10 horsepower size. Only a few are available in the 20 horsepower size. These motors are mostly powered by 30-volt power sources, although some operate from voltages as high as 500V.

Electrical energy is provided to the motor by the battery, which has sufficient capacity to power the system through the longest operating period expected between recharging operations. The battery is encased in an insulated container. The battery is heated to, and maintained at, the operating temperature prior to launching.

Considerable savings in weight can be realized by the use of solar cells for recharging the battery as compared with a system wherein the battery supplies all the energy without recharging. The weight difference becomes more pronounced as the flight duration increases.

In the more conventional utilization of solar cells, the net power per unit weight, or the power density, of an array is relatively low because a supporting structure must be provided for the array.

In this application, the supporting structure exists, since the solar cell array can be supported entirely by the balloon envelope. The two predominant types of cells (from the standpoint of status of development and availability) are silicon cells and thin film, cadmium sulfide (CdS) cells.

The solar cell array can be mounted on the uppermost surface of the balloon envelope as a stationary array, or be offset laterally for an oriented array. The power output of the cells as a function of angle of incidence of the sunlight approaches the cosine function. Thus, some power is obtained even from large angles of incidence. For convenience, however, it is estimated that on an average, full power is obtained from the stationary array over an eight hour period, which is 120 degrees included angle of incidence. This is considered to be a reasonable estimate because the curvature of the balloon would result in exposure of a portion of the cells for a longer period of time, and a small amount of power collected from large angles of incidence.

With regard to the oriented array, the center of the array would be positioned at an angle from the top of the balloon to align with the sun's elevation as much as possible. The array would be aligned with the sun in azimuth by rotating the balloon with cold gas reaction jets as signalled by light sensors. This type of array should provide the required power over a nominal 12 hour period. Variations would occur with flight location and season of the year.

In either array there will be some cells exposed to larger angles of incidence because of balloon curvature and the area required by the array. The silicon cells produce about 13 watts/ft², whereas the CdS cells produce about 4.6 watts/ft². Because of the loss of power due to the large angles of incidence, additional cells will be required to make up the difference. The end result will be to lower the overall power density value.

Silicon diodes will probably be used in series with groups of cells to prevent those cells not illuminated from loading the illuminated cells. Occasional failure of some cells, resulting in short circuits, will cause a decrease in overall solar plant performance. Also, the weight of adhesive and any other materials needed for attachment will decrease the power density. It is assumed, therefore, that for the purposes of the parametric study the power density will be about 60 watts/lb.

A major disadvantage of using a solar cell array on the surface of the balloon envelope is the large distance between the array and the gondola over which the electrical power must be collected from the solar cells and transmitted to the battery. Since the size of the conductor depends on the current, the conductor

weight can be kept low by using a high voltage, low current system. The battery and propulsion motor must be compatible with the transmitted power, unless a dc to ac converter is incorporated in the system.

30.2.3 Parametric Data for Electrically-Powered Balloons

Parametric data for the electrically powered, natural shape balloon were generated for the following range of parameters:

- Balloon volume - 500,000 to 100,000,000 cu ft
- Altitude - 60,000, 80,000 and 100,000 ft
- Airspeed - 15, 30 and 45 knots
- Flight duration - 12, 24 and 96 hours

Electrical power sources:

- No. 1 - Secondary (rechargeable) silver zinc batteries, nominal power density of 40 watt-hr/lb
- No. 2 - Primary (limited rechargeability) silver zinc batteries, nominal power density of 80 watt-hr/lb
- No. 3 - Solar cells and primary silver zinc batteries

Power cycle - half time during day and half time during night

Propeller disk loading - 0.50, 0.25 and 0.10 psf

The primary output data of the parametric study were payload capability as a function of balloon volume for the various parameters listed above. Data such as power required, propeller diameter, and electrical propulsion system component weights were also obtained.

The relationships between horsepower required and balloon size for a propeller disk loadings of 0.25 psf is shown in Figure 30.4 along with the corresponding propeller diameter required as a function of balloon volume for a 15 knot airspeed. Power requirements for an airspeed of 30 knots are shown in Figure 30.5. Substantial increases in power required are apparent. For comparison, the significantly lower power requirements for a streamlined balloon at this speed are also shown. As a reference, lines indicating this relationship for 500 pound payloads for various design conditions are superimposed on these curves.

Since payloads of around 500 pounds were considered of most interest, the relationships between balloon volume and altitude for electrically powered balloons carrying this payload were prepared and are shown in Figures 30.6 and 30.7. It is apparent from an examination of these curves that the use of power source No. 2 results in smaller balloons than power source No. 1 for a given mission. With the use of power source No. 2, very low disk loading propellers (0.10 psf) will permit flying at 30 knots over the entire altitude range of 60,000 to 100,000 feet for a 24 hour flight duration. Power source No. 3 also permits flight over the entire altitude range at 30 knots for a 24 hour flight duration and will lower balloon volume

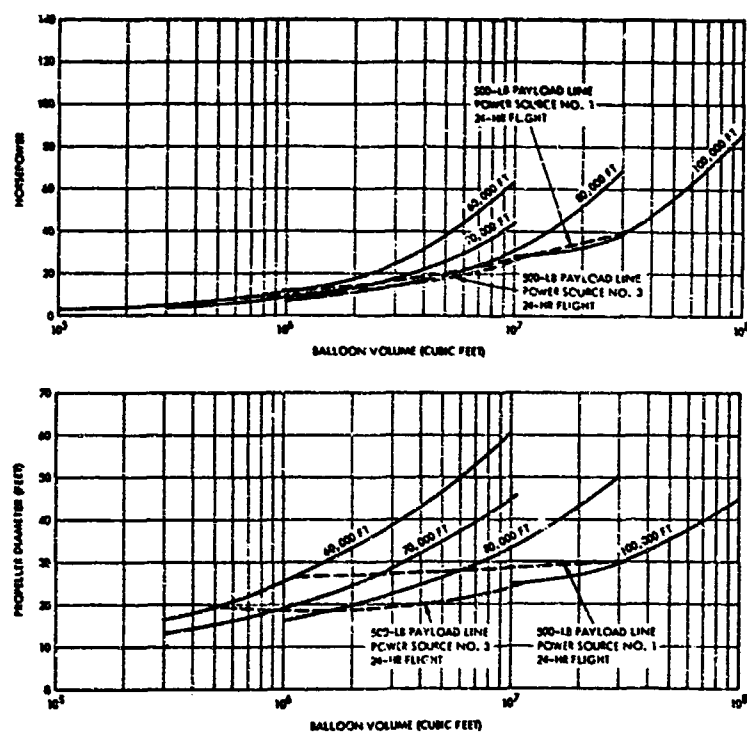


Figure 30.4. Horsepower Required and Propeller Diameter as a Function of Balloon Volume - Airspeed = 15 Knots, Disk Loading = 0.25 PSF

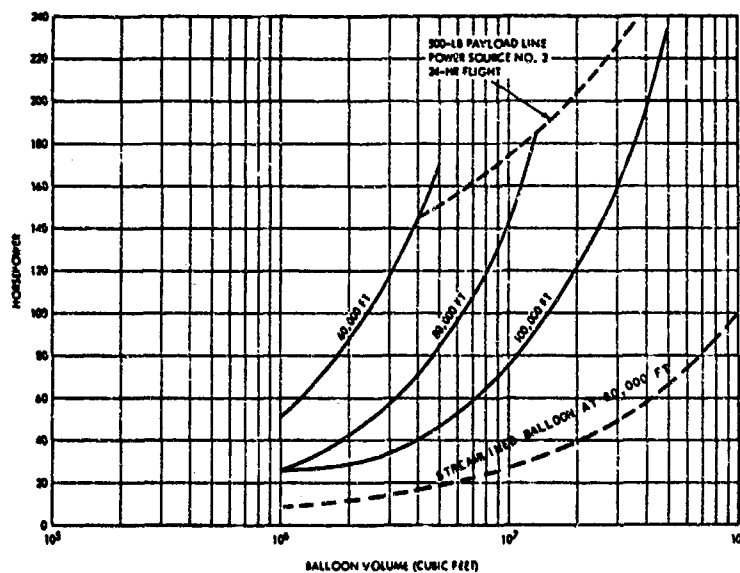


Figure 30.5. Horsepower Required as a Function of Balloon Volume Airspeed = 30 Knots, Disk Loading = 0.25 PSF

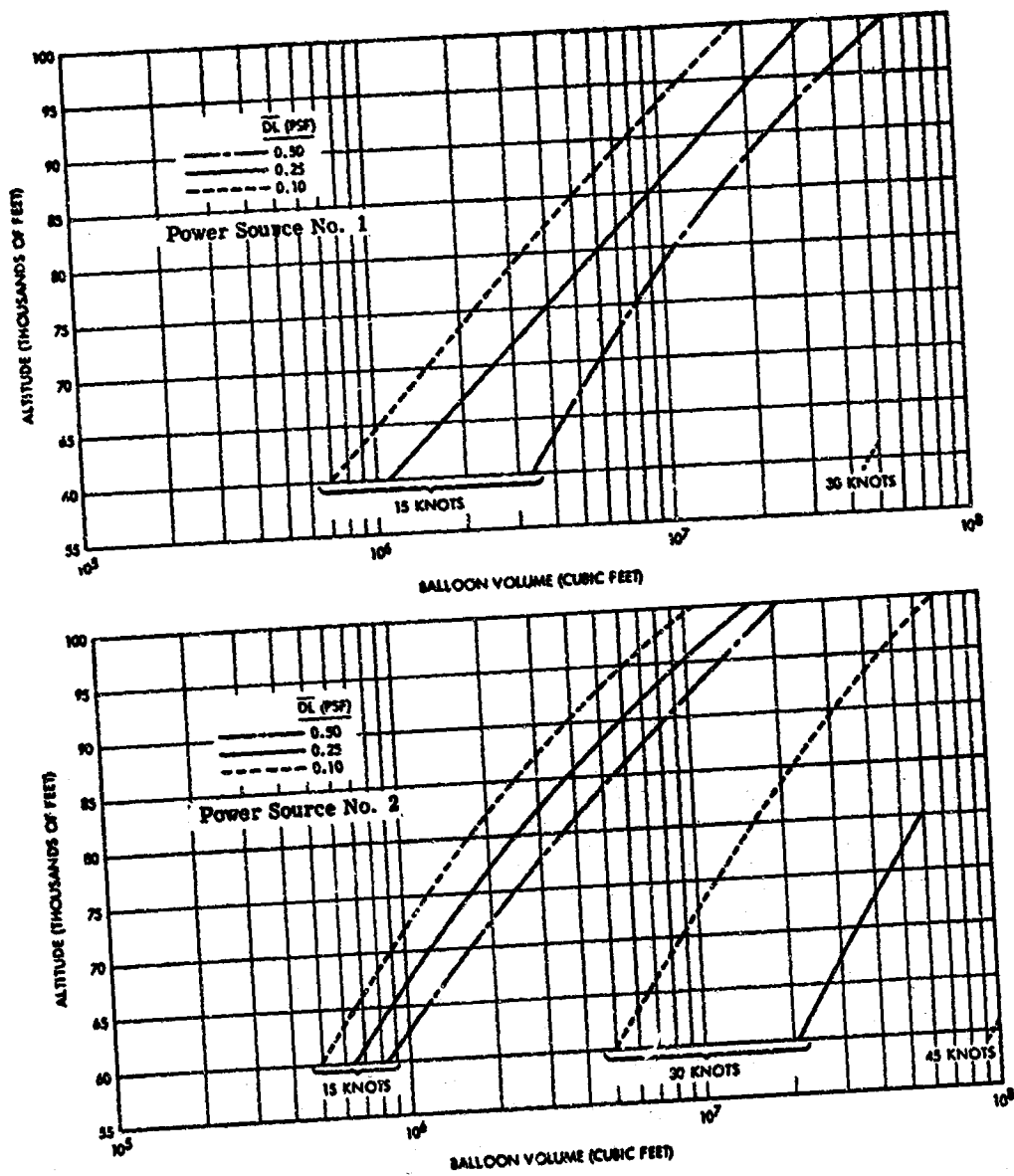


Figure 30.6. Altitude as a Function of Balloon Volume for 500 Pound Payload - Flight Duration = 24 Hours

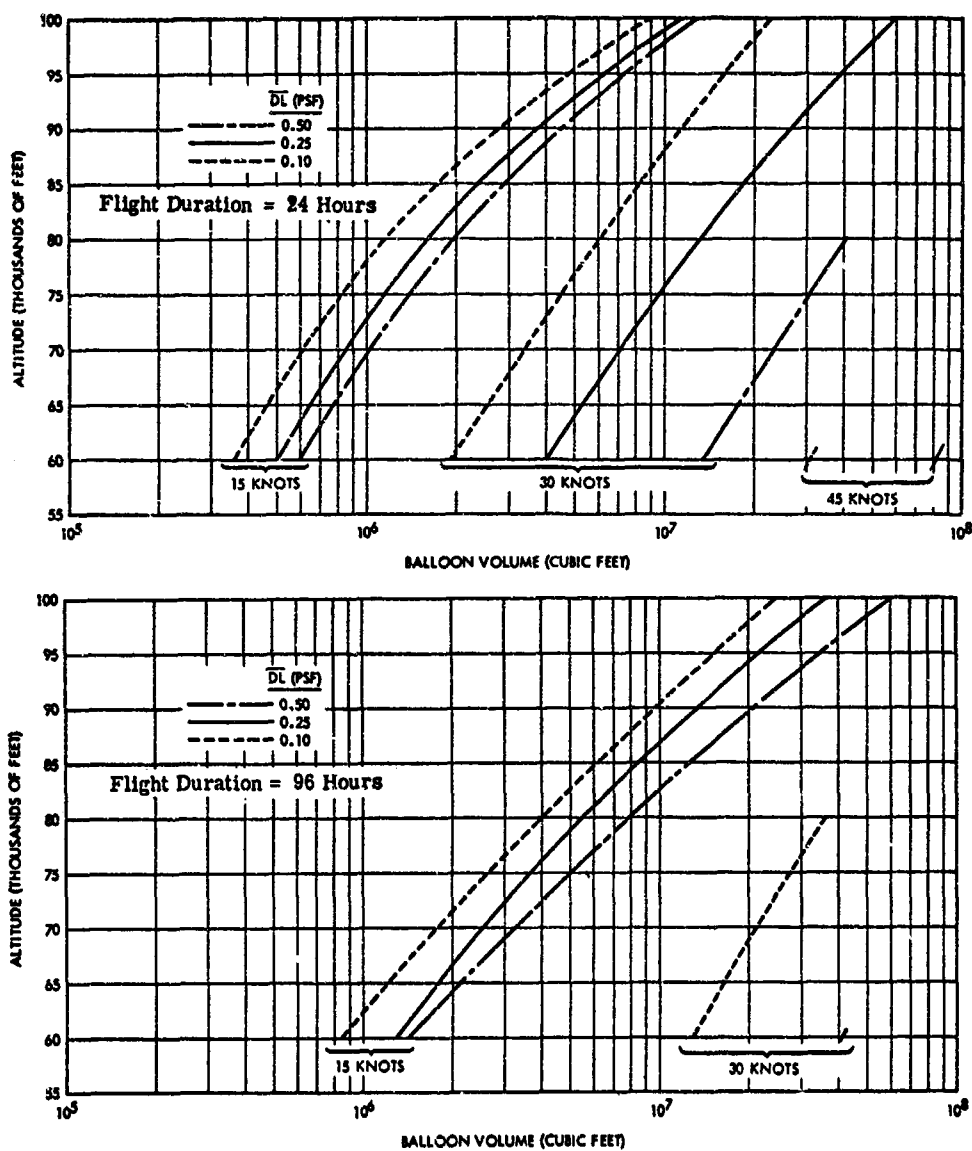


Figure 30.7. Altitude as a Function of Balloon Volume for 500 Pound Payload - Power Source No. 3

for a given mission as compared with power source No. 2. Power source No. 3 also permits flight over the entire altitude range at 15 knots for a 96 hour flight duration.

Comparative sizes of powered balloons employing the three power sources for flight at an altitude of 80,000 feet and an airspeed of 15 knots are indicated in Figure 30.8. For simplicity of representation, a spherical balloon whose volume is that of a natural shape balloon is depicted. The larger balloon sizes for a 30 knot flight condition at 80,000 feet are also shown in Figure 30.8. It was necessary to employ a battery-solar cell electrical power system to keep balloon size down. An indication of solar cell area relative to the balloon surface area is given.

In summary, the parametric study of electrically powered, natural shape balloons has established conditions for which missions can be accomplished with natural shape balloons of sizes comparable to those that have been flown. Each of the three electrical power sources - primary and secondary silver zinc batteries and solar cells combined with silver zinc batteries - provides workable systems for 24 hour flights at a 15 knot airspeed over the altitude range of 60,000 to 100,000 feet. Primary battery-powered balloon systems are significantly smaller than secondary battery-powered systems for a given mission, and battery-solar cell powered systems are even smaller than primary battery-powered balloon systems. The battery-solar cell powered systems also provide a flight capability for 96 hours at a 15 knot airspeed. A more limited number of solutions are available for the 30 knot airspeed condition. The 45 knot airspeed condition does not appear to be practical for the electrically powered, natural shape balloons that have been investigated.

30.2.4 Gondola Design

The detailed design of a gondola for an electrically powered, natural shape balloon (less command-control and telemetry system) exists for a balloon system capable of carrying scientific payloads at altitudes between 60,000 and 70,000 feet MSL. The vehicle is capable of a 15 knot airspeed; that is, ability to stay over a point on the surface of the earth when pointed and powered into a 15 knot wind. The mission duration is 24 hours with a 50 percent duty cycle on the motor. The balloon to meet this requirement has a volume of 1.5 million cubic feet. The vehicle is powered by a dc electric motor, which drives a 37-foot diameter, fixed-pitch propeller through a speed reduction unit. The propeller requires 8 brake horsepower when operating at 70,000 feet. Electrical power to the propulsion motor and a cooling blower for the motor is provided by silver zinc batteries. A payload of 1300 pounds can be carried when primary silver zinc batteries are used.

30.2.5 Air-Breathing Engine-Powered Balloon Concept

A preliminary design for an air-breathing engine powered natural balloon was based on a mission of maintaining a 1000-pound scientific payload on a station at altitudes of 60,000 to 70,000 feet against 10 knot winds for a minimum period of 24 hours. It was concluded that this mission can be accomplished with a vehicle employing a 1.1 million cubic foot, natural shape balloon. Of available engines studied, the AiResearch T76 turboprop engine offered the greatest potential for meeting the propulsion needs of the vehicle. This engine, even though carefully selected, has marginal high altitude characteristics as presently configured. Combustion instabilities and even flame blow-out may well be encountered at the operating altitudes being considered. It is expected that engine performance can be assured and improved control capability can be obtained with the addition of a dual fuel system incorporating gaseous fuel.

Balloon sizes for carrying scientific payloads greater than 1000 pounds using this propulsion system are shown in Figure 30.9. The airspeed capability for these various balloon sizes is also given.

30.3 STREAMLINED PROPELLER DRIVEN BALLOON SYSTEMS

30.3.1 Self-Powered Balloon System Concept

A general arrangement of a streamlined powered balloon is shown in Figure 30.10. The streamlined envelope is a superpressure balloon and is constructed of film-fabric laminates. A superpressure balloon is used to permit extended flight at constant density altitude. Sufficient excess helium is provided to develop a superpressure at altitude for structural stiffness and to provide for loss of helium with time. Increases in superpressure due to supertemperature are contained by the strength of the envelope.

The propulsion system consists of a stern-mounted propeller and electric motor powered by solar cells and silver zinc secondary batteries. A solar cell array of sufficient size to meet the power requirements of the vehicle is arranged on the top of the envelope. Cadmium sulfide, thin film solar cells are used. Power for daytime operation for the motor is generated by the solar cells. The solar cells also develop energy which is stored in batteries for nighttime operation. Appropriate electrical wiring is provided to transfer power.

Tail surfaces are mounted on the stern of the envelope to provide stability and control. These tail surfaces are visualized as packageable to facilitate launching and retrieval operations. A car structure for mounting the payload and batteries is submerged in the bottom of the envelope, and is supported from the top of the

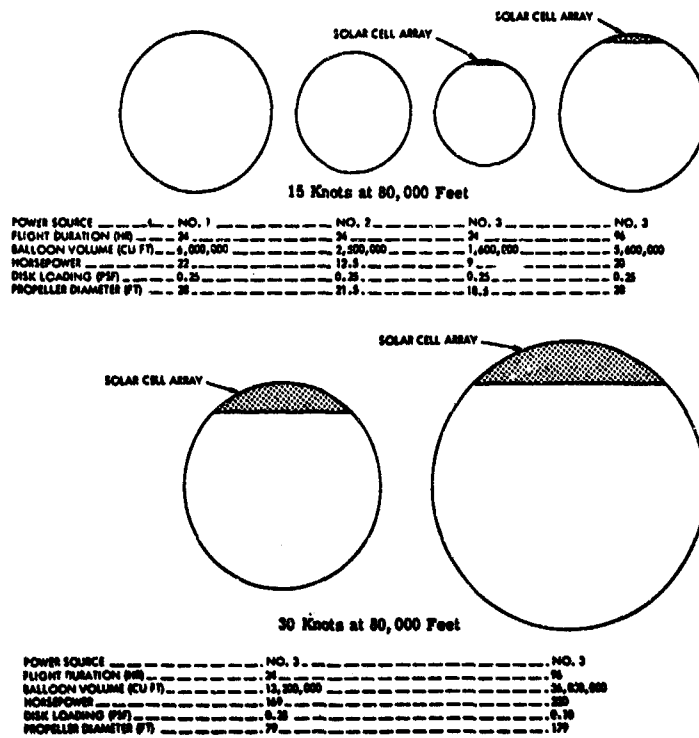


Figure 30.8. Comparative Size of Balloons with Various Electric Power Sources

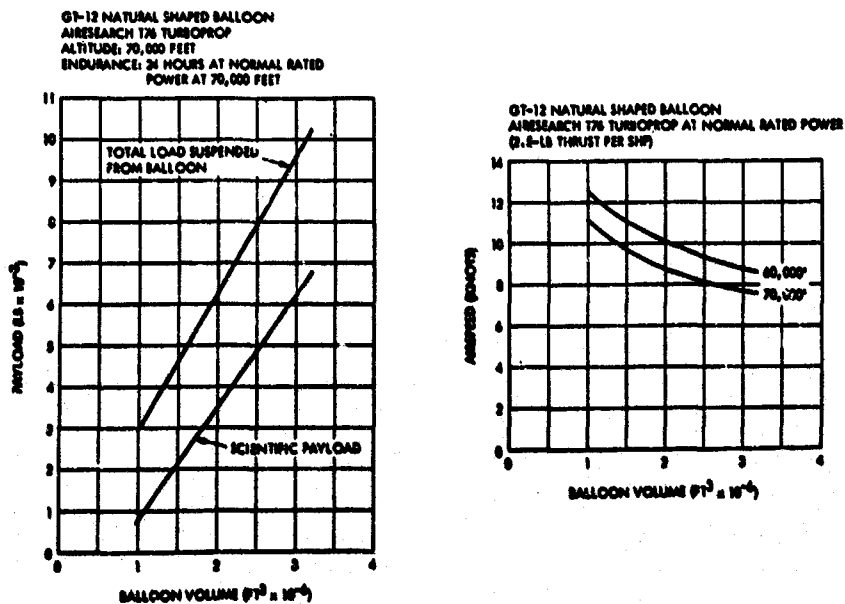


Figure 30.9. Payloads and Speed for Turboprop Powered Balloons

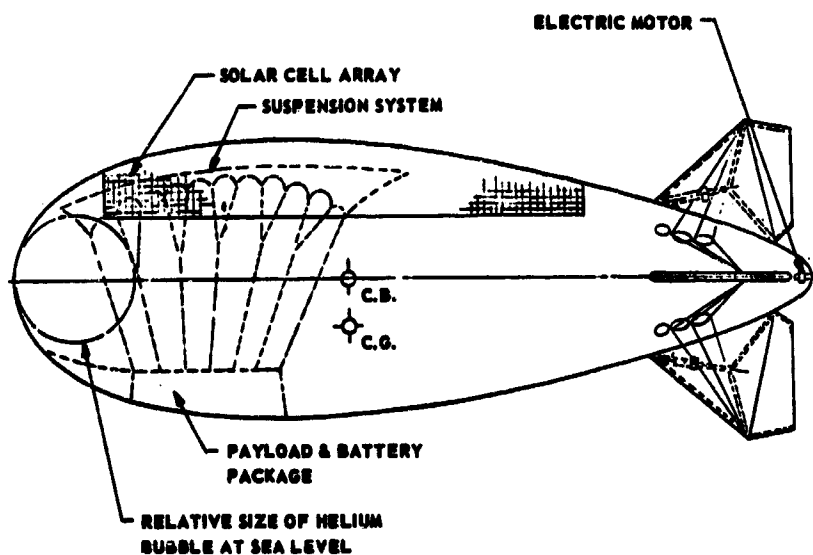


Figure 30.10. General Arrangement of Streamlined Powered Balloon

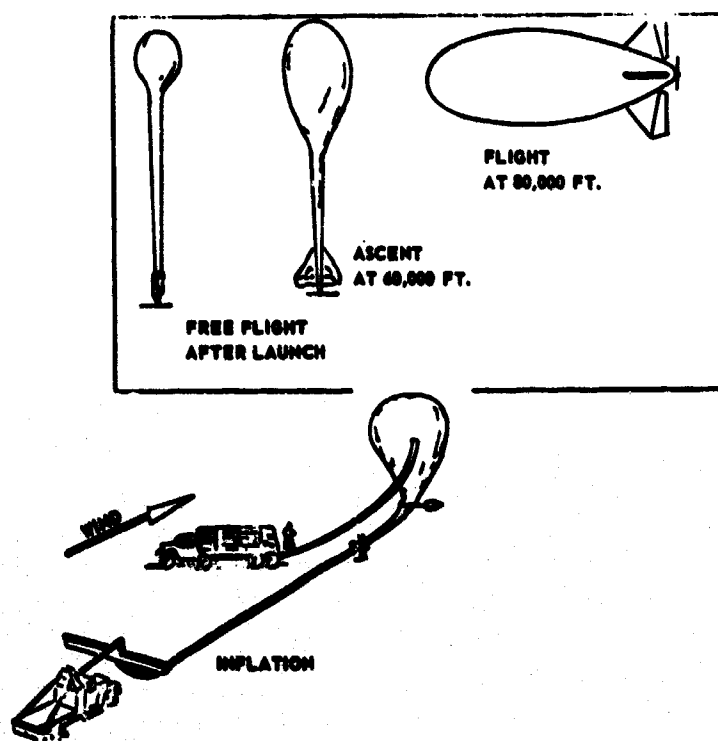


Figure 30.11. Launch and Ascent Sequence

envelope by means of a suspension system. Additional suspension toward the nose of the envelope is required for vertical ascent of the vehicle.

A sequence for launching and ascent of the vehicle is depicted in Figure 30.11. Inflation and launching of the airship is accomplished in a manner analogous to the launch of a natural balloon. Equipment and facilities presently used for natural free balloons can be used for this vehicle. The streamlined balloon ascends to float altitude in a vertical attitude and expands in volume just as a natural balloon. The relative size of the helium bubble at sea level as compared to the fully expanded envelope at 80,000 feet altitudes is depicted in Figure 30.10. During vertical ascent, the center of buoyancy is above the center of gravity providing a stable arrangement. In the flight attitude, the center of gravity is located below the center of buoyancy as shown in Figure 30.10. This location of the center of gravity causes the vehicle to rotate from the vertical to the horizontal attitude as the float altitude is approached. Once at altitude, operation of the vehicle is performed with the aid of command-control and telemetry systems.

A flexible-film, cadmium sulfide solar cell array is located along the top of the streamlined balloon and extends around the circumference of the balloon as shown in Figure 30.12. This figure also presents a trigonometric function $f(\gamma_0)$ which relates the amount of energy collected by a solar cell array of unit length and radius R to γ_0 , a measure of the arc length of solar cell upon the circumference of the balloon. This function is based on flying at the equator at the time of the equinox and can be modified for other conditions. It is apparent from Figure 30.12 that for the conditions presented, the energies collected for north - south pointing balloons and for east - west pointing balloons are nearly equal for arrays extending 40 degrees to either side of vertical.

The energy per unit length of solar cell array is given by

$$E = \frac{pR}{\psi} [f(\gamma_0)]$$

where E = energy - watt hours

p = power generated by solar cell per unit area for normal incidence of the sun's ray = 4 watts/ft² for cadmium sulfide solar cell array.

R = radius of the array - feet

ψ = rotational speed of earth = $\pi/12$ radians/hour

The expression can be expanded to cover the entire solar cell array by taking into account the length of the array.

The total energy required for 24 hours of operation is given by

$$E = \frac{748 PT}{n}$$

where P = horsepower required

T = duration of powered flight in hours

n = efficiency = 0.70

For any given power cycle the total energy required can be computed.

Equating the energy required to the energy generated gives an expression which can be used to determine the solar cell array geometry for a given balloon volume and power requirement.

Thin-film, cadmium sulfide solar cells are used for a parametric study of weights. These cells develop 60 watts/lb and 4.0 watts/sq ft in air mass 1 (on earth). For an air mass 0 these character-increase to 70 watts/lb and 4.6 watts/sq ft. The unit weight of the solar cells then is 0.066 lb/sq ft. To allow for mounting the solar cells on the balloon envelope the unit weight is increased to 0.103 lbs/sq ft. This value is used for estimating the weight of solar cell arrays.

Silver zinc secondary batteries are used since recharging is required for extensive flight durations. These batteries are reusable for 80 to 100 cycles and have a nominal energy-to-weight ratio of 40 watt-hrs/lb.

30.3.2 Self-Powered Balloon System Parametric Data

Parametric data were generated for this streamlined balloon concept to establish payload carrying capability as a function of balloon volume. The flight conditions investigated were at 80,000 feet for various airspeeds and power cycles. The effect of superpressure was also determined.

Initial data were prepared for a cycle of the equivalent of 6 hours of full power during the day and 6 hours of full power at night. This power cycle was used in the parametric studies presented earlier for natural shape balloons. Two of the curves in Figure 30.13 show the effect of superpressure based on this power cycle. It can be seen that superpressure (as differentiated by 5 percent and 15 percent free lift) has a great effect on balloon size for a given payload capability. The greater the free lift, the longer the balloon can stay aloft based on helium loss. If supertemperature can be reduced, it will provide the same effect as reducing free lift. These curves are for the 30 knot airspeed condition. It was found that, even with only 5 percent free lift, a 60 knot condition could not be achieved primarily because of the batteries required for nighttime operation. As a reference, a 36 million cubic foot zero pressure natural balloon with ballast for four days of flight is shown in Figure 30.13.

For a power cycle of 8 hours during the day, balloon size can be significantly reduced for the 30 knot speed condition as shown in Figure 30.13. This power cycle will also permit flying at 60 knots. Sufficient area for the solar cell array cannot be obtained for this power cycle for a 90 knot airspeed condition.

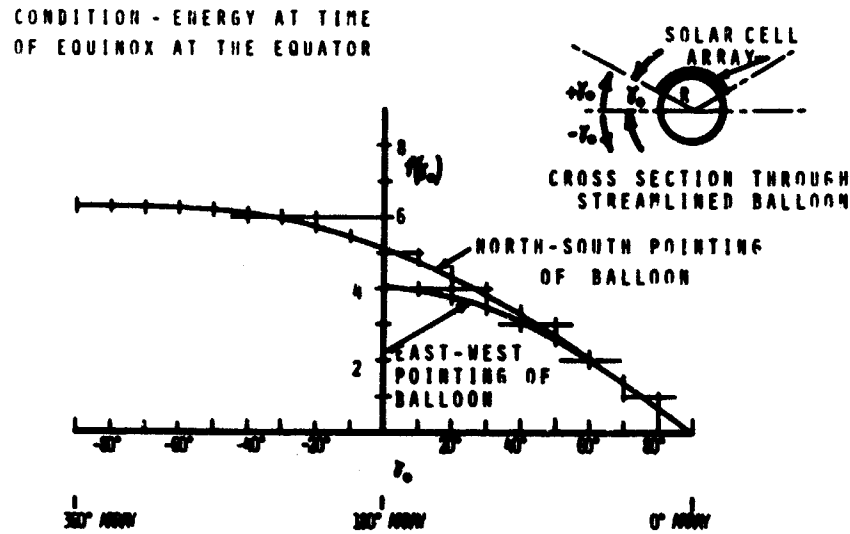


Figure 30.12. Energy Function for Solar Cells on Streamlined Balloons

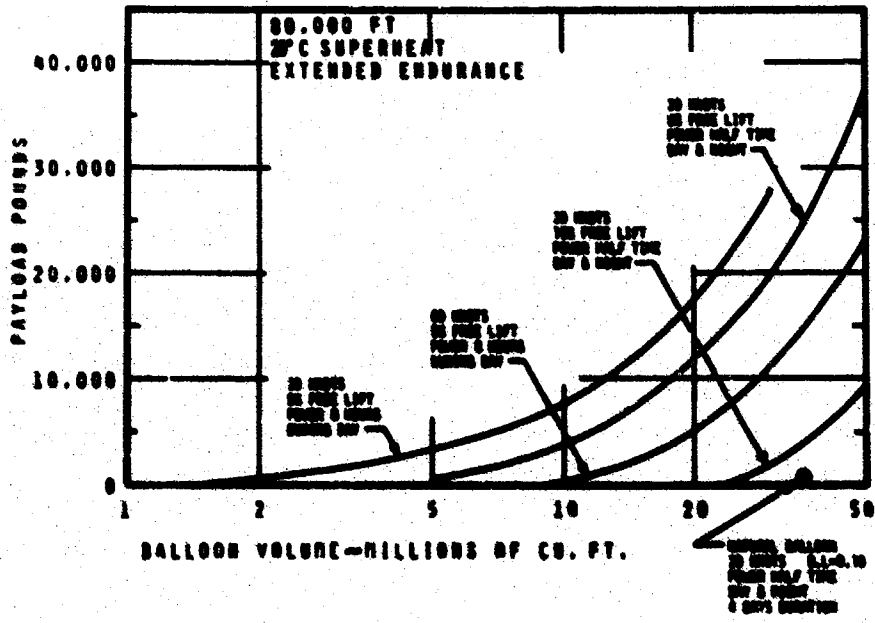


Figure 30.13. Payload for Solar Cell Powered Streamlined Balloons

A summary of balloon sizes for a 500 pound payload-carrying capability is given below.

<u>Configuration</u>	<u>Volume - Ft³</u>
30 kts - powered 1/2 time day & night	
Natural zero pressure - 4 days	36 x 10 ⁶
Streamlined superpressure - more than 1 month	5 x 10 ⁶
30 kts - powered 8 hrs during day	
Streamlined superpressure - 1 month	2 x 10 ⁶
60 kts - powered 8 hrs during day	
Streamlined superpressure - 1 month	11 x 10 ⁶

These data indicate that streamlined balloons of this type provide increased speed capability and flight duration as compared to a zero pressure natural balloon.

It should also be noted that if speed is halved and powered duration is doubled, the same distance is traversed. However, power requirements are reduced and smaller balloons can be realized. Also, for power cycles in which power is provided during the day and the night, if speed is reduced at night, power requirements will be reduced and battery weight can be saved.

30.3.3 Ground-Powered Balloon System

Another possible electric propulsion system for powered balloons employs beaming of electrical energy from the ground. The elements of this system which could replace the solar cell array used for the previous balloon concept consist of a microwave power source, a ground antenna and a device at the balloon to convert rf to dc power for propulsive power. Papers in the references discuss Raytheon Company work in the development of beamed microwave power. The primary experimental demonstrations described are of two, separate, droned helicopters. In the first case, a 5-pound helicopter with a 6-foot diameter rotor was flown continuously for 10 hours at 50 foot altitude on a delivered power at the helicopter of 270 watts. The microwave power was generated with a magnetron and delivered at a frequency of 2450 MHz.

A second drone helicopter demonstrated the positional capabilities of a microwave beam. This helicopter was powered by cable but used sensors to detect pitch, roll, yaw, "X" and "Y" positioning in the vertical beam. Altitude sensing is possible with a divergent beam.

Powering and controlling a drone helicopter at altitudes as high as 60,000 feet is also discussed. Apparently wavelengths on the order of 10 cm are necessary to avoid serious atmospheric attenuation and scattering. Refraction can occur due to atmospheric stratification so that the beam might not remain perfectly straight, but if the receiving vehicle can ride the beam this is not believed to be a serious problem.

Recently, experience has been obtained by Raytheon with a flexible diode array rectifier - antenna which is known as a "Rectenna" and provides a power-to-weight ratio of 1 KW per 2 to 5 pounds. Rectenna airborne weights are significantly lighter and require less area than solar cells, since Rectenna dc power densities in the order of 100 W/ft² are indicated. With the advent of the flexible Rectenna, it is possible to integrate the energy collection device with a balloon.

It is visualized that a streamlined balloon such as shown in Figure 30.10 can be developed wherein the solar cell array at the top of the balloon is replaced by a Rectenna array arranged on the bottom of the balloon.

Using microwave power, the Rectenna airborne weight would appear to be on the order of 10 percent of the weight of equivalent solar cells. Battery weights are reducible since beamed power is available 24 hours per day. Maximum battery weight should be that required for the maximum expected search and acquisition of the beam at altitude. Once the beam has been acquired, batteries can be recharged for emergency, off-beam maneuvering, temporary beam interruption, or flying upwind before free balloon descent.

As before, airships are envisioned as superpressure balloons designed to fly at a pressure altitude of 80,000 feet. Two percentages of "free lift" are considered: 5 percent and 15 percent. The higher figure provides a higher tolerance for small leaks, but at a cost of higher envelope design pressure. In addition, 20°C superheat is considered part of the envelope pressure requirement.

A parametric study is based on the assumptions above and those stated below.

Climb technique	- free ballooning
Rate of climb	- 1,000 fpm average
Time to 80,000 ft altitude	- 80 minutes
Average wind	- 75 fps
Downwind drift	- 80 (75) (80 sec) = 360,000 ft

Battery time to fly upwind 360,000 ft against a 15 knot wind at design altitude:

<u>Vehicle Top Speed (Knots)</u>	<u>Ground Speed (Knots)</u>	<u>Time Back (Hrs)</u>
30	15	3.95
45	30	1.98
60	45	1.32

The parametric study to establish payload-balloon size relationships is summarized in Figure 30.14. The weights calculations are for propulsion weights for 30 knot and 60 knot capabilities, Rectenna weights to accompany the necessary horsepowers, and battery capability to provide the watt-hours necessary for the 360,000 foot up-wind excursion.

30.4 TETHERED BALLOON SYSTEMS

Very high altitude tethered-balloon systems have been the subject of considerable study, including the referenced papers. Wind is one of the most important factors to be considered in their design. An essential part of the definition of tethered-balloon systems is the determination of performance parameters for balloons and tether cables under equilibrium float conditions. Balloon buoyancy and aerodynamic effects on balloons and cables from winds are primary factors in system performance.

Analytical techniques developed to investigate performance of balloons and tethers are used here to define minimum size balloon systems for the wind conditions presented in Figure 30.1. Equilibrium tether cable performance parameters are based on the 75 percentile wind condition (that is, winds at any specific altitude will be less than this value 75 percent of the time). It is expected that overall effects of this wind profile on the tether cables will not be exceeded 90 percent of the time.

A method of superposition furnishes balloon-cable solutions at a glance. The method superposes graphs whose coordinates are net lift (L_n) and net lift-to-drag ratio (L_n/D_n) or net drag (D_n). These factors of lift and drag are the only parameters common to both the balloon and cable that allow a separate solution of each component and later joining to determine compatible systems.

Typical curves of L_n/D versus L_n developed by the balloons and required by tapered glass fiber cables (designed for a factor of safety of 2) are superimposed in Figure 30.15. Data have been computed for each of three maximum altitudes; 60,000, 80,000 and 100,000 feet and represent tether requirements to support tethers from these altitudes down to 20,000 feet. An intermediate balloon and tether is required to complete the system to the ground. On Figure 30.15, the intersection of the balloon and tether curves for a given altitude provides the required balloon size. Natural shape balloon volumes are noted in cubic feet. A streamlined balloon for the 20,000 foot altitude location can be obtained in a similar manner using data such as those given in Figure 30.16 for a streamlined balloon based on 90 percentile winds. Drag and lift characteristics are plotted as a function of balloon volume and angle of attack. In selecting the lower balloon size and

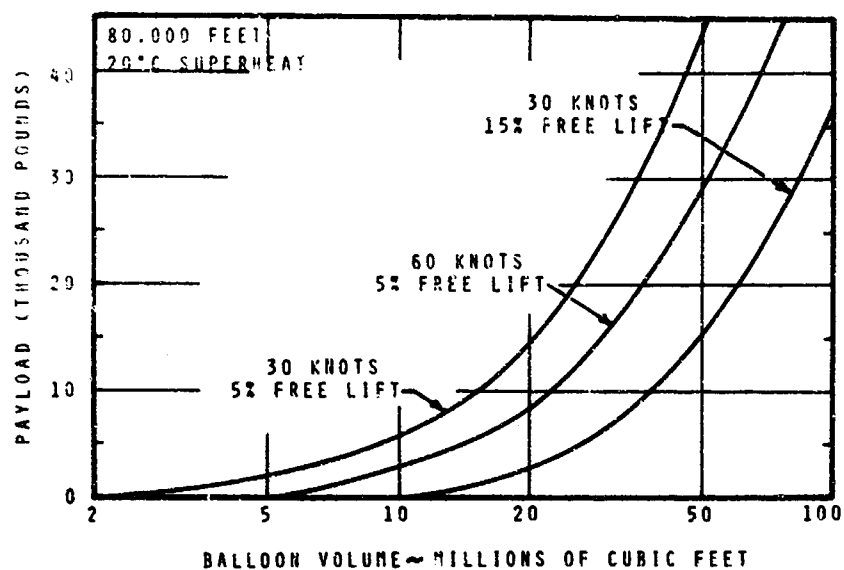


Figure 30.14. Payload for Microwave Powered Streamlined Balloons

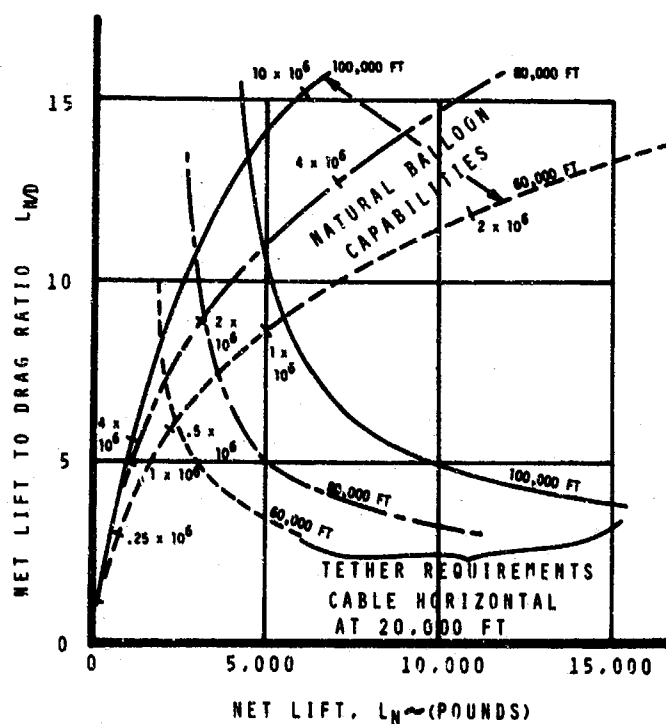


Figure 30.15. Natural Balloon Capabilities and Tether Requirements

tether, account must be taken of the tension exerted by the upper balloon and cable.

Using these techniques, a tethered balloon system for each of the three altitudes is outlined in Figure 30.17. It is desirable to keep the lower altitude balloon below the regions of maximum wind velocity to minimize structural requirements, as has been done for the 20,000 foot altitude. Volumetric change requirements are also minimized for lower altitude balloon design. The very high altitude balloon operating in low density air develops much less drag and can therefore be a natural shape balloon.

30.5 TETHERED BALLOON WITH PROPULSION SYSTEM

Using data available from previously discussed parametric studies, brief consideration was given to incorporating a balloon with an electric propulsion system for a 15 knot airspeed capability (power source No. 3) in a tethered system. It was found that a 5 million cubic foot, natural shape, powered balloon is required for the 80,000 foot altitude condition as compared to a 2 million cubic foot natural balloon used in the pure tethered balloon system. The L_n/D_n for the powered balloon was somewhat less, indicating that net drag is higher for this system in a 30 knot wind even though the propulsion system counterbalances some of the aerodynamic drag. This results because the balloon is larger. This example, therefore, does not indicate an advantage for this powered tethered balloon.

30.6 BALLOON TETHERED TO AN AIRSHIP

Payloads can be flown at an altitude of 60,000 feet or more by means of a balloon tethered to a low flying (10,000 feet above MSL) airship. The airship is the only feasible airborne vehicle for such an application. Its high speed is in the vicinity of normal wind speeds for tethered balloon design, and it is capable of very low speed and long endurance. Minimum tethered-balloon system designs for this concept are outlined in Figure 30.18.

This approach offers a flexibility to a tethered balloon system not heretofore exploited. Mobility is provided, permitting positioning regardless of terrain. Additional protection is provided the balloon-payload combination aloft by the airship's ability to vary airspeed and direction. The airship can run with the wind, if necessary, to protect the upper payload. The balloon aloft is also spared the weight of tether otherwise necessary to reach the ground.

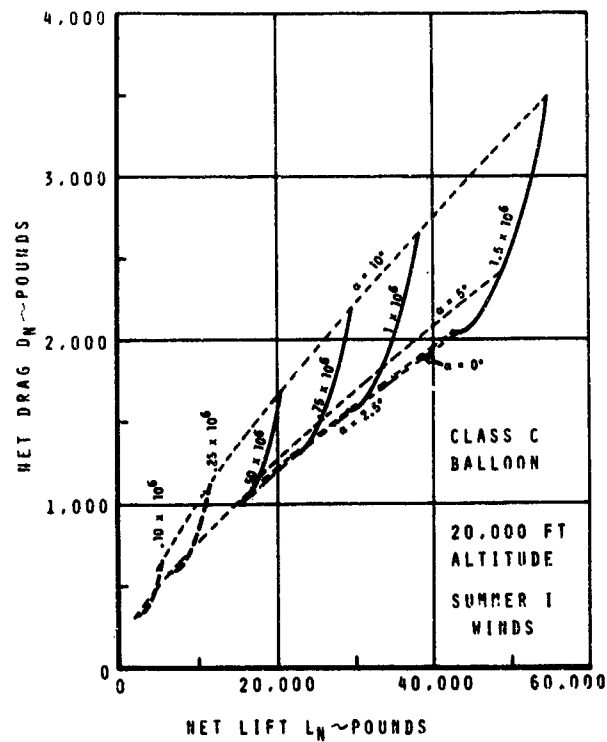
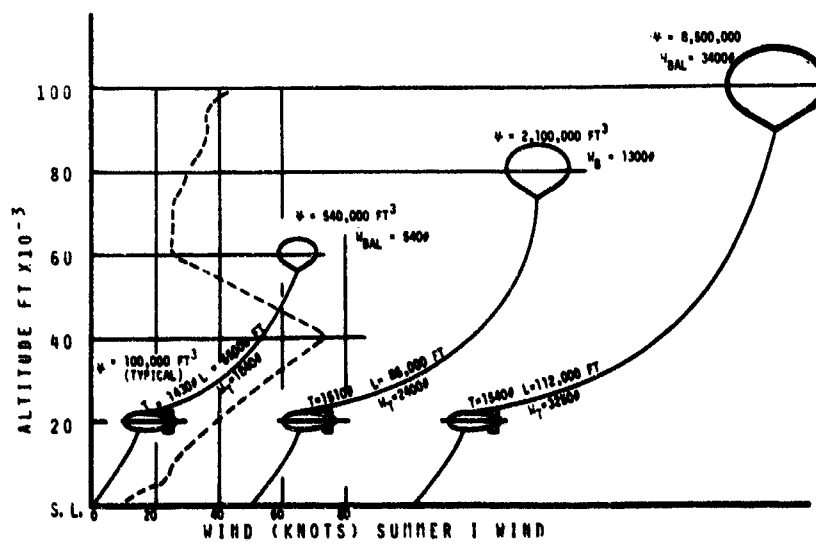


Figure 30.16. Streamlined Balloon Capabilities



The airship-launched, high-altitude, tethered balloon represents an aerial version of Elliott's mobile launch scheme. The airship has complete three-dimensional mobility, whereas Elliott's test road permitted him to run with the wind as long as the wind was reasonably along the direction of the road. The airship depicted in Figure 30.19 is a modified ZPG-3W airship stripped of electronics and radar antennas. The topside island structure is redesigned or modified to provide a large skylight opening for deploying and retrieving the high altitude balloon. The balloon room below the island (within the airship envelope) contains a handling winch, plumbing for helium, work space and storage space for the balloon. The balloon can be inflated from the airship envelope helium.

If the topside balloon is to be "transfused" with helium from the ZPG-3W airship, inflation would have to begin at about 6000 feet of altitude. If top balloon helium is not recovered by 3W, this loss (9 percent of 3W volume) for the 80,000 foot altitude balloon has to be allowed for in larger ballonnet design.

For deployment, the airship might be weighed off at 6,000 feet to neutral buoyancy by dropping disposable ballast, as necessary. Deployment of the high altitude balloon can thus be accomplished while "free ballooning" so that no relative wind exists on the two vehicles.

The balloon is paid out in a free ballooning mode until differential winds warrant flying the airship with the winds to minimize aerodynamic loads on the balloon aloft. After design altitude has been reached, the airship may be flown at speeds and directions indicated by the mission plan and the existing wind profiles.

The airship requires a winch of adequate tether storage capacity and, ideally, capable of "live" towing. A series of winches with limited storage capacity were developed during the 1950's for a number of models of Navy blimps. At that time the requirement was "live" towing of a submerged sonar listening device. The winches were hydraulically powered and capable of automatic or manual reel-out and reel-in to limit towing loads.

Recovery of the upper balloon will probably be initiated by a valving of some of the balloon's helium, to minimize reel-in loads. The airship is again flown so as to minimize aerodynamic loads on the descending balloon. Final recovery would be in a free-balloon mode. Recovery of the remaining upper balloon helium probably is not warranted as such an operation would prolong the final recovery and pose rather difficult plumbing problems.

30.7 COMPARISON OF STATION-KEEPING BALLOON CONCEPTS

In summary, a preliminary comparison of balloon systems discussed in this paper is outlined in Table 30.1. The condition chosen for comparison is support

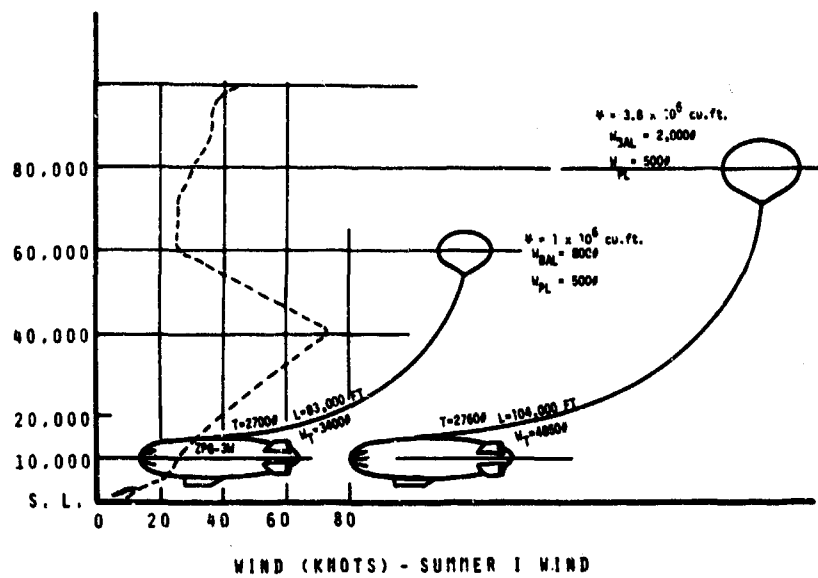


Figure 30.18. Tethered Balloons with an Airship

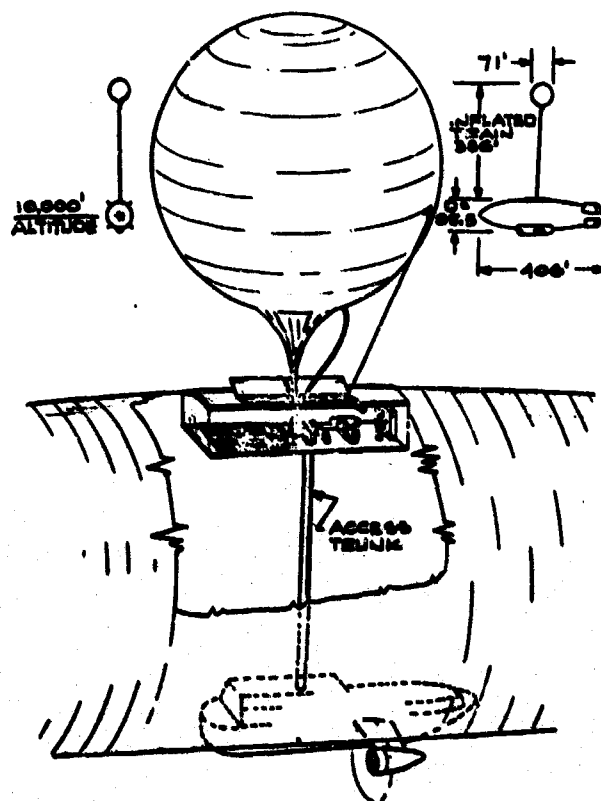


Figure 30.19. Deployment of a Tethered Balloon from an Airship

of a payload of 500 pounds at an altitude of 80,000 feet in winds up to 30 knots. It is apparent from an examination of this table that self-powered, streamlined balloons are substantially smaller than natural balloons. This is true even though the streamlined balloons employ higher strength envelopes to provide superpressure for extended flight capability.

Ground-based microwave power permits even smaller streamlined balloons. The passive, natural shape, tethered balloons are smaller yet, but are limited in endurance because of the ballast requirement for zero pressure balloons. It is possible to consider the development of natural shape superpressure balloons for extended flight to eliminate the ballasting requirement.

The major advantages and disadvantages of the station-keeping balloon concepts are listed in Table 30.2 for comparative purposes. All concepts require development work to bring them into being. Of the concepts tabulated, the natural balloon powered with batteries requires the minimum effort. The other concepts require development in varying degrees.

Before a station-keeping balloon system concept can be recommended, a more detailed definition of concepts is required. This definition for a specific mission would provide a basis for comparison and selection. However, the preliminary conceptual descriptions in this paper offer some possible solution to the general problem of station keeping and an indication of how some of the major parameters influence the nature of the balloon systems.

Table 30.1. Comparison of Station-Keeping Balloon Concepts.
Payload - 500 lb; Altitude - 80,000 ft; and Airspeed - 30 knots.

CONCEPT	ENDUR- ANCE	POWER CYCLE	BALLOON SIZE (CU FT)
1. Natural Balloon (Batteries)	1 day	Half Time Day and Night (D. L. =0.25) Half Time Day and Night (D. L. =0.10)	60×10^6 16×10^6
2. Natural Balloon (Batteries and Solar Cells)	4 days	Half Time Day and Night (D. L. =0.10)	36×10^6
3. Streamlined Balloon (Batteries and Solar Cells)	>30 days >30 days >>30 days	Daytime Only Half Time Day and Night Half Time Day and Night	2×10^6 (5% Free Lift) 5.2×10^6 (5% Free Lift) 26×10^6 (15% Free Lift)

(Continued on next page)

Table 30.1. Comparison of Station-Keeping Balloon Concepts (Cont.)

CONCEPT	ENDUR- ANCE	POWER CYCLE	BALLOON SIZE (CU FT)
4. Streamlined Balloon (Microwave Power)	>30 days >>30 days	Continuous Continuous	3.2×10^6 (5% Free Lift) 13×10^6 (15% Free Lift)
5. Tethered Balloon	1 day	None	2.1×10^6 at 80,000 ft 0.1×10^6 at 20,000 ft
6. Tethered Balloon	4 days	None	3.4×10^6 at 80,000 ft 0.1×10^6 at 20,000 ft
7. Airship with Teth- ered Balloon	1 day	570 BHP at Airship 232 lb fuel/hr	3.8×10^6 at 80,000 ft 1.5×10^6 at 10,000 ft

Table 30.2. Advantages and Disadvantages of Station-Keeping Balloon Concepts

	ADVANTAGES	DISADVANTAGES
1. Natural Balloon (Self-Electric Propulsion)	Simple Design Less Expensive Balloon Mobile Controllable	High Drag Large Power Requirements Large Volume
2. Streamlined Balloon (Self-Electric Propulsion)	Smaller Total Volume Lower Propulsion Require- ments Greater Endurance Mobile Controllable	More Complex Balloon De- sign and Construction Large Size Balloon for Super Pressure Construc- tion
3. Streamlined Balloon (Ground Power Electric Propulsion)	Minimum Sizes for Powered Remote-Controlled Flight	Same as Item 2 Above Plus: Steerable Ground Dish and Ground Power System Required Must Stay Within Range of Near-Vertical Beam
4. Tethered Balloon	Minimum Sizes for 1 to 4 Day Durations Passive Aerial Systems	Substantial Ground Winch Installation Required Two-Balloon System for Smaller Upper Balloon High Strength to Weight Tethers Require Develop- ment

Table 30. 2. Advantages and Disadvantages of Station-Keeping Balloon Concepts (Cont.)

	ADVANTAGES	DISADVANTAGES
5. Airship with Tethered Balloon	<p>Three-Dimensional Mobility with Piloted Tow Vehicle</p> <p>No Wind Deployment by Free Ballooning</p> <p>ZPG-3W Airship Design Appropriate Without Extensive Redesign</p> <p>Missions Not Limited by Ordinary Ground Wind Conditions</p> <p>Helicopter Refueling Possible for Extended Missions</p>	<p>Expensive Launch and Tow Vehicle</p> <p>Development of Large Airborne Winch Required</p>

References

- Brown, W. C. (1969) Experiments Involving a Microwave Beam to Power and Position a Helicopter, Raytheon Company, IEEE Transactions on Aerospace and Electronic Systems, September 1969 Vol. AES-5, Number 5.
- Elliott, S. D. Jr., (1964, 1965) Tethered Aerological Balloon System, in Proceedings, 1964, AFCRL Scientific Balloon Symposium - AFCRL 65-486; July 1965, Air Force Cambridge Research Laboratories.
- Graham, J. C. (1969) A Survey of the Potential of Beamed Microwave Power for Balloons, Raytheon Company, presented at the Symposium of the American Society of Photogrammetry, 6 - 7 February 1969.
- Hamilton, R. C. (1968) Performance, Analysis and Selection of Balloon Electrical Power Systems, Research Paper P-455, Institute for Defense Analyses, December 1968.
- Shirland, F. A. (1968) Forestieri, A. F., and Spakowski, A. E., Status of the Cadmium Sulfide Thin Film Solar Cell, presented at the Intersociety Energy Conversion Engineering Conference, Boulder, Colorado, 13 - 16 August 1968.
- Vorachek, J. J. (1968) Investigation of Powered Lighter-Than-Air Vehicles, AFCRL-68-0626, 27 November 1968.
- Vorachek, J. J. (1968) Concept for an Extremely High Altitude Tethered Balloon System, in proceedings, Fifth AFCRL Scientific Balloon Symposium AFCRL-68-0661, December 1968, Air Force Cambridge Research Laboratories.
- Young, E. F. Capt., (1968) Tethered Balloons: Present and Future, AIAA Paper No. 68-941, Presented at the AIAA Second Aerodynamic Deceleration Systems Conference, 23 - 25 September 1968.

Contents

31.1	Introduction	384
31.2	Description of Program	384
31.3	Description of the Equipment	385
31.4	Tests and Results	386
31.5	Conclusions	390
31.6	Super Skytacular	390

31. Recent Airship Developments and Applications

R.R. Fisher and R.S. Ross
Goodyear Aerospace Corporation
Akron, Ohio

Abstract

A recently conducted program utilized a Goodyear advertising type airship in the development of a "special mission" vehicle capable of manned or droned operation. The vehicle, which carried a variety of special hardware, demonstrated the unique capabilities of the LTA vehicle in sustained low speed flight, low altitude surveillance, and quiet operation. The flexibility of the airship in the mounting of hardware and other equipment and in its adaptation to a unique stern propulsion arrangement was also illustrated.

Envelope physical size permitted listening and direction finding on ground noise sources. The peculiar characteristics of helium also were of unique benefit in this specific program.

The latest Goodyear advertising airship, the "America", features the modified Navy "L"-ship car and a 200,000 cubic foot envelope. A larger, fan-cooled engine installation, improved envelope pressure system, improved rudder control, and a turbine-powered APU for electrical supply during the night-sign operation have been added. The four-color animated night sign, pioneered on the "Mayflower" several years ago, has been enlarged and improved with simplified electronics and animation techniques, and magnetic tape control.

PRECEDING PAGE BLANK

31.1 INTRODUCTION

Recently, under contract to Army Missile Command, Goodyear Aerospace Corporation was requested to conduct a series of tests to investigate unique capabilities of lighter-than-air vehicles for possible new mission concepts. Conventional aircraft of the fixed and rotary wing types suffer inherent limitations as they are extended into flight regimes which are quieter, slower, and smoother than previously possible.

At this particular time, Goodyear was building larger, more elaborate airships to replace the advertising fleet then in operation. One airship, the Mayflower, upon retirement became available for this test program. It was stripped of all advertising signs and supporting equipment, and placed in an experimental status so that changes could be made to it without the need for full FAA certification.

Although this airship was relatively small, limiting the payload that could be carried, it demonstrated very successfully the tremendous potential that is available in powered lighter-than-air craft as aerial platforms. This was particularly true regarding smoothness and silence of flight, as well as the ability to operate under complete control at airspeeds as low as five miles per hour. Hovering, or free ballooning where the relative velocity was zero miles per hour, was also demonstrated. The presence of the helium-filled envelope permitted listening tests never before attempted.

As a result of this program, new mission considerations for lighter-than-air vehicles can be planned with reasonable confidence of success.

31.2 DESCRIPTION OF PROGRAM

Three major objectives were to be demonstrated. First, controlled flight at airspeeds of 5 to 15 miles per hour was an unexplored region that was to be investigated with the full-scale airship. Free ballooning, or balanced uncontrolled flight at zero relative velocity, was a well known and useful emergency procedure. Controlled flight as low as 15 to 20 miles per hour was in the normal operating range. However, analytical studies, including computer runs, showed that in the region between 5 and 15 miles per hour, control reversal was probable with conventional control systems. If at some future date the airship might be under automatic control or droned, it would be advantageous to eliminate this control reversal or at least know enough about it to provide appropriate compensation. It was, therefore, decided to operate in this speed range and check the control performance so that plans for its presence could be realistically evaluated in future vehicles.

The second major objective was to demonstrate how quietly the airship could be made to operate. Many attempts at silent flight are under investigation with fixed and rotary wing vehicles; however, to support its weight, each of these types requires the relatively fast movement of some component through the air, such as the rotor or the wing. This movement in itself causes sound, limiting the minimum possible acoustic signature of the vehicle. Since the airship supports its weight primarily with the lifting gas, helium, in a completely silent manner, the major noise would result from propulsion. If this propulsion requirement were minimized, such as by reducing the speed, a completely new realm of silent operation would be possible. A quiet propulsion system was, therefore, to be demonstrated on this airship and it was to be flown at a low altitude, hopefully, undetectable by the human ear.

The third objective was to fly this quiet vehicle with GFE hardware on board and demonstrate how a stable, silent airship can be a useful platform capable of performing observation missions not completely achievable with conventional heavier-than-air craft.

With these three objectives in mind, a series of modifications, test flights, and analytical studies were performed that established the airship capability and generated the data needed for the development of a future mission vehicle. Not only were all the objectives achieved, but the airship also demonstrated several unique capabilities of safety and versatility that should be considered in evaluating the worth of the concept.

31.3 DESCRIPTION OF THE EQUIPMENT

Although very specific data were collected using a variety of instruments, for the purpose of this paper the equipment will be described only in general terms so that the impact of the overall achievements is not lost in detailed discussions of what was used and how it was used. These details are, of course, needed when trying to establish the engineering data necessary to design and build future systems, but this paper will cover primarily the importance of the broad findings which influence forward planning.

The airship used was the former Goodyear advertising airship, Mayflower, which had an envelope volume of 147,300 cubic feet, a length of 160 feet, and a diameter of 51 feet. It was propelled by two, 175 horsepower Continental engines driving variable-pitch pusher propellers. The car was 23 feet long and could carry a half dozen people when empty. The airship was stripped of all unnecessary gear to make it as light as possible so that modification and test equipment could be carried (see Figure 31.1).



Figure 31.1. Mayflower Modified for Sensor Test Program

In order to achieve silent flight at speeds between 5 and 15 miles per hour, a stern drive was installed. It consisted of a three-blade, slow turning, 20-foot diameter propeller assembled from modified helicopter blades, rigidly attached to a hub in a manner that permitted ground adjustment of the blade angles. This hub was then attached to a hydraulic motor supported by a gimbal arrangement that provided means for tipping the propeller plane for control of thrust direction. This motor was supplied by hydraulic lines from an electrically driven pump placed in the car. The entire stern propulsion

assembly was supported on a metal structure laced to the envelope. The electric motor and pump were housed in an acoustically treated container to minimize noise output (see Figure 31.2).

During one test, in order to reduce the weight of the airship even further, one engine was completely removed from the airship. The electric motor-hydraulic pump installation was mounted outside the car in place of this engine, to maintain the weight balance across the plane of symmetry. Take-offs were successfully performed with the single unsymmetrical drive system, a feat not usually even to be considered for a heavier-than-air vehicle (see Figure 31.3).

A variety of GFE hardware was attached to the envelope and also suspended below the airship on a trailing wire. The envelope was an ideal background for this equipment, and it was simple to apply another "patch" whenever a new location was desired for a piece of equipment. Even the heavy battery case that supplied the power was supported on the envelope. It was located ahead of the car to balance the weight of the stern drive system (see Figure 31.4).

Optical equipment and vibration measuring instruments were located on the car or other structure, as particular tests required. Low-light-level television was used and most of the tests were conducted at night. Data were collected on oscillograph, television and acoustic tapes, and measurements were made of performance of all the equipment.

31.4 TESTS AND RESULTS

In order to demonstrate the controllability of the airship at low velocities, it was flown with conventional engines stopped, utilizing stern drive only at varying

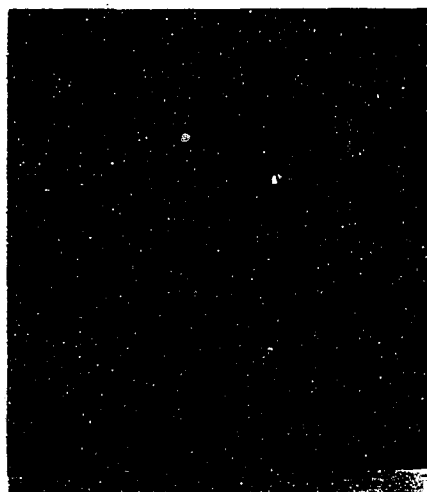


Figure 31.2. Stern Propulsion Assembly



Figure 31.3. Power Source for Stern Drive Replaced One Engine

settings of rudders, elevators, and gimbals. At all speeds from 5 to 15 miles per hour it was possible to turn the airship by the use of the rudders alone, gimbals alone, or in combination. The air flow over the control surfaces from the proximity of the stern drive improved the surface effectiveness. In this arrangement the rudders alone were more effective than the gimbal alone; however, the

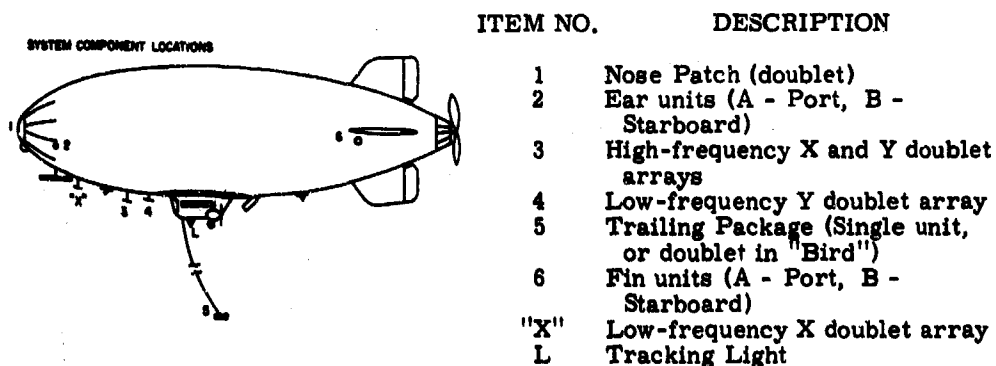


Figure 31.4. A Typical Installation

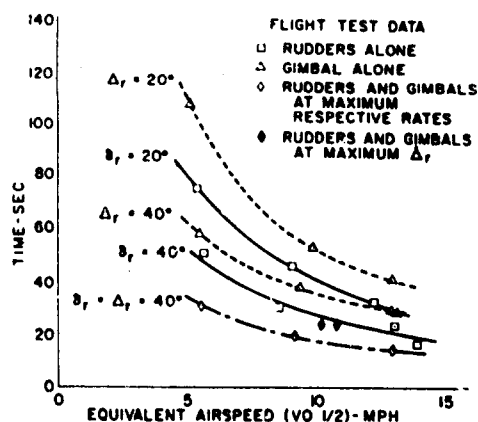


Figure 31.5. Time to Achieve 45° Heading Change

most effective system was the combination of rudders and gimbaled propeller which gave very satisfactory turning rates at all speeds tested (see Figures 31.5 and 31.6).

An attempt was made to check the reversal of control that was predicted to take place in pitch at low velocities. This was a little difficult to locate at first, because the reversal was so subtle. Actually, it does occur in the speed range between 5 and 15 miles per hour, depending on the heaviness or lightness of the vehicle. The true climb or descent rate, however, is so slow that it takes quite a

while to recognize that reversal has actually occurred. A human pilot, therefore, handles it as a flight technique. An autopilot, however, would have to anticipate it or the reversal would have to be eliminated. Several methods were studied for changing the control at this flight condition and perhaps the simplest techniques were to use bow elevators, or a ballonet system to trim the airship by movement of ballonet air fore or aft. Both can readily be accomplished and provided for on a mission vehicle. Adding bow elevators adds another feature, the ability to rise and descend without pitching the airship itself, if this should be desirable for some reason (see Figure 31.7).

Another unusual and unexpected finding was made. The airship itself, despite its size, was not visible to the naked eye during these night flights. This was despite the fact it was still silver in color and flying at altitudes between 300 and 1,000 feet. Undoubtedly under certain moonlight conditions it would have been visible; however, during these tests these conditions did not exist.

Microphones placed on the airship were used to record sounds emanating from various sources. These were both natural sounds and self-generated. It is interesting to note how the helium-filled envelope could be used to obtain stereophonic effects because of its size and the ability to separate microphones far from one another. It also acted as a deflector of sound; a nose-mounted microphone could detect far ground noises even when a nearby engine on the car was running. The difference in sound transmission properties through helium and air can be used to advantage.

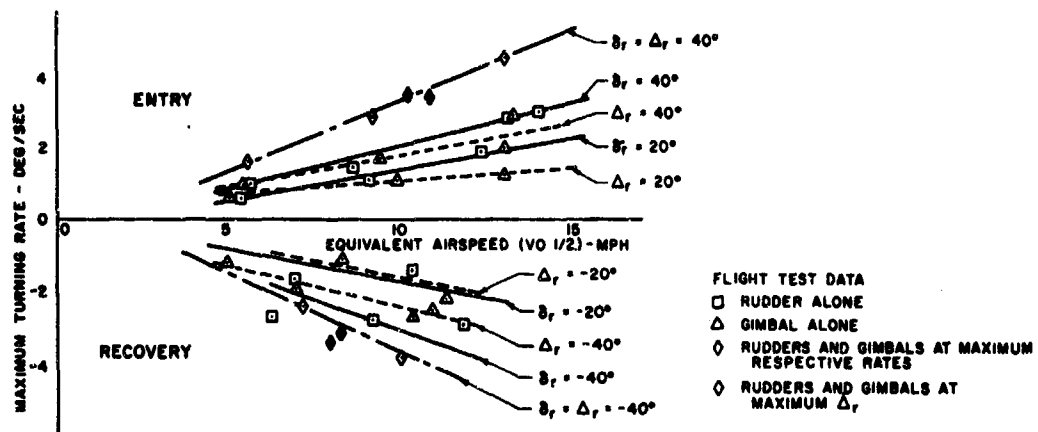


Figure 31.6. Maximum Turning Rate Performance

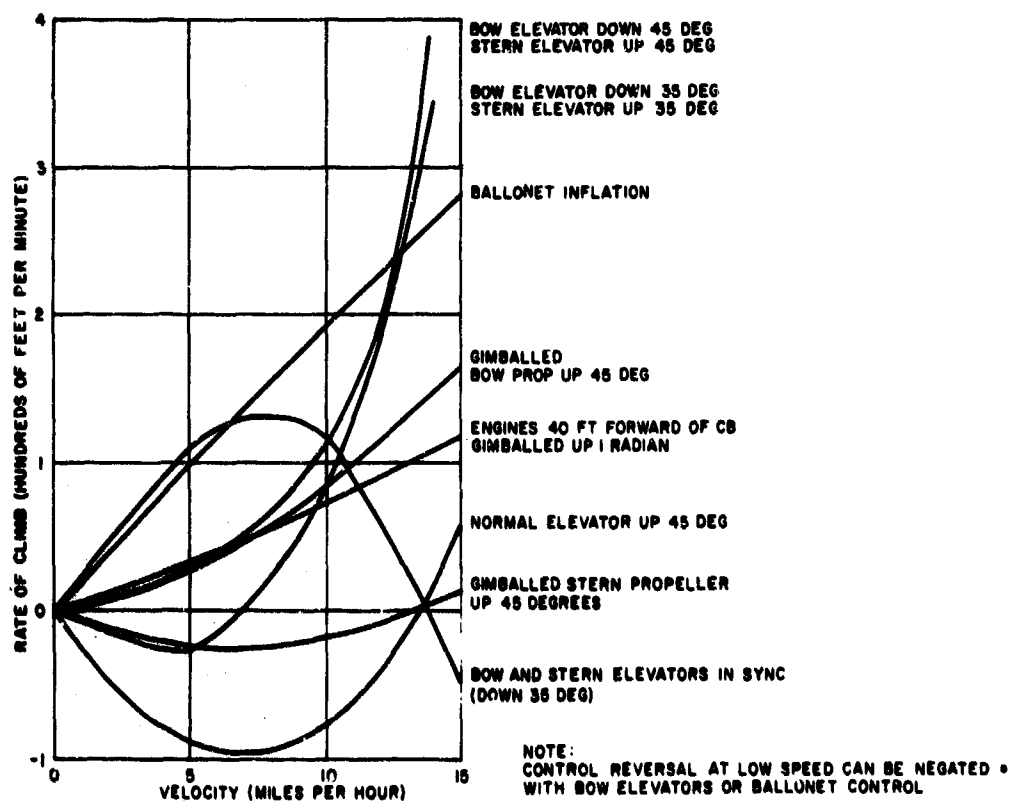


Figure 31.7. Performance of Candidate Low-Speed-Control Systems

31.5 CONCLUSIONS

From the data collected on these first tests using the airship as an observation base, the following conclusions were reached:

- (1) A silent airship can be built with complete control to minimum flight speeds of 5 miles per hour.
- (2) A low rpm stern propeller can be an effective drive for such an airship.
- (3) In the event that it is desired to drone this vehicle, reversal of control in pitch can be eliminated by the use of bow elevators or ballonnet trim.
- (4) The airship envelope is an ideal base for mounting various types of hardware because of its size and ability to shield from extraneous noises.
- (5) Under most reasonably steady wind conditions, the airship can hover relatively motionless with respect to the ground.
- (6) Microphones lowered from the airship can be used effectively to pick up discrete sounds.
- (7) The airship is surprisingly invisible to the naked eye on dark nights.
- (8) The airship possesses safety features of engine-out performance not possible in any other aircraft. Actually, the results can be summed up in one conclusive sentence. The airship possesses unique platform characteristics not possible with any other aircraft and should be given serious consideration for missions previously not believed feasible.

31.6 SUPER SKYTACULAR

This report has discussed the modification of a Goodyear advertising airship into a silent test vehicle. This part of the report will cover the upgrading of the lighter-than-air advertising fleet with a larger airship carrying a more spectacular electric sign. It illustrates the combining of a number of aerospace talents to perform a commercial, good-will project.

The blimp envelope itself has a new volume of 202,700 cubic feet instead of the former 147,300 cubic feet. This resulted in a length increase from 160 feet to 192 feet with about the same width of 50 feet. The new envelope is made of neoprene-coated Dacron and contains ballonets which give it a maximum ceiling of 7500 feet (see Figure 31.8).

The car is essentially the same one used on previous advertising airships upgraded to support twin six-cylinder, 210 hp engines instead of the previous 175 hp units. It is about 23 feet long, eight feet high and can carry six passengers plus the pilot. This gives the new airship a maximum speed of 50 mph with a cruise speed of 30-35 mph.

The major reason for the larger airship is the new sign it carries on each side of the envelope. These are 105 feet long and 24.5 feet high; each includes 3780 specially designed lamps inside red, blue, green and yellow reflectors interconnected by 80 miles of wiring. This sign, known as 'Super Skytacular', can spell out messages and enliven them with animated cartoon, all in color. Words of messages and animation can run in either direction or up and down. When the airship is flying at 1,000 feet, it can be read by people on the ground a mile away from the airship (see Figure 31.9).

The messages are made on exotic electronic equipment in a special lab in Akron. A technician "draws" the animation and copy on a cathode ray tube with a light gun. From there a computer takes over, and the process results in a magnetic data tape. A typical six-minute tape consists of 40 million pieces or bits of "on-off" information which, when run through special electronic readers aboard the airship, control lamp and color selection and the speed at which messages are run (see Figures 31.10, 31.11 and 31.12).

When this night sign is used, a special auxiliary power unit is carried underneath the car. It contains a small jet engine enclosed in a pod, driving a 500-ampere, 28-volt direct current generator.

This lighted sign, the first of its kind to employ color and animation, is used primarily for public service messages in behalf of non-profit charities and service organizations. Special animated messages in color have been developed for the holiday seasons, such as Santa, his sleigh and reindeer at

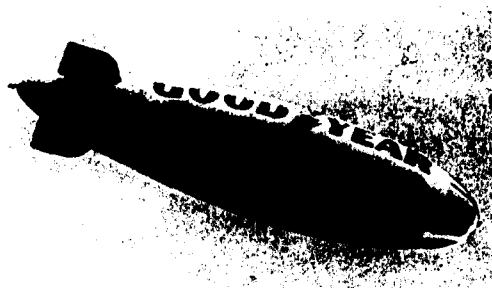


Figure 31.8. The New Airship "America" Showing the Super Skytacular Sign

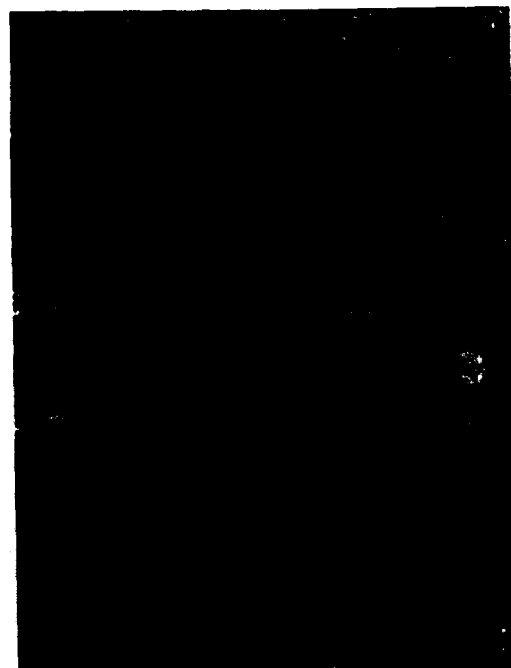


Figure 31.9. Sign at Night



Figure 31.10. Animations are "Born" in an Electronic Lab



Figure 31.11. A Light Gun is Used to "Draw" Patterns and Cartoons on a Screen

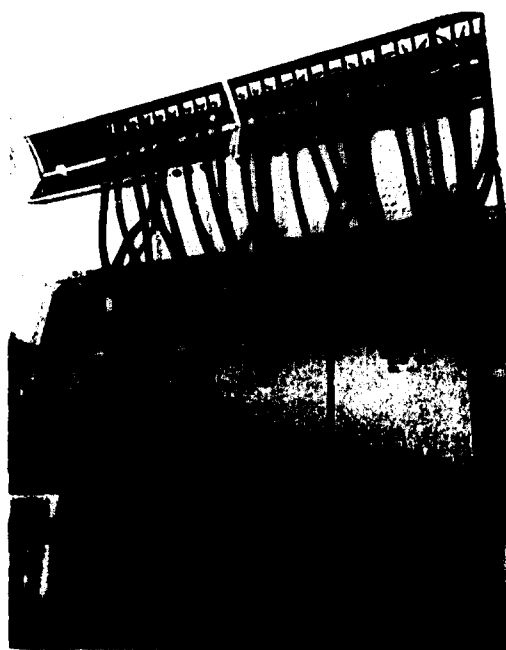


Figure 31.12. Decoding and Associated Equipment that Controls the Sign



Figure 31.13. The Star Spangled Banner Flies Proudly on the Super Skytacular Sign

Yuletide, a turkey escaping an ax-wielding man at Thanksgiving, and Fourth of July firecrackers exploding to form an American flag (see Figure 31.13).

In addition to serving Goodyear's own public relations program, the airships also are in great demand by the nation's news media, particularly television networks for use as aerial camera platforms for special events.

To maintain the airship, a crew of 22 is used; five pilots, a public relations representative and 16 crewmen, some of whom are engine, radio, electronics and structural experts. With four specially-equipped ground-support vehicles, the airship crew is almost self-sustaining in the field, as far as operation and maintenance of the blimp is concerned. The caravan of vehicles travels by highway, with the blimp flying overhead.

A bus, specifically designed for the operation, serves as a flight center and communications headquarters on tour. It is equipped with two-way aviation radio, all administrative aids necessary for the operation and a special mast for landing the blimp if it should be necessary during a cross-country mission.

A large tractor-trailer rig serves as a mobile maintenance facility. The tractor unit includes a machine shop, night sign and television equipment lab and helium purification unit. The trailer also carries the main mast, spare parts and supplementary equipment.

A station wagon and sedan round out the rolling stock, and are used for ground liaison work and crew transportation.

All special vehicles are equipped with two-way radios for contact with each other or the airship.

Safety is the primary factor in the overall airship operation.

Each airship travels more than 100,000 air miles a year and carries approximately 8,000 passengers. Goodyear airships, past and present, have operated for more than five decades without a single passenger fatality.

Contents

32.1	Introduction	395
32.2	Basic Criteria	396
32.3	Computer Sizing of Balloons	398
32.4	Tethers	400
32.5	Balloon and Tether Combination	400
32.6	Summary	404
32.7	Computer Patterning	408
32.8	Conclusions	408

32. Engineering Considerations for a Tethered Balloon System Below the Tropopause

P.F. Myers
Goodyear Aerospace Corporation
Akron, Ohio

Abstract

The trade-off considerations for a tethered system to approximately 25,000 feet above mean sea level are discussed. Considerations include payload weight, altitude, design wind, wind profile, temperature, time on station, and balloon L/D (including both static and dynamic lift).

Single balloon and multiple balloon arrangements will be suggested. The use of the computer for "blow-down" solutions of various operational wind profiles and of alternate balloon systems permits rapid and inexpensive optimizing of the system to suit specific design criteria. The computer can also generate and draw the full-size gore templates for the balloon hull shape selected and the volume determined as necessary.

32.1 INTRODUCTION

Two years ago I had the pleasure of assembling the "Tethered Balloon Handbook" under the sponsorship of our hosts, the Air Force Cambridge Research Laboratories. At that time it was apparent that though the balloon fraternity may be small in number, they are large of heart. I should like to thank those of you whom I have previously

PRECEDING PAGE BLANK

met only by phone or letter, for invaluable assistance in assembling the information in that volume.

I shall always remember the remark made to me by a gentleman from New Mexico State University. He said, "Balloons are like children. They're all different. You just have to love them!" I think we would all agree that, with balloons as well as with children, although it may be essential, love alone is not enough and there are times when love is more than difficult.

32.2 BASIC CRITERIA

32.2.1 General

This paper will describe some of the engineering methodology of tethered-balloon system design which has been developed and which makes great use of computer assistance. A considerable amount of data must, of course, be pre-digested and organized before the computer can be trusted with it.

32.2.2 Customer Requirements

The customer requirements for a tethered balloon system ordinarily specify a payload weight, flight altitude, and operational winds. The customer is frequently not knowledgeable as to the cost effects of design winds on the balloon system and must often be guided in this regard by the balloon designer.

The sizing of a balloon-tether system is a three-fold proposition. The design survival wind will generate maximum tether tensions and - for a given factor of safety - size the tether line. The "hot" atmospheric requirement will determine minimal static lift which may be insufficient to raise the weight of the previously selected tether to design altitude. Finally the operational wind will result in a down wind excursion, or "blow-down", of the balloon, necessitating a greater length of tether out to maintain design altitude. The total aerostatic and aerodynamic characteristics of the balloon and wind profile to the ground will be involved in this third aspect of the problem. Sometimes there will be additional constraints as to the down-wind excursion permissible.

32.2.3 Design Winds

Everyone here is undoubtedly familiar with the typical wind profiles, which normally peak in velocity and dynamic pressure in the neighborhood of 40,000 feet. Tethered balloon systems are sensibly engineered to stay below, or fly above, those altitudes of peak dynamic pressure. While this paper will describe the techniques of sizing a balloon system for below 25,000 feet, the techniques described are equally applicable to all altitudes.

Figure 32.1 presents the wind profiles desired by the customer whose problem I have chosen to follow for this paper. His payload was three hundred pounds, his altitude 20,000 feet above the terrain—the operating site being 2,000 feet above mean sea level. At the operational wind, the balloon was to be at design altitude despite "blow-down", and at survival it was, of course, to survive.

Figure 32.2 is a representation of the winds of 15,000 feet being carried from sea level to design altitude along lines of equal dynamic pressure. These four "survival" winds were the basis for evaluating the cost of appropriate designs for increased wind capability. The aim is to steer an optimum course between the size and cost of over-design and the disappointment of under-design.

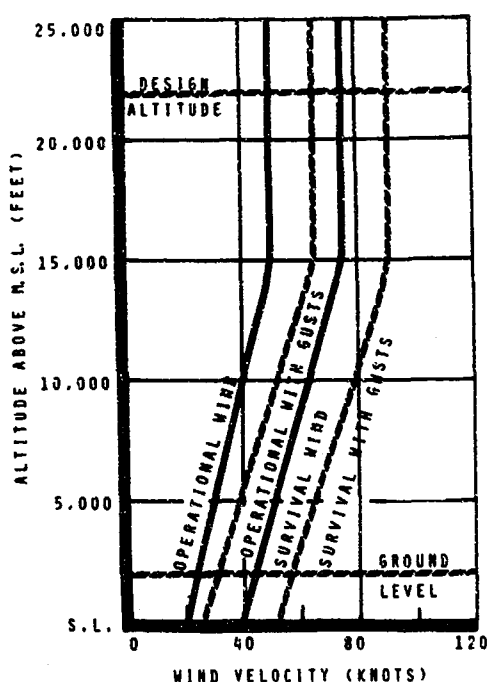


Figure 32.1 Initial Design Criteria

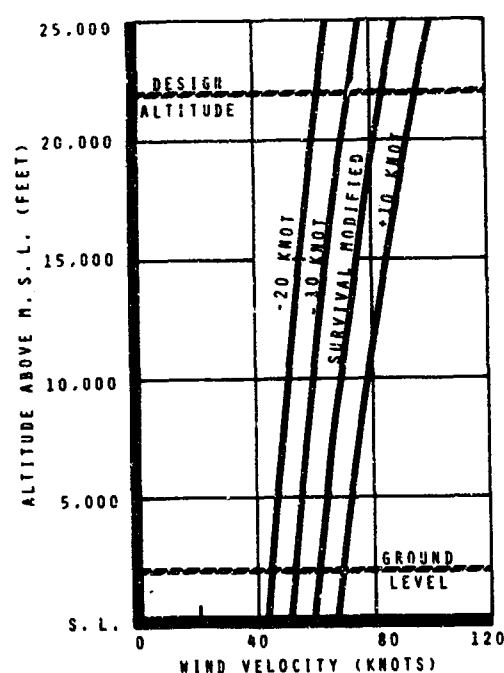


Figure 32.2 Winds for Parametric Study

32.2.4 Balloon Types

Figures 32.3 and 32.4 are the two aerodynamic balloon configurations involved in the present exercise, a single-hull shape and the VEE-BALLOON*. Other shapes, including the natural shape, could of course be used with the appropriate weight and aerodynamic characteristics fed to the computer.

*Registered Trademark, Goodyear Aerospace Corporation, Akron, Ohio

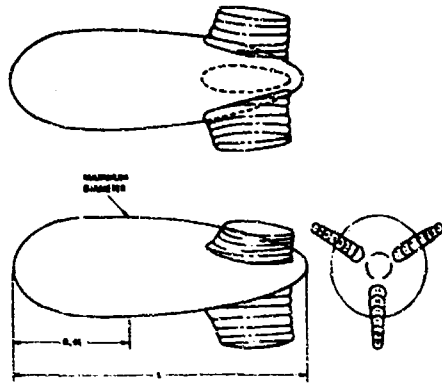


Figure 32.3. Class C and Ram Air C Configuration

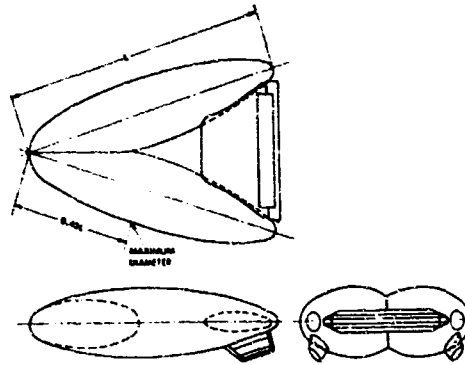


Figure 32.4. VEE-BALLOON Configuration

32.3 COMPUTER SIZING OF BALLOONS

The computer is provided the C_L and C_D values, static lift values, fabric strength and weights, dynamic pressure requirements for design, blower weights, battery weights for specified time on station, and all the multitude of details making up a specific balloon. Table 32.1 is a typical print-out for one particular balloon of single hull configuration for a given altitude, payload, and design wind.

32.3.1 Assumptions for Computer Sizing of Balloons

A number of assumptions must be made and provided the computer before it can print out such a solution. The assumptions involved in the present case are listed below:

- (1) The internal design pressure is equal to 1/4 inch of water pressure (1.30 psf) greater than the external dynamic pressure, to prevent bow cave-in.
- (2) The suspension system is assumed to distribute the tether load along the hull in such a manner that the bending moment stresses in the hull become of secondary importance and can be neglected in this "first pass" solution.
- (3) Stresses in the hull fabric are computed from three loadings: internal pressure, buoyant lift, and aerodynamic loading. These stresses are determined for the most severely loaded cross section, and result in a unit material weight which is conservatively used over the entire hull surface.
- (4) The fabric factor of safety is set at 3.00 for the stresses determined above.
- (5) The angle of attack is assumed equal to 5° as the design (survival) wind acts. A bungee system in the suspension allows the angle of attack to be $7\frac{1}{2}^\circ$ in the operational wind, for the systems studied.

Table 32.1. Computer Printout Data for a Class C Balloon Configuration

COMPUTER INPUT DATA:	. Payload	. Altitude
	. Velocity	. Angle of Attack
	. Volume	. Operating Time
	. Lift and Drag Coefficients = f (angle of attack)	
Hull unit fabric weight (lb/ft ²).....	Blower operating time at	
Stagnation pressure (lb/ft ²).....	altitude (min/day).....	
Design stress, includes	Buoyant stress by tether tension	
safety factor of 3 (lb/ft).....	(lb/ft).....	
Hull length (ft).....	Weight of hull seams (lb).....	
Projection area of 1 horiz.....	Weight of 1 horiz tail (lb).....	
tail (ft ²).....	Weight of 1 vert. tail (lb).....	
Wetted area of 1 horiz tail (ft ²).....	Weight of blower (lb).....	
Thickness of vert. tail, avg (ft).....	Weight of check valve (lb).....	
Total volume of balloon (ft ³).....	Weight of misc equip, battery and	
Wetted area of spherical	blower (lb).....	
ballonet (ft ²).....	Weight of handling lines and	
Volume lost by leakage	catenary (lb).....	
(ft ³ /day).....	Net lift (lb).....	
Volume flow thru blower (ft ³).....	Drag (lb).....	
Aerodynamic stress by tether	Wetted hull(s) area (ft).....	
tension (lb/ft).....	Location of max diameter (ft).....	
Weight of hull fabric (lb).....	Thickness of horiz tail, avg	
Weight of intersect attachments (lb).....	(ft).....	
Weight of internal partitions of	Volume of 1 vert. tail (ft ³).....	
horiz tail (lb).....	Diameter of spherical ballonet	
Weight of internal partitions of	(ft ³).....	
vert. tail (lb).....	Volume flow rate of blower	
Weight of exit value (lb).....	(ft ³ /min).....	
Weight of ballonet seams and	Volume to replace each day	
attachments (lb).....	(ft ³ /day).....	
Weight of suspension system (lb).....	Max stress due to inflation	
Buoyant lift (lb).....	(lb/ft).....	
Balloon weight (lb).....	Intersect weight (lb).....	
Unit lift (lb/ft ³).....	Weight of attachments of 1	
Internal design pressure	horiz tail (lb).....	
(lb/ft ²).....	Weight of attachments of 1	
Max hull diameter (ft).....	vert. tail (lb).....	
Projected vert. tail (ft ²).....	Weight of batteries (lb).....	
Wetted area of 1 vert. tail (ft ²).....	Weight of ballonet (lb).....	
Volume of 1 horiz tail (ft ³).....	Aerodynamic lift (lb).....	
Ballonet volume (ft ³).....	Lift coefficient.....	
Intersect area (ft ²).....	Drag coefficient.....	
Volume req'd for temp change		
(ft ³ /day).....		

Item (4) fabric factor of safety, is an unfortunate phrasing, as it does not denote the usual "margin of safety" of conventional hard structure usage. It is a necessary factor with fabric which is a material subject to creep-rupture effects. Were a factor of 1.00 to be used, very immediate and "quick-break" failure would result.

32.4 TETHERS

32.4.1 General

Tether tension will ordinarily be a maximum at the attachment to the balloon. Balloon loads applied to the tether are a combination of the total lift, both static and dynamic, and drag force. The net L/D defines the angle from the vertical at which the tether must ride at its attachment to the balloon. The angle of attack of the balloon will depend upon its static trim and the characteristics of the balloon and the suspension with which it is provided. Tether cable tension will reduce as one travels down the tether, since less and less weight is hanging below as one descends the tether.

32.4.2 Tether Constructions

A variety of tether constructions are available using different basic materials. Basic tether parameters include weight, diameter, and cost as a function of breaking strength. The best strength/weight ratio is by no means the only criterion; it could be accompanied by larger cable diameters, in which case the aerodynamic loads acting on a long length can prove to be surprisingly serious. The altitude excursion involved and the wind profile are most pertinent, and the designer must beware of making intuitive choices in his selection of a tether construction.

The example being followed in this paper makes use of the Glastran* cable, which is admittedly a controversial choice. The study from which I have extracted one example actually compared systems utilizing tethers of Glastran, rocket wire, and nylon 2-in-1 construction. The primary parameters for the computer "blow-down" solutions are cable weight per foot and cable diameter.

32.5 BALLOON AND TETHER COMBINATION

32.5.1 Minimum Lift and Survival Requirement

Table 32.2 is a typical computer determination for a particular balloon type at design altitude and for a specific design survival wind. For a series of volumes

*Trademark of Packard Electric Division of General Motors

Table 32.2. Balloon Data Selected for Class C Hull, Single-Balloon Survival Wind - 10 Knot Modified

DESIGN CONDITIONS:									
Payload		= 300 lbs		Angle of Attack		= 5.0°			
Float Altitude		= 22,000 ft		Hull Volume		= Variable			
Wind Velocity		= 124.14 ft/sec (Survival - 10k Wind) Mod		Operating Time		= 120 hours			
				Hull Type		= Single Hull			
Volume (cu. ft)	L _{buoyant} (lbs)	L _{aero} (lbs)	W _{bal} (lbs)	D _{aero} (lbs)	L _{bHot} (lbs)	Net Hot Day Lift (lbs)	T [*] Max Cable Tension (lbs)	Balloon Lifting Capacity + 20 (lbs/1000 ft)	
50,000	1,820	2,723	915	1,145	1,590	375	3,522	18.75	
100,000	3,643	4,322	1,704	1,817	3,200	1,196	6,233	59.7	
200,000	7,287	6,861	3,323	2,885	6,350	2,727	10,914	136	
300,000	10,931	8,991	5,017	3,780	9,500	4,193	15,087	207	
400,000	14,514	10,892	6,738	4,579	12,700	5,642	18,989	282	
500,000	18,218	12,639	8,485	5,314	15,850	7,095	22,703	354	
600,000	21,862	14,273	10,255	6,001	19,050	8,450	26,275	423	

$$*T = \sqrt{(L_b + L_a - W_{bal} - W_{pl})^2 + D_a^2}$$

static lifts are calculated both for a standard day and for the "Military Hot Day".* The latter condition determines minimum static lift. For the standard day, static lift combined with aerodynamic lift and drag (columns 2, 3, and 5) reduced by the calculated balloon weight and specified payload weight (column 4 + 300 pounds), determines maximum cable tension (column 8). The "Hot Day" buoyant lift (column 6) reduced by the balloon weight and payload weight, with the resultant divided by 20 (for 20,000 feet of altitude excursion) provides the balloon minimal lifting capability in units of 1,000 feet. Figure 32.5 is a plot of this balloon capability plotted with Glastran cable breaking strengths versus weight/1,000 feet. A vertical from a given size (and weight) tether to the balloon curve below indicates the minimum volume balloon which can maintain that weight tether to altitude on the "Hot Day". With a smaller balloon we have a "ground-loving" system—or at least one which cannot achieve the requisite altitude on the "Hot Day".

A horizontal from the balloon curve gives the design survival wind tether load. A vertical from the same point on the balloon curve to the cable curve gives the cable breaking strength. The ratio of the two values is the factor of safety of the tether at design wind for the specific balloon-tether combination.

The example being presented is only one of sixteen which were involved in the actual study: two balloon configurations, one- and two-balloon systems, and four design winds. Each tether construction of interest can be another sixteen problems. Only the use of computer techniques permits such voluminous comparisons.

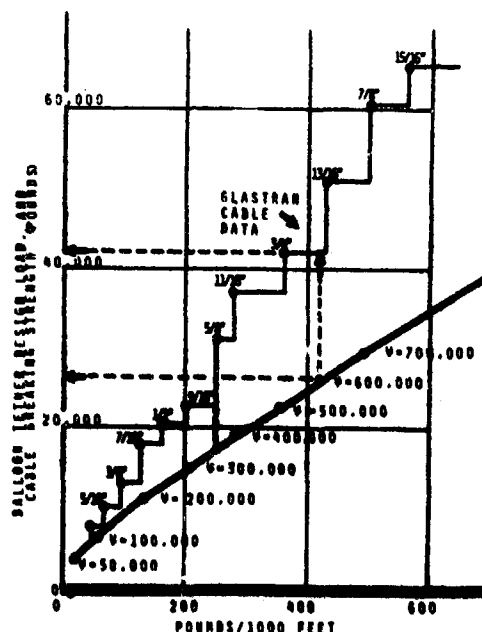


Figure 32.5 Cable Breaking Strength vs Cable Weight, and Tether Design Load vs Balloon Minimum Lift

32.5.2 Cost Comparison of Systems

The studies so far described define and compare the systems on the basis of statics. Total cost is normally a vital concern and will frequently have much to do with the final choice. For this reason, a relative cost index may be established for every element of the system providing a total comparative cost index for each system.

*M'l-Std-210-A

The components making up the cost index are those major elements which are expected to influence the final system cost by reason of variations in size or configuration. These components include the balloon, cable, winch and other ground support equipment, helium storage, and spares for all system components.

32.5.3 Safety Factors

Figure 32.6 presents the tether safety factors for a survival wind, and the operational wind. The typical sawtooth shape is a result of the "Hot Day" lift limitation, which — as one travels to the left on the curves — necessitates a lighter tether at a given balloon volume.

32.5.4 Blow-Down Solution

The "blow-down" problem is solved very neatly by a computer program. The tether of interest is hung at design altitude on the balloon as a skyhook defined by the net lift and drag of the balloon at that altitude and at the operational wind. As stated earlier, the total net L/D defines the angle off the vertical at which the tether begins its descent. The computer is provided the tether diameter, weight, wind profile, and atmospheric characteristics — either standard or non-standard. The computer then integrates the tether curve, determining tether lift and drag loadings as the tether angle changes. The print-out includes: X, the upwind displacement from the balloon; Z, the altitude descent; Phi, the angle off the vertical; T, the tether tension in pounds; and the accumulating tether total length. A tapering tether can be investigated by providing a suitable diminishing diameter and

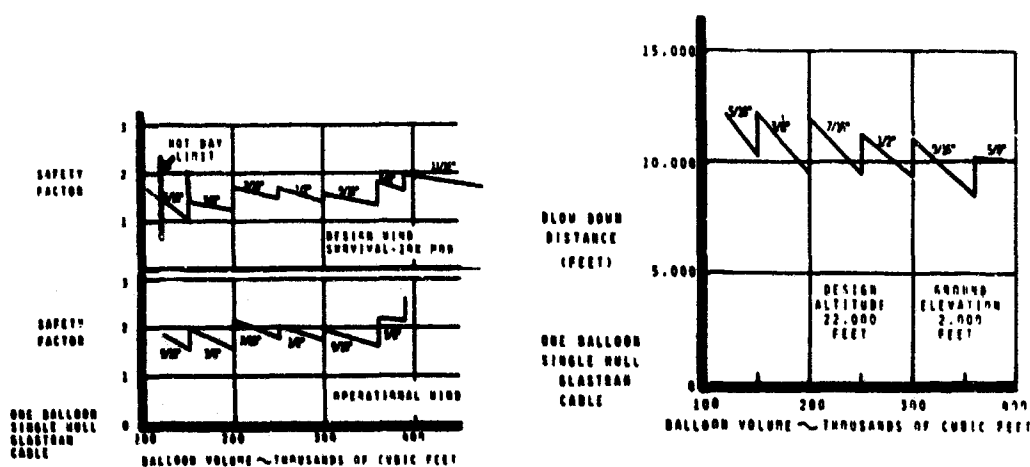


Figure 32.6 Tether Safety Factors

Figure 32.7 Balloon Downwind Displacement

weight. The program is not restricted to two-dimensional wind profiles, but can integrate the effects on a tether for varying winds from any direction of the compass.

If the angle Φ reaches 90° before the requisite lower altitude has been reached, the system under investigation does not have the operational wind and altitude capability. The altitude at which tether angle reaches 90° would represent the lowest altitude at which a second balloon would have to be brought into the total system, and practically this would be done at a higher altitude.

Figure 32.7 shows the class C, single-balloon, downwind excursion in the operational wind. The design altitude of 20,000 feet above the terrain will be accompanied by a downwind excursion of from 8,000 to 12,000 feet, a function of balloon volume and tether size.

32.6 SUMMARY

32.6.1 Cost Comparisons

Figure 32.8 presents the relative cost of the example single-hull, single-balloon system for a specific design survival wind. Figure 32.9 illustrates a number of the sixteen balloon systems studied. Where no solution is given, it merely means that — in the words of the native giving directions to the tourist — "you just can't get there from here" — with the system assumed.

Figure 32.10 illustrates the cost effect for the class C hull of one- or two-balloon systems and variation in design survival wind. Figure 32.11 presents individual class C balloon volume requirements.

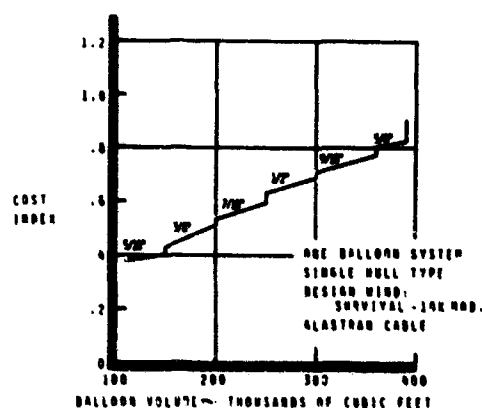


Figure 32.8. Relative Cost, Single-Balloon System

32.6.2 Wind Performance Capability

Figure 32.12 represents the per cent of wind velocities at the design altitude and desired flying site. The four design survival winds used for balloon comparison are presented as the four vertical stripes to the right of the illustration. Figure 32.13 shows a specific two-balloon system cost index as affected by design survival wind. Not surprisingly, the more expensive the system, the greater per cent of the time it may be flown — at least from a design standpoint.

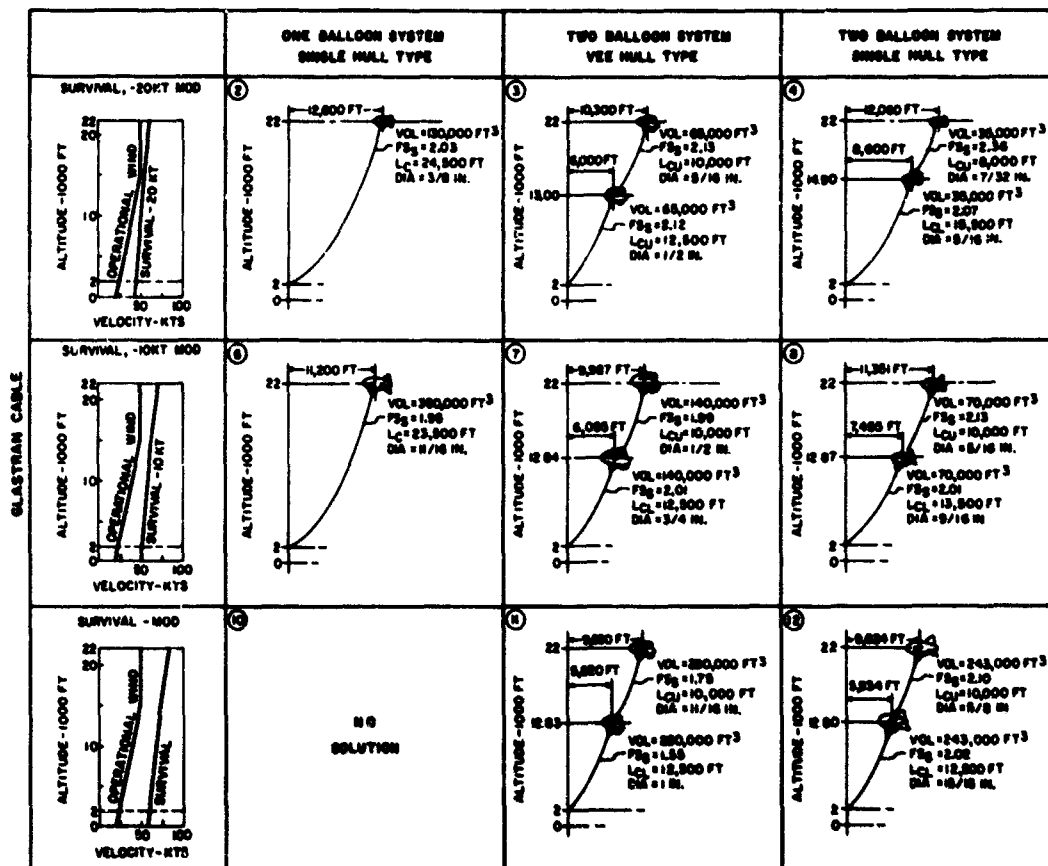


Figure 32.9. Summary of Optimum Systems

32.6.3 Tether Life Expectancy

Figure 23.14 is a presentation of creep-rupture data for three tether materials. The data is somewhat less than desirable; work in this area is far from complete.

Figure 32.15 presents, above, the average winds of Figure 32.12 and, below, a plot of a given cable safety factor at zero wind, operational wind, and design survival wind. For a significant range, the two curves are broken into four segments, the average cable safety factor determined and the percentage of winds that occur for each segment.

Table 32.3 and Figure 32.16 summarize the values on the basis of a 50-day utilization. The indication is that 8.3 percent of the tether working life has been expended, implying that the tether may be expected to provide 300 days of flying life.

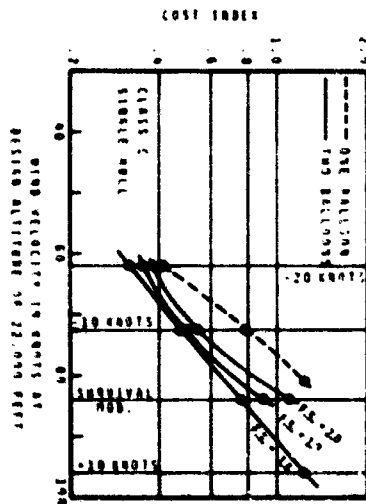


Figure 32.10. Relative Costs, Competitive Systems

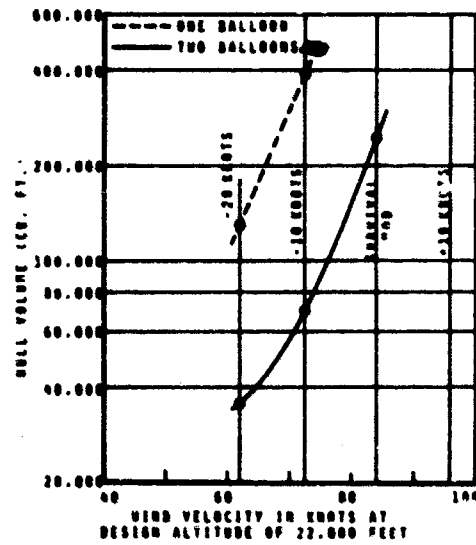


Figure 32.11. Individual Balloon Sizes, Competitive Systems

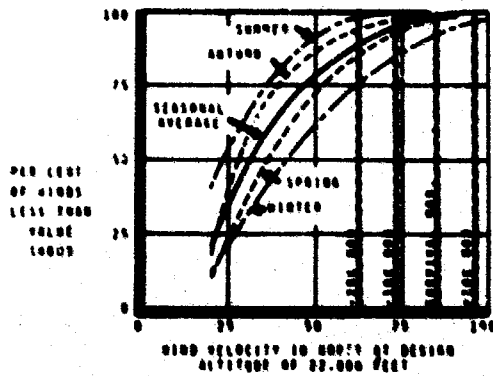


Figure 32.12. Seasonal Wind Distribution at Flying Site

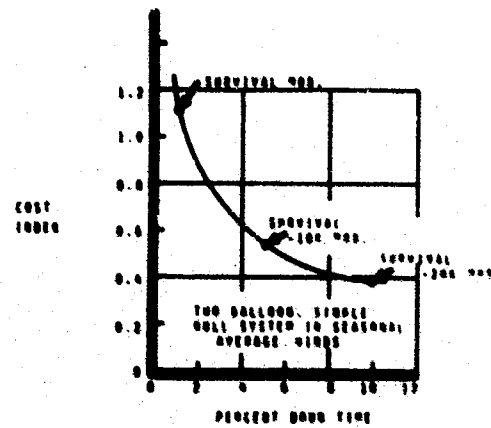


Figure 32.13. Down Time vs Relative Cost

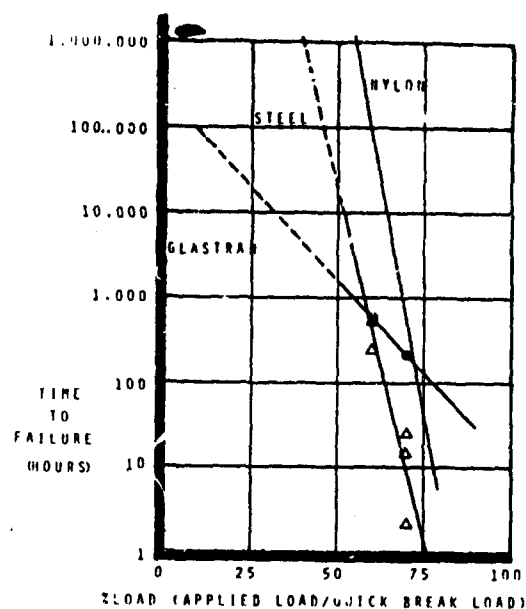


Figure 32.14. Time to Failure Data, Tethers

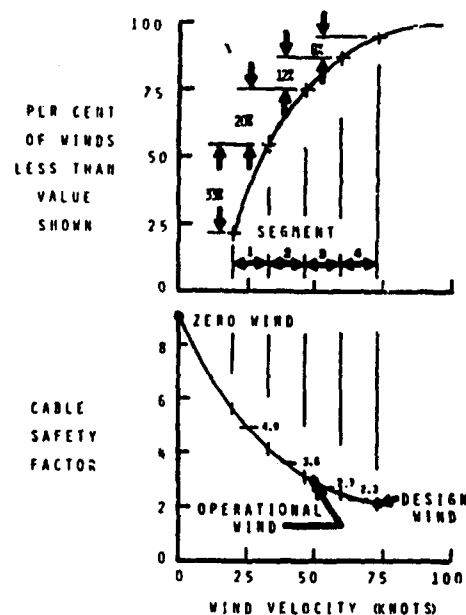


Figure 32.15. Correlation of Wind and Cable Safety Factor

Table 32.3. Summary of Creep Rupture Life Factors Glastran Cable

Segment	Average Safety Factor	% of Winds Occurring	Length of Time Winds Occur for a 50-Day Flight	Time to Failure	% of Life Used
1	4.9	33	396 hours	32,000 hours	1.24
2	3.6	20	240 hours	17,000 hours	1.41
3	2.7	12	144 hours	5,700 hours	2.52
4	2.3	8	96 hours	3,100 hours	3.10
Total					8.27
$\text{Total Life} = \frac{(50 \text{ days})}{.0827} = 604 \text{ days}$					

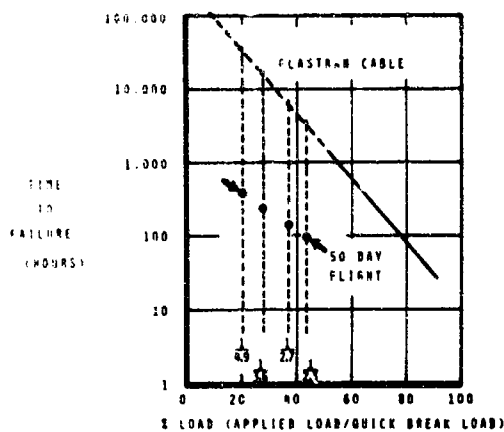


Figure 32.16. Tether Cable Life Expectancy

32.7 COMPUTER PATTERNING

One of the final problems in which the computer excels is the production of working patterns. With a balloon volume determined, a typical solid-body-of-revolution can be patterned very rapidly. All that is needed is the equation of the body and the number of gores from which it is to be patterned. Printout can be in the form of dimensional tabulation or actual full-size drawn templates. The accommodating computer will even provide a parallel lap seam line, if so programmed.

32.8 CONCLUSION

With increasing material-data accumulation and computer comparison techniques, the balloon designer is able to make more knowledgeable determinations at a minimum cost and provide his customer with the most reliable system to satisfy his specific requirements.

References

- Conley, W. F. (1967) High-Altitude Tethered Balloon Design, Goodyear Aerospace Corporation, AFCRL Tethered Balloon Workshop.
- Hoerner, S. F. (1958) Fluid Dynamic Drag (published by the author), Midland Park, New Jersey.
- Menke, J. A. (1967) High Altitude Tethered Balloon Systems Study, Goodyear Aerospace Corporation, GER 13260.
- Myers, P. F. (1968) Tethered Balloon Handbook, Goodyear Aerospace Corporation, AFCRL-69-0017.
- Speed, L. A. (1967) Some Aspects of High-Altitude Tethered Balloon Flight, Ministry of Technology, Cardington, England, AFCRL Tethered Balloon Workshop.
- Vorachek, J. J. (1968) Concept for an Extremely High-Altitude Tethered Balloon System, Goodyear Aerospace Corporation, Fifth AFCRL Scientific Balloon Symposium, AFCRL-68-0661.

Young, E. F. (1968) Tethered Balloons; Present and Future, AIAA Paper No. 68-841.

MIL-STD-210 A (1957) Climatic Extremes for Military Equipment.

U.S. Standard Atmosphere (1962) N.A.S.A., U.S.A.F., U.S. Weather Bureau.

Contents

33.1 Fair Site	412
33.2 Mark II Balloon Tether Winch	414
33.3 Summary	420

33. Fair Site and the Mark II Balloon Tether Winch

L.A. Grass
Air Force Cambridge Research Laboratories
Bedford, Massachusetts

K.J. Turner and D.C. Cox
Otis Engineering Corporation
A Halliburton Company
Dallas, Texas

Abstract

This paper discusses the Mark II Balloon Tether Winch which was developed for permanent installation at the Fair Site, White Sands Missile Range, Holloman AFB, New Mexico. This site will be operated by Detachment 1, AFCRL, Holloman AFB, New Mexico. Several unique features of the winch system and the Fair Site will be discussed.

The winch systems were designed to accommodate most known tethered balloon systems, with the ability to be expanded to future increases in balloon magnitude and altitude. Features are incorporated to take advantage of future developments in materials and physical construction of tether lines. Major winch components are arranged so that increased capacity stowage drums and more complex systems can be made with a minimum expense and alteration.

Visual aids will be employed to assist in presenting a general explanation of the Mark II Winch. The control system, main hydraulic system, capstan drive, and the stowage drum drive will be discussed. A "Servo Wind", level-wind system was developed to spool the tether line on the drum without gear adjustments when changing line sizes. A line clamp device with deceleration features is employed

PRECEDING PAGE BLANK

to clamp and hold the moving tether cable with a minimum of shock on the line or tethered balloon. In general, the Mark II Winch is a deviation from the conventional approach to line pulling mechanism.

33.1 FAIR SITE

Increasing interest in the application of tethered balloons for research studies over the past decade has involved AFCRL's Aerospace Instrumentation Laboratory - a natural outgrowth of its free ballooning activities. Many times AFCRL Detachment 1, Balloon R & D Test Branch, located at Holloman Air Force Base, New Mexico, has been called upon to support research projects using a temporary tethered site near the Detachment 1 facility.

Nearly 200 tethered balloon flights of varying configurations have been made over the past few years. Notable were: (1) the tethered balloon platforms provided for NASA's Surveyor vehicle, (2) a tether system for the Circus Day balloon which attained an altitude of 12,000 feet MSL, (3) currently, three line tethered flights to 2,000 feet above ground for the Army's Project HOMINE and (4) evaluation tests for the Athena Project, Office of White Sands Missile Range.

As a result of the increase in tethered programs and the potential for extended capabilities, a permanent tethered balloon site was obviously needed. The site should: (1) be capable of routinely handling payloads of 500 pounds or less to altitudes of 10,000 feet above ground, (2) not be encumbered by other programs, (3) be in a restricted air space area to permit flight durations of hours to weeks and (4) the area should allow for equipment expansions to accommodate development tests and operations of tethered systems of much greater payload altitude capabilities. With this in mind, the Aerospace Instrumentation Laboratory has been constructing a permanent ground handling site located on the White Sand Missile Range, New Mexico. This site, now under construction, will be called the Fair Site.

This site is located in the northwest corner of a restricted area, R-5107-B, on the White Sands Missile Range. It is approximately 70 land miles from the Detachment 1, Balloon R & D Test Branch facilities located at Holloman AFB, New Mexico. Here, tethered balloons can be flown to unlimited altitudes with the only restrictions being range scheduling. Meteorological conditions have been investigated fully, and the climatology indicates a good year-round flight capability. The site has the advantage of a fully instrumented range to provide data essential in evaluating tethered balloon systems.

Position data for tethered balloon flights can be obtained using either FPS-16 radars or cinetheodolites or both. If radar is used, a position display can be set up at the Balloon Control Center or at some Range Control Station. Velocities, accelerations and balloon altitude data can be obtained from the cinetheodolites. Data reduction can be provided through WSMR. In addition to the cinetheodolites and radars, facilities for receiving F.M. telemetry are also available.

Range Accuracy:

- (1) FPS-16 Radar (two radars available)
 - (a) Balloon at 10,000 ft. with transponder.
Max. error ± 15 yards in range.
Max. error $\pm 0.3^\circ$ azimuth and elevation.
 - (b) Balloon at 10,000 ft. with reflector.
Max. error ± 50 yards in range.
Max. error $\pm 0.3^\circ$ azimuth and elevation.
- (2) Cinetheodolite
 - (a) Balloon at 10,000 ft.
Slant range error of ± 6 ft. in position.

Figure 33.1 depicts the site layout. Two main winch systems are shown, each of which is used in conjunction with a common ground zero. The ground-zero

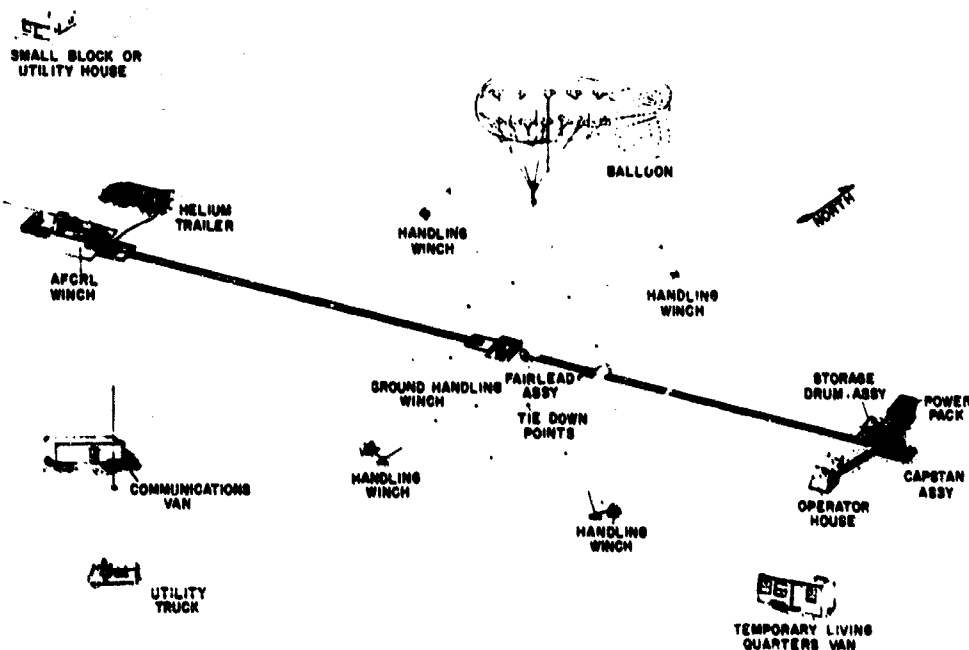


Figure 33.1. Fair Site Showing Typical Tether Operations with the Mark II Winch on the Right and the AFCRL Winch on the Trailer at Left

position incorporates both a 20-inch and 30-inch diameter sheave. Between the two sheaves is located a ground handling winch capable of handling 30,000 lbs at speeds of approximately 20 feet per minute. The purpose of this winch is to facilitate the ground handling of the balloon and payload. Located at ground zero are inner and outer anchor points. The inner anchor points are used to secure a cable system forming a pyramid used to moor barrage balloons. It is possible to moor a barrage balloon on this pyramid in winds up to 25-30 knots. In winds in excess of 30 knots, the balloon will be moored on a heavy steel cable approximately 100 feet above the ground.

The outer anchor points are used in the initial handling of the balloon. During balloon inflation, it is important that the nose of the balloon heads directly into the wind. Placement of the outer anchor points have been made to permit ten different directions. These directions will permit alignment of the balloon within 18° of any given wind direction. The ground handling winches have been positioned in such a manner that only four will be required to operate the system.

This site has been designed to handle a wide variety of tethered balloon systems. The AFCRL mobile winch on the left is capable of loads up to 4,000 pounds at speeds of approximately 300 feet per minute. The winch is capable of speeds up to 1,000 feet per minute at reduced loads in the range of a 1,000 pounds. The winch has been designed to handle cable sizes of 1/16-inch diameter to 3/8-inch diameter. The unique level wind provided by Otis Engineering Corporation can accommodate cable sizes from 1/8-inch to 3/8-inch diameter without changing drums or level wind systems. The cable is stowed on a drum at tensions between 150 to 300 pounds coming directly off the traction drive. The instrument pad is used to measure the cable speed, footage and load at ground zero. Reading at sheave is provided with approximately 1 percent accuracy of the full scale readings. The AFCRL winch positioned in Figure 33.1 illustrates the use of a mobile winch in a permanent site configuration. The winch can also be used remotely where the balloon can be flown directly from the winch at any location.

Depicted on the right is the Mark II Winch. This winch will be permanently located at the Fair Site and has been specifically designed for use at this facility. The winch is capable of controlled speeds up to 1,000 feet per minute and loads of 30,000 pounds. Mr. Turner of Otis Engineering Corporation will discuss the operational characteristics of the Mark II Winch with you in greater detail.

33.2 MARK II BALLOON TETHER WINCH

Otis Engineering Corporation, a Halliburton Company, was awarded the contract to develop and manufacture the Mark II Balloon Tether Winch in early 1969.

The performance specifications established the following requirements:

- (1) Line pull capabilities of 30,000 pounds maximum at a maximum speed of 200 feet per minute.
- (2) Line pull capabilities of 6,000 pounds at line speeds of 1,000 feet per minute.
- (3) Variable speed control in each of the above modes.
- (4) Fail-safe brake system.
- (5) Interchangeable sheave and capstan shoes.
- (6) Drum capacity to 30,000 feet of 1/2-inch diameter line.
- (7) The capability of accommodating line sizes from 3/8-inch through 3/4-inch diameter.
- (8) Level wind system capable of storing these line sizes uniformly on the stowage drum and adjustable for 3/8-inch through 3/4-inch with 1/16-inch variation in diameter.
- (9) Instrumentation consists of a line load measuring device, line footage counting device, line speed and direction measuring device.
- (10) Other instruments included those items necessary to monitor the operation of the power source and the hydraulic drive system.

The design was, then, predicated around five major components: (1) the main capstan pulling unit, (2) the main power source, (3) the stowage drum, (4) control house, and (5) the ground-zero fairlead sheaves and ground handling winch.

The main capstan assembly (Figure 33.2) consists of two 30-inch pitch diameter multi-grooved sheaves with interchangeable shoes attached to the outer periphery of the main sheave wheels. The interchangeable shoes are coated with polyurethane to provide a resilient surface for the line to bear on. The shoes are provided with six grooves to obtain the necessary friction to provide line pulls up to 30,000 pounds without the line slipping in the grooves.

The capstan unit contains a weight-indicating sheave which provides a change in direction of the high-load line leaving the capstan. This change in direction of the high-load line leaving the capstan provides a point where the resultant forces can be utilized to measure the tension in the line. The exit point



Figure 33.2. Main Capstan Drive Showing the Hydraulic Input Side with Gear Boxes

from the capstan measuring sheave to the fairlead sheave is made with no reverse bends in the line. The weight-measuring sheave is positioned in the near center of a large yoke and is free to rotate about its center axle. The yoke is pivoted at the lower end; line tension at the sheave produces a moment, exerting a force on the load cell at the upper end of the yoke. The hydraulic load-cell pressure, resulting from the force applied, is monitored by one of two pressure gauges. One is calibrated to read 0 to 30,000 pounds and one is calibrated to read 0 to 10,000 pounds. The direct-reading gauges are calibrated from the resultant of the line tension and the included angle.

The line speed and counting device is also attached to the main capstan and measures the speed in feet per minute of the line when inhauling or outhauling. It also measures the length of line payed out or pulled in.

The capstan is provided with a two-phase input power system. The high-speed phase is accomplished through an axial piston hydraulic motor, which supplies torque through a planetary-gear transmission directly into the lower capstan shaft. The low-speed, high-torque phase is provided by an axial piston hydraulic motor, applying torque directly into a planetary-gear transmission and auxiliary drive shaft. The auxiliary shaft applies torque through an air clutch to the upper capstan shaft through a chain reduction, which is sized to provide necessary torque for line pulls up to 30,000 pounds. The sprocket pinion from the auxiliary shaft is attached to the air brake, providing the fail-safe brake system.

The power unit, located adjacent to the main capstan drive opposite the control house, utilizes an 8V71 series diesel engine with a horsepower capability of 280 at 2100 rpm (Figure 33.3). The stationary power unit is provided with its own cooling system and electric starting system.

The engine is used to power an 11-cubic-inch, axial piston, pressure compensated, variable volume, hydraulic pump coupled to the flywheel. A 5.77-cubic-inch, variable volume, pressure compensated, vane type hydraulic pump is direct-coupled to the engine cam shaft drive. The engine is also equipped with an air compressor, an air storage tank, and a 300-gallon fuel tank mounted on a separate skid adjacent to the engine.

All engine controls and instruments, including the air throttle control, are located in the operator's control house.

The third, and an important part of the Mark II balloon-tether winch is the stowage drum assembly (Figure 33.4). The frame of the assembly is sized to accommodate stowage drums with capacities of 30,000 feet of 1/2-inch tether cable. The design is such that the drums are interchangeable, and can be manufactured to accommodate various line lengths and sizes. The winch is provided with two drums - one for 20,000 feet of 5/8-inch Nolato cable and one for 12,000 feet of 3/8-inch steel cable.



Figure 33.3. Mark II Balloon Tether Winch Showing Control House, Storage Drum, Main Capstan Drive and Power Unit

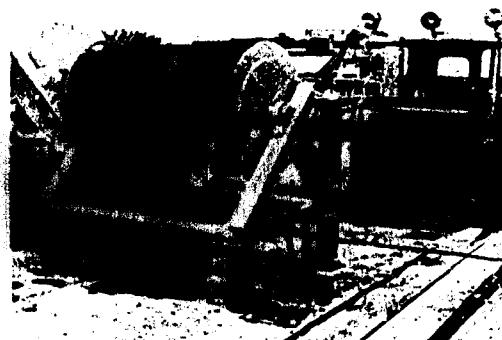


Figure 33.4. 3/8" Storage Drum

The power to rotate the drum is provided by a high-torque gear motor and chain drive to the drum shaft. The hydraulic fluid for the gear motor is furnished by the vane-type, pressure-compensated pump, mounted on the engine cam-shaft drive. This pressure can be regulated to produce line tensions from 200 to 600 pounds.

The design is such that the stowage drum is always rotating in a direction to wind the line on the drum. In the outhauling phase, the capstan must overcome this small tension and rotate the drum against the power applied to pull the line from the drum. This prevents overrunning of the drum when stopped.

In front of the stowage drum is the level wind assembly. The large 30-inch sheave traverses along its guide system, parallel to the face of the drum. Power to traverse this sheave is furnished by a hydraulic Tol-O-Matic cylinder, located just beneath the sheave support members. The direction of movement of the Tol-O-Matic cylinder is controlled by a servo valve attached to the sensing arm, located adjacent and tangent to the level wind sheave. The servo valve positions the level wind assembly by measuring the angle between the drum axis and the cable being spooled on the drum. As the line falls next to its adjacent wrap, a slight angle is formed between the line and the drum axis. This angle is sensed by the sensing arm, actuating the servo valve, directing the fluid to the side of the cylinder necessary to move the sheave, providing a near perpendicular angle between the drum and the line.

The nerve center of the Mark II balloon tether winch is the operator's control house, (Figure 33.5). All winch-operating functions are performed from the control console located inside the house. The main speed control and direction

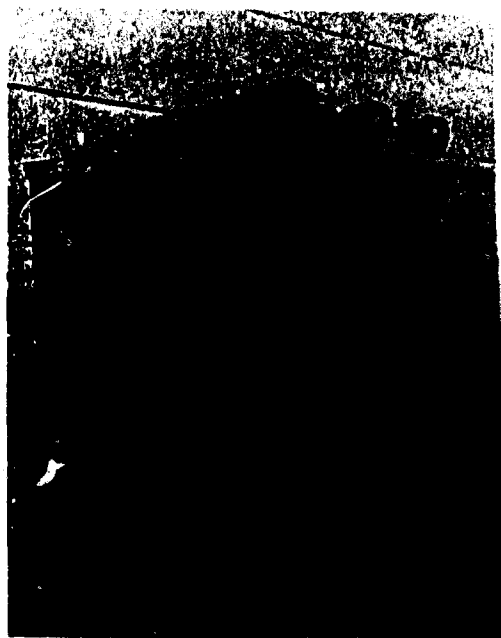


Figure 33.5. Control House



Figure 33.6. Partial Instrumentation Inside Control House Showing Control Handle, Weight Indicator Gauge, Counter and Engine Control

handle is located near the center of the panel (Figure 33.6), and is of a cam design, having a 15:1 ratio at the starting mode, reducing the ratio to 1:1 in the extended positions. This type control offers very sensitive operation in the starting phases.

The high- and low-drive phase selector is also located on the control console and is a hydraulic valve used to actuate pilots on the main control valves mounted on the capstan skid. Various engine instruments are located on the left side of the console, along with the start and stop buttons. The tension-monitoring gauge and the line counters are located near the geometric center of the panel, so that the operator has both gauges in his field of vision. The remote line-pull adjustment handle is located on this panel and is graduated to indicate the line pulls desired within certain limits. Finite line-tension adjustments are made with the winch operating.

The high-tension and low-tension alarm horn is mounted on the house and has a back-up system of lights on the panel. The operator can turn off the alarm; however, the light remains on until the cause is corrected. Another control light is provided to indicate when system pressure has reached the setting of the pressure compensator. This light indicates the maximum line pull is being obtained for the pressure range established.

There are two hydraulic systems on the Mark II balloon tether winch (Figure 33.7). The main system provides power for the capstan drives and is a closed-loop hydrostatic transmission. The pump is a variable-volume, pressure-

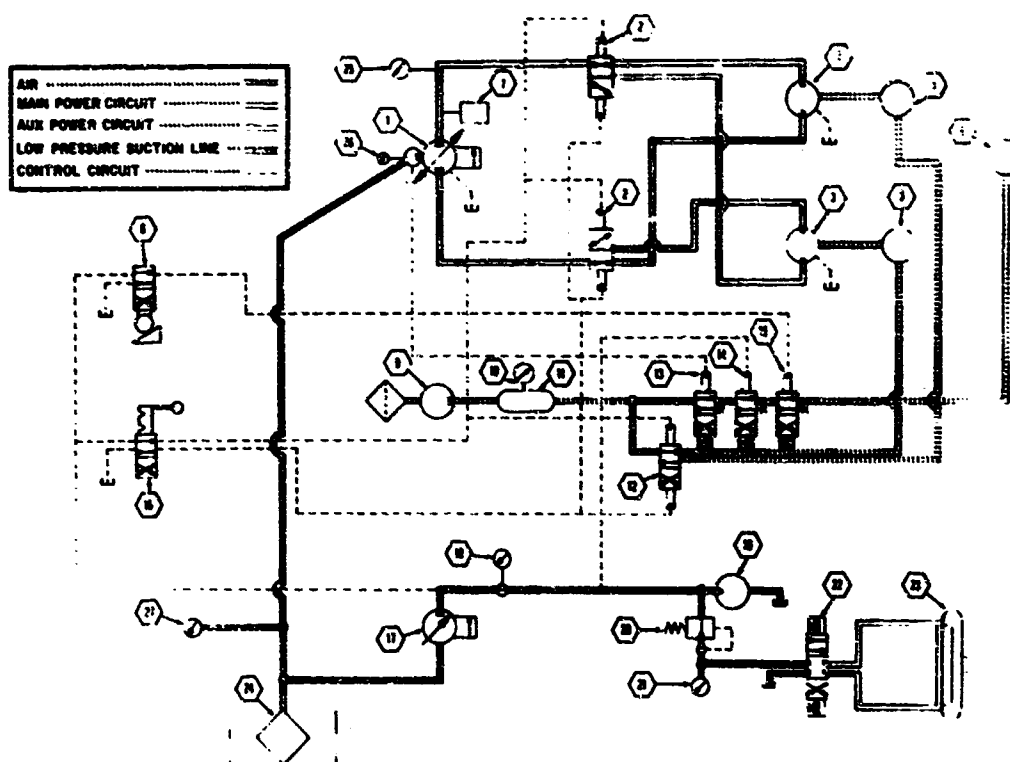


Figure 33.7. Hydraulic Circuit

compensated, axial-piston type. The pump is capable of delivering fluid in both directions. The fluid from the pump is directed to the desired motor through a pilot-operated, selector valve. Two of these valves are provided — one for the high-speed drive and one for the low-speed drive. The actuator control valve utilized to position the selector valve also actuates an air valve, engaging the air clutch for that particular drive phase.

The other hydraulic system powers the drum drive and the level-wind system. The cam shaft drives a vane type, pressure-compensated pump, supplying fluid directly to the drum drive motor. This system is automatic and requires no operator control. A portion of the secondary-system fluid is used to power the level wind system. The secondary hydraulic system also furnishes pilot pressure for manipulating the clutch and brake air valves. The air brake control is integrated with the speed and direction control handle, such that when the handle is in the center, or stop position, the brake is automatically applied. The other brake valves are utilized as fail-safe actuators in the event of failure in the secondary or primary hydraulic system.



Figure 33.8. Fairlead Assembly

The ground handling equipment provided with the Mark II Balloon Tether Winch is a 30,000-pound fairlead sheave assembly (Figure 33.8), designed to allow the line to leave the sheave in a 360° angle in the horizontal plane and 0° to 90° in the vertical plane. A small ground-handling winch, capable of exerting pulls to 30,000 pounds, and its electric hydraulic power unit are located in the cellar, adjacent to the fairlead sheave assembly.

In the line trough, near the ground zero point, a line clamping device is located to stop and hold the line in the event of an emergency. This clamping device is actuated by a control in the operator's control house. The line clamp is supported by a lineal decelerating shock absorber system to absorb

the load on the line, reducing its speed gradually to prevent shock loading on the cable.

33.3 SUMMARY

The Mark II Balloon Tether Winch is designed and manufactured as a research tool. Interchangeability of capstan and sheave shoes, as well as the stowage drums, permits operations to use different kinds and sizes of tether lines. The ability to mold other resilient materials to the shoes expands the scope of this winch to tether cables not yet developed. The arrangement of components on site will allow other stowage drums to be added along either side of the cable trough. These additional stowage capabilities can be accomplished with a minimum expenditure of time and monies. The flexibility of this system and its adaptability to future concepts will prolong the useful life of this winch system.

Meteorological Balloon Techniques

Wednesday

Afternoon: Chairman, Robert Leviton
Air Force Cambridge Research Laboratories

Contents

34.1	Introduction	424
34.2	New French Tethered Balloons of Large Volume	424
34.3	Handling Operations	430
34.4	Performance in Flight	435
34.5	Conclusion	437

34. New French Tethered Balloons of Large Volume: Development, Handling Techniques, and Safety Problems

P. Perroud, C. Aycoberry, J. Barrère, V. Coutrot,
M. Saunois, M. Sylvestre-Baron et B. Vieille*
Commissariat à l'Energie Atomique,
Direction des Applications Militaires,
Sous-Direction des Essais

Abstract

After a short historical review of French aerodynamically-shaped tethered balloons (balloon with ballonet, Caquot's type (1915), and dilatable balloon, Letourneur's type (1925), the different steps in the resumption of use of such balloons in France, which began in 1962, are presented (all materials having been completely destroyed during the Second World War). New-type requirements for heavy payloads have led to the development of operational balloons of several thousand cubic meters capacity by 1966, followed by others of yet larger volume.

A brief description of the balloons used is given. Each has a soft expendable hull of three-to-one fineness ratio, with three tail-fins in "Y" configuration equally spaced and air inflated, as well as accessory equipments.

After manufacture, these balloons are indoor-inflated with air to test gas tightness, and afterwards with hydrogen in order to make various adjustments.

The use of large quantities of hydrogen, together with synthetic fabrics (material highly electrifiable) requires unusual safety techniques to make the balloons as safe as possible.

Fitting of accessory apparatus and hydrogen inflation are carried out on special areas made of concrete. This allows easy handling of the balloon with the help of two winches and many pulleys, aided by the numerous handling ropes attached all along the hull.

* Société d'Etudes et de Travaux, SODETRA

PRECEDING PAGE BLANK

In field operation the balloons are constantly controlled, and great care is taken because of their vulnerability to bad weather and to aging of their structural materials. Two methods of anchorage are used: (1) tightly pulled down to the ground on the inflation areas, or (2) in flight, at low altitude, tethered by a single cable.

Throughout the paper, special emphasis is given to incidents which happened during the numerous test-series in France and abroad.

34.1 INTRODUCTION

During the First World War, tethered balloons were widely used as posts for observation of enemy lines.

This type of equipment gave such good service to the Allies that it was religiously preserved in France, where it was still in operation at the beginning of the Second World War. Tethered balloons were, naturally, good targets for the German Air Force, who shot down a great number; the remainder were afterwards completely destroyed or looted by the invaders.

When the use of captive balloons was again necessary in France, practically nothing was left of the past glory of military aerostatics.

Tribute must be paid at this point to some former balloon specialists (Forichon et al. and Caquot private communications), who started valiantly to work, and to some small wartime balloons rescued from a surplus dump. The revival of tethered balloons was thus possible in our country.

Resumption began in 1962, at Chambaran (Isère) where, with balloons 20 years old and of 90 to 550 and 1,000 m³ capacity, we elaborated the handling techniques and again invested the accessory apparatus (hydrogen inflation, anchorage, winches, pulleys, cables, valves, etc.) taking into account new-type requirements. In 1964, an experimental balloon of 1,500 m³ capacity, manufactured by Société AérAzur (Forichon et al) permitted the continuation of our efforts. Numerous test-series were then made, either on land or on sea, for the development of both the new balloon and its auxiliary apparatus.

This balloon soon proved to be satisfactory, and served as a model for those of larger capacity which followed (4,000, 6,500, 10,000 and 14,000 m³).

34.2 NEW FRENCH TETHERED BALLOONS OF LARGE VOLUME

For the construction of soft captive balloons, two techniques are used: (1) balloon with ballonet, BB-Caquot's type (1915), and (2) dilatable balloon, BD-Letourneur (1925). The advantages of the latter (Jouglaard, 1933), constant buoyancy lift, constant center of buoyancy and constant gas mass, have led to its choice.

34.2.1 Description of an Aérazur Balloon

Figures 34.1, 34.2, and 34.3 show schemes of a typical balloon, and a description of the parts called out in these figures is given in the Legend for Figures 34.1, 34.2, and 34.3 [parts (1.1) through (1.27), (2.1) through (2.8), (3.1) through (3.11), and (4.1) through (4.8)]. Although in the course of development during the last six years, the technique of manufacture has changed somewhat in order to meet new requirements, balloons designed and constructed by Société Aérazur of Paris (Forichon et al) have the following characteristics in common:

The hull (1), having the theoretical shape of two half-ellipsoids joined at the maximum diameter, is made of single-length gore fabric bonded with adhesive and seamed.

The fineness ratio L/D is in the range 3.1 to 3.2. Two extensible gores (1.4) and (1.5) with bellows and elastic ropes, situated at the lower part on the right and the left sides, permit extension which is completed when pressure in the hull P_c is about 3.5 mb (measured near the hull bottom).

The introduction of gas is effected by means of two valves, one for high inflation flow rate (1.16) and the other for refloat inflation (1.19) at lower flow rate. In case of accidental escape of the balloon, a calibrated relief valve (1.21) avoids a possible hull burst while a device (1.24) situated at the highest point and electrically monitored by a barocontact adjusted for a given altitude, insures rapid emptying.

Remarks: The classical rip panel formerly utilized has been finally discarded because of possible gas leaks caused by defective sealing.

The tail-fins, consisting of soft air-inflated longitudinal ribs are equally spaced in "Y" configuration, the lower one being vertical; they communicate with each other by a duct (1.14) and are removable. The constant pressure of 8 mb maintained automatically by an electrical blower (3.4) [with a standby ejection pump (3.10)] gives them the necessary rigidity which combined with the action of cross-bracings and guy ropes (made of nylon) permits maintenance of normal shape. During ascent, one or several calibrated relief valves (3.9) limit this pressure to the initial value.

The double fan-shaped harness comprises flexible metal cables (either having or not pulley-blocks) attached to the hull by gussets of reinforced fabric in the shape of goose feet, and joined at a point by a V-shaped piece from which the main mooring cable starts. This harness is adjusted so as to give to the longitudinal hull axis a positive incidence of 8° at zero wind speed.

Balloon handling on the ground (inflation and anchorage) are made possible by means of a large number of nylon handling ropes attached all along the hull by the help of glued gussets (1.7).

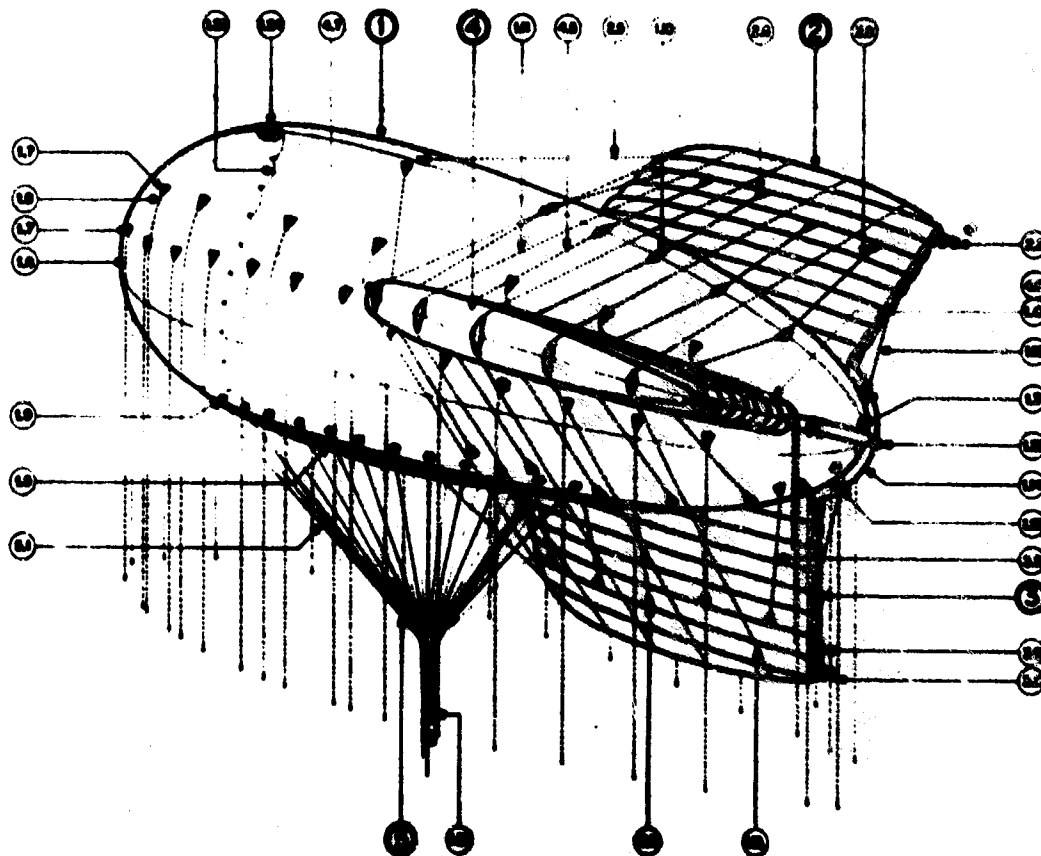


Figure 34.1. Dilatable ARZ Balloon (Side View)

Legends for Figures 34.1, 34.2, and 34.3

1 HULL

- 1.1 Hull gore
- 1.2 Bow disc
- 1.3 Stern disc
- 1.4 Right extensible gore
- 1.5 Left extensible gore
- 1.6 Fin attachment
- 1.7 Handling guy gusset
- 1.8 Handling guy
- 1.9 Harness cable gusset
- 1.10 Fin guyline gusset
- 1.11 Upper bracing
- 1.12 Right lateral bracing
- 1.13 Left lateral bracing
- 1.14 Tail-fins duct
- 1.15 Duct link

1 HULL (Ctond.)

- 1.16 Inflation valve
- 1.17 Purity and pressure test
- 1.18 Inflation sleeve and man hole
- 1.19 Refloat valve
- 1.20 Refloat hose
- 1.21 Relief valve
- 1.22 Fin air relief valve
- 1.23 Emptying hole
- 1.24 Rapid-emptying valve
- 1.25 Electrical cable for rapid-emptying valve
- 1.26 Dilation gauge band
- 1.27 Scale for in-flight pressure measurement

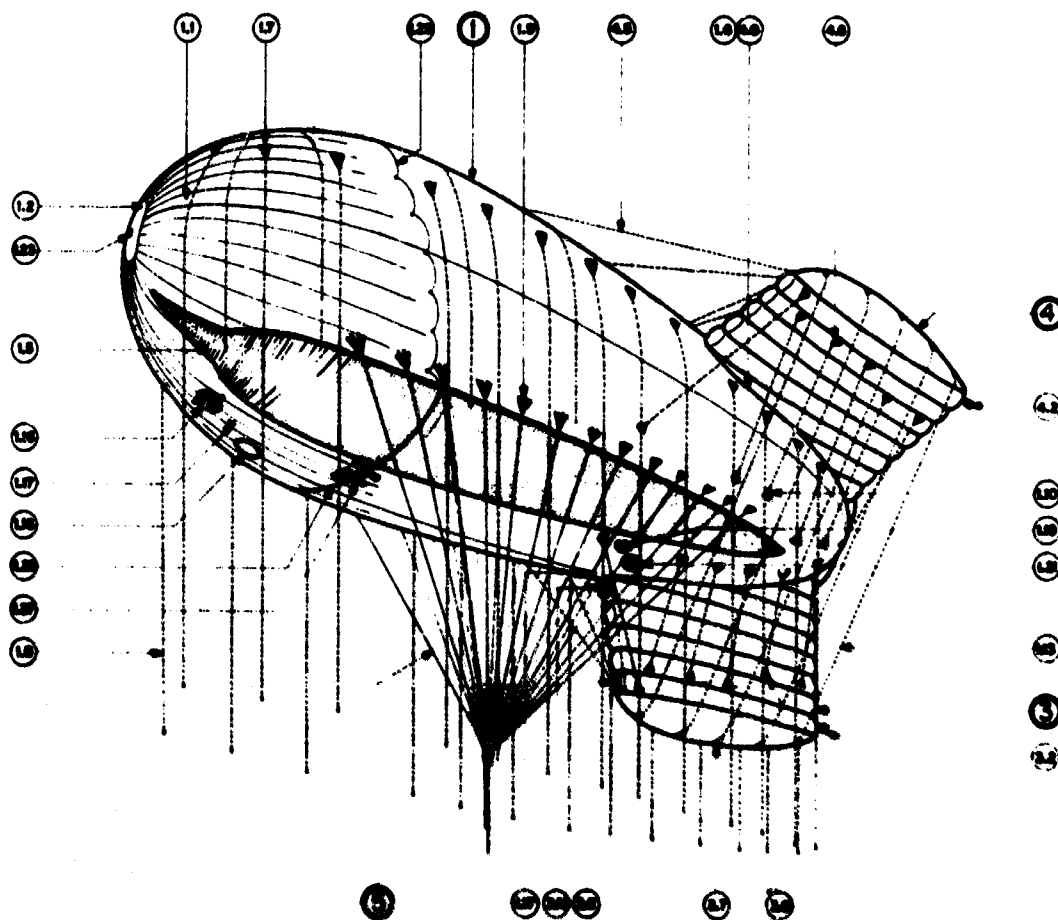


Figure 34.2. Dilatable ARZ Balloon (Side View)

Legends for Figures 34.1, 34.2, and 34.3 (Contd.)

2 RIGHT LATERAL FIN

- 2.1 Salmon (fin extremity)
- 2.2 Deflating sleeve
- 2.3 Pressure test
- 2.4 Lower bracing
- 2.5 Upper bracing
- 2.6 Bracing gusset
- 2.7 Bracing patch
- 2.8 Fin attachment

3 LOWER FIN

- 3.1 Salmon
- 3.2 Inflation sleeve
- 3.3 Pressure test
- 3.4 Right lateral bracing
- 3.5 Left lateral bracing

3 LOWER FIN (Contd.)

- 3.6 Bracing gusset
- 3.7 Bracing patch
- 3.8 Fin attachment
- 3.9 Air relief valve
- 3.10 Air ejection pump
- 3.11 Electrical blower

4 LEFT LATERAL FIN

- 4.1 Salmon
- 4.2 Deflating sleeve
- 4.3 Pressure test
- 4.4 Lower bracing
- 4.5 Upper bracing
- 4.6 Bracing gusset
- 4.7 Bracing patch
- 4.8 Fin attachment

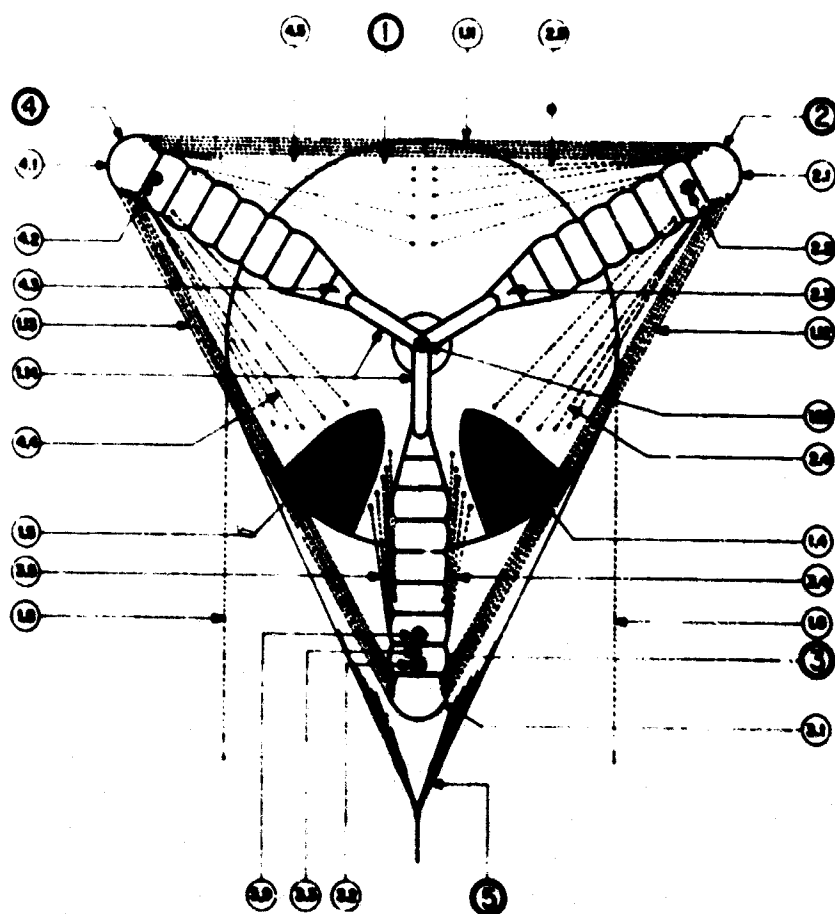


Figure 34.3. Dilatable ARZ Balloon (Stern)

34.2.2 Main Characteristics of an ARZ Balloon

By way of example, here are some characteristics of an ARZ balloon of 6,500 m³ capacity:

(1) Hull

- (a) Length: $L = 52$ m
- (b) Maximum diameter: $D = 16$ m
- (c) Capacity: $P_c = 3.5$ mb, 7,400 m³
- (d) Capacity: $P_c = 2$ mb, 6,500 m³
- (e) Angle of incidence: $i = +8^\circ$
- (f) Number of gores: 51

(2) Tail-fins

(a) Volume of one fin: 360 m^3 , length 18 m, height 15 m, area of one side 175 m^2 .

(b) Total weight of the balloon fully equipped = 2,300 daN (deka Newton).

(3) Residual lift force under the V-shaped piece, at sea level and 25°C , hydrogen inflated, zero wind speed, RLF : 4,800 daN.

34.2.3 Aerodynamic Coefficients

Figure 34.4 shows the aerodynamic coefficients: drag C_x , lift $C_z = f(i)$, and yawing-moment $C_N = f(j)$ resulting from wind tunnel measurements on a rigid model made of wood at scale 1/60. Wind speeds have reached 28 m/sec. Curve 1 corresponds to hull with fins, curve 2 to hull along; i and j are, respectively, angle of incidence and yaw angle. The high values of the ratio C_z/C_x may be noticed; an important extra lift-force due to wind speed is added to the buoyancy force.

Balloon stability in yaw motion is a delicate point; experiments have shown the desirability of having restoring moments which should be not too great.

These excellent aerodynamic properties must not, however, obscure the fact that the real balloon is soft and is deformed by strong winds (particularly the tail-fins), and that exact aerodynamic similitude is far from being achieved. Moreover, a compromise must be found between the need to obtain a good aerodynamic profile and the need to limit the wind forces on tethering cables.

34.2.4 Fabrics

The fabrics used are synthetic materials offering great mechanical strength

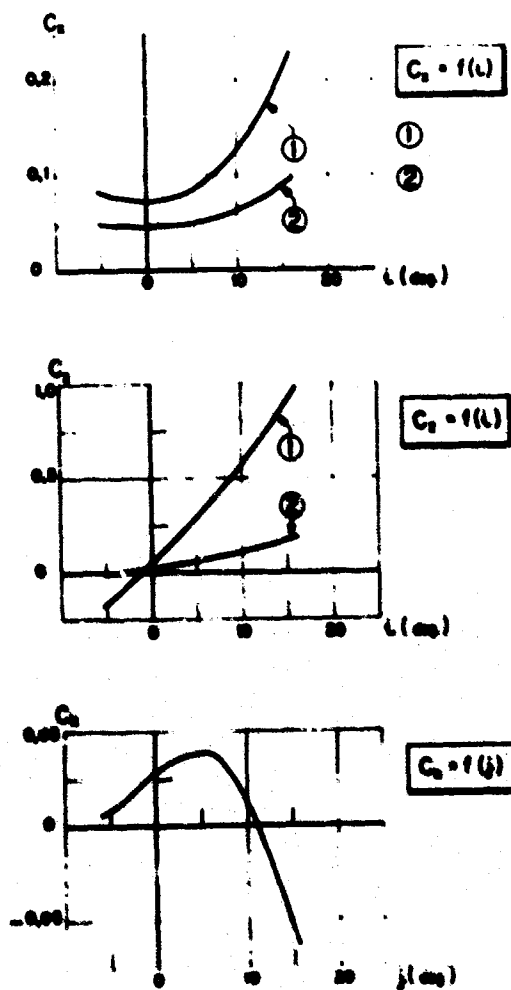


Figure 34.4. Aerodynamic Coefficients. (1) Hull with tail fins, and (2) hull without tail fins

together with high hydrogen tightness. They consist of a substrate of single or double nylon coated on the outside by yellow urethane, and on the inside by neoprene.

Here are some characteristics:

	Hull	Tail-fins
Mass g/m^2	380	280
Dead load strength daN/5 cm	250	150
Hydrogen permeability $\text{l/m}^2\text{-24 h}$	3	5

Note: Mechanical strength warp and fill are not very different; the above figures correspond to the average.

In marine tropical climates, fabrics and adhesive bonds age very rapidly. Removal of the urethane coating occurs in the laboratory at 70°C temperature and 90 percent relative humidity. The utilization of these synthetic fabrics, instead of cotton or silk, introduces a new danger when hydrogen is used because of their high capacity for electrostatic charge. Fortunately, the surface electrical resistivity decreases rapidly when the atmospheric humidity increases.

Let us note that the daily hydrogen losses for our balloons are of the order of 1/100 of their volume. Gas refilling is thus necessary every 3 or 4 days, in order to maintain the hull pressure at a sufficient value.

34.3 HANDLING OPERATIONS

34.3.1 Inflation and Anchorage Area (Figure 34.5)

Note: The parts called out in Figure 34.5 are given in the Legend for Figure 34.5, parts (1) through (12).

After manufacture, balloons are first indoor air-inflated (hull and tail-fins), for a general inspection and then they are inflated with gas in order to adjust the harness and accessory equipment.

This operation, initially carried out with some difficulty outdoors, is now easily made under an old dirigible shed, which offers the necessary space. Balloons thus leave fully tested, with the accessory apparatus well adjusted, and are then ready for service on a remote site, to which they are transported in a special packing under a dry atmosphere.

The areas where inflation and anchorage are carried out, oriented in the direction of the prevailing wind, are made of concrete with a smooth surface. They have three winches, a central one (1) permitting ascent, and two lateral ones (6) permitting anchorage on the ground.

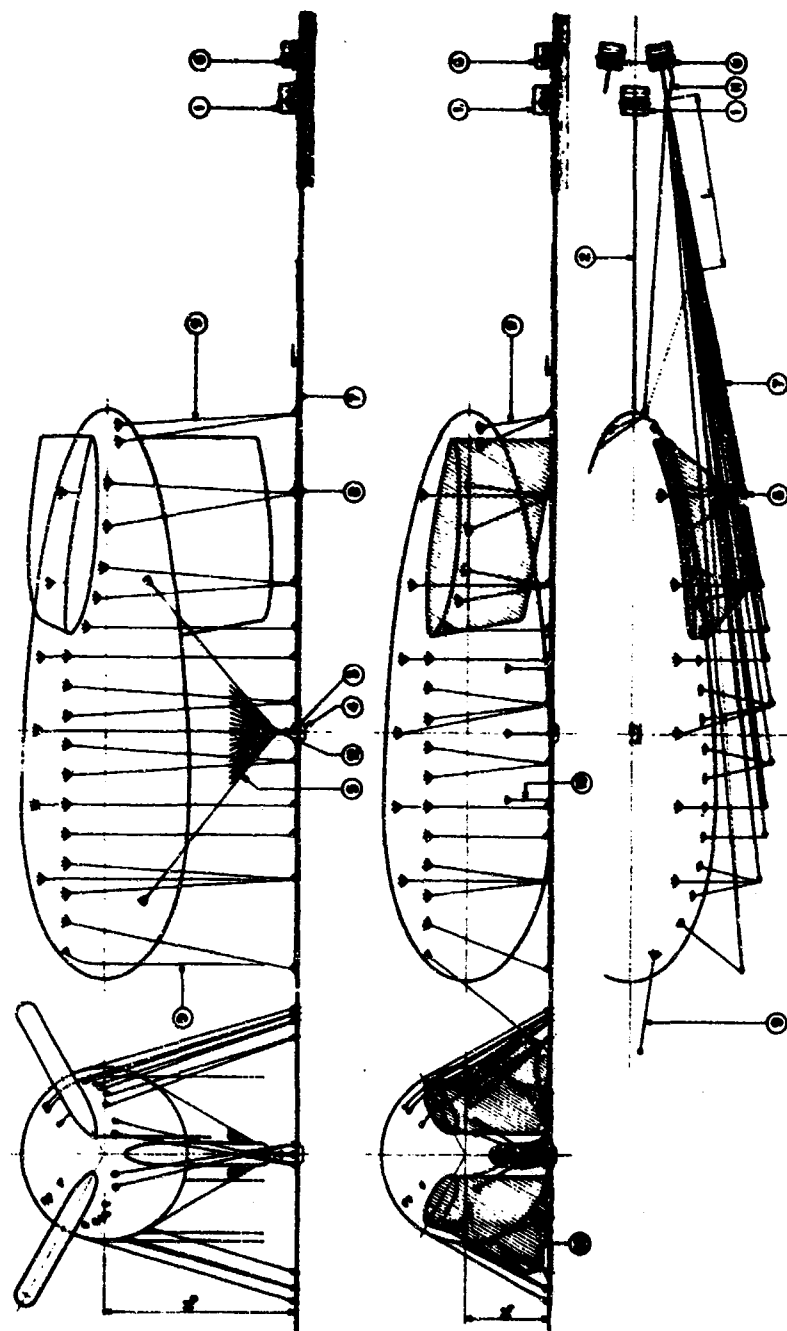


Figure 34. 5. Area of Inflation and Ground Anchorage

Legend for Figure 34.5

- | | |
|------------------------|--|
| 1. Central winch | 8. Handling line pulleys |
| 2. Central winch cable | 9. Handling lines |
| 3. Fairlead | 10. Anti-roll anchorage ropes |
| 4. Fairlead hole | 11. Safety mooring cable for lateral winch |
| 5. Harness | 12. Safety mooring cable for central winch |
| 6. Lateral winches | |
| 7. Anchorage cables | |

Balloon handling is made easier by the great number of nylon guy lines (9) attached all along the hull and joined on each side with the help of cables to a point from which starts the cable of the corresponding lateral winch, each of them passing first round a pulley block (8). When the wind does not blow in the direction of the area axis, this technique permits bringing in the balloon from positions up to 90° of the axis. Walls to provide wind-breaks arranged around the area make inflation possible, even at wind speeds greater than 10 m/sec.

Ground anchorage of the balloon in the event of bad weather, or for repair, is thus made easy. The tail-fins are then deflated and moored tightly, and all necessary safety-measures can be taken. However, in strong cross winds, tail-fins and hull can suffer. Such an anchorage has stood well, however, against cross winds of speeds greater than 30 m/sec., during an entire night under heavy rain.

34.3.2 Safety Problems Related to the Use of Hydrogen

The hydrogen used has a purity greater than 99.6 percent, and is contained in cylinders under a pressure of 200 bars. It is introduced into the hull through the inflation valve (1.16, Figure 34.2) (also see Figure 34.6) after having been depressurized to pressure slightly above atmospheric pressure. The flow rate is 5,000 to 10,000 STP m^3/h , and the desired hull pressure is 2 mb (at the bottom). The inflation operation is delicate because of: (1) fire risk, and (2) possible wind action. Operations are not carried out if the wind speed exceeds 10 m/sec with the wind-break walls, and 7.5 m/sec, without them. Knowing that hydrogen is inflammable in air at a very low ignition energy (10^{-5} Joule) within the limits of 4 to 74 percent, detonating from 18 to 59 percent, the classical principles of safety have been strictly applied: (1) avoid inflammable or detonating mixtures, and (2) eliminate ignition sources.

All metal parts of the area are electrically connected and grounded. Great care is taken to maintain a high atmospheric humidity by constant watering of known dangerous places, in order to eliminate electrostatic charges which could

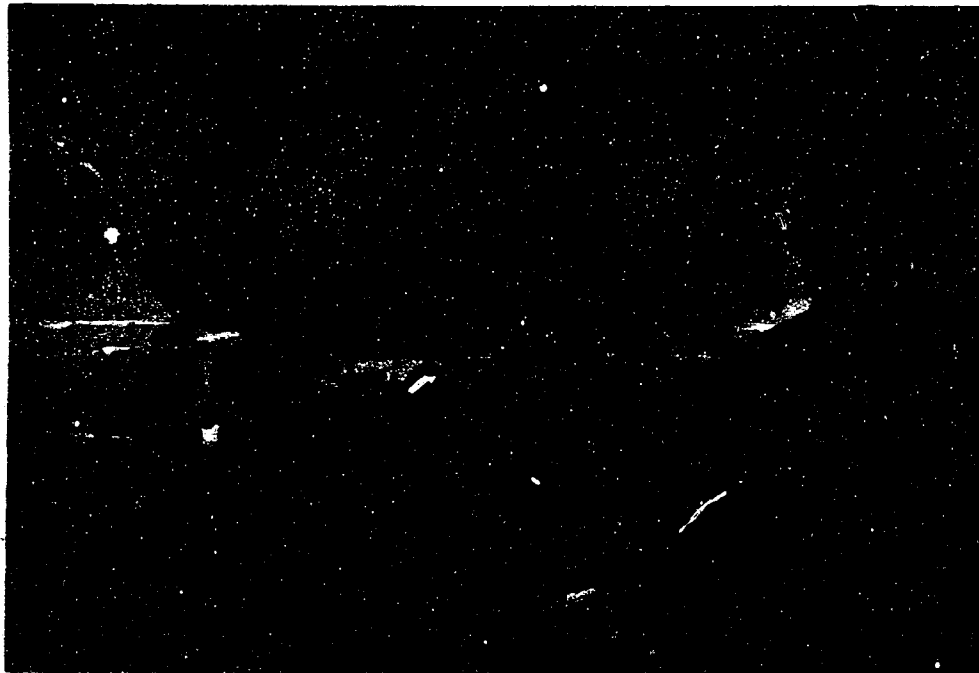


Figure 34.6. Inflation of an ARZ Balloon with Hydrogen

be generated on synthetic fabrics. The crew wear asbestos clothes and work under the careful supervision of firemen.

In spite of these precautions, an accident did occur during a balloon inflation, and 4,000 STP m^3 of hydrogen burned within about ten seconds. Thanks to rapid gas diffusion upwards, injury to personnel was fortunately light.

As laboratory experiments have shown, the fire risks due to a small hydrogen leak on the hull are relatively small (Guizouarn and Perroud, 1963).

During operation, the purity of the hydrogen in the hull is frequently checked with the help of a conductivity-type apparatus.

34.3.3 Balloon Ascent (Figure 34.7)

Note: The parts called out in Figure 34.7 are given in the Legend for Figure 34.7, parts (1) through (12).

The balloon prepared in this way on the inflation area is transported on to the launching site by a special truck, having on its rear end a winch and a fairlead permitting ascent to low altitude. In the case of marine launching sites, the truck and its aerial load are embarked on to a flat bottomed landing craft (French Navy type LCT). The transshipment is made on to the main barge (see Figure 34.7).

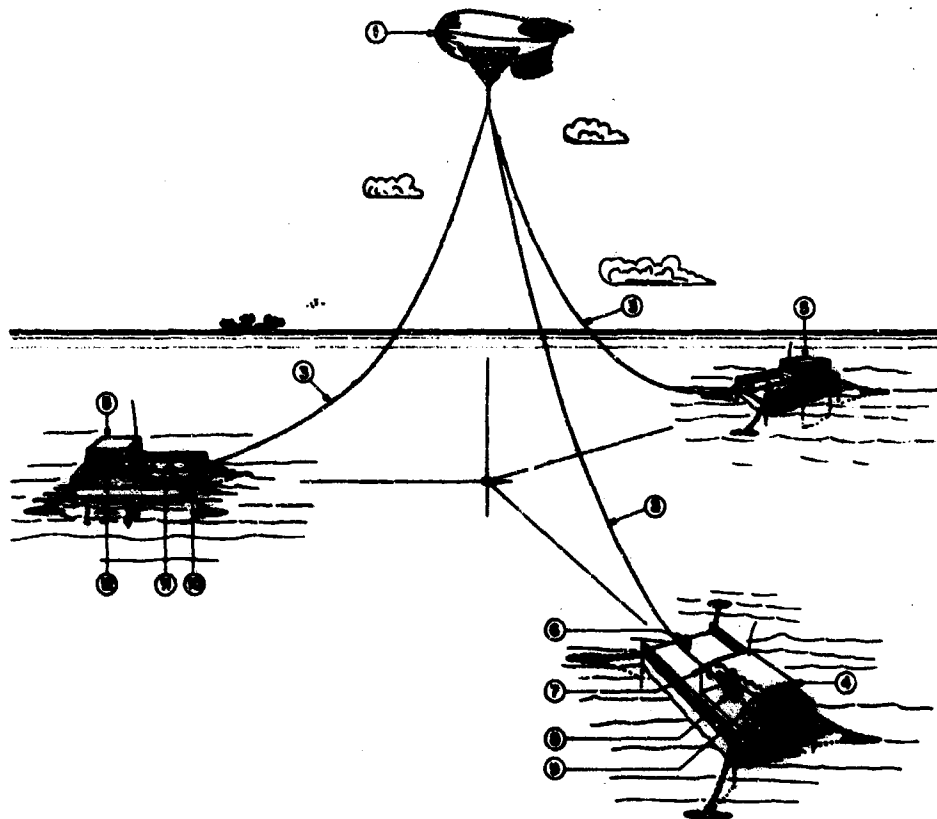


Figure 34.7. Flying the Balloon on a Tripod of Cables

- | | |
|-------------------------|---------------------------|
| 1. Balloon | 7. Cable tensiometer |
| 2. Main tethering cable | 8. Capstan of main winch |
| 3. Positioning cable | 9. Drum for cable storage |
| 4. Main barge | 10. Oscillatory fairlead |
| 5. Positioning barges | 11. Cable tensiometer |
| 6. Oscillatory fairlead | 12. Positioning winch |

Although very practical in a calm sea, this method of transport can become dangerous in a heavy sea, by reason of the whiplashes given to the cable by the action of the waves, or, more so, by wind action which increases the drag on the boat.

When a fixed position in space is required, it is necessary to make use of a regular tripod of cables (see Figure 34.7). The vertices of the equilateral triangle on the sea are then provided by barges (4) and (5), moored to the bottom in shallow water and each carrying a winch. The main barge (4) and its winch

serve for attachment and raising of the gondola and for placing the balloon on standby in the air, and the secondary winches for positioning. The winches used have each a capstan (8) and a storage drum (9). An electric motor gives a constant speed of 0.3 m/sec to the cable. The fairleads (6) and (10) are able to oscillate about a longitudinal axis, and are designed so that it is practically impossible for the cable to leave the pulley. Made up from twisted wires of special, high-tensile steel (200 daN/mm^2), the main tether cable (2) and the positioning tether cables (3) work respectively at $1/3$ and $1/2$ the rupture limit under the most unfavorable case for normal conditions. The cable tension at ground level is continuously measured by a three-pulley tensiometer.

34.4 PERFORMANCE IN FLIGHT

In flight, the following parameters are transmitted to the ground and recorded: (1) hull and fins pressure, (2) speed and direction of wind relative to balloon, and (3) warning of malfunction of one of the systems for refloating the fins (pressurizers).

The behaviour in flight is related to the aerodynamic characteristics of the balloon and to the forces applied to it. Addition of a tail parachute in certain cases improves the stability of the balloon in a wind.

34.4.1 Flight on a Single Cable (Figure 34.8)

This configuration is most often used while the balloon is "on standby" in the air. Thus, a balloon tethered by a 150 m cable can undergo, without too much strain or hazard, winds of up to 20 m/sec (lateral displacements reaching 40 m). Beyond that point, sideways drift of the balloon is so great that it can turn across the wind. The hull then curves in the form of a banana, the fins are deformed, and the aerodynamic qualities of the balloon are lost.

It can either remain in this position at low altitude, exercising a very strong force on its cable, which then makes a low angle with the horizontal, or it can continue its fall until it hits ground and is wrecked.

The good behaviour of a balloon in flight depends strongly on wind characteristics. In this respect, sudden changes in wind direction prove to be much more harmful than rapid changes in wind speed.

34.4.2 Flying on a Tripod of Cables

The stability of a tripod formed by three cables depends on the forces acting at the triple-point. The stability limit of this tripod, which also depends on the relative direction of the wind, is reached when one of the cables makes a

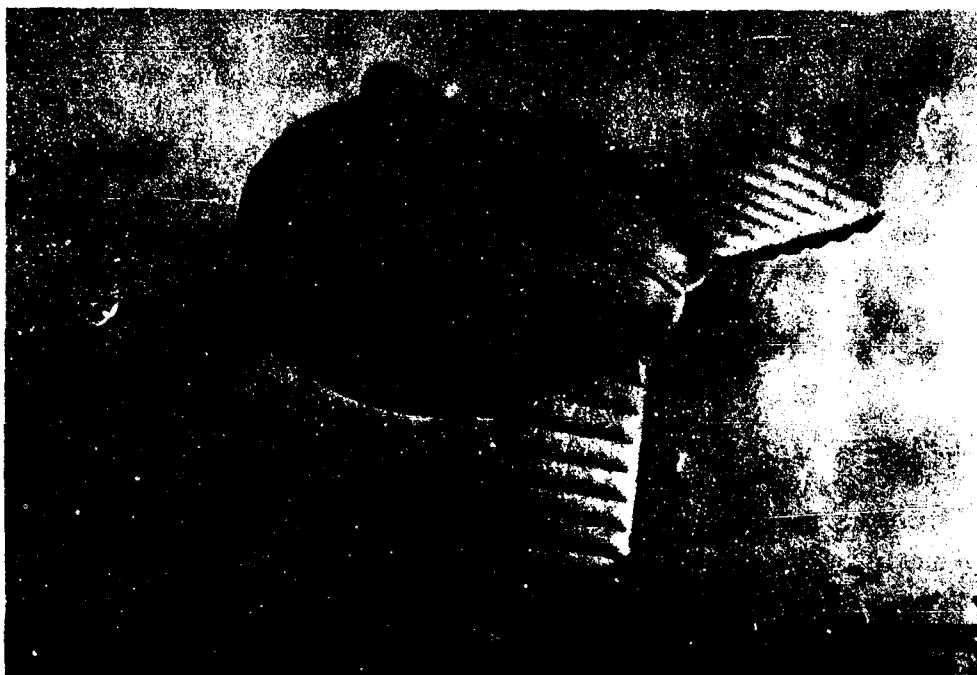


Figure 34. 8. Dilatable Balloon ARZ in Flight at Wind Speed of 10m/sec

zero tangential angle with the horizontal at its point of anchorage. After that, it is impossible to bring the triple-point to the summit of the imaginary regular tetrahedron by pulling on the cables.

For the balloons which have been used, we have calculated the limits of stability. The result of such a calculation is given in Figure 34. 9. This diagram deals with a specific tripod (altitude of the triple-point $H = 600$ m, diameter and weight of cables being known). It allows the critical wind speed V_c , as a function of its direction, and the vertical force F_v applied to the summit of the three cables to be determined. (Here the wind is defined as the direction of its force.) For example, if the wind direction is 70° and the force F_v is $4.5 \cdot 10^4$ Newton, the limit of stability of this tripod will be reached for a wind of $12 \text{ m/sec} = V_c$.

The horizontal displacements of the triple-point around the zero-point are equal to $0.075 H$ in the critical conditions of wind. For wind speeds lower than the critical value the displacements are, of course, less.

The variations in altitude of the triple-point are in the neighbourhood of one-quarter of the above-quoted values.

For wind speeds above the critical value, the cables extend and contract alternately, and the sudden tensile forces thus set up in the cables can reach their rupture limits, setting free the balloon with its load.

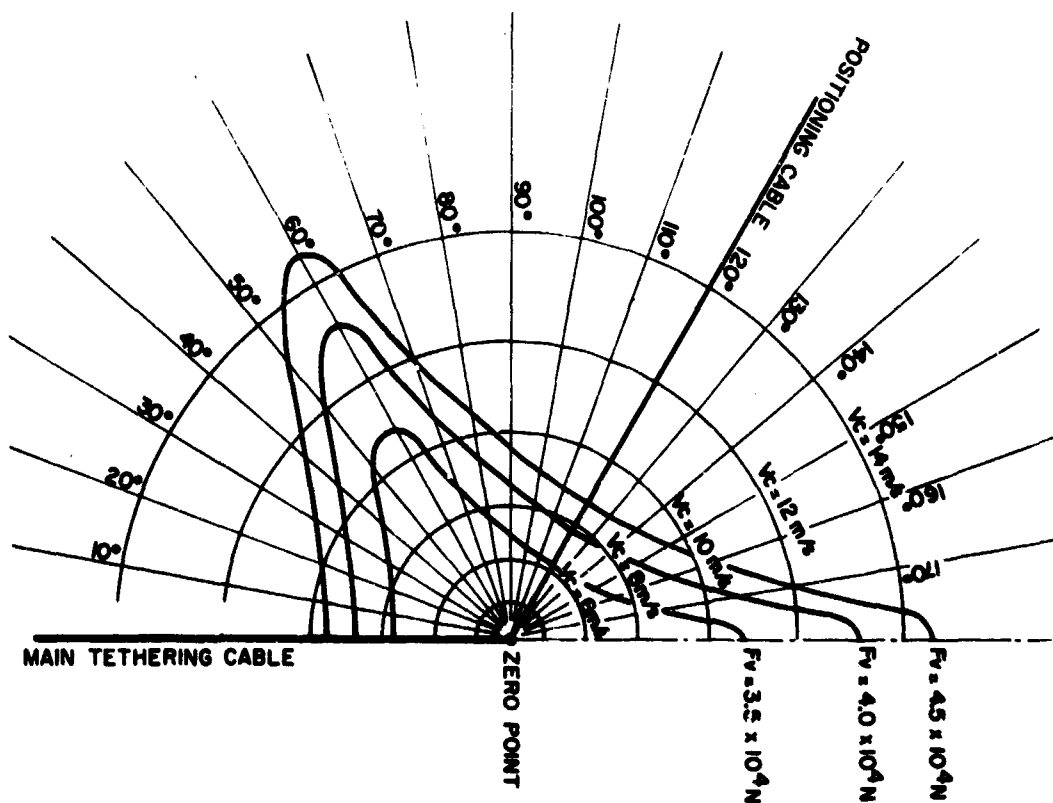


Figure 34.9. Limits of Stability of a Tripod. Altitude $H = 600$ m.

It may also be noted that the stability of the tripod has a direct effect on that of the balloon itself, the sideslip being limited if the tripod is stable.

Finally, test-series for measurements of flight parameters have been carried out, but analysis of the results has proven to be delicate, by reason of the interdependence of these parameters.

34.5. CONCLUSION

Requirements of a new type have permitted France, cradle of Aerostatics, to undertake during the last six years the development of tethered balloons of large volume. These balloons, having an expandable hull and carefully manufactured by Société Aérasur of Paris (Forichon et al), have shown outstanding performances in wind speeds up to 25 m/sec.

Inflation with hydrogen has been possible, in spite of the use of synthetic fabrics (material highly electrifiable), as a result of the inflation techniques we

have developed. Nevertheless, a potential danger still remains which should always be kept in mind. Therefore whenever it is possible, helium must be preferred.

Accessory apparatus, handling equipment and handling techniques tested out during the numerous test-series in France and abroad, are now entirely satisfactory.

In memoriam: M. Pierre Leroy (1893-1969), recently deceased, spent more than fifty years of his creative genius in the service of French Aeronautics. He was instrumental in manufacture of the balloons at Société Aératur of Paris, of which he was Technical Director.

References

Caquot, A. Paris. Communications personnelles.

Forichon, A., Lebastard M., Leroy, P. et Gaillard, A. Société Aératur. 58 boulevard Gallieni, 92 - ISSY-les-MOULINEAUX, France.

Guizouarn L. et Perroud, P. (1963) Dangers relatifs à l'emploi de l'hydrogène gazeux. Mesures de sécurité à observer pour le gonflement d'aérostats de grande capacité. Note CENG/ASP No. 63-07.

Instruction pratique sur la manoeuvre des ballons militaires (1925) Ministère de la Guerre. Imprimerie Nationale. Paris, 1925.

Jaubert, G. F. (1912) La fabrication industrielle de l'hydrogène pour le gonflement des ballons militaires. Imprimerie Nationale. Paris.

Jouglard, P. (1933) Leçons sur la mécanique des ballons et sur leur construction. Ecole Nationale Supérieure de l'Aéronautique. Paris.

Contents

35.1	Introduction	439
35.2	Symbols and Definitions	440
35.3	Equations of the Motion	441
35.4	Laplace Transform of the System	442
35.5	Stability Criteria	443
35.6	Conclusions	444

35. A Simplified Mathematical Model for the Motion of a Tethered Kite Balloon: Stability Criteria

J.M. Dubois
Commissariat à l'Energie Atomique
78 - Villecroze, France

Abstract

Some simplifying assumptions and noticing properties of streamlined balloons lead us to a system of three equations with second degree derivatives, which is valid only for small motions. Predicting large motions needs the use of computing machines and a complete system of equations. Nevertheless the simplified model is adequate to derive stability criteria of the balloon. These criteria provide important relations between mechanical and aerodynamic parameters.

35.1 INTRODUCTION

This study has been done in order to give some evidence of the importance of some balloon parameters; especially, critical wind speed, mooring altitude, lateral lift coefficient, and rotational damping coefficient.

The model is simplified. The kite has been assumed to be rigid, weight of the kite-wire negligible, and plane motions (constant altitude, constant pitch, negligible roll). All the aerodynamic parameters (lateral force and moment) are supposed to

be linear functions of yaw angle ϕ_0 . The strain due to the kite-wire is supposed to be proportional to angle α between cable and the vertical plane containing wind vector \vec{V} .

All these assumptions are valid for small motions.

35.2 SYMBOLS AND DEFINITIONS

35.2.1 Properties of Streamlined Balloons

L	Length of the kite-wire
M	Total mass: balloon, payload, additional mass of air
I	Total inertia momentum, relative to the gravity center G
δ	Distance between verticals of mooring point A and gravity center G
V	Wind speed
C_x, C_y, C_z	Aerodynamic forces coefficients: drag, lateral lift, vertical lift. The axis system is relative to the wind.
F_x, F_y, F_z	Correspondent forces. Related to their coefficients by relations as the following one:

$$F_y = C_y \rho S \frac{V^2}{2}$$

where ρ is air density, and S the main cross section of the balloon.

C_n	Aerodynamic torque coefficient relative to the vertical of point A .
M_n	Moment of the torque. H being the balloon length:

$$M_n = C_n H \rho S \frac{V^2}{2}$$

ϕ	Projection on the horizontal plane of the yaw angle
α	Angle of the kite-wire relative to the vertical plane containing wind vector \vec{V}
F_v	Kite-wire tension. Due to bouyancy and aerodynamic vertical lift plus drag
F_ϕ	Derivative of F_y force relative to angle ϕ :

$$F_\phi = \frac{\partial F_y}{\partial \phi}$$

M_ϕ	Derivative of the moment M_n relative to angle ϕ :
----------	---

$$M_\phi = \frac{\partial M_n}{\partial \phi}$$

R_ϕ Rotation damping coefficient relative to the gravity center G.

We supposed first that kite-balloon notion was plane (ϕ and α supposed to be small). Some aerodynamic considerations lead us to assume this motion linear.

If yaw angle increases from 0° to 10° , the C_x increment is 0.1 (0.3 to 0.4) when C_y increases from 0.0 to 0.8 (see Figure 35.1).

The balloon being initially in equilibrium with a yaw angle of 0° , a crosswind nonequibrated force F_y will appear, and point A will move along C_y axis. The kite-wire will provide a strain αF_y (see Figure 35.2), which is oriented along axis O_y .

Thus the motion can be described with angles α and ϕ only.

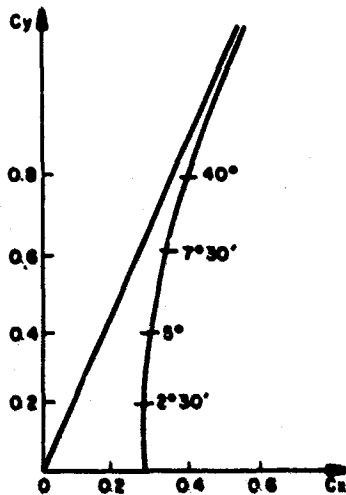


Figure 35.1

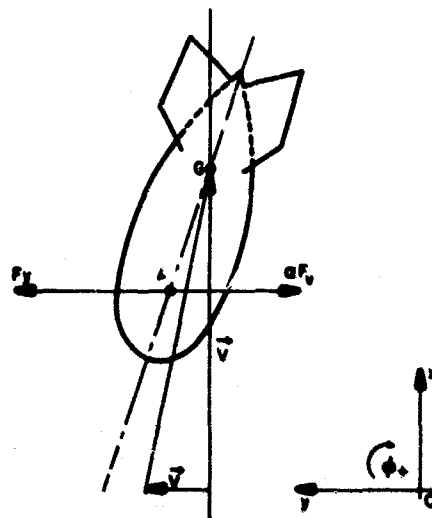


Figure 35.2

35.3 EQUATIONS OF THE MOTION

If the balloon moves with a speed v , wind speed being \vec{V} , the aerodynamic forces will be due to relative wind vector $\vec{V} - \vec{v}$. This vector has a ϕ_0 angle with the balloon axis (apparent yaw angle). Let us now examine the forces and torques system relative to gravity center G.

Forces are:

$$\begin{aligned} &F_y \\ &= \alpha F_v \end{aligned}$$

Torques are:

$$- M_n + \delta(F_y - \alpha F_v)$$

$$- g\left(\frac{d\phi_o}{dt}\right).$$

This second torque is the damping torque; due to rotation speed $\frac{d\phi_o}{dt}$. Wind tunnel tests and theoretical calculations showed that g is a linear function of $\frac{d\phi_o}{dt}$. Thus we shall write:

$$g\left(\frac{d\phi_o}{dt}\right) = R_\phi \frac{d\phi_o}{dt}.$$

The following equations describe the forces and torques system relative to point G;

$$\begin{cases} ML \frac{d^2\alpha}{dt^2} = -F_v \alpha + F_\phi \phi_o + M\delta \frac{d^2\phi}{dt^2} \\ I \frac{d^2\phi}{dt^2} = (-F_v \alpha + F_\phi \phi_o)\delta - M_\phi \phi_o - R_\phi \frac{d\phi_o}{dt} \\ \phi_o = \phi - \frac{L}{V} \frac{d\alpha}{dt} + \frac{\delta}{V} \frac{d\phi}{dt} \end{cases}$$

35.4 LAPLACE TRANSFORM OF THE SYSTEM

The initial assumptions we did lead us to have

$$F_\phi$$

$$M_\phi$$

which are the derivatives relative to ϕ of

$$F_y$$

$$M_n$$

as constants. Thus, the former system of mechanical equations can be treated by LAPLACE transform:

$$\alpha \text{ becomes } \gamma_1$$

$$\phi \text{ becomes } \gamma_2$$

$$\phi_o \text{ becomes } \gamma_3$$

As we need to derive criteria stability, we will suppose wind vector \vec{V} to be constant and the balloon in initial equilibrium. α , ϕ , and their first and second order derivatives relative to the time are zero for time zero.

Such LAPLACE transform can be written as:

$$\begin{cases} 0 = \gamma_1 [-MLs^2 - F_v] + \gamma_2 M\delta s^2 + \gamma_3 F_\phi \\ 0 = \gamma_1 [-\delta F_v] + \gamma_2 [-Is^2] + \gamma_3 [\delta F_\phi - M_\phi - R_\phi s] \\ 0 = \gamma_1 [-\frac{L}{V}s] + \gamma_2 [1 + \frac{\delta}{V}s] - \gamma_3 \end{cases}$$

These equations give a stable mechanical system if the roots of their coefficients determinant have positive real parts. Developing this determinant Δ gives a fourth degree expression:

$$\Delta = a_0 s^4 + a_1 s^3 + a_2 s^2 + a_3 s + a_4$$

with

$$a_0 = 1$$

$$a_1 = \frac{R_\phi}{I} + \frac{F_\phi}{MV}$$

$$a_2 = \frac{F_v}{ML} \frac{I + M\delta^2}{I} + \frac{M_\phi - \delta F_\phi}{I} + \frac{R_\phi}{IMLV} \delta F_v$$

$$a_3 = \frac{F_v}{ML} \left(\frac{R_\phi}{I} + \frac{\delta M_\phi}{IV} \right)$$

$$a_4 = -\frac{F_v M_\phi}{IML}$$

35.5 STABILITY CRITERIA

Respect of the former condition is given by ROUTH criteria. The three following conditions must be true:

$$(1) a_0, a_1, a_2, a_3, a_4 > 0$$

$$(2) a_2 - \frac{a_0 a_3}{a_1} > 0$$

$$(3) \ a_3 - \frac{a_1 a_4}{a_2 - \frac{a_0 a_3}{a_1}} > 0$$

In fact, mechanical parameters are such that only the term a_2 can be negative due to the expression

$$M_\phi = \delta F_\phi.$$

This expression represents the slope of aerodynamic momentum torque curve relative to the gravity center, majored of the term δF_x . This slope would be positive if the aerodynamic transversal force was located behind gravity center. Anyway we can conclude that drag increases stability.

The second condition is more restraining than the first one if damping coefficient R_ϕ or torque momentum coefficient M_ϕ (relative to the mooring point) are too important.

The third condition assigns a minimum altitude of stability.

35.6 CONCLUSIONS

For a given altitude, classical balloons have a critical wind speed. Even with streamlined wind, they move in a crosswind direction. At the same altitude, homotetical balloons have a critical wind speed proportional to the volume square root.

For a given wind speed, classical balloons have two critical altitudes of stability. If a balloon has a considerable kite effect or aerodynamic resultant behind gravity center, it will have only a minimum height of stability and no critical speed.

Some other conclusions are surprising. For instance, drag always has an improving effect. Thus, Crude-Section fins (like Caquot fins for instance) are more efficient than streamlined ones of the same shape. And streamlined hulls, class C-like can be more difficult to stabilize than cruder ones.

Lastly, to stabilize balloons it is necessary to have fins providing an important torque, less lateral lift, much vertical lift.

Thus vertical fins must be small, in a very rear position. Horizontal fins must be large in a middle position. This is possible, as far as vertical fins are concerned, if the balloon is small. Upon large ships such fins would bend the hull.

One of the solutions we experimented successfully with was to fit a parachute upon the upper fins. This device increased drag and provided a damping coefficient ten times higher. Critical wind speed was thus raised. Over critical speed, the movement amplitude was reduced by damping.

Contents

36.1 Introduction	445
36.2 Discussion	445

36. New Techniques and Developments in Meteorological Balloons

M. Sharenov
Atmospheric Sciences Laboratory
USAECON, Fort Monmouth, New Jersey

36.1 INTRODUCTION

During the past few years, studies and investigations have been pursued to meet both the existing requirements of the Army and to explore new techniques and developments in order to improve the performance of meteorological balloons. The most recent studies, devoted to the coating of neoprene balloons with various materials, have two basic goals: (1) increasing the bursting altitudes under arctic nighttime conditions, and (2) increasing ascent rates in general.

36.2 DISCUSSION

36.2.1 Metallizing

Under the first category, attempts were made to change the radiative and absorptive properties of a balloon by applying a thin, metallic coating in the expectation of keeping the balloon at a warmer than ambient temperature. Materials investigated were aluminum, magnesium, and nickel, with the greater stress on aluminum. This paper will discuss aluminizing only.

Aluminum powder is dispersed by either spraying or brushing on a neoprene adhesive. The solvents used in the preparation of the adhesive cause the vulcanized neoprene to swell and to reduce its tensile strength. However, this effect disappears upon evaporation of the solvent, unless the film has been under stress while in contact with the solvent. For example, if application was made to an expanded film, permanent distortion or rupture could occur.

36.2.2 Infrared Tests

Infrared absorption tests were carried out on small, standard, black, and aluminized films prior to any flight tests. It was found that the temperatures inside the black balloon and an expanded aluminized balloon were warmer than the temperature inside a standard balloon, presumably as the result of a greenhouse effect in the aluminized balloon (Morel et al, 1968).

Daytime and nighttime flight tests were made at Belmar, N. J., with temperature elements inside both aluminized balloons and control balloons, and the daytime comparisons exhibited quite large differences, the temperatures inside the aluminized balloons being greater in varying amounts depending on altitude by as much as 30°C and as little as 2°C. At night, the differences were small - the temperatures inside the aluminized balloons were a couple of degrees warmer up to about 30,000 feet, then they were either the same or a couple of degrees cooler than the control balloons at greater altitudes. This pattern was reversed on one pair where the nighttime balloon was aluminized only on the top half. There were five sets of flights where temperatures were measured inside.

36.2.3 Arctic Tests

A number of balloons were flown during the arctic winter night at Thule, Greenland. The first set was flown in February 1969 and another set in December 1969, and January 1970. The balloons fabricated in February 1969 were early models and were thicker-walled, shorter balloons weighing 1200 grams and approximately 80 inches long. The models for the December 1969 - January 1970 flights were 1400-1600 grams and were 110 inches long. These balloons were not intended to be 100,000-foot balloons when uninflated. Control balloons were flown with each of the aluminized balloons in February 1969.

Fifteen pairs of balloons were flown in February 1969. It was determined from the usable data (Table 36.1) that aluminized balloons performed better in altitude by 2 to 1, and in rate of rise by 4 to 1, the altitude differences varying from 4000 to 30,000 feet, and the rate of rise differences from zero to as much as 250 ft/min faster. Since all the balloons were not flown under identical conditions of complete darkness, the results can be considered only as being qualitatively correct.

Table 36.1. Aluminized Balloons, February 1969

BURST ALTITUDE (feet)				RATE OF RISE (ft/min)	
ALUMINIZED		CONTROL		ALUMINIZED	CONTROL
(feet)	TIME	(feet)	TIME		
64,429	Twilight	53,366	N	1,273	1,093
53,312	D	74,787	D	1,215	1,056
57,254	Twilight	61,027	N	1,090	1,218
80,000	D	56,539	N	1,320	1,079
76,752	D	56,319	Twilight	1,220	1,246
51,762	N	58,222	N	1,187	1,124
91,997	* Edge	55,351	Twilight	1,383	1,112
84,709	* Twilight	54,921	Twilight	1,248	1,343
81,516	Twilight	71,591	N	1,208	1,067
84,672	Edge	63,802	Twilight	1,321	1,011
48,674	N	52,795	N	1,232	1,242
72,047	Edge	55,072	Twilight	1,362	1,252

* 1/2 Aluminized (top)

Twilight = Twilight

N = Night

D = Day

The second set of balloons flown in December 1969, and January 1970, all performed under complete darkness. Unfortunately, no control balloons were flown with the second set. Five of the balloons flown in December 1969 were aluminized, ML-537 type (100,000 ft). These did not perform well (Table 36.2). Minimum temperatures were as low as -73°C . Nine other aluminized, all-zone type, ML-607 non-standard balloons were flown in January 1970. These performed better. However, the minimum temperatures had warmed up substantially by early January, 1970; therefore, no conclusions could be drawn.

The ascent rates of the all-zone aluminized balloons are considered good in spite of the fact that they were underinflated by about 300 gms. Immediately following the flights of the all-zone, aluminized balloons (1-5 January 1970), a series of all-zone, non-aluminized balloons (Table 36.3) were flown (6-13 January 1970).

Table 36.2. Aluminized Balloons, December 1969

BALLOON TYPE	ALTITUDE(ft)	RATE OF RISE (ft/min)	NOZZLE LIFT
ML-537	63,133	951	2600 grams
	59,964	919	"
	59,285	886	"
	67,664	935	"
	60,922	919	"
January 1-5 1970			
All Zone Type (ML-607)	79,754	1,066	"
	99,259	998	"
	94,472	1,098	"
	100,600	940	"
	102,110	935	"
	97,736	1,122	"
	104,170	994	"
	98,892	1,030	"
	71,959	1,010	"

Table 36.3. All Zone Non-Aluminized Balloons, 6-13 January 1970

ALTITUDE (feet)	RATE OF RISE (ft/min)
80,881	867
91,106	843
81,300	886
82,152	1,017
84,238	928
113,045	1,063
86,073	894
115,050	963
111,762	967
93,645	967
86,047	1,003

The minimum temperatures encountered on these flights were very similar to those encountered on the flights of the aluminized ones. The aluminized balloons were superior to the untreated balloons in both bursting altitude and ascent rate. Seven of the balloons exceeded 90,000 feet, compared to five of the twelve untreated balloons. Also, seven of the nine aluminized balloons were near or greater than 1000 feet per minute compared to three out of twelve for the untreated balloons, this in spite of the fact that the untreated balloons had more free lift on most flights.

36.2.4 Thermoplastic Coating

In attempts to incorporate several desirable properties into a balloon film, materials can either be incorporated into a compound or laminated to an existing film. Kraton, a thermoplastic elastomer produced by Shell Oil Corp., has shown promise both when blended with neoprene compounds and when laminated with them. Attempts to produce balloons from Kraton alone by solution-dipping have not proven successful.

Some results of the lamination technique with Kraton being sprayed or brushed on are now available. The most pronounced effect of coating with Kraton is to increase the differential pressure of a balloon. The first tests were made on 100-gm balloons in which the differential pressure was nearly doubled initially and remained well above that for an untreated balloon during inflation to burst. The differential-pressure increase was not so marked on larger balloons.

There is good indication that improvement in ascent rate is occurring in the larger balloons as a result of the Kraton coating. A balloon with higher internal pressure tends to deform less during ascent and has a better aerodynamic shape as a result. The smaller balloons are less affected by this effect; for example, normally inflated, 100-gm balloons have a fairly high differential pressure. As the balloon size increases for a given compound, the effect should be more beneficial.

Results of flights with Kraton-coated, 300-gm balloons are given in Table 36.4. These balloons were coated on the inside, resulting in an increase in balloon weight of about 25-30 percent. Initial balloon weights were 240-270 gms and increased to 320-355 gms. Ascent rates of the coated balloons exceeded those of the control balloons in five of the six flights by from 20 to 166 feet per minute. The coated balloons did not reach as high altitudes, however. Kraton is attacked by ozone - thus in some instances it might be more desirable to use it on the inside of a balloon.

Balloons were also fabricated in the 1400 gm (Table 36.5) weight range, of which 300-300 gms represented the Kraton. These balloons were essentially the

Table 36.4. Kraton-coated Balloons, 300 gm Balloon
(1400 gm free lift (F. L.) except one at 900 gm F. L.)

BURSTING ALTITUDE (feet)			RATE OF RISE (to common alt)	
Time	Kraton	Control	Kraton	Control
Night	46,400	56,400	1,255	1,094
Night	50,400	51,000	1,072	1,052
Night	43,400	46,000	1,142	1,090
Night	47,300	49,200	1,000	1,168
Day	58,700	61,300	1,210	1,044
Day	66,000	71,700	965	930

Table 36.5. Kraton-coated Balloons (1400 gm - All Day)

BURSTING ALTITUDE (feet)			RATE OF RISE (to common alt)	
Kraton	Control	Free Lift(gm)	Kraton	Control
99,800 *	-	4,000	1,414	-
108,520 *	110,932	2,850	1,398	1,173
94,485 *	103,800	2,700	1,199	1,096
100,000 *	-	2,700	1,347	-
76,800 **	115,633	1,600	1,146	921
96,800 **	-	2,700	1,358	-
45,650 **	100,148	2,700	1,237	928
102,963 **	80,400	3,600	1,388	1,020
102,000 **	105,200	2,900	1,287	1,217

* Coated inside

** Coated outside

ML-537 type, the standard 110,000 foot balloon. Flight tests were conducted on 10 samples using ML-537 as controls on some of the flights. Free lifts varied from 1600 to 4000 gms. At the higher free lifts, inflation of ML-537 was difficult since the balloon is made of a low modulus film and stretched so as to become very elongated. Launching was also difficult in all but the lightest breeze. However, no problem was encountered in inflating and launching the Kraton balloons.

Overall, the Kraton-coated balloons rose faster than the control balloons by speeds from 70 to 350 ft/min. (Comparisons were available for 6 of the 10 balloons). Most of the flights were about 200 ft/min faster. Half of the Kraton balloons were Kraton-coated on the inside, half on the outside.

While no attempt was made to fly these Kraton-coated balloons in pairs, the balloons coated on the inside appear to do better on both altitude and ascent rate than those coated on the outside. As indicated above, Kraton is attacked by ozone. Perhaps this has some effect in producing the difference in altitude and ascent rate, although more data would be required to evaluate this factor. Also, an analysis is required of the altitude regions of flight where the Kraton coating tends to improve the ascent rate.

36.2.5 Surfactant Materials

As a result of studying recent literature (Davies and Rideal, 1963; and Interfacial Circulation... 1966) on the effects of some surfactant materials on reducing evaporation from bodies of water and other surface phenomena, it was decided to investigate the effects of certain coatings on balloons. The evaporation theory (Davies and Rideal, 1963; and Interfacial Circulation... 1966) was that turbulent diffusion was responsible for the loss of water and that the use of a surfactant reduced this effect. Flow patterns in the vicinity of the air-water interface were affected by a layer of cetyl alcohol (hexadecanol) on the water. By analogy, it was thought that air flow at the air-balloon interface might be changed similarly.

A series of experiments were conducted indoors using 30-gram pilot balloons with weights in their necks, and allowing them to oscillate from the ceiling like a pendulum. Time and distance of travel were noted for 1-1/2 swings for untreated balloons and controls, followed by tests on the same balloons treated with various materials; that is, hexadecanol, corn starch, graphite (all applied both wet and dry), Tide (wet), floor wax, glycerine and ethylene glycol. The only two materials showing significant differences were wet corn starch and wet graphite. Balloons treated with these materials moved consistently through a longer path than control balloons in the same time interval.

Seven pairs of flights were made to evaluate effects on a group of 150-gram balloons carrying radiosondes aloft. Of these, four pairs were tested to determine effects of corn starch, the other three to determine effects of graphite. The balloons were treated generally by immersing them in a solution or mixture of corn starch and water, or graphite and water. After inflation and just prior to launch, the balloons were again sprayed, or the solution applied by using cheesecloth soaked in that solution. Results are shown in Table 36.6. All three graphite-coated balloons performed better than their controls. However, in the case of the corn-starch-treated balloons, 1 was a tie; two were better and two worse than their controls.

Table 36.6. Surfactant-coated Balloons

DATE ALL DAY	FLIGHT NO.	BURSTING ALTITUDE (feet)	R/R*	R/R TO COMMON ALT.	TOTAL LIFT (gm)	COATING	REMARKS
24 July 69	367	19,400	1175	1175	2700	control	
24 July 69	368	33,000	1141	1045	2700	corn starch	Immersed in solution first, then inflated and sprayed.
25 July 69	368	54,500	839	839	2700	control	
25 July 69	369	59,400	932	925	2700	graphite	Immersed in solution first, then inflated and sprayed.
28 July 69	370	40,000	983	1017	2700	control	Launch reel used.
28 July 69	371	30,000	1083	1083	2700	graphite	Turned inside-out, and solution poured in. Sprayed after inflation. Launch reel used.
30 July 69	372	41,800	873	862	2700	control	
30 July 69	373	36,000	992	992	2700	corn starch	Turned inside-out and solution poured in. Sprayed after inflation.

• Rate of Rise

Table 36. 6. Surfactant-coated Balloons (Cont.)

DATE ALL DAY	FLIGHT NO.	BURSTING ALTITUDE (feet)	R/R* COMMON ALT.	R/R TO COMMON ALT.	TOTAL LIFT (gm)	COATING	REMARKS
8 Aug 69	392	56,900	858	847	2700	control	
8 Aug 69	393	48,180	906	906	2700	corn starch	Immersed in solution, then inflated and sprayed and wiped with cheese- cloth.
8 Aug 69	394	52,360	968	968	2700	control	
8 Aug 69	395	60,100	930	929	2700	corn starch	Sprayed with solution after inflation.
8 Aug 69	401	53,600	935	935	2700	control	---
8 Aug 69	402	57,500	988	989	2700	graphite	Washed twice in cold water. Immersed in solv. before inflation. Solution applied with cheesecloth.

*Rate of Rise

Keeping the balloons moist during at least a part of the flight may be a problem. The corn-starch-coated balloons appear to dry more rapidly than the graphite-coated ones. Also, the flights were made in the summer. A problem might arise when the surface temperatures are below freezing. More data are needed to evaluate the materials more reliably, and larger size balloons or larger inflations are required to cover a wider range of Reynolds numbers. Also, other materials which do not freeze or evaporate so rapidly might be investigated.

36.2.6 Modification of Streamline Neoprene Balloons

Attaching a semi-conical neoprene tail to a spherical neoprene balloon increases its ascent rate from approximately 1000 to 1700 feet per minute. This type of balloon, in standard use by the Army for flights to 75,000 feet in the daytime, is known as Balloon ML-541. As the balloon rises and inflates, the tail is drawn up until at about 50,000 feet it becomes essentially a spherical balloon at double its initial diameter.

During an inflation test with air, at a balloon plant, it was noted that the lower 2 feet of the tail would not inflate and be drawn up on the spherical balloon. (The neck of the tail balloon is tied off since previous tests with the neck open did not provide any improvement in ascent rate over a balloon with a tied tail neck.) When two 1 inch vertical slits were cut in the tail right above its neck, the entire tail would be drawn up onto the spherical balloon as it inflated, thus allowing for complete use of the streamlining effect. Another benefit was visualized as a result of the slitting. It was felt that as the balloon approached 50,000 feet, the stresses on the tail would force it to split where the slits were placed. Once a neoprene balloon tail starts to tear, it generally tears rapidly, large sections of it ripping off. This would increase the free lift of the balloon above 50,000 feet, where the tail is no longer of any benefit.

As a result, a series of flights were made starting out at the free lift normally employed with this balloon - 2500 gms. Later this was varied to include other free lifts. At the 2500-gm free lift, significant increases in ascent rate were noted above that of control balloons having no slits. (Table 36.7). Even though in numerous instances the neck ripped off the tail at launch (the train line goes through the tail neck to an inner neck on the spherical balloon), performance was still better than that of the control balloon in each of the nine pairs of flights. In one case, the slit-tail balloons rose by more than 300 feet per minute faster than the control balloons.

Another series of flights was made at 3,500 gm free lift, but the results showed no improvement. This is possibly due to the fact that the greater the inflation, the lower in altitude the slit will rip. It is believed that the slitting

Table 36.7. Streamlined Balloons.
(Two slits near tail neck) 2500 gm Free Lift

BURSTING ALTITUDE (feet)		RATE OF RISE (ft/min)	
Slit Tail	Control	Slit Tail	Control
79,700	83,350	1,775	1,740
77,400	76,550	1,887	1,686
83,800	84,400	1,976	1,620
82,500	78,300	1,950	1,813
74,400	75,800	1,797	1,747
76,800	80,300	1,864	1,712
81,250	82,300	1,751	1,718
SLITS AT MIDTHAIL			
79,100	83,800	1,766	1,693
83,700	54,875	1,820	1,764

Table 36.8. Streamlined Balloons
(with two slits in tail) 3500 gm Free Lift

BURSTING ALTITUDE (feet)		RATE OF RISE (ft/min)	
Slit Tail	Control	Slit Tail	Control
71,000	81,000	2,052	1,858
68,450	78,700	1,860	1,892
50,890*,**	72,000	1,621	1,853
72,500*	76,550	1,898	1,963
71,000*	72,000	1,802	1,837
81,600*	78,500	1,858	1,813
76,000	73,000	1,818	1,751
74,100	57,000	1,760	1,932
77,500	82,200	2,013	1,724

* Slits midway up tail

** Hole tied off

technique will have applicability to the development of higher-altitude, fast-rise balloons currently being initiated.

36.2.7 New Fabrication Technique

Streamline neoprene balloons, type ML-541, are more cumbersome and time-consuming to manufacture than spherical balloons. Generally, the streamline balloon involves the manufacture of two spherical balloons and cementing or gel-adhering of one balloon to a semi-conical section of the other. Considerable space and rigging are required for these processes.

A new technique has been conceived and is being tried on an experimental basis. It consists of dipping the form into a coagulant and then into a tank of latex to form the spherical or top balloon. The form and gel are then dipped into a second coagulant to exactly two-thirds of the fluted section of the form. It is then withdrawn and dipped into a tank of latex to a depth of two inches above the depth of the second coagulant. The tip of the neck of the second gel is snipped, then each gel is separately inflated as indicated in Figure 36.1, "Procedure for Making Integral Tail Streamlined Balloon." After drying, the top balloon is pulled through the neck of the tail balloon to provide a longer tail. A number of details on the processing are omitted for brevity.

A limited number of balloons were fabricated using this process - mostly small ones weighing approximately 250 grams. Some were flight-tested and showed promise. Effort is continuing to produce the full-scale balloons of the ML-541 size.

36.2.8 Fast-rise Balloons for Artillery Applications

Radiosonde soundings in Southeast Asia for artillery purposes are seldom required to exceed 35,000 feet. Use of the larger, more expensive balloons such as the ML-537 and ML-541 is not economical. It was proposed that a low-cost, small-volume, low-altitude, fast-rise balloon be developed for such applications. Initially, requirements were drafted for a balloon to achieve an altitude of 11 kilometers (36,000 feet) at a minimum ascent rate of 475 meters per minute (1,560 feet per minute) with an ultimate goal of 550 meters per minute. A small, streamlined, neoprene balloon was visualized weighing perhaps 300 gms, which would provide the necessary performance. While awaiting receipt of a formal directive, an effort was made to determine the size and shape of the top spherical part of such a balloon. Data were obtained on a balloon 40-inches long weighing 150 gms. This balloon provided a minimum ascent rate of 400 meters per minute (1300 feet per minute) when inflated with 75-80 cubic feet of hydrogen. In response to informal inquiries from artillery users as to the availability of such a balloon,

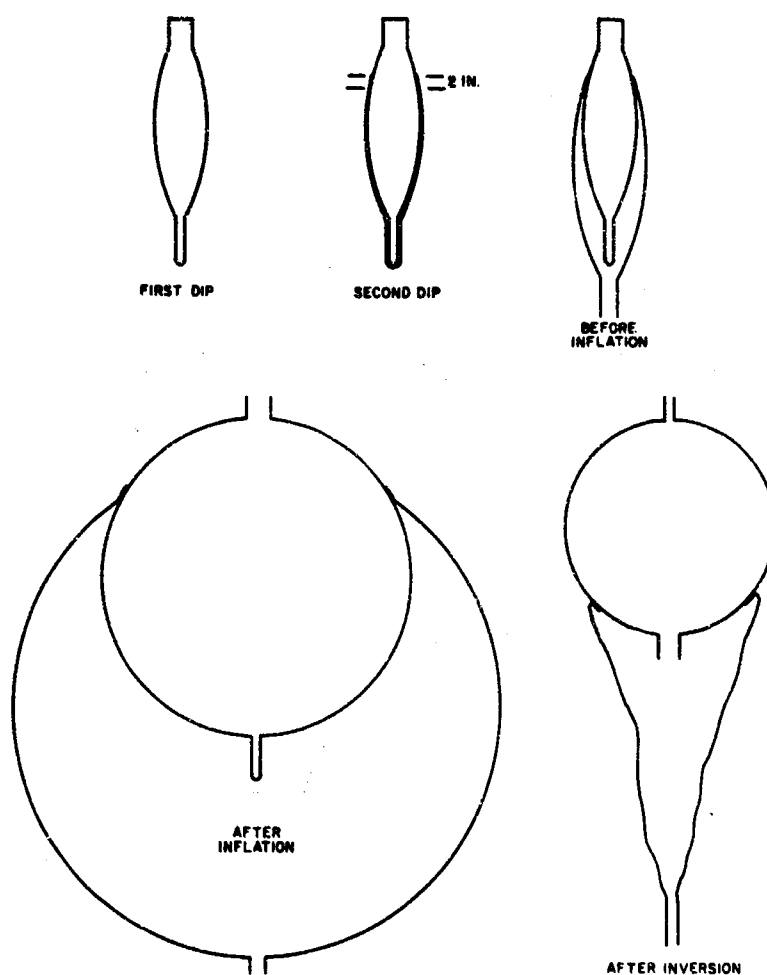


Figure 36.1. Procedure for Making Integral Tail Streamlined Balloon

200 models were tested further. It was found that better than 85 percent met the minimum ascent rate and altitude, with many exceeding 1400 and 1500 feet per minute. A directive has been issued to buy a large quantity of these balloons for use in Southeast Asia.

Acknowledgments

Appreciation is expressed to Kaysam Corporation of America, in particular to Mr. Eric Nelson, for participation and guidance in the effort, and to Mr. Robert Leviton of AFCRL for supporting the effort and arranging to evaluate balloon models at Thule AFB, Greenland.

References

- Davies and Rideal (1963) Interfacial Phenomena, Academic Press, New York.
- Interfacial Circulation Due to Surface Active Agents in Steady Two-Phase Flow, J. Fluid Mech. 24:293-306.
- Morel, P., Fourier, J., and Sitbon, P. (1968) The occurrence of icing on constant level balloons J. Appl. Meteor. 7.

Contents

37.1	Introduction	460
37.2	Development of Free-Flying Aerodynamically Shaped Balloons	462
37.3	Wind Response Considerations	465
37.4	Conclusions	468

37. Fast-rising Stable Streamlined Balloon for High Resolution Wind Measurements

R.M. Henry and C.V. Echstrom
NASA Langley Research Center
Hampton, Virginia

Abstract

Problems involved in the use of balloons for small-scale wind measurement are reviewed and several special purpose balloons designed for this purpose are briefly described. The development of a stable streamlined balloon for small-scale wind measurements is discussed in greater detail. The realization of accurate small-scale wind measurement with streamlined balloons requires careful attention to the balloon's static and aerodynamic stability. The appropriate stability criteria are outlined and some balloon configurations which meet these criteria are shown.

The stable streamlined balloon avoids the problems associated with vortex shedding by spherical balloons and achieves a greater ascent rate, which reduces the required tracking time (ascent rates up to 4,000 feet per minute have been observed in prototype balloons). Since the streamlined balloon is an aerodynamic lifting body, the response distance of the balloon does not increase in proportion to its velocity as does a pure drag sensor. In addition to reducing required tracking time, the higher ascent rate avoids low elevation angles which might cause loss or degradation of tracking data during very high winds.

37.1 INTRODUCTION

Radar reflective balloons have been used for small-scale horizontal wind measurements since the introduction of precision radar systems (Leviton, 1962). Smooth, spherical, 2-meter-diameter balloons were first used for the wind sensor until the identification of the problem of self-induced balloon motions (Henry and Scoggins, 1963). A multiexposure photograph of self-induced motion of a spherical balloon during ascent in still air is presented as Figure 37.1.

An examination of the problem of self-induced motions and a review of the literature on the subject revealed that the probable cause was vortex shedding in the wake of the spherical balloon, especially under conditions of super-critical Reynolds number flow. Once the problem of self-induced balloon motion has been identified, several modified balloon configurations were investigated. The most widely used of these is the Jimsphere balloon system shown in Figure 37.2 (Scoggins, 1967; and Eckstrom, 1965). The Jimsphere, which has been an operational system for some time, has a roughened surface to help prevent random shedding of large-scale vortex patterns, and also a 100-gram weight which helps provide rotational stability. Because the induced motions of smooth spherical balloons occurred primarily at Reynolds numbers greater than about 2×10^5 , an additional solution to the problem was to use a smaller size balloon of lighter weight which operates primarily in the subcritical Reynolds number range. Balloons of this type (Wright, 1967) are also currently in operational use.

Because the self-induced motions of spherical balloons were due primarily to the shifting wake or pressure field on the aft surface of the balloon, a partially filled balloon such as shown in Figure 37.3 was tried by Langley Research Center as a wind sensor. This partially filled balloon deforms rather than translates due to the shifting airflow in the wake. As a result, this balloon turned out to be an excellent sensor of small-scale winds. However, the ascent rate of a small partially filled balloon is about 2.5 m/sec (500 ft/min) no matter how much free lifting gas was used. Therefore, the time required to traverse the altitude range of interest was excessively long. The low ascent rate also results in low elevation angles for radar tracking due to horizontal drift with the wind.

Before the Jimsphere or other modified balloon systems were operational, Langley Research Center became interested in the possibility of using a streamlined balloon of shape similar to those used for many years as powered airships, blimps, and tethered or kite balloons. Such a streamlined balloon would greatly reduce the problems associated with vortex shedding, and would provide a rapid ascent rate by virtue of the low drag configuration. It is the purpose of this paper to present details of the development of such a fast-rising stable streamlined balloon system.



Figure 37.1. Self-induced Motion of a Smooth Spherical Balloon in Still Air

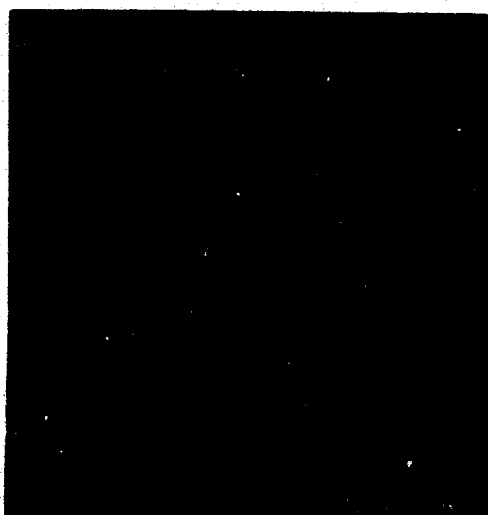


Figure 37.2. Jimsphere Balloon System



Figure 37.3. Partially Filled Deformable Balloon Wind Sensor

37.2 DEVELOPMENT OF FREE-FLYING AERODYNAMICALLY SHAPED BALLOONS

The effort to develop a stable, free-flying, streamlined balloon began with a study of the literature concerning tests of airships, dirigibles, blimps, and kite balloons. Of primary interest was information on drag and stability as a function of system shape, volume, and fin size. Most of the literature relating to airships was dated in the years 1915 to 1932. Information relating to blimps was of a little more recent origin, with the bulk of the information available on the Navy Class C shape. It was also determined that most of the information available on tethered, aerodynamically-shaped balloons also related to Navy Class C shapes or close modifications. Zahn et al (1928) and Van Mises (1959) provided information on the drag of the Navy Class C hull shape as a function of fineness ratio f . Data indicated that a hull shape of fineness ratio $f = 2.1:1$ had the least total drag based on frontal area. However, of more importance to this application would be the drag per unit of volume. Data presented showed the minimum drag per unit volume to occur at a fineness ratio of 4.5 to 4.63 for the Class C shape. However, it was also determined that the drag of inflated fin stabilizer surfaces would probably be greater than the drag of the streamlined hull. Because the bulk of the available literature related to the Navy Class C shape, the first series of experimental balloons were of Class C shape with three inflated fin stabilizer surfaces, as shown in Figure 37.4. These balloons had variations in fineness ratio of 2, 3, and 4 to 1. Although all of these first streamlined balloons were statically stable, as defined by Figure 37.5, flight tests revealed that they were aerodynamically unstable, as defined by Figure 37.6. As can be seen from Figure 37.6, aerodynamic instability results from the improper location of the center of pressure (c.p.) with respect to the center of buoyancy (c.b.) and center of gravity (c.g.). The first series of Class C streamlined balloons were released in a noseup position; however, as the ascent velocity increased, the balloons changed from a vertical to a near horizontal position, indicating that the center of pressure of the balloon configuration was too far forward.

After the first series of tests were completed, it was concluded that a streamlined balloon design was needed which located the center of buoyancy as far forward as possible, and the center of pressure as far aft as possible. Carrying this concept to the extreme, the nose of the balloon was made a hemisphere, with the remainder of the body being a long slender cone which located the fins as far aft as possible. In addition, the fin size was increased and the number of fins increased from 3 to 4. The resulting balloon, which had a fineness ratio of 4 to 1, is shown in Figure 37.7. After the solution of a few fabrication problems, this type balloon successfully flew in a noseup position at a rise rate of about 15 m/sec (3,000 ft/min) from ground level to a float altitude of about 12 km (40,000 ft).



Figure 37.4. Experimental Class C Balloon

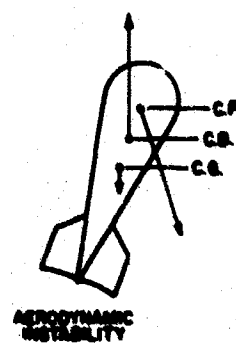
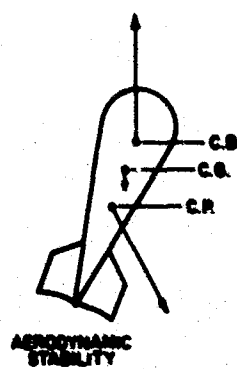
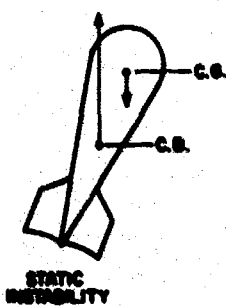
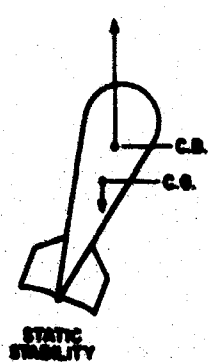


Figure 37.5. Static Stability Conditions

Figure 37.6. Aerodynamic Stability Conditions

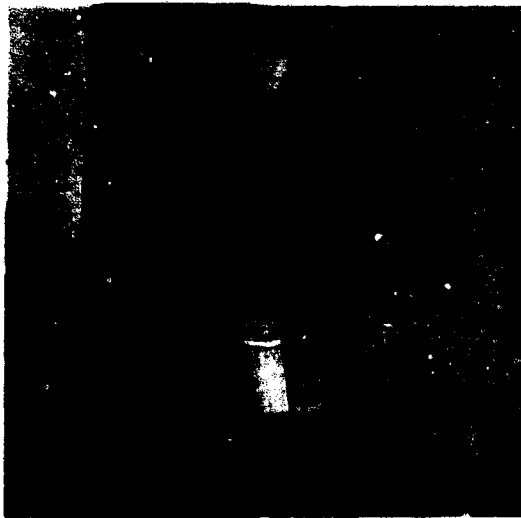


Figure 37.7. Hemisphere-cone Streamlined Balloon



Figure 37.8. Combination Class C Conical Balloon

After the successful completion of this second series of flight tests with the balloons referred to as the hemisphere-cone shapes, it was of interest to deter-

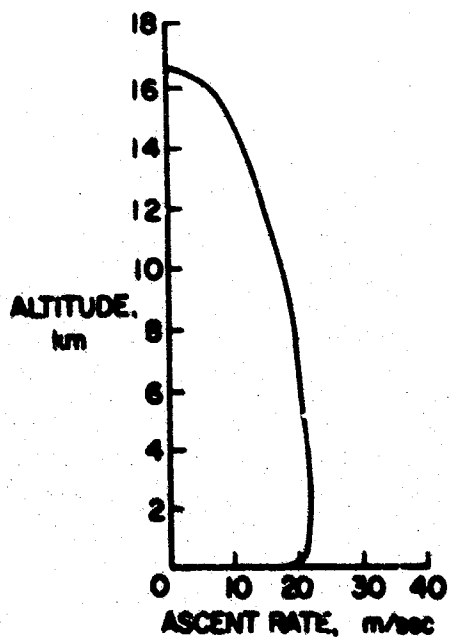


Figure 37.9. Streamlined Balloon Ascent Rate

mine if higher float altitudes could be attained with balloons of more efficient volume-to-mass characteristics. For this purpose, a large series of balloon designs were considered and a few selected designs were flight-tested. As a result of the third series of flight tests, the balloon configuration shown in Figure 37.8 was selected as about an optimum design. This balloon consists of a Class C shape forebody of fineness ratio of 2 to 1 with a conical aft section increasing the total length to give an overall fineness ratio of 3 to 1. This balloon has a rise rate of about 20 m/sec (4,000 ft/min) and the useful altitude range has been increased to about 16 km (52,000 ft), as shown in Figure 37.9.

The combination Class-C-conical streamlined balloons tested to date have been 6.1 m (20 ft) in length and are constructed of 1/2-mil (0.0005 in.) thick, metalized Mylar material with fins constructed of dacron-scrim reinforced, clear Mylar film. The basic weight of the balloon is 1.42 kg (3.1 lb). At standard sea-level conditions, the balloons have an approximate volume of 9.2 m³ (325 ft³) and provide a free lift of 21 N (18.3 lb).

After completion of the development phase of the streamlined balloon program, an additional reference was discovered (Halfman and Ashley, 1953) which considered the theoretical aspects of developing a fast-rising streamlined balloon system. The report, which predated the experimental effort reported here, concluded that a fast-rise balloon system was a distinct possibility and predicted ascent rates as great as 25 m/sec (5,000 ft/min). After locating this particular reference, it was interesting to note that most of the recommended experimental tests were actually performed during the Langley Research Center development effort.

Although several streamlined, aerodynamically-shaped balloons have been successfully flown in a stable vertical flight path at rise rates of at least 20 m/sec (4,000 ft/min), there are still some engineering developments needed to make the system operationally competitive. The most obvious improvement needed is a simplified fin design to reduce the cost of the balloons on a unit basis. Also, the long, slender, metalized balloons do not present a point target for the radar-tracking system, apparently causing the radar to search in the vertical direction. It is believed that replacing the metalized surface with an internal corner reflector or a crumpled aluminum foil target would solve this problem. Additional minor improvements in balloon accessory design would aid in problems associated with inflation, handling, and release of the balloon for radar tracking.

37.3 WIND RESPONSE CONSIDERATIONS

In evaluating the capabilities of any wind sensor, it is of interest to know just how closely or quickly the sensor will respond to varying horizontal wind inputs as the sensor traverses the atmosphere in a vertical direction. Eckstrom (1965) presented a method of determining a characteristic lag distance L of a pure drag wind sensor as follows:

$$L = \left[\frac{(m_s + m_g)}{\rho Vol + (m_s + m_g)} \right] \frac{V_{zB}^2}{g} \quad (37.1)$$

where

m_s = mass of balloon skin, fins, and so forth

m_g = mass of balloon inflation gas

ρ = atmospheric density

Vol = balloon volume

V_{zB} = vertical rise rate of the balloon

g = gravitational constant

As can be seen from Eq. (37.1), the response capability of a pure drag device is a function of its total mass, the mass of the displaced air, and the square of the rise rate.

If the center of gravity of a streamlined balloon were coincident with its center of bouyancy, the balloon would be statically stable at any angle, but dynamically stable at zero angle of attack only (assuming it is an aerodynamically stable balloon). Such a balloon would be essentially a pure drag device as it would always go to zero angle of attack to the relative air velocity. We could, therefore, compare the response capability of such a balloon to a spherical sensor such as the Jimsphere which is theoretically a pure drag sensor. The streamlined balloon rise rate is about four times greater than that of the Jimsphere, and the mass-to-volume ratio is also greater because the streamlined shape encloses less volume per unit surface area and the streamlined balloon has the added mass of the fin stabilizers. As a result, at the altitude of 3 km (10,000 ft), the characteristic lag distance of a pure drag streamlined balloon would be about 41 m (135 ft), whereas that of the Jimsphere is only about 1.5 m (5 ft). Clearly, just increasing the rise rate of a pure drag sensor results in considerable loss of wind sensitivity. However, in actuality, the streamlined balloon is not a pure drag sensor since it experiences large lift forces in addition to the drag forces. As mentioned earlier, the fins have substantial mass and are located on the aft end of the balloon. Typically, the center of bouyancy is at about 40 percent of the balloon length aft of the nose, whereas the balloon center of gravity is at about 70 percent aft of the nose. As a result, the balloon would normally have a significant degree of static stability and the only time the streamlined balloon would fly at zero angle of attack would be under the "no wind gradient" condition.

A vertically rising, aerodynamically stable streamlined balloon with static stability would respond to a horizontal wind shear layer by both lift and drag forces, as shown by the following equations of motion:

x (horizontal)

$$(m_s + m_g)\dot{V}_{xB} = (C_D \sin \gamma + C_L \cos \gamma)1/2 \rho V_R^2 S - m'(\dot{V}_{xB} - \dot{V}_{xw}) \quad (37.2)$$

z (vertical)

$$(m_s + m_g)\dot{V}_{z_B} = (C_L \sin \gamma - C_D \cos \gamma) \frac{1}{2} \rho V_R^2 S - (m_s + m_g)g - m'(\dot{V}_{z_B} - \dot{V}_{z_w}) \quad (37.3)$$

where

- m_s = mass of balloon skin, fins, and so forth
- m_g = mass of balloon inflation gas
- m' = apparent mass of system
- C_D = drag coefficient
- C_L = lift coefficient
- S = reference area
- ρ = atmospheric density
- V_R = relative velocity between air and balloon
- V_{x_B} = horizontal velocity of balloon relative to earth
- V_{x_w} = velocity of wind relative to earth
- V_{z_B} = vertical velocity of the balloon
- V_{z_w} = vertical velocity of the wind
- γ = angle of resultant velocity from vertical

Dots over symbols denote differentiation with respect to time.

The magnitude of the lift force generated will be a function of the balloon angle of attack to the resultant airflow. As a result of the balloon center of mass being aft of the balloon center of buoyancy, the balloon will fly at some angle of attack α to the resultant airflow as shown in Figure 37. 10, where the moment due to aerodynamic force balances the moment due to buoyant and gravitational forces. The lift force of the balloon is generally greater than the drag force (C_L/C_D ranges from 3 to 5) in the range of possible angles of attack, and the angle γ of the resultant velocity from the vertical is also small ($\gamma \leq 13^\circ$ for balloon ascent rates of 4,000 ft/min and wind shears of 0.1 sec^{-1} or less) so that $C_L \cos \gamma \gg C_D \sin \gamma$.

In comparing the wind response capabilities of the streamlined balloon with lift to a spherical, pure-drag sensor, it should be remembered that the increased response of the streamlined balloon due to lifting forces is balanced somewhat by virtue of its greater mass per unit volume and its faster rise rate, as mentioned earlier.

A comparison of winds as measured by different sensor systems is presented in Figure 37. 11. The profiles of wind velocity versus altitudes are for a combination Class C - conical streamlined balloon sensor, a parachute altitude wind sensor (PAWS) system (Silbert, 1970), and the smoke-trail method (Henry et al,

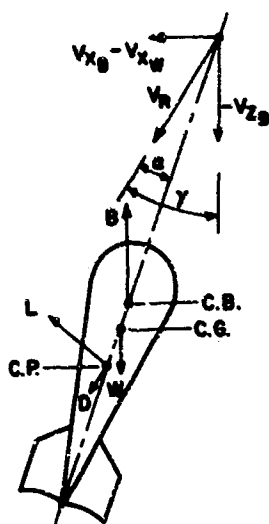


Figure 37.10. Streamlined Balloon Flight Conditions

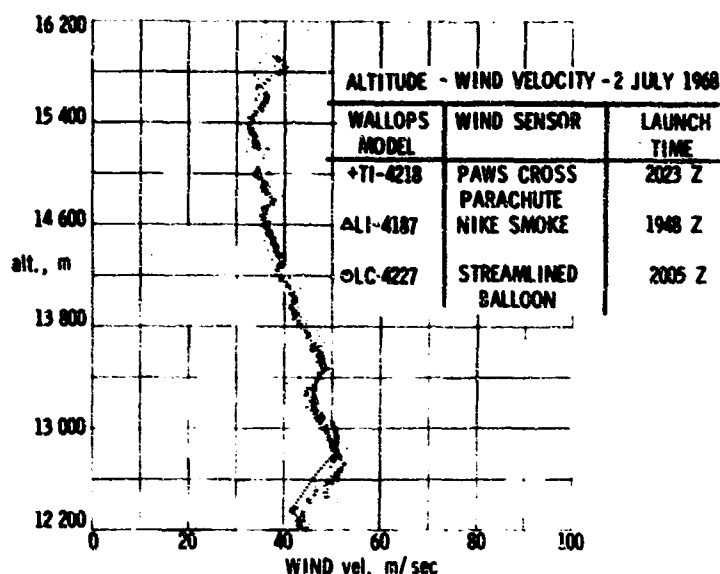


Figure 37.11. Wind Velocity Measurements by Various Systems

1960). The balloon sensor data presented have relatively large scatter over some parts of the profile but, in general, are in close agreement with both the smoke-trail data and the parachute sensor data. The reason for the scatter in the streamlined balloon data has not been fully determined but is believed to be a radar-tracking error. The use of a discrete radar target might substantially reduce this scatter.

37.4 CONCLUSIONS

Langley Research Center investigations of balloons as sensors of small-scale horizontal winds lead to the following conclusions:

- (1) Vertical rising, stable, streamlined balloons having rise rates of 20 m/sec (4,000 ft/min) and float altitudes of about 16 km (52,000 ft) have been successfully flight-tested.
- (2) Vertically rising, streamlined balloons which are both statically and aerodynamically stable respond to changing winds by both aerodynamic drag and lift forces.
- (3) Experimental flight tests have proven the capability of the streamlined balloon concept, but additional engineering efforts are required before the system becomes operationally competitive with existing modified spherical balloon sensors.

(4) The streamlined balloon system would be applicable to a requirement for greater ascent rates than are possible with the currently operational balloon sensor systems.

(5) A partially filled, deformable balloon is also an excellent wind sensor as it changes in shape rather than translates as a result of shifting airflow in the wake. However, the low rise rate of about 2.5 m/sec (500 ft/min) results in radar-tracking problems for many applications.

References

- Eckstrom, C.V. (1965) Theoretical Study and Engineering Development of Jim-sphere Wind Sensor, NASA CR-64966.
- Halfman, R.L., and Ashley, H. (1953) Stability of Streamline Balloons, Final Report on Contract No. DA-36-039 SC-42570, Dept. of Army Project No. 3-36-05-037, Signal Corps Project No. 24-723L, by Massachusetts Institute of Technology, Cambridge, Massachusetts.
- Henry, R.M., Brandon, G.W., Tolefson, H.B., and Lanford, W.E. (1961) The Smoke-Trail Method for Obtaining Detailed Measurements of the Vertical Wind Profile for Application to Missile-Dynamic-Response Problems, NASA TN D-976.
- Henry, R.M., and Scoggins, J.R. (1963) Self-induced balloon motions, Astronautics and Aerospace Engineering, 1 (No. 9).
- Leviton, R. (1962) A Detailed Wind Profile Sounding Technique, Air Force Surveys in Geophysics, No. 140, Vol. 1, pp. 187-195, Geophysics Research Directorate, Bedford, Massachusetts.
- Scoggins, J.R. (1967) Sphere Behavior and the Measurement of Wind Profiles, NASA TN D-3994.
- Silbert, M.N. (1970) The Parachute Altitude Wind Sensor, paper presented at the Fourth Conference on Aerospace Meteorology sponsored by the American Meteorological Society, the American Institute of Aeronautics and Astronautics, and the Institute of Environmental Sciences, Las Vegas, Nevada.
- Von Mises, R. (1959) Theory of Flight, Dover Publications, Inc., New York, New York.
- Wright, J.B. (1967) Reynolds number effects on ascending spherical balloons, AIAA Journal of Spacecraft, 4 (No. 3):407-408.
- Zahm, A.F., Smith, R.H., and Loudon, F.A. (1928) Drag of C-Class Airships Hulls of Various Fineness Ratios, NACA Report 291.

38. An Analysis of the Boundary Layer Associated With Floating Balloon Systems

R.D. Reynolds and A.L. Wallis, Jr.
U.S. Army Electronics Command
White Sands Missile Range, N.M.

Ney, et al (1961) discussed the boundary layer associated with floating balloon systems for flights during the day and at night. They devised two methods to obtain the "undiluted" ambient temperature from a floating balloon system in daytime. In one method, a boom was extended horizontally at least three feet from the balloon payload so that the thermistor would be outside the boundary layer, and in the second method a thermistor was suspended several feet below the balloon payload.

The suspended or "dangling" thermistor technique was utilized by Reynolds and Lamberth (1966) on superpressure balloon flights (Figure 38.1). It was found that although the dangling thermistor provided ambient daytime temperatures that agreed with temperatures measured by other methods at the same altitude at approximately the same time and point in space, the technique was inadequate for nighttime measurements since the thermistor was inundated in the drainage down the balloon system.

The nighttime boundary layer and drainage (Figure 38.2) were reported in detail by Ney et al (1961) who showed that at night the gas in a floating balloon approached a blackbody equilibrium temperature. The balloon gas temperature is often 15°C colder than ambient. The modeling of nighttime drainage (Figure 38.3) by Wagner (1965) resulted in a visual presentation of the drainage phenomenon.

PRECEDING PAGE BLANK

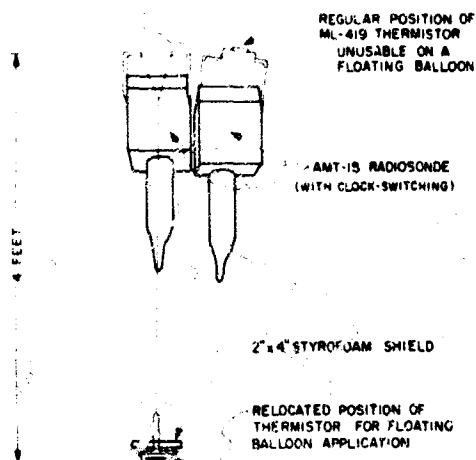


Figure 38.1. Dangling Thermistor Used by Reynolds and Lamberth to Obtain Ambient Temperatures from Floating Superpressure Balloons During Daytime

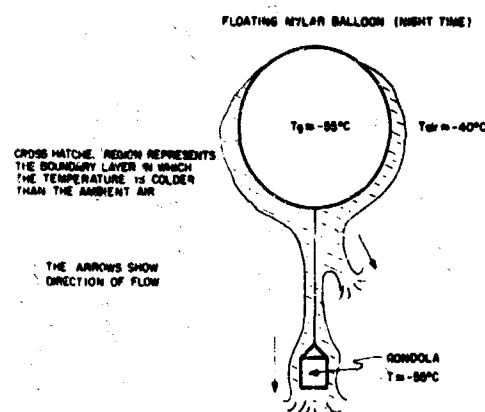


Figure 38.2. Nighttime Drainage Associated with Floating Balloon Systems as Shown by Ney, Maas, and Huch. (Note: Their drainage flow was found to be more lamirar so they suggested suspending a boom out three feet or more from the load line or the widest part of the payload to obtain ambient temperatures)

In September 1968, a 29-million cubic foot balloon, the largest flown to that date, was launched for the Atmospheric Sciences Laboratory at White Sands Missile Range by the Air Force Cambridge Balloon R&D Test Branch. At the float altitude (155,000 feet) of the balloon, its diameter was 412 feet. The payload was eight-feet wide and exposed the instrumentation 65 feet below the balloon, with the thermistor and other sensors being at the lower extremity of the system. Daytime temperatures measured by the thermistor in this configuration were 10°C higher than the temperature measured by a spacially and temporally comparable rocket-sonde. This difference led to questions regarding the reliability of the temperatures obtained and the possible contamination of the other sensors, because of the relative positions of the balloon and instrumentation in this configuration.

To insure accurate measurements, an attempt was made to determine the extent of the daytime and hightime boundary associated with the balloon system. While the daytime measurements were expected to be in close agreement with ambient temperatures (1,2), three daytime tests were conducted to determine the superheat of the balloon fabric. Superheat is defined in balloon terminology as any heat in excess of ambient. Three nighttime tests were conducted to determine the thermal drainage about the balloon system. In all of these tests, the ambient temperatures used in the comparisons were taken from regular radiosonde flights

at approximately the same location and normally within four hours of the test balloons. For these tests the geometry of sensor exposure on the small balloons was proportional to that of the large balloon configuration. The nighttime tests were conducted in September 1968 and January and March 1969. The balloons used were 18 feet in diameter and fabricated of 3/4 mil thick polyethylene. For the first two tests, three thermistors were mounted on each of two booms, the first two feet and the second approximately 22 feet below the balloon, with the position of each sensor as shown in Figure 38.4. As can be noted from the figure, the thermistors six feet from the center of the boom were still in the nighttime drainage since the balloon radius was nine feet. The thermistor in line with the outer edge of the balloon measured 9°C colder than the ambient. All three thermistors on the lower boom yielded identical temperatures, still 7°C lower than ambient.

For the third night test, the balloon was at a float altitude of 54,000 feet and was equipped with a grid of thermistors as shown in Figure 38.5. Although one of the thermistors was exposed three feet above the top of the balloon and was shielded from the balloon by a large, one-inch-thick sheet of StyroFoam, its temperature readings indicated the effect of blackbody radiation from the balloon.

There are two main points of interest in this figure. First, the shape of the drainage is delineated by the isotherms. The flow appears to be turbulent and not laminar as shown by Ney et al (1961). When viewed in a horizontal rather than a vertical plane, the drainage about the balloon resembles the flow through a diffusion nozzle. Note that the flow differs somewhat from the model reported by Wagner (1965), although his model with the Froude number similar to atmospheric conditions agrees in many respects with the results of these tests. The temperature differences at this altitude (the lowest float level included in this study) were the least that were encountered during the tests, suggesting that the blackbody radiation temperature and the ambient were possibly about the same.

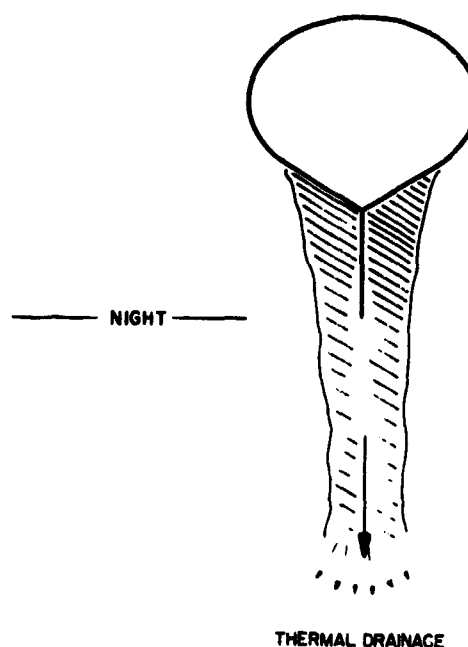


Figure 38.3 Model After Wagner Showing Nighttime Drainage Pattern Obtained in Fluid Tank Where Grashoff Number is of Same Order of Magnitude as that of a Balloon of Medium Size at High Altitude, Balloon Material Being Mylar. Temperature differences for polyethylene balloons are usually smaller due to the lower absorption coefficient of polyethylene in the infra-red range

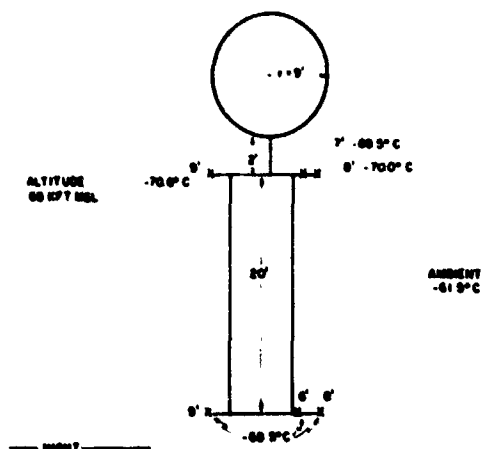


Figure 38.4. Test with a Polyethylene Balloon — Third in a Series. The initial test modeled the same geometry as the 29-million cubic foot balloon launched by Byers & Ballard; since the first test was inundated with the cold drainage the thermistors were progressively moved out until this one shown as the same distance out as the outer limit of the balloon

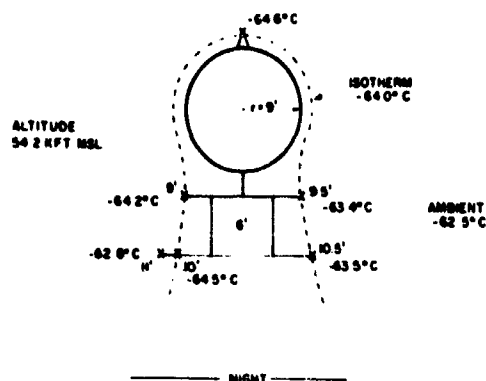


Figure 38.5. Isotherm Pattern Shown Delineates Shape of Drainage Flown Down from Balloon. This test was the lowest flown in altitude and had the least spread between ambient and balloon sensors. Note that the thermistor out 11 feet on the bottom boom was essentially ambient.

Three daytime tests were conducted in April and May 1969 to test the superheat of the balloon fabric. Two of the balloons were 18 feet in diameter and made of polyethylene; the third was a 200-foot-gore-length tetrahedron fabricated of 1/4 mil mylar. The float level of all three balloons was 70,000 feet. The test configuration was as shown in Figure 38.6. AMT-15 radiosondes with clock-switching were modified to provide three temperature readings in lieu of the standard pressure, humidity, and temperature. The superheat of the polyethylene was 40°C and of the mylar was 43°C . Note that the dangling thermistor and the thermistors on the three-foot boom were indicating 12 to 14°C higher than the ambient temperature. This is of the same order of superheat experienced on the September 1968 flight of the large balloon.

In September 1969, a 30-million cubic foot balloon was launched from White Sands. The balloon was launched with payload 65 feet below balloon (same as 1968 flight). The launch was during the night, and the instrumentation recorded temperatures well below ambient when the balloon reached 135,000 feet altitude. As the sun rose on the balloon, the instrumentation indicated a large temperature rise along with a large height rise. Before the instrumentation was lowered 1000

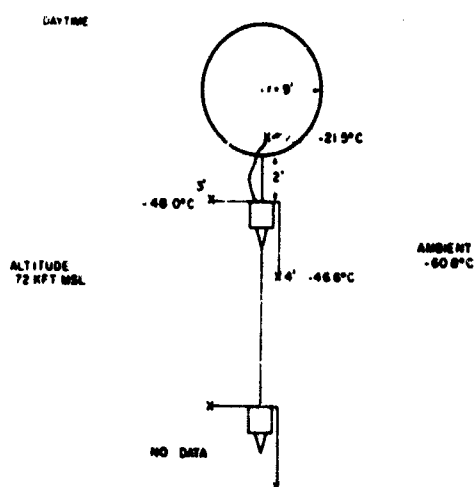


Figure 38.6. Daytime Flights Flown with Both Mylar and Polyethylene Balloons. This test was with polyethylene, but it was found that the superheat was identical using either film. Note the superheat of the balloon of approximately 40°C . The balloon affects also both of the thermistors on the radio-sonde

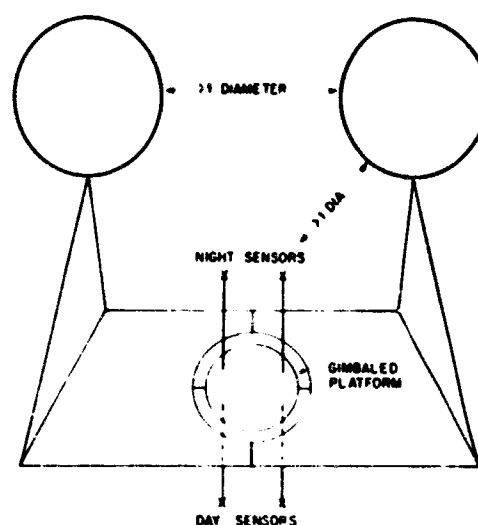


Figure 38.7. Proposed Launch Configuration that is a Real Balloon Launcher's Nightmare. It should enable an experimenter to obtain true day and night ambient temperatures

feet below the balloon, a superheat of 10°C was noted. After the payload was lowered, the instrumentation indicated a temperature near ambient.

In summary, daytime tests with small (for the most part 18-foot diameter) balloons at 70,000 feet have shown that the superheat of both mylar and polyethylene balloons is approximately 40°C , and that instrumentation within less than $1/2$ the balloon diameter may experience superheat of 10 to 14°C above the ambient.

At night, the thermal drainage about a balloon system is quite extensive, resulting in temperatures that range from a few degrees to 15° lower than ambient, depending on sensor exposure on the balloon system.

One means of possibly obtaining "undiluted" temperature measurements in the atmosphere would be a system such as is shown in Figure 38.7. The configuration would include a gimbaled platform supported between two balloons so that there would be nothing above or below the sensors for night or day flights, respectively.

References

- Ney, E., Maas, R.W. and Huch, W.F. (1961) The measurement of atmospheric temperature J. Meteor., 18:60-80.
- Reynolds, R.D., and Lamberth, R.L. (1966) Ambient temperature measurements from radiosondes flown on constant-level balloons J. Appl. Meteor., 5:304-307.
- Wagner, W.C. (1965) Temperature Measurements from Floating Balloons, Proceedings 1964 AFCL Scientific Balloon Symposium, Air Force Surveys in Geophysics, No. 167, pp. 157-169.

Contents

39.1	Introduction	477
39.2	Load Attachment System	478
39.3	Balloon Films	478
39.4	Launch Techniques	480
39.5	Ascent Controls	480
39.6	Performance Summary	481
39.7	Conclusion	482

39. Nimbus-D/IRLS Superpressure Balloons in the Tropical Stratosphere

J.D. Tefft
National Center for Atmospheric Research
Boulder, Colorado

Abstract

A summary of twenty-two, tropical, experimental superpressure balloon flights is presented. These flight data describe the launch technique, ascent controls, balloon films investigated, balloon design, environmental conditions, and anticipated durational float altitudes of 30 mb and 50 mb.

This program is a joint NCAR-GSFC meteorological experiment utilizing the Nimbus-D/IRLS system to provide quantitative measurements of wind speed, wind direction and ambient temperature on a global scale.

39.1 INTRODUCTION

On 8 April 1970, near midnight, the Nimbus-4 weather satellite was launched successfully into polar orbit. Along with remote sensors and weather cameras, the Interrogation, Recording and Location System (IRLS) will make the most comprehensive study yet undertaken of the earth's atmosphere.

NCAR's responsibility in this NASA weather program is to develop the appropriate launch techniques, and provide suitable stratospheric super-pressure

balloons to study the oscillation in the stratospheric winds which appears to vary in a quasi-biennial fashion. During the past 2 1/2 years, 22 test flights have been made and evaluated from Ascension Island. The final flight program is currently underway from Ascension, with the Nimbus-4 satellite tracking the balloon packages and relaying the data to the Goddard Space Flight Center computer center.

39.2 LOAD ATTACHMENT SYSTEM

The poor performance of the Ascension balloons during the early flights was attributed to cold tropopause, excessive ascent rate and oscillation, or a combination of these. Two flights at 30 mb were made from Christchurch, New Zealand, with Raven balloons which averaged 160 days, but the cold tropical tropopause and high ascent rate were eliminated. Two Schjeldahl balloons were launched similarly from Christchurch, but failed. In the second Ascension series a Schjeldahl balloon failed in the same manner as the two bursts in the first series, as well as one burst from Christchurch - the balloon shattered as it became spherical but prior to developing any superpressure.

In Table 39.1 is a tabulation which has led us to conclude that failures just prior to entering float altitude were due to a faulty load-attachment fitting, which overstressed the attachment point when the balloon is spherical and the load exceeds ten pounds.

Figures 39.1 and 39.2 show several types of load attachment schemes that have been investigated. It was observed during the cold chamber tests at Wright-Patterson AFB that the nylon caps and webbing systems tended to shrink at low temperatures (-80°F), and stress that part of the balloon to failure.

After this analysis and several launches, we elected to use the great-circle design on the Nimbus-D flight balloons. This eliminated any bonding of material to the balloon wall, and uniformly distributed the load entirely around the balloon along the bi-taped seals.

39.3 BALLOON FILMS

Several polyester film laminates were evaluated during the test series, such as bilaminates of mylar, Celanar and Scotchpar, and trilaminates of mylar-saran and mylar-thick adhesive.

A double envelope of mylar and saran-coated mylar was tested, but it exhibited additional fabrication problems as well as a weak saran-coated material. This design was not explored further.

Table 39.1. Load Attachments

Launch Site	Balloon Manufacturer	Attachment Type*	Flight Results
Ascension	Raven	R-1	2 days
Ascension	Schjeldahl	S-1	10 days
Ascension	Schjeldahl	S-1	burst
Ascension	Raven	R-1	2 days
Ascension	Raven	R-1	2 days
Ascension	Schjeldahl	S-1	burst
Christchurch	Raven	R-1	O.K.
Christchurch	Raven	R-1	O.K.
Christchurch	Schjeldahl	S-2	2 days
Christchurch	Schjeldahl	S-2	burst
Ascension	Raven	R-2	O.K.
Ascension	Schjeldahl	S-2	burst
Ascension	Raven	R-2A	O.K.
Ascension	Schjeldahl	S-2A	O.K.

*R-1 = 4 lines attached 6 ft from bottom.

S-1 = End cap mesh attached around periphery of cap section.

S-2 = Two crossed bands of nylon netting attached 40 inches from bottom.
No excess material.

R-2 = Similar to S-2 but with less stress concentration on attachment corner.

S-2A = Field modification, adding 2 inches to nylon bands.
R-2A =

The mylar-thick adhesive balloons (1/2-mil mylar x 1/2-mil adhesive x 1/2-mil mylar) indicated an initial period of creep and then catastrophic failure.

The trilaminate balloons of mylar-saran (3/4-mil mylar x 3/4-mil saran x 3/4-mil mylar) showed reasonable overpressure throughout their lifetime, but suddenly ruptured. These two flights averaged 60 days at 50 mb in the tropics. The lamination of saran adds considerably to the balloon weight and not necessarily to an extended duration. Therefore, this film was not investigated further.

Since the longest duration flights have been made with the conventional bi-laminated mylar, this design was selected for the final flight series with the Nimbus-D/IRLS packages.

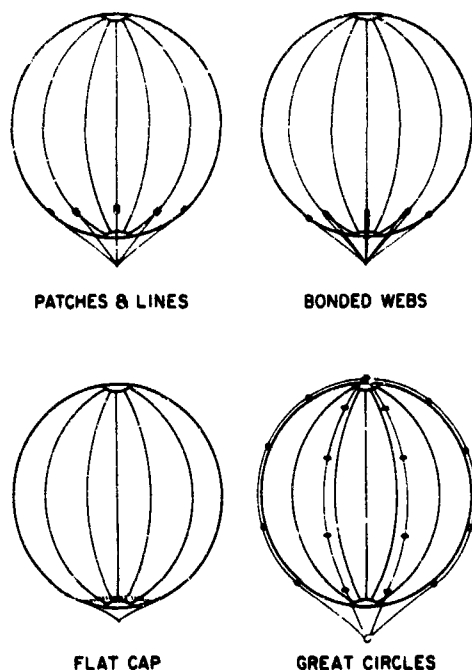


Figure 39.1. Load Attachments

39.4 LAUNCH TECHNIQUES

The balloon trailer and launch truck (Figure 39.3) have been used satisfactorily throughout the test series, to launch balloons in the trade winds which blow continuously across Ascension Island ($8^{\circ}\text{S} \times 14^{\circ}\text{W}$) at an average velocity from 14-25 miles per hour. The original GHOST wagon was modified by the addition of heavier wheels and axles and a wider track, all of which greatly increased its stability.

The use of this mobile launch technique has been developed to the point of complete reliability and safety for the launching of the large superpressure balloon and electronic packages.

39.5 ASCENT CONTROLS

Some of the early balloon failures in the program were attributed in part to a relatively high rate of ascent (1000 to 1500 ft/min) through the tropopause.

In order to reduce the ascent rate to less than 1000 ft/min through the cold tropopause, the superpressure balloon is ballasted for a net freelift of 1 percent. Freon (FR-11) is used for ballast and is carried aloft in a vented, black plastic jug. FR-11 has a boiling temperature near $+25^{\circ}\text{C}$ at sea level. During ascent, the Freon temperature remains below boiling point. At float altitude heating of the black jug causes a slow evaporation of the liquid, with a gradual increase in balloon superpressure.

With this ascent-control system, the average ascent rate is 600 ft/min from surface to 40,000 ft, then slowly increases to float altitude. The maximum rate is attained at the time the balloon becomes spherical and begins to overpressure. This final maximum rate is around 1000 ft/min.

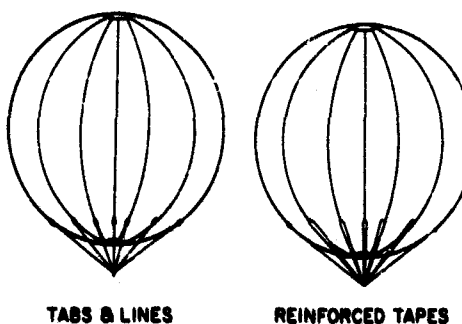


Figure 39.2. Load Attachments

Ground tests performed at Ascension showed a 2 gm/min evaporation rate for the black bottle outdoors in the shade, and 8 gm/min in bright sunlight. Our best estimate is four to five hours at altitude to evaporate 4000 grams of Freon.

Another control used for stability during ascent was an 8.5 ft diameter, natural shaped, zero-pressure polyethylene balloon. This balloon performed the following four functions during the launch and ascent phases:

- (1) Acted as a guide or pilot balloon to determine proper launch truck wind speed.
- (2) Launched the GHOST locator package prior to the Nimbus balloon.
- (3) Provided the required freelif for the FR-11 Freon ballast during the early phase of ascent.
- (4) Used as a drag stabilizer during ascent of Nimbus balloon.

This small balloon was permanently attached to the lower end of the 190-ft flight train.



Figure 39.3. Balloon Trailer and Launch Truck

39.6 PERFORMANCE SUMMARY

Out of the 22 test flights, eight failed within a few days after launch and the remainder averaged the following durations:

30 mb = 67 days

50 mb = 109 days

Tests are nearly complete on the balloon film from a 50 mb balloon that flew 81 days and was recovered from the Congo. The film is being investigated for ultraviolet deterioration, changes in the chemistry of the polyester plastic through IR tests, and biaxial strength tests. Initially, it appears that the shorter lifetime in the cold tropical stratosphere is due to a loss in film strength in areas of the balloon directly exposed to ultraviolet radiation (top sections). The top area received 521 hours of equivalent normal exposure from the sun and showed 44 to 50 percent loss of strength, as compared to the equatorial areas where only a 6 percent loss of strength was observed (balloon equator received 233 hours of equivalent normal sun exposure). Seal strength deterioration appears to be more marked in the case of the top sections (53 to 58 percent loss of strength compared

to 16 to 23 percent loss for seals in lower portions of the sphere). The areas adjacent to the seals developed more holes during testing than film samples from the center of the gore. From these initial biaxial tests it appears that the top polar area was weaker and more brittle.

39.7 CONCLUSION

The current May-June series of Ascension Island launches consist of ten 50-mb balloons and five 30-mb balloons launched during a five-week period. Sixty days after the last balloon is launched the second series of fifteen flights will be made, with the same number of balloons as launched in the first series.

Contents

40.1	Introduction	483
40.2	Block Diagram Description of IRLS	484
40.3	IRLS Modulation and Coding	486
40.4	IRLS Synchronization Techniques	487
40.5	IRLS Ranging Technique	487
40.6	IRLS Spacecraft and BIP RF Hardware	488
40.7	Spacecraft Receiver	488
40.8	Spacecraft Transmitter	489
40.9	Platform Receiver	490
40.10	Platform Transmitter	491
40.11	Diplexers	492

40. Nimbus 4 Interrogation, Recording and Location Subsystem

A. Gottesman
General Instrument Corporation
Hicksville, New York

40.1 INTRODUCTION

The Interrogation, Recording, Location Subsystem (IRLS) experiment provides for the periodic collection of scientific data from both the surface of the earth and its atmosphere on a global basis. IRLS additionally provides position determination and tracking (in latitude-longitude coordinates) of its various fixed and mobile data-gathering stations. Since existing data collection is limited to a regional basis, and in general does not contain position or tracking capability, it is expected that an operational IRLS will contribute significantly to the field of meteorology.

IRLS achieves global coverage by using the earth-oriented Nimbus satellite as an active relay station to periodically collect and store data obtained from remote data gathering stations. These stations can take the form of buoys, weather stations and high altitude balloons. The data collected by the satellite is subsequently transmitted to a ground station when the two are in communication range. The specific objectives of IRLS are:

- (1) Provide a data relay and location system for remote platforms.
- (2) Prove feasibility of selective interrogations of a remote platform from a satellite and receipt of an automatic response.

- (2) Provide data collection from platforms on a global scale.
- (4) Trace atmospheric motion by direct measurement of the flight path of a free-floating, constant-level balloon.

To date, two Nimbus satellites containing IRLS operational hardware have been successfully launched. The first of these, designated as Nimbus 2, was launched in April, 1969, while the second, designated as Nimbus 4, was launched in April, 1970. The Nimbus 4 IRLS hardware includes newly designed receivers and transmitters to perform functions similar to Nimbus 2 IRLS. Advanced features permit lighter, less expensive data-gathering packages. The overall IRLS system tests conducted thus far on a limited number of ground-based, fixed and mobile data-gathering stations have been successful. Specific recent tests that have received wide publicity include tracking an ocean buoy in the South Atlantic (Nimbus 2) and tracking an elk in Colorado (Nimbus 4). The first IRLS balloon-borne data gathering package is scheduled for launch, at the time of this writing, from New Zealand under the auspices of NCAR. Currently, thirty IRLS balloon-borne data-gathering electronics packages (designated as BIP's) are being manufactured for NASA at General Instrument Corporation's Electronic Systems Division.

40.2 BLOCK DIAGRAM DESCRIPTION OF IRLS

The block diagram of IRLS is shown in Figure 40. 1. IRLS consists of three basic components:

- (1) Remote data-gathering packages or platforms
- (2) A satellite
- (3) A ground station

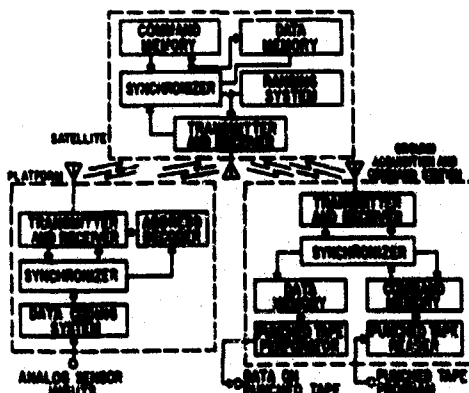


Figure 40. 1. IRLS Simplified Block Diagram

The platform may be functionally divided into a data coding system, a synchronizer, an address decoder, and a transmitter and receiver. Upon reception and demodulation of the rf PCM/FM coded signal from the spacecraft by the receiver, the receiver output is fed to the synchronizer and then to the address decoder. The synchronizer establishes the timing for all platform operations, and its timing is synchronized to the received PCM signal. When the address decoder recognizes its unique address

(each platform is assigned a unique address which is hard-wired in the unit at the factory), the transmitter is energized and the platform address is retransmitted to the spacecraft as an acknowledgement. The spacecraft, in turn, acknowledges the platform reply after acquiring synchronization to the received PCM code train. When the platform receives and recognizes the spacecraft acknowledgement, the platform data-coding system, which accepts inputs from the analog sensors, is energized. The BIP then transmits its frame of data to the spacecraft. A frame of data consists of two platform address complements, the data obtained from the platform sensors, and an additional platform address complement. The analog inputs from the sensors to the data coding system are sequentially encoded into a serial binary PCM pulse train. The spacecraft uses the first platform address complement in the reply frame to perform the satellite-to-platform range measurement. After transmission of the data frame, the platform transmitter is de-energized. The entire satellite-BIP communication sequence described above lasts for a period of approximately 3 seconds.

The satellite IRLS equipment may be functionally divided into a command and data memory, a synchronizer, ranging system, and transmitter and receiver. The command memory stores the commands it receives from the ground station when the two stations are in communications view during each orbital pass around the earth. This command information contains the addresses of each of the platforms which are to be interrogated during the subsequent orbit, together with the time the interrogation should commence. When the command time and the Nimbus spacecraft clock time coincide, the transmitter is energized and the spacecraft begins transmission of a platform address signal. The spacecraft receiver demodulates the interrogated platform's acknowledgement and data frame signals. The spacecraft synchronizes to the platform PCM signal during platform acknowledgement transmission (which precedes the data frame transmission). This enables the ranging system to perform a valid range measurement on the first address complement in the data frame, and to correctly recognize the received data which follows. Both the received data and the computed range (from the ranging system) are transferred to and stored in the data memory. When the satellite is in communications range of the Ground Station, the data memory contents are transmitted to and stored in the data memory in the ground station. This transmission is initiated upon command from the Ground Station. New platform address and time commands for the next orbit are then transmitted to the spacecraft from the Ground Station.

The Ground Station (commonly referred to as the Ground Acquisition and Command Station, GACS) contains the same functional components as the satellite, with the addition of a tape perforator and a tape reader. The punched tape program, which contains the platform interrogation command data, is read into the Ground Station command memory and subsequently transferred to the satellite command

memory following reception of the stored satellite data. The latter data is stored in the Ground Station data memory and then put on paper tape for further processing.

10.3 IRLS MODULATION AND CODING

The selection of IRLS transmission parameters has been governed by the following considerations:

(1) Transmit the required amount of data (with the specified resolution) in the minimal time in order to reduce average power consumption in the spacecraft and balloon.

(2) Provide a transmission code which can provide rapid synchronization so that data transfer can start as quickly as possible.

(3) Provide a sufficiently wide bandwidth so that signal rise times are short to permit an accurate ranging measurement to be performed on the spacecraft.

PCM/FM transmission has been chosen to most nearly satisfy the system requirements. The data, command and address bit rate is 1.041 kHz, and each data bit modulates 8 bits of a group of 12-12.5 kHz pulse trains. The remaining four bits of the 12.5 kHz pulse train group are used for synchronization, and the group of 12 bits comprise a word. The eight bit configuration (referred to as an M word) for a "1" is 10101100, and for "0" zero it is 01010011 or the complement of the "1" representation. Sixteen words are grouped together to form a pattern. The last four bits (referred to as the N word) in all but the first M word of a pattern have the configuration 1001, while the corresponding N word for the first word in the pattern is 0110. The N words permit the receiving equipment to establish both word and pattern synchronization.

Data transmission from the platforms to the spacecraft, and from the spacecraft to the Ground Station is in a frame format. A frame consists of a number of patterns; the BIP data frame format, for example, is shown in Figure 40.2 and consists of 10-16 word patterns. The first two patterns in the frame contain the complement of the 10 word address of the responding platform. The following seven patterns contain the coded sensor data, while the tenth pattern repeats the address complement of the platform. The sampled data from each analog sensor is encoded into 7 words (or major bits) plus a parity check word. As seen from Figure 40.2, two data word groups from two analog sensors are combined into a pattern in the frame. The total time required to transmit the BIP data frame format is 0.1536 seconds.

The 12.5 KC pulse train frequency shifts the transmitted UHF frequency about its unmodulated value. A "1" causes the frequency to increase by 25 kHz, and a "0" causes the frequency to decrease by 25 kHz. This non-return-to-zero (NRZ)

modulation technique results in an average frequency equal to the unmodulated frequency, since both the M and N words contain an equal number of 1's and 0's. This fact makes it easier to implement automatic frequency control on the received signal.

40.4 IRLS SYNCHRONIZATION TECHNIQUES

Each of the IRLS receiving equipments employs phase-lock loops to lock or synchronize to the demodulated 12.5 kHz pulse train directly. Synchronization is derived from each of the seven or eight transitions of the 12.5 kHz bits that occur in each word. The phase-lock loop is narrow band to permit synchronization at low carrier-to-noise ratio, and to provide a "coasting" effect or memory when the received signal momentarily fades.

The 12.5 kHz synchronized regenerated signal is divided down by 12 and then by 16 times to establish the word and pattern rates, respectively. The first divider (divide by 12) is reset or synchronized from the word sync pulses, while the second divider is reset or synchronized by pattern sync pulses. Word sync pulses are generated when any of the four possible 12 bit word configurations are recognized. Pattern sync pulses are generated when either of the two possible 8 bit groups is found together with the 0110 N word configuration.

40.5 IRLS RANGING TECHNIQUE

By using certain geometrical relationships, the platform location, in latitude-longitude coordinates, may be computed from the following data:

- (1) Two slant range measurements between the spacecraft and the platform.
- (2) The trajectory of the spacecraft and the distance it travels between each of the two slant range measurements. IRLS performs a slant range measurement during each interrogation cycle with the platform by, in effect, measuring the round trip propagation time of the satellite reply sequence to the platform acknowledgement signal.

Platform reception of the satellite reply initiates transmission of the data frame. The first line of the data frame (see Figure 40.2) contains the platform address complement. Satellite recognition of this pattern causes a 15 stage

2 ¹⁵	2 ¹⁴	2 ¹³	2 ¹²	2 ¹¹	2 ¹⁰	2 ⁹	2 ⁸	2 ⁷	2 ⁶	2 ⁵	2 ⁴	2 ³	2 ²	2 ¹	2 ⁰	BIT LINE
UNIT ADDRESS COMPLEMENT															1	
UNIT ADDRESS COMPLEMENT															2	
UNSPECIFIED DATA															3	
UNSPECIFIED DATA															4	
UNSPECIFIED DATA															5	
P ₁₅		DATA WORD 2						P ₈		DATA WORD 1						6
P ₁₅		DATA WORD 4						P ₈		DATA WORD 3						7
P ₁₅		DATA WORD 6						P ₈		DATA WORD 5						8
UNSPECIFIED DATA															9	
UNIT ADDRESS COMPLEMENT															10	

NOTES: 1. MSB ABOVE IS ON LEFT IN ALL LINES.
 2. P₁₅ IS ODD PARITY FOR BITS 20-29.
 3. P₈ IS ODD PARITY FOR BITS 30-39 EXCLUDING BIT 27.
 4. OUTDOWN MODE FORMAT WILL CONTAIN UNIT ADDRESS INSTEAD OF UNIT ADDRESS COMPLEMENT.

Figure 40.2. BIP Data Frame Format

counter driven by a 1.6 Mhz clock to be started. The counter is stopped at the beginning of the following satellite reply sequence, and its contents at this time are a measure of the platform-to-satellite slant range. The range number is transferred to the data memory and subsequently transmitted to the ground station. Accuracy of the slant range is ± 500 meters, and accuracy of the platform location is ± 2 kilometers.

40.6 IRLS SPACECRAFT AND BIP RF HARDWARE

The most challenging and critical parts of the IRLS equipment design were the spacecraft and BIP rf components. Both units contain a receiver, transmitter and diplexer. Photographs of these Nimbus 4 components developed and manufactured by General Instrument Corp., are shown in Figures 40.3 through 40.7.

40.7 SPACECRAFT RECEIVER

The Spacecraft Receiver (Figure 40.3) acquires the platform and ground station transmitted signals. The Nimbus 4 spacecraft receiver contains several advanced features, compared to the Nimbus 2 equipment, which result in approximately 6 dB sensitivity enhancement. Consequently, platform transmitter power requirements are reduced from 25 watts to 6 watts. Among the advanced features contained in the IRLS Nimbus 4 spacecraft receiver are:

- (1) Very low noise RF amplifier.
- (2) Highly symmetrical AFC system with operation down to -3 dB IF carrier-to-noise ratios.
- (3) Rapid-quench, matched crystal filters for optimum 12.5 kHz bit detection under high noise conditions.
- (4) Separate narrow-band synchronization channel which provides the 12.5 kHz bit transition information for synchronization of the 12.5 kHz phase lock loop.
- (5) Type II narrow-band phase-lock loop which provides a more optimum trade-off of open loop gain and noise bandwidth.

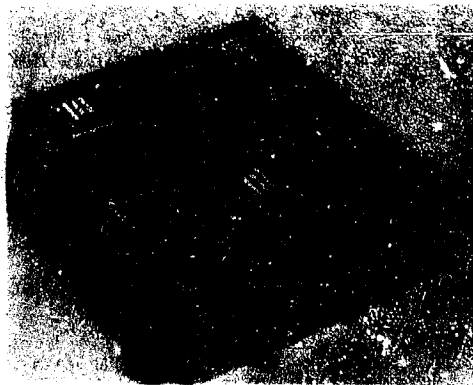


Figure 40.3. IRLS Nimbus D Spacecraft Receiver

Some of the salient measured performance characteristics of the IRLS

Nimbus 4 spacecraft receiver presently in orbit are:

- (1) Noise figure - 2.5 dB
- (2) 12.5 kHz bit error rate - less than 2×10^{-2} at -120 dBm received signal
- (3) Time delay uncertainty - less than ± 1.5 μ secs for 98 percent of the time, 800 m secs after signal reception under all conditions
- (4) Spurious frequency response - down 70 dB.

40.8 SPACECRAFT TRANSMITTER

The IRLS Spacecraft Transmitter (Figure 40.4) transmits the PCM/FM signal at a 25 watt UHF level to the platform and to the Ground Station. The transmitter is pressurized and features all solid-state construction, high frequency stability, excellent FM deviation linearity, and high efficiency. The signal to be transmitted is derived from a wideband temperature-compensated, voltage-controlled crystal oscillator. The oscillator signal is amplified and frequency multiplied before application to the final power amplifier. The latter consists of two recently developed

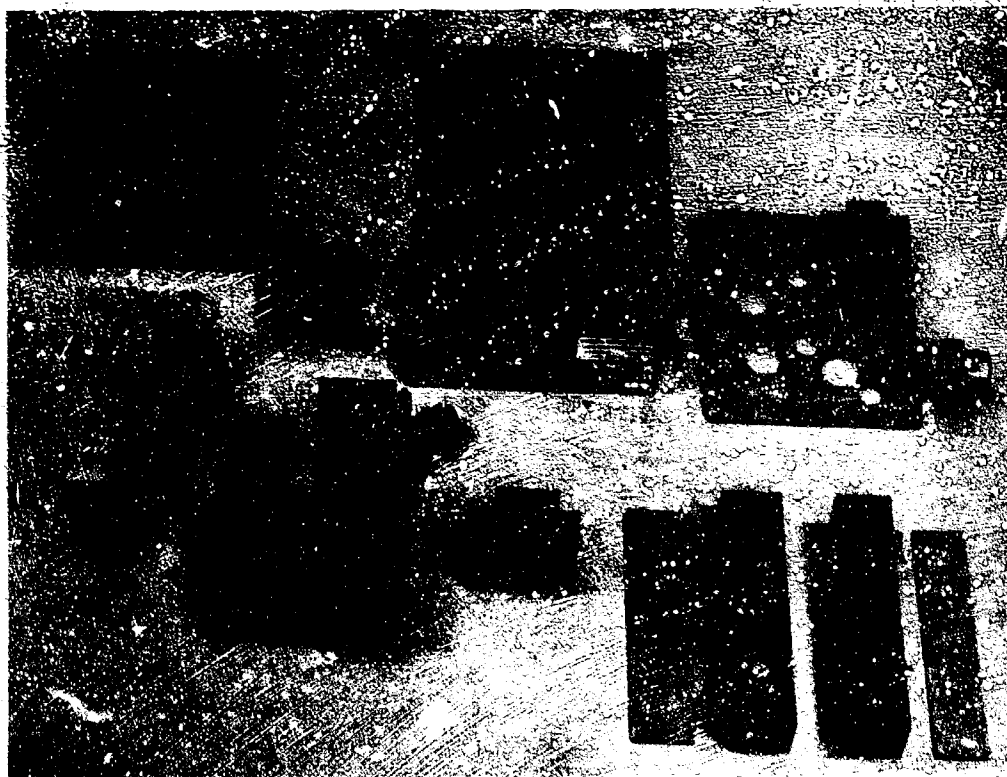


Figure 40.4. Nimbus D IRLS Spacecraft Transmitter

UHF power transistors. The power output of these two transistors is added in a hybrid power combiner and then applied to the diplexer for transmission.

Salient measured performance characteristics of the IRLS Nimbus 4 spacecraft transmitter presently in orbit are:

- (1) Power Output (CW) - 25 watts
- (2) Frequency Stability - ± 8 ppm (aging, temp. and voltage variation)
- (3) Frequency deviation non-linearity - less than 2 percent over ± 25 kHz deviation.
- (4) Power Consumption - 80 watts (when energized)
- (5) On Time - may be continuously energized for a 5 minute period when heat sunk to the spacecraft sensory ring.
- (6) Spurious - 60 dB down
- (7) Over-voltage capability - can handle 40 percent over-voltage for a five minute period and 60 percent over-voltage for transients.

40.9 PLATFORM RECEIVER

The Platform Receiver (Figure 40.5) demodulates the transmitted PCM/FM signal from the orbiting spacecraft. Features of the platform receiver include high sensitivity (3 dB noise figure), small volume (less than 12 in³), light weight (less than 8 ounces) and low average power consumption (30 mw). The low average power consumption is primarily achieved by switching the receiver power ON and OFF with a 50 percent duty cycle until recognition of a correct platform address. Salient measured performance data on the platform receiver are:

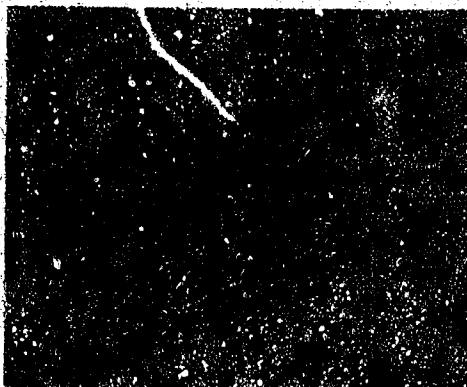


Figure 40.5. IRLS Platform Receiver

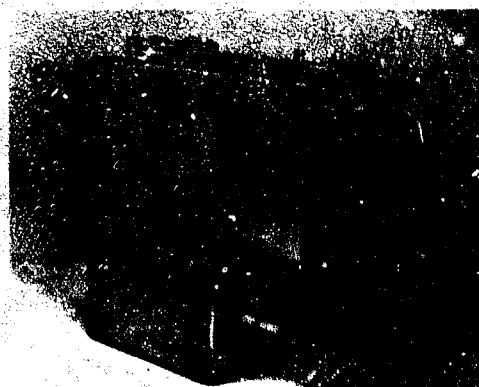


Figure 40.6. IRLS Platform Transmitter

- (1) Noise Figure - 3 dB
- (2) Time Delay uncertainty - ± 0.70 u secs (under all conditions)
- (3) Power Consumption - 30 milliwatts average
- (4) Center Frequency Stability - ± 5 ppm (referred to the receiver center frequency of 401.5 MHz).
- (5) Operating Temperature Range - -20°C to $+45^{\circ}\text{C}$
- (6) Spurious Response - 60 dB down
- (7) Volume - 12 in³
- (8) Weight - 8 ounces

(A photograph of the Platform Receiver inserted in the BIP assembly is shown in Figure 40.7.)

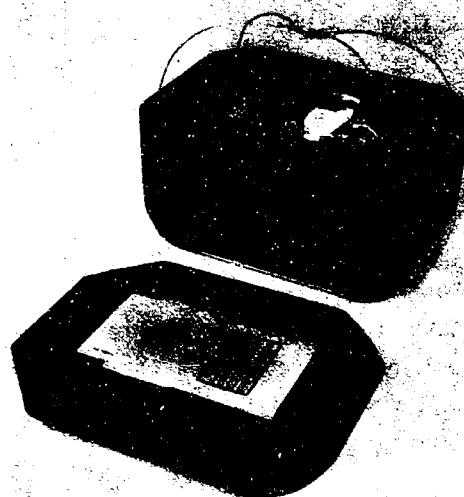


Figure 40.7. Electronics-Unit Housing and Module Configuration

40.10 PLATFORM TRANSMITTER

The Platform Transmitter (Figure 40.6) transmits the PCM/FM signal at a 6 watt level to the spacecraft. Features of the platform transmitter include high efficiency (30 percent overall), light weight (1 lb exclusive of the diplexer), full operational performance over ± 20 percent supply voltage variation and over the temperature range of -20°C to $+45^{\circ}\text{C}$, and excellent frequency stability and FM deviation linearity. The platform transmitter is energized after platform recognition of an address, and is SHUT-OFF after data-frame transmission or after a 2 second period following address recognition, whichever event occurs first.

Salient measured performance data on the platform transmitter are:

- (1) Power Output - 6 watts
- (2) Frequency Stability - ± 10 ppm
- (3) Frequency deviation non-linearity - 3 percent
- (4) Power Consumption - 21 watts total
- (5) Temperature Range - -20°C to $+45^{\circ}\text{C}$
- (6) Spurious - greater than 50 dB

A photograph of the Platform Transmitter inserted in the BIP assembly package is shown in Figure 40.7.

40.11 DIPLEXERS

The spacecraft and platform diplexer assemblies are packaged integrally with the associated transmitter and permit independent transmission and reception with 15 percent frequency separation (the platform transmit and receive frequencies are 466 MHz and 401.5 MHz, respectively, while the corresponding spacecraft frequencies are the reverse). The diplexers are helical resonator, multiplepole bandpass filters with extremely low insertion loss. Each diplexer assembly contains a three-pole transmitter section which has 0.4 dB insertion loss, and a five-pole receiver section which has 1 dB insertion loss. Isolation between transmitter and receiver is greater than 95 dB at the transmitter frequency and greater than 30 dB at the receiver frequency.

References

Cressey, J. R., and Hogan, G. D. (1965) The Interrogation, Recording and Location System Experiment, Proceedings 1965 National Telemetry Conference; P. 98-101.

GSFC Specification, S-733-P-8-A (1969) Nimbus D/IRLS Balloon Interrogation Package, Goddard Space Flight Center, Greenbelt, Maryland.

Appendix A

Publications of Proceedings of Past AFCRL Balloon Symposia and Workshops

Due to interest expressed in the proceedings of past AFCRL balloon symposia and workshops, and because the report series for these reports has been changed, a listing of the proceedings of all past AFCRL balloon symposia and workshops follows.

<u>TITLE</u>	<u>AFCRL REPORT NO. AND DATE</u>
Proceedings of the AFCRL Balloon Symposium	AFCRL-63-919, Dec. 1963 (AD614065)
Proceedings, 1964 AFCRL Scientific Balloon Symposium	AFCRL-65-486, Jul. 1965 (AD619695)
Proceedings, AFCRL Scientific Balloon Workshop, 1965	AFCRL-66-309, May 1966 (AD634765)
Proceedings, Fourth AFCRL Scientific Balloon Symposium	AFCRL-67-0075, Jan. 1967 (AD656692)
Proceedings, AFCRL Tethered Balloon Workshop, 1967	AFCRL-68-0097, Mar. 1968 (AD676037)
Proceedings, Sixth AFCRL Scientific Balloon Symposium	AFCRL-68-0661, Dec. 1968 (AD685726)

Unclassified
Security Classification

DOCUMENT CONTROL DATA - R&D		
<i>(Security classification of title, body of abstract and indexing annotation must be entered when the overall report is classified)</i>		
1. ORIGINATING ACTIVITY <i>(Corporate author)</i> Air Force Cambridge Research Laboratories (LC) L.G. Hanscom Field Bedford, Massachusetts 01730		2a. REPORT SECURITY CLASSIFICATION Unclassified 2b. GROUP
3. REPORT TITLE PROCEEDINGS, SIXTH AFCRL SCIENTIFIC BALLOON SYMPOSIUM		
4. DESCRIPTIVE NOTES <i>(Type of report and inclusive dates)</i> Scientific. Interim.		
5. AUTHOR(S) <i>(First name, middle initial, last name)</i> Lewis A. Grass, Editor		
6. REPORT DATE 27 October 1970	7a. TOTAL NO. OF PAGES 477	7b. NO. OF REFS 159
8a. CONTRACT OR GRANT NO. NASA b. PROJECT, TASK, WORK UNIT NOS. 6665 c. DOD ELEMENT 63404 F d. DOD SUBELEMENT N/A		9a. ORIGINATOR'S REPORT NUMBER(S) AFCRL-70-0543 9b. OTHER REPORT NO(S) <i>(Any other numbers that may be assigned this report)</i> Special Reports, No. 105
10. DISTRIBUTION STATEMENT 1-This document has been approved for public release and sale; its distribution is unlimited.		
11. SUPPLEMENTARY NOTES This work was supported in part by the National Aeronautics and Space Admini- stration.		12. SPONSORING MILITARY ACTIVITY Air Force Cambridge Research Laboratories (LC) L.G. Hanscom Field Bedford, Massachusetts 01730
13. ABSTRACT This publication contains the papers presented at the Sixth AFCRL Scientific Balloon Symposium held in June, 1970 to promote the exchange of current information among balloon designers, developers, and flight managers and re- searchers engaged in scientific balloon programs. Subjects include: Balloon- borne experiments in high-energy astrophysics, detection of atmospheric tides near 48 km, sun-oriented atmospheric optics, a proposed balloon mission in the Venus atmosphere, a panel on balloon materials and testing, telemetry and balloon-control instrumentation, advanced balloon technology, high altitude station-keeping balloons, the AFCRL tethered-balloon facility, advances in meteorological balloons, and superpressure balloons in the tropical stratosphere.		

DD FORM 1473
1 NOV 68

Unclassified
Security Classification

Unclassified
Security Classification

14.	KEY WORDS	LINK A		LINK B		LINK C	
		ROLE	WT	ROLE	WT	ROLE	WT
	Balloons Balloon-borne experiments Tethered balloons Balloon-materials testing Atmosphere Cosmic rays						

Unclassified
Security Classification